

ИЗБРАННЫЕ НАУЧНЫЕ ТРУДЫ ПРОФЕССОРА В.С. ЛЕТОХОВА

Составители:
В.И. Балыкин, В.Н. Задков, Е.А. Рябов, С.В. Чекалин

МОСКВА
2023

УДК 539.1
ББК 22.38+72
И 32

Балыкин В.И., Задков В.Н., Рябов Е.А., Чекалин С.В. / Избранные научные труды В.С. Летохова. – М.: РАН, 2023. – с. 532

ISBN 978-5-907645-36-3

© В.И. Балыкин, В.Н. Задков,
Е.А. Рябов, С.В. Чекалин, 2023



Владилен Степанович Летохов (1939–2009) в своем рабочем кабинете
в Институте спектроскопии РАН в День науки 24 марта 2007 года

Каждый выбирает для себя
Женщину, религию, дорогу.
Дьяволу служить или пророку –
Каждый выбирает для себя.

Каждый выбирает по себе
Слово для любви и для молитвы.
Шпагу для дуэли, меч для битвы
Каждый выбирает по себе.

Каждый выбирает по себе.
Щит и латы, посох и заплаты,
Меру окончательной расплаты
Каждый выбирает по себе.

Каждый выбирает для себя.
Выбираю тоже – как умею.
Ни к кому претензий не имею.
Каждый выбирает для себя!

Ю.Д. Левитанский
(1922–1996)

СОДЕРЖАНИЕ

ПРЕДИСЛОВИЕ 8

КНИГИ, ОПУБЛИКОВАННЫЕ В.С. ЛЕТОХОВЫМ 12

ИЗБРАННЫЕ СТАТЬИ В.С. ЛЕТОХОВА 14

1. ЛАЗЕРЫ 15

1.1. *Басов Н.Г., Амбарцумян Р.В., Зуев В.С., Крюков П.Г., Летохов В.С.* Нелинейное усиление импульса света // ЖЭТФ. 1966. Т. 50 (1). С. 23–34 ... 16

1.2. *Амбарцумян Р.В., Басов Н.Г., Крюков П.Г., Летохов В.С.* Лазер с нерезонансной обратной связью // Письма в ЖЭТФ. 1966. Т. 3 (6). С. 261–264 30

1.3. *Летохов В.С.* Генерация света рассеивающей средой с отрицательным резонансным поглощением // ЖЭТФ. 1967. Т. 53 (10). С. 1442–1452 33

1.4. *Летохов В.С.* Автостабилизация частоты световых колебаний лазера нелинейным поглощением в газе // Письма в ЖЭТФ. 1967. Т. 6 (4). С. 597–600 46

1.5. *Летохов В.С.* Генерация ультракоротких импульсов света в лазере с нелинейным поглотителем // ЖЭТФ. 1968. Т. 55, 3 (9). С. 1077–1089 50

1.6. *Kryukov P.G., Letokhov V.S.* Fluctuation mechanism of ultrashort pulse generation by laser with saturable absorber // J. Quant. Electron. QE. 1972. Vol. 8 (10). P. 766–782 65

1.7. *Жерихин А.Н., Кошелев К.Н., Летохов В.С.* Об усилении в области далекого вакуумного ультрафиолета на переходах многозарядных ионов // Квант. электроника. 1976. Т. 3 (1). С. 152–156 98

1.8. *Жерихин А.Н., Кошелев К.Н., Крюков П.Г., Летохов В.С., Чекалин С.В.* Поиски усиления в далекой ВУФ области на переходах многозарядных ионов в протяженной лазерной плазме // Квант. электроника. 1981. Т. 8 (1). С. 88–97 104

2. ЛАЗЕРНАЯ СПЕКТРОСКОПИЯ 117

2.1. *Bekov G.I., Letokhov V.S., Mishin V.I.* Isotopically selective Rb atoms ionization through Rydberg states by laser and electric fields // Opt. Commun. 1977. Vol. 23 (1). P. 85–89 118

2.2. *Antonov V.S., Knyazev I.N., Letokhov V.S., Matiuk V.M., Movshev V.G., Potapov V.K.* Stepwise laser photoionization of molecules in a mass spectrometer: a new method for probing and detection of polyatomic molecules // Opt. Lett. 1978. Vol. 3 (2). P. 37–39 126

2.3. *Летохов В.С., Мовшев В.Г., Чекалин С.В.* Фотоотрыв ионов молекул родамина 6G, адсорбированных на поверхности, под действием ультракороткого лазерного импульса // ЖЭТФ. 1981. Т. 81 (8). С. 480–485 133

2.4. *Antonov V.S., Letokhov V.S.* Laser multiphoton and multistep photoionization of molecules and mass spectrometry // Appl. Phys. 1981. Vol. 24. P. 89–106 140

2.5. *Bekov G.I., Letokhov V.S.* Laser atomic photoionization spectral analysis of element traces // Appl. Phys. B. 1983. Vol. 30. P. 161–176 169

2.6. *Chekalin S.V., Farztdinov V.M., Golovlyov V.V., Letokhov V.S., Lozovik Yu.E., Matveets Yu.A., Stepanov A.G.* Femtosecond spectroscopy of $YBa_2Cu_3O_7$-δ: electron-phonon-interaction measurement and energy-gap observation // Phys. Rev. Lett. 1991. Vol. 67 (27). P. 3860–3863 196

3. ЛАЗЕРНЫЙ КОНТРОЛЬ ДВИЖЕНИЯ АТОМОВ 202

3.1. *Летохов В.С.* Сужение доплеровской линии в стоячей световой волне // Письма в ЖЭТФ. 1968. Т. 7 (9). С. 348–351 203

3.2. *Letokhov V.S., Minogin V.G., Pavlik B.D.* Cooling and trapping of atoms and molecules by a resonant laser field // Opt. Commun. 1976. Vol. 19 (1). P. 72–75 207

3.3. *Андреев С.В., Балыкин В.И., Летохов В.С., Миногин В.Г.* Радиационное замедление и монохроматизация пучка атомов натрия до 1,5 К во встречном лазерном луче // Письма в ЖЭТФ. 1981. Т. 34 (8). С. 463–467 213

3.4. *Балыкин В.И., Летохов В.С., Сидоров А.И.* Радиационная коллимация атомного пучка путем двухмерного охлаждения лазерным излучением // Письма в ЖЭТФ. 1984. Т. 40 (6). С. 251–253 218

3.5. *Balykin V.I., Letokhov V.S.* Laser optics of neutral atomic beams // Physics Today. 1989. Vol. 42 (4). P. 23–28 222

3.6. *Балыкин В.И., Летохов В.С., Овчинников Ю.Б., Сидоров А.И.* Отражение атомного пучка от градиента светового поля // Письма в ЖЭТФ. 1987. Т. 45 (6). С. 282–284 235

3.7. *Balykin V.I., Letokhov V.S., Ovchinnikov Yu.B., Sidorov A.I.* Quantum-state-selective mirror reflection of atoms by laser light // Phys. Rev. Lett. 1988. Vol. 60 (21). P. 2137–2140 239

3.8. *Balykin V.I., Letokhov V.S., Ovchinnikov Yu.B., Sidorov A.I., Shul'ga S.V.* Channeling of atoms in a standing spherical light wave // Opt. Lett. 1988. Vol. 13 (11). P. 958–960 246

3.9. *Grimm R., Ovchinnikov Yu.B., Sidorov A.I., Letokhov V.S.* Observation of a strong rectified dipole force in a bichromatic standing light wave // Phys. Rev. Lett. 1990. Vol. 65 (12). P. 1415–1418 251

3.10. *Balykin V.I., Letokhov V.S.* The possibility of deep laser focusing of an atomic beam into the Å-region // Opt. Commun. 1987. Vol. 64 (2). P. 151–156 259

4. ЛАЗЕРЫ И ЯДЕРНАЯ ФИЗИКА 269

4.1. *Летохов В.С.* Узкие резонансы испускания и поглощения γ-излучения ядер, индуцируемые лазерным излучением // Письма в ЖЭТФ. 1972. Т. 16 (7). С. 428–431 270

4.2. *Letokhov V.S.* Narrow-frequency tunable γ-ray nuclear resonances induced by laser radiation // Phys. Rev. Lett. 1973. Vol. 30 (16). P. 729–732 274

5. ЛАЗЕРНЫЕ ФОТОСЕЛЕКТИВНЫЕ ПРОЦЕССЫ И ЛАЗЕРНОЕ РАЗДЕЛЕНИЕ ИЗОТОПОВ 279

5.1. *Амбарцумян Р.В., Калинин В.Н., Летохов В.С.* Двухступенчатая селективная фотоионизация атомов рубидия лазерным излучением // Письма в ЖЭТФ. 1971. Т. 13 (6). С. 305–307 280

5.2. *Ambartzumian R.V., Letokhov V.S.* Selective two-step (STS) photoionization of atoms and photodissociation of molecules by laser radiation // Appl. Opt. 1972. Vol. 11 (2). P. 354–358 282

5.3. *Амбарцумян Р.В., Летохов В.С., Макаров Г.Н., Пурецкий А.А.* Лазерное разделение изотопов азота // Письма в ЖЭТФ. 1973. Т. 2. С. 91–94 291

5.4. *Амбарцумян Р.В., Летохов В.С., Рябов Е.А., Чекалин Н.В.* Изотопически селективная химическая реакция молекул BC_{13} в сильном инфракрасном поле лазера // Письма в ЖЭТФ. 1974. Т. 20 (9). С. 597–600 295

5.5. *Ambartzumian R.V., Chekalin N.V., Doljikov V.S., Letokhov V.S., Ryabov E.A.* The visible luminescence kinetics of BCl3 in the field of a high-powerful CO_2 laser // Chem. Phys. Lett. 1974. Vol. 5 (4). P. 515–518 298

5.6. *Амбарцумян Р.В., Горохов Ю.А., Летохов В.С., Макаров Г.Н.* Разделение изотопов серы с коэффициентом обогащения $>10^3$ при воздействии излучения CO_2-лазера на молекулу SF6 // Письма в ЖЭТФ. 1975. Т. 21 (6). С. 375–378 303

5.7. *Bagratashvili V.N., Doljikov V.S., Letokhov V.S., Makarov A.A., Maljavkin L.P., Ryabov E.A., Silkis E.G., Vainer Yu.G.* Stochastization limit of vibrational energy in SF6 and CF3I molecules at IR multiple photon excitation // Opt. Commun. 1981. Vol. 38 (1). P. 31–34 307

5.8. *Makarov A.A., Petrova I.Yu., Ryabov E.A., Letokhov V.S.* Statistical inhomogeneous broadening of infrared and Raman transitions in highly vibrationally excited XY6 molecules // J. Phys. Chem. A. 1998. Vol. 102. P. 1438–1449 312

6. ЛАЗЕРНАЯ БИОМЕДИЦИНА 339

6.1. *Абильсиитов Г.А., Беляев А.А., Брагин М.А., Велихов Е.П., Жданов В.С., Кару Т.Й., Летохов В.С.* и др. Изучение фотоабляции атеросклеротических бляшек лазерным излучением // Квант. электроника. 1985. Т. 12 (10). С. 1991–1993 340

6.2. *Kara T., Tiphlovaa O., Esenaliev R., Letokhov V.* Two different mechanisms of low-intensity laser photobiological effects on Escherichia coli // Lasers Surg. Med. 1993. Vol. 13. P. 470–484 344

6.3. *Esenaliev R.O., Oraevsky A.A., Letokhov V.S., Karabutov A.A., Malinsky T.V.* Two different mechanisms of low-intensity laser photobiological effects on Escherichia coli studies of acoustical and shock waves in the pulsed laser ablation of biotissue // J. Photochem. Photobiol. B: Biol. 1994. Vol. 24. P. 155–161 355

6.4. *Karabutov A.A., Podymova N.B., Letokhov V.S.* Time-resolved laser optoacoustic tomography of inhomogeneous media // Appl. Phys. B. 1996. Vol. 63. P. 545–563 377

7. НАНООПТИКА 415

7.1. *Летохов В.С.* Применение лазерного излучения в автоэлектронной и автоионной микроскопии для наблюдения биологических молекул // Квант. электроника. 1975. Т. 2 (5). С. 930–937 416

7.2. *Chekalin S.V., Letokhov V.S., Likhachev V.S., Movshev V.G.* Laser photoion projector // Appl. Phys. B. 1984. Vol. 33. P. 57–61 426

8. АСТРОФИЗИЧЕСКАЯ СПЕКТРОСКОПИЯ 434

8.1. *Летохов В.С.* О стимулированном радиоизлучении межзвездной среды // Письма в ЖЭТФ. 1966. Т. 4 (11). С. 477–481 435

8.2. *Летохов В.С.* Астрофизические лазеры // Квант.электроника. 2002. Т. 32 (12). С. 1065–1079 438

ПОЛНЫЙ СПИСОК НАУЧНЫХ ПУБЛИКАЦИЙ В.С. ЛЕТОХОВА 472

ПРЕДИСЛОВИЕ

Владилен Степанович Летохов – советский и российский физик, пионер лазерной физики, в частности метода лазерного охлаждения атомов. Доктор физико-математических наук (1970), профессор. Автор более 850 статей и 17 монографий, наиболее цитируемый советский ученый во всех областях науки за период 1973–1988 годов.

В.С. Летохов родился в Тайшете (Иркутская область). В 1963 году окончил Московский физико-технический институт и поступил в аспирантуру ФИАН, где учился под руководством академика Н.Г. Басова, а затем работал в его же отделе. В 1970 году по приглашению профессора С.Л. Мандельштама (первого директора Института спектроскопии АН СССР, ИСАН) перешел в ИСАН, где и работал до конца своей жизни – руководил отделом лазерной спектроскопии, был заместителем директора по науке. Одновременно с 1972 года являлся профессором МФТИ. Среди учеников – 60 кандидатов и 12 докторов наук.

В.С Летохов был соредактором и членом редколлегий многих научных журналов и серий книг: соредактором серии монографий Laser Science and Technology (Harwood Academic Publ, ed. by V.S. Letokhov, C.V. Shank, Y.R. Shen and H. Walther; вышло 20 томов); соредактором журналов Lasers in the Life Sciences (1986–2009), Laser Chemistry (1982–2009), Nonlinear Optics (1991–2009), а также членом редколлегий журналов «Вестник Российской академии наук», «Журнал экспериментальной и теоретической физики» (ЖЭТФ) (1980–1982), «Квантовая электроника» (1974–2009), Optics Communications (1976–2009), Optics Letters (1977, 1979–1980, 1982–1986, 1988–1990), Comments on Atomic and Molecular Physics (1977–2009), Journal of Modern Optics (part “Optics Acta”) (1986–2009), Chemical Physics (1981–2009), Chemical Physics Letters (1991–2009), Nuovo Cimento B (1977–1982), Nuovo Cimento D и P (1995–2009), Chinese Journal of Lasers (1989–1997), Applied Physics B (1980–1992), Laser Focus (1971–1982), Spectrochimica Acta B и Journal of Applied Spectroscopy.

В.С. Летохов был удостоен за его научные заслуги Ленинской премии (совместно с В.П. Чеботаевым в 1978 году – за цикл работ по нелинейным узким резонансам в оптике и их применению), награжден почетной медалью в честь 600-летнего юбилея Гейдельбергского университета (Германия, 1986), премией в области квантовой электроники и оптики Европейского физического общества за пионерский вклад в изучение физики взаимодействия лазерного излучения с веществом, включая атомную оптику, лазерное охлаждение атомов, лазерную химию и методы лазерной аналитической спектроскопии (1998); Государственной премией России (в составе группы, в 2002 году – за цикл работ «Физико-технические основы лазерного разделения изотопов методом селективной многофотонной диссоциации молекул»), Премией им. Д.С. Рождественского (совместно с В.И. Балыкиным, в 2001 году – за цикл работ «Лазерное охлаждение и пленение атомов»), грантом Эрландера (Швеция, 2000).

Он также был избран почетным гражданином города Троицк (2000), почетным профессором Эколь Нормаль (Франция), университетов Аризоны, Беркли и Айовы (США), Лундского университета (Швеция), почетным членом Американского оптического общества (OSA, США, 1977), внешним членом Общества Макса Планка (Германия, 1989), членом Европейской академии искусств и наук (1996), почетным членом Всемирного инновационного фонда (2000), членом Европейской академии (2002) и членом общества Лейбница (Германия, 2003).

Признание выдающихся заслуг В.С. Летохова. В честь признания выдающихся заслуг В.С. Летохова в области лазерной физики и фотоники в 2011 году Оптическим обществом им. Д.С. Рождественского учреждена медаль имени В.С. Летохова, которая присуждается раз в два года молодым ученым за новаторские работы по лазерной физике, нелинейной оптике и их приложениям. В 2018 году Европейское физическое общество (EPS) учредило свою высшую награду – премию EPS имени Владилена Летохова (EPS Vladilen Letokhov award) за исключительные достижения в области взаимодействия лазерного излучения с веществом, чтобы признать его выдающийся вклад в развитие лазерной физики, в частности в спектроскопию атомов и молекул, лазерную манипуляцию атомами и изучение процессов в сильных полях. Медаль вручается каждый нечетный год на одной из ключевых конференций в Европе.

Также пионерские работы профессора В.С. Летохова были отмечены в 2018 году при присуждении Институту спектроскопии РАН (ИСАН) знака отличия Европейского физического общества – EPS Historic Site, на памятной доске которого указано, что «здесь в творческой атмосфере группа молодых исследователей, возглавляемая Владиленом Летоховым, выполнила первые в мире эксперименты по лазерному захвату и охлаждению атомов, что привело к созданию новых направлений в физике, а также пионерские эксперименты по лазерному разделению изотопов с использованием методов селективного лазерного возбуждения атомов и молекул, что привело к созданию новой области лазерной химии».

По постановлению президиума Российской академии наук № 181 от 14 сентября 2010 года в ИСАН установлена мемориальная доска «В.С. Летохов. ИСАН. 1970–2009» и кабинет Летохова сохранен как мемориальный кабинет.

Научная деятельность. Профессор В.С. Летохов внес существенный вклад в различные области лазерной физики и ее применения, включая лазерную спектроскопию, лазерное управление движением атомов, фотоселективную многофотонную химию, применение лазеров в ядерной физике и биомедицине, нанооптику и астрофизическую спектроскопию. Его ключевые научные достижения кратко описаны ниже.

В области лазерной спектроскопии В.С. Летохов выполнил вместе с коллегами пионерские работы по спектроскопии насыщения, предложил и реализовал резонансную ионизационную спектроскопию (RIS), включая лазерное обнаружение одиночных атомов со многими приложениями в аналитике, исследование высоковозбужденных состояний редких атомов. Им и его коллегами вы-

полнены первые эксперименты по детектированию молекул с помощью метода RIS и метода многофотонной ионизации с резонансным усилением (REMPI) с масс-спектрометрией. Кроме того, предложена флуоресцентная спектроскопия фотонного всплеска (photon-burst spectroscopy) для обнаружения одиночных атомов и очень редких изотопов, а также фотоакустическая и фототермическая спектроскопия в сочетании с газовой хроматографией и оптоакустической томографией пространственно неоднородных сред. Методы сверхбыстрой спектроскопии использовались также для изучения процессов сверхбыстрой релаксации в высокотемпературных сверхпроводниках и фуллеренах.

В.С. Летохов получил также ключевые результаты в области лазерной спектроскопии с субволновым пространственным разрешением. Он предложил и в своей лаборатории экспериментально реализовал лазерную резонансную фотоэлектронную микроскопию с пространственным разрешением около 30 нм и лазерную резонансную фотоионную микроскопию с разрешением около 5 нм. Кроме того, им был предложен новый тип сканирующей оптической микроскопии с нанометровым пространственным разрешением, основанный на резонансном возбуждении флуоресценции из одноатомного возбужденного центра.

В области лазерного управления движением атомов В.С. Летохов с сотрудниками выполнил с 1968 по 1973 год пионерские работы по захвату (каналированию) атомов с помощью градиентной дипольной силы, предложил так называемые оптические решетки (optical lattices, molasses) и ввел определение доплеровского предела для лазерного охлаждения атомов. Впервые также в 1979 году были проведены эксперименты по охлаждению и монохроматизации, коллимации и отражению атомного пучка с помощью лазерного излучения. Впервые было предложено использовать резонатор, подобный резонатору лазера, для ансамбля атомов с высоким вырождением и острой фокусировкой (до ангстрема) атомного пучка. Несомненно, В.С. Летохов и его группа внесли решающий вклад в формирование новой области исследований в сфере атомной лазерной физики, в частности атомной оптики.

В области селективного взаимодействия лазерного излучения с веществом В.С. Летоховым изучено резонансное взаимодействие лазерного излучения с атомами и молекулами. Он с коллегами предложил, открыл и разработал новую область исследований, имеющих принципиальное значение, – фотоселективную многофотонную химию. В этой области ими были выполнены пионерские работы, приведшие к созданию резонансной ступенчатой ионизационной спектроскопии и новой технологии лазерного разделения изотопов. Была предложена и успешно продемонстрирована многофотонная резонансная ионизация молекул (REMPI) в масс-спектрометрии. Сегодня этот метод играет исключительно важную роль в исследовании молекулярной динамики с помощью молекулярных пучков и т.д. В.С. Летохов впервые объединил идею фотоселективного возбуждения колебательных состояний молекул с последующим возбуждением реактивных электронных состояний. В настоящее время фотоселективная многофотонная химия является одним из самых мощных инструментов фотохимии. В.С. Летохов выступил соавтором пионерских работ, в

которых было обнаружено явление многофотонного фотоселективного (изотопически-селективного) колебательного фотовозбуждения и фотодиссоциации многоатомных молекул мощным импульсом ИК-лазера. Эти и последующие работы привели к возникновению новой области исследований: многофотонной ИК-лазерной фотофизики и фотохимии молекул в основном электронном состоянии, а также к разработке нового метода разделения изотопов ИК-излучением, который был реализован на промышленном уровне.

В.С. Летохов также занимался исследованиями лазеров с сильно разупорядоченной средой усиления (random lasers) нанооптики, нанофотоники и наноплазмоники, а в последние годы – изучением лазерных эффектов в атмосферах звезд, которые он предсказал в начале своей карьеры.

Идеи и исследования В.С. Летохова не только сохраняют актуальность в настоящее время, но и определяют развитие многих научных направлений. Идея и исследования Летохова послужили основой для работ Чу, Коэн-Таннуджи и Филлипса по лазерным методам охлаждения атомов, за которые они получили в 1997 году Нобелевскую премию по физике.

В данной книге мы публикуем ключевые, на наш взгляд, статьи В.С. Летохова по указанным выше основным научным направлениям его деятельности (на языках оригинала, без купюр), что позволяет не только проследить развитие В.С. Летоховым многих новых научных направлений, но и оценить его пионерский вклад в развитие современной лазерной физики и фотоники.

Составители выражают глубокую благодарность и признание всем коллегам и друзьям В.С. Летохова за поддержку и полезные советы при составлении данной книги. Наша отдельная благодарность Ольге Татьянченко и Татьяне Иголкиной за огромную помощь в подготовке рукописи данной книги.

КНИГИ, ОПУБЛИКОВАННЫЕ В.С. ЛЕТОХОВЫМ

1. Летохов В.С., Чеботаев В.П. Принципы нелинейной лазерной спектроскопии. М.: Наука, 1975. 279 с.

2. Letokhov V.S. Laser-Spectroskopie. Berlin: Verlag, 1977. 221 pp.

3. Letokhov V.S., Chebotayev V.P. Nonlinear Laser Spectroscopy. Berlin: Springer, 1977. 466 pp.

4. Баграташвили В.Н., Летохов В.С., Макаров А.А., Рябов Е.А. Многофотонные процессы в молекулах в ИК-лазерном поле. Ч. I. М.: ВИНИТИ, 1980. Ч. II. М.: ВИНИТИ, 1981.

5. Летохов В.С., Устинов Н.Д. Мощные лазеры и их применение. М.: Советское радио, 1980. 112 с.; V.S. Letokhov, N.D. Ustinov. Powerful Lasers and their Applications. New York: Harwood Acad. Publ., 1983. 128 pp.

6. Letokhov V.S. Nonlinear Laser Chemistry. Multiple-Photon Excitation. Springer Series in Chemical Physics. Vol. 22. Berlin: Springer, 1983. 417 pp.

7. Летохов В.С. Нелинейные селективные фотопроцессы в атомах и молекулах. М.: Наука, 1983. 408 с.

8. Велихов Е.П., Баранов В.Ю., Летохов В.С., Рябов Е.А., Старостин А.Н. Импульсные СО2-лазеры и их применение для разделения изотопов. М.: Наука, 1983. 304 с.

9. Жаров В.П., Летохов В.С. Лазерная оптико-акустическая спектроскопия. М.: Наука, 1984. 320 с.; Zharov V.P., Letokhov V.S. Laser Optoacoustical Spectroscopy. Springer Series in Optical Sciences. Vol. 37. Berlin: Springer, 1986. 327 pp.

10. Bagratashvili V.N., Letokhov V.S., Makarov A.A. and Ryabov E.A. Multiple Photon Infrared Laser Photophysics and Photochemistry. New York: Harwood Acad. Publishers, 1986. 512 pp.

11. Летохов В.С. Лазерная фотоионизационная спектроскопия. М.: Наука, 1987. 317 с.; Letokhov V.S. Laser Photoionization Spectroscopy. New York: Academic Press, 1987. 357 pp.

12. Летохов В.С., Матвеев Ю.А., Шарков А.В. и др. Лазерная пикосекундная спектроскопия и фотохимия биомолекул. М.: Наука, 1987.

13. Миногин В.Г., Летохов В.С. Давление лазерного излучения на атомы. М.: Физматгиз, 1986. 222 с.; Minogin V.G., Letokhov V.S. Laser Light Pressure on Atoms. New York: Gordon and Breach, 1987. 248 pp.

14. Летохов В.С., Чеботаев В.П. Нелинейная лазерная спектроскопия сверхвысокого разрешения. М.: Наука, 1990. 512 с.

15. Balykin V.I., Letokhov V.S. Atom Optics with Laser Light. New York: Harwood Acad. Publ., 1995. 115 pp.

16. Letokhov V.S. Laser Control of Atoms and Molecules. Oxford: Oxford University Press, 2007. 320 pp.

17. Letokhov V.S. From Siberia to Laser Science (Dalla Siberia alla Scienza del Laser). Rome: Di Renzo Editore, 2008. 125 pp.

18. Letokhov V.S., Johansson S. Astrophysical Lasers. Oxford: Oxford University Press, 2009. 252 pp.

19. Физик В.С. Летохов – жизнь в науке (http://www.rfbr.ru/rffi/ru/books/o_1781409#1) / под ред. Е. Рябова, Т. Кару, В. Балыкина. М.: Физматлит, 2012. 260 с.

Составители книги:

В.И. Балыкин, В.Н. Задков, Е.А. Рябов, С.В. Чекалин
Институт спектроскопии РАН

ИЗБРАННЫЕ СТАТЬИ В.С. ЛЕТОХОВА

ЛАЗЕРЫ

1. Басов Н.Г., Амбарцумян Р.В., Зуев В.С., Крюков П.Г., Летохов В.С. Нелинейное усиление импульса света // ЖЭТФ. 1966. Т. 50 (1). С. 23–34.

2. Амбарцумян Р.В., Басов Н.Г., Крюков П.Г., Летохов В.С. Лазер с нерезонансной обратной связью // Письма в ЖЭТФ. 1966. Т. 3 (6). С. 261–264.

3. Летохов В.С. Генерация света рассеивающей средой с отрицательным резонансным поглощением // ЖЭТФ. 1967. Т. 53 (10). С. 1442–1452.

4. Летохов В.С. Автостабилизация частоты световых колебаний лазера нелинейным поглощением в газе // Письма в ЖЭТФ. 1967. Т. 6 (4). С. 597–600.

5. Летохов В.С. Генерация ультракоротких импульсов света в лазере с нелинейным поглотителем // ЖЭТФ. 1968. Т. 55, 3 (9). С. 1077–1089.

6. Kryukov P.G., Letokhov V.S. Fluctuation mechanism of ultrashort pulse generation by laser with saturable absorber // J. Quant. Electron. 1972. QE-8 (10). P. 766–782.

7. Жерихин А.Н., Кошелев К.Н., Летохов В.С. Об усилении в области далекого вакуумного ультрафиолета на переходах многозарядных ионов // Квант. электроника. 1976. Т. 3 (1). С. 152–156.

8. Жерихин А.Н., Кошелев К.Н., Крюков П.Г., Летохов В.С., Чекалин С.В. Поиски усиления в далекой ВУФ области на переходах многозарядных ионов в протяженной лазерной плазме // Квант. электроника. 1981. Т. 8 (1). С. 88–97.

ЛАЗЕРЫ

1.1. *Басов Н.Г., Амбарцумян Р.В., Зуев В.С., Крюков П.Г., Летохов В.С.* Нелинейное усиление импульса света // ЖЭТФ. 1966. Т. 50 (1). С. 23–34.

1.2. *Амбарцумян Р.В., Басов Н.Г., Крюков П.Г., Летохов В.С.* Лазер с нерезонансной обратной связью // Письма в ЖЭТФ. 1966. Т. 3 (6). С. 261–264.

1.3. *Летохов В.С.* Генерация света рассеивающей средой с отрицательным резонансным поглощением // ЖЭТФ. 1967. Т. 53 (10). С. 1442–1452.

1.4. *Летохов В.С.* Автостабилизация частоты световых колебаний лазера нелинейным поглощением в газе // Письма в ЖЭТФ. 1967. Т. 6 (4). С. 597–600 .

1.5. *Летохов В.С.* Генерация ультракоротких импульсов света в лазере с нелинейным поглотителем // ЖЭТФ. 1968. Т. 55, 3 (9). С. 1077–1089.

1.6. *Kryukov P.G., Letokhov V.S.* Fluctuation mechanism of ultrashort pulse generation by laser with saturable absorber // J. Quant. Electron. QE. 1972. Vol. 8 (10). P. 766–782.

1.7. *Жерихин А.Н., Кошелев К.Н., Летохов В.С.* Об усилении в области далекого вакуумного ультрафиолета на переходах многозарядных ионов // Квант. электроника. 1976. Т. 3 (1). С. 152–156.

1.8. *Жерихин А.Н., Кошелев К.Н., Крюков П.Г., Летохов В.С., Чекалин С.В.* Поиски усиления в далекой ВУФ области на переходах многозарядных ионов в протяженной лазерной плазме // Квант. электроника. 1981. Т. 8 (1). С. 88–97.

ЖЭТФ. 1966. Т. 50 (1). С. 23–34

НЕЛИНЕЙНОЕ УСИЛЕНИЕ ИМПУЛЬСА СВЕТА

Н.Г. Басов, Р.В. Амбарцумян, В.С. Зуев, П.Г. Крюков, В.С. Летохов
Физический институт им. П.Н. Лебедева АН СССР

Теоретически и экспериментально исследовано прохождение мощного импульса света через оптический квантовый усилитель, работающий в режиме насыщения. Показано, что максимум импульса при усилении без существенного сокращения длительности импульса перемещается со скоростью, значительно превышающей скорость света. Для сокращения длительности импульса при нелинейном усилении необходимо увеличивать крутизну переднего фронта входного импульса. В эксперименте крутизна увеличивалась срезанием переднего фронта дополнительным затвором. Длительность импульса со срезанным передним фронтом при нелинейном усилении сократилась до 4,7 нс.

I. Введение

Стремление получить импульсы света с максимальной энергией и мощностью неизбежно приводит к использованию оптических квантовых усилителей, работающих в нелинейном режиме, связанном с эффектом насыщения [1]. Ожидалось [2], что при нелинейном усилении будет происходить дальнейшее увеличение мощности за счет преимущественного усиления переднего фронта и сокращения длительности входного импульса. Однако экспериментально до настоящего времени не удавалось получить существенного сокращения длительности импульса при усилении. Эксперименты, приведенные в [6], показывают, что при нелинейном усилении импульса оптического квантового генератора (ОКГ) с модулированной добротностью происходит не сокращение длительности переднего фронта, а перемещение импульса в целом, причем максимум усиленного импульса значительно опережает максимум усиливаемого, так как скорость распространения максимума импульса существенно превышает скорость света. Распространение максимума импульса в усиливающей среде со скоростью, превышающей скорость света, не нарушает принципа причинности, поскольку такое распространение происходит за счет усиления фотонов, испущенных задающим ОКГ в более ранние моменты времени. Перемещение импульса может происходить лишь до момента включения затвора задающего ОКГ. Одновременно с приближением импульса к моменту включения затвора должно наблюдаться сокращение длительности импульса.

В настоящей работе для сокращения длительности импульса при нелинейном усилении был использован дополнительный затвор (ячейка Керра),

который увеличивал крутизну переднего фронта усиливаемого импульса. При этом удалось наблюдать существенное сокращение длительности импульса.

II. Теория нелинейного усиления

Теоретически нелинейное усиление импульса света рассматривалось рядом авторов [4, 5, 7–14]. Было показано, что длительность импульса при распространении в среде с инверсной заселенностью должна сокращаться; в среде с потерями излучения энергия импульса после прохождения определенного расстояния становится практически постоянной; минимальная длительность импульса, которую можно получить при нелинейном усилении, порядка обратной ширины радиационного перехода. Ниже рассматриваются особенности, связанные с распространением импульса со скоростью, превышающей скорость света.

1. Основные уравнения

Рассмотрим среду из двухуровневых «атомов» с инверсной заселенностью уровней. Хотя мы имеем в виду случай примесных ионов в кристалле, полученные результаты справедливы для любой квантовой системы с однородным уширением уровней. Для описания среды воспользуемся уравнением Больцмана для матрицы плотности $\hat{\rho}$ с продольной и поперечной релаксацией, а для описания поля $\mathbf{E}$ — уравнением Максвелла в среде, обладающей также нерезонансными потерями излучения:

$$\frac{\partial^2 \mathbf{E}}{\partial t^2} + c^2 \mathrm{rot}\,\mathrm{rot}\mathbf{E} + \gamma c \frac{\partial \mathbf{E}}{\partial t} = -4\pi N_i \frac{\partial^2}{\partial t^2} \mathrm{Sp}(\boldsymbol{\mu}\hat{\rho}), \tag{1}$$

$$i\hbar \frac{\partial \hat{\rho}}{\partial t} = [\mathcal{H}_0 - \boldsymbol{\mu}\mathbf{E}, \hat{\rho}] - i\hbar\Gamma\hat{\rho}, \tag{2}$$

где c — скорость света в среде без ионов, γ — коэффициент потерь излучения на единицу длины в среде, N_i — плотность ионов, $\mathcal{H}_0$ — невозмущенный гамильтониан иона, $\boldsymbol{\mu}$ — оператор электрического дипольного момента иона. Член $\Gamma\hat{\rho}$ феноменологически описывает релаксацию элементов матрицы плотности: диагональные элементы $(\Gamma\hat{\rho})_{nn} = (\rho_{nn} - \rho_{nn}^0)/T_1$, недиагональные элементы $(\Gamma\hat{\rho})_{mn} = \rho_{mn}/T_2 (m, n = 1, 2)$, где T_1 — время продольной релаксации, равное времени жизни иона в возбужденном состоянии, T_2 — время поперечной релаксации, определяемое в основном взаимодействием иона с фононами, которое приводит к однородному уширению уровней. В кристаллах, в которых достигается инверсная заселенность, $T_1 \gg T_2$.

В представлении, в котором $\mathcal{H}_0$ диагонален, уравнение для матрицы плотности (2) можно привести к уравнениям для поляризации $\mathbf{P} = N_i \mathrm{Sp}(\boldsymbol{\mu}\hat{\rho})$ и плотности инверсной заселенности $N = N_i(\rho_{22} - \rho_{11})$:

$$\frac{\partial^2 \mathbf{P}}{\partial t^2} + \frac{2}{T_2}\frac{\partial \mathbf{P}}{\partial t} + \omega_0^2 \mathbf{P} = -N\mathbf{E}\frac{\omega_0}{\hbar}|\mu_{12}|^2, \tag{3}$$

$$\frac{\partial N}{\partial t} + \frac{1}{T_1}(N - N_0) = \mathbf{E}\frac{\partial \mathbf{P}}{\partial t}\frac{2}{\hbar\omega_0}, \tag{4}$$

где $N_0 = N_i(\rho_{22}^0 - \rho_{11}^0)$ — плотность инверсной заселенности в отсутствие поля, $\omega_0 = \omega_{21}$ и опущены малые члены в предположении $\omega_0 \gg 1/T_2$. Для случая $T_1 = T_2$ эти уравнения получены Файном [15] и Ораевским [16].

Уравнение поля (1) и материальные уравнения (3) и (4) вместе с начальными условиями полностью описывают резонансное взаимодействие импульса света, распространяющегося в среде с инверсной заселенностью.

В люминесцентных кристаллах обычно $\sigma_0 N_0, \gamma \ll k$, и $T_2 \gg 1/\omega_0$, где σ_0 — введенное ниже сечение радиационного перехода между уровнями, k — волновой вектор. Поэтому можно перейти к «медленным» переменным $\mathcal{E}, \mathcal{P}, \varphi, \psi$[1]:

$$\begin{aligned} E &= \tfrac{1}{2}\mathcal{E}(t,\mathbf{r})\exp\{i[\varphi(t,\mathbf{r}) + \omega t - \mathbf{kr}]\} + \text{с. с.}, \\ P &= \frac{1}{2}\mathcal{P}(t,\mathbf{r})\exp\{i[\varphi(t,\mathbf{r}) + \omega t - \mathbf{kr}]\} + \text{с. с.} \end{aligned} \tag{5}$$

Тогда уравнение для поля и материальные уравнения сводятся к следующей системе пяти уравнений:

$$\begin{aligned} &\frac{\partial \mathcal{E}}{\partial t} + c\frac{\partial \mathcal{E}}{\partial x} + \frac{\gamma}{2}c\mathcal{E} = 2\pi\omega\mathcal{P}\sin(\psi - \varphi), \\ &\mathcal{E}\left(\frac{\partial \varphi}{\partial t} + c\frac{\partial \varphi}{\partial x}\right) = -2\pi\omega\mathcal{P}\cos(\psi - \varphi), \\ &\frac{\partial \mathcal{P}}{\partial t} + \frac{1}{T_2}\mathcal{P} = \frac{\sigma_0 c}{4\pi\omega T_2}N\mathcal{E}\sin(\psi - \varphi), \\ &\frac{\partial \psi}{\partial t}\mathcal{P} + (\omega - \omega_0)\mathcal{P} = \frac{\sigma_0 c}{4\pi\omega T_2}N\mathcal{E}\cos(\psi - \varphi), \\ &\frac{\partial N}{\partial t} + \frac{1}{T_1}(N - N_0) = -\frac{1}{\hbar}\mathcal{P}\mathcal{E}\sin(\psi - \varphi), \end{aligned} \tag{6}$$

где введено обозначение для сечения радиационного перехода между уровнями на центральной частоте ω_0:

$$\sigma_0 = 4\pi T_2\omega_0|\mu_{12}|^2/\hbar c. \tag{7}$$

Прежде чем исследовать уравнения (6), выясним условия, при которых они переходят в обычные скоростные уравнения переноса излучения. Интегрируем уравнение поляризации (6_3) при начальном условии $\mathcal{P}(-\infty) = 0$ и подставляем

[1] Для простоты ограничимся одномерным случаем распространения линейно поляризованного света.

полученное выражение в уравнения поля (6_1) и плотности инверсной заселенности (6_5):

$$\frac{\partial \mathcal{E}}{\partial t} + c\frac{\partial \mathcal{E}}{\partial x} + \frac{\gamma}{2}c\mathcal{E} = \frac{\sigma_0 c}{2T_2}\sin(\psi-\varphi)\int_{-\infty}^{t} N(t')\mathcal{E}(t') \times \sin(\psi-\varphi)\exp\left(\frac{t'-t}{T_2}\right)dt',$$
$$\frac{\partial N}{\partial t} + \frac{1}{T_1}(N-N_0) = -\frac{\sigma_0 c}{4\pi\hbar\omega_0 T_2}\mathcal{E}\sin(\psi-\varphi) \times \int_{-\infty}^{t} N(t')\mathcal{E}(t') \times \sin(\psi-\varphi)\exp\left(\frac{t'-t}{T_2}\right)dt'. \quad (8)$$

Если изменения поля, инверсной заселенности и разности фаз поляризации и поля пренебрежимо малы за время T_2, то интеграл в (8) сводится к $T_2 N(t)\mathcal{E}(t)\sin(\psi-\varphi)$, а множитель $\sin^2(\psi-\varphi)$ равен $T_2^{-2}/[(\omega-\omega_0)^2 + T_2^{-2}]$, то есть описывает лоренцевскую форму линии излучения. Тогда $\sigma_0\sin^2(\psi-\varphi) = \sigma(\omega)$ — сечение радиационного перехода на частоте ω. Переходя к плотности потока излучения

$$I = \frac{1}{\hbar\omega_0}\frac{c}{8\pi}\mathcal{E}^2[\text{фотон/сек}\cdot\text{см}^2],$$

уравнение (8) при выполнении указанных условий можно записать в обычном виде:

$$\frac{\partial I}{\partial t} + c\frac{\partial I}{\partial x} + \gamma c I = \sigma(\omega)cIN, \quad \frac{\partial N}{\partial t} + \frac{1}{T_1}(N-N_0) = -2\sigma(\omega)IN. \quad (9)$$

Таким образом, предположение о медленности изменения всех переменных за время T_2 является существенным при переходе от строгих уравнений (6) к скоростным уравнениям (9). При рассмотрении процессов, развивающихся за время, сравнимое с временем поперечной релаксации T_2, необходимо пользоваться уравнениями (6).

2. Динамика импульса света при нелинейном усилении

Рассмотрим теперь взаимодействие импульса излучения с длительностью, гораздо большей времени поперечной релаксации T_2. В этом случае допустимо использование (см. п. 1) скоростных уравнений (9), которые сводятся к нелинейному уравнению в частных производных:

$$\frac{\partial I}{\partial t} + c\frac{\partial I}{\partial x} = cI\left[\sigma_0 N_0 \exp\left(-2\sigma_0\int_{-\infty}^{t} I(t',x)dt'\right) - \gamma\right], \quad (10)$$

причем мы пренебрегаем спонтанным распадом инверсной заселенности, поскольку практически всегда длительность импульса $\tau_{\text{имп}} \ll T_1$.

Нестационарное решение (10) при $\gamma \neq 0$ аналитически найти не удается. Случай нулевых потерь излучения ($\gamma = 0$) допускает аналитическое решение

[4, 5, 10, 11], но является слишком идеализированным, поскольку, как будет показано ниже, именно потери излучения существенно определяют развитие импульса. Однако основные выводы можно сделать, не рассматривая нестационарные решения уравнения (10).

Уравнение распространения (10) имеет стационарное решение вида $I(t - x/v)$ $(v \neq c)$. Стационарное решение отвечает сформировавшемуся при достаточно длительном распространении в среде импульсу, движущемуся со скоростью v, и определяется уравнением

$$I\left(\frac{1}{c}-\frac{1}{v}\right) = I\left[\sigma_0 N_0 \exp\left(-2\sigma_0 \int_{-\infty}^{\tau} I(\tau')d\tau'\right) - \gamma\right], \tag{11}$$

где $\tau = t - x/v$. Переходя к функции

$$R(\tau) = \int_{-\infty}^{\tau} I(\tau')d\tau'$$

и интегрируя при начальном условии $\dot{R}(-\infty) = 0$, уравнение (11) сводим к уравнению

$$\left(\frac{1}{c}-\frac{1}{v}\right)\dot{R} = \frac{N_0}{2}\left(1 - e^{-2\sigma_0 R}\right) - \gamma R. \tag{12}$$

Как видно из уравнения (12), стационарное решение, имеющее физический смысл (полная энергия импульса $R(+\infty)$ удовлетворяет условию $0 < R(+\infty) < +\infty$), существует и устойчиво при условиях

$$\sigma_0 N_0 > \gamma > 0, \quad v > c. \tag{13}$$

Первое условие тривиально: начальное усиление среды $\sigma_0 N_0$ больше ненулевых потерь γ. Второе условие означает, что скорость распространения сформировавшегося стационарного состояния импульса превышает скорость света в среде *c*. Физический смысл этого заключается в следующем.

В стационарном состоянии энергия импульса $\mathcal{E}_m = R(+\infty)$ определяется из уравнения (12) при условии $R(+\infty) = 0$, что приводит к выражению

$$1 - \exp\left(\frac{\mathcal{E}_m}{\mathcal{E}_s}\right) = \frac{\gamma}{\sigma_0 N_0}\frac{\mathcal{E}_m}{\mathcal{E}_s}, \tag{14}$$

где $\mathcal{E}_s = 1/2\sigma_0$ имеет смысл величины энергии насыщения, уменьшающей инверсию в *e* раз. В дальнейшем ограничимся практически интересным случаем $\gamma/\sigma_0 N_0 < 0{,}5$ (практически $\gamma/\sigma_0 N_0 \ll 1$). В этом случае $\mathcal{E}_m \gg \mathcal{E}_s$, поэтому энергии передней части импульса вполне достаточно для полного высвечивания активных частиц среды. В результате передняя часть импульса забирает себе всю энергию активных частиц, а задняя часть импульса распространяется

в среде с потерями. Этот механизм обеспечивает дополнительное перемещение вперед максимума импульса. Таким образом, за счет существенно нелинейного взаимодействия импульса излучения с инверсно заселенной средой происходит непрерывная деформация импульса, обеспечивающая его движение вперед с эффективной скоростью $v > c$.

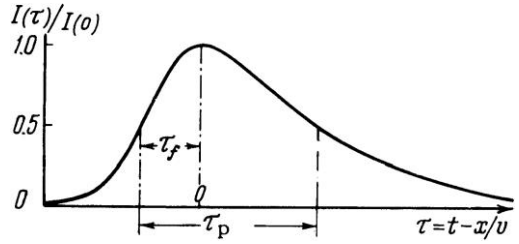


Рис. 1. Форма импульса света в стационарном состоянии с длительностью много больше T_2 $(\gamma/\sigma_0 N_0 = 0{,}17)$

Форму импульса в стационарном состоянии можно получить приближенным решением (12), разлагая $\exp(-2\sigma_0 R)$ в ряд до R^3 включительно. Ради краткости это решение не приводится, поскольку все основные параметры стационарного состояния найдены ниже другим способом, а для сравнения на рис. 1 приведена типичная форма импульса в стационарном состоянии, полученная численным решением уравнения (12).

Заметим, что о стационарных состояниях реального импульса, имеющего конечную протяженность переднего фронта, можно говорить в тех случаях, когда время установления стационарного состояния гораздо меньше полной длительности переднего фронта. Ниже показано, что экспоненциальный импульс приближается к стационарному состоянию за время $\Delta t_s \approx (c\gamma)^{-1}$. Полная протяженность переднего фронта импульса ОКГ с модулированной добротностью (время задержки Δt_3) практически всегда много больше $(c\gamma)^{-1}$.

Оценим величину эффективной скорости импульса в стационарном состоянии. Поскольку импульс перемещается в целом со скоростью v, то достаточно найти, например, скорость перемещения переднего фронта. Из (11) следует, что передний фронт, распространяющийся в среде с практически неизменной инверсной заселенностью N_0, возрастает экспоненциально:

$$I_f(t,x) \sim I_0 \exp(vt - x/c\tau_0).$$

Кроме того, передний фронт удовлетворяет нестационарному уравнению (10), что приводит к следующему выражению для эффективной скорости импульса:

$$v/c = 1 + c(\sigma_0 N_0 - \gamma)\tau_0. \qquad (15)$$

Крутизна переднего фронта τ_0 связана с длительностью переднего фронта импульса τ_f соотношением $\tau_f = f(\alpha)\tau_0$, где $\alpha = \gamma/\sigma_0 N_0$ — безразмерный параметр. Рассматривая уравнения (12) в моменты времени $\tau_{\max}$, $\tau_{\max}$-τ_f и $\tau \to -\infty$, можно найти функцию $f(\alpha)$. В случае $\alpha > 10^{-2}$ имеем

$$\frac{\tau_f}{\tau_0} = f(\alpha) \approx \frac{(1-\alpha)\ln(1/\alpha)}{(1-\alpha)-\alpha\ln(1/\alpha)}. \qquad (16)$$

Наконец, можно найти полную длительность импульса $\tau_{\text{имп}}$ в стационарном состоянии. Полная энергия импульса $\mathcal{E}_m \approx N_0/2\gamma$. Из условия стационарности мощности импульса в максимуме следует

$$\sigma_0 N_0 \exp\left(-2\sigma_0 \mathcal{E}_f\right) = \gamma, \quad \mathcal{E}_f = \int_{-\infty}^{\tau_{max}} I(\tau')d\tau',$$

где $\mathcal{E}_f$ — энергия переднего фронта импульса. Приближенно $\tau_f/\tau_p = \mathcal{E}_f/\mathcal{E}_m$ и, следовательно,

$$\tau_f/\tau_{\text{имп}} \approx \alpha \ln(1/\alpha). \qquad (17)$$

Для того чтобы полностью проследить динамику импульса и приближение к стационарному состоянию, находились нестационарные решения уравнения (10) путем численного интегрирования на электронной вычислительной машине. Приведем результаты решения для случая, соответствующего распространению импульса в кристалле рубина с обычными параметрами. Начальный импульс на границе среды имеет экспоненциальную форму

$$I_0(t) = \frac{\mathcal{E}_0}{\tau_0}\frac{\exp(-t/\tau_0)}{[1+\exp(-t/\tau_0)]^2},$$

хорошо аппроксимирующую передний фронт импульса мощного ОКГ с мгновенным включением добротности. Реальный импульс ОКГ имеет несколько асимметричную форму из-за большей длительности заднего фронта, но это несущественно, поскольку только передний фронт определяет динамику импульса. Одно из типичных решений приведено на рис. 2, где изображены зависимости $I(t, x)$ в системе координат, движущейся со скоростью c после прохождения расстояния x в среде с инверсной заселенностью. Отчетливо видно, что как только энергия в передней части импульса достигает значения энергии насыщения $\mathcal{E}_s$, все активные частицы высвечиваются на переднем фронте, что ведет к дополнительному движению переднего фронта импульса. Затем после прохождения расстояния $\sim v/c\gamma$ энергия импульса достигает максимального значения $\mathcal{E}_m$, и при дальнейшем движении импульс принимает стационарную форму, распространяющуюся со скоростью v. Кроме того, τ_f импульса в стационарном состоянии близко к длительности переднего фронта τ_f^0 начального импульса.

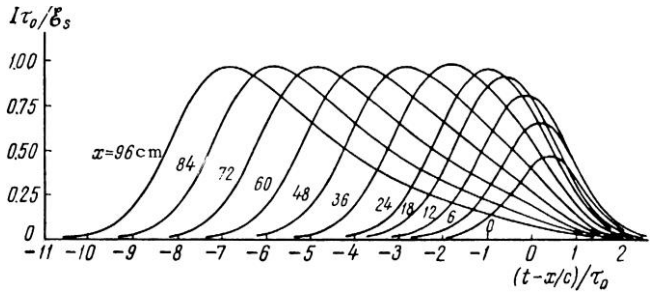


Рис. 2. Изменение формы экспоненциального импульса с начальной энергией $\mathcal{E}_0 = \mathcal{E}_s$ при распространении в среде с инверсной заселенностью ($\sigma_0 N_0 = 0{,}2$ см$^{-1}$); $\gamma = 0{,}03$ см$^{-1}$, x — расстояние, пройденное импульсом в среде

Таким образом, световой импульс с экспоненциальным передним фронтом крутизны τ_0, распространяясь в среде с инверсной заселенностью, за время $\sim(\gamma c)^{-1}$ нелинейного усиления достигает стационарного состояния с длительностью $\tau_{\text{имп}} \approx \tau_f[\alpha \ln(1/\alpha)]^{-1}$, движущегося со скоростью $v = c[1 + c\tau_0(\sigma_0 N_0 - \gamma)]$. В этом случае преимущественное усиление переднего фронта не приводит к сокращению длительности начального импульса.

3. Сокращение длительности импульса

Для того чтобы получить сокращение длительности импульса, необходимо существенно увеличить крутизну переднего фронта. Для этого начальный импульс можно предварительно пропустить через затвор, открывающийся к моменту прохождения максимума импульса. В случае нулевого начального пропускания затвора, когда происходит полное срезание переднего фронта, преимущественное усиление переднего фронта ведет к эффективному сокращению длительности импульса. На рис. 3 показано изменение длительности и энергии импульса при распространении в среде с инверсной заселенностью. После того как энергия импульса достигает значения энергии насыщения, начинается резкое сокращение длительности импульса. При ненулевом начальном пропускании затвора имеется определенный предел сокращения длительности.

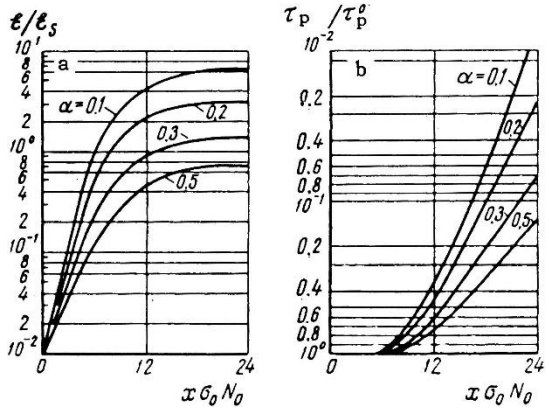


Рис. 3. Изменение энергии (*а*) и длительности (*б*) импульса, передний фронт которого срезан затвором с нулевым пропусканием, при распространении в среде с инверсной заселенностью ($\mathcal{E}_0 = 10^{-2}\mathcal{E}_s$)

Нелинейное поглощение [17–19] переднего фронта импульса при распространении в двухкомпонентной среде (один компонент — усиливающие атомы, а другой — поглощающие) также приводит к подавлению «убегания» переднего фронта и позволяет получить эффективное сокращение длительности импульса. На рис. 4 показано изменение формы экспоненциального импульса при распространении в двухкомпонентной среде, полученное численным интегрированием уравнений (10), и уравнения для числа поглощающих атомов. Отчетливо видно, что передний фронт импульса непрерывно поглощается, просветляя среду и обеспечивая эффективное усиление максимума импульса.

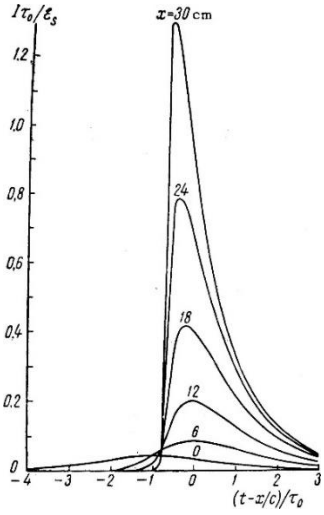


Рис. 4. Изменение формы экспоненциального импульса при распространении в двухкомпонентной среде, когда начальная энергия импульса $\mathcal{E}_0$ больше пороговой ($\sigma_0^{(2)}/\sigma_0^{(1)} = 50$, $\sigma_0^{(2)}N_0^{(2)}/\sigma_0^{(1)}N_0^{(1)} = 5$, $\sigma_0^{(1)}N_0{}^{(1)} = 0.2$ см$^{-1}$, где индекс 1 относится к усиливающим атомам, а 2 — к поглощающим, $\gamma = 0{,}03$ см$^{-1}$)

Заметим, что существует предел сокращению длительности импульса. Рассматривая строгие уравнения (6), можно показать, что форма импульса с минимальной длительностью ~T_2 имеет вид ($\gamma/\sigma_0 N_0 < 0{,}5$).

$$I(\tau) = \frac{2(\sigma_0 N_0/\gamma - 1)^2 \exp(-t/\tau_0)}{\sigma_0 T_2 [1+\exp(-t/\tau_0)]^2}, \quad \tau_0 = \frac{T_2}{2}\left(\frac{\sigma_0 N_0}{\gamma} - 1\right)^{-1}. \tag{18}$$

Энергия импульса в предельном стационарном состоянии $N_0(1/\gamma - 1/\sigma_0 N_0)$ почти в два раза превышает энергию импульса $\mathcal{E}_m$ при длительности $\gg T_2$, так как при длительности импульса $\gg T_2$ инверсная заселенность после прохождения импульса уменьшается до нуля, а в предельном стационарном состоянии инверсная заселенность изменяется следующим образом:

$$N(\tau) = N_0 - \frac{2\gamma(\sigma_0 N_0/\gamma - 1)}{\sigma_0 [1+\exp(-t/\tau_0)]}, \tag{19}$$

то есть после прохождения импульса света атомы инвертируются.

III. Экспериментальное исследование

1. Измерение скорости распространения максимума импульса

Распространение мощного светового импульса было изучено экспериментально с помощью установки, состоящей из ОКГ с модулированной добротностью и оптического квантового усилителя. Схема эксперимента показана на рис. 5.

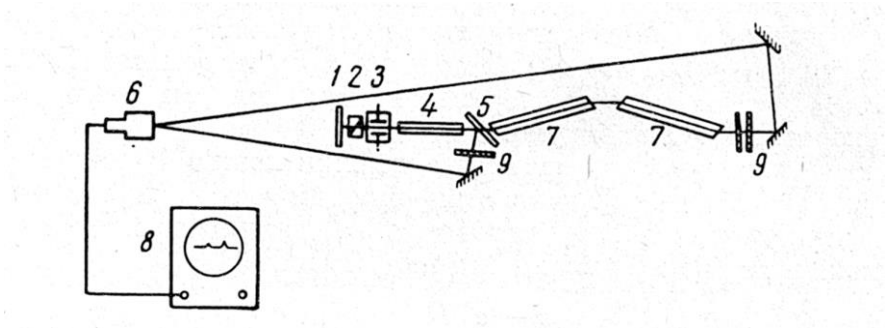


Рис. 5. Схема установки: *1* — зеркало генератора, *2* — поляризатор, *3* — ячейка Керра, *4* — кристалл рубина генератора, *5* — стеклянная пластина, *6* — коаксиальный фотоэлемент, *7* — кристаллы рубина усилителя, *8* — осциллограф С1-14, *9* — нейтральные светофильтры. Выходным зеркалом ОКГ служит торец кристалла *4*

Импульс света получался с помощью генератора, описанного в [3]. Малая часть светового потока генератора отводилась стеклянной пластинкой *5* на коаксиальный фотоэлемент *6.* Большая часть подавалась на вход оптического

квантового усилителя, состоящего из двух кристаллов рубина *7* длиной 24 см и диаметром 1,6 см каждый. Для устранения обратной связи торцы кристаллов срезались под углом Брюстера. Общее усиление оптического усилителя для слабого сигнала было около 50.

Регистрация импульсов света до и после усилителя осуществлялась с помощью одного и того же фотоэлемента *6*, причем усиленный импульс проходил дополнительный путь около 20 м и попадал на фотоэлемент спустя 56 нс после прихода входного импульса.

Импульсы от фотоэлемента регистрировались на осциллографе С1–14. Световые потоки соответствующим образом ослаблялись с помощью нейтральных светофильтров *9*, чтобы обеспечить линейный режим работы фотоэлемента и осциллографа. На рис. 6а приведена типичная осциллограмма входного и выходного импульсов при слабом входном сигнале. Импульс генератора при этом был ослаблен в $3 \cdot 10^3$ раз с помощью нейтральных светофильтров.

Параметры входного неослабленного импульса следующие: энергия — 1,3 Дж; длительность по полувысоте — 16 нс; начало импульса, определяемое моментом включения затвора генератора, отстоит на 45 нс от вершины импульса; длительность переднего фронта (от уровня 0,5 до максимума) — 8 нс. На рис. 6б приведена осциллограмма входного и выходного импульсов при неослабленном сигнале.

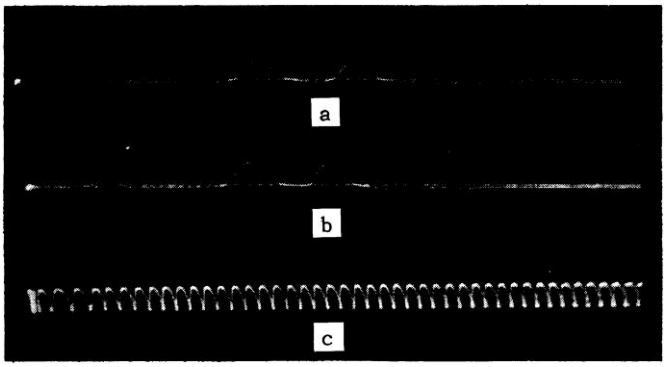


Рис. 6. Осциллограммы входного (слева) и усиленного (справа) импульсов света: *а* — случай слабого сигнала — линейное усиление; *б* — случай сильного сигнала — нелинейное усиление; *в* — калибровочные метки с периодом 8 нс

Из сравнения осциллограмм на рис. 6а и 6б можно отметить, что существенного сокращения импульса не происходит, зато выходной импульс на рис. 6б оказывается на более близком расстоянии по отношению к входному импульсу, чем на рис. 6а (световая задержка не изменялась!). Обработка осциллограмм дает значение для этого сдвига $\Delta t_{\text{эксп}} = 9 \pm 0{,}5$ нс как для максимумов, так и для полувысот передних фронтов. В соответствии с представлениями, развитыми выше, этот эффект связан с нелинейным усилением импульса света, имеющим экспоненциально нарастающий передний фронт.

По оценкам, плотность энергии импульса достигала энергии насыщения $\mathcal{E}_s \approx 4$ Дж/см^2 на расстоянии $L = 10 \div 15$ см от выходного торца усилителя. (Энергия импульса на выходе усилителя достигала 17 Дж.) Опережение импульса на Δt означает его перемещение в пространстве на $c\Delta t$. Эффективная скорость перемещения максимума импульса определяется из соотношения $(v - c)L/c = c\Delta t$. Таким образом, получаем в эксперименте соотношение $v/c = 10 \div 15$, или скорость перемещения максимума была в $6 \div 9$ раз больше скорости света в вакууме.

Теоретическое значение времени задержки можно оценить по формуле (15) для скорости импульса в стационарном состоянии, так как величина скорости при нелинейном усилении даже вдали от стационарного состояния близка к стационарному значению. Согласно (15),

$$\Delta t_{\text{теор}} = \frac{v-c}{c}\frac{L}{c} = (\sigma_0 N_0 - \gamma) L \tau_0.$$

Крутизна входного импульса $\tau_0 \approx 4 \times 10^{-9}$ с. Поэтому $\Delta t_{\text{теор}} = 5 \div 7$ нс. Поскольку механизм перемещения максимума импульса начинает работать несколько раньше, чем энергия импульса достигает 4 Дж/см^2, экспериментальное опережение должно превышать эту оценку. Полученное экспериментальное значение $9 \pm 0{,}5$ нс не противоречит развитым выше представлениям.

2. Сокращение длительности импульса

Как было показано выше (п. 3 раздела II), для сокращения длительности переднего фронта и всего импульса необходимо срезать пологую часть переднего фронта начального импульса. Такое срезание осуществлялось с помощью дополнительного затвора Керра, который помещался после генератора перед отводящей пластинкой 5 (рис. 5). Дополнительный затвор открывался с задержкой в 48–50 нс по отношению к затвору генератора. Время открывания затвора Керра от уровня 0,1 до 0,9 составляло $\tau_{\text{вкл}} = 8$ нс. В закрытом состоянии затвор пропускал около 3% света ($\eta_1 = 0{,}03$), а в открытом состоянии — $\eta_2 = 50\%$. Для компенсации потерь в затворе добавлялся еще один каскад усилителя.

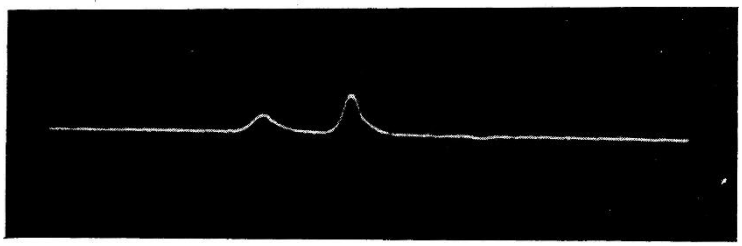


Рис. 7. Осциллограммы входного (слева) и усиленного (справа) импульсов света при дополнительном срезании переднего фронта импульса генератора. Усиление на двух каскадах

Задержка между моментом открывания затвора генератора и появлением максимума импульса зависит от величины инверсной заселенности кристалла. Поэтому можно было, изменяя накачку генератора, срезать импульс с любого уровня интенсивности.

На рис. 7 приведена осциллограмма импульсов до усилителя (но после второго затвора) и после усилителя на двух каскадах, когда нелинейный режим только начинает проявляться. Из осциллограммы видно, что передний фронт начинает сокращаться.

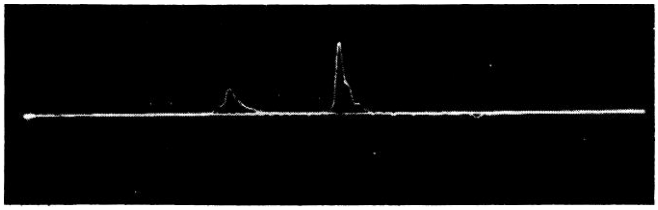


Рис. 8. То же, что и на рис. 7. Усиление на трех каскадах

На рис. 8 показаны импульсы до и после усиления на трех каскадах усилителя. В этом случае срезание импульса осуществлялось по более высокому уровню. Длительность входного импульса по полувысоте равна $\tau^0_{\text{имп}} = 8{,}7 \pm 0{,}5$ нс, длительность усиленного импульса $\tau_{\text{имп}} = 4{,}7 \pm 0{,}5$ нс. Длительности передних фронтов от уровня 0,5 до максимума составляют $\tau^0_f = 3{,}7 \pm 0{,}5$ нс и $\tau_f = 1{,}9 \pm 0{,}5$ нс соответственно для входного и выходного импульсов. Теоретическая оценка возможного сокращения длительности в нашем эксперименте дает сокращение в два раза, что согласуется с экспериментальным значением. В нашем эксперименте начальное пропускание дополнительного затвора $\eta_1 \neq 0$. Именно это дает предел длительности переднего фронта усиленного импульса.

Литература

1. *Karplus R., Schwinger J.* // Phys. Rev. 1948. Vol. 73. P. 1020.

2. *Geusic J.E., Scovil K.E.P.* // Quantum Electronics. Proc. 3 Intern. Congress, Paris, 1964.

3. *Басов Н.Г., Амбарцумян Р.В., Зуев В.С., Крюков П.Г., Стойлов Ю.Ю.* // ЖЭТФ. 1964. Т. 47. С. 1595.

4. *Bellman R., Birnbaum G., Wagner W.G.,* // *J. Appl* Phys. 1963. Vol. 34. P. 780.

5. *Frantz L.M., Nodvik J.S.* // Ibid. 1963. Vol. 34. P. 2346.

6. *Басов Н.Г., Амбарцумян Р.В., Зуев В.С., Крюков П.Г., Летохов В.С.* // ДАН СССР. 1965. Т. 165. С. 58.

7. *Басов Н.Г., Летохов В.С.* // Оптика и спектроскопия. 1965. Т. 18. С. 1042.

8. *Микаэлян А.Л., Тер-Микаэлян М.Л., Турков Ю.Г.* // Радиотехника и электроника. 1964. Т. 9. С. 1788; *Тер-Микаэлян М.Л., Микаэлян А.Л.* // ДАН СССР. 1964. Т. 155. С. 1298.

9. *Прохоров А.М.* // Оптика и спектроскопия. 1963. Т. 14. С. 73.

10. *Таланов В.И.* // Изв. вузов. Радиофизика. Т. 7. С. 491 (1964).

11. *Schulz-Du Bois E.O.* // Bell System Techn. J. 1964. Vol. 43. P. 625.

12. *Wittke J.P. and Warter P.J.* // J. Appl. Phys. 1964. Vol. 35. P. 1668.

13. *Басов Н.Г., Летохов В.С.* Препринт ФИАН. 1965. № А-2.

14. *Ильинова Т.М., Хохлов Р.В.* // Изв. вузов. Радиофизика. 1965.

15. *Файн В.М.* // ЖЭТФ. 1957. Т. 33. С. 945.

16. *Ораевский А.Н.* // Радиотехника и электроника. 1959. Т. 4. С. 718.

17. *Ривлин Л.А.* // Радиотехника и электроника. 1965. Т. 10. С. 665.

18. *Sorokin P.P., Luzzi J.J., Lankard J.P. and Pettit G.D.* // IBM J. Res. a. Devel. 1964. Vol. 8. P. 182.

19. *Bret G., Gires F.* // Appl. Phys. Lett. 1964. Vol. 4. P. 175.

Письма в ЖЭТФ. 1966. Т. 3 (6). С. 261–264

ЛАЗЕР С НЕРЕЗОНАНСНОЙ ОБРАТНОЙ СВЯЗЬЮ

Р.В. Амбарцумян, Н.Г. Басов, П.Г. Крюков, В.С. Летохов
Физический институт им. П.Н. Лебедева АН СССР

1. В квантовом генераторе радио- и оптического диапазонов обратная связь является резонансной [1, 2]. Последнее есть следствие применения резонаторов (объемного в радиодиапазоне и Фабри — Перо в оптическом диапазоне), которые имеют минимум потерь электромагнитной энергии в области сравнительно узких интервалов частот. Поэтому генераторы с резонансной обратной связью излучают один или несколько типов колебаний, которые обычно слабо взаимодействуют между собой и могут рассматриваться как изолированные.

В настоящем письме сообщается о получении генерации с нерезонансной обратной связью на кристаллах рубина, имеющих высокое усиление. Нерезонансная обратная связь осуществлялась при обратном рассеянии на рассеивающем объеме или поверхности. При падении световой волны на рассеиватель часть энергии рассеивается в другие типы колебаний «резонатора», а другая часть — покидает его. В результате типы колебаний резонатора сильно взаимодействуют и, строго говоря, не являются изолированными. Спектр собственных частот такого «стохастического» резонатора является сплошным. Отсутствие резонансных свойств у стохастического резонатора означает, что частота генерации не должна зависеть от длины резонатора, а определяется резонансной частотой активного вещества.

2. Схема лазера приведена на рис. 1. Активной средой являются два последовательных кристалла рубина *2* и *3* длиной 24 см и диаметром 1,8 см каждый, торцы которых для предотвращения самовозбуждения срезаны под углом Брюстера. Обратная связь осуществлялась с помощью зеркала *4*, отражавшего 99% света, и объемного или поверхностного рассеивателя *1*. В качестве объемного рассеивателя использовалась взвесь частиц мела диаметром не более 2×10^{-3} см в воде, а в качестве поверхностного рассеивателя — пластинка со слоем напыленного MgO. Световой поток, пропущенный зеркалом *4* и ослабленный светофильтром *5*, для регистрации поступал на фотоэлемент *6* и осциллограф *7*, а для измерения спектра — на эталон Фабри — Перо. Усиление слабого сигнала на двух кристаллах за проход достигало 900.

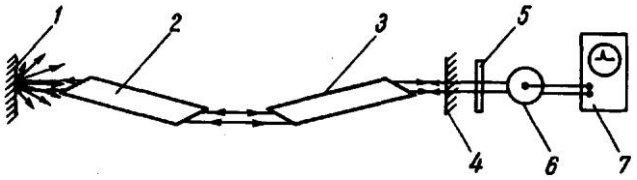


Рис. 1. Схема эксперимента

3. Условие самовозбуждения лазера в нашем случае ($\Omega_{\text{расс}} \gg \Omega_{\text{генер}}$) имеет вид:

$$k^2\tau\frac{\Omega_{\text{генер}}}{\Omega_{\text{расс}}}\frac{\alpha}{2} = 1, \qquad (1)$$

где k — усиление за проход; τ — коэффициент отражения зеркала; $\Omega_{\text{генер}}$ — эффективный телесный угол, в котором распространяется генерируемое излучение; $\Omega_{\text{расс}}$ — эффективный телесный угол обратного рассеяния; α — коэффициент обратного рассеяния в угол 2 (стер); множитель 1/2 возникает из-за полной деполяризации излучения при рассеянии. Приближенно $\Omega_{\text{генер}} = (P/L)^2$, где P — диаметр кристалла, L — среднее расстояние между зеркалом и рассеивателем. Для идеального рассеивателя $\Omega_{\text{расс}} = 2\pi$. В эксперименте $L = 100$ см, $P = 1{,}8$ см, $\tau \simeq 1{,}0$. При рассеянии на поверхности $\alpha \simeq 0{,}9$, $\Omega_{\text{расс}} = 2\pi$, а при объемном рассеянии $\alpha \simeq 0{,}5$, но $\Omega_{\text{расс}} < 2\pi$. Поэтому пороговое усиление на проход в обоих случаях одного порядка $k \simeq 4 \cdot 10^4$.

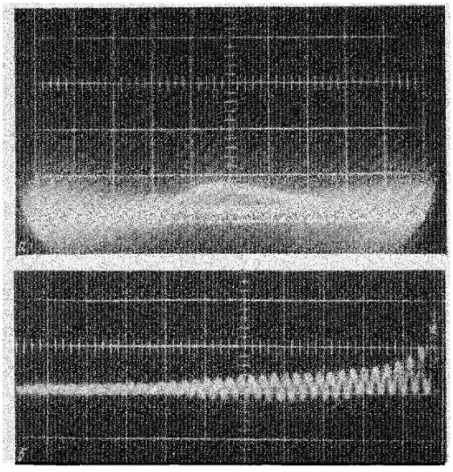


Рис. 2. Излучение лазера до порога (*а*) и выше порога (*б*). Письма ЖЭТФ. 1966. Т. 3 (6)

4. На рис. 2а (см. вклейку) приведена осциллограмма излучения лазера при накачке ниже пороговой, а на рис. 2б — при накачке выше пороговой при обратной связи на объемном рассеивателе. На рис. 2б отчетливо видны затухающие пульсации, характерные для режима генерации. Порог практически не

зависит от угла наклона рассеивателя в широких пределах, но повышается при удалении рассеивателя от кристалла, что согласуется с условием (1). Исследование спектра производилось с помощью эталона Фабри — Перо с воздушным промежутком 3 см. Ширина линии излучения была менее 0,015 $см^{-1}$ и определялась разрешающей способностью эталона (ширина линии спонтанного излучения рубина 15 $см^{-1}$). Исследование спектра биений излучения показало отсутствие частот типа $c/2L$, характерных для лазеров с резонансной обратной связью. Угловая расходимость излучения $\sim P/L$, а распределение поля излучения в дальней зоне является весьма однородным. При модуляции добротности стохастического резонатора был получен импульс с длительностью 200 нс.

5. Средняя частота генерируемого излучения в лазере с нерезонансной обратной связью определяется положением центра атомного перехода, а не резонанса обратной связи. Следовательно, на основе лазера с нерезонансной обратной связью можно создать оптический стандарт частоты. Для этого следует использовать атомные переходы с большим коэффициентом усиления в газовом разряде Ne, Xe и др. в непрерывном режиме, а также рассеиватели с узкой диаграммой обратного рассеяния.

6. Следует отметить, что генерация с обратной связью за счет рассеяния на неоднородностях кристалла и боковой матированной поверхности кристалла может ограничить максимальное усиление. Теоретически случай генерации на «случайных модах» боковой матированной поверхности кристалла рассматривался в работе Флека [3]. В наших экспериментах такая генерация возникала при максимальной накачке. В этом случае генерация происходит в определенном конусе углов.

Литература

1. *Басов Н.Г., Прохоров А.М.* // ЖЭТФ. 1954. Т. 27. С. 431; *Gordon J.P., Zeiger H.J. , Townes C.H.* // Phys. Rev. 1954. Vol. 95. P. 282.

2. *Прохоров А.М.* // ЖЭТФ. 1958. Т. 34. С. 1658; *Shawlow A.L., Townes C.H.* // Phys. Rev. 1958. Vol. 112. P. 1940.

3. *Fleck Jr. J.A.* // Appl. Phys. 1965. Vol. 36. P. 1301.

ЖЭТФ. 1967. Т. 53 (10). С. 1442–1452

ГЕНЕРАЦИЯ СВЕТА РАССЕИВАЮЩЕЙ СРЕДОЙ С ОТРИЦАТЕЛЬНЫМ РЕЗОНАНСНЫМ ПОГЛОЩЕНИЕМ

В.С. Летохов
Физический институт им. П.Н. Лебедева АН СССР

Теоретически рассмотрена генерация света рассеивающей средой с отрицательным резонансным поглощением в случае, когда длина пробега фотона за счет рассеяния гораздо меньше размеров области. Обратная связь в таком квантовом генераторе является нерезонансной. Найден порог генерации квантового генератора, рассмотрена динамика установления стационарного режима и сужения спектра излучения. Найдена предельная ширина спектра излучения в режиме генерации, вызванная флуктуационным движением рассеивающих частиц. Обсуждается применение такого квантового генератора в качестве источника световых колебаний стабильной частоты.

1. Введение

Известные оптические квантовые генераторы представляют собой оптически однородную среду с отрицательным поглощением и конфигурацию элементов, возвращающих часть излучения обратно в среду для достижения обратной связи. Если возвращение излучения осуществляется с помощью системы зеркал типа резонатора Фабри — Перо [1], то обратная связь является резонансной, а если же с помощью обратного рассеяния, то обратная связь является нерезонансной [2]. В нашей работе [3] рассматривался случай генерации в межзвездной среде, когда обратная связь осуществляется рассеивающими частицами (электроны, пылинки и др.), распределенными в активной среде, но и здесь среда с отрицательным поглощением являлась по существу «оптически» однородной, поскольку длина свободного пробега кванта за счет рассеяния гораздо больше размеров генератора.

В настоящей работе рассматривается генерация света рассеивающей средой с отрицательным резонансным поглощением в случае, когда длина свободного пробега фотона за счет рассеяния гораздо меньше размеров области, то есть когда движение фотонов является диффузионным. Возможность режима генерации света в этом случае была показана в нашей работе [4]. Рассматриваемый квантовый генератор, представляющий фактически лишь рассеивающую среду с отрицательным поглощением, является разновидностью квантового генератора с нерезонансной обратной связью. Интерес к исследованию его свойств связан с перспективой создания высокостабильного оптического стандарта

частоты [2, 4]. Настоящая работа посвящена теоретическому исследованию такого квантового генератора. Найден порог генерации рассеивающей области с отрицательным поглощением. Рассмотрена динамика установления стационарного режима генерации и сужения спектра излучения. Найдена предельная ширина спектра излучения в режиме генерации, вызванная флуктуационным движением рассеивающих частиц.

2. Основные уравнения

Рассмотрим ансамбль одинаковых диэлектрических частиц с плотностью N_0 и комплексной диэлектрической проницаемостью $\varepsilon = \varepsilon + i\varepsilon''$, где $\varepsilon'' > 0$ в окрестности частоты ω_0. Пусть Q_s — сечение рассеяния, Q_ω — сечение отрицательного поглощения света частоты ω на одной частице. Будем рассматривать случай, когда длина свободного пробега фотона за счет рассеяния $\Lambda_s = 1/N_0 Q_s$, средний размер занимаемой ансамблем области R и длина волны излучения λ удовлетворяют соотношению

$$R \gg \Lambda_s \gg \lambda, \tag{1}$$

а $N_0^{-1/3} \gg \lambda$. Тогда изменение плотности потока фотонов $\Phi_\omega(\mathbf{r}, t)$ частоты ω в точке $\mathbf{r}$ можно описывать в диффузионном приближении[1)]:

$$\frac{1}{c}\frac{\partial \Phi_\omega(\mathbf{r},t)}{\partial t} = D\Delta\Phi_\omega(\mathbf{r}, t) + Q_\omega(\mathbf{r}, t)N_0\Phi_\omega(\mathbf{r}, t), \tag{2}$$

здесь D — коэффициент диффузии, Δ — оператор Лапласа, c — средняя скорость света в области, занимаемой ансамблем. Зависимость плотности фотонов от частоты связана с резонансным характером отрицательного поглощения. Сечение $Q_\omega(\mathbf{r}, t)$ не остается постоянным, поскольку мнимая часть диэлектрической проницаемости $\varepsilon''_\omega(\mathbf{r}, t)$ зависит от плотности потока фотонов (эффект насыщения [6]).

Процесс диффузионного размножения фотонов, описываемый уравнением (2), во многом напоминает диффузию нейтронов в гомогенном ядерном реакторе. Поэтому ниже мы будем использовать ряд результатов, известных для диффузии нейтронов (например, условие критичности), со ссылкой на монографию [5]. В тоже время в нашем случае имеется ряд существенных отличий, связанных с резонансным характером и нестационарностью сечения поглощения $Q_\omega(\mathbf{r}, t)$.

[1)] Строго говоря, необходимым условием диффузионного приближения является также требование, чтобы длина пробега за счет рассеяния была гораздо меньше длины пробега фотона за счет поглощения (в данном случае рождения) фотонов [5]. Как будет видно из дальнейшего, в стационарном режиме генерации это условие является следствием условия (1). В нестационарном случае может быть не так и необходимо с самого начала потребовать, чтобы $\Lambda_s \ll \Lambda_a$.

Коэффициент диффузии в поглощающей среде с анизотропным рассеянием имеет вид [5]

$$D = \Sigma_s/3\Sigma(\Sigma - \bar{\mu}\Sigma_s), \tag{3}$$

где $\Sigma_s = Q_s N_0$; $\Sigma_a = Q_\omega N_0$ — макроскопические сечения рассеяния и отрицательного поглощения; $\Sigma = \Sigma_s + \Sigma_a$; $\bar{\mu}$ — средний косинус угла рассеяния. В рассматриваемом нами случае $\Sigma_s \gg \Sigma_a$, и, следовательно,

$$D \approx \frac{1}{3\Sigma_s(1-\bar{\mu})} = \frac{\Lambda_s}{3(1-\bar{\mu})}. \tag{4}$$

Для осесимметричного рассеяния (типа релеевского) $\bar{\mu} = 0$. В случае преимущественного рассеяния вперед ($\bar{\mu} > 0$) коэффициент диффузии возрастает.

Мнимую часть диэлектрической проницаемости частиц $\varepsilon''_\omega(\mathbf{r}, t)$ в случае однородного уширения линии можно представить в виде

$$\varepsilon''_\omega(\mathbf{r}, t) = a(\omega)\varepsilon''(\mathbf{r}, t), \tag{5}$$

где $a(\omega)$ — нормированная на единицу в максимуме форма линии поглощения. В случае, например, лоренцовой формы

$$a(\omega) = \frac{(\Delta\omega_0/2)^2}{(\omega-\omega_0)^2+(\Delta\omega_0/2)^2}. \tag{6}$$

величина $\varepsilon''(\mathbf{r}, t)$ определяется мощностью накачки и зависит от интенсивности потока фотонов (эффект насыщения). Уравнение для $\varepsilon''(\mathbf{r}, t)$ можно записать в виде

$$\frac{\partial\varepsilon''(\mathbf{r},t)}{\partial t} + \frac{1}{T_1}\varepsilon''(\mathbf{r}, t) = -2\sigma_0\varepsilon''(\mathbf{r}, t)\int a\omega\Phi_\omega(\mathbf{r}, t)d\omega + \frac{1}{T_1}\tilde{\varepsilon}''(\mathbf{r}), \tag{7}$$

где $\sigma_0 = \sigma(\omega_0)$ — сечение радиационного перехода «атомов» диэлектрических частиц, ответственных за резонансное отрицательное поглощение; T_1 — время продольной релаксации, описывающее спонтанный распад отрицательного поглощения; $\tilde{\varepsilon}''(\mathbf{r})$ — член, пропорциональный мощности накачки. В стационарном случае в отсутствие поля (ниже порога) $\tilde{\varepsilon}''(\mathbf{r}, t) \equiv \tilde{\varepsilon}''(\mathbf{r})$.

Система уравнений (2) и (7) полностью описывает стимулированное излучение ансамбля рассеивающих частиц с отрицательным поглощением. Для решения ее необходимо задать граничные условия. Плотность фотонов очень мала на внешней границе среды. Однако она не может быть равна нулю, так как фотоны диффундируют из среды и могут проходить через поверхность. Можно ввести расстояние d, на котором поток фотонов, линейно экстраполированный наружу от границы среды, был бы равен нулю. Это расстояние, называемое длиной линейной экстраполяции, определяется выражением [5].

$$d = 2/3\Sigma \approx 2/3\Lambda_s. \tag{8}$$

3. Условие порога генерации

Правая часть уравнения (2) описывает затухание излучения за счет диффузионного «расплывания» и усиление за счет резонансного отрицательного поглощения. Существует, очевидно, порог, при котором потери излучения компенсируются отрицательным поглощением. При пороге насыщением усиления можно пренебречь и считать $\varepsilon(\mathbf{r},t)=\tilde{\varepsilon}''(\mathbf{r})$. Ограничимся случаем однородной накачки $\tilde{\varepsilon}''(\mathbf{r})=\varepsilon_0''$, когда комплексная диэлектрическая проницаемость одинакова для всех рассеивающих частиц. Тогда решение задачи сводится к решению (2) с постоянным по ансамблю и времени сечением $Q_\omega(\mathbf{r},t)\equiv Q_\omega$.

Общее решение уравнения (2) имеет вид

$$\Phi_\omega(\mathbf{r},t)=\sum_n a_n\psi_n(\mathbf{r})\exp[-(DB_{n^2}-Q_\omega N_0)ct], \tag{9}$$

где $\psi_n(\mathbf{r})$ и B_n — собственные функции и собственные значения уравнения

$$\psi_n(\mathbf{r})+B_{n^2}\psi_n(\mathbf{r})=0 \tag{10}$$

с граничным условием $\psi_n=0$ на расстоянии d от границы области, a_n — произвольные постоянные, определяемые начальным распределением Φ (**r**, *t)* при $t=0$.

Из (9) сразу следует условие порога

$$DB^2-N_0Q_0=0, \tag{11}$$

где B — наименьшее собственное значение B_n (обычно $B=B_1$), $Q_0=Q_{\omega_0}$, ω_0 — частота максимального усиления.

Если область, занимаемая ансамблем рассеивающих частиц, имеет форму сферы радиуса R, то[2)] [5]:

$$\psi_n=\frac{1}{r}\sin\frac{n\pi r}{R},\quad B_n=\frac{n\pi}{R},\quad B=\frac{\pi}{R}. \tag{12}$$

Для цилиндра высоты H и радиуса R наименьшее собственное значение B есть

$$B=\left[\left(\frac{2{,}4}{R}\right)^2+\left(\frac{\pi}{H}\right)^2\right]^{1/2}, \tag{13}$$

а для параллелепипеда со сторонами *a, b, c* равно

$$B=\left[\left(\frac{\pi}{a}\right)^2+\left(\frac{\pi}{b}\right)^2+\left(\frac{\pi}{c}\right)^2\right]^{1/2}. \tag{14}$$

[2)] Из (12) и (11) следует, что отношение длин свободного пробега за счет рассеяния и усиления $\Lambda_s/\Lambda_a=\pi^2(\Lambda_s/R)^{\,2}/3(1-\bar{\mu})$ при выполнении условия (1) гораздо меньше единицы.

Строго говоря, все размеры областей нужно увеличить на длину линейной экстраполяции (8), но это из-за условия (1) дает малую поправку, которой будем пренебрегать.

Сечения Q_s и Q_0 определяются геометрией и значением комплексной диэлектрической проницаемости $\varepsilon = \varepsilon_0 + i\varepsilon_0''(\omega_0)$ рассеивающих частиц. Вычисление их при произвольном соотношении между размером частиц и длиной волны даже для определенной формы частиц является весьма сложной задачей [7]. Поэтому мы ограничимся параметрами сферических частиц с радиусом a, гораздо меньшим или гораздо бóльшим длины волны λ.

Случай k$a \ll 1$ рассчитывается точно [7]:

$$Q_s = \frac{8}{3}(ka)^4 \left|\frac{\varepsilon-1}{\varepsilon+2}\right|^2 G, Q_0 = 4ka\mathrm{Im}\frac{\varepsilon-1}{\varepsilon+2}G, \bar{\mu} = 0 \tag{15}$$

($G = \pi a^2$ — геометрическое сечение). Мнимая часть диэлектрической проницаемости $\varepsilon_0'' = \alpha_0/k \ll 1$, где α_0 — коэффициент усиления на единицу длины в веществе рассеивающих частиц, k — волновой вектор. Тогда имеем

$$Q_s = \frac{8}{3}(ka)^4 \left(\frac{\varepsilon_0-1}{\varepsilon_0+2}\right)^2 G, \quad Q_0 = \frac{4}{\varepsilon_0+2} a\alpha_0 G. \tag{16}$$

Соотношения (11) и (16) определяют пороговый (критический) размер области генерации или пороговое усиление α_0. Например, выражение для порогового размера $\pi/R_{\text{пор}}$ (в случае сферы — критического радиуса $R_{\text{пор}}$) имеет вид

$$\frac{\pi}{B_{\text{пор}}} = \frac{g^3}{(ka)^2}\left(\frac{\varepsilon_0+2}{\varepsilon_0-1}\right)\sqrt{\frac{2(\varepsilon_0+2)a}{\alpha_0}}, \tag{17}$$

где $g = N_0^{-1/3}/2a$ — отношение среднего расстояния между частицами к их диаметру.

В случае ka >> 1 вычисление точных значений сечений и диаграммы является громоздким. Однако для приближенных оценок в области $\varepsilon_0 - 1 \approx 1$ можно принять, что

$$Q_s \approx G, \;\; Q_0 \approx 2\eta a\alpha_0 G, \;\; \bar{\mu} = 0, \tag{18}$$

где η — среднее пропускание границ диэлектрического шара. Тогда выражение для критического размера имеет вид

$$\frac{\pi}{B_{\text{пор}}} = g^3\sqrt{\frac{32a}{3\eta\alpha_0}}. \tag{19}$$

Например, для сферического распределения частиц рубина ($\lambda = 7 \times 10^{-5}$ см) с радиусом $a = 2\times10^{-4}$ см, $\eta \approx 1$, $g = 2$, и усилением $\alpha_0 \approx 1\,\text{см}^{-1}$ (при 77° К) критический радиус области $R_{\text{пор}} \approx 4$ мм.

Выше рассмотрен случай однородного распределения накачки при отсутствии какого-либо отражения фотонов на границе области. В ряде случаев это не так.

В частности, при оптической внешней накачке рассеивающих частиц из-за диффузии и поглощения света накачки распределение $\tilde{\varepsilon}_0''(\mathbf{r})$ максимально на границе области и минимально внутри. Решая уравнение диффузии с поглощением и притоком фотонов накачки на границе, можно найти распределение интенсивности накачки и, следовательно, функцию $\tilde{\varepsilon}_0''(\mathbf{r})$.

Решение для сферической области имеет вид

$$\tilde{\varepsilon}''(\mathbf{r}) = \tilde{\varepsilon}_m'' \frac{R}{r} \frac{e^{\varkappa r} - e^{-\varkappa r}}{e^{\varkappa R} - e^{-\varkappa R}}, \tag{20}$$

где $\tilde{\varepsilon}_m''$ — значение $\tilde{\varepsilon}_0''(\mathbf{r})$ на границе области, R — радиус области, $\varkappa = \sqrt{N_0 Q_a / D_{\text{н}}}$, $D_{\text{н}}$ и D_a — коэффициент диффузии и сечение поглощения света накачки. Величины $D_{\text{н}}$ и D_a определяются прежними выражениями (4), (16) и (18) с учетом отличия длины волны света накачки от длины волны генерируемого излучения, а также коэффициента поглощения света накачки $\alpha_{\text{н}}$ от коэффициента усиления α_0. Учет неоднородности $\tilde{\varepsilon}_0''(\mathbf{r})$ существенен лишь при $\varkappa R \lesssim 1$ или, полагая $R = R_{\text{пор}}$, при $|\alpha_{\text{н}}| \gtrsim |\alpha_0|$. Однако условие порога (11) и в этом случае остается прежним, но величина B является наименьшим собственным значением следующего уравнения:

$$\Delta\psi_n(\mathbf{r}) + B_{n^2} \frac{\tilde{\varepsilon}''(\mathbf{r})}{\tilde{\varepsilon}_m''} \psi_n(\mathbf{r}) = 0. \tag{21}$$

Очевидно, учет неоднородности повышает величину B и, следовательно, порог генерации.

Наличие отражения (зеркального или диффузного) на границе области, наоборот, понижает порог. Рассчитать порог в этом случае можно либо заменой нулевых граничных условий, либо переносом границы на эффективное расстояние, определяемое коэффициентом отражения.

4. Рассеивающие частицы в газовой усиливающей среде

Особый интерес представляет случай, когда рассеивающие частицы распределены в газовой среде с отрицательным поглощением (например, в смеси газов He–Ne или He–Xe, возбуждаемой электрическим разрядом [8]). В этом случае рассеивающие частицы осуществляют нерезонансную обратную связь, а газовая активная среда — резонансное усиление. Использование газовой активной среды обеспечивает более высокую стабильность частоты центра

линии усиления и представляет интерес для создания оптического стандарта частоты.

Существенным свойством газовой усиливающей среды в рассматриваемом случае является «однородное уширение» линии излучения. Как известно, в газовых лазерах с резонатором Фабри — Перо в пределах неоднородно уширенной эффектом Доплера линии в сильном монохроматическом поле происходит образование «провалов» за счет эффекта насыщения [9, 10]. Физически образование «провалов» связано с генерацией светового поля в виде направленных волн. В нашем случае длина свободного пробега фотона гораздо меньше размеров генерируемой области и поэтому излучение существенно изотропно. В монохроматическом изотропном поле вероятность индуцированного излучения не зависит от направления скорости атома и образование «провалов» невозможно. В этом смысле линия усиления является «однородно уширенной», а частота максимального усиления не зависит от напряженности поля. Это является весьма существенным для создания оптического стандарта частоты.

Пороговое условие (11) остается справедливым и в этом случае, если усиление на единицу длины в рассеивающей среде $Q_\omega N_0$ заменить на эффективное усиление в газовой среде $\alpha_{\text{эфф}}(\omega)$. Строго говоря, эффективное усиление при наличии рассеивающих частиц несколько отличается от усиления в чистой газовой среде $\alpha_0(\omega)$ за счет возможного проникновения поля внутрь частиц, которые могут быть поглощающими. Для оценки можно принять, что

$$\alpha_{\text{эфф}}(\omega) = f\alpha_0(\omega) + (1-f)\varkappa_0, \tag{22}$$

где $(1-f)$ — параметр, описывающий относительную величину среднего пути фотона внутри рассеивающих частиц при случайном блуждании внутри области; $\varkappa_0$ — коэффициент поглощения на единицу длины в веществе рассеивающих частиц. Если поле свободно проникает внутрь рассеивающих частиц, приближенно можно считать, что $(1-f) \approx (V_\text{S}/V_0)^{1/3}$, где V_s — объем всех рассеивающих частиц; V_0 — объем области генерации.

Критический радиус области генерации имеет вид

$$R_{\text{пор}} = \pi[\Lambda_s/3(1-\bar{\mu})]\alpha_{\text{эфф}}(\omega_0)^{1/2}. \tag{23}$$

Например, на смеси Не-Хе $\lambda = 3{,}51$ μ реально получить $\alpha_{\text{эфф}}(\omega) \approx 0{,}1$ см$^{-1}$ [11]. При $\Lambda_\text{S} \approx 0{,}1$ см, $\bar{\mu} \approx 0$ критический радиус $R_{\text{пор}} \approx 1{,}8$ см.

5. Динамика генерации

Процесс генерации, включая переходный процесс, установление стационарного режима генерации, сужение спектра излучения и др., описывается нелинейными уравнениями (2) и (7). Прежде чем решать их, качественно обсудим поведение решения.

После перехода порога происходит экспоненциальное возрастание интенсивности излучения, начиная от уровня спонтанного шума. Этот процесс еще описывается линейным решением (9). Из-за резонансного характера отрицательного поглощения скорость возрастания максимальна для частот вблизи центра линии ω_0, что ведет к одновременному сужению спектра. Экспоненциальное возрастание интегральной интенсивности $\Phi(\mathbf{r},t) = \int \Phi_\omega(\mathbf{r},t)d\omega$ продолжается до тех пор, пока не наступит уменьшение отрицательного поглощения $\varepsilon''(\mathbf{r}, t)$ за счет эффекта насыщения. Этот процесс описывается уравнением (7). В результате резкого насыщения система оказывается ниже порога и интенсивность излучения падает, но затем за счет накачки $\tilde{\varepsilon}''(\mathbf{r})$ происходит превышение над порогом и пульсации повторяются. Такие пульсации (пички) являются обычным переходным процессом квантового генератора [12]. Постепенно они затухают, и генерация переходит в стационарный режим.

Исследуем сначала нестационарное решение уравнений (2) и (7). Для этого проинтегрируем (2) по частоте и учтем, что

$$\int \Phi_\omega(\mathbf{r},t)Q_\omega(\mathbf{r},t)d\omega \simeq Q_0(\mathbf{r},t)d\omega.$$

Последнее справедливо на том основании, что уже к началу первого пичка ширина спектра излучения становится гораздо меньше ширины резонанса отрицательного поглощения $\Delta\omega_0$. Тогда уравнения (2) и (7) приобретают следующий вид:

$$\frac{1}{c}\frac{\partial\Phi(\mathbf{r},t)}{\partial t} = D\Delta\Phi(\mathbf{r},t) + Q_0(\mathbf{r},t)N_0\Phi(\mathbf{r},t), \tag{24}$$

$$\frac{\partial\varepsilon''(\mathbf{r},t)}{\partial t} = -2\sigma_0\varepsilon''(\mathbf{r},t)\Phi(\mathbf{r},t) + \frac{\tilde{\varepsilon}''(\mathbf{r})-\varepsilon''(\mathbf{r},t)}{T_1}. \tag{25}$$

Сечение $Q_0(\mathbf{r},t)$ пропорционально $\varepsilon''(\mathbf{r}, t)$ (см. раздел 3). Решение уравнения в частных производных (24) будем искать в виде ряда по собственным функциям уравнения (10):

$$\Phi(\mathbf{r},t) = \sum_{k=1}^{\infty}\alpha_k(t)\psi_k(\mathbf{r}). \tag{26}$$

Подставляя (26) в (24) и учитывая, что функции $\psi_k(\mathbf{r})$ образуют полную ортонормированную систему, после стандартных преобразований находим:

$$\frac{d\alpha(t)_m}{dt} = -cDB_{m^2}\alpha_m(t) + cN_0\sum_{k=1}^{\infty}\alpha_k(t)Q_{km}(t), \tag{27}$$

где

$$Q_{km}(t) = \langle\psi_k(\mathbf{r})|Q_0(\mathbf{r},t)|\psi_m(\mathbf{r})\rangle, \tag{28}$$

а $Q_0(\mathbf{r}, t)$ подчиняется уравнению (25). Решение системы уравнений (25), (27) полностью определяет развитие генерации, но найти его аналитически невозможно. Поэтому производилось численное интегрирование уравнений на электронной вычислительной машине.

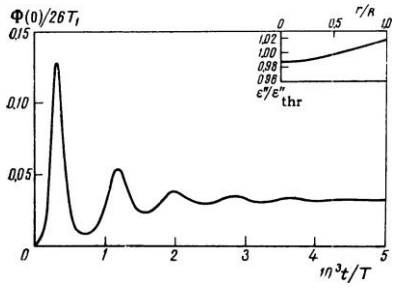


Рис. 1. Динамика установления стационарного режима генерации в сферической рассеивающей области с отрицательным поглощением. Начальное превышение над порогом $\eta = 1{,}02$; $T/T_1 = 3 \times 10^{-3}$. В верхнем углу — радиальное распределение ε'' в стационарном режиме

Рассматривался случай сферической области радиуса R, когда собственные функции и значения определяются выражением (12). Распределение накачки $\tilde{\varepsilon}''(\mathbf{r})$ было однородным. Параметр T/T_1, где T — среднее время жизни фотона в области при $\varepsilon'' \equiv 0$, определяемое выражением

$$T = 1/DB^2c, \tag{29}$$

а T_1 — время продольной релаксации, был гораздо меньше единицы. На рис. 1 приведены результаты решения для случая $T/T_1 = 3 \times 10^{-3}$ при величине превышения накачки над пороговой $\eta = 1{,}02$. Отчетливо видно возникновение пульсаций плотности фотонов и переход к стационарному режиму генерации. В верхней части рисунка показано радиальное распределение $\varepsilon''(\mathbf{r})$ в стационарном режиме. Неоднородность распределения $\varepsilon''(\mathbf{r})$ вызвана преимущественным насыщением отрицательного поглощения в центре области.

Стационарное решение уравнений (24) и (25), соответствующее установившейся генерации, удовлетворяет уравнению:

$$\Delta\Phi(\mathbf{r}) + \frac{N_0}{D}\frac{\tilde{Q}(\mathbf{r})}{1+2\sigma_0 T_1 \Phi(\mathbf{r})}\Phi(\mathbf{r}) = 0, \tag{30}$$

где $\tilde{Q}(\mathbf{r})$ — стационарное значение $Q_0(\mathbf{r}, t)$ в отсутствие поля, определяемое значением $\tilde{\varepsilon}''(\mathbf{r})$. При малом превышении накачки над порогом, когда эффектом насыщения можно пренебречь ($2\sigma_0 T_1 \Phi \ll 1$), решением (30) является собственная функция уравнения (10) (ограничиваемся случаем однородной накачки), соответствующая наименьшему собственному значению, а

нелинейность уравнения (30) определяет амплитуду решения. Если B_n — наименьшее собственное значение, то решение имеет вид

$$\Delta\Phi(\mathbf{r}) = \frac{\eta-1}{2\sigma_0 T_1 \eta}\left(\int \psi_{n^3}(\mathbf{r})\, d\mathbf{r}\right)^{-1}\psi_n(\mathbf{r}),\ \ \eta - 1 \ll 1, \tag{31}$$

где $\eta = \tilde{Q}N/DB_n^2$ — коэффициент превышения накачки над пороговым значением. При увеличении накачки над порогом становится существенным искажение потенциала в уравнении (30) за счет насыщения. В результате в решении появляется примесь других собственных функций. При слабом насыщении ($2\sigma_0 T_1 \Phi \lesssim 0{,}1$) решение можно найти по теории возмущений, рассматривая «деформацию» потенциала в (30) как возмущение. В первом приближении решение имеет вид [13]

$$\Delta\Phi(\mathbf{r}) = \frac{\eta-1}{2\sigma_0 T_1 \eta U_{nn}}\left[\psi_n(\mathbf{r}) + (\eta-1)\frac{B_{n^2}}{U_{nn}}\sum_{p\neq 1}\frac{U_{np}}{\eta B_{n^2} - B_{p^2}}\psi_p(\mathbf{r})\right], \tag{32}$$

где

$$U_{np} = \int \psi_{n^2}\psi_p d\boldsymbol{r}. \tag{33}$$

Интенсивность выходного излучения квантового генератора определяется диффузией фотонов через границу области. Этот процесс аналогичен «утечке» нейтронов из реактора, и интенсивность выходного излучения в стационарном случае определяется выражением [5]:

$$P = \frac{\Lambda_s}{6}\left|\mathrm{grad}_n \Phi(\boldsymbol{r})\right|, \tag{34}$$

где n — нормаль к границе области. Интенсивность выходного излучения пропорциональна отношению длины свободного пробега $\sim\Lambda_s$ к размерам области. Физически это связано с тем, что фотоны диффундируют наружу преимущественно из приповерхностного слоя с толщиной $\sim\Lambda_s$. Поэтому излучение такого генератора, подобно излучению «черного тела», изотропно.

6. Спектр излучения

При стационарном значении интегральной интенсивности излучения $\Phi(\mathbf{r}, t)$ спектральная плотность $\Phi_\omega(\mathbf{r}, t)$, вообще говоря, не является стационарной. Нестационарность спектра заключается в том, что после начала генерации происходит непрерывное сужение спектра излучения. Этот эффект является особенностью лазеров с нерезонансной обратной связью и впервые был теоретически и экспериментально изучен в работе [14]. В нашем случае в этом нетрудно убедиться, рассматривая уравнение для спектральной плотности (2) при стационарном значении сечения отрицательного поглощения Q_0 и стационарном

пространственном распределении плотности фотонов. Для простоты будем пренебрегать искажением Q_0 за счет насыщения, так что $\Delta\Phi_\omega = -B^2\Phi_\omega$. Тогда уравнение (2) сводится к следующему:

$$\frac{1}{c}\frac{\partial\Phi\omega}{\partial t} = -DB^2\Phi\omega + a(\omega)Q_0N_0\Phi_\omega. \tag{35}$$

Поскольку $a(\omega_0)Q_0N_0 = DB^2$, то

$$\Phi_\omega(t) \sim exp\{-[a(\omega) - a(\omega_0)]Q_0N_0ct\}. \tag{36}$$

Разлагая функцию формы линии (6) $a(\omega)$ вблизи центра линии ω_0, находим закон сужения спектра в стационарном режиме генерации:

$$\Delta\omega(t) = (Q_0N_0ct/\ln 2)^{-1/2}\Delta\omega_0, \tag{37}$$

который аналогичен найденному в [14].

Сужение спектра, как обычно, происходит до некоторого флуктуационного предела. В идеальном случае предельная ширина линии определяется спонтанным излучением. Однако практически существенную роль играет флуктуационное (броуновское) движение рассеивающих частиц, которое ведет к случайному изменению (блужданию) частоты фотона за счет эффекта Доплера на рассеивающих частицах. Пусть при каждом рассеянии частота фотона изменяется на среднюю величину $\delta\omega \ll \Delta\omega_0$. Тогда изменение спектра можно найти, рассматривая диффузию фотонов только по частоте:

$$\frac{1}{c}\frac{\partial\Phi\omega}{\partial t} = \Gamma\frac{\partial^2\Phi\omega}{\partial\omega^2} + Q(\omega)N_0\Phi_\omega, \tag{38}$$

где Г — коэффициент диффузии частоты, определяемый в принятой модели выражением

$$\Gamma = (\delta\omega)^2/2\Lambda_s. \tag{39}$$

Найдем предельную ширину линии излучения в этом случае.

Уравнение стационарного состояния Φ_ω имеет вид

$$\frac{\partial^2\Phi\omega}{\partial\omega^2} + Q_\omega\frac{N_0}{\Gamma}\Phi_\omega = 0. \tag{40}$$

Так как $\delta\omega$ гораздо меньше $\Delta\omega_0$ — ширины резонанса Q_ω, ширина Φ_ω также должна быть гораздо меньше $\Delta\omega_0$. Следовательно, в уравнении (40) функцию Q_ω можно разложить вблизи центра линии ω_0 с точностью до квадратичного члена. Для лоренцовой формы линии (6) уравнение (40) тогда принимает вид

$$\frac{\partial^2\Phi\omega}{\partial\omega^2} + \frac{N_0Q_0}{\Gamma}\left[1 - \left(2\frac{\omega-\omega_0}{\Delta\omega_0}\right)^2\right]\Phi_\omega = 0, \tag{41}$$

совершенно аналогичный уравнению Шредингера для гармонического осциллятора [15], где $Q_0 = Q_{\omega_0}$. Форма линии Φ_ω определяется собственной

функцией основного состояния уравнения (41), так как это единственная функция, удовлетворяющая условию $\Phi_\omega > 0$. Следовательно,

$$\Phi_\omega = A\exp\left[-\left(\frac{\omega-\omega_0}{\Delta\omega_0}\right)^2\sqrt{\frac{N_0 Q_0}{\Gamma}}\right], \tag{42}$$

или, подставляя значения Γ и Λ_s:

$$\Phi_\omega = A\exp\left[-\left(\frac{\omega-\omega_0}{\Delta\omega_0\delta\omega}\right)^2\sqrt{2\frac{Q_0}{Q_s}}\right], \tag{43}$$

где A — нормировочная постоянная. Выражение для предельной ширины спектра по полумаксимуму $\Delta\omega_{min}$ имеет вид[3)]

$$\Delta\omega_{min} = \left(4\ln 2\,\Delta\omega_0\delta\omega\sqrt{Q_s/2Q_0}\right)^{1/2}. \tag{44}$$

В рассматриваемом приближении не учтен вклад спонтанного излучения в уширение линии генерации. Можно предполагать, что величина его, как и в обычных лазерах, значительно меньше ширины (44), связанной с флуктуационным движением элементов обратной связи. Вычисление уширения линии генерации за счет спонтанного излучения должно учитывать статистические свойства излучения такого лазера, которые существенно отличны от статистических свойств излучения обычных лазеров.

7. Заключение

С точки зрения «мод» «стохастический резонатор» в виде рассеивающей среды представляет систему с большим числом «мод» (волн различных направлений), сильно связанных рассеянием и обладающих большими радиационными потерями. Высокие радиационные потери и сильное взаимодействие «мод» приводят к полному перекрытию их спектра частот. Понятие «моды» здесь теряет обычный смысл, и спектр становится сплошным. Если число взаимодействующих «мод» N достаточно велико, обратная связь становится нерезонансной [2]. Число связанных рассеянием «мод» N определяется выражением:

$$N \simeq \Omega_{\text{ген}}/(\lambda/D)^2, \tag{45}$$

где $\Omega_{\text{ген}}$ — телесный угол генерации, D — диаметр области генерации. В лазерах, описанных в работах [2, 14] ($\Omega_{\text{ген}} \approx 10^{-3} \div 10^{-4}$ стерад), $N \simeq 10^5$ и

[3)] Условием справедливости раздельного рассмотрения диффузии по частоте и в пространстве является $\Delta\omega_{\min} \ll \Delta\omega_0$.

обратную связь можно считать нерезонансной[4]. Чем больше число взаимодействующих «мод», тем эффективнее осуществляется разрушение резонансных свойств. Для получения максимальной стабильности частоты генерации необходимы лазеры с максимальным $\Omega_{\text{ген}}$. Поэтому рассмотренный в настоящей статье лазер в наибольшей степени обладает нерезонансным характером обратной связи, так как телесный угол генерации его максимален ($\Omega_{\text{ген}} = 4\pi$). Например, при $D \approx 1$ см на $\lambda \approx 10^{-4}$ см число взаимодействующих «мод» достигает $10^8 \div 10^9$.

В заключение автор выражает глубокую благодарность академику Н.Г. Басову за поддержку и обсуждение настоящей работы и ценные советы, А.Т. Матачун — за помощь в численных расчетах, Р.В. Амбарцумяну и П.Г. Крюкову — за обсуждение работы.

Литература

1. *Прохоров А.М.* // ЖЭТФ. 1958. Т. 34. С. 1658. *Schawlow A.L., Townes C.H.* // Phys. Rev. 1958. Vol. 112. P. 1940.

2. *Амбарцумян Р.В., Басов Н.Г., Крюков П.Г., Летохов В.С.* // Письма в ЖЭТФ. 1966. Т. 3. С. 261; ЖЭТФ. 1966. Т. 51. С. 724.

3. *Летохов В.С.* // Письма в ЖЭТФ. 1966. Т. 4. С. 477.

4. *Летохов В.С.* // Письма в ЖЭТФ. 1967. Т. 5. С. 262.

5. *Вейнберг А., Вигнер Е.* Физическая теория ядерных реакторов. М.: Изд-во иностр. лит., 1961.

6. *Karplus R. and Schwinger J.* // Phys. Rev. 1948. Vol. 73. P. 1020.

7. *Хюлст Г. ван де.* Рассеяние света малыми частицами. М.: Изд-во иностр. лит., 1961.

8. *Javan A., Bennett Jr. W.R. and Herriott D.R.* // Phys. Rev. Lett. 1961. Vol. 6. P. 106.

9. *Bennett Jr. W.R.* // Phys. Rev. 1962. Vol. 126. P. 580.

10. *Lamb Jr. W.E.* // Phys. Rev. 1964. Vol. 134. P. A 1429.

11. *Paananen R.A. and Bobroff D.L.* // Appl. Phys. Lett. 1963. No. 2. P. 99.

12. *Statz H. and de Mars G.* Quantum Electronics / ed. by C.H. Townes. N.Y., 1960.

13. *Морс Ф.М., Фешбах Г.* Методы теоретической физики. Т. II. М.: Изд-во иностр. лит., 1966.

14. *Амбарцумян Р.В., Крюков П.Г., Летохов В.С.* // ЖЭТФ. 1966. Т. 51. С. 1669.

15. *Ландау Л., Лифшиц Е.* // Квантовая механика. М.: Физматгиз, 1963.

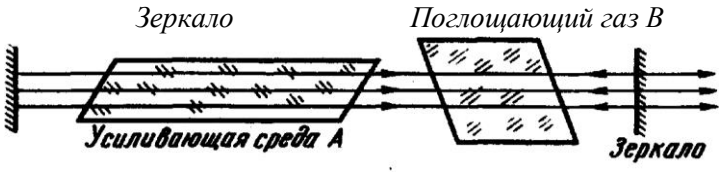
[4] Однако при малых углах генерации, когда N мало (например, при $\Omega_{\text{ген}} \simeq (\lambda/D)^2$, перекрытие «мод» невелико и возможно появление случайных «резонансов» на некоторых частотах (С.Н. Townes, частное сообщение), но в этом случае понятие нерезонансной обратной связи теряет смысл.

Письма в ЖЭТФ. 1967. Т. 6 (4). С. 597–600

АВТОСТАБИЛИЗАЦИЯ ЧАСТОТЫ СВЕТОВЫХ КОЛЕБАНИЙ ЛАЗЕРА НЕЛИНЕЙНЫМ ПОГЛОЩЕНИЕМ В ГАЗЕ

В.С. Летохов
Физический институт им. П.Н. Лебедева АН СССР

1. Известно, что для создания квантового генератора с высокой стабильностью частоты колебаний (стандарта частоты) необходимо иметь узкий резонанс усиления активной среды со стабильным положением максимума резонанса и широкий резонанс потерь в резонаторе. Этот принцип лежит в основе стандартов частоты радио- [1, 2] и оптического [3] диапазонов. В настоящем письме предлагается принципиально другой метод стабилизации частоты лазера, который основан на возникновении в поле стоячей волны лазера узкого резонансного «провала» в линии поглощения газа, помещенного в резонатор, при широком и менее стабильном резонансе усиления активной среды. Предложенный метод представляет интерес для создания оптического стандарта частоты.



2. Пусть газ низкого давления находится в поле стоячей световой волны $Ee^{i\omega t}\cos kz$, частота которого совпадает с линией резонансного поглощения газа на частоте ω_b. В «слабом» световом поле, не вызывающем насыщения поглощения газа, форма линии поглощения является доплеровской. В «сильном» световом поле происходит насыщение поглощения атомов, наиболее эффективно взаимодействующих с полем стоячей волны. В результате форма линии поглощения существенно изменяется и, если доплеровская ширина линии значительно больше однородной ширины, на частоте ω и зеркальной ей относительно ω_b частоте $2\omega_b - \omega$ выжигаются «дырки». Коэффициент поглощения стоячей световой волны приобретает «провал» на частоте ω_b, из-за совпадения зеркально-симметричных «дырок» при $\omega = \omega_b$. Это явление было подробно изучено Лэмбом [4] для случая усиливающей газовой среды и носит название лэмбовского «провала».

Если газ имеет низкое давление, а вероятность радиационного перехода поглощающих атомов A_{21}^{b} мала, «провал» в линии поглощения может быть весьма узок. Ширина его $\Delta\omega_b$ определяется временем пролета атомов через луч $\tau_0 = d/\mathrm{v}_0$ (d — диаметр луча, v_0 — средняя скорость атомов) и уширением линии за счет столкновений $\Delta\omega_{\text{ст}}$:

$$\Delta\omega_b = \frac{1}{\tau_0} + \Delta\omega_{\text{ст}}, \tag{1}$$

если $A_{21}^{b} \ll 1/\tau_0$. Например, при давлении газа 10^{-2} тор, когда обычно $\Delta\omega_{\text{ст}} \simeq 10^4 \div 10^5$ Гц, для луча диаметром $d \simeq 1$ см ($\mathrm{v}_0 \simeq 10^5 - 10^6$ см/сек) ширина «провала» $\Delta\omega_b \simeq 2 \cdot 10^4 \div 10^5$ Гц.

3. Пусть в резонаторе лазера находится кювета с поглощающим газом, линия поглощения которого на частоте ω_b совпадает с линией усиления активной среды на частоте ω_a (рис.1). При достаточном превышении накачки над порогом, когда образуется «провал» в линии поглощения, частота генерации ω автоматически стабилизируется в области минимума потерь на частоте «провала» ω_b, переход в режим автостабилизации достигается, если частота генерации ω поддерживается в пределах «провала» ($|\omega - \omega_b| \lesssim \Delta\omega_b$). Если активная среда лазера имеет доплеровскую неоднородную линию уширения с шириной $\Delta\omega_{\text{доп}}$ однородной шириной $\Delta\omega_a \ll \Delta\omega_{\text{доп}}$, то условия автостабилизации имеют следующий вид:

$$S_1 = \frac{1}{p_b}\frac{\Delta\omega_b}{kc}, S_2 = \frac{1}{p_b}\frac{\alpha}{k}\frac{\Delta\omega_b}{\Delta\omega_{\text{доп}}}, S_3 = \frac{\alpha a}{kb}\frac{\Delta\omega_b}{\Delta\omega_a} \ll 1, \tag{2}$$

где c — скорость света; $p_a = aE^2$, $p_b = bE^2$ — параметры насыщения усиления и поглощения соответственно; α, k — коэффициенты усиления и поглощения на единицу длины соответственно. Частота генерации ω в режиме автостабилизации определяется выражением:

$$\omega = \omega_b + S_1(\Omega - \omega_b) + (S_2 - S_3)(\omega_a - \omega_b), \tag{3}$$

где Ω — частота резонатора. В случае активной среды с однородной линией усиления выражение (3) остается справедливым, если в S_2 заменить доплеровскую ширину на однородную $\Delta\omega_a$ и положить $S_3 = 0$. Выражение (3) получено в предположении $p_a p_b \ll 1$, но эффекты автостабилизации существуют и при больших значениях параметров насыщения*. Из (2) и (3) следует, что стабилизирующее действие поглощающего газа объясняется возникновением узкого «провала» с шириной $\Delta\omega_b \ll \Delta\omega_a, kc, \Delta\omega_{\text{доп}}$, за счет которого параметры $S_1, S_2, S_3 \ll 1$.

* Результаты для случая сильного насыщения и условия устойчивости будут изложены в подробной публикации.

4. Для осуществления предложенного лазера необходимо подобрать атомы или молекулы, обладающие линией поглощения на частоте излучения лазера непрерывного действия. Укажем на следующие две возможные пары: 1) линия 3,3913 мк He–Ne лазера совпадает с линией поглощения 2947,906 см$^{-1}$ молекулы CH_4 с точностью 0,003 см$^{-1}$ при коэффициенте поглощения k = 0,17 см$^{-1}$/тор и $\Delta\omega_{\text{ст}} = 5$ мГц/тор [5]; 2) линия 3,5070 мк He–Xe лазера совпадает с линией поглощения 2850,608 см$^{-1}$ молекулы H_2CO с точностью 0,007 см$^{-1}$ при $k \simeq 0{,}1$ см$^{-1}$/тор [6]. При давлении газа 10^{-2} тор можно получить глубокий «провал» с шириной $\Delta\omega_b \simeq 5 \cdot 10^4$ Гц под действием поля с интенсивностью 10^{-2} Вт/см^2.

В качестве поглощающих молекул в ряде случаев можно использовать молекулы активной среды при отсутствии возбуждения, так как условие совпадения частот усиления и поглощения в этом случае выполняется автоматически.

Приведенные примеры поглощающих молекул являются далеко не оптимальными, так как для них $A_{21}^b \simeq$ сек$^{-1}$. Наиболее выгодны атомы или молекулы с $A_{21}^b \simeq 10^3 - 10^5$сек$^{-1}$. При таких значениях A_{21}^b можно использовать весьма низкие давления поглощающего газа (~10^{-4} тор), что гарантирует высокую стабильность положения линии поглощения ω_b. При столь низких давлениях длина свободного пробега составляет десятки сантиметров, и, следовательно, при многократном пропускании луча через поглощающий газ строго параллельно самому себе за счет молекул, пересекающих последовательно несколько лучей, можно получить весьма узкий «провал» с шириной $\Delta\omega_b \simeq 10^3$ Гц. Кроме того, при $A_{21}^b \simeq 10^3 \div 10^5$с$^{-1}$ существенно снижается мощность, необходимая для образования «провала».

5. Вполне реальны получение «провала» поглощения с шириной $\Delta\omega_b \simeq 10^5$ Гц и стабилизация частоты резонатора Ω и частоты линии усиления ω_a с точностью 10^{-9}. В этом случае при $p_b \simeq 0{,}1 \div 0{,}3$ и $\Delta\omega_a, kc \gtrsim 10^8$ Гц можно ожидать стабильности частоты генерации ω относительно ω_b порядка 10^{-11}. Поэтому абсолютная стабильность частоты генерации будет определяться стабильностью частоты линии поглощения ω_b. При низких давлениях газа ($10^{-3} \div 10^{-4}$ тор) стабильность центра линии поглощения будет определяться взаимодействием молекул со стенками кюветы и, по-видимому, может быть не хуже 10^{-11}.

Автор глубоко благодарен академику Н.Г. Басову за обсуждение и поддержку настоящей работы.

Литература

1. *Басов Н.Г., Прохоров А.Н.* // ЖЭТФ. 1954. Т. 27. С. 431; *Gordon J.P., Zeiger K.J., Townes C.H.* // Phys. Rev. 1954. Vol. 95. P. 282.

2. *Goldenberg H.M., Kleppner D., Ramsey N.F.* // Phys. Rev. Lett. 1960. Vol. 5. P. 361.

3. *Басов Н.Г., Летохов В.С.* // Письма в ЖЭТФ. 1965. Т. 2. С. 6.
4. *Lamb Jr. W.E.* // Phys. Rev. 1964. Vol. 134A. P. A 1429.
5. *Edwards B.N., Burch D.E.* // JOSA. 1965. Vol. 55. P. 174.
6. *Sakurai K., Shimoda K., Takami M.* // J. Phys. Soc. of Japan. 1966. Vol. 21. P. 1838.

ЖЭТФ. 1968. Т. 55, 3 (9). С. 1077–1089

ГЕНЕРАЦИЯ УЛЬТРАКОРОТКИХ ИМПУЛЬСОВ СВЕТА В ЛАЗЕРЕ С НЕЛИНЕЙНЫМ ПОГЛОТИТЕЛЕМ

В.С. Летохов
Физический институт им. П.Н. Лебедева АН СССР

Теоретически рассмотрены образование и эволюция ультракороткого импульса света в лазере с насыщающимся поглотителем. Оценена вероятность возникновения случайного выброса интенсивности за счет флуктуаций интенсивности излучения в наборе аксиальных мод. Показано, что в линейной области генерации происходит расширение начального флуктуационного выброса интенсивности за счет усиливающей среды, а в нелинейной области — сжатие импульса нелинейным поглотителем. Показано, что минимальная длительность импульса в лазере с бесконечно быстрой релаксацией просветленного состояния в несколько раз больше предельной и для достижения предельной длительности необходимо устранять естественную селекцию мод в лазере. Рассмотрена эволюция формы импульса в случае поглотителя с конечным временем релаксации просветленного состояния. Показана возможность весьма быстрой релаксации просветленного состояния ($\sim 10^{-13}$ с) за счет переходов молекул по возбужденным синглетным уровням.

Введение

В последнее время достигнут значительный прогресс в области генерации мощных ультракоротких импульсов света методом самофазировки аксиальных мод твердотельного лазера, насыщающегося поглотителем [1, 2]. Нелинейный поглотитель (обычно просветляющийся раствор красителя) осуществляет включение добротности лазера и последовательное сжатие импульса, движущегося внутри резонатора. Этого удается достигнуть одновременно, если время жизни возбужденных частиц поглотителя T_{1b} гораздо короче времени прохода импульсом резонатора T ($T = 2L/\upsilon$, где T — длина резонатора, υ — средняя групповая скорость в резонаторе), то есть если нелинейный поглотитель является «быстрым» или малоинерционным. Самосжатие импульса в резонаторе эквивалентно самовозрастанию числа сфазированных мод, которое обычно называют самофазировкой или самосинхронизацией мод (*self-mode-locking*). Об эффективности этого метода можно судить по тому, что лазер на

неодимовом стекле с «быстрым» просветляющимся раствором генерирует цуг ультракоротких импульсов с длительностью импульса порядка 10^{-11}–10^{-12}с и энергией порядка 10^{-3}Дж [3, 4].

Теоретически ряд вопросов установившейся генерации лазера с насыщающимся поглотителем рассматривался в [5, 6]. В этих работах исследовались эффекты положения поглотителя внутри резонатора [5, 6] и ограничение длительности импульса за счет конечного времени жизни частиц поглотителя в возбужденном состоянии T_{1b} [6]. Ряд вопросов развития ультракоротких импульсов в лазере с бесконечно «быстрым» поглотителем ($T_{1b} = 0$) рассматривался в [7, 8]. Однако до настоящего времени нет теоретического рассмотрения, на основании которого можно было бы объяснить результаты существующих экспериментов и предложить пути достижения предельной длительности импульсов, определяемой шириной полосы усиления. Цель настоящей статьи — восполнить этот пробел.

В настоящей статье рассмотрены возникновение и эволюция ультракороткого импульса в лазере с нелинейным поглотителем, включая все стадии генерации: образование начального ультракороткого выброса интенсивности за счет флуктуаций интенсивности излучения, расширение флуктуационного выброса в линейной области из-за конечной полосы усиления и сжатие импульса в нелинейной области за счет поглотителя. В частности, показано, что для достижения предела длительности импульсов необходимо устранять расширение импульса в линейной области развития с помощью, например, частотно-селективных потерь в резонаторе. Рассмотрено влияние конечного времени T_{1b} релаксации просветленного состояния поглотителя на эволюцию импульса и механизмы достижения предельно малых значений T_{1b} для молекул в растворе. Предлагаемая теория объясняет результаты существующих экспериментов и позволяет указать пути получения мощных ультракоротких импульсов с длительностью порядка 10^{-13} с.

1. Качественное рассмотрение

Будем рассматривать следующую модель лазера с «быстрым» насыщающимся поглотителем. В резонаторе находится возбужденная среда, обладающая усилением в полосе частот $\Delta\omega_a$ с центром на частоте ω_0, и невозбужденная среда, обладающая поглощением в полосе частот $\Delta\omega_b$, внутри которой находится полоса усиления. В дальнейшем параметры усиливающей среды будем обозначать индексом a, а поглощающей среды — индексом b.

При накачке активной среды в некоторый момент времени ($t = t_0$) усиление компенсирует потери в поглощающей среде и на зеркалах. С этого момента времени усиление превышает потери и в резонаторе происходит нарастание интенсивности излучения в типах колебаний первоначально по закону

$$\exp\left\{\frac{1}{T}\int_{t_0}^{t}[\alpha(t')-\alpha_0]dt'\right\},$$

где $\alpha(t)$ — усиление на проход активной среды, $\alpha_0 = \alpha(t_0)$ — пороговое усиление на проход. Через некоторое время τ_1 интенсивность излучения становится достаточной для насыщения поглощения. Приближенно время задержки τ_1 момента просветления относительно момента порога определяется выражением

$$\tau_1 = T\left[\frac{2\tau_н}{\alpha_0 T}\ln\left(\frac{I_S}{I_0}\frac{1}{\varkappa_0}\sqrt{\frac{\alpha_0 T}{2\tau_н}}\right)\right]^{1/2}, \quad (1)$$

где T — время прохода светом резонатора, $\tau_н$ — время, характеризующее скорость нарастания усиления за счет накачки при прохождении порога $\tau_н^{-1} = \alpha^{-1}d\alpha/\mathrm{dt}|_{t=t_0}$, I_0 — начальная интенсивность, определяемая спонтанным излучением в типах колебаний, I_s — интенсивность насыщения поглощения, $\varkappa_0$ — начальные потери на проход в поглотителе. Для двухуровневой системы с временем жизни частиц на верхнем уровне T_{1b} и сечением радиационного перехода σ_b интенсивность насыщения определяется выражением

$$I_s = \hbar\omega_0/2\sigma_b T_{1b}. \quad (2)$$

В момент времени $t \approx t_0 + \tau_1$ потери в поглощающей среде резко уменьшаются — самовключается добротность резонатора [9–11]. Вслед за тем происходит более быстрое нарастание интенсивности и через относительно короткое время $\tau_2 << \tau_1$ — насыщение усиливающей среды ($\sigma_a << \sigma_b$), сопровождающееся высвечиванием запасенной в ней энергии в виде гигантского импульса.

В резонаторе неизбежно возбуждается несколько аксиальных типов колебаний[1)], из-за биений которых возникают флуктуации интенсивности с характерным временем $\sim T/m$, где m — число возбужденных типов колебаний. Число флуктуационных выбросов на интервале времени T порядка m, а амплитуда их случайна. Если время релаксации просветленного состояния поглотителя T_{1b} гораздо короче T/m, то в области нелинейности поглотитель «раскачивает» флуктуации интенсивности. Это происходит из-за того, что потери в поглотителе уменьшаются с увеличением мгновенной интенсивности излучения. В результате наиболее интенсивные флуктуационные выбросы усиливаются и сжимаются значительно быстрее остальных и, в конце концов, вызывают насыщение поглощения, а затем усиление их в резонаторе. При каждом отражении от полупрозрачного зеркала часть излучения покидает резонатор, и поэтому выходное излучение лазера представляет собой последовательность ультракоротких импульсов с интервалом T между ними.

[1)] Исключение составляет случай, когда в резонаторе находятся частотно-селективные элементы. Влияние их на число возбужденных аксиальных мод исследовалось в работе [12].

2. Метод решения

Цуг эквидистантных импульсов света, очевидно, можно описывать набором аксиальных мод с определенными фазовыми соотношениями между ними. Такой подход, в принципе, эквивалентен изложенному выше подходу, но анализ взаимодействия очень большого числа мод весьма сложен, и его удалось последовательно развить только для случая внешней периодической модуляции потерь (в стационарном [13] и нестационарном [14] режимах генерации). В рассматриваемом случае более пригоден подход, основанный на анализе изменения формы импульса, использовавшийся для этой цели в ряде работ [6–8, 15].

В соответствии с этим будем рассматривать распространение импульса в резонаторе, внутри которого находятся усиливающая и поглощающая среды. Взаимодействие импульса с усиливающей средой в данном случае будем описывать обычными скоростными уравнениями. Так как энергия импульсов на два-три порядка меньше энергии насыщения усиления $\mathscr{E}_{as}$, то это означает, что мы ограничиваемся случаем, когда длительность импульса $\tau >> 2\pi/\Delta\omega_a$. В этой области будет исследована эволюция импульса и найдены условия, при которых длительность импульсов уже ограничивается конечной полосой усиления.

Взаимодействие импульса с поглощающей средой также будем описывать скоростными уравнениями, предполагая, что $\Delta\omega_b >> \Delta\omega_a$. Тогда уравнения, описывающие преобразование импульса за один проход резонатора, имеют вид

$$\partial I_k(t)/\partial k = I_k(t)[\alpha_k(t) - \varkappa_k - \gamma], \tag{3а}$$

$$\partial N_{ak}(t)/\partial t + (N_{ak} - N_a^0)/T_{1a} = -2\sigma_a/I_k(t)N_{ak}(t), \tag{3б}$$

$$\partial N_{bk}(t)/\partial t + \left(N_{bk} - N_b^0\right)/T_{1b} = -2\sigma_b/I_k(t)N_{bk}(t), \tag{3в}$$

где $-1/2T \le t \le 1/2\,T$; $I_k(t)$ — форма импульса после k-го прохода; $\alpha_k(t)$ — усиление в активной среде на k-ом проходе, связанное с плотностью инверсной заселенности уровней $N_{ak}(t)$ соотношением $\alpha_k = \sigma_a N_{ak} L_a$ (L_a — длина усиливающей среды); $\varkappa_k(t)$ — потери в поглощающей среде на k-ом проходе, связанные с плотностью разности заселенностей уровней поглотителя $N_{bk}(t)$ аналогичным соотношением: $\varkappa_k = \sigma_b N_{bk} L_b$ (L_b — длина поглощающей среды); γ — линейные потери излучения на одном проходе; N_a^0 и N_b^0 — стационарные разности заселенностей уровней в усиливающей и поглощающей средах при нулевой амплитуде поля. Заселенности N_{ak} и N_{bk} в начале k-го прохода, очевидно, равны заселенностям после k – 1-го прохода:

$$N_{ak}(t - T/2) = N_{a,k-1}(t + T/2),\ \ N_{bk}(t - T/2) = N_{b,k-1}(t + T/2).$$

Уравнение (3а) справедливо в приближении малости изменения формы импульса за проход. Так как энергия импульса недостаточна для насыщения усиления за один проход ($\mathscr{E} << \mathscr{E}_{as}$), то это условие накладывает ограничение лишь на величину насыщаемых потерь:

$$\varkappa_0 \ll 1. \tag{4}$$

Условие (4) с достаточной точностью выполняется в лазерах ультракоротких импульсов, так как для них обычно $\varkappa_0 \approx 30\%$ [1, 2].

Эволюцию импульса удобно рассматривать последовательно на двух стадиях: возникновение и эволюция флуктуационного выброса интенсивности в области линейного поглощения и затем деформация импульса в области нелинейности поглощения. В свою очередь, эволюцию импульса в нелинейной области удобно рассматривать на двух следующих друг за другом этапах:

$$\tau \gg T_{1b}, \tag{5а}$$

$$\tau \approx T_{1b}. \tag{5б}$$

3. Образование и эволюция импульса в линейной области

Пусть спектр первоначально возбужденных аксиальных мод имеет ширину $\Delta\omega_0$. Фазы излучения в модах случайны, и, следовательно, мгновенная интенсивность излучения в модах $I(t)$ является случайной функцией времени. Средняя длительность флуктуаций интенсивности $\tau_ф \approx 2\pi\Delta\omega_0^{-1}$. Если число возбужденных мод $m \gg 1$, то суммарное излучение можно считать подобным некогерентному излучению [16]. Функция распределения флуктуаций интенсивности определяется соотношением [16, 17]:

$$W(I) = \frac{1}{\langle I\rangle}\exp\left(-\frac{I}{\langle I\rangle}\right). \tag{6}$$

Вероятность флуктуации интенсивности с амплитудой, в β раз превышающей среднее значение $\langle I\rangle$, определяется соотношением:

$$\mathcal{P}(\beta) = \int_{\beta\langle I\rangle}^{\infty} W(I)\,dI = e^{-\beta}. \tag{7}$$

Частота появления выбросов интенсивности равна $\sim 1/\tau_ф$. Следовательно, флуктуационный выброс с амплитудой $\beta\langle I\rangle$ с вероятностью единица возникает в среднем за интервал времени $\tau(\beta)$:

$$\tau(\beta) \approx \tau_ф e^{\beta} = \frac{2\pi}{\Delta\omega_0} e^{\beta}. \tag{8}$$

Флуктуационный выброс с амплитудой, в 10 раз превышающей среднее значение, появляется, например, в неодимовом лазере при $\Delta\omega_0 = \Delta\omega_a/5$ за среднее время $\tau(10) \approx 10^{-8}$ с. При прохождении порога импульс начинает усиливаться. Он усиливается в е раз за время τ_y после порога, определяемое выражением

$$\tau_y \approx (\tau_н T/2\alpha_0)^{1/2}. \tag{9}$$

Условие возникновения отчетливого флуктуационного выброса интенсивности, который может быть начальным импульсом в лазере, можно записать в виде

$$\tau(10) \lesssim \tau_y. \tag{10}$$

В лазере с включением добротности насыщающимся поглотителем это условие вполне реально выполнить[2)].

В области линейного развития происходит естественная селекция мод усиливающей средой за счет преимущественного усиления мод вблизи центра линии усиления. Естественная селекция особенно существенна в лазерах с насыщающимся поглотителем из-за большой величины времени задержки τ_1 [19]. В результате селекции происходит сужение спектра возбужденных мод в течение времени задержки или, другими словами, расширение начальных флуктуаций интенсивности. Это следует иметь в виду при оценке длительности ультракоротких импульсов [20]. Если τ_0 — длительность начального флуктуационного выброса интенсивности, то длительность τ_0' к моменту насыщения поглощения становится равной

$$\tau' = \tau_0 \left[1 + \alpha_0 \frac{\tau_1}{T}\left(\tau_0 \frac{\Delta\omega_\alpha}{8}\right)^{-2}\right]^{1/2}, \tag{11}$$

где для простоты форма начальной флуктуации и форма линии усиления считаются гауссовыми. Величина $8/\Delta\omega_a$ равна предельной длительности импульса $\tau_{пред}$, определяемой лишь шириной полосы усиления. Если $\tau_0 \ll \tau_{пред}\sqrt{\alpha_0\tau_1/T}$, то длительность флуктуации к концу линейного развития не зависит от начальной длительности:

$$\tau' = \tau_{пред}\sqrt{\alpha_0\tau_1/T}. \tag{12}$$

Выражение (12) определяет минимальную длительность флуктуационного выброса к моменту начала сжатия его нелинейным поглотителем.

[2)] Рассмотренный механизм образования флуктуационных выбросов вполне объясняет также наблюдавшееся в работах [18] спонтанное образование пикосекундных импульсов в твердотельных лазерах без нелинейного поглотителя.

4. Эволюция импульса в области $\tau \gg T_{1b}$

Если длительность импульса $\tau \gg T_{1b}$, то прозрачность поглотителя определяется мгновенным значением интенсивности $I(t)$. Кроме того, в этом случае заведомо $T \gg T_{1b}$ и, следовательно, к следующему проходу импульса поглотитель успевает релаксировать к начальному состоянию с поглощением $\varkappa_0$. На первой стадии, очевидно, можно пренебречь насыщением усиления. Тогда изменение формы импульса описывается одним уравнением:

$$\frac{\partial P_k(t)}{\partial k} = P_k(t)\left[\alpha_k - \frac{\varkappa_0}{1+P_k(t)} - \gamma\right], \tag{13}$$

где введена безразмерная интенсивность $P = I/I_s$, *а* I_s — интенсивность насыщения, определяемая соотношением (2).

Зависимость усиления от k обусловлена эффектом накачки в течение времени задержки τ_1. Это изменение весьма мало, и его можно представить в виде

$$\alpha(k) = \alpha_0 + \left.\frac{d\alpha}{dt}\right|_{t=t_0} Tk, \tag{14}$$

где $\alpha_0 = \alpha(t_0) = \gamma + \varkappa_0$ — пороговое усиление. Наиболее существенно в (14) то, что $\alpha_k > \alpha_0$, то есть усиление превышает потери. Вместо того чтобы рассматривать изменение α_k, достаточно учесть основное следствие этого измерения — отличие α_k от порогового значения α_0. Для этого естественно ввести среднее за время задержки τ_1 значение $\alpha(k)$:

$$\alpha = \alpha_0 \frac{\partial \alpha}{\partial t}\frac{\tau_1}{2} = \alpha_0\left(1 + \frac{\tau_1}{2\tau_{\text{н}}}\right), \tag{15}$$

где $\tau_{\text{н}}$ — введенная выше константа, характеризующая скорость накачки в момент порога; τ_1 — время задержки, определяемое соотношением (1). При постоянном значении α уравнение (13) интегрируется и его решение $P_k(t)$ определяется неявно выражением

$$P_k^{-1}(t)[(\alpha - -\varkappa_0 - \gamma) + \alpha P_k(t)]^{\frac{(\varkappa_0+\gamma)}{\alpha}} =$$
$$= P_0^{-1}(t)\,[(\alpha - \varkappa_0 - \gamma) + \alpha P_0(t)]^{\frac{(\varkappa_0+\gamma)}{\alpha_e} - (\alpha - \varkappa_0 - \gamma)^k}, \tag{16}$$

где $P_0(t)$ — начальная форма импульса.

Определим эффективную длительность импульса τ_k соотношением

$$\frac{1}{\tau_k^2} = -\frac{1}{P_k(t)}\frac{\partial^2 P_k(t)}{\partial t^2}\Big|_{t=0}, \tag{17}$$

где $t = 0$ — точка максимума импульса, которая в рассматриваемом приближении неизменна. Дифференцируя дважды соотношение (16) в точке $t = 0$, после преобразования находим

$$\tau_k^2 = \tau_0^2 \frac{1+P_k}{1+P_0}\frac{(\alpha-\varkappa_0-\gamma)+\alpha P_0}{(\alpha-\varkappa_0-\gamma)+\alpha P_k}, \tag{18}$$

где P_k и P_0 — интенсивности в максимуме ($t = 0$). Поскольку интенсивность импульса $P_0(t = 0)$ заведомо удовлетворяет условию $P_0 << (\alpha\text{-}\varkappa_0\text{-}\gamma)/\alpha$, то изменение длительности определяется выражением

$$\tau_k^2 = \tau_0^2(1 + P_k)\left(1 + \frac{\alpha}{(\alpha-\varkappa_0-\gamma)}P_k\right)^{-1}. \tag{19}$$

Из соотношения (19) следует, что сжатие импульса конечно, даже при бесконечно быстрой релаксации поглотителя. Действительно, полагая $P_k \gg 1$, находим минимальную длительность импульса:

$$\tau_{min} = \tau_0\left(\frac{\alpha-\varkappa_0-\gamma}{\alpha}\right)^{1/2} = \tau_0\left(\frac{\tau_1}{2\tau_н}\right)^{1/2}. \tag{20}$$

Окончательно максимальное сжатие импульса определяется следующим выражением:

$$\frac{\tau_{min}}{\tau_0} = \left[\frac{T}{2\alpha_0\tau_н}\ln\left(\frac{I_s}{I_0}\frac{1}{\varkappa_0}\sqrt{\frac{\alpha_0 T}{2\tau_н}}\right)\right]^{1/2}, \tag{21}$$

где мы воспользовались выражением (2) для времени задержки τ_1. Из (21) следует, что сжатие возрастает с увеличением $\tau_н$, то есть при более медленном прохождении через порог. Максимально возможная величина $\tau_н$ ограничивается техническим требованием, чтобы время задержки τ_1 было заметно меньше длительности накачки и времени релаксации усиления T_{1a}. Рассмотрим следующий численный пример: $\tau_1 \approx 3 \times 10^{-4}$ с, $T \approx 6 \times 10^{-9}$ с,

$\alpha_0 \approx 0{,}5$, $\varkappa_0 \approx 0{,}2$, $I_0/I_s \approx 10^{-10}$. В этом случае $\tau_н = 0{,}25$ с и $\frac{\tau_{min}}{\tau_0} \approx 2{,}5 \cdot 10^{-2}$. Отсюда ясно, что для получения импульсов с длительностью короче 10^{-12} с необходимо, чтобы $\tau_0 < 0{,}5 \times 10^{-10}$ с, то есть чтобы в образовании флуктуационных выбросов к началу нелинейного развития участвовало свыше 10^2 аксиальных мод. Однако число их ограничивается естественной селекцией мод. Если в качестве τ_0 взять длительность флуктуационного выброса в конце линейного развития (12), то минимальная длительность импульса к концу сжатия, согласно (21), определяется соотношением

$$\tau_{min} = \tau_{пред}\left[\ln\left(\frac{I_s}{I_0}\frac{1}{\varkappa_0}\sqrt{\frac{\alpha_0 T}{2\tau_н}}\right)\right]^{1/2}. \qquad (22)$$

При стандартных параметрах лазера $\tau_{min} \approx (4 \div 5)\tau_{пред}$. Таким образом, в идеальном случае полного отсутствия селективных элементов в резонаторе и бесконечно «быстрого» нелинейного поглотителя минимальная длительность импульса в $4 \div 5$ раз больше предельной, определяемой шириной линии усиления.

5. О генерации импульсов предельной длительности

Для того чтобы достигнуть предельной длительности импульсов $\tau_{пред}$, необходимо подавить естественную селекцию аксиальных мод усиливающей средой. Этого можно добиться, устраняя максимум усиления в центре линии, например, следующим методом. Пусть внутрь резонатора введена линейная поглощающая среда, центр линии поглощения которой совпадает с центром линии усиления ω_0, а ширина полосы поглощения несколько меньше ширины линии усиления $\Delta\omega_a$. Если дополнительное поглощение меньше α_0, то суммарная линия эффективного усиления этих двух сред имеет минимум в центре. В результате очевидно, что вместо сужения спектра мод происходит расширение спектра. Длительность флуктуационного выброса интенсивности в лазере с таким дополнительным резонансным поглотителем не должна возрастать в течение линейного развития генерации, то есть τ' может быть порядка τ_0, а минимальная длительность импульса может быть равна $\tau_{пред}$.

Отметим, что в предлагаемом лазере ультракоротких импульсов нелинейный поглотитель уже не играет роли как элемент, сжимающий импульс света. Нелинейный поглотитель лишь выделяет наиболее интенсивный флуктуационный выброс на фоне остальных, менее интенсивных выбросов. Естественно, что для этого необходимо, чтобы $T_{1b} \lesssim \tau_{пред}$. Если $T_{1b} > \tau_{пред}$, то, помимо интенсивного флуктуационного выброса с предельной длительностью, усиливаться будут также следующие за ним на интервале $\sim T_{1b}$ флуктуационные выбросы с меньшей амплитудой. В результате ультракороткий импульс с длительностью $\tau \ll T_{1b}$ может иметь слабый, но длительный хвост.

Если длительность импульса становится сравнимой с временем релаксации просветленного состояния поглотителя T_{1b}, необходимо учитывать инерционность поглотителя.

6. Эволюция импульса в области $\tau \sim T_{1b}$

Эволюцию импульса, включая область, в которой становится существенной инерционность поглотителя, можно рассмотреть, точно решая систему уравнений (3). Отметим, что распространение импульса в нелинейно поглощающей среде с релаксацией просветленного состояния исследовалось в работе Зуева и Щеглова [21] и позднее обсуждалось в работе Харциева и др. [22]. Рассматриваемый случай отличается присутствием усиления, которое значительно превышает потери, по крайней мере, в те моменты времени, когда $\tau \sim T_{1b}$.

Основной эффект конечного времени релаксации просветленного состояния поглотителя заключается в том, что поглотитель не успевает «захлопнуться» на заднем фронте импульса, имеющего длительность $\tau < T_{1b}$. В результате поглощение происходит лишь на переднем фронте, а задний фронт импульса практически не деформируется. Поэтому форма импульса с длительностью $\lesssim T_{1b}$ становится асимметричной.

Приведем сначала результаты численного интегрирования полной системы уравнений (3) на вычислительной машине. В этих расчетах одновременно учитывался эффект насыщения усиления. Такая модель уже близка к реальному лазеру. Решение приведем для случая, когда параметры лазера таковы, что длительность импульса $\tau_{\min}$ с бесконечно «быстрым» поглотителем была бы в несколько раз короче T_{1b}. В этом случае длительность импульса ограничивается именно инерционностью поглотителя T_{1b}. На рис. 1а показано изменение длительности τ и пиковой мощности P_m импульса, а также изменение усиления активной среды в зависимости от числа проходов резонатора k, а на рис. 1б приведена форма импульса для трех характерных моментов развития генерации: начало, максимум и конец гигантского импульса.

На этом примере отчетливо видны основные особенности эволюции импульса, рассмотренные выше и в нашей работе [8]. Во-первых, на рис. 1а видно, что сжатие импульса действительно начинается при $P_m \approx (\alpha - \varkappa_0 - \gamma)/(\varkappa_0)$ и продолжается до тех пор, пока P_m опять не станет значительно больше единицы. В конце генерации, когда P_m опять становится порядка единицы, вновь происходит некоторое сжатие импульса.

Это хорошо согласуется с найденной в работе [8] зависимостью скорости сжатия импульса за проход от интенсивности импульса в максимуме P_k:

$$W = \frac{\partial \tau}{\partial k} = -\frac{\varkappa_0 P_k}{(1+P_k)(2+P_k)}. \qquad (23)$$

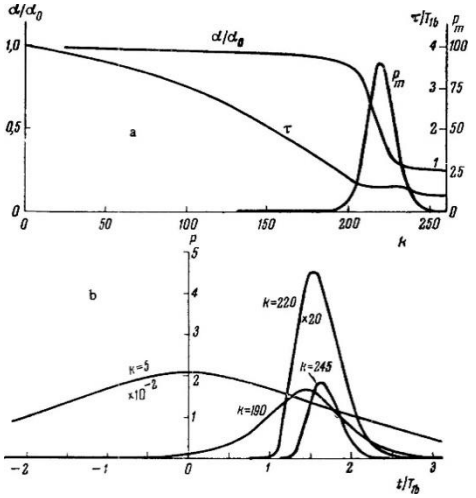


Рис. 1. Развитие генерации ультракороткого импульса: *а* — изменение длительности импульса τ, максимальной мощности P_m и усиления α активной среды в зависимости от числа проходов резонатора k (начало отсчета числа проходов произвольно); *б* — форма ультракороткого импульса в различные моменты генерации (k = 5, 190, 220, 245). Параметры лазера: $\sigma_a/\sigma_b = 10^{-3}$; $\varkappa_0 = \gamma = 0{,}3$; $(\alpha - \alpha_0) \approx 3 \times 10^{-2}$ at $k = 0$. Пиковая интенсивность импульса $P_m \approx 2 \times 10^{-2}$ at $k = 0$

Из (23) следует, что скорость сжатия импульса максимальна при $\boldsymbol{P_k = \sqrt{2}}$ и стремится к нулю в предельных случаях малых и больших интенсивностей.

Во-вторых, на рис. 1б видно, что, когда длительность импульса становится порядка $\boldsymbol{T_{1b}}$, возникает асимметрия импульса и передний фронт становится значительно круче заднего. В конце генерации длительность импульса $\boldsymbol{\tau \approx 0{,}5\, T_{1b}}$. В принципе, могут генерироваться еще более короткие импульсы. Для этого необходимо, чтобы потенциальная минимальная длительность импульса $\boldsymbol{\tau}_{\min}$, которая достигается в лазере с безынерционным поглотителем, была значительно короче времени релаксации $\boldsymbol{T_{1b}}$, используемого в лазере реального поглотителя. На рис. 2а приведен пример развития генерации в таком случае. В этом примере длительность импульса достигает значения $\boldsymbol{\sim 0{,}2\, T_{1b}}$ уже к середине генерации, и далее она остается неизменной. Форма импульса $P(t)$ и соответствующее ему изменение поглощения $\boldsymbol{\varkappa(t)}$ изображены на рис. 2б.

Влияние поглотителя на эволюцию импульса в области, когда длительность импульса мала ($\tau << \boldsymbol{T_{1b}}$), а мощность велика ($\boldsymbol{P_m \gg 1}$), можно понять, если рассмотреть изменение поглощения $\boldsymbol{\varkappa(t)}$ под действием такого импульса. Изменение поглощения во время прохождения импульса можно, очевидно, рассматривать, пренебрегая релаксацией. Тогда уменьшение поглощения описывается выражением

$$\varkappa_1(t) = \varkappa_0 \exp\left\{-\frac{1}{T}\int_{-\infty}^{t} P(t')\partial t'\right\}. \qquad (24)$$

Поглощение уменьшается до величины $\boldsymbol{\varkappa_{min} \approx \varkappa_0 \exp(-\tau P_m / T_{1b})}$ за время $\boldsymbol{\tau' \approx T_{1b}/P_m}$. После прохождения импульса поглощение релаксирует за время порядка $\boldsymbol{T_{1b}}$ к начальному состоянию практически независимо от импульса:

$$\varkappa_2(t) = \varkappa_{min} \exp\left(-\frac{t}{T_{1b}}\right) + \varkappa_0[1 - \exp(-t/T_{1b})]. \qquad (25)$$

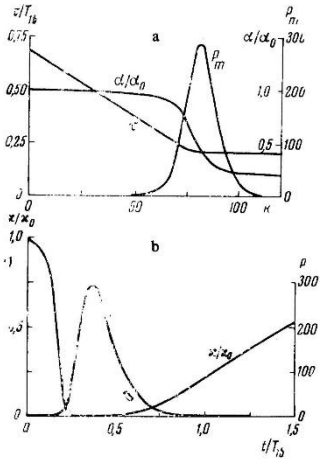


FIG. 2

Рис. 2. Генерация ультракороткого импульса, когда его длительность ограничивается инерционностью поглотителя

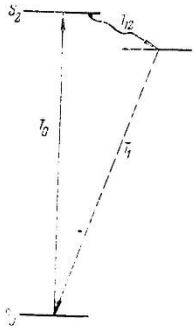


FIG. 3

Рис. 3. Схема двухступенчатой релаксации просветленного состояния раствора красителя

Время «открывания» поглотителя пропорционально мощности импульса и поэтому может быть весьма мало. Время «закрывания» поглотителя не зависит от мощности и определяется временем релаксации $\boldsymbol{T_{1b}}$. Поэтому крутизна переднего фронта импульса может быть значительно выше крутизны заднего фронта. Передний фронт, в принципе, может стать ступенчатым, но практически в лазере это не достигается, так как из-за насыщения усиления мощность импульса довольно быстро падает. Однако длительность переднего фронта может стать на порядок короче времени релаксации $\boldsymbol{T_{1b}}$[3)].

[3)] Отметим, что, если поперечная релаксация молекул в растворе короче T_{1b} не более чем на порядок, то исходное скоростное уравнение (36) в этом случае становится несправедливым. Его надо заменить уравнениями для плотности поляризации $\mathcal{P}_b(t)$ и заселенности $N_b(t)$ поглощающей среды. В результате отклик поглотителя на мощный импульс с длительностью $\sim T_{2b}$ становится осцилляторным. Возникающие осцилляции поглощения типа $n\pi$-импульса, вообще говоря, могут привести к осцилляциям в импульсе [23]. Однако в данном случае этого не происходит из-за присутствия в лазере усиления $\alpha \gtrsim \varkappa$, которое увеличивает интенсивность импульса и тем самым препятствует накоплению искажений его формы. Осцилляции в импульсе могут появиться лишь в случае $\alpha \ll \varkappa$, который в рассматриваемом лазере не реализуется.

Теперь нетрудно понять, как влияет дисперсия среды внутри резонатора на эволюцию импульсов в лазере, работающем в нестационарном режиме. На тех стадиях развития импульса, когда велика его длительность или имеется заметная скорость сжатия длительности, дисперсия, очевидно, не влияет на развитие импульса. Однако в области $\boldsymbol{P_m \gg 1}$, когда длительность импульса мала, а скорость сжатия импульса равна нулю, возможно уширение импульса. Это уширение приближенно описывается выражением

$$\tau \approx \tau_m \left\{1 + \left[\frac{2kL}{\tau_m^2 c}\left(\frac{\partial n}{\partial \omega} + \frac{\omega_0}{2}\frac{\partial^2 n}{\partial \omega^2}\right)\right]^2\right\}^{1/2}, \qquad (26)$$

где $\boldsymbol{\tau_m}$ — длительность импульса в момент, когда сжатие прекращается; $\boldsymbol{k}$ — число проходов, отсчитываемое от момента прекращения сжатия; $Ln(\omega)$ — суммарный оптический путь диспергирующей среды в резонаторе. Основным диспергирующим элементом является обычно стекло или кристалл активной среды. При длине $L = 10$ см и дисперсии $\boldsymbol{\partial}n/\partial\omega \approx 10^{-17}$ с$^{-1}$, например, за 30 проходов уширение будет сказываться только для импульсов с длительностью $\boldsymbol{\tau_m} \approx 5\times10^{-13}10$ с.

7. Замечание о релаксации просветляющегося раствора

«Быстрый» просветляющийся раствор красителей, применяемых в лазерах ультракоротких импульсов, обычно рассматривают как двухуровневую систему с коротким эффективным временем жизни $\boldsymbol{T_{1b}}$ молекул на верхнем уровне, которое определяется излучательными и безизлучательными переходами в основное состояние. Вероятность излучательной релаксации возбужденного уровня для разрешенных переходов с силой осциллятора $f \approx 1$ в видимом диапазоне не превышает 10^9 с$^{-1}$. Безизлучательная релаксация может заметно понизить время жизни возбужденных молекул. Однако скорость безизлучательной деградации возбуждения не может достигать предельных значений порядка $10^{12} \div 10^{13}$ с$^{-1}$, так как величина kT (T — температура раствора) значительно меньше энергии возбуждения молекулы.

Тем не менее скорости релаксации просветленного состояния раствора порядка 10^{13} с$^{-1}$ могут быть достигнуты практически. Дело в том, что помимо возбужденного синглетного состояния S_2, в которое переходит молекула из основного состояния S_0, молекула может иметь нижележащее электронное состояние S_1 (рис. 3). Все эти состояния обладают также набором колебательных уровней. Возбужденные молекулы в состоянии S_2 за счет безизлучательных переходов релаксируют на нижние уровни возбужденного состояния S_1. Скорость такой релаксации, называемой внутренней конверсией, весьма велика и, согласно [24] (см. также обзоры [25, 26]), составляет $T_{12}^{-1} = 10^{10} \div 10^{13}$ с$^{-1}$. Из нижнего возбужденного состояния S_1 молекулы возвращаются в основное состояние гораздо более медленно за время $T_1 >> T_{12}$. В результате быстрых

переходов молекул по возбужденным уровням просветленное состояние раствора релаксирует к поглощающему (но не к начальному!) состоянию с поглощением $\boldsymbol{\varkappa_0/2}$ за характерное время T_{12}, а затем в результате перехода молекул в основное состояние раствор релаксирует к начальному состоянию с поглощением $\boldsymbol{\varkappa_0}$ за более длительное время T_1. Просветляющийся раствор с такой двухступенчатой релаксацией вполне пригоден для получения ультракоротких импульсов[4)]. Первая релаксация обеспечивает сжатие импульсов до величины T_{12}, а вторая релаксация возвращает раствор к начальному состоянию до следующего прихода импульса $T_1 << T$. Сжатие импульса в лазере с таким просветляющимся раствором во многом сходно с рассмотренной выше картиной. Более детальное рассмотрение этого вопроса будет представлено позже.

Заключение

В статье изложена теория генерации ультракоротких импульсов в лазере с нелинейным поглотителем, включающая все фазы развития генерации. Из теории следует, что практически вполне реально достигнуть предельной длительности ультракоротких импульсов, определяемой шириной полосы усиления. Для этого предложено устранять расширение импульса в линейной фазе генерации и применять просветляющиеся растворы с двухступенчатой релаксацией просветленного состояния молекул. Последняя фаза развития генерации в лазере предельно коротких импульсов света, заключающаяся в формировании импульса предельной стационарной длительности, настоящей теорией не описывается. Для рассмотрения ее необходимо учитывать форму линии усиления. Этот вопрос будет изложен в следующей статье. По-видимому, необходимо также принимать во внимание поперечную структуру импульсов, так как при длительности 10^{-12} с поперечный размер импульса становится значительно больше продольного, то есть импульс в пространстве имеет вид сильно сплющенного электромагнитного сгустка.

В заключение автор выражает глубокую благодарность академику Н.Г. Басову за поддержку и обсуждение настоящей работы.

Литература

1. *De-Maria A.J., Stetser D.A., Heynau H.* // Appl. Phys. Lett. 1966. Vol. 8. P. 174.

2. *De-Maria A.J., Stetser D.A., Glenn. Jr. W.H.* // Science. 1967. Vol. 156. P. 1557.

3. *Armstrong J.A.* // Appl. Phys. Lett. 1967. Vol. 10. P. 16; *Glenn W.H., Brienza M.J.* // Appl. Phys. Lett. 1967. Vol. 10. P. 221.

[4)] Не исключено, что этот механизм имеет место в полиметиловом красителе, с помощью которого удается получать ультракороткие импульсы с длительностью 10^{-12} с [27, 28].

4. *Giordmaine J.A., Rentzepis P.M., Shapiro S.L., Wecht K.W.* // Appl. Phys. Lett. 1967. Vol. 11. P. 216; *Rentzepis P.M., Duguay M.A.* // Appl. Phys. Lett. 1967. Vol. 11. P. 218.

5. *Кузнецова Т.И., Малышев В.И., Маркин А.С.* // ЖЭТФ. 1967. Т. 52. С. 438.

6. *Garmire E., Yariv A.* // IEEE J. Quantum Electronics QE-3. P. 222 (1967).

7. *Кузнецова Т.И.* Препринт ФИАН. 1967. № 25; Тезисы III Всес. симп. по нелинейной оптике. Ереван, 1967.

8. *Летохов В.С.* //. Письма в ЖЭТФ. 1968. Т. 7. С. 35.

9. *Sorokin P.P., Luzzi J.J., Lankard J.R., Pettit G.D.* // IBM J. Res. and Develop. 1964. Vol. 8. P. 182.

10. *Bret G., Gires F.* // Appl. Phys. Lett. 1964. Vol. 4. P. 175.

11. *Борович Б.Л., Зуев В.С., Щеглов В.А.* // ЖЭТФ. 1965. Т. 49. С. 1031.

12. *Малышев В.И., Маркин А.С., Сычев А.А.* // ЖЭТФ. 1967. Т. 6. С. 503.

13. *Летохов В.С., Морозов В.Н.* // ЖЭТФ. 1967. Т. 52. С. 1296.

14. *Летохов В.С.* // ЖЭТФ. 1968. Т. 54. С. 1392.

15. *Беспалов В.И.* // Изв. вузов. Радиофизика. 1968. Т. 11. С. 320.

16. *Mandel L., Wolf E.* // Rev. Mod. Phys. 1965. Vol. 37. P. 231.

17. *Летохов В.С.* // ЖЭТФ. 1966. Т. 50. С. 765; Препринт ФИАН. 1965. № А-45.

18. *Duguay M.A., Shapiro S.L., Rentzepis P.M.* // Phys. Rev. Lett. 1967. Vol. 19. P. 1014; *Shapiro S.L. , Duguay M.A., Kreuzer L.B.* // Appl. Phys. Lett. 1968. Vol. 12. P. 36.

19. *Sooy W.R.* // Appl. Phys. Lett. 1965. Vol. 7. P. 36.

20. *Малышев В.И., Маркин А.С., Масалов А.В., Сычев А.А.* Препринт ФИАН. 1968. № 34.

21. *Зуев В.С., Щеглов В.А.* // Журн. прикл. спектроск. 1966. Т. 5. С. 604.

22. *Харциев В.Е., Стаселько Д.И., Овчинников В.М.* // ЖЭТФ. 1967. Т. 52. С. 1457.

23. *McCall S.L., Hahn E.L.* // Phys. Rev. Lett. 1967. Vol. 18. P. 908.

24. *Kasha M.* // Disc. Farad. Soc. 1959. Vol. 9. P. 14.

25. *Лоуэр С., Эль-Сайед М.* // УФН. 1968. Т. 94. С. 289.

26. *Ермолаев В.Л.* // УФН. 1963. Т. 80. С. 3.

27. *Басов Н.Г., Крюков П.Г., Летохов В.С., Сенатский Ю.В.* Доклад на V Межд. конф. по квантовой электронике. Майами, США, 1968.

28. *Кайтмазов С.Д., Красюк И.К., Пашинин П.П., Прохоров А.М.* // ДАН СССР. 1968. Т. 180. С. 1331.

J. Quant Electron. 1972. QE-8 (10). P. 766–782

FLUCTUATION MECHANISM O ULTRASHORT PULSE GENERATION BY LASER WITH SATURABLE ABSORBER

P.G. Kryukov,[*] V.S. Letokhov[**]
[*]*P.N. Lebedev Physical Institute, Academy of Sciences USSR, Moscow,*
[**]*Institute of Spectroscopy, Academy of Sciences USSR, Moscow,*

This paper presents a theoretical treatment of the fluctuation mechanism involved in the generation of picosecond laser pulses with saturable absorbers. The processes responsible for the shortening of the pulsewidth and for selection of the most intense pulse are treated. Some experimental results that confirmed the treatment are presented. The influence of inertia of saturable absorber and nonlinear losses (self-focusing and self-modulation) is discussed.

Introduction

Remarkable progress in obtaining high-power short light pulses was achieved in 1966 [1, 2]. Measurements of pulse duration [3, 4] showed the ability of lasers with saturable absorbers to generate trains of pulses a few picoseconds in time duration. The study of emitted radiation from lasers having saturable absorbers in their feedback cavity was appreciably expanded after the introduction of the two-photon fluorescence method for time-duration measurements [5, 6]. The simplicity of this makes it very attractive. Unfortunately, the two-photon fluorescence method has no explicit definiteness, as it produces similar records for both mode-locked pulses and for irregular fluctuation spikes occurring from the multimode radiation from any laser [7–9]. The difference lies in the value of the contrast ratio, which changes from 3 for an ideal ultrashort pulse train to 1.5 for incoherent multimode radiation (Gaussian noise) [8, 10–11]. It is thus necessary to measure the contrast ratio with very high accuracy if one has to be sure of the presence of ideal mode-locked pulses [12]. In addition, it was found that the actual pulse duration of the Nd:glass laser with a saturable absorber is an order of magnitude greater than the limiting duration defined by the spectral width of the radiation [2]. To explain this fact, the author of paper [13] has proposed a frequency “chirping” mechanism due to dispersion, which broadens the time duration of the subpicosecond light pulses. On the basis of this mechanism, the use of the pulse compression method to obtain shorter time-duration pulses [13, 14] was suggested. By contrast, in [15, 16] the authors succeeded in finding a subpicosecond structure within the ultrashort pulses with no compensation for

the frequency chirping. Many papers, besides those mentioned here, have been concerned with the study of these two facts. Detailed information on the question may be found in [17–18].

Far less attention has been paid to the study of the dynamics of ultrashort pulse formation process. Creation of the regular train of ultrashort pulses was considered to be an evident process, the so-called "self-mode locking by a saturable absorber." Previously, mode locking in gas and solid-state lasers by intracavity active-loss modulation was studied [19–21]. In this case, the periodic disturbance of the resonator gradually increases the number of modes and, finally, results in the strict periodic sequence of pulses with time duration $\tau_p \simeq T/m$, where m is a number of locked modes and T is the repetition period. A laser utilizing a saturable absorber also emits a strictly periodic sequence of very short pulses with a broad radiation spectrum. This formal resemblance gives reason to suppose that these processes are analogous. In particular, such a point of view is described in [17]. This is quite true for lasers operating in CW or quasi-CW regimes but not for lasers with a saturable absorber, in which the formation of ultrashort pulses and Q-switch modulation take place simultaneously. The Q-switched case deals with a transient process and not with a stable self-oscillating system.

In fact, the mechanism of ultrashort pulse formation in a laser with a saturable absorber has quite a different character and a typical feature of the mechanism is an oscillation of the laser on a great number of modes from the very beginning. The first consistent treatment of ultrashort pulse formation from the threshold of oscillation was done in [23]. A number of results were briefly treated in [24]. The treatment is based on the fluctuation mechanism of ultrashort pulse formation. According to [23] the picture of oscillation is the following.

In the linear stage of generation, the fluctuations of intensity arise due to the interference of a great number of modes having a random phase distribution so that the radiation consists of a chaotic collection of ultrashort peaks. In the nonlinear stage, where bleaching of the absorber takes place, the most intensive fluctuation peaks are compressed and amplified faster than all the weaker ones. One or several ultrashort pulses are amplified during each round trip in the cavity until all the stored energy in the active medium is emitted. In [23] it was shown that the shortening of the pulses during the nonlinear stage has a finite value (10–20 times). Therefore, the appearance of mode-locked ultrashort pulses cannot be attributed to the effect of gradual time reduction of an initial fluctuation arising from the beating of several axial modes in the nonlinear medium (as postulated in a number of papers with analogy to CW lasers without Q switching [2, 17]). Formation of picosecond pulses takes many axial modes (over 10^2). Since the radiation undergoes spectral narrowing in the initial stage of oscillation, the limiting pulse duration defined by the spectral width is not achieved at all [23]. Independently, Fleck has arrived at similar conclusions from a detailed calculation of the oscillation process beginning at threshold, under the multimode excitation [25–26].

Experiments that were carried out in the last two years confirm the hypothesis that ultrashort pulses are initiated from short fluctuations in the spontaneous emission from lasers with a saturable absorber. With the help of a high-speed image-converter streak

camera [27–28] the main ultrashort pulse was observed to be systematically accompanied by satellite pulses that were spaced in a random way in the train period. Their appearance cannot be explained by accidental reflections from different parts of the laser. The emission spectrum in the initial stage of oscillation is quite wide and contains many modes even in the absence of a saturable absorber [29]. The emission spectrum remains broad even if one observes no periodical pulse train [28]. A careful investigation of the emission spectrum [30] has shown the presence of a fluctuation structure in the spectrum that appeared due to the fluctuation structure in the emission intensity. Besides, the study of many-passage propagation of the multimode emission through a saturable absorber and an amplified medium, demonstrated the appearance of ultrashort pulses from the original fluctuation structure [31–32]. Moreover, many authors have indicated the presence of background radiation between regular pulses of the train [18, 27–28, 33–34, 58]. Although the ratio between background energy and energy of the regular pulses appears to be greatly dependent on the laser construction, this effect is typical for lasers with saturable absorbers. It finds a natural explanation in terms of the fluctuation mechanism.

A consistent treatment of the fluctuation mechanism of ultrashort pulse generation in the laser with a saturable absorber is presented in this paper. Theoretical analysis of a model of the laser with an ideal instant-relaxation-time nonlinear absorber is presented in Section II. Previously, results of Section II were only available in preprint [35] as a continuation of [23]. In this paper, a total comparison of two processes of ultrashort pulse formation is made. Mechanisms for shortening of the pulse duration and selection of the most intensive pulses will also be given. In addition, a parameter of nonlinearity has been found that is essential for the evolution of the fluctuation peak. The paper shows that a mode of operation quite distinct from the case of ideal mode locking is possible. Inertness of the absorber (finite relaxation time) leads to a greater deviation from the perfect picture.

Experimental results on ultrashort pulse formation and a discussion in terms of the fluctuation mechanism are presented in Section III. In addition, the influence of inertness of the absorber and the influence of the spectral width on the operation of a laser with a saturable absorber is discussed. The laser with an absorber having a rather large relaxation time for its bleachable state was experimentally studied. These experiments made it possible to investigate the influence of the absorber's inertness on laser operation. The evolution of the temporal structure of ultrashort pulses during oscillation was also treated. An increase in the number of additional pulses (satellite pulses) at the end of oscillation has been found. This fact is explained by the power saturation of the most intensive pulses due to nonlinear effects and development of weaker additional pulses. Measurement of the second-harmonic generation (SHG) versus the number of pulses in the train was also carried out. It helped explain the SHG efficiency decrease effect that was observed in [4] and interpreted in terms of ultrashort pulse broadening. On the basis of the ultrashort pulse-generation process, a special scheme has been suggested and studied experimentally [36]. This scheme makes it possible to significantly decrease the ratio between background energy and energy of the regular pulses. Hence, by means of this scheme, one can get ultrashort pulses of enhanced energy without any satellites.

II. Theoretical Considerations

A. Qualitative Picture

Let us consider an excited medium with amplification in a frequency band width $\Delta\omega_a$ and a nonexcited medium having absorption in the bandwidth $\Delta\omega_a$. Band $\Delta\omega_a$ is centered at $\Delta\omega_0$ and lies within the $\Delta\omega_b$ band. We shall define the parameters of the amplifying medium as *a* and of the absorbing ones as *b*. During pumping, the gain coefficient of the active medium becomes equal to the losses of the absorber and the mirrors of the cavity at a certain time ($t = t_0$). After this time, the gain exceeds the losses and an initial increase of radiation of the cavity modes occurs according to the following relationship:

$$exp\left\{\frac{1}{T}\int_{t_0}^{t}[\alpha(t') - \alpha_0]\partial t'\right\},$$

where $T = 2L/c$ cavity round-trip time required for the radiation in the laser, L length of the optical cavity, c light velocity, $\alpha(t)$ gain coefficient of the active medium during a whole round trip of the light in the laser, $\alpha_0 = \alpha(t_0)$ threshold gain. After some time, interval τ_1 the intensity of the radiation becomes sufficient for saturating the absorber. If one assumes that the time at which the absorber bleaches is the time when the total gain per round trip doubles, i.e., when the bleaching value is equal to the gain excess over the threshold:

$$x_0 - x(t_0 + \tau_1) = \alpha\,(t_0 + \tau_1) - \alpha_0 \tag{1}$$

one can find the following expression for the time delay τ_1 between the time of bleaching and the time when threshold is reached

$$\tau_1 = \left\{2T\left(\frac{d\alpha}{dt}\right)^{-1}\ln\left[\frac{I_s}{I_0 x_0}\left(\frac{T}{2}\frac{d\alpha}{dt}\right)\right]^{\frac{1}{2}}\right\},^{\frac{1}{2}} \tag{2a}$$

where $\frac{\frac{d\alpha}{dt}}{t} = t_0$ speed of the gain increases due to pumping at time $t = t_0$, x_0 initial losses of the absorber per round trip of light in the laser, I_0 initial intensity defined by the spontaneous radiation into modes, I_s absorber saturation intensity. The saturation intensity for a two-level system with decay time of the upper level T_1^b and a radiative transition cross-section σ_b is defined by the expression

$$I_s = \hbar\omega_0(2\sigma_b T_1^b)^{-1}. \tag{3}$$

At $\Delta\omega_\alpha \gg 1/T = \frac{c}{2L}$ a great number of axial modes having random phase relation between them are inevitably excited. Beating of the great number of axial modes gives rise to quasi-periodical intensity fluctuations $I(t)$ having characteristic time ~ $T/_{m0}$ and period T, where m_0 is the number of the exciting axial modes. During the linear stage of the intensity fluctuation buildup, the number of axial modes slightly decreases due to the natural selection towards the center of amplification line given by:

$$m = m_0(\alpha_0(\tau_1/T)^{-1/2} \tag{4}$$

where m_0 is the initial number of axial modes. The time broadening of the fluctuation intensity yields pulsewidths $\tau_{fl} \simeq \frac{T}{m}$ during this stage. In the ideal case, when the bleachable absorber relaxes to the initial state within a time interval $T_1^b \ll \tau_{fl}$, the absorber is predominantly bleached by the most intensive peaks. In terms of Q switching, one can say that at time $t = t_0 + \tau_1$ self-Q-switching by the most intensive peaks takes place. As a result, the pulsewidth is reduced and a significant intensity discrimination of large peaks against the background of numerous weaker peaks takes place. A different situation is realized when the absorber relaxation time T_1^b exceeds τ_{fl} by several times. In this case, appreciable pulsewidth reductions of the peak by the absorber do not occur and efficiency of discrimination in favor of the most intensive peaks decreases.

The creation process of ultrashort pulses is accompanied by the rapid rise in radiative intensity, and saturation of the amplifying medium occurs in a rather short time, $\tau_2 << \tau_1$. During saturation, the energy of the active medium is released in the form of a train of ultrashort pulses. Time delay τ_2 of such a giant pulse with respect to the moment of self-Q-switching is approximately defined by the expression:

$$\tau_2 \simeq \frac{T}{\alpha_0 - x_0} \ln \frac{\hbar\omega_0}{2\sigma_a T I_s} = \frac{T}{\alpha_0 - x_0} \ln \left(\frac{\sigma_h}{\sigma_a} \frac{T_1^b}{T} \right), \tag{5}$$

where $\sigma_b T_1^b \gg \sigma_a T$. A schematic of the kinetic processes in the laser with the saturable absorber is shown in Fig. 1

According to this qualitative picture, the ultrashort pulse creation is a statistical event. The probability of the occurrence of this event may be close to unity when a rather high degree of amplitude discrimination of fluctuation peaks occurs. However, there always exists a distinct nonzero probability for the generation of satellite pulses, background radiation between pulses, etc. The problem is first to calculate the nonlinear characteristics of the pulse development and second to find the probabilistic characteristics describing the growth of a train of short pulses using a specific statistical model for the initial fluctuations in the radiation field.

B. Pulse Evolution in Nonlinear Absorbing Stage (Inertialess Absorber)

1) Model: Let us consider a model of a multimode laser with a saturable absorber under the following assumptions, which simplifies the problem and exposes the essential behavior of the fluctuation mechanism of ultra-short generation.

a) Assumption that the radiative transition cross section for absorbing medium is much greater than for the amplifying one σ_b:

$$\sigma_b >> \sigma_a. \tag{6}$$

This assumption is accurate for presently operated systems (e.g. $\sigma_a = 2.5 \cdot 10^{-20}$ cm^2 for ruby and $\sigma_a = 1.7 \cdot 10^{-16}$ cm^2 for cryptocyanine [37]). However, σ_a may differ only slightly from σ_b in dye lasers. Condition (6) allows a clean separation between the saturation stages of amplification and absorption. For the optimal laser operation, the emission of energy stored in the active medium should take place after the complete formation of ultra- short pulses by the nonlinear absorber. The formation is practically over when the pulse power exceeds by several times the absorber saturation power I_s. As the relaxation time of the absorber $T_1^b \ll T$, the absorber bleach and relax many times during a round trip. In order for the pulse power to exceed the absorber saturation power, energy $\sim I_s \cdot T$ is required. This energy must apparently be much less than the energy of amplification saturation $\frac{(\hbar_1 \omega_0)}{2\sigma_a}$. Hence, a stricter condition than (6) must be met in order to have a clear operation between nonlinear absorption and amplification saturation. This stricter condition is

$$\sigma_b T_1^b \gg \sigma_a T. \tag{7}$$

Let us note that (7) can be obtained from (5). Condition (7) means that for absorbers that have T_1^b in the picosecond range, the amplification saturation stage borders with the ultrashort pulse formation stage. We shall suppose in what follows that condition (7) is fulfilled for an ideal laser. However, in real devices, the time duration of the nonlinear absorption stage may not be sufficient for the total formation of ultrashort pulses.

b) Assumption of the absorber's fast relaxation. Let us consider that the pulse duration τ_p is much greater than the relaxation time of the bleaching state of the absorber: $\tau_p >> T_1^b$. For the best nonlinear absorbers that are available for ruby and Nd-glass lasers, the value of T_1^b about 10^{-11}s (for Eastman Kodak 9740 $T_1^b = 35$ ps [38], for Eastman Kodak 9860 $T_1^b = 6$ ps, for DDI $T_1^b = 14$ ps, for cryptocyanine $T_1^b = 22$ ps [39]). Therefore, this approximation is true only for pulses of tens of picosecond time duration. However, the "fast relaxation" absorber model is very important since it allows us to recognize the limitations of an ideal laser. The influence of absorber inertia will be qualitatively considered later and it will be shown that for a pulse with $\tau_p < T_1^b$ statistical effects become more important.

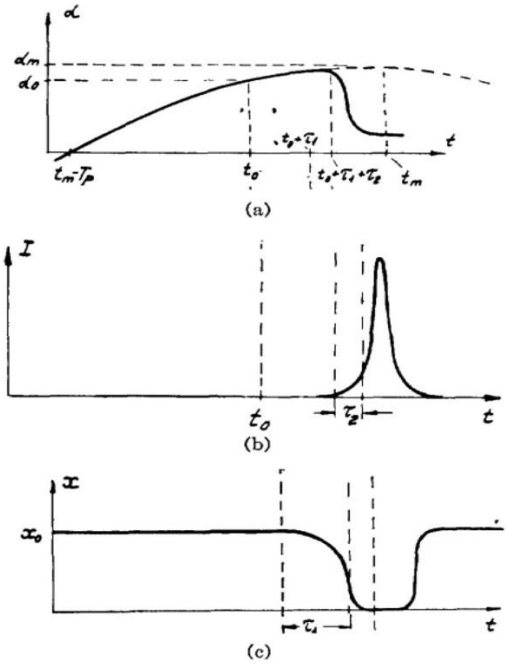


Fig. 1. Kinetics of processes in a laser with a nonlinear absorber. (a) Time dependence of amplification saturation (dotted curve) and with the saturation under oscillation (solid line). (b) The changing absorption of the bleachable absorber under the action of the average intensity. (c) Evolution of the average radiative intensity $I_{av}(t)$ with the time (averaged over the round-trip period T). Notation: t_0 — threshold time; τ_1 — period of delay from the time of absorber bleaching to threshold, i.e., the period of linear evolution of the laser field; τ_2 — delay from the beginning of the giant pulse to the beginning of the absorber bleaching

c) Assumption that the spatial distribution of the power is uniform over the laser cross section. This assumption corresponds to the case of axial modes excitation. As has been experimentally shown, this condition is necessary for good self-mode-locking.

d) Assumption that the initial absorption per pass in the absorber x_0 is rather small:

$$x_0 << 1. \tag{8}$$

Usually, $x_0 = 0.2–0.4$. This assumption is not as stringent as assumptions (a)–(c) for the generation of ultrashort pulses. However, it does simplify calculations since it allows one to consider the laser gain and losses to be uniformly distributed along the cavity.

In view of assumption (b), bleaching of the absorber under the effect of pulse $I(t)$ may be written in a two-level approximation:

$$x(t) = x_0(1 + I(t)/I_s)^{-1} \tag{9}$$

where x_0 is the initial coefficient of absorption, $I(t)$ the radiation intensity (watts/square centimeters), and I_s the saturation intensity, defined by (3). The simplicity of (9) allows one to advance rather far in the calculations of the statistical behavior of the radiation. Some possible effects of absorber darkening by high power intensity are neglected in this model. The influence of such effects will be considered qualitatively in Section III.

2) Equation-Time Delay: We are now interested in the changing random intensity $I(t)$ at consecutive passes in the laser. Function $I(t)$ is random in any interval of duration T, but this random pattern is repeated with some distortions in T due to interaction with absorbing and amplified media (Fig. 2). In order to retrace the accumulated change in the temporal intensity pattern after consecutive passes in the laser, it is convenient to write the function $I(t)$ as a function of two variables $I(\tau, k)$, where

$$t = kT + \tau = t_k + \tau, \quad k = 0, 1, 2, \ldots, \quad 0 < \tau T \tag{10}$$

where $\tau = t - t_k$ is the time interval counted from the beginning of the kth passage and k the number of a given passage.

The change in the temporal intensity pattern after consecutive passes in the laser may then be written by a single equation:

$$\frac{\partial P(\tau,k)}{\partial k} = \left[\alpha(k) - \gamma - \frac{x_0}{1+P(\tau,k)}\right] P(\tau,k) \tag{11}$$

where $P(\tau,k) = I_s^{-1} I(\tau,k)$ is a dimensionless intensity in a fixed point inside the laser, $\alpha(k)$ the gain per pass at the beginning of the kth passage after threshold ($t_0 = 0$), and γ the linear losses per pass including the losses of the mirrors. In (11) assumption (b) is taken into account, and the dependence of the absorption on intensity is put in the simplest form (9). In (11) the dependence of the amplification α on intensity is neglected. This is quite possible in view of assumption (a). The gain coefficient at first changes only as a result of pumping during time delay τ_1 and then later it also changes as a result of gain saturation. This change may be approximated by expression:

$$\alpha(k) = \alpha_0 + k\left(\frac{d\alpha}{dk}\right) = \alpha_0 + kT\left(\frac{d\alpha}{dk}\right) \tag{12}$$

where $\alpha_0 = x_0 + \gamma$ a threshold gain and $d\alpha/dt$ the speed of the gain increases due to pumping at the time of threshold. The value $d\alpha/dt$ is small but it is necessary to take it into account because the difference between $\alpha(k)$ and the threshold value α_0 defines the time delay τ_1 and the degree of discrimination of pulses having different amplitudes. First, let us express the quantity $d\alpha/dt$ and the time delay τ_1 in terms of the excess pumping over the threshold.

At a small value of pumping above threshold, the maximum gain α_m, which is possible at the given pumping level, just exceeds the threshold gain α_0. Then the gain curve $\alpha(t)$ in the range where $\alpha > \alpha_0$ may be approximated by a parabolic relationship [Fig. 1(a)]:

$$\alpha(t) = \alpha_m \left[1 - \left(\frac{t - t_m}{T_p}\right)^2\right] \tag{13}$$

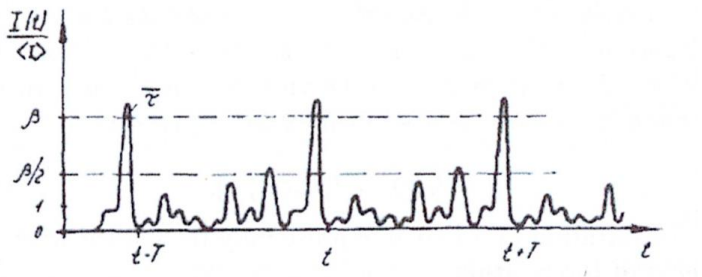


Fig. 2. Time profile of the incident intensity $I(t)$ that results from the interference of many axial modes (T = 2L/c — repetition period)

where $\alpha(t_m) = \alpha_m$ and T_p is the typical pumping time during which inverse population takes place. The speed of the gain growth at the threshold point when $t_0 = 0$ is defined by expression

$$d\alpha/dt = (2\alpha/T_p)(\eta - 1)^{1/2} \tag{14}$$

where $\eta = \alpha_m/\alpha_0$ is the excess pumping over the threshold.

The duration of the linear stage of laser action buildup is defined by (2a), which has the following form with regard to (14):

$$\tau_1 = \left\{\frac{1}{\alpha_0} T T_p (\eta - 1)^{-1/2} \ln\left[(P_0 x_0)^{-1}\left(\frac{T}{T_p}\sqrt{\eta - 1}\right)^{1/2}\right]\right\}^{1/2} \tag{2b}$$

where $P_0 = I_0/I_s$. For this case, the total growth of amplification during the linear stage, i.e., the gain excess over the threshold at the moment when the nonlinear interaction between the radiation with the absorber begins is given by:

$$\Delta\alpha = \tau_1 \frac{d\alpha}{dt} = 2\left\{\alpha_0 (\eta - 1)^{-1/2} \frac{T}{T_p} \ln\left[(P_0 x_0)^{-1}\left(\frac{T}{T_p}\sqrt{\eta - 1}\right)^{1/2}\right]\right\}^{1/2}. \tag{15}$$

Strictly speaking, (12) and (15) are only true provided $d^2\alpha/dt^2 = (\tau_1^2/2) \ll \Delta\alpha$. This condition may be expressed as

$$(\eta - 1)^{1/2} \gg \tau_i/2T_p). \tag{16}$$

If the excess pumping over threshold is so small that (16) is not fulfilled, it is necessary to take into account the higher order terms of expansion $\alpha(t)$. However, for a typical case (α_0 = 0.5; x_o = 0.3, $T_p = 10^{-3}$ s; $T = 10^{-8}$ s, $P_0 = 10^{-10}$), e.g., $(\eta - 1) = 3 \cdot 10^{-2}$corresponds to a 3-percent excess pumping over threshold, time delay $\tau_1 = 6 \cdot 10^{-5}$ s; $\Delta\alpha = 10^{-2}$; (16) is fulfilled.

3) Solution of the Equation — Nonlinearity Parameter: Equation (11) has a general solution $P_k = f(P_0, k)$, where $P_0 = P$ at $k = 0$. Obviously, the change in the shape of the pulse is described by the expression:

$$P_k(\tau) = f[P_0(\tau), k]. \tag{17}$$

The duration of a bell-like pulse may be defined with the help of the relation

$$\tau = \left(\frac{a}{P}\frac{\partial^2 P}{\partial \tau^2}\right)^{-1/2} \tag{18}$$

where the derivative is taken at the pulse maximum, a is a coefficient of order unity that is constant for a given pulse form (e.g., $a = 1/\sqrt{2}$ for a Gaussian-shaped pulse). Differentiating (17) twice, one can find the pulse duration after the kth passage with the help of (18):

$$\tau_k = \tau_0 \left(\frac{P_0}{P_k}\frac{\partial P_k}{\partial P_0}\right)^{-1/2} \tag{19}$$

where P_0 and P_k are the peak pulse intensities. Pulse compression is defined by a single parameter that characterizes the nonlinearity of the solution (17):

$$\mu_k = \frac{P_0}{P_k}\frac{\partial P_k}{\partial P_0} \tag{20}$$

Now let us consider the development of two pulses having close initial amplitudes P_{01} and P_{02}. During a nonlinear development their intensities are

$$P_{k,1} = f(P_{01}k); \quad P_{k,2} = f(P_{02}k). \tag{21}$$

If $\Delta P_k = P_{k,1} - P_{k,2} \ll P_{k,1};\ P_{k,2}$, then

$$\Delta P_k = \Delta P_0 \frac{\partial f}{\partial P_0} \tag{22}$$

or

$$\frac{\Delta P_k}{P_k} = \frac{\Delta P_0}{P_0}\left(\frac{P_0}{P_k}\frac{\partial P_k}{\partial P_0}\right) = \mu_k \frac{\Delta P_0}{P_0} \tag{23}$$

where μ_k is the nonlinearity parameter introduced previously. In the general case of an arbitrary ratio of maximal amplitudes P_{01} and P_{02}, we obtain an expression for the discrimination degree of two pulses having different amplitudes from the differential expression (23):

$$P_1/P_2 = (P_{01}/P_{02})^{\mu k}. \tag{24}$$

Thus, pulse compression and selection of most intensive pulses are defined by the same parameter μ_k.

An evident expression for parameter μ_k can be found using a solution of (11), which has been obtained in paper [23]:

$$\begin{aligned} &P_k^{-1}(\tau)[\alpha - x_0 - \gamma] + (\alpha - \gamma)P_k(\tau)^{x_0/(\alpha-\gamma)} \\ &= P_0^{-1}(\tau)[\alpha - x_0 - \gamma] + (\alpha - \gamma)P_0(\tau)^{x_0/(\alpha-\gamma)} \\ &\exp\left[-(\alpha - x_0 - \gamma)/k\right]. \end{aligned} \tag{25}$$

When solving (11) μ_k was replaced by $\alpha = \alpha_0 + \Delta\alpha$ in the end of the linear stage. It is possible because the duration of a nonlinear stage is small compared to the linear stage, and the growth of α_k is a negligible quantity during the nonlinear stage. With the help of (25), it is possible to obtain the following expression for parameter μ_k:

$$\mu_k = \frac{1+P_0}{1+P_k}\frac{\Delta\alpha+(x_0+\Delta\alpha)P_k}{\Delta\alpha+(x_0+\Delta\alpha)P_0}. \tag{26}$$

As the initial intensity $P_0 << \Delta\alpha$ and $\Delta\alpha << \alpha_0$, x_0 (26) can be simplified:

$$\mu_k = (x_0/\Delta\alpha)(P_k/1 + P_k). \tag{27}$$

It can be seen that the nonlinearity parameter tends to a constant value

$$\mu = x_0/\Delta\alpha \tag{28}$$

at $P_k \gg 1$. Physically this is connected with the fact that the speed of pulse compression by a nonlinear absorber attains a maximum at $P = \sqrt{2}$ and decreases at $P \ll 1$ and $P \gg 1$.

The expression for the nonlinearity parameter μ_k can be found by solving (11) without substituting a constant value for α_k. The general form of the solution for (11) $P_k = f(P_0, k)$ s shown in Fig. 3. First, when the linear term α_k is predominant, the growth of the peak intensity is very slow. With the growth of P_k the contribution of the last nonlinear term becomes considerable and the relationship becomes very steep. When the initial value P_0 is increased, the solution is displaced to the left along the k axis. This displacement corresponds to an acceleration of the nonlinear stage of development. The relationship

$$(\partial P_k/\partial P_0) = (\partial P_k/\partial k)(\partial k/\partial P_0) \tag{29}$$

holds where $\partial P_k/\partial k$ is defined by the right part of (10), and $\partial k/\partial P_0$ characterizes the displacement of the $f(k)$ curve for a given change in the initial value P_0. Since the curve is displaced as a whole, it is sufficient to evaluate the amount of displacement, e.g., in the linear stage. This becomes possible with the help of (11) by neglecting the nonlinearity of the last term, which we can do when $P_k << d\alpha/dk$. This condition is true at the beginning of the linear stage when $P_0 \lesssim 10^{-10}$. Solution of (11) results in the following expression of the displacement value:

$$k = \left(2\ln \frac{P_{01}}{P_{02}} \Big/ \frac{d\alpha}{dk} \Big/\right)^{1/2}; \tag{30}$$

hence it follows:

$$\frac{dk}{dP_0} = \left(\mathrm{k_{lin}} \frac{d\alpha}{dk} P_0\right)^{-1} = \frac{1}{P_0 \Delta\alpha} \tag{31}$$

where $\Delta\alpha$ is the growth of amplification over the threshold value during the linear development of k_{lin}. Expression for μ_k coincided with (27) and was obtained with the help of (29), (31), and (11).

Using (15) for $\Delta\alpha$ we obtain the value for the nonlinearity parameter at the end of the nonlinear stage:

$$\mu = \frac{1}{2} x_0 \left\{ \alpha_0 (\eta - 1)^{1/2} \frac{T}{T_p} \ln \left[\frac{1}{P_0 x_0} \left(\frac{T}{T_p} \sqrt{\eta - 1} \right)^{1/2} \right] \right\}^{-1/2}, \tag{32}$$

Where η is the excess pumping over the threshold value and T_p the duration of pumping.

Now let us consider the efficiency of two mechanisms affecting the development of the temporal intensity pattern (the mechanism of pulse shortening and the mechanism of pulse amplitude discrimination) from the viewpoint of ultrashort pulse generation. For this purpose let us consider a typical numerical example.

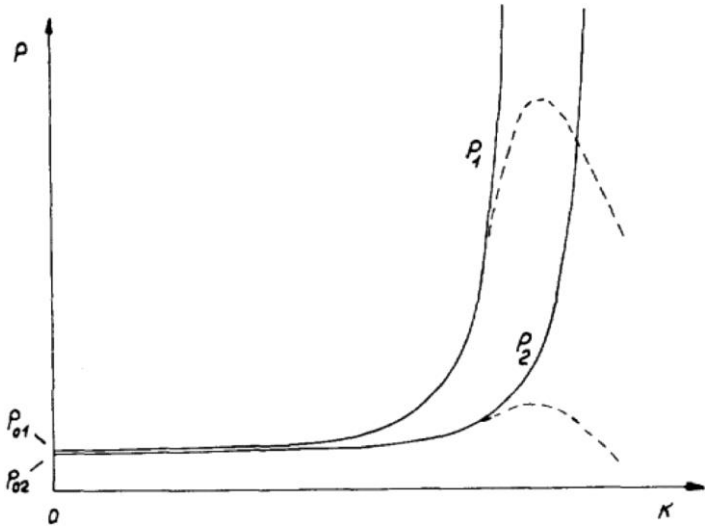


Fig. 3. Dependence of the pulse peak power P on the number of passes for two different values of the initial intensity P_{01} and P_{02} (before the saturation of amplification), which is obtained from a solution of (10). The saturation of amplification restricts the growth of intensity as shown by the dotted curves

4) Numerical Example: Let us consider a laser having total optical length $2L$ = 300 cm ($T = 10^{-8}$ s), threshold gain per round trip through the active medium α = 0.5, an initial transmission for the nonlinear absorber per round trip $x = 0.3$, and total linear losses per round trip $\gamma = 0.2$. Assume that the lifetime of the inverted population that characterizes pumping duration is $T_p = 10^{-3}$ s and that the excess pumping over threshold is $(\eta - 1) = 0.03$. In this case, the duration of linear growth is $\tau_1 = 0.85 \cdot 10^{-4}$ s due to (2b). The maximal value of the nonlinearity parameter is $\mu = 30$ according to (32). The value μ and the time delay increase when the threshold is approached $\mu, \tau_1(\eta - 1)^{-1/4}$. This relationship is rather weak. For example, μ increases by 30 percent only, i.e., $\mu = 40$ when we have 1-percent excess of pumping over threshold in the above example, when $(\eta - 1)$ is 3 times smaller.

5) Pulse Compression: According to (19) and (32) total pulse compression in the nonlinear stage of the developing is

$$\frac{\tau_p}{\tau_0} = (\mu)^{-1/2} = \left(\frac{2}{x_0}\right)^{1/2} \left\{\alpha_0 \sqrt{\eta - 1}\, \frac{T}{T_p} \ln\left[\frac{1}{P_0 x_0}\left(\frac{T}{T_p}\sqrt{\eta - 1}\right)^{1/2}\right]\right\}^{1/4}. \qquad (33)$$

The amount of time compression increases as threshold is approached. This fact has been already noted in previous works on lasers with a saturable absorber [40]. However, this relationship is very weak and it is not likely that it influences the development of ultrashort pulses, the compression method was considered as the mechanism of ultrashort pulse generation in [40].

If the spectral gain profile of the medium has a regular shape (Lorentzian, Gaussian, etc.), account must be taken of the broadening of the fluctuation peaks due to natural selection of axial modes (spectral narrowing) in the linear stage [42]. The influence of this process on ultrashort pulse generation has been considered in [23]. A broadening value in the linear stage is defined by (4) and (2b):

$$\frac{\tau_p}{\tau_0} = \left(\alpha_0 \frac{\tau_1}{T}\right)^{-1/2} = \left\{2\alpha_0(\eta-1)^{-1/2}\frac{T_p}{T}\ln\left[\frac{1}{P_0 x_0}\left(\frac{T}{T_p}\sqrt{\eta-1}\right)\right]\right\}^{1/4}. \qquad (34)$$

The total change in the duration defined by simultaneous action of the broadening in the linear stage and the compression in the nonlinear stage is

$$\frac{\tau_p}{\tau_0}\left\{2\sqrt{2\frac{\alpha_0}{x_0}\ln\left[\frac{1}{P_0 x_0}\left(\frac{T}{T_p}\sqrt{\eta-1}\right)^{1/2}\right]}\right\}^{1/2} > 1. \qquad (35)$$

Value τ_p/τ_0 is always more than 1, i.e., the pulse broadening in the linear stage always exceeds its compression in the nonlinear stage [23, 28]. The value of ratio τ_p/τ_0 does not, in fact, depends on the excess pumping over threshold (for small excesses). Hence, the compression of pulses by the nonlinear absorber cannot become a mechanism of picosecond pulse formation in the laser with a saturable absorber.

For the above numerical example the pulse shortening in the nonlinear stage is $\mu^{1/2}$ = 5.5 times, and the possible broadening in the linear stage is $[\alpha_0(\tau_1/T)]^{1/2}$ = 65 times, i.e., it greatly exceeds the compression. Note that the pulse compression mechanism in a laser with a saturable absorber has been considered in [41] and there the inefficiency of the pulse compression mechanism was also mentioned.

6) Amplitude Discrimination of Pulses: According to (24), a small difference in the initial amplitudes is sufficient for a significant discrimination of their intensities in the nonlinear stage. So, in the preceding numerical example μ = 30 and the 10-percent difference of initial amplitudes produces a 10-time ratio of amplitudes at the end of the nonlinear stage. This mechanism allows formation of ultrashort pulses of a few picoseconds duration when the following conditions are fulfilled.

a) The initial radiation contains fluctuation peaks of picosecond duration.

b) Within the period T of the fluctuation structure $I(t)$ there is a peak whose amplitude differs substantially from the amplitudes of the rest of the fluctuation pulses.

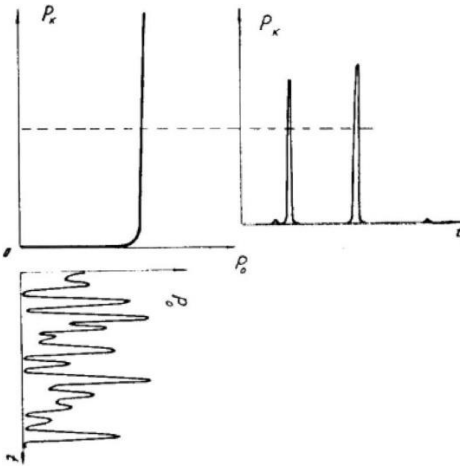


Fig. 4. Ultrashort pulse formation due to the nonlinear evolution of the initial fluctuation profile of the multimode radiative intensity

The ultrashort pulse formation due to the nonlinear evolution of initial fluctuation structure is shown in Fig. 4. Condition a) is fulfilled if a sufficiently great number of axial modes are excited, i.e., if the initial spectrum of radiation is broad. This condition requires removing all frequency selectors out of the laser cavity. Condition b) is fulfilled only with some probability even in the ideal case. The presence of reflecting elements in the cavity and nonaxial mode excitation "multiplies" and "smoothes" the fluctuation peaks and thereby decreases this probability. Thus, the generation of a regular train of ultrashort pulses is a statistical event. The fluctuation mechanism of ultrashort pulse generation admits the presence of background radiation between the pulses, satellite pulse generation within the period T and so on. This subject deserves a more detailed analysis.

C. Statistics of Ultrashort Pulse Generation in an Ideal Laser

As before we shall consider a laser model with an inertialess absorber and with only axial mode excitation. It will be shown that substantial deviations from the regular picture of the ultrashort pulse train are possible even in the ideal model. These deviations arc typical for the fluctuation mechanism of ultrashort pulse formation. Further it will be shown that the inertia of the absorber tends to decrease the probability of generating a regular train of isolated pulse generation.

1) Statistics of Initial Radiation: In the linear stage of oscillation, it is possible to treat multimode radiation with the randomly distributed phases as narrow-band Gaussian noise (thermal light). The properties of such radiation are well known in statistical radiophysics [43–45]. The distribution function of intensity fluctuations averaged over the light period has the form:

$$W(I) = \frac{1}{\langle I \rangle} \exp\left(-\frac{I}{\langle I \rangle}\right) \tag{36}$$

The mean number of intensity peaks that exceed the level $\beta\langle I\rangle$ is defined by [45]:

$$\bar{N} = \left(-\frac{1}{2\pi}\rho''(0)\right)^{1/2}(2\beta)^{1/2}e^{-\beta} \tag{37}$$

where $\rho''(0)$ is the second derivative of the amplitude of correlation function for narrow-band noise evaluated at zero argument:

$$k(t) = \sigma^2\rho(\tau)\cos(2\pi\nu_0\tau) \tag{38}$$

where $\sigma^2 = 2\langle I\rangle$ is the noise dispersion, $\rho(0) = 1$. If the envelope of the mode spectrum has, e.g., a Gaussian form

$$S(\nu) = S_0\exp\left[-4\ln 2\left(\frac{\nu-\nu_0}{\Delta\nu}\right)^2\right], \tag{39}$$

then $\rho(\tau) = \exp[-3.5(\tau\Delta\nu)^2]$ and according to (37) the mean number of intensity peaks exceeding a level $\beta\langle I\rangle$ per unit time is equal to

$$\bar{N} = \Delta\nu(2\beta)^{1/2}e^{-\beta}. \tag{40}$$

Except for a multiplication constant of the order of unity, this expression also holds for other forms of the mode spectrum envelope.

The following expressions [45] (Fig. 2) hold for the mean values of peak duration $\bar{\tau}$ and time interval between peaks $\bar{\theta}$:

$$\bar{\tau} = (-\beta\rho''(0)/\pi)^{-1/2} \tag{41}$$

$$\bar{\theta} = (-\beta\rho''(0)/\pi)^{-1/2}(e^{\beta}-1). \tag{42}$$

For the Gaussian form of the mode spectrum envelope, these expressions are

$$\bar{\tau} = (\Delta\nu\sqrt{2\beta})^{-1} = T/m(2\beta)^{-1/2} \tag{43}$$

$$\bar{\theta} = (\Delta\nu\sqrt{2\beta})^{-1}(e^{\beta}-1) = T/m(2\beta)^{-1/2}(e^{\beta}-1), \tag{44}$$

where *m* is the number of axial modes at the end of the linear stage of buildup and *T* the round-trip time in the cavity.

The random intensity *I*(t) becomes a quasi-periodical function of the period *T* at the end of the linear stage buildup. The condition for the appearance of a reiterated peak with amplitude $\beta\langle I\rangle$ is

$$\bar{\theta}(\beta) = T. \tag{45}$$

When $m >> 1$, (45) has the following approximate solution:

$$\beta = \ln[m(2\ln m)]^{1/2} \simeq \ln m. \tag{46}$$

The mean duration of the fluctuation peak having such an amplitude is

$$\bar{\tau}(\beta) = \frac{T}{m}\left\{2\ln\left[m(2\ln m)^{1/2}\right]\right\}^{-1/2} \simeq \frac{T}{m(2\ln m)^{1/2}} \tag{47}$$

and the mean duration at half maximum is rather more (Fig. 2):

$$\bar{\tau} \simeq \frac{T}{m}(\beta)^{-1/2} = \frac{T}{m}(\ln m)^{-1/2}. \tag{48}$$

Note that the duration of the peak with maximum amplitude is $(\ln m)^{1/2}$ times less than the mean duration of the fluctuations having a mean amplitude. This fact may be interpreted as a result of the contribution of spectral wings to the formation of peaks with maximum amplitude.

2) Nonlinear Stage: During the nonlinear stage of buildup, compression of the fluctuation pulses and preferential growth of the most intensive of them take place. The most intensive peaks with amplitude $\langle P_0\rangle(\ln m)$ and duration $\bar{\tau}$ at the end of the nonlinear stage have durations according to (19) and (48):

$$\tau_p = \tau/(\mu)^{1/2} = T/m(\mu\ln m)^{-1/2}. \tag{49}$$

The ratio of its peak power to the mean background power resulting from the growth of the pulses with the mean amplitude ($\beta = 1$) is

$$P_m/P_{\text{backgr}} \simeq \beta^{\mu}(\ln m)^{\mu}. \tag{50}$$

Strictly speaking, to calculate this ratio the averaging of the random intensity after the nonlinear transformation growth [24] should be made. In this case, an increase in the mean background power due to a contribution of peaks with amplitude $\beta > 1$ during the nonlinear growth having $\mu >> 1$ would be taken into account. A similar calculation was performed in [46].

As a criterion of laser perfection, not the ratio of peak pulse power to the mean background power but the ratio of ultrashort pulse energy to the entire background and satellite pulse energy at time interval *T,* must be taken. Such a criterion has been introduced in [46] and a related calculation may be found there. In 3) we shall calculate the probability of another statistical event, which characterizes the perfection of laser pulsing, namely, the probability of generating a train of double pulses.

3) Probability of Appearance of Double Pulses: From the point of view of the fluctuation mechanism one can expect the appearance of two peaks having nearly equal amplitudes that the discrimination of one versus the other in the nonlinear stage will be

poor and will leave the two peaks with their comparable amplitudes. The ratio of the amplitudes of the two pulses at the end of the nonlinear stage will not be more than $S > 1$, if their initial amplitudes satisfy the following condition according to (24):

$$(P_{01}/P_{02} \leq S^{1/\mu} \simeq 1 + (\ln S/\mu)) \tag{51}$$

where we are limited only by the case $(\ln S/\mu \ll 1$. Now let us estimate the probability for the appearance of two initial peaks, the amplitude of which satisfy condition (51).

Let $\omega(h)$ be the distribution of the maxima of the intensity peaks, and $M >> 1$ be an average number of maxima in the interval *T*. Then the probability that a peak will have an amplitude exceeding *h* is

$$P_h = \int_h^\infty \omega(h')dh' \tag{52}$$

The probability for another peak to have the same amplitude within $\pm\Delta h$ is $\omega(h)2\Delta h$ if $\Delta h \ll h$. The probability of the fact that the remaining peaks $(M - 2)$ will have amplitudes less than *h* is, obviously, $(1 - P_h)^{M-2}$. Since the maximal peaks may be distributed among all *M* peaks in C_M^2 ways, therefore, according to the binomial theorem, the probability that among *M* peaks two maximal ones will have a difference between their amplitudes of less than Δh is

$$\rho_{\Delta h}(2) = C_M^2 P_h 2\Delta h\omega(h)(1 - P_h)^{M-2}. \tag{53}$$

In (53), instead of *h*, the most probable value of an amplitude of the maximal peak should be substituted, and we denote this value by *II*. In the case of a distribution of intensity fluctuations of the type (36) the distribution of peak maxima has the same type as [45]:

$$\omega(h) = e^{-h} \tag{54}$$

and $H = \ln M$. After transformation one obtains ($P_h = M^{-1}$):

$$\rho_{\Delta h}(2) = (1/e)M\omega(\ln M)\Delta h = \Delta h/e. \tag{55}$$

Since according to (51) $\Delta h/h = \ln S/m$, the probability of generation of a double-pulse train with an amplitude ratio between pulses not exceeding *S* is

$$\rho_s(2) = h \ln S/e_\mu = \frac{\ln S \cdot \ln m}{e_\mu}. \tag{56}$$

Similarly, it can be shown that the probability for the appearance of a train of triple pulses in the interval *T* with an amplitude ratio less than *S* is

$$\rho_s(3) = (2/3e)(\ln S\ \ln m/\mu)^2. \tag{57}$$

Let us consider the example of a laser, in which the number of modes at the end of the linear stage buildup is $m = 10^2$ and the nonlinearity parameter is $\mu = 30$. In this case the duration of the ultrashort pulses (USP) in the train is $\tau_p = 2/10^{-3}$. The probability for the appearance of a double-pulse train with an amplitude ratio less than 2 is $\rho_2(2)\ 0.03$. It means that there is a definite probability for the generation of the satellite pulses even for an ideal laser (an inertialess absorber, axial modes).

It should be noted that the presence of several independent USP's in the interval T corresponds (in terms of modes) to the generation of several independent sets of locked axial modes with coincidental frequencies but displaced in phases. *A priori*, the number of satellites USP's is not known and is determined by a stochastic process. That is why the method of expanding the field into the cavity modes, a method that has been used in many published papers for describing USP generation, does not suit a physical picture of the phenomenon and cannot fully inform us about the characteristics of the USP laser.

The preceding estimations of the probability for the appearance of a satellite pulse are valid provided the various fluctuation peaks buildup independently. Strictly speaking, this takes place only in a unidirectional traveling-wave laser. In the conventional laser there are two waves running in opposite directions. In this case, the most intensive peak bleaches the nonlinear absorber at times when it coincides with other peaks inside the cell. Because of such an overlap of two pulses, a small pulse can also be amplified and two USP's will be created in the laser, with a fixed interval between them. This interval is determined by the distance from the absorber cell to the rear mirror.

D. Qualitative Analysis of the Influence of a Nonlinear Absorber

1) Inertia: If the relaxation time of the absorber T_1^b is greater than the mean duration τ of the fluctuation peaks at the end of the linear buildup, then the interaction of a fluctuation structure with an inertial absorber has a more complex character and calls for a special treatment. Here we have restricted ourselves to the qualitative remarks that point out the worsening of USP-generation statistics in this case.

Let $T_1^b \gg \tau$. Such an inertial absorber does not follow the fast intensity fluctuation of the pulses; its response to the intensity peaks has a diminished amplitude and lasts during time T_1^b. Essentially, the response of an absorber is the same, as if it were under the influence of a fluctuating radiation field that is averaged over the period T_1^b:

$$I_{eq}(t) = \int_{t-T_1^b}^{t} I(t')dt'. \tag{58}$$

If the random intensity $I(t)$ has a maximal peak of amplitude $\beta = \ln m.$ in the period T, in $I_{eq}(t)$ this peak has a relative amplitude:

$$\begin{aligned}\beta_{\text{eq}} &= \left(1/T_1^b\right)\left[\tau\beta + \left(T_1^b - \tau\right)\right] \\ &= 1 + (\ln m - 1)(\tau/\beta_1^b)\end{aligned} \tag{59}$$

where for the sake of the estimate we have neglected the presence of other peaks having $\beta \gg 1$ in the time interval $\left(T_1^b - \tau\right)$. The inertia of the absorber is equivalent to a decrease in the fluctuation dispersion and therefore hampers the most intensive peak discrimination in the nonlinear stage. Under this condition, the probability of double USP generation rises sharply. It is associated with the fact that the permissible interval, in which maximal amplitudes of initial peaks should be found in order for their amplitudes to remain comparable in the linear stage, is growing in proportion $\left(T_1^b/\tau\right)$. The probability for the generation of a double USP is

$$\rho_s(2) = (\ln S \cdot \ln m/e\mu)\left(T_1^b/\tau\right). \quad (60)$$

Let us now consider a Nd-glass laser with a nonlinear absorber. Let the radiation spectrum width be $\Delta\nu = 20$ cm^{-1} at the end of the linear stage, and the period $T = 5.10^{-9}$ s ($m = 3.10^3$. Then, according to (48) the duration of the largest peak is $\tau = 10^{-12}$ s. The saturable absorber relaxation time for this type laser is $T_1^b \simeq 10^{-11}$ s [38, 39]. For a nonlinear parameter $\mu = 30$, the probability of double-pulse generation with an amplitude ratio less than 2 is $\rho_2(2) \simeq 0.7$. Of course, there are fluctuations of duration τ inside each pulse and the pulse should have an asymmetrical form [23].

Thus, this approximate estimate shows that the inertia of the absorber sharply decreases the stability of the generation of a single USP train.

That is why in the case of an absorber having a slow relaxation rate there is no need for attaining a wide spectrum of modes because the most intensive ultrashort peaks having duration $\ll T_1^b$ are poorly selected against the background of the other pulses. The case is likely to be optimal when the mode spectrum width at the end of the linear buildup is about $(T_1^b)^{-1}$ or the number of the mode is $m \simeq T/T_1^b$. In this case the intensive peak will be selected very effectively and the probability of appearance of satellite pulses will be very small. Moreover, time reduction of the widths of the peaks by a factor of 2 to 3 times will take place during the nonlinear buildup [23]. Naturally, in the case of a laser with an ideal inertialess absorber, it is advisable to broaden the mode spectrum width, e.g., by the method proposed in [23], since the probability of satellite pulse generation rises in proportion to ln *m*, i.e., rather slowly.

III. Experimental Results and Discussion

The main feature of experimental lasers with nonlinear absorbers intended for USP generation is their “instability”. It appears that not every shot of the laser produces a train of regular isolated pulses. Even with careful control of operating

conditions, one observes satellite pulses[1] in the period T, which may become a sequence of irregular ultrashort pulses as shown in Fig. 5.

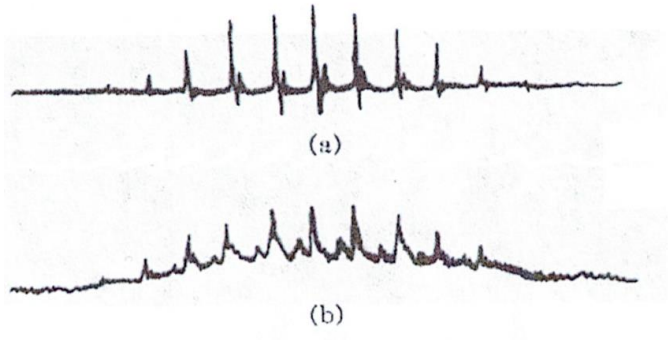


Fig. 5. Oscillograms of ultrashort pulses (a) Regular USP train, (b) USP train with satellite pulses

This feature was noted by all experienced investigators [18, 27–28]. At first sight, it might seem that this deviation from an ideal picture of mode locking is associated with the technical imperfections in the experimental devices, namely, excitation of off-axial modes, the presence of several mode-selective elements in the cavity, distortion of the cavity due to pumping, etc. In fact, all of these effects degenerate the USP laser operation, but even carefully avoiding and compensating for these effects does not allow one to obtain an ideal USP train in every shot. Such a behavior in this type laser has a natural explanation in terms of the fluctuation mechanism of USP generation, which was suggested in [23–24, 28] and is treated in this paper.

According to the preceding theory, there is a definite probability for the generation of an irregular sequence of USP. This is a fundamental finding of the theory describing a USP laser with a nonlinear absorber. This probability has been calculated previously and it represents a physical limit of "ideality" for such a laser. However, in real devices there occur different physical processes that increase the deviation from an ideal picture. Among these are the following: 1) inertia of the saturable absorber; 2) nonlinear losses in the optical media due to powerful radiation; and 3) insufficient duration of the nonlinear absorption built-up stage of the pulse train generation cycle.

It is of interest to perform some experiments that could reveal a contribution of each physical mechanism to the imperfection of the operation of the laser. A number of such experiments are described.

[1] The irregular satellite pulses in the axial period T are meant here. In addition to these pulses, regular satellite pulses may appear, the position of which is associated with the position of a bleachable absorber cell in the cavity [53]. One can eliminate this effect either by traveling-wave operation (the ring laser) [54] or by locating the absorber in a thin cell in contact with the rear mirror of the cavity [55, 56].

A. Influence of the Relation Between Spectral Width and Relaxation Time of the Absorber

According to the preceding theoretical analysis, the probability for the formation of a train of isolated pulses is sharply decreased if the mode spectrum width exceeds the inverse of the absorber relaxation time. Two operating regimes are considered.

1) The regime of the inertial absorber (or the broad spectrum), when

$$\Delta\nu \gtrsim (T_1^b)^{-1}. \tag{61}$$

2) The regime of the inertialess absorber (or the narrow spectrum), when

$$\Delta\nu \lesssim (T_1^b)^{-1}. \tag{62}$$

The influence of the spectral width on the "stability" of the USP laser operation has been studied experimentally in [30], and it has been found that the radiation spectrum has an irregular structure. This structure has been explained as the spectral interference of several USP in the train period *T*. Therefore, from the shape of the spectrum, it was possible to judge whether a train of single pulses had been generated or not. The smoothness of the spectrum was an indication of the appearance of a train of single isolated pulses. With the help of this method, it was found that the probability for the generation of single-pulse trains grew as the lasing spectrum narrowed up to certain values. These values are specific for ruby and Nd glass. In [30] this effect was explained in terms of the influence of a number of modes *m* on the probability of appearance of satellite pulses, i.e., by a relationship similar to (56). But this relationship for the laser with an inertialess absorber is too weak (~ ln m) to explain this effect. That is why in [48], the degeneration of operation when the lasing spectrum is broad was explained as due to the finite value of the absorber relaxation time.

In addition to the degeneration, the complex internal pulse structure should be expected in view of the fluctuation mechanism for USP oscillation. The envelope duration is determined by the relaxation time of the absorber, and the internal structure is determined by the intensity fluctuations $\tau_{fl} \simeq (\Delta\nu)^{-1}$. The accurate measurements of two-photon fluorescence patterns constitute independent evidence for the existence of an internal structure [15–16, [48]. The time resolution of existing electronic instruments does not allow the direct observation of this internal structure. The best time resolution that has been achieved with the help of a high-speed image-converter streak camera is 4–7 ps [49] and it permits the measurement of the overall pulse shape only.

Investigations aimed at studying the influence of absorber inertia on the USP laser operation were carried out on a laser with an absorber of rather slow relaxation time [50]. In this case, the time resolution of the image-converter streak camera was quite sufficient for the observation of the form and structure of the pulse. The experimental setup is shown in Fig. 6. The ruby rod was the active medium and the vanadium phtalocianyne solution in nitrobenzene was the nonlinear absorber. Measurements of the absorber's relaxation time gave a value for $T_1^b = 1.2 \pm 0.6$ ns. For the

excitation of a sufficiently large number of modes in the spectral interval $(T_1^b)^{-1}$ it is necessary that $T_1^b \ll T = 2L/c$. For this purpose, the cavity length was made to be sufficiently long (L = 600 cm, T = 40 ns). A system of two lenses was used to compensate for the waveform distortion in the ruby, and an iris with a diameter from 2 to 4 mm was used for mode selection. To change the spectral width, the plane-parallel glass plates of different thickness used as frequency-selecting elements were inserted in the cavity. An overall view of the laser oscillation was recorded with a fast oscilloscope and a coaxial photodiode. The pulse substructure was observed with the help of an image-converter streak camera (time resolution was about 0.1 ns). The laser spectrum was recorded with a Fabry-Perot etalon. The experimental setup permitted the investigation of three regimes of laser operation: 1) $\tau_{fl} \simeq (\Delta\nu)^{-1} \ll T_1^b$, 2) $-\tau_{fl} \simeq T_1^b$ and 3) $-\tau_{fl} \gg T_1^b$.

In the first regime the spectral width was $\Delta\nu = 0.2 - 0.5$ cm^{-1}. It corresponds to $\tau_{fl} \simeq 0.1$ ns, i.e., ten times less than the relaxation time of the absorber. In this case the time profile of the ruby's output radiation was very unstable. Generally, the output radiation took the form of a group of USP's that followed one another one axial period apart. Between the groups of pulses, the satellite pulses were usually present. The envelope of the group had an asymmetrical form with a short leading edge and a slowly falling trailing edge (Fig. 7). Based on the measurement of the envelope, the exponential decay time of the trailing edge was around T_1^b.

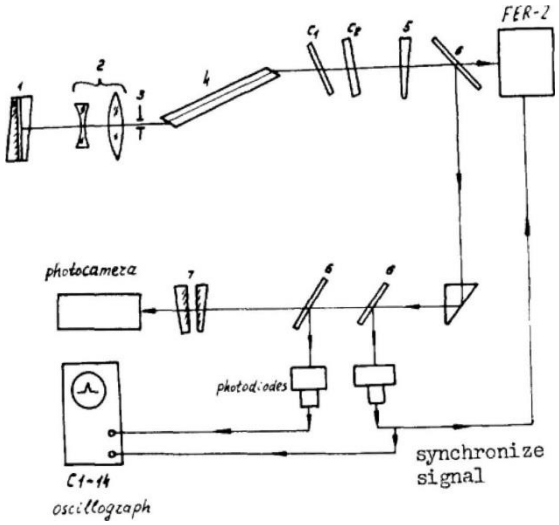
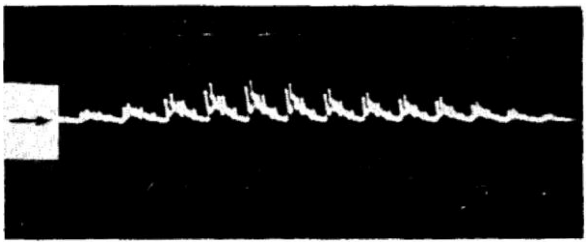


Fig. 6. Experimental scheme for measuring the pulse shape produced by a laser with a relatively slow relaxation absorber

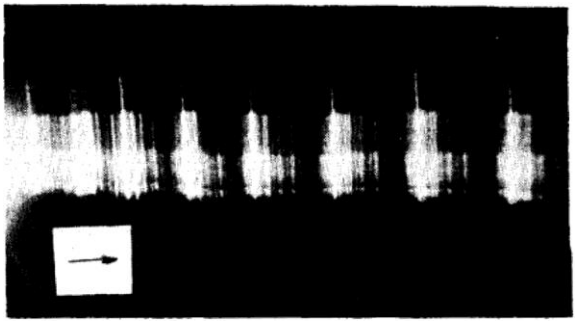
To operate the laser in the second regime ($T_1^b \simeq \tau_{fl}$), the mode selector was inserted in the cavity. It narrowed the axial mode spectrum up to $\Delta\nu = 0.04 - 0.08$ cm^{-1}, i.e., $\tau_{fl} \simeq$0.04–0.08 ns. In this case, the laser operation stability sufficiently increased. Photographs on which the entire period T was filled by pulses were

seldom obtained. More often a damping sequence of pulses that followed the largest pulse was observed (see Fig. 8). The decay constant of the amplitudes of the pulses was also about T_1^b. The duration of each pulse, taken separately, was approximately τ_{fl}.

In the third regime, the radiation spectrum narrowed up to a value less than 0.02 cm^{-1} when τ_{fl} >>1.7 ns. In this regime the stability of laser action became greater and the most probable was the generation of a train of single isolated pulses. From the photometry data taken, the form of these pulses was found to be asymmetrical (see Fig. 9), with a 2–4 times faster dropping trailing edge than the rise time of the leading edge. The pulse duration at half height was approximately τ_p = 2.0 ns, it was close to the relaxation time T_1^b.



(a)



(b)

Fig. 7. Complex structure of the USP train when the spectral width $\Delta\nu \gg 1/T_1^b$ where T_1^b is the relaxation time, and repetition period T = 40 ns. (a) Oscillogram. (b) Photograph taken with an image-converter streak camera

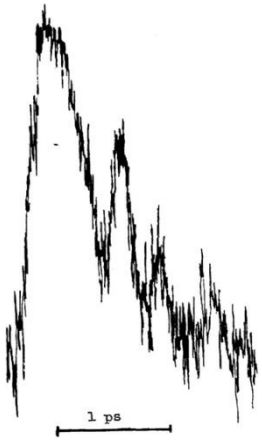


Fig. 8. Microdensitometer trace of a streak image-converter camera photograph that shows the intensity versus time pulse structure when $\Delta\nu \sim 1/T_1^b$

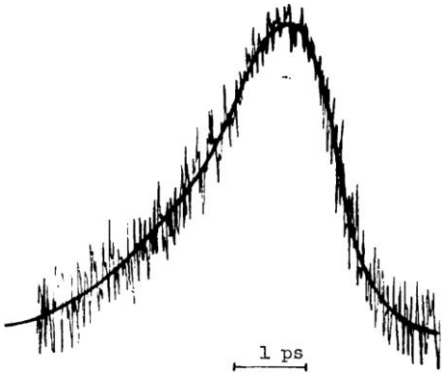


Fig. 9. Asymmetrical pulse shape when $\Delta\nu < 1/T_1^b$. (Experimental arrangement same as for Fig. 8)

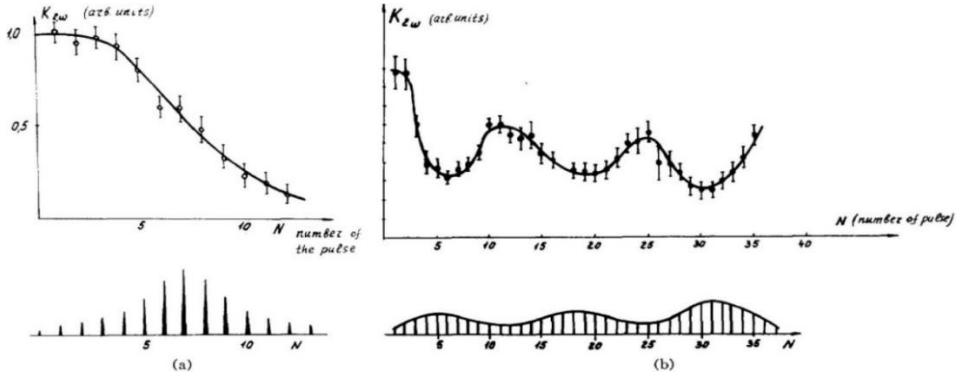


Fig. 10. Dependence of the efficiency of second-harmonic generation on the pulse number in the train. (a) When the total train energy density is equal to 10^{-2} J/cm^2. (b) When the total train energy is equal to 10^{-3} J/cm^2

Real USP lasers operate, as a rule, in a regime where broad spectrum is obtained. This regime, as indicated by theory and measurements, is characterized by an insufficiently stable operation and a complex pulse substructure.

B. Influence of Nonlinear Losses on the Satellite Pulse Evolution

The formation of a USP by a nonlinear absorber occurs when the USP power becomes greater than the absorber saturation power. After this point, a predominant amplification of the USP takes place with each consecutive pass through the active medium until saturation of the laser medium takes place, i.e., until partial emission of the energy stored in the active medium begins. USP power may reach a level at which a nonlinear nonresonant interaction with the substance of any element inside the cavity becomes important [52]. The most important is the change in the refractive index of the laser glass matrix due to the intensive radiation field of the USP. This change results in the self-focusing of the radiation and spectral broadening. Both effects give rise to losses that increase with the growth of pulse intensity. Self-focusing throws radiation out of the cavity because of diffraction, and spectral broadening the frequency of the radiation out of the amplifying line profile of the laser [18].

The nonlinear losses that increase with the field intensity must influence the USP formation mechanism in the following way. Beginning from a certain level of intensity, amplification of the most intensive USP decreases, i.e., there occurs a limitation on the USP power. At the same time, less intensive USP can be amplified and reach the same power level as the most intensive pulses. In other words, nonlinear losses, which increase with the intensity growth, lead to a process opposite to the one that takes place in the bleaching of the nonlinear absorber. Experimentally, this should result in an increase in the number of satellite pulses at the end of the train. Note that such a fact has been observed experimentally in [27]. Moreover, the nonlinear losses may be the reason why USP trains last longer than conventional giant pulses for the same value of laser parameters [18].

Experiments on the influence of nonlinear losses on USP laser operation have been carried out in [51–52]. In [51], it has been shown that self-focusing of the radiation takes place in USP lasers. It causes the deterioration of laser operation, especially in those cases where one uses long rods for the active medium and a large thickness of saturable absorber, and one operates in the regime of large output energy. To eliminate this effect the USP output energy density should be decreased. Decreasing the energy density of the USP train generated by a Nd-glass laser down to $5 \cdot 10^{-3}$ J/cm^2 led to a probability for the appearance of a single-pulse train (within the limits of a time resolution of 20 ps) that was not less than 90 percent.

In [52] the change in the number of satellite pulses in the USP train was studied. This change could be judged from the change in the efficiency of second-harmonic generation (SHG). The amplitudes of the fundamental I_ω and second harmonics $I_{\omega 2}$ were measured by an oscilloscope. The amplitude of the signal on the oscilloscope screen is defined by the light pulse energy, which is integrated over the resolution time of a photodiode and an oscilloscope (τ_{reg} 1-2 ns). Let us assume that several pulses of total energy ε are situated within the resolution time of the apparatus. If the

number of pulses increases while the total energy remains constant, the mean intensity will drop correspondingly. This will be displayed as a corresponding decrease in the conversion coefficient for the SHG. One can therefore observe the kinetics of the growth of the satellite pulses on a time scale of τ_{reg} by measuring the conversion coefficient for SHG for each period T of the train.

The change in the SHG conversion coefficient was first observed in [4]. In that work, this effect was attributed to a gradual increase in the pulse duration as the train developed. We think that the effect should be explained by an increase in the number of satellite pulses due to the nonlinear losses. To support this explanation a measurement of the SHG conversion coefficient for the USP laser was performed [52]. The laser operated in two regimes, in which the densities of output energy substantially differed. The relationship between the measured conversion coefficient and the pulse number in the train is shown in Fig. 10(a). In this case the output energy density was 10^{-2} J/cm^2. From this curve it is obvious that at the beginning of the train the coefficient remains constant during several periods, i.e., the nonlinear losses are not sufficient at that time, but then their influence grows and the coefficient falls. In Fig. 10(b), a similar relationship is presented for a lower output energy density (~10^{-3} J/cm^2), which is reached when the bleachable absorber has a small initial absorption. In this case a long (more than 500 ns) USP train with an oscillating envelope is observed. The relationship between the conversion coefficient and the pulse number in the train also displays an oscillatory behavior. Maximum laser energy corresponds to the minima in the value of the conversion coefficient and vice versa. Such oscillatory behavior is likely to be due to the transient process in the laser, which operated with an absorber having a small initial absorption coefficient. This oscillatory behavior can be explained by the periodical growth and decrease of the number of satellite pulses. In this case the role of the nonlinear losses was less than in the former one because the change of the conversion coefficient was also smaller.

From these data it follows that there are nonlinear losses that deteriorate laser operation, even when the energy density of the output energy is small. This effect prevents one from achieving the theoretical limit for the ratio between USP power and background power for an "ideal" laser. That is why it is interesting to develop a special method for increasing the ratio of USP energy (power) to background energy (power). The following is a way of achieving such method.

C. The Method of Increasing the Ratio of the Pulse Energy to the Background Energy Ratio

To increase the ratio between the energy of the pulse and the background due to residual fluctuation and satellite pulses the USP was amplified in a stable two-component amplifier [36]. The two-component amplifier consists of two parts: an amplifying medium and a nonlinear bleachable dye with fast relaxation of the bleachable state. This system is stable because it is below the self-oscillation threshold. Such a system acts as a good discriminator since it is absorbing for weak pulses and amplifying for strong ones. The discrimination becomes better as the number of passes increase.

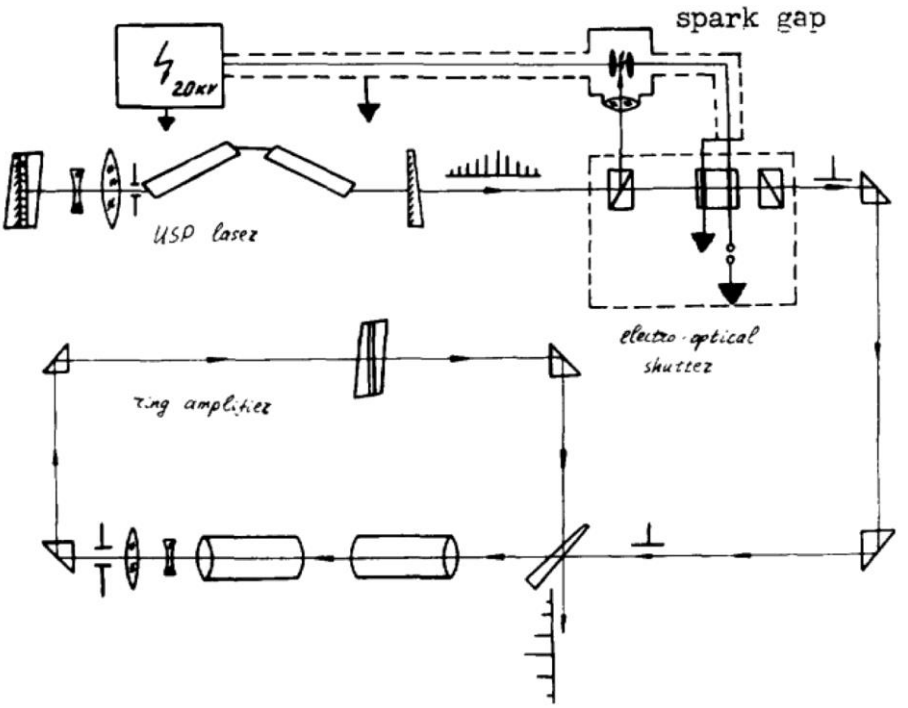


Fig. 11. Experimental scheme for USP amplification in the stable two-component amplifier.

Note that this situation cannot be realized in conventional USP lasers with nonlinear absorbers. In a laser, oscillation begins from spontaneous noise and passes through a stage of linear amplification when the nonlinear absorber is not bleached and only causes linear losses. All fluctuation peaks are equally amplified independently of their amplitudes. When weak pulses begin saturating the absorber, discrimination of amplitudes is ended. To get a greater discrimination per passage one could use an absorber with a greater initial absorption, but in this case the gain has to be increased to achieve self-oscillation conditions. This gain increase in turn results in a decrease in the duration of the nonlinear stage and therefore deteriorates the discrimination between large and small pulses.

It is not necessary to fulfill the self-oscillation conditions in a two-component stable amplifier. First, it allows one to use a nonlinear absorber with low initial transmission and to get a greater degree of discrimination per passage. In this case the amplifying component must compensate only rather small losses in the bleached absorber. Secondly, if one has losses in the bleached absorber close to the gain, it will be possible to increase the duration of the nonlinear stage. There is, however, an actual limit to this, which is due to the unsteadiness of the critical point in a two-component amplifier [32]. The important feature of this system is the possibility of a regime where the largest pulse goes through the system without great gain or decay, while all the weaker pulses decay. This is how the two-component amplifier differs from the conventional USP laser.

The experiment is shown in Fig. 11. To obtain the largest pulse-to-background ratio the input-signal power and the initial absorber transmission were chosen so as to make the system operate with a slight net gain for the largest pulse. The initial transmission of the absorber was about 15 percent. An oscillogram of the input and output signals is shown in Fig. 12. This oscillogram illustrates a case where the input signal consisted of two pulses of different amplitudes. One can see that the smaller second pulse is absent in the output signal. From this oscillogram we estimate that the ratio between amplitudes increased by at least two orders of magnitude. The effective gain of the larger pulse was about 10^2. The detailed investigation of this system shows that it is a promising method for obtaining a USP with high reproducibility and low background level.

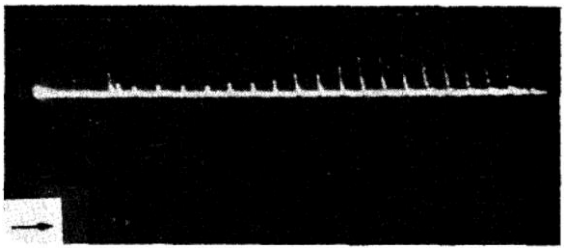


Fig. 12. Oscillogram that shows the effect of discrimination of satellite pulses as they propagate in the stable two-component amplifier

Since laser pulses but not the noise fluctuation pulses are fed to the input of this system, condition (7) does not have to be met. In addition, it allows the use of nonlinear absorbers that require high powers for bleaching. Such absorbers must include dyes with a very short bleachable state relaxation time (of the order of about and less than 10^{-12} s), and they are necessary for obtaining subpicosecond pulses. Such absorbers can probably exist, but due to the short relaxation time they need such high intensities that saturation of amplification becomes noticeable. In other words, saturation of amplification occurs earlier than saturation of the absorber, and Q switching does not take place.

Indeed, for bleaching of the absorber within time T_1^b a fluctuation peak-energy density $\hbar\omega/2\sigma_b$ is required. In this case all fluctuation peaks in interval T carry an energy $(1/\beta)(\hbar\omega/2\sigma_b)$ (T/T_1^b) where β is the, ratio between the largest peak and the average background amplitude. For some pulse discrimination, several passages are required, e.g., $N = 10$ and more. The total energy in time interval $N \cdot T$ must be sufficiently less than the energy for saturation of amplification, i.e.,

$$\frac{N}{\beta}\frac{\hbar\omega}{\sigma_b}\frac{T}{T_1^b} \ll \frac{\hbar\omega}{\sigma_a}. \tag{63}$$

Only in this case is it possible to extract an ultrashort fluctuation pulse before the saturation of amplification takes place. In this respect absorbers are available for which:

$$T_1^b \gg \frac{\sigma_a}{\sigma_b} T \frac{N}{\beta}. \tag{64}$$

The parameter σ_a/σ_b for ruby and Nd-glass and suitable dyes is about 10^{-4}. Even if one assumes a minimum value of about 1 for N/β we must have $T_1^b \gg 10^{-4}T$, i.e., in practice when T is about several nanoseconds, T_1^b must be greater than several tenths of a picosecond. This means that it is not possible to use dyes having subpicosecond relaxation time in conventional schemes for USP generation.[2] But such dyes can operate in the two-component medium. In this case a sufficiently powerful signal can bleach the absorber. Saturation of the active medium will only cause some decay of the pulse train, but discrimination of large versus small pulses will he considerable. Dyes with subpicosecond relaxation time may be found by this method and be used to obtain subpicosecond pulses.

IV. Conclusion

At present, we believe that the fluctuation mechanism is mainly responsible for generating ultrashort pulses in lasers Q switched by nonlinear absorbers. According to this mechanism there always exist ultrashort pulses in multimode lasers and the nonlinear absorber selects the most intensive ones. Selection of a single pulse, and hence, formation of a regular sequence is a statistical phenomenon, the probability of which is conditioned by physical and technical circumstances.

With the use of an inertial absorber with a relaxation time $T_1^b \gg 1/\Delta\nu$ ($\Delta\nu$ is the spectral width) a "single" pulse will have a complex fluctuation substructure. Inside an envelope with duration T_1^b chaotic subpulses with a shorter duration of the order $1/\Delta\nu$ will exist. The effect of dispersion, which has not been considered in this article, will influence the character of this internal structure [57]. Due to dispersion the broadening and overlapping of the internal subpulses will take place without a significant change in the envelope. Shortening of the USP envelope duration down to a subpicosecond level is the most important point. In this case broadening due to dispersion will take place but this could be compensated by a method that is described in [13–14].

References

1. *DeMaria A.J., Stetser D.A., Heynau H.* Self-mode-locking of laser with saturable absorbers // Appl. Phys. Lett. 1966. Vol. 8. P. 174–176.

2. *DeMaria A.J., Stetser D.A., Glenn Jr. W.H.* Ultra-short light pulses // Science. 1967. Vol. 156. P. 1557–1568.

3. *Armstrong J.A.* Measurement of picosecond laser pulse widths // Appl. Phys. Lett. 1967. Vol. 10. P. 16–18.

[2] It. is possible to soften condition (64) by using a laser beam expander. In this case, condition (64) has the form:

$$T_1^b \gg T\left(\frac{d_b}{d_a}\right)^2 \frac{\sigma_a}{\sigma_b}\frac{N}{\beta} \tag{65}$$

where d_a and d_b are the diameters of beams in the active medium and in the dye, respectively.

4. *Glenn W.H., Brienza M.J.* Time evolution of picosecond optical pulses // Appl. Phys. Lett. 1967. Vol. 10. P. 221–224.

5. *Giordmaine J.A., Rentzepis P.M., Shapiro S.L., Wecht K.W.* Two-photon excitation of fluorescence by picosecond light pulses // Appl. Phys. Lett. 1967. Vol. 11. P. 216–218.

6. *Rentzepis P.M., Duguay M.A.* Picosecond light pulse display using two different optical frequencies // Appl. Phys. Lett. 1967. Vol. 11. P. 218–220.

7. *Duguay M.A., Shapiro S.L., Rentzepis P.M.* Spontaneous appearance of picosecond pulses in ruby and Nd: glass lasers // Phys. Rev. Lett. 1967. Vol. 19. P. 1014–1019.

8. *Weber H.P.* Comments on pulse width measurement with two-photon excitation of fluorescence // Phys. Lett. 1968. Vol. 27A. P. 321–322.

9. *Letokhov V.S.* Ultrashort fluctuation pulses of light in a laser // Zh. Eksp. Teor. Fiz. 1968. Vol. 55. P. 191–1946.

10. *Klauder J.R., Duguay M.A., Giordmaine J.A., Shapiro S.L.* Correlation effects in the display of picosecond pulses by two-photon techniques // Appl. Phys. Lett. 1968. Vol. 13. P. 174–176.

11. *Harrach R.J.* Effect of partial mode-locking on contrast ratios in two-photon excitation of fluorescence // Phys. Lett. 1968. Vol. 28A. P. 393–394.

12. *Kuznetsova T.I.* Concerning the problem of registration of ultrashort light pulses // Zh. Eksp. Teor. Fiz. 1968. Vol. 55. P. 2453–2458.

13. *Treaey E.B.* Compression of picosecond light pulses // Phys. Lett. 1968. Vol. 28A. P. 34–35.

14. Measurement of picosecond pulse substructure using compression techniques // Appl. Phys. Lett. 1969. Vol. 14. P. 112–114.

15. *Shapiro S.L., Duguay M.A.* Observation of subpicosecond components in the mode-locked Nd:glass laser // Phys. Lett. 1969. Vol. 28A. P. 698–699.

16. *Bradley D.J., New G.H.C., Caughey S.J.* Subpicosecond structure in mode-locked Nd:glass lasers // Phys. Lett. 1969. Vol. 30A. P. 78–79.

17. *DeMaria A.J., Glenn W.H., Brienza Jr. M.J., Mack M.E.* Picosecond laser pulses // Proc. IEEE. 1969. Vol. 57. P. 2–25.

18. *Duguay A., Hansen I.W., Shapiro S.L.* Study of the Nd:glass laser radiation // IEEE J. Quantum Electron. 1970. QE-6. P. 725–743.

19. *Hargrove L.E., Fork R.L.* Locking of He-Ne laser modes induced by synchronous intracavity modulation // Appl. Phys. Lett. 1964. Vol. 5. P. 4–5.

20. *DeMaria A.J., Ferrar C.M., Danielson Jr. G.E.* Mode-locking of a Nd3+-doped glass laser // Appl. Phys. Lett. 1966. Vol. 8. P. 22–24.

21. *DiDomenico M., Geusic Jr. J.E., Marcos H.M., Smith R.G.* Generation of ultrashort optical pulses by mode-locking the YAG:Nd lasers // Appl. Phys. Lett. 1966. Vol. 8. P. 180–183.

22. *Culler C.O.* The regenerative pulse generator // Proc. IRE. 1955. Vol. 43. P. 140–148.

23. *Letokhov V.S.* Generation of ultrashort light pulses in a laser with a nonlinear absorber // Zh. Eksp. Tear. Fiz. 1968. Vol. 55. P. 1077–1089.

24. *Basov N.G., Kriukov P.G., Letokhov V.S., Senatskii Yu.V.* Generation and amplification of ultrashort, optical pulses // IEEE J. Quant. Electron. 1968. QE-4. P. 606–609.

25. *Pieck Jr. J.A.* Evolution of a Q-switched laser pulse from noise // Appl. Phys. Lett. 1968. Vol. 13. P. 365–367.

26. *Fleck J. A.* Ultrashort pulse generation by Q-switched lasers // Phys. Rev. B. 1970. Vol. 1. P. 84–100.

27. *Malyutin A.A., Shehelev M.Ya.* Investigation of the temporal structure of neodymium-laser emission in the mode self-locking regime // Pis'ma Zh. Eksp. Teor. Fiz. 1969. Vol. 9. P. 445–448.

28. *Basov N.G., Kryukov P.G., Letokhov V.S.* Ultrashort light pulses // FIAN Preprint. Sept. 1969. No. 122; also Opt. Laser Technol. 1970. Vol. 2. P. 126–131; also Laser. 1969. Vol. 3. P. 39–45.

29. *Malyshev V.I., Markin A.S., Sychev A.A.* Kinetics of free generation spectra of solid-state laser at traveling wave regime and elimination of mode discrimination // Pis'ma Zh. Eksp. Teor. Fiz. 1969. Vol. 9. P. 3–6.

30. *Malyshev V.I., Masalov A.V., Sychev A.A.* Spectral-temporal method of study of partial self-mode-locking in ruby and Nd:glass lasers // Zh. Eksp. Teor. Fiz. 1970. Vol. 59. P. 48.

31. *Basov N.G. et al.* Fluctuation structure of a giant light, pulse and its variation when passing through nonlinear absorber // Pis'ma Zh. Eksp. Teor. Fiz. 1969. Vol. 8. P. 428–432.

32. *Basov N.G., Kriukov P.G., Letokhov V.S., Matveetz Yu.A.* Investigation of the formation of an ultrashort light pulse propagating in two-component medium // Zh. Eksp. Teor. Fiz. 1969. Vol. 56. P. 1546–1556.

33. *Wang C.C., Baardsen E.L.* Optical third harmonic generation using mode-locked and non-mode-locked lasers // Appl. Phys. Lett. 1969. Vol. 15. P. 396–397.

34. *Eckardt R.C., Lee C.K.* Optical third harmonic measurements of subpicosecond light pulses // Appl. Phys. Lett. Dec. 1969. Vol. 15. P. 425–427.

35. *Letokhov V.S.* Generation of ultrashort pulses in laser with nonlinear absorber, II. FIAN Preprint. 1969. Vol. 181.

36. *Basov N.G., Kriukov P.G., Letokhov V.S., Matveetz Yu.A., Chekalin S.V.* Amplification of ultrashort pulses in two-component medium // Pis'ma Zh. Eksp. Teor. Fiz. 1969. Vol. 10. P. 479–482.

37. *Giuliano C.R., Hess L.D.* Nonlinear absorption of light: optical saturation of electronic transitions in organic molecules with high intensity laser radiation // IEEE J. Quantum Electron. 1967. QE-3. P. 358–367.

38. *Shelton J.W., Armstrong J.A.* Measurement of the relaxation time of the Eastman 9740 bleachable dye // IEEE J. Quantum Electron. 1967. QE-3. P. 696– 697.

39. *Duguay M.A., Hansen J.W.* Direct measurement of picosecond lifetimes // Opt. Commun. 1969. Vol. 1. P. 254–256.

40. *Kuznetsova T.I.* On problem of light pulse shortening in lasers with a fast relaxing bleachable absorber // Izv. Vyssh. Ucheb. Zaved. Radiofiz. 1968. Vol. 11. P. 1560–1566; also FIAN Preprint 1967. No. 25.

41. *Gurevich G.L., Otmakhov Yu.A.* Nonstationary processes in traveling wave lasers with bleachable absorber // Izv. Vyssh. Ucheb. Zaved. Radiofiz. 1969. Vol. 12. P. 208–220.

42. *Sooy W.R.* The natural selection of modes in a passive Q-switched laser // Appl. Phys. Lett. 1965. Vol. 7. P. 36–37.

43. *Rytov S.M.* Introduction to statistical radiophysics. Izv. Akad. Nauk., 1966.

44. *Mandel L., Wolf E.* Coherence properties of optical fields // Rev. Mod. Phys. 1965. Vol. 37. P. 231–287.

45. *Tikhonov V.I.* Bursts of random processes//Usp. Fiz. Nauk. 1962. Vol.77. P. 449.

46. *Kuznetsova T.I.* On the statistics of appearance of ultra-short light pulses in a laser with a bleachable absorber // Zh. Eksp. Teor. Fiz. 1969. Vol. 57. P. 1673–1683.

47. *Salzmann H.* Mode-locking of giant pulse ruby lasers // Phys. Lett. 1970. Vol. 32A. P. 40–41.

48. *Malishev V.I., Sychev A.A., Babenko V.A.* Investigation of radiation of Nd:glass laser with blechable dyes having finite time of relaxation // Pis'ma Zh. Eksp. Teor. Fiz. 1971. Vol. 13. P. 588–592.

49. *Bradley D.J., Liddy B., Sleat W.E.* Direct linear measurement of ultrashort light pulses with a picosecond streak camera // Opt. Commun. 1971. Vol. 2. P. 391–395.

50. *Kriukov P.G., Matveetz Yu.A., Churilova S.A., Shatberashvili O.B.* Investigation of the shape of the radiation pulse from a mode-locked laser // Zh. Eksp. Teor. Fiz. 1972. Vol. 62. P. 2036–2043.

51. *Basov N.G. et al.* Nonlinear losses in ultra-short light pulse generators and amplifiers, Zh. Eksp. Teor. Fiz. 1971. Vol. 60. P. 533–540.

52. *Bykovskii N.E. et al.* Enhancement of ultrashort laser pulse/background energy ratio // Quantum Electron. Symp. 1972. Vol. 7. P. 68–70.

53. *Kuznetsova T.I., Malyshev V.I. and Markin A.S.* Self-locking of axial modes in lasers with saturable filters // Zh. Eksp. Teor. Fiz. 1967. Vol. 52. P. 438–466.

54. *Krasyk I.K., Pashinin P.P., Prokhorov A.M.* Ring laser of ultra-short pulses // Pis'ma Zh. Eksp. Teor. Fiz. 1968. Vol. 7. P. 117–119.

55. *Bradley D.J., Caughey S.J., New G.H.C.* Relationship between saturable absorber cell length and pulse duration in passively mode-locked lasers // Opt. Commun. 1970. Vol. 2. P. 41–44.

56. *Volak T.B., Kaitmazov S.D., Medvedev A.A., Pogorelskii I.V.* Obtaining of single picosecond pulses in laser with thin bleaching dye // P.N. Lebedev Phys. Inst., Moscow, USSR (Short Phys. Commun.), 1970. Vol. 4. P. 15.

57. *Letokhov V.S., Morozov V.N.* Generation of ultra-short duration coherent light pulses // Zh. Eksp. Teor. Fiz. 1967. Vol. 52. P. 1296–1302.

58. *Duguay M.A., Mattick A.T.* Ultrahigh speed photography of picosecond light, pulses and echoes // Appl. Opt. 1971. Vol. 10. P. 2162–2170.

59. *Eckardt R.C., Lee C.H., Bradford J.N.* Temporal and spectral development of mode-locking in a ring-cavity Nd:glass laser // Appl. Phys. Lett. 1971. Vol. 10. P. 420–423.

Квант. электроника. 1976. Т. 3 (1). С. 152–156

ОБ УСИЛЕНИИ В ОБЛАСТИ ДАЛЕКОГО ВАКУУМНОГО УЛЬТРАФИОЛЕТА НА ПЕРЕХОДАХ МНОГОЗАРЯДНЫХ ИОНОВ

А.Н. Жерихин, К.Н. Кошелев, В.С. Летохов

Институт спектроскопии АН СССР, Москва

Показана возможность получения усиления порядка 10–25 $см^{-1}$ в области 300–700 Å на переходах 3s–3p многозарядных ионов с основной электронной конфигурацией $1s^2\ 2s^2\ 2p^6$ при быстром нагреве электронов предварительно созданной плазмы мощным ультракоротким импульсом света (двухступенчатый нагрев плазмы).

1. В настоящее время ведется интенсивный поиск путей создания лазеров в области далекого вакуумного ультрафиолета и мягкого рентгена на электронных переходах атомов и ионов. Для получения усиления предлагается создавать инверсию населенностей уровней внутренних рентгеновских переходов атомов или ионов малой кратности ионизации [1–3] либо высокоэнергетических переходов внешнего оптического электрона в многозарядных ионах [4–9]. В первом подходе накачку предлагается осуществлять путем фотоионизации электрона с нижней *K*-оболочки под действием мощного импульса рентгеновского излучения. При втором подходе предложено несколько методов создания инверсии между возбужденными уровнями многозарядных ионов в лазерной плазме: быстрое возбуждение отдельных уровней ионов электронами плазмы с сильно отличающимися электронной и ионной температурами [4–6], возбуждение определенного уровня иона за счет перезарядки ионов на нейтральных атомах [5], возбуждение уровней в процессе рекомбинации в быстрорасширяющейся плазме [7–9].

Поскольку время существования инверсии для коротковолновых переходов мало, во многих предложениях рассматривается возбуждение в режиме бегущей волны, позволяющее генерировать однонаправленное лазерное излучение с расходимостью, определяемой угловым размером активной области [10]. Такой метод, например, успешно использовался в ВУФ-лазере на H_2 с временем существования инверсии короче 10^{-9} с [11]. Для обеспечения возбуждения за время короче 10^{-12} с в области далекого вакуумного ультрафиолета в работе [4] был предложен метод двухступенчатой накачки лазерной плазмы. Он заключается в быстром нагреве электронной компоненты предварительно

приготовленного шнура лазерной плазмы при распространении вдоль него ультракороткого импульса (УКИ) мощного лазерного излучения. В этом методе автоматически осуществляется пространственно-временное согласование движения области инверсии и генерируемого импульса коротковолнового излучения. В зоне УКИ накачки энергия электронов быстро возрастает и происходит эффективное возбуждение уровней ионов за время, короче 10^{-12} с, что позволяет надеяться на возникновение инверсии даже на так называемых самоограниченных переходах.

Однако в работе [4] не была рассмотрена кинетика возбуждения уровней ионов электронным ударом, а также не были выбраны подходящие переходы многозарядных ионов. Цель данной работы состоит в том, чтобы дополнить этот метод именно таким анализом. Мы покажем, что ранее предложенный метод накачки лазеров в области 300–700 Å может быть осуществлен на многозарядных ионах с основной электронной конфигурацией $2\,p^m$.

2. Рассмотрим процессы заселения возбужденных состояний ионов, возникающие при нагреве заранее подготовленной лазерной плазмы, отвлекаясь от метода ее создания. Будем считать, что УКИ света накачки распространяется вдоль плазменного шнура с электронной концентрацией N_e и ионами ионизации z. За время взаимодействия УКИ с плазмой происходит быстрый нагрев электронной компоненты, при этом ионная температура меняется слабо [4]. Рассмотрим кинетику заселения возбужденных состояний ионов и возможность создания инверсии за счет неупругих электрон-ионных столкновений.

В работе [12] было показано, что электронные столкновения могут привести к созданию инверсии в ионах с основной электронной конфигурацией $1s^22s^22p^3$ на переходе $2p^23s$–$2p^23p$. Наш анализ показал, что конфигурация $2p^3$ не является исключительной среди всех конфигураций $2p^m$. Поэтому мы сразу рассмотрим более общий случай любой конфигурации типа $2p^m$.

Система уровней ионов этого типа обладает следующими важными особенностями. Верхнее состояние $2p^{m-1}3p$ распадается наиболее эффективно в состояние $2p^{m-1}3s$, которое, в свою очередь, испытывает очень быстрый радиационный распад в основное состояние, в то время как радиационный распад состояния $2p^{m-1}3p$ в основное состояние запрещен. Заселение обоих рабочих уровней происходит в результате возбуждения электронным ударом из основного состояния, причем анализ атомных констант показал, что заселение состояния $2p^{m-1}3p$ идет значительно эффективнее, чем состояния $2p^{m-1}3s$. Все процессы, участвующие в заселении уровней, схематически показаны на рисунке 1.

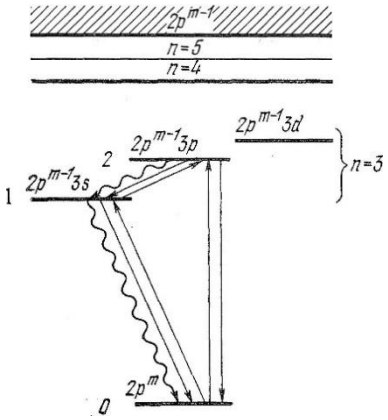


Рис. 1. Схема уровней иона с основной электронной конфигурацией $1s^2 2s^2 2p^m$. Прямыми стрелками обозначены переходы, вызванные неупругими электрон-ионными столкновениями, волнистыми — радиационные переходы. Слева от уровня стоит условное обозначение, используемое в тексте

Населенности уровней могут быть получены из решения полных уравнений баланса частицы, включающих все процессы столкновительных и радиационных переходов между этими уровнями. В квазистационарном случае, приравнивая скорости возбуждения и девозбуждения уровней 1 и 2 иона, имеем

$$N_0 N_e \langle \upsilon\sigma_{01} \rangle + N_2 N_e \langle \upsilon\sigma_{21} \rangle + N_2 A_{21} = N_1 N_e \langle \upsilon\sigma_{12} \rangle + N_1 N_e \langle \upsilon\sigma_{10} \rangle + N_1 A_{10}, \quad (1а)$$

$$N_0 N_e \langle \upsilon\sigma_{02} \rangle + N_1 N_e \langle \upsilon\sigma_{12} \rangle = N_2 N_e \langle \upsilon\sigma_{21} \rangle + N_2 N_e \langle \upsilon\sigma_{20} \rangle + N_2 A_{21}, \quad (1б)$$

где N_i — плотность частиц на i-м уровне иона; $\langle \upsilon\sigma_{ij} \rangle$ — усредненное значение сечения перехода между уровнями i и j иона, вызванного электронным ударом; A_{ij} — вероятность радиационного перехода i–j.

Анализ показал, что можно выделить две различные области электронной плотности, для которых достаточно легко найти выражение для населенности состояний 1 и 2. Первая область определяется условием

$$N_e < A_{21}/\langle \upsilon\sigma_{21} \rangle, \quad (2)$$

вторая условием

$$A_{21}/\langle \upsilon\sigma_{21} \rangle N_e < A_{10}/\langle \upsilon\sigma_{34} \rangle, \quad (3)$$

где $\langle \upsilon\sigma_{34} \rangle$ — усредненное сечение перехода между всеми уровнями с главными квантовыми числами n = 3 и 4.

При выполнении условия (2), соответствующего случаю так называемой чистой короны [13], основной вклад в заселение вносят процессы

возбуждения $3s$- и $3p$-состояний электронным ударом из основного состояния с учетом каскадного заселения и радиационные переходы $3p$–$3s$ и $3s$–$2p$. В этой области значений электронной плотности величина инверсии определяется выражением

$$\Delta N_{21} = \frac{N_2}{g_2} - \frac{N_1}{g_1} = N_0 N_e \left(\frac{\langle \upsilon\sigma_{02} \rangle}{g_2 A_{21}} - \frac{\langle \upsilon\sigma_{01} \rangle + \langle \upsilon\sigma_{02} \rangle}{g_1 A_{10}} \right), \quad (4)$$

где g_i — статистический вес i-го уровня. Учет вышележащих состояний с главными квантовыми числами $n = 4, 5$ приводит к тому, что для ионов низкой кратности ионизации ($A_{21} \approx A_{10}$) в области чистой короны инверсия может отсутствовать. В случае ионов высокой кратности ионизации ($z > 30$, $A_{10} >> A_{21}$) уровни $3s$ и $3p$ могут быть инверсно населены, однако абсолютная величина инверсии оказывается очень малой.

При выполнении условия (3), когда основную роль в переходах между $3s$ и $3p$ состояниями играют неупругие столкновения электронов и ионов, выражение для величины инверсии имеет вид

$$\Delta N_{21} = \frac{N_0}{g_1} \frac{\langle \upsilon\sigma_{02} \rangle}{\langle \upsilon\sigma_{12} \rangle} = \frac{N_e}{z g_1} \frac{\langle \upsilon\sigma_{02} \rangle}{\langle \upsilon\sigma_{12} \rangle}. \quad (5)$$

Ограничение на существование инверсии со стороны больших электронных плотностей связано с включением состояний $2p^{m\text{-}1}3s$ и $2p^{m\text{-}1}3p$ в термальную зону с больцмановским распределением ионов по возбужденным состояниям. Расчеты показали, что инверсия достигает максимального значения при

$$N_e^{\text{опт}} \approx 0{,}1 N_e^{\text{кр}}, \text{ где } N_e^{\text{кр}} = A_{10} / \langle \upsilon\sigma_{34} \rangle.$$

Время существования инверсии на переходе $3s$–$3p$ может быть довольно значительным, так как определяется в основном временем перехода в состояние следующей кратности ионизации. Однако для получения максимально возможной инверсии необходимо, чтобы нагрев электронов происходил достаточно быстро, причем в начальный момент ионы должны находиться в основном состоянии. Поэтому электронная температура, определяющая заселение возбужденных состояний, должна быть мала по сравнению с энергией возбуждения рабочих состояний. Это позволяет сделать выбор среди всех конфигураций типа $2p^m$ при использовании лазерной плазмы в качестве активной среды. Известно, что в разлетающейся плазме происходит довольно быстрая рекомбинация ионов по степеням ионизации, причем наиболее долгоживущими являются неоноподобные ионы с конфигурацией $2p^6$. Вызвано это скачком потенциала ионизации при переходе от ионов с внешней L-оболочкой к ионам с M-электронами. Поэтому неоноподобные ионы являются наиболее удобными в данном случае.

В таблице приведены результаты расчетов коэффициента усиления на переходе 3*s*–3*p* для некоторых ионов. Величины атомных констант рассчитаны с помощью данных [14]. В таблице приведены значения оптимальной электронной плотности $N_e^{\text{опт}}$ энергии 3*s*–3*p*-перехода ΔE, длина волны того же перехода λ, коэффициент усиления α и потенциал ионизации иона *I*. Электронная температура в расчетах была выбрана равной половине потенциала ионизации соответствующего иона. Как видно из таблицы, в диапазоне длин волн 300–700 Å можно рассчитывать на получение существенных коэффициентов усиления.

Коэффициент усиления на переходе 3s–3p для Ne-подобных ионов

Ион	$N_e^{\text{опт}} = 0{,}1N_e^{\text{кр}}$ 10^{20} см$^{-3}$	$\Delta E(3s-3p)$, эВ	λ, Å	α, см$^{-1}$	I, эВ
SVII	0,2	17,5	700	7	281
KX	1,5	21,7	570	15	502
TiXIII	10	29,0	430	25	787
MnXVI	30	37,0	330	40	1136

3. Оценим энергию УКИ, необходимую для нагрева плазменного шнура при оптимальном значении электронной плотности. Для иона КХ $N_e^{\text{опт}} = 1{,}5 \cdot 10^{20}$ см$^{-3}$, плазму необходимо нагреть до температуры 250 эВ. Пусть для нагрева используется излучение неодимового лазера с длительностью импульса 10^{-11} с и сечением пучка 10^{-3} см^2. С помощью формулы (7) из работы [4] находим, что необходимая энергия импульса составляет 5 Дж.

При оценке величины инверсии следует учесть также, что если плазма содержит достаточно большое количество Na-подобных ионов с основным состоянием $1s^22s^22p^63s$, то импульсный нагрев приведет к усилению процессов типа $1s^22s^22p^63s + e^- \rightarrow 1s^22s^2p^53s + e^- + e^-$. Расчет показал, что в плазме, содержащей равное количество Ne- и Na-подобных ионов калия, указанный выше процесс может уменьшить величину инверсии не более чем на 20%.

4. Для продвижения в область $\lambda < 300$ Å необходимо использовать ионы более высокой кратности ионизации. Однако анализ ситуации, возникающий при переходе к очень высоким зарядам ионов, весьма затруднителен. Это вызвано исключительно сильным вкладом релятивистских взаимодействий в энергетическую структуру ионов и вероятности переходов для высоких *z* [15]. Во-первых, из-за большой величины спин-орбитального взаимодействия при $z \gtrsim 60$ происходит перегруппировка уровней так, что, по нашему мнению, в противоположность выводу работы [12], становится невозможным выделить

группы уровней, относящиеся к возбуждению электрона в 3*s*-, 3*p*- или 3*d*-состояние. Во-вторых, радикальным образом меняется соотношение вероятностей переходов между этими состояниями и основным состоянием, а также величины скоростей возбуждения каждого из этих состояний. Поэтому вопрос о создании инверсии в области $\lambda<300$ Å на неоноподобных ионах остается пока неясным.

5. Таким образом, метод двухступенчатого нагрева плазмы [4] дает возможность получить инверсию на 3*s*–3*p*-переходе в ионах с основной конфигурацией $1s^2 2s^2 2p^6$. По проведенным оценкам предлагаемая схема позволяет получить коэффициент усиления $\alpha = 10 – 25$ см$^{-1}$ для длин волн $700 > \lambda > 300$ Å и может быть использована для создания лазера в этой области спектра.

Литература

1. *Duguay M.-A., Rentzepis P.M.* // Appl. Phys. Letts. 1967. Vol. 10. P. 350.
2. *Станкевич Ю.Л.* // ДАН СССР. 1970. Т. 191. С. 805.
3. *Malozzi P.J., Epstein K.M., Jung R.C., Appelbaum D.C., Fairand P.P., Gallagher W.J.* In Fundamental and Applied Laser Physics. Proceedings of Efsahan Symposium, Sept., 1971. Ed. by M. S. Feld, A. Javan, N. Kurnn. N.Y. John Wiley and Sons, 1973. P. 165.
4. *Knyazev I.N., Letokhov V.S.* // Optics Comm. 1971. Vol. 3. P. 332; Оптика и спектроскопия. 1972. Т. 23. С. 110.
5. *Виноградов А.В., Собельман И.И.* // ЖЭТФ. 1972. Т. 63. С. 2113.
6. *Bristow T.C., Lubin M.J., Foesyth J.M., Goldman E.B., Soures J.M.* // Optics Comm. 1972. Vol. 5. P. 315.
7. *Carillon A., Jamelot G., Sorean A., Jeagle P.*//Phys. Rev. Letts. 1972. 38A. P. 2.
8. *Bohn W.L.* // Appl. Phys. Letts. 1974. Vol. 24. P. 15.
9. *Кононов Э.Я., Кошелев К.Н.* // Квантовая электроника. 1974. Т. 1. С. 2411.
10. *Shipman J.D.* // Appl. Phys. Letts. 1967. Vol. 10. P. 3.
11. *Антонов В.С., Князев И.Н., Летохов В.С., Мовшев В.Г.* // Письма в ЖЭТФ. 1973. Т. 17. С. 545.
12. *Duguay M.-A.* Report on Laser Physics School. Erice, Sicily, 1973; Laser Focus. 1973. Vol. 9. P. 41.
13. *Макуиртер Р.* Диагностика плазмы / под ред. Ходдлстоуна и С. Леонарда. М.: Мир, 1967.
14. *Вайнштейн Л.А., Собельман И.И., Юков Е.А.* Сечения возбуждения атомов и ионов электронами. М.: Наука, 1943.
15. *Иванова Л.Н., Рабинькина И.В., Сафронова У.И.* Препринт ИСАН. 1974. № 14.

Квант. электроника. 1981. Т. 8 (1). С. 88–97

ПОИСКИ УСИЛЕНИЯ В ДАЛЕКОЙ ВУФ ОБЛАСТИ НА ПЕРЕХОДАХ МНОГОЗАРЯДНЫХ ИОНОВ В ПРОТЯЖЕННОЙ ЛАЗЕРНОЙ ПЛАЗМЕ

А.Н. Жерихин, К.Н. Кошелев, П.Г. Крюков, В.С. Летохов, С.В. Чекалин
Институт спектроскопии АН СССР

С целью поиска усиления на переходах многозарядных ионов в протяженной плазме исследованы спектры плазменного шнура, создаваемого субнаносекундными лазерными импульсами на различных мишенях. Обнаружены аномалии в поведении интенсивности ряда линий NaIX и CVI при наблюдении вдоль оси шнура. Показано, что эти аномалии можно интерпретировать как следствие усиления на переходах 2p–4d, 2p–3d и 2s–3p иона NaIX и на переходе 3–4 иона CVI.

1. Введение

Проблема получения лазерного эффекта в диапазоне вакуумного ультрафиолета (ВУФ) и мягкого рентгена привлекает внимание исследователей уже более десятилетия. Однако, несмотря на усилия целого ряда исследовательских групп, она еще весьма далека от решения. Ключевым этапом в этой проблеме является создание активной среды. Самым подходящим материалом является высокотемпературная плазма, поскольку она обладает значительной прозрачностью в требуемом диапазоне длин волн и, кроме того, энергетические интервалы между уровнями ионов высокой кратности ионизации лежат в ВУФ и рентгеновском диапазоне. Все это позволяет рассчитывать на использование этих уровней в качестве рабочих. Весьма перспективным представляется использование лазерной плазмы, так как в этом случае можно обеспечить требуемую очень высокую скорость накачки.

Теоретическому рассмотрению различных схем создания усиливающих сред на базе лазерной плазмы посвящено большое число публикаций (см. обзоры [1–2]), однако экспериментальная их реализация встречает серьезные трудности. Одна из главных трудностей связана с тем, что во всех предложенных схемах, отвечающих реальным условиям эксперимента, для достижения лазерного эффекта необходимо создавать плазму с помощью весьма мощных лазеров. Действительно, лазер должен обладать, с одной стороны, большой

мощностью для обеспечения высокой скорости энерговклада в плазму, а с другой стороны — достаточной энергией, чтобы можно было создать высокотемпературную плазму большой протяженности. Последнее требование связано с тем очевидным условием, что только в протяженной активной среде можно достичь усиления на один проход, достаточного для возникновения лазерного эффекта. Усиление на проход в безрезонаторной схеме должно для этого превышать 10^9. Оценки, основанные на экспериментальных данных [3], показывают, что для достижения лазерного эффекта на переходе 3–2 (λ = 18,2 Å) иона CVI лазерный импульс, создающий плазму, должен обладать энергией в несколько сот джоулей при длительности около 10^{-10} с. Требование к величине усиления на проход можно существенно ослабить благодаря использованию резонатора [2], но практическая реализация этого чрезвычайно сложна. Во-первых, отсутствуют зеркала с достаточно высоким коэффициентом отражения в области ВУФ и мягкого рентгена; во-вторых, время существования инверсии в плазме слишком мало, чтобы обеспечить достаточное число проходов между зеркалами. Лишь в одном эксперименте [4] удалось зарегистрировать излучение с высокой направленностью в диапазоне длин волн ~600 Å от лазерной плазмы, помещенной в резонатор.

Ввиду трудностей, связанных с постановкой экспериментов по непосредственному наблюдению лазерного эффекта, используются альтернативные методы поиска активной среды. В большинстве опубликованных экспериментальных работ сообщается о наблюдении инверсии между возбужденными уровнями многозарядных ионов [5–9]. В исследованиях такого рода наличие инверсии регистрируется по отношению интенсивностей спектральных линий, не принадлежащих инвертированному переходу. При этом используется небольшой объем оптически тонкой плазмы, так что требования к энергии нагревающего лазерного импульса довольно скромны. Именно поэтому этот метод использован в большинстве опубликованных работ. Кроме того, он позволяет регистрировать очень малую инверсную населенность. Это, в свою очередь, дает возможность следить за тенденциями изменения инверсной населенности при изменении условий нагрева и таким образом подбирать оптимальные условия. Но существование инверсии не означает существования усиления в плазме, которое определяется величиной инверсии.

Непосредственное обнаружение усиления возможно в протяженной среде, даже если ее длина много меньше требуемой для возникновения лазерного эффекта. В этом случае исследуется поведение именно тех линий, на которых можно получить лазерный эффект. Такая постановка задачи является следующим приближением к схеме реального лазера.

В настоящей работе излагаются результаты экспериментов, проведенных с целью обнаружения усиления в плазменном шнуре. Спектры такого шнура исследовались при различных условиях. Мы рассчитывали зарегистрировать усиление по возрастанию интенсивности линий, соответствующих инвертированным переходам, при наблюдении спектра вдоль оси шнура.

2. Экспериментальная установка

Для создания и нагрева плазмы использовался лазер с задающим генератором на АИГ: Nd^{3+} и многокаскадным усилителем на неодимовом стекле [10]. Энергия лазерного импульса составляла 8–10 Дж, длительность 0,25 нс, расходимость излучения 0,3 мрад. С помощью системы оптических задержек выходной импульс преобразовывался в пару импульсов с соотношением энергий 1:10. Вначале на мишень посылался более слабый импульс для создания плазмы с малой электронной температурой, затем через время Δt — более мощный импульс, служащий для окончательного разогрева плазмы. Задержка Δt могла варьироваться от 0 до 5 нс. При этом за счет разлета изменялась электронная плотность рабочего объема плазмы. Изменение электронной температуры плазмы могло осуществляться изменением интенсивности лазерного излучения. Таким образом, мы имели возможность подобрать лучший с точки зрения получения усиления режим.

Для создания плазменного шнура излучение лазера фокусировалось на мишень при помощи цилиндрических линз с фокусным расстоянием $f = 1$ и 0,5 м и четырехкомпонентного объектива, исправленного на сферическую аберрацию, с $f = 45$ мм. Для регистрации спектров плазмы использовались спектрографы скользящего падения ДФС-6 или Е-580. Мишень помещалась в вакуумную камеру, закрепленную на спектрографе. Расстояние от мишени до щели спектрографа было около 10 см. Для получения одного спектра достаточно было 7–10 лазерных вспышек.

3. Наблюдение аномалий интенсивности спектральных линий иона NaIX

Ранее мы сообщали о наблюдении аномалий интенсивности ряда линий в области 58–78 Å в спектрах плазменного шнура, создаваемого парой мощных субнаносекундных лазерных импульсов при фокусировке на поверхность кристалла KCl [11]. В этой работе наблюдалось значительное (до пяти крат) увеличение относительной интенсивности некоторых линий в спектре при наблюдении вдоль оси плазменного шнура по сравнению с наблюдением поперек оси. Линиями сравнения служили резонансные переходы в Ne-подобном ионе ClVIII (58,67 и 59,19 Å), для которых отсутствовали признаки эффектов поглощения при любой из геометрий наблюдения. Кроме того, при нагреве плазмы одиночным импульсом длительностью 1,2 нс интенсивность линии 58,2 Å возрастала не менее чем в пять раз при увеличении длины шнура от 1,5 до 3 мм, причем плотность потока излучения на мишени поддерживалась одинаковой ($\sim 10^{13}$ Вт/см^2).

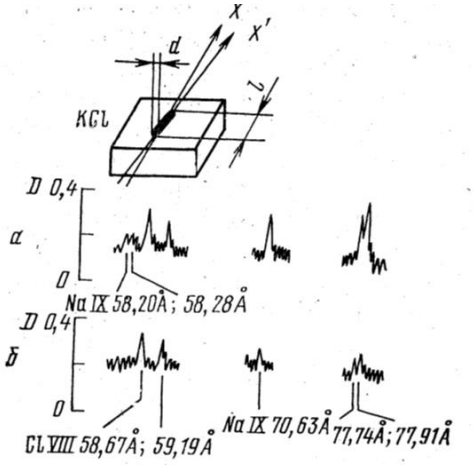


Рис. 1. Денситограммы спектров плазменного шнура, наблюдаемых вдоль оси X(*а*) и под углом 15° к оси X (X')(*б*). Вверху мишень из KCl, $d\sim100$ мкм, $l=5$ мм, $\Delta t=0{,}6$ нс

Линии с аномальным поведением были ошибочно приписаны в [11] переходам из автоионизационных состояний ClVII. В действительности, как было указано в [12], они принадлежат переходам 2*p*–4*d* (58,2 и 58,28 Å), 2*p*–3*d* (77,14 и 77,91 Å) и 2*s*–3*p* (70,63 Å) Li-подобного иона NaIX. Наличие линий NaIX в спектре обусловлено, как выяснилось, малой (< 0,3%) примесью Na в кристаллах KCl, использовавшихся в качестве мишени [13]*.

В настоящей работе мы продолжили изучение эффекта, наблюдаемого нами в [11], и попытались создать модель механизма возникновения инверсии населенности на переходах NaIX.

3.1. Экспериментальные данные. Изучение лазера, аналогичного использованному в [11], фокусировалось на поверхность мишени в пятно размерами 0,1 × (2,5 – 5) мм. Спектры плазменного шнура регистрировались спектрографом Е-580. Положение плазменного шнура относительно оси спектрографа контролировалось с точностью 10 мкм.

В первой серии экспериментов проводилось сравнение спектров плазменного шнура, полученных при наблюдении вдоль его оси и под сравнительно малым (15°) углом к ней (рис. 1). Как видно из рис. 1, при наблюдении вдоль оси пятимиллиметрового плазменного шнура относительные интенсивности вышеуказанных линий NaIX увеличиваются. Возрастание максимально для линий 2*p*–4*d*. Сравнение спектров, полученных при различных длинах плазменного шнура (рис. 2), показывает, что при увеличении его длины от 2,5 до 5 мм относительная интенсивность линий 2*p*–4*d* возрастает по крайней мере в три раза.

* Авторы признательны А.В. Зыбину за помощь в определении концентрации Na в использовавшихся кристаллах KCl.

Нормировка спектров, как и в [11], проводилась по резонансным линиям ClVIII $2p^6\ ^1S_0$-$2p^5 3s\ ^1P_1$; $2p^6\ ^1S_0$-$2p^5 3s\ ^3P_1$, отношение интенсивностей которых не зависело от направления наблюдения, а общая интенсивность оставалась постоянной в пределах воспроизводимости экспериментов. Для контроля нормировки использовались линии 2–2' переходов ClIX, ClX, KXI, соотношение интенсивностей которых также не зависело от направления наблюдения.

Эти спектры, в которых подтвердились аномалии интенсивностей, были получены при использовании одной и той же мишени. Кроме того, во избежание влияния возможных неоднородностей в распределении примеси Na по кристаллу KCl, спектры снимались таким образом, что кратеры одной серии располагались на мишени в промежутках между кратерами другой серии. Результаты экспериментов показывают, что полностью воспроизвести условия опытов [11] не удалось, так как аномалии в настоящих экспериментах наблюдались лишь при длине плазменного шнура 5 мм.

При использовании мишени из NaCl в спектрах плазменного шнура, снятых вдоль его оси, наблюдались интенсивные линии NaIX. Однако в этом случае их относительная интенсивность возрастала при уменьшении длины шнура, что, по-видимому, вызвано поглощением в плазме на переходах NaIX.

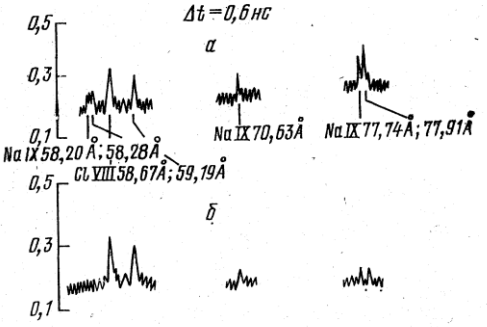


Рис. 2. Денситограммы спектров плазменного шнура, наблюдаемых вдоль его оси при длине шнура l=5 (*а*) и 2,5 мм (*б*)

3.2. Интерпретация данных. Полученные данные позволяют рассматривать в качестве одной из возможных причин наблюдаемых аномалий существование усиления на переходах $2p$–$4d$ и, возможно, $2p$–$3d$ и $2s$–$3p$ иона NaIX. Попытка построить модель возникновения инверсии между уровнем $4d$ и близким к основному состоянию уровнем $2p$ (ΔE = 17,7 эВ) связана с известными трудностями. Однако учет процессов фотоионизации в неоднородной лазерной плазме позволяет построить такую модель.

Инверсия может создаваться следующим образом. Первый (более слабый) лазерный импульс создает вблизи поверхности мишени плазму, плотность которой вследствие разлета падает до $N_e = (5 - 10)\cdot 10^{20}$ см$^{-3}$ к моменту прихода второго импульса [14]. Радиационное охлаждение на L-ионах Cl и K может существенно понизить электронную температуру плазмы T_e [7], так что на расстоянии 100–200 мкм от поверхности мишени она составляет 30. Эти спектры, в которых подтвердились аномалии интенсивностей, были получены при использовании одной и той же мишени. Кроме того, во избежание влияния возможных неоднородностей в распределении примеси Na по кристаллу KCl, спектры снимались таким образом, что кратеры одной серии располагались на

мишени в промежутках между кратерами другой серии. Результаты экспериментов показывают, что полностью воспроизвести условия опытов [11] не удалось, так как аномалии в настоящих экспериментах наблюдались лишь при длине плазменного шнура 5 мм 50 эВ. При электронной плотности $N_e = 5 \cdot 10^{20}$ см$^{-3}$ возбужденные состояния Li-подобного иона NaIX (n = 3, 4) оказываются захваченными в термальную зону, так что их населенности N^*_{IX} описываются уравнением Саха — Больцмана по отношению к населенности основного состояния Не-подобного иона NaX N_X:

$$\frac{N^*_{IX}}{g^*_{IX}} = N_e N_x \frac{1}{g_x}\left(\frac{h^2}{2\pi m}\right)^{3/2} \frac{\exp(\Delta E/kT_e)}{2(kT_e)^{3/2}}, \quad (1)$$

где ΔE — энергия возбужденного состояния, отсчитанная от границы ионизации; g — статистический вес соответствующего состояния. Отметим, что даже при интенсивной ударно-радиационной рекомбинации инверсия населенности по отношению к основному состоянию не возникает.

Под действием второго, существенно более мощного лазерного импульса вблизи мишени образуется горячее «ядро», нагретое до температуры 0,5 кэВ. Фотоионизация коротковолновым излучением горячего ядра может существенно изменить ионизационное равновесие во внешней «холодной» плазме лазерного факела. Тогда ионизационное равновесие в этой зоне будет описываться уравнением Саха с эффективной температурой T_ν, определяемой температурой излучения горячего ядра и геометрией разлета:

$$\frac{N_{IX}}{g_{IX}} = \frac{N_e N_x}{g_x}\left(\frac{h^2}{2\pi m}\right)^{3/2} \frac{\exp(I/kT_\nu)}{2(kT_\nu)^{3/2}}. \quad (2)$$

Из сравнения (1) и (2) следует соотношение для приведенных населенностей основного и возбужденного состояния:

$$\frac{N^*_{IX}}{g^*_{IX}} = \frac{N_{IX}}{g_{IX}} = \left(\frac{T_\nu}{T_e}\right)^{3/2} \exp\left(\frac{\Delta E}{kT_e} - \frac{I}{kT_\nu}\right), \quad (3)$$

Для рассматриваемого иона NaIX с потенциалом ионизации I = 300 эВ и глубиной залегания возбужденного (n = 4) уровня ΔE = 70 эВ инверсная населенность в плазме с $T_e \sim 30$ эВ возникает при $T_\nu \sim 150$ эВ. При расчете абсолютной величины инверсии и коэффициента усиления следует иметь в виду, что в результате фотоионизации значительная часть ионов натрия находится в основном состоянии Не-подобного NaX. Оценки показывают, что при $N_e = 5 - 10 \cdot 10^{20}$ см$^{-3}$, T_e = 30–40 эВ и $T_\nu \sim 150$ эВ возможно достижение коэффициента усиления $\varkappa \sim 1$–5 см$^{-1}$ на переходе $2p$–$4d$ (58,2 Å) NaIX. Время существования инверсии определяется временем выравнивания T_e и T_ν, обусловленного теплопроводностью плазмы.

Тот факт, что при использовании мишени из NaCl линии NaIX не проявляют аномалий в поведении интенсивностей, объясняется в рамках описанной модели отсутствием в плазме *L*-ионов К. Замена калия на натрий приводит к существенному снижению скорости радиационного охлаждения плазмы, так как натрий в условиях эксперимента существует в основном в виде Не-подобных ионов, которые не обеспечивают эффективного охлаждения [15]. Кроме того, для ионов калия суммарная интенсивность линейчатого излучения, способного ионизовать NaIX, существенно превышает соответствующую величину для ионов Na.

Для эффективного действия изложенного механизма создания инверсии плазменный факел должен быть сильно неоднородным: в нем должны присутствовать области высокой и низкой T_e, расположенные достаточно близко друг от друга. Распределение T_e по плазменному факелу задается угловым распределением нагревающего лазерного излучения, так что от этого фактора может существенно зависеть величина инверсии, а также интенсивность линий NaIX в спектре. В связи с этим следует отметить, что используемый нами лазер работал в предельном режиме, когда его выходная яркость ограничивается мелкомасштабной самофокусировкой излучения в усиливающих каскадах [10]. В этих условиях самофокусировка очень существенно влияет на угловые характеристики выходного излучения лазера, приводя к образованию вокруг коллимированного лазерного луча ореола с много меньшей направленностью [10]. Мелкомасштабная самофокусировка является трудноконтролируемым процессом, так что доля энергии, заключенная в ореоле, а также его угловое распределение зависят от таких причин, как взаимное расположение усилительных каскадов, сорт и качество материала активных элементов, наличие в них объемных и поверхностных повреждений и т.д. В установке, использованной в [11], в апертуру фокусирующей системы попадала значительно бóльшая доля энергии ореола, чем в настоящих экспериментах. Весьма возможно, что именно этим обстоятельством объясняется тот факт, что в спектрах [11] линии NaIX были ярче и аномальное поведение их интенсивностей проявлялось при длине плазменного шнура 1,5 мм.

Аномальные линии NaIX соответствуют переходам в основное состояние 2*s* или близкое к основному 2*p*, поэтому не исключена возможность того, что их интенсивность определяется эффектами поглощения. Такое положение действительно имеет место в плазме NaCl. При интерпретации результатов, полученных с мишенью из KCl, возникает более сложная ситуация. Зависимость интенсивностей NaIX от направления наблюдения (рис. 1) может быть, в принципе, объяснена поглощением в зоне разлета, как это было сделано в работах [16–18] для объяснения результата [19]. Однако нам не удалось объяснить эффектами поглощения нелинейного роста интенсивности перехода 2*p*–4*d* при удлинении плазменного шнура (рис. 2).

4. Аномалии интенсивности перехода 3–4 H-подобного иона CVI

В литературе рассмотрено довольно большое число схем, предсказывающих возникновение инверсии между возбужденными уровнями ионов в лазерной плазме [1–3, 5–9, 15, 20–22]. Одной из наиболее удобных в этом отношении атомных структур представляются водородоподобные ионы, в частности CVI. В отличие от случая, рассмотренного в п. 3, поглощение на инвертированных переходах водородоподобных ионов в холодной зоне плазмы должно заведомо отсутствовать, что значительно облегчает интерпретацию результатов.

4.1. Возможный механизм создания инверсии. Хорошо известно, что в переохлажденной рекомбинирующей плазме возможны условия, при которых уровни многозарядных ионов инверсно заселены (см., например, [20–22]). Инверсная населенность для уровней $n = 2, 3, 4$ иона CVI наблюдалось в работах [5, 6] при разлете лазерной плазмы на расстоянии ~3 мм от мишени, причем возникновение эффекта было связано с охлаждением и «закалкой» плазмы при разлете. Из-за весьма низкой плотности лазерной плазмы вдали от мишени абсолютная величина инверсии была крайне мала ($\sim 10^{11}$ см$^{-3}$) и соответствовала коэффициенту усиления на переходах в области 130. Эти спектры, в которых подтвердились аномалии интенсивностей, были получены при использовании одной и той же мишени. Кроме того, во избежание влияния возможных неоднородностей в распределении примеси Na по кристаллу KCl, спектры снимались таким образом, что кратеры одной серии располагались на мишени в промежутках между кратерами другой серии. Результаты экспериментов показывают, что полностью воспроизвести условия опытов [11] не удалось, так как аномалии в настоящих экспериментах наблюдались лишь при длине плазменного шнура 5 мм 180 Å $\varkappa \sim 10^{-5}$. Эти спектры, в которых подтвердились аномалии интенсивностей, были получены при использовании одной и той же мишени. Кроме того, во избежание влияния возможных неоднородностей в распределении примеси Na по кристаллу KCl, спектры снимались таким образом, что кратеры одной серии располагались на мишени в промежутках между кратерами другой серии. Результаты экспериментов показывают, что полностью воспроизвести условия опытов [11] не удалось, так как аномалии в настоящих экспериментах наблюдались лишь при длине плазменного шнура 5 мм 10^{-6} см$^{-1}$. Очевидно, что при столь малом коэффициенте усиления линейные размеры плазмы и соответственно мощность возбуждающего лазерного излучения, необходимые для наблюдения нелинейных эффектов, представляются фантастическими. В работе [15] было показано, что использование для охлаждения плазмы излучения ионов с низкоэнергетическими резонансными состояниями (например, ионов с заполняющейся *L*-оболочкой) позволяет эффективно охлаждать плазму достаточно близко от мишени, так что процесс рекомбинации идет при высоких плотностях плазмы (10^{20}–10^{21} см$^{-3}$). Экспериментальное изучение спектров Li-подобных ионов AlXI [7] показало, что инверсия на

переходе 3–4 (λ~150 Å) имеет место вблизи мишени на расстояниях больше 50 мкм и соответствует коэффициенту усиления ~0,1 см$^{-1}$.

В связи с этим представлялось весьма перспективным использовать наиболее выгодную атомную схему H-подобных ионов, обеспечив охлаждение за счет излучения L-ионов более тяжелых элементов (в нашем эксперименте Cl и K). Высокий потенциал ионизации *L*-ионов K и Cl (0,5–1 кЭв) позволяет им существовать в плазме одновременно с H-подобными ионами CVI (I ~ 490 эВ) и эффективно охлаждать плазму после окончания возбуждающего лазерного импульса.

Выбор ионов Cl в качестве охлаждающей примеси особенно удобен в связи с тем, что у ионов ClXV и CVI имеются две пары совпадающих линий [23] (рис. 3):

$$\text{ClXV } 1s^2\,2p^2\,P_{3/2}\text{-}1s^2\,3d\,^2D_{3/2}\ (\lambda = 28{,}42\ \text{Å}) - \text{CVI } 1 - 3\ (\lambda = 28{,}466\ \text{Å}),$$

$$\text{ClXV } 1s^2\,2s\,^2S_{1/2}\text{-}1s^2\,3p\,^2P_{3/2}\ (\lambda = 26{,}67\ \text{Å}) - \text{CVI } 1 - 4\ (\lambda = 26{,}99\ \text{Å}).$$

При достаточной интенсивности линий ClXV такое совпадение может служить причиной возникновения или увеличения инверсии между уровнями n = 2 и n = 3, 4 иона CVI. Механизм резонансной накачки был предложен в работе [24] и экспериментально исследован на совпадающих парах H- и He-подобных ионов магния и углерода [8]. Оценки показывают, что рассогласование ~5,5 эВ для пары (26,67 Å – 26,99 Å) не препятствует резонансной накачке из-за сильного штарковского сдвига и уширения перехода 1–4 CVI в плазме с ионной плотностью ~10^{20} см$^{-3}$.

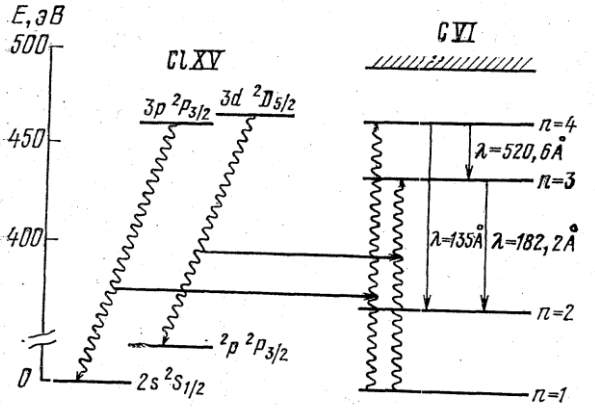


Рис. 3. Схема создания инверсии населенности при накачке уровней иона CVI излучением иона ClXV

Отметим, что «накачивающие» переходы ClXV являются одним из основных каналов ударно-радиационной рекомбинации ClXVI–ClXV и поэтому могут обладать значительной интенсивностью в плазме с электронной температурой, недостаточной для возбуждения этих переходов из основного состояния электронным ударом.

Оба описанных выше механизма создания инверсии весьма чувствительны к параметрам плазмы — электронной температуре и плотности [24, 25]. Мы уже отмечали, что задержка охлаждения приводит к резкому уменьшению абсолютной величины «рекомбинационной» инверсии. С другой стороны, при охлаждении плазмы в непосредственной близости от мишени, когда ее плотность достаточно велика ($N_e \sim 10^{22}$ см$^{-3}$), быстрая рекомбинация не влечет за собой создания инверсии из-за большой роли столкновительных переходов между уровнями. Известно также, что и механизм резонансной накачки требует подбора оптимальных параметров плазмы [8], например, из-за чувствительного к плотности штарковского сдвига линий пары совпадений. Как указывалось выше, подбор оптимальных параметров плазмы может быть осуществлен при использовании двух импульсов с варьируемой задержкой и интенсивностью.

Оценки показывают, что в условиях реального эксперимента каждый из указанных механизмов может обеспечить коэффициент усиления $\varkappa \sim 10$ см$^{-1}$ [24, 25]. Кроме того, как показано в работе [8], оба механизма могут действовать одновременно. Поэтому можно было рассчитывать на регистрацию эффектов усиления при длине плазменного шнура 1,5 мм. В наших экспериментах указанием на усиление излучения на инвертируемых переходах служило изменение отношения интенсивностей двух линий с общим верхним уровнем: перехода 2–4 ($\lambda = 135$ Å) и 3–4 ($\lambda = 520{,}6$ Å) в ионе CVI.

4.2. Эксперимент с ионом CVI. Для реализации изложенных механизмов создания инверсии необходимо одновременное присутствие в плазме ионов углерода, хлора и калия. В наших экспериментах использовалась слоистая мишень, предложенная в [24]. В такой мишени рабочее вещество (углерод) помещается в тонком поверхностном слое, нанесенном на подложку из материала, ионы которого используются для накачки или охлаждения плазмы. Величина инверсии весьма критична к толщине слоя рабочего вещества. Если этот слой слишком тонок, то в образовавшейся плазме будет содержаться малое количество рабочих ионов и нельзя будет достичь высоких значений инверсии. При слишком толстом слое за время действия лазерного импульса не успеет испариться достаточное количество материала подложки, что приведет к уменьшению скорости охлаждения и интенсивности излучения накачки, а это, в свою очередь, приведет к падению абсолютного значения инверсии.

В наших экспериментах использовалась подложка из кристалла KCl. Нанесение прочного слоя чистого углерода нужной толщины на ее поверхность оказалось чрезвычайно сложным, поэтому мы решили использовать какое-либо вещество с большим содержанием углерода, наносимое на поверхность мишени в виде пленки. Наиболее подходящей для этой цели оказалась вакуумная

смазка. Она растворялась в бензине, затем капля раствора наносилась на поверхность мишени и высушивалась. К сожалению, мы не могли контролировать толщину получающейся пленки; критерием правильно подобранной толщины пленки служило одновременное присутствие в спектре плазмы достаточно интенсивных линий ионов материала как пленки, так и подложки. Для грубой оценки толщины пленки были сняты спектры плазмы пленок железа различной толщины, нанесенных на стеклянную подложку. Линии ионов кремния и железа наблюдались в спектрах одновременно при толщине слоя от 50 до 500 нм. Из этого мы заключили, что правильно подобранная толщина пленки в экспериментах составляла несколько сотен нанометров.

Невозможность контролировать толщину пленки не позволила сравнить спектры при наблюдении вдоль и поперек оси плазменного шнура, так как при такой постановке эксперимента пришлось бы сравнить спектры, полученные на разных мишенях. Выполнить же две серии измерений на одной мишени не представлялось возможным, поскольку при каждой лазерной вспышке пленка испаряется с большой площади вокруг кратера и для получения двух спектров достаточной яркости не хватает поверхности мишени. Поэтому надежная информация могла быть получена только из сравнения интенсивностей линий CVI в одном и том же спектре, снятом вдоль оси плазменного шнура.

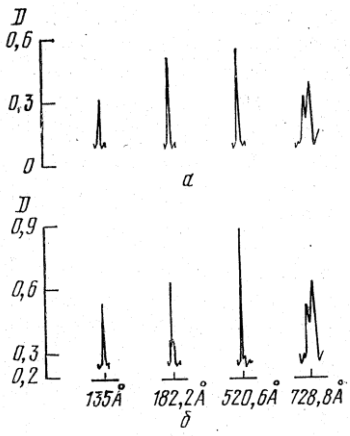


Рис. 4. Денситограммы спектров оптически тонкой плазмы CVI (*а*) и плазмы слоистой мишени при наблюдении вдоль оси 1,5-миллиметрового плазменного шнура (*б*)

В экспериментах сравнивались интенсивности линий, соответствующих переходам 4–3, 4–2 и 3–2 иона CVI, при наблюдении вдоль оси 1,5 мм плазменного шнура. Оказалось, что соотношение этих интенсивностей одинаково в спектрах углеродной мишени и в спектрах мишени из KCl с толстой пленкой смазки (линии K и Cl отсутствовали). Это соотношение не менялось при укорачивании плазменного шнура вдвое. Кроме того, отношение интенсивностей спектрально разрешенных компонент перехода 2–3 указывает на его опти-

ческую прозрачность во всех полученных спектрах. Все это говорит об оптической прозрачности плазмы для вышеуказанных переходов в названных случаях (спектр приведен на рис. 4*а*). При использовании мишени из KCl с оптимально подобранной толщиной пленки (см. выше) было зарегистрировано увеличение отношения I_{34}/I_{24} в 1,5 раза (рис. 4*б*). Ошибки измерения интенсивностей в спектрах не превышали 15%.

Увеличение отношения I_{34}/I_{24} может быть связано как с эффектами усиления на этих переходах (при равных величинах инверсной населенности коэффициент усиления $\varkappa_{34}$ примерно в 30 раз превышает $\varkappa_{24}$), так и с дополнительным поглощением излучения на переходе 2–4, которое могло бы возникнуть из-за каких-либо изменений в населенностях уровней CVI в многокомпонентной плазме. Однако отсутствие следов поглощения в дублете перехода 2–3, таких как выравнивание интенсивностей линий дублета, указывает, что и переход 2–4 не обладает поглощением в плазме.

Таким образом, существуют основания полагать, что увеличение отношения I_{34}/I_{24} вызвано усилением на переходе 3–4. Зарегистрированное возрастание интенсивности I_{34} соответствует коэффициенту усиления $\varkappa \sim 6$ см$^{-1}$.

5. Заключение

Эксперименты с плазменным шнуром показали, что в протяженной лазерной плазме возможны создание и регистрация усиления в диапазоне ВУФ и мягкого рентгена. Данные по аномальному поведению интенсивностей линий NaIX и модельные оценки показывают, что такое поведение может быть связано с возникновением усиления на переходах 2*p*–4*d* и, возможно, 2*p*–3*d* и 2*s*–3*p* в результате опустошения нижних состояний при фотоионизации излучением горячего ядра плазмы. При этом коэффициент усиления должен составлять ~10 см$^{-1}$. Объяснить наблюдаемые аномалии поглощением в плазменном шнуре и в окружающей его холодной зоне плазмы не удается. Возрастание интенсивности на переходе 3–4 иона C VI, зарегистрированное в экспериментах со сложной мишенью, наиболее разумно связать с возникновением усиления, так как поглощение на переходах 2–3, 2–4 и 3–4 в этом случае отсутствует.

В заключение авторы считают своим приятным долгом выразить благодарность Э.Я. Кононову, А.Н. Рябцеву и С.С. Чурилову за помощь в работе и полезные обсуждения.

Литература

1. *Waynant R., Elton R.C.* // Proc. IEEE. 1976. Vol. 64. P. 1059.

2. *Vinogradov A.V., Sobelman L.I., Yukov E.A.* // J. de Physique. 1978. Vol. 39. P. 61.

3. *DeWhurst R.J., Jacoby D., Pert G.J., Ramsden S.A.* // Phys. Rev. Letts. 1976. Vol.37. P. 1265.

4. *Ильюхин А.А., Перегудов Г.В., Рагозин Е.Н., Собельман И.И., Чирков В.А.* // Письма в ЖЭТФ. 1977. Т. 25. С. 569.

5. *Irons F.E., Peackock N.J.* // J. Phys. B. 1974. Vol. 7. P. 1109.

6. *Irons F.E., Peackock N.J.* // J. Phys. B. 1974. Vol. 7. P. 2084.

7. *Кононов Э.Я., Кошелев К.Н., Левыкин Ю.А., Сидельников Ю.В., Чурилов С.С.* // Квантовая электроника. 1976 Т. 3. С. 576.

8. *Bhagavatula V.A.* // Appl. Phys. Letts. 1978. Vol. 33 (8). P. 726.

9. *Bhagavatula V.A., Yaakobi B.* Optics Comms. 1978. Vol. 24. P. 4331.

10. *Жерихин А.Н., Матвеец Ю.А., Чекалин С.В.* // Квантовая электроника. 1976. Т. 3. С. 1585.

11. *Жерихин А.Н., Кошелев К.Н., Крюков П.Г., Летохов В.С., Чекалин С.В.* // Письма в ЖЭТФ. 1977. Т. 25. С. 325.

12. *Elton R.C., Dixon R.H.* // J. Opt. Soc. Amer. 1977. Vol. 67. P. 1384.

13. *Жерихин А.Н., Кошелев К.Н., Крюков П.Г., Летохов В.С., Чекалин С.В.* Тезисы IX Всес. конф. по когерентной и нелинейной оптике. 1978. Ч. 1. С. 39.

14. *Баянов В.И., Гулидов С.С., Мак А.А., Перегудов Г.В., Собельман И.И., Стариков А.Д., Чирков В.А.* // Квантовая электроника. 1976. Т. 8. С. 2253.

15. *Кононов Э.Я., Кошелев К.Н.* // Квантовая электроника. 1974. Т 1. С. 2411.

16. *Valero F.P.J.* // Appl. Phys. Letts. 1974. Vol. 25. P. 64.

17. *Кошелев К.Н., Чурилов С.С.* // Квантовая электроника. 1975. Т. 2. С. 723.

18. *Silfvast W.T., Green J.M., Wood O.R.* // Phys. Rev. Letts. 1975. Vol. 35. P. 435.

19. *Jaegle P., Carillon A., Dhez P., Hamelot G., Sureau A., Cukier M.* // Phys. Letts A. 1971. Vol. 36. P. 167.

20. *Гордиец Б.Ф., Гудзенко Л.И., Шелепин Л.А.* // ЖЭТФ. 1968. Т. 55. С. 942.

21. *Bohn W.* // Appl. Phys. Letts. 1974. Vol. 24. P. 15.

22. *Pert G.J., Ramsden S.A.* // Optics Comms. 1974. Vol. 11. P. 270.

23. *Kelley R.L., Palumbo L.J.* Atomic and Ionic Emission Lines Below 2000 A. NRL Rep. 7599, NRL, Washington D. C., 1973.

24. *Виноградов А.В., Собельман И.И., Юков Е.А.* // Квантовая электроника. 1975. Т. 2. С. 105.

25. *Pert G.J.* // J. Phys. B. 1976. Vol. 9. P. 15.

ЛАЗЕРНАЯ СПЕКТРОСКОПИЯ

1. *Bekov G.I., Letokhov V.S., Mishin V.I.* Isotopically selective Rb atoms ionization through Rydberg states by laser and electric fields // Opt. Commun. 1977. Vol. 23 (1). P. 85–89.

2. *Antonov V.S., Knyazev I.N., Letokhov V.S., Matiuk V.M., Movshev V.G., Potapov V.K.* Stepwise laser photoionization of molecules in a mass spectrometer: a new method for probing and detection of polyatomic molecules // Opt. Lett. 1978. Vol. 3 (2). P. 37–39.

3. *Летохов В.С., Мовшев В.Г., Чекалин С.В.* Фотоотрыв ионов молекул родамина 6G, адсорбированных на поверхности, под действием ультракороткого лазерного импульса // ЖЭТФ. 1981. Т. 81 (8). С. 480–485.

4. *Antonov V.S., Letokhov V.S.* Laser multiphoton and multistep photoionization of molecules and mass spectrometry // Appl. Phys. 1981. Vol. 24. P. 89–106.

5. *Bekov G.I., Letokhov V.S.* Laser atomic photoionization spectral analysis of element traces // Appl. Phys. B. 1983. Vol. 30. P. 161–176.

6. *Chekalin S.V., Farztdinov V.M., Golovlyov V.V., Letokhov V.S., Lozovik Yu.E., Matveets Yu.A., Stepanov A.G.* Femtosecond spectroscopy of $YBa_2Cu_3O_7$-δ: electron-phonon-interaction measurement and energy-gap observation // Phys. Rev. Lett. 1991. Vol. 67 (27), P. 3860–3863.

Opt. Commun. 1977. Vol. 23 (1). P. 85–89

ISOTOPICALLY SELECTIVE RB ATOMS IONIZATION THROUGH RYDBERG STATES BY LASER AND ELECTRIC FIELDS

G.I. Bekov, V.S. Letokhov, V.I. Mishin
Institute of Spectroscopy, Academy of Sciences USSR, 142092 Moscow, USSR

Ionization by a pulsed electric field of rubidium isotopes ^{85}Rb and ^{87}Rb selectively excited to Rydberg states by dye lasers radiation has been carried out. We have obtained the values of the critical electric field strength for d-states of Rb atom with $n = 15 - 22$. Experimentally measured critical strength correlates with the theoretical one and is proportional to $(n^*)^{-4}$, where n^* is the effective quantum number. It is shown, that in the electric field with strength larger than the critical one highly excited atoms are ionized with the ultimate ion yield equal to one. In this case atomic ionization cross section is equal to the cross section of high lying state excitation.

1. Introduction

Considerable attention has been paid recently to the investigation of selective stepwise photoionization of atoms by laser radiation. With this method one expects to solve the following tasks: isotopes and nuclear isomers, separation, purification of substance, single atoms detection.

In this method chosen atoms are selectively excited by narrow band laser radiation to an intermediate state. Then excited atoms are ionized by the additional laser radiation. Such way of photoionization has been suggested for the first time and carried out in ref. [1] on the example of Rb atom. The same method has been applied to carry out the selective photoionization of isotope ^{40}Ca [2] and to obtain a weight amount of uranium concentrated by isotope ^{235}U [3]‡. Using a dye laser with a tunable frequency for excitation, and the radiation of a ruby laser and its second harmonic for ionization, we carried out rubidium atoms photoionization with ion yield approximate to one [5]. The ions and electrons concentration in the formed plasma reached 10^{13} cm^{-3}.

However, in spite of the high selectivity and efficiency of the selective photoionization method obtained in some experiments its wide application is impeded. This is connected with the fact that because of the small value of the atomic photoionization cross section ($\sigma_{ion} \approx 10^{-17} - 10^{-19}$ cm^2) the photoionization rate ($W_{ion} = \sigma_{ion} I$) becomes equal to the radiation decay rate only in laser fields with an intensity I in the order of MW/cm^2. Therefore, to extract the maximum number of atoms from the atomic beam, high rate repetition pulsed lasers with average output power of one or more kW are required.

The use of autoionization states permits to increase the cross section of atomic ionization (about one order) but the enhancement is still low. Besides not all the atoms have autoionization states, the latter are known only for a limited number of elements. Therefore, the search of ways to increase atomic ionization cross section from the excited states is rather actual.

2. Ionization of highly excited atoms by the electric field

To increase the atomic ionization cross section, it was suggested in ref [6] to use the autoionization decay of a highly excited atom in an external electric field. The essence of the process is in the following. Under the action of the electric field the part of high lying states passes into a continuous spectrum, while the others become autoionized because of a tunnelling of the electron. The closer the state to the ionization limit the larger is the rate of its autoionization decay, the rate quickly increasing with the increase of the principal quantum number and the strength of the electric field. The transition of discrete states to continuum, i.e. their ionization, takes place in the field with the strength [7]

$$E \geq E_{crit} = \frac{1}{16n^{*4}} \text{[atomic units]}, \qquad (1)$$

where 1 at $u = 5 \times 10^9$ V/cm, n^* is the effective principal quantum number.

The strength of the electric field may be taken in such a way, that the autoionization rate for the selected level will be equal or will exceed the radiative decay rate. The quantum yield of atomic ionization from the highly excited state W_{auto} here approaches to one, and the ionization cross section from the selectively excited state, if we determine it like $\sigma_{ion} = \sigma_2 W_{autoton}$ becomes equal to the cross section of high lying state excitation σ_2 (usually $\sigma_2 = 10^{-12} - 10^{-15}$ cm^2) Thus, the application of the electric field allows to increase the atomic photoionization cross section four to five orders.

The proposed method of photoionization has been experimentally realized in ref [8] on the example of a sodium atom. Ionization was carried out in a d.c. electric field. It was shown that this phenomenon has a distinctly expressed threshold behavior. For states excited by the laser with a wavelength $\lambda_2 = 4167$Å (the principal quantum number n=15), the threshold strength was 12 kV/cm.

It is noteworthy that at field strengths, when the autoionization becomes appreciable, the strong Stark-effect takes place. As a result, high lying levels split into a large number of components and the levels with different n intersect [9], all this led to uncertainty in the quantum numbers of the state which is excited. More preferable is the scheme where the electric field is switched on after laser pulses. In this case the states of which the positions are known with a great accuracy are excited. Ionization of sodium atoms ($n = 26 - 37$), xenon atoms ($n = 24 - 28$ f-states), uranium atoms ($n = 40 - 50$) and rubidium atoms (n = 28–65) by a pulsed electric field was investigated in refs [10–13].

The absorption linewidth at the transition to a high lying state is of Doppler broadening order, therefore a narrow band continuously tunable on the frequency laser is required for excitation of these states. Generation efficiency of such lasers is usually of about few percents. If we take this circumstance into consideration, the ionization through high lying states will be more advantageous in comparison with the ionization directly from the selectively excited state in the case, when the efficiency η_{narr} of the laser with a line width comparable with the Doppler width and the efficiency of a wideband laser η_{wide} for the direct ionization through continuum satisfies the condition

$$\eta_{narr}/\eta_{wide} \geq \sigma_{ion}/\sigma_2 W_{auto}$$

σ_2 excitation cross section is proportional to n^{-3}. Therefore, the maximum enhancement at the application of high lying states will be for not too large values of n.

On the other hand, the critical field, i.e., the field where the ion quantum yield is close to one, sharply increases with the decrease of n. The optimum case will be the case when the electric field strength will be about ten kV/cm. In such a field the states with $n \sim 15$ are easily ionized.

In this work we utilize the method of highly excited atoms ionization in an electric field for selective ionization of rubidium isotopes ^{85}Rb and ^{87}Rb. The ionization of d-states of Rb atom with $n = 15 - 22$ is investigated.

3. Experiment and results

For the elements of average masses (K, Ca, Rb and so on) the isotope shift of levels is small (0.008 cm^{-1} for K, 0.002 cm^{-1} for Rb). For such elements hyperfine splitting of the ground state considerably exceeds the isotope shift. Therefore, the difference in hyperfine splitting for different isotopes of the element can be used during isotopically selective atomic excitation by means of dye lasers radiation with a narrow line and a tunable frequency.

For rubidium of the natural isotope abundance the ground state is presented by four levels (fig. 1) The maximum shift between sublevels of different isotopes is 0.08 cm^{-1}.

Rubidium atoms in a beam (concentration $\approx 10^8$ cm^{-3}) were excited to high lying states by the radiation of two tunable dye lasers simultaneously pumped by a pulsed nitrogen laser. The scheme of energy levels of a rubidium atom and the used transitions are shown in fig. 1.

The first step dye laser (POPOP solution in toluol, $\lambda_1 \approx 4202$ Å, generation spectrum width $\Delta\nu_1 = 0.05$ cm^{-1}) excited rubidium isotopes to $\sigma^2 P_{3/2}$ state. As a result of the subsequent radiation decay $5\,^2P_{3/2}$ state was populated. The radiation pulse of the second step dye laser reached the region of atomic and light beams interaction 50 ns later after the first step laser pulse at the expense of an additional optical delay. The second laser wavelength (acid solution 4-MU in ethanol, $\Delta\lambda_2 = 0.2$ Å) was tuned within the range of 4950–4850 Å that allowed to excite Rb atoms from $5\,^2P_{3/2}$-state to the states with the principal quantum number $n = 15–22$.

Light beams intersected the atomic beam (fig. 2) in the region between the electrodes. The electric field pulse of rectangular shape was sent on the electrodes. The voltage pulse on the electrodes was formed during a discharge of a charged piece of a coaxial cable via concordant spark gap with a light ignition on the transferring line. To start up the spark gap a part of a nitrogen laser radiation was focused on one of the electrodes. Such a system allowed to form at a concordant load a single voltage pulse of a rectangular shape with a duration of 10 ns and an amplitude from 1 to 20 kV, synchronized to good accuracy with the laser pulses. The voltage pulse delay after the spark gap relatively to the starting pulse of N2-laser did not exceed 5 ns with a variation of the pressure in the spark gap from 4 to 10 atm. The transferring line length was such, that the voltage pulse appeared on the electrodes 75 ns after the first step laser pulse appearance.

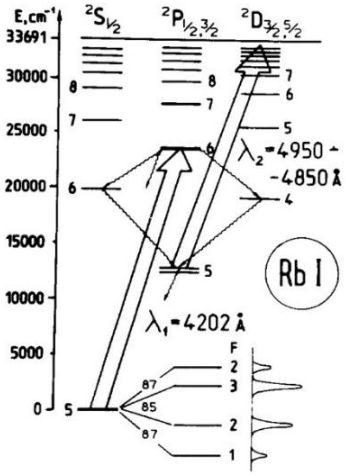


Fig 1. Diagram of Rb atom energy levels and used transitions

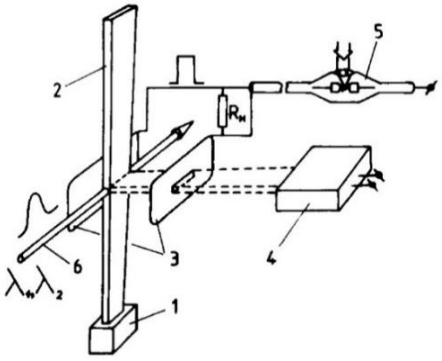


Fig. 2. Experiment scheme *1*. Oven with a collimating diaphragm for atom beam formation, *2*. Rubidium atom beam, *3*. Electrodes, *4*. Secondary emission multiplier, *5*. Concordant spark gap with laser ignition, *6*. Light laser beams

Rubidium ions, which are formed as a result of highly excited atom ionization during an electric field pulse were extracted through a slit in the electrode under a zero potential by the electric field of the cathode of a secondary emission multiplier, which was under the potential of -4 kV. To decrease the dependence of the multiplier signal on the energy of detected ions, the pulse duration formed by a spark gap was chosen to be 10 ns. The maximum energy accumulated by an ion in the region between the electrodes did not exceed 0.3 keV, and in the cathode field was 4 keV. The signal from the secondary emission multiplier was transferred to a boxcar integrator and registered by a recorder.

In fig. 3 is shown the ion yield dependence on the electric field strength at rubidium atom excitation to $15\,^2D$ state. The dependence has a evidently expressed threshold. At field absence an ion signal, selective on the first step laser frequency is detected. With the field strength increasing up to a critical value the signal increases slightly. When the critical value is achieved the signal sharply increases 20–50 times. Further electric field strength increase leads to an ion signal saturation.

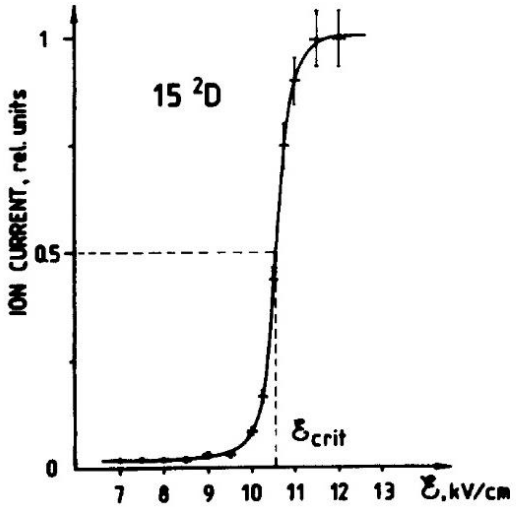


Fig. 3. Ion yield dependence on electric field strength at $15\,^2D$ level excitation

The ion signal detected at electric field absence is conditioned mainly by the rubidium atom ionization from $6\,^2P_{3/2}$ state of the second step laser radiation. With the field strength growth, the signal increase is connected with a more complete ion extraction from the space between electrodes, as the autoionization probability at such fields is very small. The sharp signal increase at the strength crossing through a critical value is conditioned by a very strong dependence of ionization probability on the electric field strength. The signal saturation is connected with an ionization during an electric field pulse of practically all the atoms, excited into high lying state.

Analogous threshold dependences were obtained also for d-states of $n = 16 - 22$. From the obtained curves we have determined the critical values of the electric field strength. The field strength, at which the half of highly excited atoms

was ionized, was accepted as a critical value; this corresponded to an ion signal two times smaller than with the saturation.

Fig. 4 shows the ion yield dependence on the first step laser frequency during rubidium atoms excitation to the 15 d-state and an electric field strength of $E = 13.5$ kV/cm which is larger than critical. Such a shape of the ion current is conditioned by a hyperfine structure of the ground state of rubidium of natural isotope abundance. Two central maxima correspond to the 85Rb isotope. One of the hyperfine structure components of the 87Rb isotope was distinctly resolved. Our results correlate well with the results of ref. [14], where the hyperfine splitting structure of the ground Rb state by the methods of classical spectroscopy has been observed. At the first step laser line tuning to the isotope ^{85}Rb (or ^{87}Rb) absorption line, the ionization selectivity, determined like the ratio

$$\frac{N_{ion}^{85}/N_{ion}^{85}}{N_{atom}^{85}/N_{atom}^{87}}$$

was not less than ten. The ionization cross section of rubidium isotopes from the $5\,^2P_{3/2}$ state is determined by the excitation cross section of the 15 d-state and reaches the value of 10^{-14} cm^2. We have used in our work not the optimum scheme of Rb atoms excitation to $15\,^2P_{3/2}$ state. A direct atoms excitation by a laser pulse from the ground state to $5\,^2P_{3/2}$ state will allow to make the whole process of ionization and rubidium isotope separation highly effective.

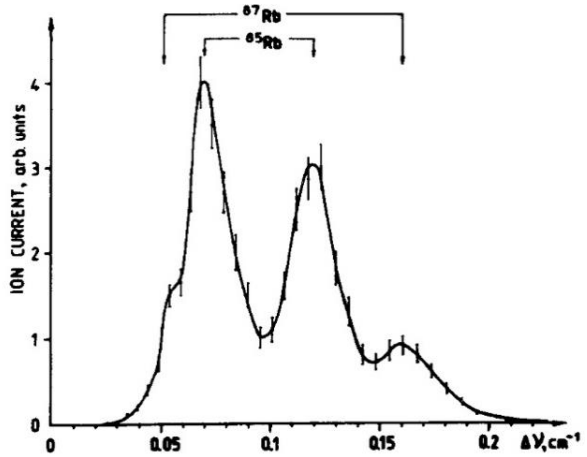


Fig. 4. Ion yield dependence on the first step laser frequency at $15\,^2D$ level excitation and an electric field strength $E = 13.5$ kV/cm larger than the critical one

In fig. 5 is shown the dependence of the critical electric field strength on the effective quantum number n^*. The low straight line is the classical dependence $E_{crit} = 1/16n^{*4}$. In this formula the level shift because of the Stark-effect and the electron tunneling were not taken into consideration. This has been done in ref. [6], where in

first order perturbation theory an analytical expression for the autoionization rate has been obtained. The upper straight line has been computed with this formula for a pulsed electric field with a duration equal to the lifetime of a high lying state. On the same figure are shown experimental values of the critical strength, which were obtained in this work for Rb and also for sodium from our previous paper [15] and paper [10], and data on uranium [12]. Experimental values of all the works differ from the both theoretical dependences. The difference of experimental and theoretical results is outside the experiment accuracy and is 15% in average. The approximated dependence (dashed line) drawn on the experimental values of all the works is parallel to the classical dependence and can be described by a formula $E_{crit}^{exper.} = 0.07(n^*)^{-4}$ cm^2.

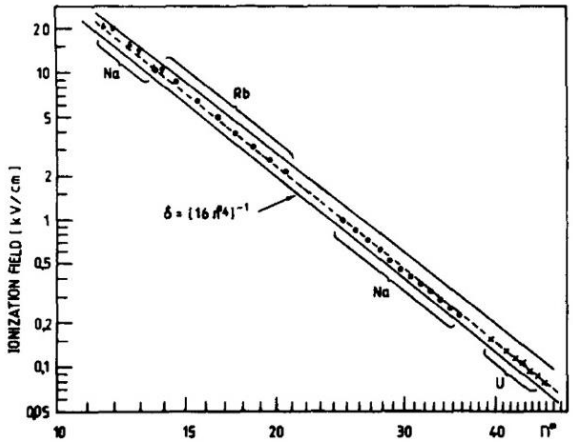


Fig. 5. Critical electric field strength dependence E_{crit} on the effective principal quantum number n^* of the excited level ▲, ▼ results of ref. [15] for s- and d-states respectively; ○ results of the present work; • results of ref. [10]; × results of ref. [12]

4. Conclusion

The effective selective ionization of rubidium isotopes ^{85}Rb and ^{87}Rb from the $5\,^2P_{3/2}$ state has been carried out. Highly excited atoms in an electric field larger than the critical one are ionized with the ion quantum yield equal to one. The cross section of the ionization is determined by the resonance excitation cross section of a high lying state. The ionization cross section in the electric field with the strength a little bit more than 10 kV/cm can reach the value of 10^{-14} cm^2. The measured critical strength of the electric field is proportional to $(n^*)^{-4}$ and apparently does not depend on the element.

The considered method of ionization of highly excited atoms by an electric field may be effectively used with already existing dye laser types with a tunable frequency and in set ups of laboratory scale for isotope separation and purification of substances. In connection with this the method is undoubtedly of practical interest.

References

1. *Ambartzumian R.V., Kalinin V.P., Letokhov V.S.* // JETP Lett. 1971. Vol. 13. P. 217.

2. *Brinkman U., Hartig W., Telle H., Walther H.* // Appl. Phys. 1974. Vol. 5. P. 109.

3. *Tuccio S.A., Foley R.J., Dubrin J.W., Krikonan O.* // IEEE J. of Quant. Electr. 1975. QE-11. P. 101.

4. *Letokhov V.S., Mishin V.I., Puretsky A.A.* // Prog. of Quant. Electr. 1977. Vol. 23. P. 85.

5. *Ambartzumian P.V. et al.* // Zh ETF. 1976. Vol. 70. P. 1660.

6. *Ivanov L.N., Letokhov V.S.* // Sov. Quant. Electr. 1975. Vol. 5. P. N3.

7. *Bethe H.A., Salpeter E.A.* Quantum mechanics of one and two electron atoms. New York: Academic Press, 1957.

8. *Ambartzumian R.V., Bekov G.I., Letokhov V.S., Mishin V.I.* // JETP Lett. 1975. Vol. 21. P. 279.

9. *Liftman M.G., Zimmerman M.L., Ducas T.W., Freeman R.R., Kleppner D.* // Phys. Rev. Lett. 1976. Vol. 36. P. 788.

10. *Ducas T.W., Littman M.G., Freeman R.R., Kleppner D.* // Phys. Rev. Lett. 1975. Vol. 35. P. 366.

11. *Stebbings R.F., Latimer C.J., West W.P., Dunning F.B., Cook T.B.* // Phys. Rev. A. 1975. Vol. 12. P. 1453.

12. *Paisner J.A., Carlson L.P., Worden E G., Johnson S.A., May C.A., Solarz R.W.* Report to the p/d session of the IX Int. Quant. Electr. Conf., June 1976, Amsterdam, The Netherlands.

13. *Tuan D.H., Liberman S., Pinard J.* // Opt. Comm. 1976. Vol. 18. P. 533.

14. *Brechignac C., Gerstenkorn S., Luc P.* // Physica B + C. 1976. Vol. 409. P. 82.

15. *Bekov G.I., Letokhov V.S., Mishin V.I.* // ZhETF. 1977. Vol. 1. P. 73.

Opt. Lett. 1978. Vol. 3 (2). P. 37–39

STEPWISE LASER PHOTOIONIZATION OF MOLECULES IN A MASS SPECTROMETER: A NEW METHOD FOR PROBING AND DETECTION OF POLYATOMIC MOLECULES

V.S. Antonov, I.N. Knyazev, V.S. Letokhov, V.M. Matiuk,
V.G. Movshev, V.K. Potapov
Institute of Spectroscopy, Academy of Sciences USSR

Laser spectroscopy and kinetic mass spectrometry of polyatomic isolated molecules have been carried out by using stepwise laser ionization of molecules in a mass spectrometer. The optical absorption spectrum of NO_2 has been recorded, for example, by using pulsed dye-laser excitation and H_2 vacuum-ultraviolet laser ionization of molecules. The kinetics of excited electron states and of the production of molecular and fragmented ions of some polyatomic molecules have been investigated with high temporal resolution. The sensitivity achieved is 10^{-10} cm^{-1} of the absorption coefficient and 10^9 (10^5) molecules in the ground (electronically excited) state in the irradiated volume.

Recent progress in development of far-ultraviolet (UV) and vacuum-ultraviolet (VUV) lasers has opened the way for applying the photoionization methods of laser spectroscopy to molecular systems. Especially promising in this respect is the combination of stepwise laser photoionization of molecules with the mass spectrometric analysis of photoions [1]. This combination should provide exceptional selectivity (of both optical spectrum and e/m ratio), high sensitivity, and (by using controllable time delay between laser pulses) high temporal resolution.

A laser detector of trace quantities of polyatomic molecules can be created on this basis, and thus one of the most difficult problems of physics can be solved. On the other hand, a new, powerful method of investigation of the basic features of polyatomic isolated molecules in excited states can be developed.

In this work, the optical absorption spectrum of the NO_2 molecule has been recorded by using two-step laser photoionization of molecules in a mass spectrometer. The kinetics of stepwise photoionization processes of benzaldehyde, benzophenone, nitrobenzene, and para- and ortho- nitrotoluene have been investigated.

Two-step laser photoionization of polyatomic molecules by time-delayed frequency-tuned double-pulse laser radiation was first carried out in a gas [2] and then (after one-step photoionization experiments [3]) the method developed was directly

transferred to the mass spectrometer. Two-step laser photoionization of some of the simplest diatomic alkali molecules was also recently carried out [5,6].

The experimental setup included a chemical photoionization mass spectrometer MX1311 [7] and time-synchronized exciting and ionizing pulsed lasers [Fig. 1(a)]. The excitation of intermediate electronic states of the molecules was carried out by means of a nitrogen UV laser ($\lambda = 337$ nm) with a laser-pulse energy output in the photoionization volume, $\epsilon = 0{,}2$ mJ, and a laserpulse duration, $\Delta t = 12$ ns. A 4-methylumbelliferon dye laser pumped by a nitrogen laser with $\epsilon = 40$ μJ, $\Delta t = 12$ ns was used in the investigation of the NO_2 absorption spectrum. The spectral width of laser radiation was 0.5 Å, and the laser frequency was tuned in the 440–470-nm region.

The ionization of excited molecules was carried out by a pulsed hydrogen VUV laser [2] at $\lambda = 160$ nm with $\epsilon = 0.5$ μJ, $\Delta t \lesssim 1$ ns, and a repetition rate of 10–20 Hz. In the case of one-step ionization of molecules in the mass spectrometer, the use of a H_2 VUV laser with appropriate strobing and with integration of the signal increases the relative sensitivity of registration more than 5 orders of magnitude compared with the traditionally used H_2 lamp [Fig. 1(b)]. A sensitivity of 0.1 ion per pulse was achieved at a repetition rate of 10 Hz, an integration time of 1–10 s, a strobe-pulse duration of 10 μs, and an optimal delay of the strobe pulse relative to the H_2 laser pulse, of 40 μs. The sensitivity threshold was determined by the background photoion current but apparently arose from surface ionization, scattered laser radiation, and ionization by electrons accelerated in the ionizing electric field.

The N_2, or dye, laser beam was focused by a lens of focal length F = 20 cm and crossed with a H_2 laser beam, thus forming a photoionization region $0.1 \times 0.1 \times 1$ cm^3. The position of this region relative to the exit slit of the ionization volume was properly adjusted to achieve a maximum ionization efficiency of about 5%. The vapors of the molecules flowed into the ionization volume at a pressure of 10^{-4}–10^{-6} Torr through a multichannel glass inlet.

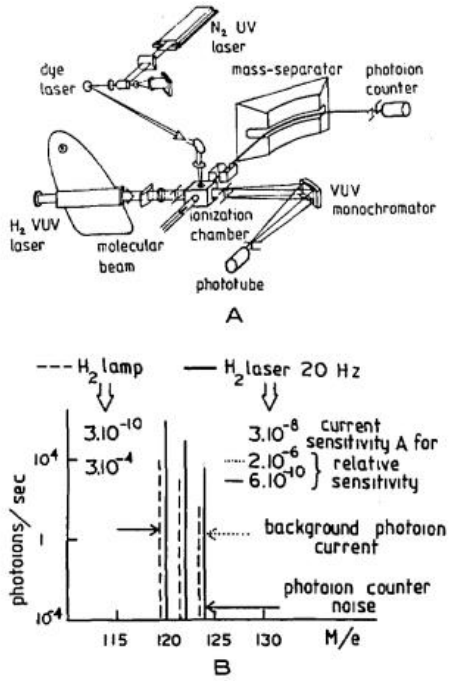


Fig. 1. One-step photoionization of dimethylaniline using a H_2 lamp and a H_2 laser. A, Experimental setup; B, sensitivity of the system

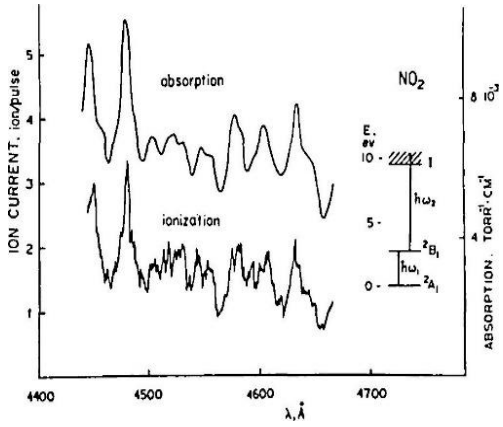


Fig. 2. Dependence of the two-step photoionization yield and the absorption [8] of NO_2 on the dye-laser wavelength. An energy-level diagram is shown at the right

The time behavior of the excited electronic states of molecules was investigated by using a controllable 010 ± 0.003 μs time delay of the probing pulse of the H_2 VUV laser relative to the exciting laser pulse. Mass spectra of photoionization products, as well as the dependence of peak intensities in mass spectra on the frequency and intensity of the exciting laser radiation and on gas pressure, were investigated.

Fig. 2 shows the two-step ionization yield of NO_2^+ (the only observed photoion in NO_2) compared with the optical absorption spectrum [8] of the $^2A_1$–$^2B_1$ transition. The two-step photoionization spectrum is determined in general by both the molecular absorption spectrum on the first step and the spectral dependence of ionization on the second step. The latter is determined mainly by Franck-Condon factors for ionization of molecules in transition between vibrational levels of the electronically excited molecule and the molecular ion. As can be seen from Fig. 2, in the case of the NO_2 molecule the two-step ionization spectrum is determined mainly by the absorption spectrum of the molecule on the first step.

The two-step ion current does not decrease significantly for a time delay of $\Delta t = t(H_2) - t(N_2) \lesssim 2\mu$s. This can be connected with the relatively long lifetime of the intermediate electron state $^2B_1$ (44 μs) [9].

The minimum registered absorption coefficient in NO_2 is of the order of 10^{-7} cm [1]. Figures 3–5, respectively, show examples of the mass spectra of stepwise ionization, the dependence of the photoion current on the time delay between laser pulses, and assumed ionization schemes of some polyatomic molecules.

The benzaldehyde molecule is an example of the relatively simple two-step ionization scheme. As can be seen from the mass spectra [Fig. 3(a)], the relative yield of the fragmented ion $C_6H_5CO^+$ for two-step ionization (solid line) is twice of that for one-step ionization [10] (dashed line). The photoion current depends linearly on the N_2 laser intensity, in accordance with the two-step ionization scheme. The energy of two laser quanta (3.7 + 7.7 eV = 11.4 eV) exceeds the ionization potential of the molecule 1.9 eV. This provides favorable conditions for fragmented ion formation.

The two-step photoion current rapidly increases for time delay $\Delta t = 0 - 15$ ns and then slowly decreases [Fig. 3(b)]. The former time interval is determined by the N_2 laser-pulse duration. The slight decrease of signal during the following 300-ns time interval is associated mainly with the diffusion of the excited molecules from the irradiated region with a characteristic time of 2 μs. The absence of a fast decrease of ion current for $\Delta t \lesssim 21\ \mu$s in the case of excitation of the singlet state can be explained by the quick conversion of molecules to the relatively long-lived[11] triplet state [Fig. 3(c)]. The large rate of radiationless singlet-triplet conversion $\kappa_{ST} \sim 10^{12}$ s^{-1} is characteristic of the benzaldehyde molecule as well as of other aromatic molecules in the carbon group [12]. The molecule converted to the triplet state acquires a large excess of vibrational energy, ~0.6 eV, which is located mainly in the CHO group. This may explain the observed increase in the yield of the fragmented ion $C_6H_5CO^+$ for two-step photoionization.

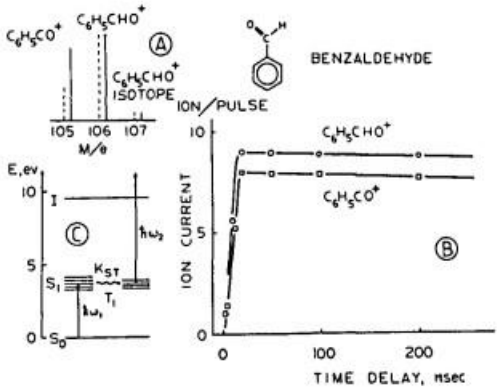


Fig. 3. Two-step photoionization of benzaldehyde. A, Mass spectra of molecular $C_6H_5CHO^+$ and fragmented $C_6H_5CO^+$ ions. Solid and dashed lines mark two-step and one-step photoionization, respectively. B, Dependence of the two-step photoion current on the time delay $\Delta t = t(H_2) - t(N_2)$ between laser pulses. C, Energy-level diagram of molecule

The photoionization kinetics of the benzophenone molecule are more complex. The fragmented ion $C_6H_5CO^+$, as well as the molecular ion $(C_6H_5)_2CO^+$, is observed in the mass spectrum. The dependence of yields for molecular and fragmented ions on the time delay between the laser pulses is shown in Fig. 4(a). The fragmented-ion yield becomes a maximum immediately after the nitrogen-laser pulse. It follows an approximately exponential decay with a time constant of 14 ± 2 ns, after which it remains stable at a level of 7% relative to the molecular-ion yield.

The peak amplitude in Fig. 4 depends quadratically on the nitrogen-laser intensity. This may confirm two-step absorption of N_2 laser radiation for $\Delta t \gtrsim 12$ ns.

The following preliminary explanation of the results obtained can be given. The benzophenone molecule in the excited singlet state is quickly converted into the triplet state $S_1 \rightarrow T_1$, $\kappa_{ST} \sim 10^{11}$ s^{-1} (Ref. 13.) [Fig. 4(b)]. Therefore, molecular and fragmented ions for time delay $\Delta t \gtrsim 70$ ns should be formed mainly by ionization from the T_1 state [14]. The possible second channel for production of the fragmented ions is connected with the absorption of a second quantum of nitrogen-laser radiation, giving rise to the transition $T_1 \rightarrow T_n$. The energy of the excited triplet state T_n in this case is 3.7 + 3.7 eV = 7.4 eV, and the molecule should quickly dissociate; otherwise the ionization by three quanta from the nitrogen laser would be observed. Finally, ionization of the supposed electronically excited radical $C_6H_5CO^*$ by hydrogen-laser radiation can produce the $C_6H_5CO^+$ ion. The signal decay with the time $\tau = 14$ ns probably corresponds to the radiative lifetime of the excited radical $C_6H_5CO^* \rightarrow C_6H_5CO^+ + h\nu$.

In the case of benzophenone, the minimum recorded absorption coefficient on the first step, $S_0 \rightarrow S_1$, is 10^{-10} cm^{-1}, and on the second step, $T_1 \rightarrow$ molecular ion, is 10^{-14} cm^{-1}. This corresponds to 10^9 molecules in the ground state and 10^5 electronically excited molecules.

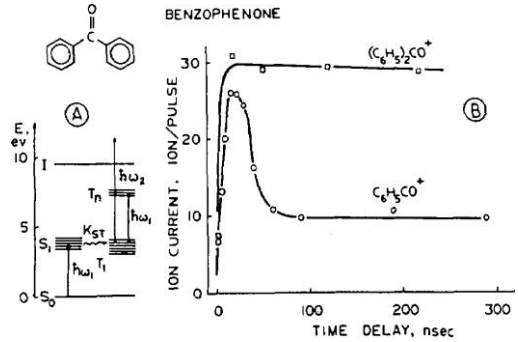


Fig. 4. Stepwise photoionization of benzophenone. A, Dependence of the photoion current on the time delay Δt for molecular $(C_6H_5)_2CO+$ and fragmented $C_6H_5CO^+$ ions. B, Energy-level diagram of molecule

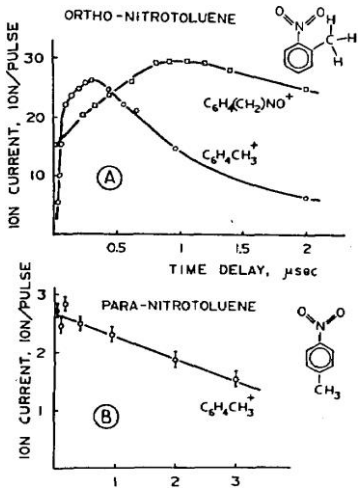


Fig. 5. Stepwise photoionization of A, ortho- nitrotoluene and B, para-nitrotoluene. Dependence of photoion current on time delay Δt

The kinetics of the stepwise ion formation of the nitrobenzene and *para*- and *ortho*-nitrotoluene molecules, as it follows from rough analysis, should be more complicated and is not quite clear yet. Here we present some preliminary results of investigations. Stepwise photoionization of nitrobenzene and *para*- nitrotoluene occurs only by breaking of the C–N bond with the formation of carbon-hydrogen ions C_7H^{7+} and $C_6H_5^+$. For *ortho*- nitrotoluene, besides these types of processes, the production of fragmented ions $C_7H_6NO^+$ with an OH yield is observed (Fig. 5). The latter can be attributed to the intramolecular rearrangement process. The yields of carbon-hydrogen and $C_7H_6NO^+$ ions depend quadratically and linearly on the N_2-laser intensity. This may be considered as proof of two-step and one-step photoexcitation, respectively, by the N_2 laser.

For *ortho*-nitrotoluene, an increase of the ion current is observed after N_2-laser excitation [Fig. 5(a)]. This can be explained by the formation of intermediate particles from electronically excited molecules after N_2-laser excitation. The photoionization of these particles can lead to the formation of fragmented ions $C_7H_7^+$ and $C_7H_6NO^+$.

Further improvements of the system considered above may be accomplished. Increase of power and better focusing of the VUV and dye-laser radiation, accompanied by a corresponding decrease of background photoion current and increase of ion-detaching efficiency, could increase the overall sensitivity of the system by 5–7 orders of magnitude. Subnanosecond time resolution may be obtained by decreasing the pulse duration of the lasers used. Simultaneous laser action on 1600 and 1200 Å bands of H_2 could simplify the analysis of the molecular decomposition products.

References

1. *Letokhov V.S.* // Sov. Phys. Usp. 1976. Vol. 118. P. 199.
2. *Antonov V.S., Knyazev I.N., Letokhov V.S., Movshev V.G.* // Zh. Eksp. Teor. Fiz. 1977. Vol. 73. P. 1325.
3. *Potapov V.K., Movshev V.G., Letokhov V.S., Knyazev I.N., Evlasheva T.I.* // Quantum Electronics (in Russian). 1976. Vol. 3. P. 2610.
4. *Antonov V.S., Knyazev I.N., Letokhov V.S., Matiuk V.M., Movshev V.G.* // Pis'ma Zh. Tekh. Fiz. 1977. Vol. 3. P. 1287.
5. *Feldman D.L., Lengel R.K., Zare R.N.* // Chem. Phys. Lett. 1977. No. 52. P. 413.
6. *Herrmann A., Leutwyler S., Schumacher E., Wöste L.* // Chem. Phys. Lett. 1977. Vol. 52. P. 418.
7. *Akopian M.E., Vilesov F.I., Komarov M.S., Pavlenko V.A., Potapov V.K., Shereschevkii A.M.* // High Energy Chem (USSR). 1969. Vol. 3. P. 483.
8. *Hall T.C., Blacet F.E.* // Chem J. Phys. 1952. Vol. 20. P. 1745.
9. *Nenberger D., Duncan A.* // J. Chem. Phys. 1954. Vol. 22. P. 1693.
10. *Iskakov L.I., Potapov V.K.*//High Energy Chem (USSR). 1971. Vol. 5. P. 265.
11. *Berger M., Gotdblatt I.L., Steel C.* // J. Am. Chem. Soc. 1973. Vol. 95. P. 1717.
12. *Stockburger M.* // J. Phys. Chem. 1962. Vol. 31. P. 350.
13. *Dym S., Hochstrasser R.M.* // J. Chem. Phys. 1969. Vol. 51. P. 2458.
14. *Hochstrasser R.M., Wessel J.E.* // Chem. Phys. Lett. 1973. Vol. 19. P. 156.

ЖЭТФ. 1981. Т. 81 (8). С. 480–485

ФОТООТРЫВ ИОНОВ МОЛЕКУЛ РОДАМИНА 6G, АДСОРБИРОВАННЫХ НА ПОВЕРХНОСТИ, ПОД ДЕЙСТВИЕМ УЛЬТРАКОРОТКОГО ЛАЗЕРНОГО ИМПУЛЬСА

В.С. Летохов, В.Г. Мовшев, С.В. Чекалин
Институт спектроскопии АН СССР

Наблюдалась фотодесорбция тяжелых ионизированных фрагментов родамина 6G с поверхности вольфрамовой мишени под действием пикосекундного лазерного импульса с длиной волны $\lambda = 0{,}53$ мкм, интенсивностью 10^7 Вт/см^2. При этом для излучения с длиной волны $\lambda = 1{,}06$ мкм десорбция ионов не наблюдалась вплоть до интенсивностей 10^9 Вт/см^2. Делается вывод о нетепловом характере фотодесорбции.

1. Введение

В работе [1] было предложено использовать лазерное излучение ультракороткой длительности для визуализации, то есть получения прямых данных о пространственно-химическом строении сложных молекул, в частности, биомолекул. Эта идея основана на предположении о возможности селективной фотоионизации отдельных фрагментов молекул, адсорбированных на поверхности иглы ионного микроскопа. До самого последнего времени не было экспериментальных данных о фотоотрыве молекулярных ионов или ионизированных фрагментов с поверхности под действием лазерного излучения. В то же время было опубликовано несколько интересных предложений о возможности воздействия лазерным излучением на молекулы, адсорбированные поверхностью [2–4].

Для экспериментального исследования такого рода процессов и возможности селективной фотоионизации нами был выбран следующий экспериментальный подход. Исследуемая поверхность с адсорбированными на ней молекулами помещается в камеру времяпролетного масс-спектрометра. Ионы, образующиеся при воздействии лазерного излучения различных длин волн на эту поверхность, могут быть идентифицированы по массам. Таким образом, можно выяснить, отрываются ли от поверхности ионные фрагменты сложной молекулы и, если отрываются, то какие именно.

Недавно [5] было сообщено об успешных экспериментах по фотоотрыву молекулярных ионов оснований нуклеиновых кислот и антрацена с поверхности

молекулярного кристалла под действием интенсивного УФ-лазерного излучения наносекундной длительности.

В настоящей работе впервые сообщается об экспериментах по фотоотрыву адсорбированных на поверхности вольфрама тяжелых ионов родамина 6G (Rh6G) под действием ультракоротких импульсов (УКИ) излучения второй гармоники YAG:Nd^{3+} лазера на длине волны $\lambda = 0{,}53$ мкм длительностью 30 пс и интенсивностью 10^7 Вт/см^2. В то же время отрыв таких ионов не наблюдался при облучении импульсом с длиной волны $\lambda = 1{,}06$ мкм, лежащей вне полосы электронного поглощения (Rh6G), при интенсивности вплоть до 10^9 Вт/см^2.

2. Экспериментальная установка

Экспериментальная установка (рис. 1) состояла из времяпролетного масс-спектрометра, в ионизационную камеру которого помещалась мишень, и YAG:Nd3+-лазера УКИ. YAG:Nd^{3+}-лазер, собранный по обычной схеме «генератор — затвор — усилитель», позволял получать одиночный импульс длительностью 30 пс с энергией до 10^{-2} Дж на длинах волн 0,53 или 1,06 мкм. Излучение лазера направлялось на мишень под углом 80°. Мишень представляла собой пластину из вольфрама размером 6×6 мм^2. Перед нанесением адсорбата мишень электрополировалась и промывалась дистиллированной водой и спиртом.

Раствор Rh6G в этаноле (10^{-3}–10^{-4} моль/л) наносился на поверхность мишени в виде капли и затем высушивался. После этого мишень помещалась в ионизационную камеру масс-спектрометра, которая откачивалась до 5×10^{-8} мм рт. ст. с помощью магнитодиодного насоса.

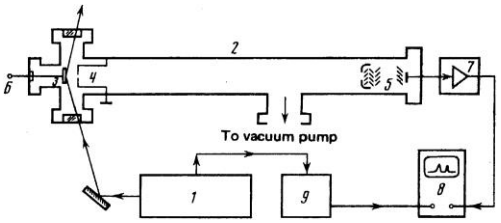


Рис. 1. Схема экспериментальной установки. *1* — лазер УКИ, *2* — времяпролетный масс-спектрометр, *3* — мишень, *4* — диафрагма, *5* — ВЭУ, *6* — ввод высокого напряжения на мишень, *7* — усилитель, *8* — осциллограф, *9* — генератор задержки

Каждый масс-спектр снимался за одну лазерную вспышку. При съемке масс-спектров на мишень подавался постоянный потенциал +0,5 кВ. Такое малое ускоряющее напряжение в сочетании с большой длиной пространства дрейфа давало возможность оценивать плотность ионов на мишени по уширению масс-пика (см. разд. 4). Для формирования ионного пучка использовалась диафрагма диаметром 3 мм из нержавеющей стали, размещенная на оси масс-спектрометра в 15 мм от поверхности мишени. Диафрагма имела нулевой потенциал. Длина пространства дрейфа масс-спектрометра составляла 155 см.

Положительные ионы регистрировались вторичным электронным умножителем (ВЭУ), сигнал с которого подавался после соответствующего усиления на вертикально отклоняющие пластины запоминающего осциллографа С-8-12. Запуск развертки осциллографа осуществлялся импульсом с электрооптического затвора лазера, жестко связанным по времени с выделенным лазерным импульсом. С помощью генератора Г-5-28 можно было задерживать запуск развертки на интервал от 0 до 90 мкс, меняя тем самым диапазон исследуемых масс. Подчеркнем, что эксперименты были выполнены в условиях, когда лазерное излучение не создавало плазмы на облучаемой мишени. Эти условия могли четко контролироваться, так как при возникновении плазмы наблюдалось резкое увеличение амплитуды сигнала на три-четыре порядка и аномальное уширение масс-пиков.

3. Результаты эксперимента

Было обнаружено, что при воздействии на мишень одиночного УКИ на длине волны 0,53 мкм в масс-спектре на пороге его появления ($1{,}4 \times 107$ Вт/см^2) наблюдается лишь один пик, соответствующий времени пролета 10^3 мкс, что соответствует массе m/e = 434 (рис. 2а, г). При увеличении энергии лазера происходит существенное уширение этого пика как в сторону бóльших, так и в сторону меньших времен пролета (рис. 2б, в, д, 3). Кроме того, появляются еще два пика, которые мы идентифицировали как Na и K (23,6 и 30,6 мкс), а также иногда широкий пик в области 150 мкс, соответствующий двойной массе молекулярного иона 2Mi (рис. 2д).

При облучении мишени излучением с длиной волны 1,06 мкм масс-спектр появлялся лишь при интенсивности $1{,}2 \times 10^8$ Вт/см^2 и содержал только пики K и Na вплоть до 10^9 Вт/см^2 (рис. 2е).

Отметим, что значительное уширение (до 20 мкс) при увеличении энергии лазера испытывал лишь пик родамина, ширина же пиков K и Na не превышала 0,5 мкс. Уширение пика можно приписать различным причинам. Одной из таких причин могла бы быть вторичная ионизация электронами и отрицательными ионами, возникающими при бомбардировке первичными ионами диафрагмы.

Был проведен контрольный эксперимент, позволивший исключить эту причину. Для этого излучение лазера направлялось на диафрагму масс-спектрометра (рис. 1). При этом получался масс-спектр мишени, бомбардируемой электронами (и, возможно, отрицательными ионами), вылетевшими из материала диафрагмы и ускоренными полем до энергий около 5 кэВ. Порог появления такого спектра был по крайней мере на порядок выше, чем при стрельбе по мишени. Типичный вид масс-спектра изображен на рис. 2ж. Видно, что, в отличие от рис. 2г, д, здесь наблюдаются лишь довольно легкие фрагменты.

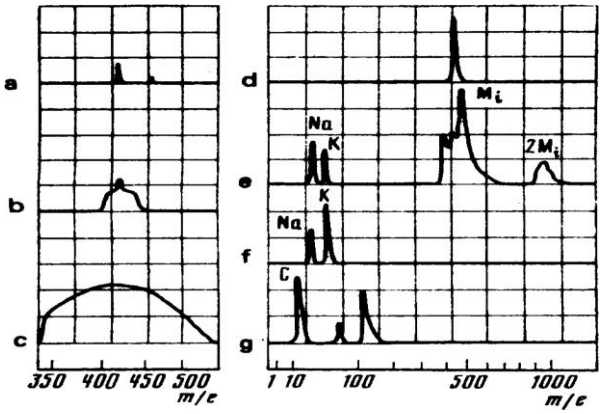


Рис. 2. Масс-спектры, полученные при различных условиях облучения слоя Rh6G. *а–в* — 5 мкс/дел, задержка запуска 90 мкс; *г–ж* — 20 мкс/дел, задержка запуска 0; *а–д* — облучение λ = 0,53 мкм; *е* — λ = 1,06 мкм; *ж* — электроны 0,5 кэВ. Интенсивность лазерного излучения на мишени *I* в Вт/см^2: *а* — 1,4 × 10^7, *б* — 1,6 × 10^7; *в*) 2,8 × 10^7; *г*) 2,2 × 10^7; *д*) 2,5 × 10^7; *е*) 1,2 × 10^8

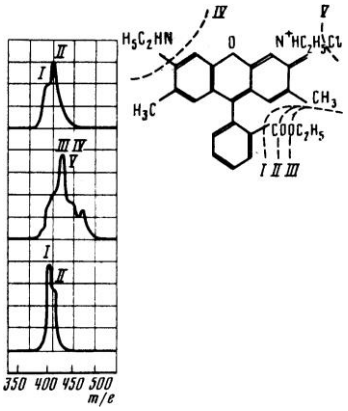


Рис. 3. Возможная идентификация структуры масс-пика Rh6G. Задержка запуска 90 мкс, 5 мкс/дел. λ = 0,53 мкм, *I* = 2×10^7 Вт/см^2. *I* — Rh6G без $COOC_2H_5$ (*m*/*e* = 406); *II* — Rh6G без OOC_2H_5 (*m*/*e* = 418); *III* — Rh6G без OC_2H_5 (*m*/*e* = 434); *IV* — Rh6G без H_5C_2HN (*m*/*e* = 435); *V* — Rh6G без Cl (*m*/*e* = 444)

Ширина пика родамина на пороге его появления в масс-спектре на превышает 0,5 мкс (рис. 2а). Пик соответствует времени пролета иона 102,5 ± 0,5 мкс. Точная идентификация массы зарегистрированного иона невозможна без калибровки масс-спектра по пикам ионов с близкими и точно заранее известными массами. Поэтому мы можем предположить, что наблюдаемый пик принадлежит ионам, попавшим в ускоряющий промежуток со значительной начальной скоростью (при этом она должна быть одинакова для всех ионов). На рис. 3 приведены несколько масс-спектров, имеющих структуру, и дана возможная идентификация наблюдаемых пиков в предположении, что каждый из них соответствует определенной массе.

Порог появления масс-спектров непрерывно возрастал по мере облучения мишени лазерными импульсами. Кроме того, после нескольких серий экспериментов на диафрагме масс-спектрометра появился заметный налет Rh6G. Это говорит о том, что в ходе экспериментов происходила очистка поверхности мишени лазерным излучением.

В отдельной серии экспериментов в условиях вакуума 5×10^{-8} торр были сняты масс-спектры чистой подложки (рез родамина) при облучении УКИ с разными длинами волн и энергичными электронами (рис. 4). Как видно из рис. 4а, б, существенного отличия масс-спектров, полученных при облучении λ = 1,06 и 0,53 мкм, нет.

Интересной особенностью спектров представляется появление интенсивной и узкой линии водорода при интенсивности лазерного излучения $I > 10^8$ Вт/см^2 (потенциал ионизации водорода 13,6 эВ) как для λ = 0,53 и 1,06 мкм (рис. 4а, б).

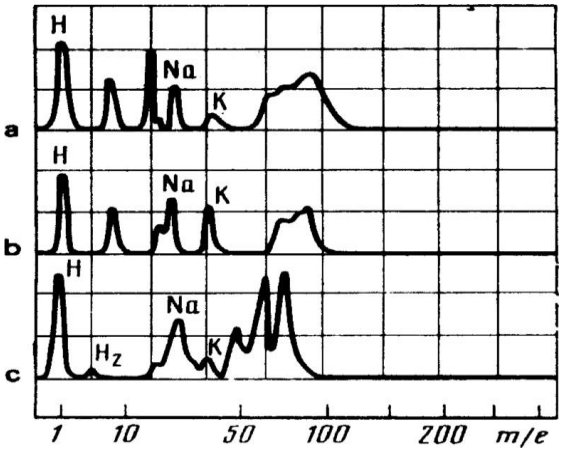


Рис. 4. Масс-спектры, полученные на мишени без родамина при различных способах возбуждения. *а* — излучение λ = 0,53 мкм ($I = 1{,}2 \times 10^8$ Вт/см^2); *б* — излучение λ = 1,06 мкм ($I = 1{,}1 \times 10^8$ Вт/см^2); *в* — электроны или отрицательные ионы 0,5 кэВ. Задержка запуска 0; 10 мкс/дел

4. Обсуждение результатов

Наиболее интересным фактом нам представляется отрыв тяжелых ионов Rh6G в отсутствие их значительной фрагментации под действием излучения с λ = 0,53 мкм ($\hbar\omega$ = 2,36 эВ). Отсутствие Rh6G в масс-спектрах при облучении мишени излучением с λ = 1,06 мкм, не поглощающимся в родамине, свидетельствует о незначительной роли подложки в процессе ионизации. О том же говорят и оценки нагрева подложки. Поэтому первичным процессом, приводящим к появлению ионов Rh6G, несомненно, является поглощение излучения с λ = 0,53 мкм в слое родамина. В наших экспериментах этот слой был, по-видимому, неоднороден по толщине в силу известной склонности молекул красителей

к образованию агрегатов при адсорбции за счет действия межмолекулярных вандерваальсовских сил притяжения [6]. Поэтому толщина покрытия в разных точках мишени, вероятно, варьировалась от нуля до нескольких сотен монослоев. Ориентация поверхности слоя красителя при таком расположении может быть также весьма разнообразной в разных точках мишени, и от нее может отражаться от 36% (при падении под прямым углом) до практически 100% излучения в области полосы поглощения красителя. Оценки термического нагрева Rh6G в местах наибольшего поглощения излучения 0,53 мкм при условии, что вся поглощенная энергия уходит в тепло, дают величину около 100°C, что недостаточно для тепловой ионизации. В этих оценках брались плотность энергии $1{,}4 \times 10^7$ Вт/см^2 на пороге появления масс-спектра, сечение поглощения в электронной полосе в окрестности $\lambda = 0{,}53$ мкм, $\sigma = 2{,}5 \times 10^{-16}$ см^2; теплоемкость твердого Rh6G считалась равной 0,3 кал/г·град. Отсюда можно заключить, что процесс фотоионизации Rh6G в наших экспериментах носит нетепловой характер. Выяснение конкретного механизма ионизации требует дополнительных экспериментов. Одним из возможных механизмов могут быть, например, коллективные процессы передачи энергии от одной электронно-возбужденной молекулы другой электронно-возбужденной молекуле [7].

Отметим, что процесс ионизации K и Na сенсибилизируется поглощающими молекулами родамина. Это следует из того экспериментального факта, что при облучении излучением с $\lambda = 0{,}53$ мкм порог появления ионов K и Na в присутствии Rh6G на порядок меньше, чем для мишени без родамина. При облучении же излучением $\lambda = 1{,}06$ мкм, не поглощающимся в Rh6G, порог появления ионов K и Na в случае чистой мишени такой же, как и для мишени с родамином.

Уширение пика Rh6G при увеличении лазерной энергии (рис. 2а–в) происходит как в сторону меньших, так и в сторону бóльших времен пролета. Поэтому оно связано, по-видимому, главным образом не с увеличением начальных скоростей ионов, а с их кулоновским расталкиванием. Кулоновское расталкивание должно приводить к бóльшим (по времени) уширениям масс-спектра для бóльших масс, что согласуется с нашими наблюдениями.

По уширению масс-пиков можно оценить поверхностную плотность заряда вылетающего пакета ионов [8]. Эта величина составляет 10^6–10^7 ион/см^2 в плоскости диафрагмы масс-спектрометра в предположении равномерного распределения заряда и малой расходимости пучка ионов.

5. Выводы

Итак, во-первых, под действием ультракороткого импульса с длиной волны 0,53 мкм может происходить нетепловой отрыв ионов молекул Rh6G из толстого слоя без существенной фрагментации. Этот факт представляется важным для развития метода лазерной визуализации молекулярных связей с помощью селективно-возбуждаемой лазерным излучением химической метки [1], в частности интеркалирующих красителей в случае молекулы ДНК. Пометив

биомолекулу соответствующим красителем, можно адсорбировать ее на игле ионного проектора и затем облучить лазерным импульсом на длине волны поглощения красителя. Оторванные ионы красителя дадут на экране проектора карту мест интеркаляции, то есть расположения определенных пар соединений. Имея набор красителей, интеркалирующих с разными парами и имеющих при этом существенную разницу в полосах поглощения, можно получить карту строения биомолекулы, облучая ее импульсами разных частот. Существенным преимуществом этого метода является то обстоятельство, что полосы поглощения красителей лежат в видимом диапазоне, а сами биомолекулы прозрачны в этой области (полосы поглощения большинства из них лежат в УФ-области), так что, вероятно, можно возбуждать красители, не затрагивая самих биомолекул. Кроме того, представляется вполне возможной идентификация места возбуждаемой и вырываемой химической метки и ее массы по времени пролета в импульсном автоионном проекторе [9].

Во-вторых, обнаружена сенсибилизация отрыва ионов K и Na молекулами Rh6G, электронно-возбужденным ультракоротким световым импульсом.

В-третьих, при интенсивностях УКИ, превышающих 10^8 Вт/см^2, происходит отрыв ионов водорода от поверхности, причем этот эффект наблюдается как для $\lambda = 1{,}06$ мкм, так и для $\lambda = 0{,}53$ мкм.

Литература

1. *Летохов В.С.* // Квант. электрон. 1975. Т. 2. С. 930.

2. *Аскарьян Г.А., Намиот В.А.* // Письма в ЖЭТФ. 1975. Т. 21. С. 646.

3. *Гольданский В.И., Намиот В.А., Хохлов Р.В.* // ЖЭТФ. 1976. Т. 70. С. 2349.

4. *Djidjoev M.S., Khokhlov R.V., Kiselev A.V., Lygin V.I., Namiot V.A., Osipov A.I., Panchenko V.I., Provotorov M.V.* In: Tunable Lasers and Applications. V. 3, Springer Series in Optical Sciences / ed. by Mooradian et al. Proceedings of the Loen Conference. Norway: Springer-Verlag, 1976. P. 100.

5. *Антонов В.С., Летохов В.С., Шибанов А.Н.* // Письма в ЖЭТФ. 1980. Т. 31. С. 471.

6. *Теренин А.Н.* Фотоника молекул красителей и родственных органических соединений. Л.: Наука, 1967. С. 483.

7. *Campillo A.J., Hyer R.C., Shapiro S.L., Swenberg C.E.* // Chem. Phys. Lett. 1977. Vol. 48. P. 495.

8. *Сысоев А.А., Чупахин М.С.* Введение в масс-спектрометрию. М.: Атомиздат, 1977. С. 174.

9. *Panitz J.A.* // Rev. Sci. Instrum. 1973. Vol. 44. P. 1034.

Appl. Phys. 1981. Vol. 24. P. 89–106

LASER MULTIPHOTON AND MULTISTEP PHOTOIONIZATION OF MOLECULES AND MASS SPECTROMETRY

V.S. Antonov, V.S. Letokhov
Institute of Spectroscopy, Academy of Science of the USSR, Moscow-Troitzk, USSR

A review of laser-induced photoionization of polyatomic molecules and the application of this process in mass-spectrometry is presented. Combination of laser selective photoionization and mass spectral analysis of fragments as a promising tool for the detection of trace amounts of complex molecules is considered particularly.

Laser photoionization of molecules has recently received much attention. The progress made towards the development of laser engineering and, particularly, lasers in the vacuum ultraviolet range has pushed photoionization laser spectroscopy of molecules to one of the most advanced fields of laser spectroscopy at present. At the initial stage of its development there were different approaches to laser photoionization of molecules.

1. Background

1.1. Idea of Two-Dimensional Mass-Optical Spectrometer

The first approach was related to the use of selective two-step IR-VUV molecular photoionization in mass spectrometers [1]. On the basis of this idea the possibility of creation a universal detector for trace amounts of complex molecules as a so-called two-dimensional mass-optical spectrometer has been discussed many times [2]. This is illustrated in Fig. 1. A laser with the tunable frequency ω_1 excites selectively the vibrational (electronic for some molecules) state of molecules. Due to such excitation the photoionization band-edge usually lying in the VUV region shifts by a small amount. The second laser operating in the VUV range performs photoionization of molecules, with its frequency ω_2 in the region of maximum slope of the photoionization band-edge. In this case the selective preexcitation of molecules by the tunable laser (a rather small value of $E_{\text{exc}} = 0.1 \div 0.5$ eV) brings about a detectable photoionization cross-section (10^{-1} to 10^{-2}% with molecular distribution over rotational states allowed for), i.e., a change in photocurrent. The photoions enter a standard mass-spectrometer where the mass spectrum, i.e., the photocurrent $i = f(M/e)$, is measured. Besides, this modification of a mass spectrometer is able to measure the photocurrent for a given value of M/e as a function of the tunable laser frequency ω_1. In this case the IR spectrum of traces of complex molecules will be measured

since, the tunable laser frequency ω_1 and the frequency of molecular absorption are coincident, the molecules will be excited and hence the ionic photocurrent amplitude will vary. The laser mass- spectrometer with selective molecular photoionization, instead of usual nonselective ionization by an electron beam (or by wide-band VUV radiation), will produce simultaneously an optical (IR and visible) absorption spectrum and a mass spectrum.

Since the photon energy must be $E > 5 \div 7$ eV to photoionize most molecules from intermediate vibrational and even electron-excited states the systematic studies into this method began with the development of hydrogen VUV lasers [3]. The first experiments on single-photon molecular ionization in gases [4] and in the mass spectrometer beam [5] demonstrated a high efficiency of this laser as an ionization source. At single-step molecular photoionization in the mass spectrometer the use of a H_2 VUV laser with proper strobing and integrating of the signal increased the sensitivity of recording by more than five orders [6] compared to the hydrogen lamp usually used as a source of VUV radiation for photoionization.

1.2. Early Experiments on Stepwise Photoionization

The early experiment on selective two-step photoionization [7] was performed on formaldehyde molecules in gas with exciting the intermediate electron state $^1A_2$ and with subsequent ionization by the H_2 laser pulse. The use of controllable delay between laser pulses made it possible to investigate the kinetics of excited-state population decay. Further experiments on stepwise photoionization of polyatomic molecules in the mass spectrometer proved that the mass spectra of stepwise molecular photoionization were very sensitive to the time delay between laser pulses [6, 8]. This suggests that intramolecular processes taking place between laser pulses manifest themselves in the mass spectrum of fragmentary ions and provide a new possibility of studying photophysical processes in isolated molecules. The spectra of electron absorption of NO_2 molecules produced by the method of two-step photoionization, with a tunable dye laser used at the first step [6, 9], agreed well with the absorption spectrum measured by the standard method. Even with the use of a rather low-power H_2 VUV laser the minimum detectable absorption coefficient was around 10^{-10} cm^{-1}.

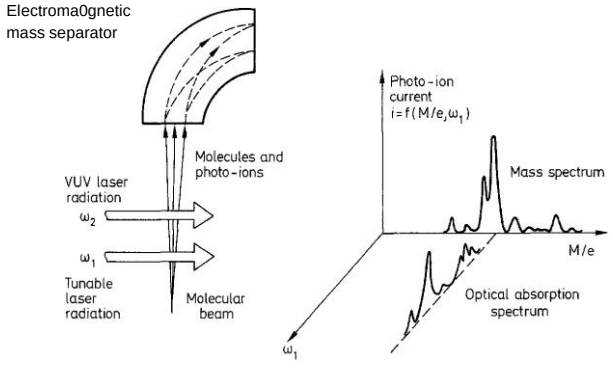


Fig. 1. Scheme of a two-dimensional mass-optical spectrometer [1]

Another approach to laser photoionization of molecules resulted from experiments on atomic photoionization. As cesium was photoionized in the atomic beam by neodymium laser pulses with $\lambda = 1.06$ μm there was a molecular component Cs_2^+ found by time-of-flight mass analysis of the ionization products [10]. The resonance with the intermediate molecular levels of Cs_2 leads to an essential ionization yield of molecular dimers despite their low content in the beam [11]. The molecules of such alkali metals as Cs_2, Rb_2, and RbCs were a very convenient object for the first studies into the basic features of two-step molecular photoionization [12] due to their low ionization potential and the possibility of using of simple time-of-flight technique to record molecular fragmentation according to the laser radiation wavelength. The experiments on two-step photoionization of Na_2 molecules in a supersonic free jet and BaCl molecules resulted from the Ba + HCl reaction [13], proved the efficiency of this technique for the study of molecular beams. Of particular importance here is that it is possible to obtain information as two-dimensional mass-optical spectra [2] and to study the spectroscopy of certain atomic clusters, such as K_n and Na_n with $n > 2$ in molecular beams with different aggregates of K_x and Na_x [14]. The high spectral selectivity achieved in two-step photoionization of the Li_2 dimer by cw Ar^+ laser radiation allowed selective photoionization of different isotopes of this molecule [15].

1.3. First Experiments on Multiphoton Ionization

Photoionization of polyatomic molecules is of principal scientific and practical interest. As noted above, extensive studies into selective stepwise photoionization of such molecules were impossible for lack of proper VUV lasers. One more approach to molecular photoionization was demonstrated in [16]. The essence of the technique proposed consists of using a tunable dye laser with strong focusing of the laser beam to the diffraction limit. In this case the power density in the focus may be as great as 10^{10} W/cm^2 which effectively promotes the processes of multiphoton absorption and ionization of molecules. When the laser wavelength is tuned resonances appear at the double or triple laser frequencies with subsequent one- or two-photon molecular photoionization. The presence of intermediate resonances drastically increases the ion yield and hence a multiphoton ionization spectrum is formed. Despite its simplicity, this method has proved very efficient in studying the spectroscopy of electron states and particularly those forbidden for single-photon transitions. Even in the first experiments on benzene molecules a new electron state $^1E_{1g}$ forbidden for single-photon transitions was found by multiphoton ionization (MPI) spectra [17]. It was also possible to observe spectra of three-photon resonances with Rydberg states resembling usual single-photon spectra. Some works on MPI spectroscopy of I_2 [18, 19] and NO molecules in a supersonic cooled molecular jet [20], trans-1,3-butadiene [21, 22], transhexatriene [23], two caged amines [24], ammonia [25], cyclopropane and ethylenimine [26], pyridine and pyrazine [27, 28] were performed in a similar way. In many cases unknown electron states were found for the first time and their symmetry types were identified with polarization measurements [29]. It should be noted that reliable identification of MPI spectra with certain resonances often presents some problems. Besides, in some cases it is difficult to explain why there are no transitions in the spectra which are allowed by the selection rules for MPI. Furthermore, in photoionization of the I_2

molecule there is no normal optical spectrum at all when the radiation wavelength is tuned to the lines of the transition $B \leftarrow X$ [19].

Considerable progress in understanding the processes of MPI of polyatomic molecules was achieved during mass-spectral study of photoionization products [30]. It had been expected before that the number of photons absorbed per molecule corresponded to the minimum number required for the lowest ionization potential to be achieved. The formation of fragments with high appearance potentials was neglected. But in experiments on multiphoton ionization of bensene and trans-l,3-butadiene molecules in a mass spectrometer through an intermediate two-photon resonance, extensive fragmentation of the molecules was observed up to C^+ fragments [31]. In the case of benzene this corresponds to absorption of no less than 9 photons with their total energy about 28 eV. The studies into the formation of a spectrum in MPI were impeded due to the fact that the photoion yield was limited by two-photon absorption from the ground state while the rest of the transitions were near saturation. As the dye laser wavelength was tuned the yield of different ion fragments agreed well with the spectrum of two-photon resonances except for the molecular ion which had a considerable contribution of non-resonant 3-photon ionization. The analysis of the products of MPI of the I_2 molecule [31] has shown that both the I_2^+ and I^+ components contribute to the total ionic signal, and the ratio of ion yields, I^+/I_2^+, depends greatly on wavelength. Therefore, the analysis of the spectroscopic constants of intermediate state proceeded from assumptions of negligible contribution to the signal of the I^+ component [18] is apparently not valid.

Below we shall restrict ourselves to considering laser mass spectrometry of polyatomic molecules since the combination of laser selective photoionization and mass spectral analysis for this class of molecules is obviously of particular interest both for obtaining new information about molecules and practical detection of trace amounts of complex molecules.

2. Multiphoton Ionization of Polyatomic Molecules

2.1. Frequency Dependence of Cross-Section

Multiphoton processes are usually described by the first nonzero expansion term of the nonstationary perturbation theory. The general expression for the probability of *n*-photon ionization has the form $W^{(n)} = \sigma_n I^n$ where I is the radiation intensity, σ_n is the cross-section of the *n*-photon process. The expression for σ_n includes the summation over all molecular states as well as the continuum. For the case $n = 4$ which is typical of multiphoton molecular ionization the expression has the form

$$\sigma_4^{(\omega_L)} \infty \left| \sum_1 \sum_2 \sum_3 \cdot \frac{\langle f|V|3\rangle\langle 3|V|2\rangle\langle 2|V|1\rangle\langle 1|V|i\rangle}{(E_3 - E_i - 3\omega_L)(E_2 - E_i - 2\omega_L)(E_1 - E_i - \omega_L)} \right|^2. \qquad (1)$$

In this expression "*i*" and "*f*" correspond to the initial bound state and the final ionization continuum of states; the indexes "1", "2", and "3" denote, respectively, the intermediate first, second and third quantum states; ω_L is the laser frequency; V is the

Hamiltonian of the molecule-field interaction. The numbers in the matrix elements denote virtual states with one, two or three photons absorbed. When the radiation frequency ω_L is tuned according to the position of intermediate molecular levels, resonances may arise on the basic, double and triple frequencies. The ionization yield in this case increases greatly provided that the selection rules for multiphoton transitions are satisfied and so the spectrum of MPI is formed. Since the electron absorption bands of most molecules begin in the UV region of the spectrum, the most typical case in using tunable dye lasers is recording the spectra of two- and three-photon resonances.

2.2 Experiments in Gas

First, we shall consider briefly the experimental technique and then discuss the experimental results for various molecules.

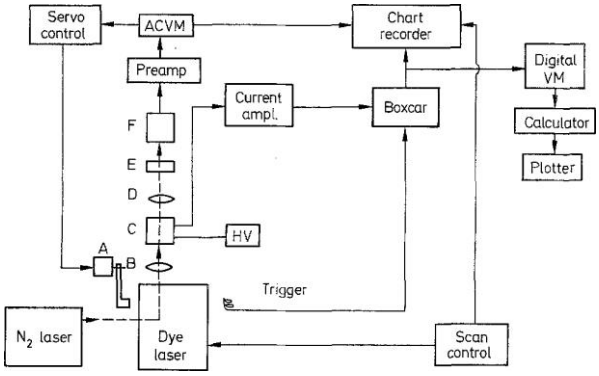


Fig. 2. Experimental setup for investigation of MPI spectra of molecules [17]

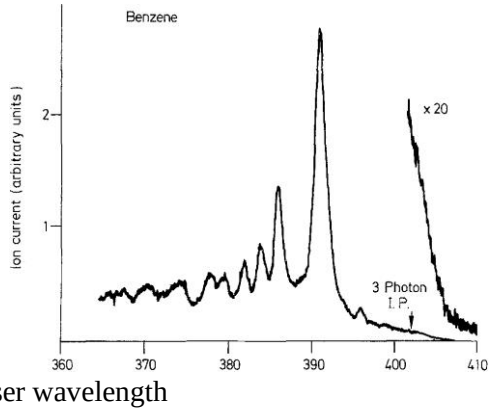


Fig. 3. MPI spectrum of two-photon resonances ($^1E_{1g} \leftarrow {}^1A_{1g}$) in benzene [17]

2.2.1 Experimental Technique

Figure 2 shows a typical scheme of the experimental setup used in recording MPI spectra [17]. A powerful (about 1 MW) nitrogen laser pumps a dye laser which can be tuned in the range 360 to 700 nm with the output line width of 0.02 nm. The dye laser

beam is focused at diffraction limit into the ionization cell using a special lens with a focal length of 25 mm. The photoionization cell contains a wire electrode inside a cylindric electrode. The voltage across the cylindric electrode was +200 V. The wire electrode is connected to a current amplifier. The signal from its output is fed to a boxcar integrator and then to chart-recorder. In experiments on benzene, with the pressure 50 Torr and the repetition rate 10 pulse/s, the mean signal value was 10^{-11} A. Since the signal of multiphoton ionization greatly depends on radiation intensity, special measures are being taken to prevent the intensity in the focus and the focal area size from being varied as the dye laser wavelength is scanned. For this purpose, the radiation intensity was measured at the ionization cell output and the control signal was fed to the servo mechanism which attenuated the dye laser pumping radiation. The right choice of laser intensity is of importance in measuring MPI spectra. At high intensities the signal of MPI builds up, but due to saturation the contrast in spectra reduces.

2.2.2 Experimental Results for Various Molecules

Spectra are the main source of information in MPI. It is essential that at multiphoton transitions the selection rules differ from those at one-photon transitions. For example, the transition between levels with the same parity is forbidden for one-photon transitions but allowed for two-photon ones. Thus, the spectroscopic information obtained from MPI supplements conventional one-photon spectroscope. In some cases it is possible to study such electronic molecular states which have not been known so far at all.

Benzene Molecule. The MPI spectra of benzene were measured in the ranges 365 to 400 nm (Fig. 3) and 400 to 450 nm [17]. The first question arising in the analysis of MPI spectra is how to identify the resonances in the MPI spectrum under observation. As shown in Fig. 3, the three-photon ionization potential of benzene corresponds to the wavelength of 402 nm. Therefore, at shorter wavelengths the signal corresponds to three-photon ionization and in the range 400 to 450 nm to four-photon ionization. The spectral structure observed in the region 365 to 400 nm may, in principle, occur both due to resonances with bound molecular states at the double laser frequency and due to autoionization states above the ionization limit at a three-photon transition. The analysis of the vibrational structure and its comparison with the well-known one-photon spectrum in the region of autoionization states show however that the structure observed is caused by two-photon resonances. The only known state in this region is $^1B_{1u}$. The two-photon transition to this state may be vibrationally allowed, and explained the spectrum of MPI. But the position of the maximum peak in the spectrum as well as the shifts observed in deuteration are inconsistent with this assumption. There are four different types of states $^1A_{1g}$, $^1E_{1g}$, $^1E_{2g}$ and $^1A_{2g}$, which are allowed in two-photon transitions from the ground $^1A_{1g}$ state in D_{6h}. The transitions to the $^1A_{2g}$ state are forbidden if two photons are identical. The presence of E_{2g} vibrations in the transition may indicate a Jahn-Teller effect in the excited state and would therefore speak for either $^1E_{1g}$ or $^1E_{2g}$. The MPI yield measured at linear and circular polarization has enabled the symmetry of the $^1E_{1g}$ state to be ascertained [29]. So, the new $^1E_{1g}$ electron state predicted theoretically has been detected and identified from MPI spectra.

The spectrum of three-photon resonances in benzene in the range 400 to 500 nm corresponds almost completely to transitions to Rydberg states, and the three- photon Rydberg structure is identical, in fact, with the spectrum of single-photon absorption, exclusive of the difference in their intensities which points to a strong influence of $^1A_{1g}$ components in the two-photon virtual state.

Other Molecules. The MPI spectra of trans-1,3-butadiene were measured at the wavelength ranging from 365 to 468 nm [21, 22]. In four-photon ionization at wavelengths over 405 nm there were many three- photon resonances due to Rydberg states observed and a new series with the quantum defect 0.04 identified. At wavelengths below 405 nm two-photon resonances with the *B* state were observed. From the vibrational structure of the spectrum, it has been found that the symmetry of this electron state corresponds to the ^1B_g symmetry.

The studies into the vibrational structure of two-photon resonances in MPI of trans-hexatriene in the range 370 to 400 nm [23] made it possible to ascertain that this transition was allowed for two-photon transitions of the $g \leftrightarrow g$ type. Subsequent polarization measurements showed that the state had the ^1A_g symmetry.

There was a new electron state in ammonia revealed by the method of MPI [25]. Besides, three-photon absorption spectra of NH radicals were observed. They were formed in the dissociation of ammonia after absorbing three photons.

MPI spectra of other molecules [24, 26–28, 32–41] were studied in a similar way. In the recent work on MPI of l,4-diazabicyclo(2,2,2) octane two lasers were used [42]. The first laser pulse produced two-photon excitation of the molecules and the second pulse ionized these molecules. It was shown that in the typical case of four-photon ionization the loss of efficiency of MPI usually takes place due to the dissociation of molecules after the third photon absorbed. This competitive channel may be removed by using different lasers for excitation and ionization. Despite the fact that the method of molecular MPI has been developed rather recently, at present it is a standard method widely used to study electron molecular spectra.

2.3 Experiments with Mass Spectrometers

It was expected that the number of photons absorbed by a molecule in MPI was equal to the minimum number required for photoionization. The result of mass-spectroscopic analysis of MPI products for some molecules was unexpected. It has been found that, beside molecular ions, there are also fragment ions in the mass spectrum, up to C^+, and the yield of fragment ions may greatly exceed that of molecular ions. This means that molecules absorb a much greater number of photons than that required of usual ionization.

2.3.1 Experimental Technique

In Fig. 4 the scheme of an experimental setup for studying MPI in the mass spectrometer is given [31]. To ionize molecules, it is also used a dye laser pumped by a nitrogen laser with power of about 1 MW. The output power of the dye laser was about 250 kW with the repetition rate 12 pps. The generation line width was 0.01 nm, the pulse duration 5-6 ns. The horizontal laser beam was focused into the central part of the ion source in the quadrupole mass filter, transversely to the molecular

beam. The power density in the focus was 10^9 W/cm^2, with the laser beam diameter in the focus of about 0.2 mm. The ions formed in MPI were pushed out by the 100 V/cm field, they pass through the axial ionic lenses into the quadrupole analyzer and then through some additional ionic lenses and come to the cathode of the magnetic ion-electron multiplier. The signal from the multiplier was amplified and fed to the boxcar integrator, gated open from 20–35 μs following the laser trigger pulse. The output signal was directed to a Varian signal averager and/or to a stripchart recorder.

2.3.2 Experimental Results for Various Molecules

Benzene Molecule. The MPI spectrum was studied with the radiation wavelength scanned in the region 365 to 400 nm [31] which corresponded to the Johnson band of two-photon transitions $^1E_{1g} \leftarrow {}^1A_{1g}$. Under weak focusing the experiment was performed with low mass resolution. The results of the experiment are graphically presented in Fig. 5. The C_n "clumps" denote a relative yield of the ionic components with the same number n of carbon atoms according to the laser radiation wavelength. The spectral dependence of C_n, excluding the C_6 component, are the same and correspond, for the most part, to the MPI spectrum measured before. The dependence of the ion yield of C_6 on the wavelength has a considerable nonresonance contribution that increases as the wavelength is decreased. It has been found that the intensity dependence of the ion yield of C_6 measured between resonances is cubic. These ions are believed to be formed in a direct nonresonance three-photon process. Under strong focusing the fragmentation is more extensive and the C^+ ion yield in the mass spectrum is maximum (Fig. 6). The signal in this case is sufficient for the mass filter to operate under unit mass resolution. It follows from the potentials of fragment ion appearance that at least 9 photons, with the energy of each being 3.17 eV, are needed to form the C^+ and C_3^+ ions. The intensity dependence of the yield of light fragments in this case is stronger than for heavy ones. Nevertheless, even for the C^+ ion the power dependence does not exceed 3.5 which is indicative of strong saturation of multiphoton absorption.

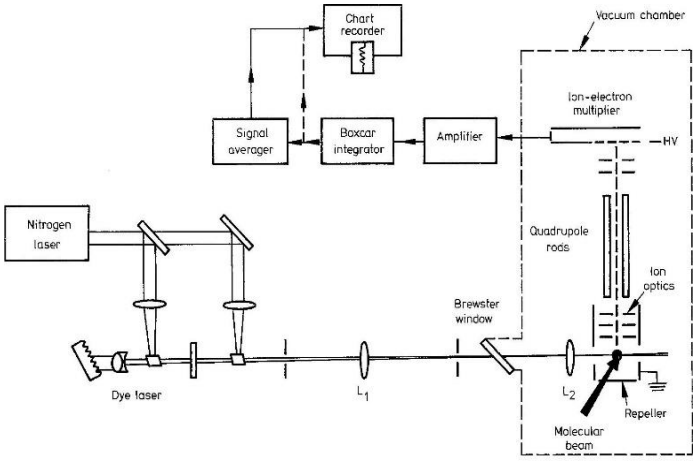


Fig. 4. Schematic drawing of the laser MPI mass spectrometer [31]

Trans-1,3-Butadiene Molecule. The results of the experiment on MPI of trans-1,3-butadiene [31] are similar in many respects to those in the case of benzene. The mass spectrum of MPI in trans-1,3-butadiene, like in benzene, displays extense fragmentation which points to absorption of a great number of photons by the molecule being ionized (or its fragments). Figure 7 shows the MPI mass spectrum of trans-1,3-butadiene, with the radiation wavelength tuned to one of vibrational peaks with λ=386.8 nm at the transition identified before as a two-photon transition to the ^1B_g Rydberg state [21]. In Fig. 7 there is also seen a mass spectrum of ionization by electron impact with an electron energy of 100 eV. Their comparison shows that the fragmentation of the molecule is more intensive in MPI, which is also characteristic for benezene molecules.

Similar results were obtained during the experiments with acetaldehyde [43]. As in the benzene case a great number of fragment ions were present in the MPI mass spectrum. As the wave-length of dye laser was scanned within the range 360-364 nm the output of all mass peaks was of the equal spectral dependence.

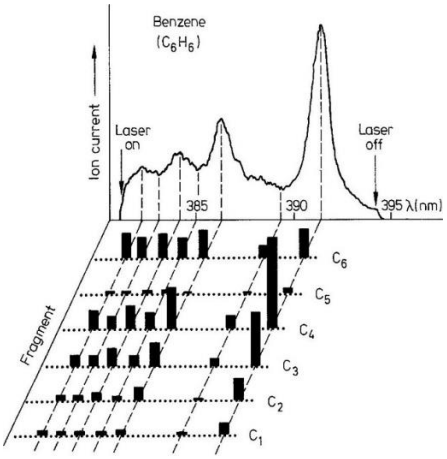


Fig. 5. Two-dimensional optical-mass spectrum of benzene [31]

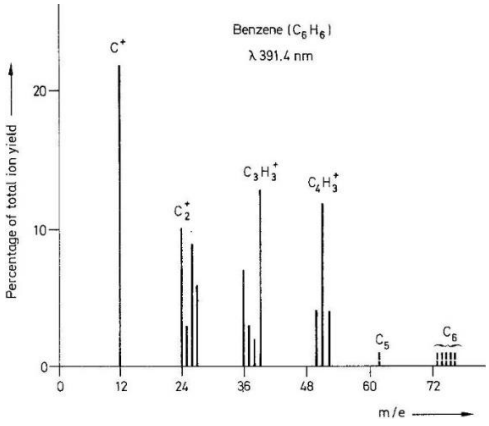


Fig. 6. MPI mass spectrum of benzene (at 391.4 nm) [31]. The dashed lines for the C_5 and C_6 groups are uncertain: only the unresolved total for these groups could be measured

2.4 Conclusions

The method of MPI is widely used at present to investigate the spectroscopy of excited states of polyatomic molecules, forbidden for one-photon transitions. An essential advantage of the method is that it is possible to study the Rydberg states lying in the VUV region of the spectrum and also to ionize almost any molecule using lasers of the visible and ultraviolet ranges. The fact is that it is often difficult to identify the structure of MPI spectra with certain resonances. Besides, in some cases it is difficult to explain the absence of transitions in the MPI spectra which are allowed by the selection rules and must be observed [19]. Of great importance is apparently molecular dissociation from excited states being a competitive process relative to

photoionization. Mass-spectral analysis aids in understanding MPI processes. The recording of MPI spectra on controllable mass components substantially improves and supplements spectral information. Yet the presence of two- or three-photon absorption from the ground state at the first step needs high radiation intensities, and the mass spectrum of ionization products in this case is rather complicated. The fragmentation of molecules in MPI exceeds that in ionization by electron impact. With decreasing intensity, the mass spectrum becomes simpler but this is followed by a considerable attenuation of the MPI signal.

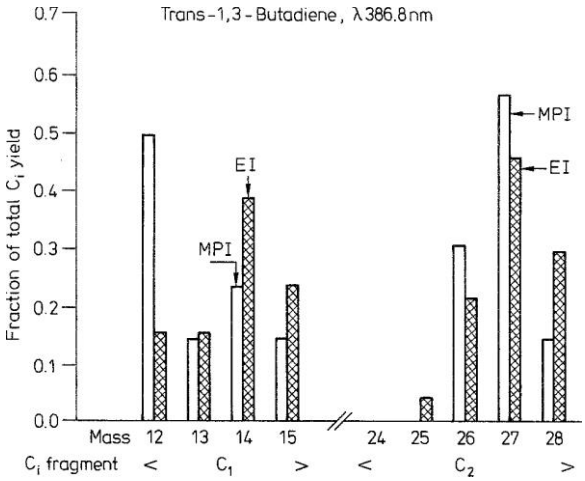


Fig. 7. MPI mass spectrum (open bars) and electron impact data (cross-hatched bars) of C_1 and C_2 groups of butadiene [31]

3. Multistep Photoionization of Polyatomic Molecules

As opposed to MPI, in multistep photoionization (MSPI) the quantum transition at each step is a resonant single-photon transition. In the important particular case of two-step photoionization (TSPI) the energy of the first photon corresponds to the transition of molecules to a real excited state. Since the transition to the ionization continuum occurs at the second step, the resonance condition is satisfied automatically. Due to a complicated quasi-degenerate level structure of polyatomic molecules in the intermediate electron- excited state and because of various intramolecular relaxation processes, the phase memory of the system in the intermediate state can be lost very quickly. This enables us to consider two-step processes as incoherent and to describe them by rate equations [44]. As for ionization selectivity, the method of TSPI has the important advantage that wavelengths for the exciting and ionizing radiations can be chosen independently with the use of two time-synchronized lasers. Scanning the delay time of the ionizing pulse relative to the exciting one provides an additional possibility for studying the kinetics of photophysical processes in excited intermediate molecular states.

3.1. Two-Step Photoionization in Gas

The first experiments on TSPI were performed on formaldehyde and nitrogen dioxide molecules in gas, the total ion current recorded in the ionization chamber. The H_2 VUV laser was used as a source of ionizing light [3]. The photon energy of the H_2 VUV laser being equal to 7.7 eV is, as a rule, sufficient to ionize polyatomic molecules excited by the first-step laser radiation in the visible and ultraviolet region.

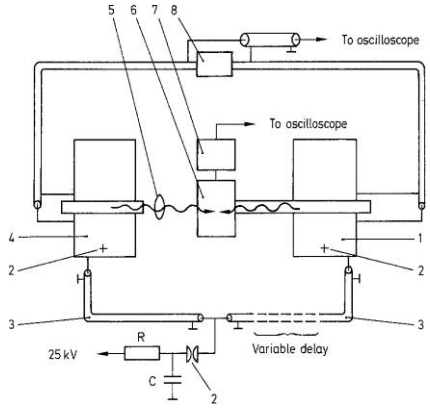


Fig. 8. Experimental setup to investigate TSPI of molecules with time-synchronized lasers (1: H_2 VUV laser, 2: sparkgap, 3: charging cables, 4: N_2 UV laser, 5: quarz lens, 6: ion cell, 7: amplifier, 8: shunt) [7]

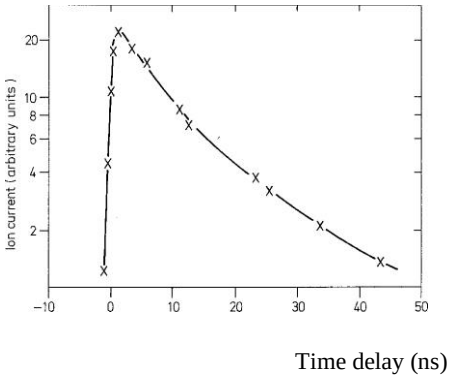


Fig. 9. The photoion current of TSPI in formaldehyde vs time delay between the two laser pulses [7]

3.1.1. Experimental Technique

The use of two pulsed time-synchronized lasers is a specific feature of the experimental setup for molecular TSPI [7]. During two-step photoionization of formaldehyde the molecule is excited to the $^1A_2$ electron state by the nitrogen laser pulse with the wavelength of 337 nm, the generation pulse duration of 2 ns, and the output power of 150 kW. Synchronization with the nanosecond H_2 VUV laser was accomplished through pulsed charging of the Blumlein lines of both lasers (Fig. 8). The laser pulse of the H_2 VUV laser was delayed by making longer the line charge cable. The error in determining the time delay between laser pulses was no larger than ±1 ns. In the NO_2 molecule the long-lived electron state was excited by the radiation of a dye laser pumped by a nitrogen laser. The requirements on accuracy of delay between laser pulses were less rigid in this case. The H_2 laser pulse was directed into a cylindrical photoionization cell without focusing. The N_2 laser radiation was focused by a lens with a focal length of 10 cm. The amplified ion signal was fed either to the oscilloscope or after the boxcar integrator to the chart recorder.

3.1.2. Experimental Results for Various Molecules

Formaldehyde Molecule. Figure 9 shows the dependence of the yield of formaldehyde TSPI on the delay between the exciting and ionizing laser pulses [7]. The

building-up time near the zero delays is related to the final duration of the laser pulses. The subsequent reduction of ionic current corresponds to the decay of the excited $^1A_2$ state. The fact that the decay observed is not exponential is connected with vibrational relaxation of the excited state or with simultaneous excitation of two vibrational states. For formaldehyde the radiative life time of the $^1A_2$ state lies in the microsecond range. The nanosecond decay observed at the excitation wavelength of 337 nm is fully related to nonradiative processes. In this connection the fluorescence quantum yield is rather low which apparently impedes fluorescence measurements and causes the life times of excited states measured in different works [45] to vary greatly. We should note that the advantage of the TSPI method is its applicability for studying predissociating and radiationless molecular states.

Nitrogen Dioxide Molecule. In this case the TSPI method was used to measure the absorption in the range 447 to 457 nm [9]. Figure 10 shows the dependence of ion photocurrent on the wavelength of the exciting dye laser. Part of the laser pulse was directed into an additional cell with NO_2 and the absorption was measured by scanning the spectrum. For comparison, this figure shows the measured absorption spectrum. As follows from Fig. 10, the signal of TSPI copies the absorption spectrum at the first step to a good degree. This points to the fact that transitions from the excited state to the ionization continuum have a weaker spectral dependence.

Other Molecules. Two-step photoionization of paraterphenyl [46] and tertiary amines [47] has been investigated under single laser-frequency condition. It was revealed that deactivation of dye-molecule excited states through the photoionization channel can be very effective and prevent formation of laser action. Detection possibilities to trace aniline amounts in the atmosphere were demonstrated in the experiment on two-step photoionization in an ordinary ionizing cell [48].

Recently selective photoionization of NO molecules via vibrational excited states with subsequent multiphoton ionization by dye laser [49] has been demonstrated for the first time. Photocurrent spectra were registered during wavelength tuning of both IR and dye lasers.

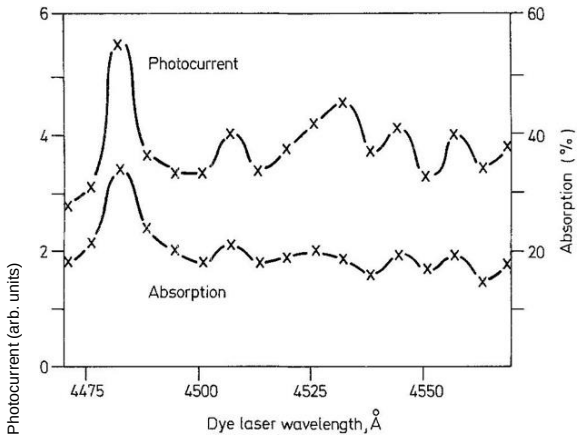


Fig. 10. Absorption spectrum of NO_2 measured by means of TSPI (upper curve) and the simultaneously recorded ordinary absorption spectrum (lower curve), for comparison [9]

3.2. Two-Steps Photoionization in the Mass-Spectrometer

In experiments on TSPI of formaldehyde and nitrogen dioxide molecules, recording the total ion current, the energy of two laser quanta suffices to form molecular ions only. Of great interest is the study into stepwise photoionization in mass spectrometers when along with the molecular ion it is possible to observe fragment ions. In this case we deal with a new method where we not only probe the population of the excited molecular state but also study the ability of a molecule to produce various fragments in a two-step process. In recording absorption spectra in the mass spectrometer the information obtained is two-dimensional by character – the spectrum produced can be simultaneously identified with the mass of the initial molecule or its fragment.

3.2.1. Experimental Technique

The experimental setup for studying the stepwise photoionization of polyatomic molecules in the mass spectrometer [6] comprises an MX 1311-type magnetic static mass spectrometer and time-synchronized exciting and ionizing lasers. The intermediate electron states of benzaldehyde, benzophenone, para- and ortho-nitrotoluene molecules were excited by a nitrogen laser (λ = 337 nm), with a laser pulse energy of 0.2 mJ and pulse duration 12 ns. To measure the absorption spectrum of NO_2 by the method of TSPI at the first step a dye laser was used, its wavelength was tuned in the range 440 to 470 nm. In all cases the excited molecules were ionized by an H_2 VUV laser with the generation energy of 0.5 μJ and pulse duration of about 1 ns. The laser pulses were directed into the ion source of the mass spectrometer transversely to each other (Fig. 11). The region of laser beam intersection was 0.1 × 0.1 × 1 cm^3. The photoions formed passed through the cylindrical ion optics and the magnetic separator, and were recorded by a secondary electron multiplier. The vapor of the molecules was admitted into the ionization chamber through a glass multichannel inlet at the estimated pressure of 10^{-4} to 10^{-6} Torr.

3.2.2. Experimental Results for Various Molecules

Benzaldehyde Molecule. The mass spectrum of benzaldehyde TSPI (Fig. 12a) consists of molecular ion and fragment $C_6H_5CO^+$ ions arising when the hydrogen atom of the aldehyde group breaks away [6, 8]. The characteristic feature of TSPI is that the fragment ion yield here is almost twice as much as compared to the case of single-photon ionization where the photon energy is equal to the total energy of two laser quanta. This suggests that the theory of mass spectrum formation based on assumptions that the excess ion energy is uniformly distributed over the degrees of freedom (statistic approximation) is of limited use. At the first stage the molecule is subjected to electronic excitation of the $n \leftrightarrow \pi^*$ type, which is connected with the transition of the *p*-electron of the oxygen atom to the antibonding orbital. The vibrational energy in this case is localized basically in the aldehyde group. This apparently increases the probability of eliminating the hydrogen atom from the aldehyde group in subsequent ionization of the molecule from the excited state.

Figure 12b illustrates the dependence of the yield of molecular and fragmentary photoions on the ionizing pulse time delay. The build-up of signal in the zero-delay

range occurs due to final duration of the laser pulses. A small drop in the region up to 1 ps is caused by scattering of excited molecules from the region of their interaction with the laser radiation. The absence of a rapid drop in ion current at delays below 1 ps agrees with the available data on fast $\tau_{st} \simeq 10^{-12}$s [50] conversion of the molecule to the triplet state.

Benzophenone Molecule. During stepwise photoionization of benzophenone molecules in the mass spectrometer molecular and fragment $C_6H_5CO^+$ ions can be observed [6, 8]. The dependence of the yield for molecular and fragment ions on the delay between laser pulses is shown in Fig. 13. The fragment ion yield becomes maximum right after the nitrogen laser pulse, then drops exponentially with the time of 14 ns and finally comes to the stationary level. The yield of ions at a maximum is quadratically dependent on the exciting radiation intensity, which points to two-step excitation. When excited to the first singlet electron state the benzophenone molecule also undergoes fast conversion to the triplet state from which it is either ionized by the H_2 laser pulse or absorbs the second photon of the nitrogen laser and dissociates from the highly excited triplet state. The excited C_6H_5CO*radical may be further ionized by the H_2 laser. The drop in signal with the time of 14 ns corresponds probably to the radiative life time of radical.

Other Molecules. The kinetics of formation of para- and ortho-nitrotoluene ions during stepwise photoionization is more complicated by nature and not clearly understood yet [6]. In TSPI of ortho- nitrotoluene one can observe only the fragmentary ions $C_6H_4CH_3^+$ and $C_6H_4(CH_2)NO^+$ with a rather complex time dependence of their formation. In paranitrotoluene only one ion $C_6H_4CH_3$ is observed which is related to the elimination of the NO_2 group. The appearance of the $C_6H_4(CH_2)NO^+$ ion in nitrotoluene with a substituent in the ortho-position can be explained by rearrangement dissociation with an elimination of the OH group either in the excited state of the molecule or in the ion. The absence of molecular ion in the mass spectrum enables us to suggest that dissociation occurs in the excited molecular state.

Nitrogen Dioxide Molecule. The TSPI spectrum of the NO_2 molecule was measured by scanning the laser wavelength at the first step from 445 to 470 nm [6]. In the general case the TSPI spectrum depends both on the absorption spectrum at the first step and the dependence of ionization yield at the second step. The latter is determined mainly by Franck-Condon factors for molecular photoionization at transitions between the vibrational states of the electron-excited molecule and ion. The experimental results show that the TSPI spectrum of NO_2 is governed basically by the absorption at the first step. The minimum recordable coefficient of absorption in NO_2 equals 10^{-7} cm^{-1}. For benzaldehyde and benzophenone molecules with more favorable cross-sections of ionization from excited states it comes to about 10^{-10} cm^{-1}.

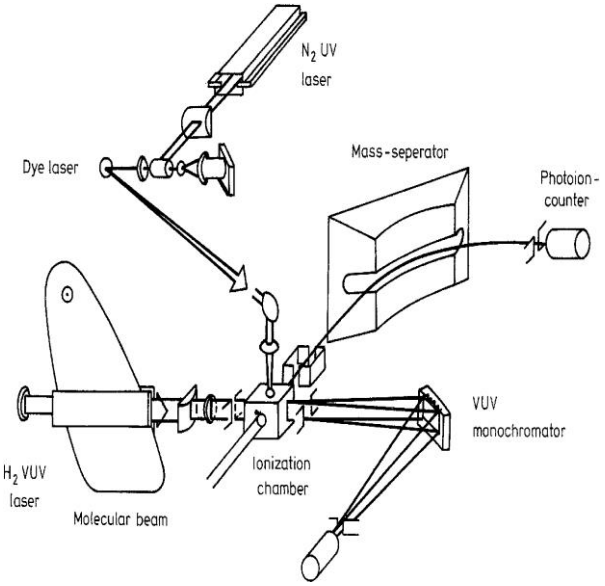


Fig. 11. Experimental arrangement for two-step photoionization by a mass spectrometer [6]

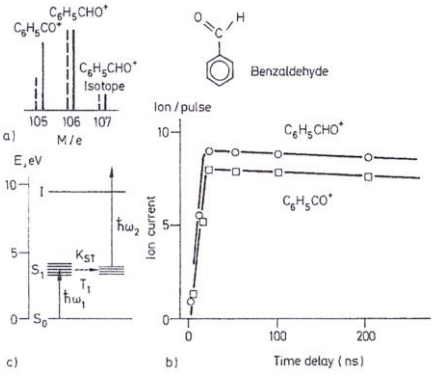


Fig. 12*a–c*. TSPI of benzaldehyde (*a*) mass spectra (solid lines) and one-photon ionization (dashed lines), (*b*) dependences of molecular and fragment photoions on time delay between pulses, (*c*) scheme of TSPI [6]

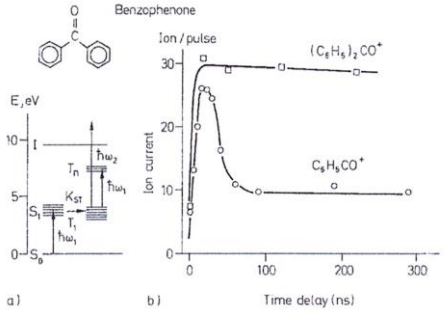


Fig. 13*a* and *b*. Stepwise photoionization of benzophenone (*a*) scheme of stepwise photoionization, (*b*) dependences of molecular and fragment photoions yields on time delay between the laser pulses [6]

The aniline two-step photoionization spectrum [51] with the dye laser wavelength tuned in the region of 293–298 nm of the $^1B_2 \leftarrow^1 A_1$ transition was also in good agreement with the ordinary absorption spectrum. The main peak in the spectrum was due to a molecular ion; the fraction of fragment ions did not exceed 1%. The excited state photoionization cross-section was 3.5×10^{-17} cm^2 at the wavelength of 293.9 nm.

Isotopically selective two-step photoionization was realized in the experiments with tetrazine [52] and NO [53].

A great improvement of the selective photoionization method was the use of pulsed supersonic cooled molecular beams. Maximum photoionization efficiency (nearly 100%) was achieved in the experiments with cooled molecules of metal-carbonils [54] and aniline [55]. In the latter case under deep cooling $T_{rot} = 0.2$ K the ultimate ionization efficiency was reached with aniline ionization by two UV photons and a radiation intensity equal to just 2×10^7 W/cm^2.

3.3. Photoionization and Photofragmentation Induced by Intense UV Laser Radiation

Recent years have seen interest in photoionization and photofragmentation of polyatomic molecules induced by an intense laser radiation. This is due to the necessity to use powerful lasers in order to achieve the ultimate efficiency of the selective photoionization of molecules in the mass-spectrometer. On the other hand, the investigation of polyatomic molecular interaction with powerful laser radiation is of independent interest and allows to obtain novel information on the excited states of a molecule, its neutral and ionized fragments. It was a successful development of powerful excimer and UV and VUV lasers that made an essential contribution to the realization of such experiments [56].

The above-described experiments on selective two-step photoionization of polyatomic molecules were performed at fairly low intensities of laser radiation. In the photoionization mass spectra there were a few ions observed whose appearance potentials were smaller than the energy of two laser quanta. Other situation took place when molecules are irradiated by UV or visible radiation with an intensity higher than 10 MW/cm^2. In this case, at an average, a molecule deals with a great number of absorbed quanta, which results in formation of a severely fragmentated mass spectrum.

In the general case three possible mechanisms are being discussed which, in principle, contribute to PIMS (photoionization mass spectrometry) formation of molecules (Fig. 14). The first mechanism (Fig. 14*a*) is parent ion fragmentation (PIF) corresponding to the subsequent dissociation of ions in the laser radiation field, beginning with a molecular ion [57–59] as a rule. According to the second mechanism (Fig. 14*b*) — "autoionization tree" (AT) — the excitation of neutral molecules proceeds through resonant or near-resonant levels beyond the ionization limit with subsequent autoionization and fragmentation of molecules [31, 60]. The third mechanism (Fig. 14*c*) deals with neutral fragments photoionization (NFP) of the molecules. They can be produced very efficiently under absorption of the initial photons [61, 57].

In the experiments on MPI of polyatomic molecules the mass spectra of photoions are, as a rule, rather complicated. Under the high radiation intensities necessary for two or three photon transitions from the ground state the subsequent transitions which cause molecular fragmentation, are usually close to saturation. By the stepwise photoionization method, the transition to the ionization continuum occurs via resonant intermediate levels with high efficiency. This permits one to investigate a photoionization mass spectrum of molecules in a wide range of intensities. It is of a great interest for probing the mechanism of formation of polyatomic molecules photoionization mass spectra.

3.3.1. Experimental Setup

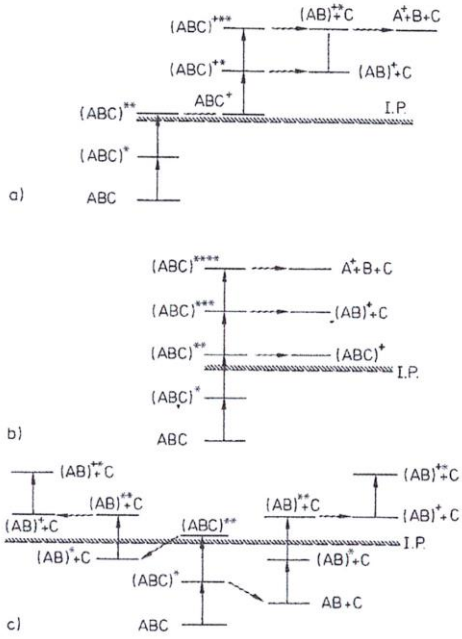


Fig. 14 *a–c*. Schemes of different mechanisms of photoionization mass-spectrum formation: (*a*) parent ion fragmentation (PIF), (*b*) through the autoionization states, "autoionization tree" (AT) model, (*c*) neutral fragments photoionization (NFP)

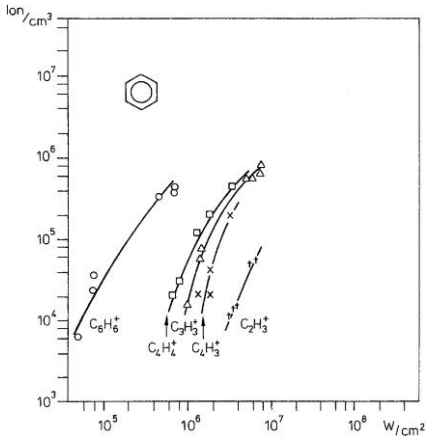


Fig. 15. Dependences of photoions yields in benzene on laser radiation intensity (λ = 249 nm) [57]

3.3.2. Experimental Results for Various Molecules

Benzene Molecule. Figure 15 shows yield dependences of the most characteristic ions in benzene PIMS on laser radiation intensity with λ = 249 nm [57]. Under a radiation intensity of less than 1 MW/cm^2 PIMS reveals a molecular ion only, which is formed under two-step photoionization via the intermediate electronic state $^1B_{1u}$. When radiation intensity increases, more light ions appear. When the intensity exceeds 300 MW/cm^2 C^+ ion begins to dominate in PIMS [59]. The total ion yield is very large and reaches almost 10% at a radiation intensity close to 1 GW/cm^2 [57]. With comparison to benzene MPI by visible radiation with a wavelength of λ = 504 nm the ion yield of two-step photoionization is 150 times larger despite that the UV radiation intensity is more than two orders lower. Apart from a high sensitivity benzene ionization by an excimer laser is selective: that is under maximum intensities there were practically no such atmospheric components as H_2, H_2O in the mass spectrum.

The lifetime of benzene molecule in the intermediate electronic state is longer than the laser pulse duration. This causes high efficiency of the molecular ion formation. The presence of fragment ions under relatively low radiation intensity

(nearly 10 MW/cm^2) can not be explained by an AT mechanism taking into consideration very short lifetimes of autoionization states (usually equal to $10^{12} + 10^{-13}$ s). Moreover, it was shown that there is a lack of doubly charged benzene ions in PIMS although their formation threshold (26 eV) is lower than the appearance potential of the C^+ ion [59]. This also demonstrates that AT mechanism plays a minor role in PIMS formation.

The experiment on benzene molecule photoionization by joint action of UV and visible lasers with wavelengths of 241 and 483 nm, respectively, [58] was an additional confirmation of the PIF mechanism of fragment ion formation for the case of a high intensity of the laser radiation. Below an intensity of 3 MW/cm^2 the action of only UV radiation caused formation of a molecular ion. On the contrary the intensity of visible radiation was 0.4 GW/cm^2, which is sufficient for benzene MPI if two-photon transition from the ground state is allowed by the selection rules. When the frequencies of visible radiation correspond to two- photon forbidden transitions to the vibrational sublevel of the S_1 state the MPI signal was not observed. Under these conditions joint UV and visible radiations caused extensive molecular fragmentation typical for MPI [31]. However, it remains somewhat vague as to whether a powerful visible-radiation induced fragmentation through the excited autoionization states, or a visible radiation itself provokes parent ion fragmentation. To clear up this point the visible radiation was delayed relative to UV pulse by 17 ns, a time sufficient for the decay of an intermediate state. This revealed that PIMS turned out to be analogous to the previous case. Apart from this the total charge of all ions in one- colour and two-colour experiments was just the same. All above-said strongly argues against any ladder climbing in the neutral molecule above the ionization potential.

Other Molecules. The experiment using benzaldehyde molecule [57, 63] was conducted with a radiation wavelength of 249 nm. A molecular transition at the first step occured at highly excited vibrational levels of the second singlet S_2. Energy of two UV photons was also sufficient to ionize this molecule.

Figure 16 shows photoionization mass spectra of benzaldehyde for two intensities of laser radiation — 2 MW/cm^2 and 1 GW/cm^2. It is characteristic that under relatively low radiation intensity the fragment ions prevail in PIMS. The mass spectra below I = 1 GW/cm^2, which is a typical intensity for MPI experiments, reveal very strong fragmentation of a molecule with maximum C^+ ion yield. Figure 17 demonstrates the dependences of the most characteristic photoion yields on the laser radiation intensity. A general trend in PIMS transformation under high intensity consists in the appearance of lighter ions with a simultaneous yield saturation of heavy ones. The total yield of benzaldehyde photoionization is two orders less than in benzene case. This fact and the observed domination of the fragment ions in the mass-spectrum at all intensities reveal that for this molecule an important part in PIMS formation is played by the NFP mechanism (Fig. 14*c*).

An interesting peculiarity of benzaldehyde photoionization is the high yield of an ion with m/e = 78, which corresponds to the benzene ion $C_6H_6^+$ (Fig. 16), under low radiation intensity. It is evident that benzene cannot be produced by simple elimination of arbitrary parts of the benzaldehyde molecule. To produce it one needs to strip the aldehyde CHO group with transferring the aldehyde hydrogen atom to the

benzene ring. The analysis of the experimental data reveals [57] that appearance of the fragment with m/e = 78 corresponds to the collisionless rearrangement dissociation of a benzaldehyde molecule in the electronically excited state resulting in benzene and CO molecules (Fig. 17).

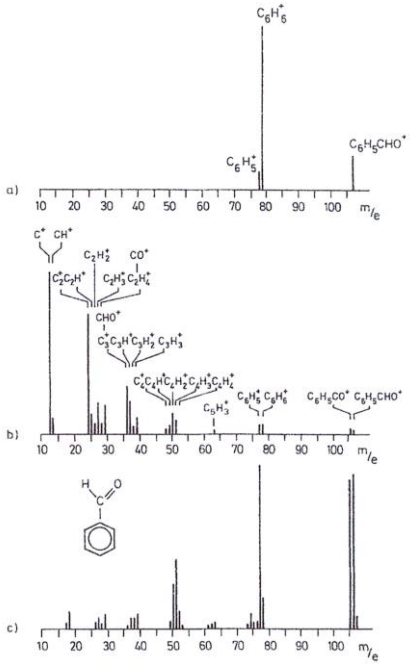


Fig. 16*a–c*. Mass spectra of benzaldehyde (*a*) photoionization, I = 2 MW/cm^2, (*b*) I = 1 GW/cm^2 [63], (*c*) electron impact data, for comparison [71]

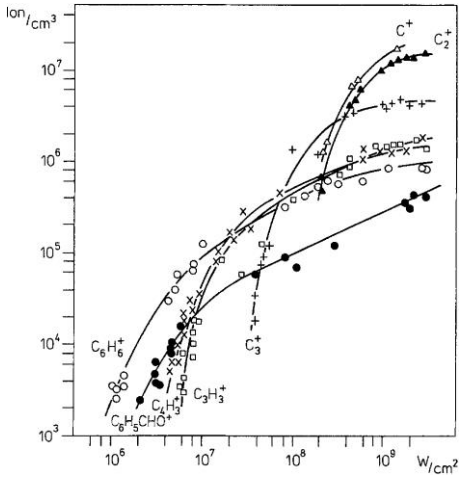


Fig. 17. Dependences of particular photoions yields in benzaldehyde on laser radiation intensity (λ = 249 nm) [57]

One of the first works [61] on molecular photoionization by the intensive UV radiation vividly demonstrated the importance of molecular dissociation from the electronically excited states up to the ionization limit in the mass-spectra formation. In case of the acetaldehyde the energy of two UV photons was a little lower than the molecule ionization potential. This resulted in disappearance of the molecular ion due to a high dissociation rate from the highly excited state. The analysis of the data on benzene photoionization yield [59] using ArF laser (λ = 193 nm) radiation allowed to evaluate the lifetime of the excited state making certain assumptions regarding the photoionization cross-section from this state. It turned out to be 20 ps. Nevertheless, the role of the NFP mechanism in the photoionization mass-spectrum formation can be essential even under stability of intermediate electronic states. Photoionization of molecules from the intermediate electronic state with large storage of vibrational energy or with a nuclear configuration of this state differing from that of an ion can result in a sharp increase of molecular dissociation as the competitive channel with respect to autoionization [57]. This channel of neutral-fragments formation seems important for the experiments with benzaldehyde with an excitation wavelength of 249 nm.

A detailed theoretical description of the ionization processes of molecules induced by intense laser radiation [43, 59, 65] faces serious problems due to lack of data on the appearance potentials of various fragment ions, electronic terms location, absorption cross-section, etc. A qualitative similarity of PIMS under moderate radiation intensity with mass-spectra during the electronic impact testifies that mass-spectra formation is determined to an essential degree by the energetics of bonds in molecules. Using the statistic approach this permits to calculate, in the first approximation, the dependences of PIMS on the absorbed energy [66], being in qualitative agreement with the experiment.

4. Towards a Laser Selective Molecular Detector

The analysis of matter by the mass-spectroscopic method lies in transforming the molecules of a sample into ions with further separation and analysis by the mass-to-charge ratio. Mass spectrometrists have always been aiming their efforts at creating ion sources with a high ionization efficiency at moderate molecular fragmentation. The progress made in this direction makes the mass-spectrometric method of analysis one of the most sensitive ones. In favorable cases it is possible to analyze substances with no higher than 2.5×10^{-14} g [67]. The characteristic efficiency of transformation of molecules into ions with their subsequent detection in present-day mass spectrometers amounts to 10^{-5} of the number of molecules [68] and hence is far from being ultimate. The case is somewhat worse with selectivity. As a rule, molecular mass spectra consist of a lot of fragment ions where there are often no molecular ions at all. Despite the fact that the analysis of fragments gives valuable information on the molecular structure, it is rather difficult to analyze multicomponent mixtures. Due to the overlap of mass spectra it is especially difficult to analyze molecular components at low percentage. Preliminary separation of mixture components in a chromatograph can partially overcome this problem [68] but not completely yet.

In [1, 2] the authors proposed and developed for the first time a basically new approach to the analysis of trace amounts of complex molecules. It consists in selective multistep laser photoionization of molecules with subsequent mass-spectroscopic analysis of the ionization products. In this method the molecular ionization selectivity is determined by the selectivity of molecular excitation to vibrational and electronic states, and may be rather high. As the wavelength of exciting laser radiation is tuned, the photoion spectrum is modulated by the optical absorption spectrum and thus the information on molecules results from highly selective two-dimensional mass-optical spectra. Besides, as it has been demonstrated in the experiments on two-step photoionization [55, 57], this method may be very sensitive due to high efficiency of molecular ionization by intense laser radiation.

4.1. Comparison Between Multiphoton and Multistep Molecular Photoionization

The method of MPI of polyatomic molecules is widely used at present for systematic studies of the spectroscopy of excited molecular states particularly forbidden for single-photon transitions. The attractive feature of the method is that it is rather simple to produce multiphoton spectra, and its sensitivity is much higher compared to that in fluorescence measurements. Another advantage is the possibility of using visible and near-ultraviolet radiation for studying the electron states in the vacuum ultraviolet range of the spectrum. Though multiphoton ionization in mass spectrometers gives a lot of new information on photoionization and photofragmentation of molecules under intense laser radiation, systematic use of molecular MPI can hardly be applicable to mass analysis because of a high degree of fragmentation and rather low efficiency of molecular ionization.

The method of multistep photoionization of polyatomic molecules in the mass spectrometer was developed from the very beginning to detect trace amounts of complex molecules. Using one or several lasers tuned in resonance to appropriate molecular transitions, including vibrational ones, it is possible to excite successively the molecule to any state with very high selectivity from which it is ionized with high efficiency (Fig. 18).

4.2. Optimum Scheme of Selective Stepwise Molecular Photoionization

There are several basic schemes for stepwise molecular photoionization. Below we shall consider them from the standpoint of maximum selectivity and efficiency of ionization.

4.2.1. Through Intermediate Electron States

In this case the molecules are excited to the lower electron states by visible or ultraviolet radiation with subsequent ionization by VUV or far UV laser radiation (Fig. 18). The main advantage of this scheme rests in the fact that the quantum energy of ionizing radiation may be taken much smaller than the molecular ionization potential, and so only excited molecules can be ionized. An additional channel of information arises when an ionizing laser pulse with a controllable delay is used [6, 7]. In some cases this may essentially increase the selectivity of the two-step process.

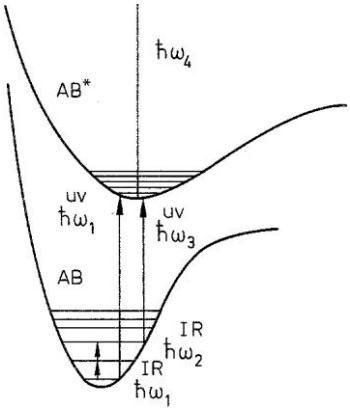


Fig. 18. Schemes of selective multistep photoionization of molecules

It should be noted that in this rather simple scheme other photoionization channels may exist, which cause the selectivity to be reduced. In the typical case when $2\hbar\omega_1 < I < 2\hbar\omega_2$, where ω_1 and ω_2 are the laser radiation frequencies, respectively, at the first and second steps and I is the molecular ionization potential, two-step molecular photoionization is possible through high-lying electron states by two-step laser radiation. Besides, three-step photoionization may exist when in the presence of resonance, the molecule absorbs in succession two photons of the exciting laser with frequency ω_1. In the experiments on selective stepwise photoionization [6–8], however, where lasers in the visible or UV ranges were used for the first step with ionization conducted by a delayed pulse of the VUV laser and the laser pulse sequence inverted, no signals of TSPI have been observed for all molecules under study. This is apparently due to the fact that, when polyatomic molecules are excited to high-lying electron states, nonradiative processes causing dissociation complete with the ionization from these states. These ionization channels mut therefore be suppressed effectively. Such suppression must be particularly strong in recording molecular ions.

At $2\hbar\omega_1 > I$ two-step photoionization of molecules in a one-frequency field becomes possible. In this case the only limitation on the laser radiation intensity is the loss of mass-spectral information due to strong molecular fragmentation. Yet for many molecules at such radiation frequencies rather high-lying electron states become excited. The molecules from these states can dissociate quickly and the absorption spectra are often structureless.

To attain the maximum sensitivity of molecular detection, the laser-pulse energy flux at each step should be close to the saturation energy flux $\mathcal{E}_{\text{sat}} = \hbar\omega/2\sigma$ where σ is the cross-section of an appropriate transition. For a characteristic value of the cross-section $\sigma = 10^{-18}\text{cm}^{-2}$ the saturation energy flux equals 0.1 J/cm^2. This value is quite accessible for present-day lasers even in the VUV region of the spectrum. The studies into ultimate efficiencies of stepwise photoionization for benzene and benzaldehyde molecules have shown that even with the laser energy close to the absorption saturation energy at the first step there will be fragment ions in the mass

spectrum. At higher intensities of laser radiation, the information on the molecule may be lost because of mass spectrum degradation. Nevertheless, it follows from [57, 59] that when the molecule has no time to dissociate from the intermediate electron state during a laser pulse, and the total energy of laser quanta exceeds the potential of molecular ionization from the intermediate electron vibrational state (this corresponds to a small fraction of molecules decaying in the photodissociation channel which competes with photoionization), the ion yield in stepwise photoionization amounts to 10% of the number of molecules. So, the efficiency of laser two-step photoionization is four orders higher than the value obtainable in standard mass spectrometers with nonselective ionization by electron impact, and approaches its natural limit.

Under optimum conditions, in the absence of secondary photoionization channels, the ionization selectivity is governed by electronic spectra of molecular absorption. Yet it is known that the electronic absorption spectra of polyatomic molecules in gas are less characteristic than vibrational, IR spectra and in this case it is difficult to obtain reasonable photoionization selectivity. Radical increase in photoionization selectivity through electron states can be accomplished using a cooled supersonic molecular jet. In recent works supersonic molecular beams were used to cool such complex molecules as phthalocyanine ($C_{32}N_8H_{18}$) [69]. The absorption spectrum of this molecule under deep cooling of vibrational and rotational degrees of freedom consisted of lines with width of 0.5 to 1.0 cm^{-1}. In the electronic absorption spectrum of oxalyl fluoride ($C_2O_2F_2$) cooled in a pulsed supersonic beam to 0.17 K [38] single vibrational-rotational lines were resolved completely. In this respect we can speak about ultimate spectral selectivity in radiation absorption.

In the two-step photoionization spectrum of aniline cooled in the supersonic free jet [55] line widths also did not exceed 1 cm^{-1} at radiation intensities less than 1 MW/cm^2. By intensity increase lines were broadened up to 5 cm^{-1} when I=10÷13 MW/cm^2. We should note that an increase in selectivity at the first step during molecular cooling is beneficial for obtaining the ultimate sensitivity since to saturate the first step takes a much smaller intensity of laser radiation and, hence, subsequent nonselective transitions under this radiation will essentially be suppressed.

Let us evaluate the ultimate sensitivity of the scheme for detection of impurities in the air with cooling of molecules in a supersonic free jet. The number of ions selectively formed during a pulse may be expresses as

$$\mathcal{N}_{\text{ion}} = \eta \cdot \gamma_{\text{ph.ion}} \cdot P_{\text{atm.}}/P_{\text{buf}} \cdot \kappa \cdot n_{\text{beam}} \cdot V_{\text{ph.ion.}}, \qquad (2)$$

where η is the recording efficiency of photoions, $\gamma_{\text{ph.ion}}$ is the two-step photoionization yield, P_{buf} is the buffer gas pressure, κ is the fraction of admixed molecules, n_{beam} is the molecular concentration in the beam, $V_{\text{ph.ion.}}$ is the photoionization volume. Taking the recording of one selectively formed photoion as the molecular detection threshold, and substituting the values η = 0.5 [57], $\gamma_{\text{ph.ion}}$ = 0.1 [57], P_{buf} = 10 atm, $n_{\text{beam}} = 2 \times 10^{15}\text{cm}^{-3}$ which corresponds to the maximum gas pressure of 5×10^{-2} Torr when collisionless extraction of ions from the beam is still possible

and which is practicable in cooled supersonic beams [70], $V_{\text{ph.ion.}} = 0.1\ \text{cm}^3$, we have $\kappa = 10^{-12}$.

In some cases, due to high sensitivity the two-step photoionization through intermediate electronic states is of interest for detecting impurities in the air in the simplest case without using mass-spectrometric equipment. Work [48] has demonstrated the detection of aniline with the help of TSPI-spectrum measurements in the ionization chamber with the air at 1 atm and relative concentration of aniline of 10^{-5}.

4.2.2. Through Intermediate Vibrational States

Vibrational spectra carry the most information about polyatomic molecules and so, from the standpoint of trace-detection selectivity, the stepwise photoionization through intermediate vibrational states is of particular interest. It is rather difficult to realize this scheme because during vibrational excitation the photoionization-limit shift is smaller than the width of the photoionization band-edge and single-photon ionization of unexcited molecules is unlike. Besides, when a short-wave radiation quantum $\hbar\omega_2$ absorbed, photodissociation competes with the process of photoionization since the total energy of laser photons exceeds slightly the molecular ionization potential and the Franck-Condon factors for transitions with ionization may be small in the general case. The potentialities of this scheme can be estimated by considering the simplest model of TSPI when the tunable laser radiation with the frequency ω_1 selectively excites the molecular vibrations active in a photoionization transition under radiation with the frequency ω_2 chosen in the region of maximum variation of the photoionization cross-section value [9].

Let us assume that as the molecule is photoionized from the excited vibrational state the photoionization cross-section changes by some value $\Delta\sigma$. The case when the maximum number of molecules is excited at the frequency ω_1 is optimum for molecular detection. In this case the energy flux of the first laser pulse should satisfy the condition

$$\mathcal{E}(\omega_1) \gtrsim \mathcal{E}_{\text{sat}}^{(1)} = \hbar\omega_1/2\sigma_{\text{exc}} \tag{3}$$

where σ_{exc} is the cross-section of molecular excitation to the intermediate state. Then the number of molecules transferred to the excited state equals

$$\mathcal{N}_{\text{exc}} \simeq \mathcal{N}_0 q/2, \tag{4}$$

where $\mathcal{N}_0$ is the number of molecules in the ground state, q is the fraction of molecules being in resonance with the exciting radiation. For a maximum photoion yield the laser pulse at the frequency ω_2 must have the energy flux

$$\mathcal{E}(\omega_2) \lesssim \mathcal{E}_{\text{sat}}^{(2)} = \hbar\omega_2/\left(\sigma_{\text{ph.ion.}} + \sigma_{\text{ph.dis.}}\right). \tag{5}$$

In this case each excited molecule becomes broken up, with a probability close to unity, through photoionization and photodissociation channels. The buildup in the

number of ions formed under these conditions by virtue of selective two-step photoionization is determined by the simple expression

$$\Delta\mathcal{N}_{\text{ion}}^{(2)} = \mathcal{N}_{\text{exc}} \frac{\Delta\sigma}{(\sigma_{\text{ph.ion.}}+\sigma_{\text{ph.dis.}})} = \mathcal{N}_0 \cdot \frac{q}{2} \cdot \frac{\Delta\sigma}{(\sigma_{\text{ph.ion.}}+\sigma_{\text{ph.dis.}})} \qquad (6)$$

Thus, molecular detection results in recording a small number of selectively formed ions $\Delta\mathcal{N}_{\text{ion}}^{(2)}$ against the fluctuation $\left(N_{\text{ion}}^{(2)}\right)^{1/2}$ of a great number of nonselective ions. This makes it possible to evaluate the minimum number of detectable molecules

$$\boldsymbol{\mathcal{N}_0^{\min} = 1/\eta \cdot (2/q)^2 \cdot \left(\sigma_{\text{ph.ion.}}/\Delta\sigma\right) \cdot (\sigma_{\text{ph.ion.}} + \sigma_{\text{ph.dis.}})/\Delta\sigma.} \qquad (7)$$

Substituting the numerical values $\eta = 0.5$, $q = 0.01$, $\sigma_{\text{ph.ion.}}/\Delta\sigma = 10$, $\sigma_{\text{ph.dis.}}/\sigma_{\text{ph.ion.}} = 10$ into (7) we have $\mathcal{N}_0^{\min} = 10^7$. The efficiency of selective photoionization, in this case, is rather high, but still six orders lower than in the ionization scheme through electronic states. Besides, it may be much worse due to overlapping of intense mass spectra of single-photon ionization from molecules of a different type with a lower ionization potential.

The sensitivity and selectivity of this scheme can be substantially increased, first, through multistep vibrational excitation. This will lead to a considerable shift of the photoionization limit from the excited state and hence to an increase of the fraction of selective ions. Secondly, they can be increased using a cooled molecular beam. In this case the population factor q of a molecular state being in resonance with the laser field may be close to unity, and this will materially increase the selectivity and sensitivity of detection. The efficiency of selective photoionization will be governed by the competitive process of dissociation during absorption of short-wavelength photons.

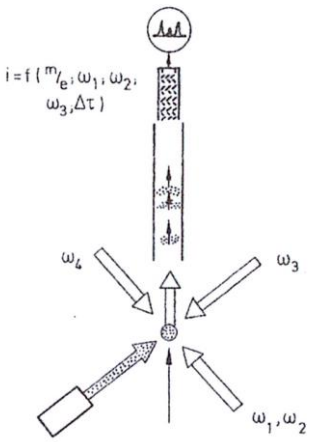


Fig. 19. Optimum scheme of highly selective detector for trace amounts of molecules by laser photoionization

4.2.3. Successive Excitation of Intermediate Vibrational and Electronic States

This scheme (Fig. 18) is a combination of the two above mentioned schemes, having the high degree of selectivity of vibrational molecular spectra and the merits of photoionization through electronic states as the absence of background single-photon ionization and the acquisition of data on lifetime of electronically excited molecules. The use of supersonic pulsed-cooled molecular beams here is an important constituent of the technique like in the previous cases. Adequate mass- spectrometric equipment must ensure recording of photoionic mass spectra during a pulse. Thus, the optimum scheme of laser molecular detector shown in Fig. 19 will enable us to come close to detecting smelles, one of the most difficult and important analytical problems of today.

References

1. *Ambartzumian R.V., Letokhov V.S.* // Appl. Opt. 1972. Vol. 11. P. 354.

2. *Letokhov V.S.* In: Frontiers in Laser Spectroscopy, Proc. Les Houches School. 1975. Vol. 2 / ed. by R. Balian, S. Haroche, S. Liberman. North-Holland, Amsterdam, 1977. P. 771; also, in Tunable Lasers and Applications / ed. by A. Mooradian, T. Jaeger, P. Stokseth. Berlin, Heidelberg, N.Y.: Springer, 1976. P. 122; Phys. Today. 1977. Vol. 30. P. 23.

3. *Antonov V.S., Knyazev L.N., Movshev V.G.* // Kvant. Elektron. (Russ.). 1975. Vol. 2. P. 1305; *Knyazev L.N. , Letokhov V.S., Movshev V.G.* // IEEE J. Quantum Electron. 1975. Vol. 11. P. 805.

4. *Andreyev S.V., Antonov V.S., Knyazev L.N., Letokhov V.S., Movshev V.G.* // Phys. Lett. 1975. Vol. 54 A. P. 91.

5. *Potapov V.K., Movshev V.G., Letokhov V.S., Knyazev L.N., Evlasheva T.I.* // Sov. Quantum Electron. 1977. Vol. 6. P. 1437.

6. *Antonov V.S., Knyazev L.N., Letokhov V.S., Matiuk V.M., Movshev V.G., Potapov V.K.* // Opt. Lett. 1978. Vol. 3. P. 37.

7. *Andreev S.V., Antonov V.S., Knyazev I.N., Letokhov V.S.* // Chem. Phys. Lett. 1977. Vol. 45. P. 166.

8. *Antonov V.S., Knyazev I.N., Letokhov V.S., Matink V.M., Movshev V.G., Potapov V.K.* // Sov. Tech. Phys. Lett. 1977. Vol. 3. P. 531.

9. *Antonov V.S., Knyazev I.N., Letokhov V.S., Movshev V.G.* // Zh. Eksp. Teor. Fiz. 1977. Vol. 73. P. 1325.

10. *Held B., Mainfray G., Manuc C., Morellec J.* // Phys. Rev. Lett. 1972. Vol. 28. P. 130.

11. *Collins C.B., Johnson B.W., Mirza M.Y., Popescu D., Popescu I.* // Phys. Rev. A. 1974. Vol. 10. P. 813.

12. *Granneman E.H.A., Klewer M., Nygaard K.J., Van der Wiel M.J.* // J. Phys. B. 1976. Vol. 9. P. 865.

13. *Klewer M., Beerlage M., Los J., Van der Wiel M.J.* // J. Phys B. 1977. Vol. 10. P. 2809.

14. *Feldman D.L., Lengel R.K., Zare R.N.* // Chem. Phys. Lett. 1977. Vol. 52. P. 413.

15. *Herrman A., Leutwyler S., Schumacher E., Wöste L.* // Chem. Phys. Lett.

1977. Vol. 52. P. 418; *Herrmann A., Schumacher E., Wöste L.* // J. Chem. Phys. 1978. Vol. 68. P. 2327.

16. *Mathur B.P., Rothe E.W., Reck G.P., Lightman A.J.* // Chem. Phys. Lett. 1978. Vol. 56. P. 336.

17. *Johnson P.M., Berman M.R., Zakheim D.* // J. Chem. Phys. 1975. Vol. 62. P. 2500; *Petty G., Tai C., Dalby F.W.* // Phys. Rev. Lett. 1975. Vol. 34. P. 1207.

18. *PJohnson M.* // J. Chem. Phys. 1975. Vol. 62. P. 4562; Johnson P.M. // J. Chem. Phys. 1976. Vol. 64. P. 4143.

19. *Dalby F.W., Petty-Sil G., Pryce M.H.L., Tai C.* // Can. J. Phys. 1977. Vol. 55. P. 1033; *Tai C., Dalby F.W.* // Can. J. Phys. 1978. Vol. 56. P. 183.

20. *Lehmann K.K., Smolarek J., Goodman L.* // J. Chem. Phys. 1978. Vol. 69. P. 1569.

21. *Zakheim P., Johnson P.M.* // J. Chem. Phys. 1978. Vol. 68. P. 3644.

22. *Johnson P.M.* // J. Chem. Phys. 1976. Vol. 64. P. 4638.

23. *Vaida V., Turner R.E., Casey J.L., Colson S.D.* // Chem. Phys. Lett. 1978. Vol. 54. P. 25.

24. *Parker D.H., Sheng S.J., El-Sayed M.A.* // J. Chem. Phys. 1976. Vol. 65. P. 5534; *Parker D.H., Berg J.O., El-Sayed M.A.* // Chem. Phys. Lett. 1978. Vol. 56. P. 197.

25. *Parker D.H., Avouris P.* // Chem. Phys. Lett. 1978. Vol. 53. P. 515.

26. *Neiman G.C., Colson S.D.* // J. Chem. Phys. 1978. Vol. 68. P. 5656.

27. *Robin M.B., Kuebler N.A.* // J. Chem. Phys. 1978. Vol. 69. P. 806.

28. *Berg J.O., Parker D.H., El-Sayed M.A.* // Chem. Phys. Lett. 1978. Vol. 56. P. 411.

29. *Turner R.E., Vaida V., Molini C.A., Berg J.O., Parker D.H.* // Chem. Phys. 1978. Vol. 28. P. 47.

30. *Berg J.O., Parker D.H., El-Sayed M.A.* // J. Chem. Phys. 1978. Vol. 68. P. 5661.

31. *Zandee L., Bernstein R.B., Lichtin D.A.* // J. Chem. Phys. 1978. Vol. 69. P. 3427; *Zandee L., Bernstein R.B.* // J. Chem. Phys. 1979. Vol. 70. P. 2574.

32. *Zandee L., Bernstein R.B.* // J. Chem. Phys. 1979. Vol. 71. P. 1359.

33. *Heath B.A., Kuebler N.A., Robin M.B.* // J. Chem. Phys. 1979. Vol. 70. P. 3362.

34. *Krogh-Jespersen K., Rava R.P., Goodman L.* // Chem. Phys. 1979. Vol. 44. P. 295.

35. *Williamson A.D., Compton R.N., Eland J.H.D.* // J. Chem. Phys. 1979. Vol. 70. P. 590.

36. *Rava R.P., Goodman L., Krogh-Jespersen K.* // Chem. Phys. Lett. 1979. Vol. 68. P. 337.

37. *Krogh-Jespersen K., Rava R.P., Goodman L.* // Chem. Phys. 1980. Vol. 47. P. 321.

38. *Murakami J., Kaya K., Ito M.* // J. Chem. Phys. 1980. Vol. 72. P. 3263.

39. *Parker D.H., Pandolfi R., Stannard P.R., El-Sayed M.A.* // Chem. Phys. 1980. Vol. 45. P. 27.

40. *Heath B.A., Robin M.B., Kuebler N.A., Fisanick G.J., Eichelberger T.S.* // J. Chem. Phys. 1980. Vol. 72. P. 5565.

41. *Heath B.A., Fisanick G.J., Robin M.B., Eichelberger T.S.* // J. Chem. Phys. 1980. Vol. 72. P. 5991.

42. *Glownia J.H., Riley S.J., Colson S.D.* // J. Chem. Phys. 1980. No. 72. P. 5998.

43. *Parker D.H., Avouris P.* // J. Chem. Phys. 1979. Vol. 71. P. 1241.

44. *Parker D.H., El-Sayed M.A.* // Chem. Phys. 1979. Vol. 42. P. 379.

45. *Fisanick G.J., Eichelberger T.S., Heath B.A., Robin M.B.* // J. Chem. Phys. 1980. Vol. 72. P. 5571.

46. *Letokhov V.S., Chebotayev V.P.* Nonlinear Laser Spectroscopy. Springer, 1977.

47. *Sakurai K., Capelle G., Broida H.P.* // J. Chem. Phys. 1971. Vol. 54. P. 1412.

48. *Aoki T., Morikawa T., Sakura K.* // J. Chem. Phys. 1973. Vol. 59. P. 1543.

49. *Zubarev I.G., Kotov A.V., Logunov O.A., Stoilov Yu.Yu.* // Sov. J. Quant. Electron. 1978. Vol. 8. P. 24.

50. *Zapka W., Schäfer F.P.* // Appl. Phys. 1979. Vol. 20. P. 287.

51. *Brophy J.H., Rettner C.T.* // Opt. Lett. 1979. Vol. 4. P. 337.

52. *Esherick P., Anderson R.J.M.* // Chem. Phys. Lett. 1980. Vol. 70. P. 621.

53. *Stockburger M.* // J. Phys. Chem. 1962. Vol. 31. P. 350.

54. *Brophy J.H., Rettner C.T.* // Chem. Phys. Lett. 1979. Vol. 67. P. 351.

55. *Boesl U., Neusser H.J., Schlag E.W.* In Laser-Induced Processes in Molecules / ed. by K.L. Kompa, J.D. Smith. Springer, 1979. P. 219; *Boesl U., Neusser H.J., Schlag E.W.* In Laser Spectroscopy IV / ed. by H. Walther, K.W. Rothe. Springer, N.Y. P. 164.

56. *Zaccharias H., Schmiedle R., Welge K.H.* // Appl. Phys. 1980. Vol. 21. P. 127.

57. *Duncan M.A., Dietz T.G., Smalley R.E.* // Chem. Phys. 1979. Vol. 44. P. 415.

58. *Dietz T.G., Duncan M.A., Liberman M.G., Smalley R.E.* // Chem. Phys. Lett. 1980. Vol. 70. P. 246.

59. *Rhodes C.K.* (ed.). Excimer Lasers. Topics Appl. Phys. Springer, 1979. Vol. 30.

60. *Antonov V.S., Letokhov V.S., Shibanov A.N.* // Zh. Eksp. Teor. Fiz. (Russian). 1980. Vol. 78. P. 2222.

61. *Boesl U., Neusser H.J., Schlag E.W.* // J. Chem. Phys. 1980. Vol. 72. P. 4327.

62. *Reilly J.P., Kompa K.L.* // J. Chem. Phys. (in press, 1981).

63. *Lubman D.M., Naaman R., Zare R.N.* // J. Chem. Phys. 1980. Vol. 72. P. 3034.

64. *Reilly J.P., Kompa K.L.* // Adv. Mass Spectrom. 1980. Vol. 9.

65. *Rockwood S., Reilly J.P., Hohla K., Kompa K.L.* // Opt. Commun. 1979. Vol. 28. P. 175.

66. *Antonov V.S., Letokhov V.S., Shibanov A.N.* // Appl. Phys. 1980. Vol. 22. P. 293.

67. *Seaver M., Hudgens J.W., Decorpo J.J.* // Int. J. Mass. Spectrom. Ion Phys. 1980. Vol. 34. P. 159.

68. *Zakheim D.S., Johnson P.M.* // Chem. Phys. 1980. Vol. 46. P. 263.
69. *Silberstein J., Levine R.D.*: to be published.
70. *Hunt D.F., Crow F.W.* // Anal. Chem. 1978. Vol. 50. P. 1781.
71. *Ligon W.V.* // Science. 1979. Vol. 151. P. 205.
72. *Fitch P.S.H., Wharton L., Levy D.H.* // J. Chem. Phys. 1978. Vol. 69. P. 3424.
73. *Liberman M.G., Beck S.M., Monts D.L., Smalley R.E.* // J. Chem. Phys. 1979. Vol. 70. P. 192.
74. Atlas of Mass Spectral Data / ed. by E. Stenhagen, S. Abrahamson, F.W. McLafferty. New York: Wiley Interscience, 1969.

Appl. Phys. B. 1983. Vol. 30. P. 161–176

LASER ATOMIC PHOTOIONIZATION SPECTRAL ANALYSIS OF ELEMENT TRACES

G.I. Bekov and V.S. Letokhov
Institute of Spectroscopy, Academy of Sciences USSR, Troitzk

A new method for determining trace amounts of elements in a substance has been developed. It is based on thermal evaporation and atomization of a substance in vacuum and detection of the released trace atoms by the laser stepwise photoionization technique. A rather effective way of detecting atoms is their multistep excitation to Rydberg states by the radiation of tunable dye lasers with their subsequent ionization by electric field pulses. The analytical laser spectrometer consisting of several tunable, pulsed dye lasers, a vacuum chamber with an atomizer and a recording system is described. The microimpurities of elements have been detected in pure materials: the contents of Na impurities in CdS crystals (2×10^{-6} %) and Al impurities in germanium (2×10^{-7} %). The detection limit of about 10^{-9} % was determined. A technique for direct determination of the content of elements in natural water and human blood is described. A high sensitivity, universality and other merits of the method enable it to be used in determining traces of many important elements at a level of 10^{-8} to 10^{-11} % almost in any matrix.

1. Method of Laser Stepwise Photoionization of Atoms

In this method the atoms are excited by laser radiation to an intermediate state in one or several steps, and then only the excited atoms are photoionized by laser radiation.

To detect a single atom it is apparently necessary that photoionization should be provided during its period in the laser beam. This period is usually much longer than the lifetime of intermediate atomic states with the exception of rare cases when metastable states are used. So for reliable photoionization of each atom by the method of multistep excitation (Fig. la) it is necessary that the rate of laser-induced transitions at every excitation step W_{kn} should be much higher than the population relaxation rate of each of the intermediate states $1/\tau_k$ and $1/\tau_n$.

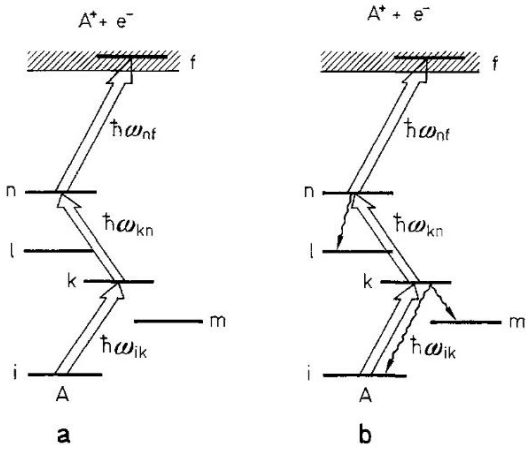


Fig. la and b. Multistep excitation and ionization of an atom: (a) General scheme of atomic excitation by short laser pulses without decay to intermediate states; (b) Irradiation of atoms with prolonged pulses ($\tau_p \gg \tau_k$) when accumulation of atoms at intermediate levels (*l, m*) takes place

The optimum case will be when a multilevel system is irradiated simultaneously by several laser pulses of the same duration $\tau_p \ll \tau_k (k = i, \dots, f)$ at resonant frequencies ω_{kn} of successive quantum transitions (Fig. la). If the energy fluence $E(\omega_{kn})$ for each of these pulses complies with the saturation condition

$$E(\omega_{kn}) \gg E_{kn}^{sat}, \tag{1}$$

where E_{kn}^{sat} is the saturation energy fluence of the resonant transition $k \to n [E_{kn}^{sat} = \hbar\omega_{kn}/2\sigma_{kn}$, σ_{kn} being the excitation cross-section of the transition $k \to n]$, the population n_k of the quantum system is in the average uniformly distributed, under multi-frequency laser radiation action, over the initial, all the intermediate and the final levels:

$$n_i/g_i \approx n_k/g_k \approx \cdots \approx n_f/g_f, \tag{2}$$

where g_k is the statistical weight of the kth state. If the statistical weight grows with the number of quantum states, there will be a considerable fraction of atoms in the final state.

When the condition (1) for saturation of intermediate quantum transitions is clearly fulfilled, the distribution of quantum systems over intermediate levels (2) sets in at a short time, being shorter than the pulse duration

$$\tau_{exc} \approx \sum_k \frac{1}{W_{kn}} \lesssim \tau_p\,, \tag{3}$$

where $W_{kn} = \sigma(\omega_{kn}) \cdot I(\omega_{kn})$, $I(\omega_{kn})$ is the laser radiation intensity.

A highly excited atom can pass to the continuum, i.e. be ionized, either spontaneously or under irradiation or some additional perturbation. If the rate of transfer to the continuum W_{fc} is small as compared to the photoexcitation rate $1/\tau_{exc}$ and decay occurs mainly after irradiation, the value of absolute yield to the continuum is limited by the relative population of the final excited state:

$$\beta \leqq g_f / \sum_k g_k \,. \tag{4}$$

Yet, if in the process of photoexcitation the decay channel of the quantum system is open and the rate of such a decay W_{fc} is large enough

$$W_{fc} \gtrsim 1/\tau_{exc}, \tag{5}$$

under the action of such single-time irradiation, with a set of laser pulses it is possible to deplete the initial, all the intermediate and the final levels, and hence to realize a maximum yield of photoionization $\beta \approx 1$.

Conditions (1) and (3) may turn out to be too rigid. But, as a rule, an atom stays in the region of irradiation much longer than the lifetime of excited states. Therefore at longer irradiation reliable photoionization can be ensured even with each excitation step being far from saturation. In principle, this is valid for ideal three- or four-level atoms. But actually an atom usually has many other intermediate states into which it may decay at slow excitation and from which it cannot be photoionized by radiation at several strictly fixed frequencies (Fig. 1b). It is because of this that the regime of pulsed irradiation with the pulse duration

$$\tau_p \lesssim \tau_k \tag{6}$$

is optimum to realize a quantum yield approaching unity. Only this case will be considered below.

If it is necessary to detect each atom during its stay τ_{cr} in the region of interaction with the radiation, the laser-pulse repetition period must satisfy the condition

$$T_{rep} \leqq \tau_{cr}. \tag{7}$$

From this the requirement on the necessary average laser radiation power at each step follows, i.e.,

$$P_{kn}^{av} = E_{kn}^{sat} S / T_{rep}, \tag{8}$$

where S is the laser beam cross-section.

To fulfill condition (1) or (3), it is desirable to use quantum transitions with the largest cross-section. This condition is especially critical for the last quantum transition from an intermediate state to the ionization continuum.

Three approaches to the method of stepwise photoionization may be singled out, each differing by the way of ionization of the atom from an intermediate state (Fig. 2):
1) nonresonance photoionization of excited atoms to the continuum;
2) ionization of atoms from Rydberg states by an electric field or as a result of their collisions with the buffer gas and so on; and
3) resonance photoionization of excited atoms through excitation to a narrow autoionization state.

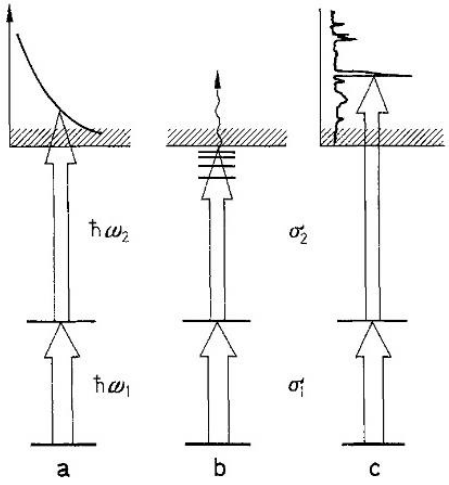


Fig. 2*a–c*. Methods of selective stepwise photoionization of atoms: (*a*) photoionization through continuum; (*b*) atom ionization from Rydberg states by the electric field; (*c*) atomic ionization through autoionization states

In the first case the excited atom is ionized by additional laser radiation or by the radiation used at one of the steps of resonant excitation. Such nonresonant photoionization is characterized by relatively a small cross-section $\sigma_{ion} = 10^{-17} - 10^{-18}$ cm^2 as opposed to the cross-section of resonant excitation at intermediate levels $\sigma_{exc} = 10^{-11} - 10^{-14}$ cm^2. For effective excitation and subsequent photoionization of excited atoms the pulse energy fluences must comply with the following conditions being a particular case of the general conditions (1):

$$E_{exc} \gtrsim E_{exc}^{sat} = \hbar\omega_{exc}/2\sigma_{exc}, \qquad E_{ion} \gtrsim E_{ion}^{sat} = \hbar\omega_{ion}/2\sigma_{ion}. \tag{9}$$

For the ionizing pulse the saturation energy fluence E_{ion}^{sat} varies between 0.01 and 1 J/cm^2 (for exciting pulses the corresponding values of E_{exc}^{sat} are smaller by a factor of $2\sigma_{exc}/\sigma_{ion}$). Such laser radiation parameters can be obtained with up-to-date pulsed lasers if the necessary pulse repetition rate lies within several tens of Hz. At the same time, according to requirement (7), to ionize every atom passing through the laser beam, the interval between pulses must be shorter than the time of flight of an atom through the beam τ_{cr}. For an atom moving with the thermal velocity, $\tau_{cr} \simeq 2 \times 10^{-5}$ s. Thus, the laser pulse repetition rate should be $f_{rep} \gtrsim 1/\tau_{cr} = 50$ kHz.

Under these conditions the average power of laser radiation required for effective ionization comes to several kW.

In the second method suggested in [14] an atom from an intermediate state is excited to a Rydberg state and then ionized by an electric field pulse. Rydberg atoms can be ionized rather easily in electric fields no matter what type of atom. Every Rydberg state is characterized by its value of the critical electric field near the normal threshold of ionization [15–18]. The dependence of the critical electric field strength on the effective principal quantum number n* of the state for a considerable part of the elements is described well by the classical formula:

$$\mathcal{E}_{crit} = 1/16(n^*)^4 \text{ at. un. (1 at. unit } \approx 5 \times 10^9 \text{V/cm}). \qquad (10)$$

With the electric field strength being higher than the critical strength for the given Rydberg state, the atoms excited to this state are ionized with an ion yield approximating unity. In this case the ionization cross-section of an atom from an intermediate state is determined by the cross-section of its resonance excitation to a Rydberg state. This cross-section is several orders higher than that of nonresonance ionization to the continuum.

The excitation of an atom to a Rydberg state can be carried out in two or three steps with the radiation of pulsed dye lasers synchronized with each other. The choice of an excitation scheme depends on the type of the atom. Since the processes of stepwise excitation of atoms to Rydberg states are resonant, the saturation of transitions requires comparatively low energy fluences of the laser pulses attainable with the existing dye lasers. Typical values of saturation energy fluence lie within $E_{exc}^{sat} = 10^{-6} - 10^{-4}$ J/cm^2. Therefore, even at a high laser pulse repetition rate necessary for detecting atoms moving with thermal velocity, the required average power of laser radiation will be rather moderate (about 1W).

It is most convenient to act on an atom with an electric field pulse after the laser pulse is over. In this case the atomic spectrum is not complicated by the Stark shift and splitting of Rydberg states. But the absolute photoionization yield in this case is limited by the relative population of the last excited discrete state determined by (4).

The third approach is based on using of atomic autoionization states lying above the ionization limit of the atom, i.e. in the continuum. For multielectron atoms such states may be narrow enough, and the cross-section of such an autoionization transition can exceed, by several orders, the cross-section of nonresonance photoionization [19, 20]. On the other hand, even at a very small width of the autoionization state, for example, $\Delta\nu_{AS} \simeq 0.01$ cm-1, its lifetime relative to the decay to the continuum comes to several nanoseconds. Therefore, if such a state is excited by a laser pulse with its typical duration of 10^{-8} s, it will be effectively depleted during a laser pulse. This makes it possible to reach the ultimate absolute ionization yield of $\beta = 1$.

Systematic study of autoionization states became possible with the development of stepwise excitation methods of high-lying atomic states by tunable laser radiation. Such states are both of practical value for increasing the cross-section of atomic photoionization by laser radiation and of scientific interest for understanding and deciphering spectra of multi-electron atoms. Since the autoionization states have been

studied only for a few elements, it is an urgent matter to carry out experiments on their search and study. In [21] the autoionization states (AS) of the gadolinium atom were studied. In the region of 300 cm-1 above the limit an autoionization state was found with the lifetime of 0.5 ns ($\Delta\nu_{AS} \simeq 0.05$ cm-1) and an excitation cross-section of about 10^{-15} cm2 comparable to that of Rydberg states. The experimental and theoretical studies of narrow autoionization states of the ytterbium atom [22] showed that the method of multistep laser excitation is most promising for such studies and the theoretical approach applied can be used to calculate the autoionization states of other multielectron systems with good accuracy.

2. Photoionization-Analytical Spectrometer

2.1. Choice of Ionization Technique

Each of the stepwise photoionization schemes considered in Sect. 1 has its pros and cons as far as their application in the photoionization spectral analysis is concerned.

The method of nonresonance ionization allows almost all the atoms, interacting with the laser radiation, to be ionized during a laser pulse. However this method cannot be applied if a high pulse repetition rate is required.

The method of ionization of Rydberg atoms by an electric field reduces the requirements on the energetics of the ionizing radiation by several orders. This enables effective ionization of atoms in an atomic beam when a high pulse repetition rate is necessary. The atomic beam provides a maximum spectral resolution, and the use of a multistep excitation scheme provides an extremely high ionization selectivity. This is due to the fact that the processes of excitation at each step are independent and so the selectivity of the whole process of multistep excitation and ionization of the atom equals the product of excitation selectivities at each step [23]. This method provides for only about one half the atoms interacting with the radiation to be excited to a Rydberg state. As a result, every second atom will be ionized.

The method of an ionization of atoms through narrow autoionization states holds more promise since it is a sort of synthesis of the above ionization methods when the excitation remains resonant in the presence of a constant channel of ionization decay of the final discrete quantum state. A disadvantage of this method, however, is the absence of such states near the ionization limit for a considerable number of elements.

The most universal and accessible method of ionization of atoms for their detection is selective excitation of Rydberg states of atoms by laser radiation, and their subsequent ionization by an electric field. As far as the use of this method in analytical tasks is concerned, we consider it important to emphasize its advantages. As it has already been said, the method of multistep excitation features extremely high selectivity, and so, even when there are close absorption lines of the element and the matrix at the first step, the selectivity of detecting the traces of this elements is very high.

Since the excitation of transitions at all steps is resonant, comparatively low values of laser radiation energy fluence are required to saturate these transitions (3 or 4 orders lower than those for ionization to the continuum). In this case the nonselective ion background conditioned by multiphoton ionization of the basic substance will be several orders less than in the case of direct ionization to the continuous spectrum by

a powerful pulse. As shown in [24], for the coefficient of atomic yield from the sample being about 0.01 only 10^8 atoms in the sample will be sufficient to detect this element. The value 0.01 is typical for the degree of thermal atomization for most compounds over the temperature range from 2000 to 2800 °C. So, one can expect that it is possible to detect the traces of an element in the substance when the content of its atoms in the sample studied is also around 10^8. The mass of the sample being 10 mg (the total number of atoms is about 10^{20}), this corresponds to a detectable concentration of about 10^{-3} ppb.

2.2. Laser Spectrometer

The laser analytical spectrometer consists of a set of a tunable lasers, a vacuum chamber with an atomizer and a registration system. The laser setup for resonance stepwise photoionization of atoms through Rydberg states is built up of two or three tunable dye lasers pumped simultaneously with one standard nitrogen laser (its pulse power is 350 kW and the pulse repetition rate is 12 Hz). The dye laser contain the following elements: an output mirror with a reflectivity of $4 - 10\%$, a cell with a dye solution without through-pump, a correcting lens with focal $f = 15$ cm, a prism expander with $K = 20 \div 25$ and a diffraction grating with 1200 groove/mm in the first order. The spectrum width of the dye lasers was $\Delta\nu_l = 1$ cm-1, the pulse duration $\tau_p = 7$ ns. To increase the laser pulse energy an amplifier was used that consisted of a cell with a dye solution excited by nitrogen laser radiation. Such a laser system generated tunable laser radiation in the range of $350 - 750$ nm with a pulse energy of up to 50 μJ. The pulse power was sufficient to generate the second harmonic of radiation in the range from 245 to 350 nm with a conversion of up to 5% using the nonlinear crystals $HCOOLi{\cdot}H_2O$, KDP, etc. Thus, the laser system allowed effective multistep excitation of more than 80% of the elements of the periodic table.

The laser beams were directed into the vacuum chamber and crossed the atomic beams between the electrodes (Fig. 3). The residual pressure in the chamber did not exceed 10^{-6} Torr. The sample to be studied was put into a tantalum crucible with a bore diameter from 2 to 3 mm and a heights of $15 - 20$ mm. In analyzing the solutions the sample was first evaporated. Then the crucible was placed inside a thin-wall tantalum tube heated by electric current where it could be heated by thermal radiation to a temperature of about 2000 °C. To suppress a strong background from thermal ions and electrons there was, above the heater, a set of several diaphragms at electric potentials of alternating signs. As a result, the residual ion background was no higher than one ion per second.

The evaporating substance was guided, with the same diaphragms, into an atomic-molecular beam that intersected the laser beams between the two electrodes at an angle of 90°. For exact tuning of the laser radiation to the transitions of the element under analysis an additional oven was placed in the vacuum chamber to form a reference beam for this element. The reference beam formed by thermal evaporation of the element crossed the laser beams at an angle of 45° in the opposite direction. This resulted in a long-wavelength shift of the absorption line

($\delta\nu = 0.015$ cm-1) and a small broadening unessential for laser lines with width $\Delta\nu_l = 1$ cm-1. The basic and reference beams crossed the laser beams in the same region opposite the hole in one electrode.

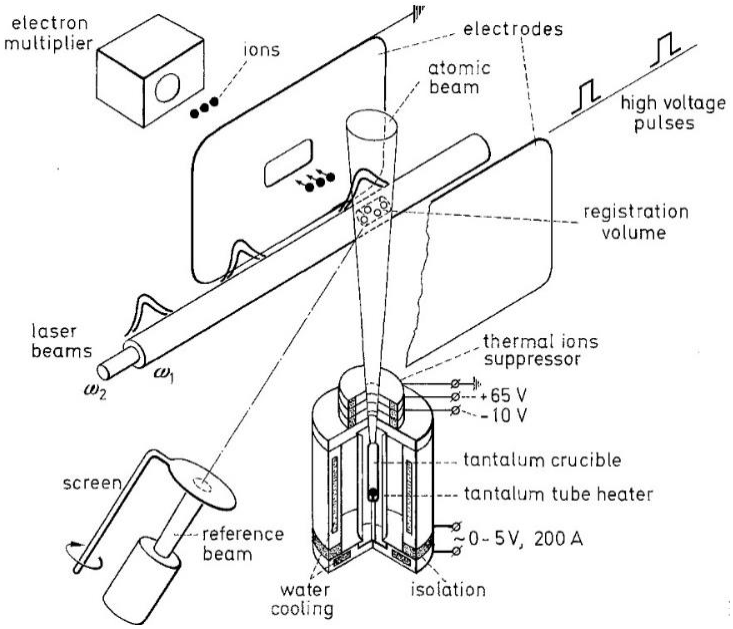


Fig. 3. Arrangement of elements in the vacuum chamber

After exciting the atoms to a Rydberg state by dye laser pulses a rectangular electric pulse with duration of 10 ns and amplitude of up to 20 kV was fed to the electrodes with a delay of 20 ns (the distance between the electrodes was 1 cm). The pulses were generated by a spark-gap concordant with cable-line and triggered by a nitrogen laser pulse.

The ions formed under Rydberg-atom ionization by electric field pulse acquired, in the same pulsed field, a normal component to its thermal velocity in the atomic beam. The value of this component was two orders higher than the average velocity in the beam, and so the ions moved between the electrodes almost normally to the motion of atoms. Having reached the zero-potential electrode the ions were extracted through the hole in this electrode by the electric field of the cathode of the electron multiplier (EM). The excitation volume, that is, the volume where the atomic beam crossed the laser beams, was a cylinder with a diameter of $1 - 2$ mm and a length of $5 - 7$ mm. The hole in the electrode was 3×10 mm^2 in size. The estimation of efficiency of ion extraction from the interelectrode space shows that ions can be extracted almost completely. The efficiency of ion detection by the electron multiplier was measured and came to $\varepsilon = 0.35 - 0.5$.

The signal from EM was amplified and fed to a boxcar averager and then to a recorder. The recording of the ion signal dependence on the evaporation time was carried out at a stepwise increase of the atomizer temperature.

3. Analysis of Element Impurities in Pure Materials

3.1. Determination of Sodium Impurity in CdS Crystals

The present-day level of development of quantum electronics places heavy demands on the purity of appropriate materials — one atom of impurity per 10^{10} to 10^{12} atoms or molecules of the basic substance. First of all this refers to laser semiconductor crystals and particularly CdS crystal. This crystal is used to make e-beam pumped laser screens. The question how impurities affect the growth of such crystals is not clear yet. In [25] sodium impurities into CdS crystals were investigated. The crystals were grown by the method of resublimation of CdS from the gas phase in an argon flow.

The sodium impurities were registered in the following way. A sample of CdS crystal with a mass of several tens of milligram was put into a tantalum crucible with an outlet channel of 1 mm across and was heated in vacuum ($p \simeq 10^{-6}$ Torr) to a temperature from 800 to 1050 °C. At such temperatures an intense sublimation of the CdS crystal occures [$t_{melt}(CdS) = 1475$ °C] with formation of atoms and molecules of the compounds comprising the crystal: Cd, CdS, S_2, S_4, Na, etc. The wavelengths of the dye lasers were tuned for two-step excitation of sodium atoms to the Rydberg state $14d$ by the scheme

$$3^2S_{1/2} \xrightarrow{\lambda_1=589\text{ nm}} 3^2P_{3/2} \xrightarrow{\lambda_2=418\text{ nm}} 14^2D_{3/2,\ 5/2}.$$

Then the Rydberg atoms were ionized by an electric field pulse and the ions were detected by an electron multiplier.

To determine the number of sodium atoms in the atomic-molecular beam from the crucible a calibrating atomic beam of sodium formed by heating metallic sodium in an additional oven was used (Fig. 3). This beam was directed into the area of intersection of the laser beams with the atomic beam so that the both beams had one and the same excitation volume. The parameters of laser radiation, the electric field, the excitation volume and the registration system being constant, the ion current i_1 was measured separately as a function of the sodium flux ϕ_1 in the reference beam (the basic beam closed) and the ion current i_2 as a function of the sodium flux ϕ_2 in the basic beam (the reference one closed). The flux of sodium atoms ϕ_1 through the excitation volume for the calibrating reference beam was estimated by the standard method [26] on the basis of the oven temperature, sodium thermodynamic constants and atomic beam geometry. When the ion current registration system operates in the linear regime, the ion signal is proportional to the atomic flux, that is, the relation $\phi_2 = \phi_1 \times i_2/i_1$ holds true. Thus, given the ratio between the signals from the basic and reference beams and the atomic flux in the reference beam, it is possible to determine the flux of the element to be investigated in the basic beam. Thereby we realize absolute calibration of the registration system with the reference beam.

Figure 4 shows the dependence of the ion current of sodium, i_2, on the evaporation time at $t = 940$ °C for a CdS sample with its mass of 30 mg. A sharp maximum at the beginning of evaporation is conditioned by the evaporation of sodium

compounds from the external polluted surface of the crystal. Similar dependences were obtained for several samples of CdS crystals over the temperature range from 800 to 1050 °C. In some cases, stronger fluctuations of ion current i_2, as compared to those in Fig. 4, were recorded which most probably was due to a nonuniform distribution of impurities in the sample volume.

The area under the ion signal curve determines the total atomic yield of the element from the sample. To make the description more convenient one can characterize every sample by the average value of impurity ion current, $< i_2 >$, (and so with the average flux of impurity, $< \phi_2 >$) and the average evaporation time T so that their product gave the area under the ion signal curve. In this case the basic substance flux from the crucible can be also characterized by the mean value $< \phi >= M/mT$, M being the crystal mass, and m the mass of a basic substance molecule. The flux through the excitation volume $< \phi_0 >$) is K times smaller than $< \phi >$), and the K coefficient is governed only by the geometry of the basic beam and the evaporator. The flux ratio $\eta_1 = < \phi_2 > / < \phi_0 >$ gives the relative content of impurity atoms in the basic substance flux. It differs from the real content η_0 of impurity in the crystal by the coefficient $\xi (\eta_0 = \eta_1/\xi)$ that depends on the degree of atomization of the impurity compounds during crystal evaporation. Crystals with a regular structure and a low level of impurities are characterized by the fact that the impurity molecule in it is dissociated [27]. As such crystals evaporate, the impurity molecule dissociates completely to form free atoms of the impurity element. Thus, in our case for the impurity of sodium in CdS crystals $\xi \approx 1$ takes place, i.e. $\eta_0 \approx \eta_1$.

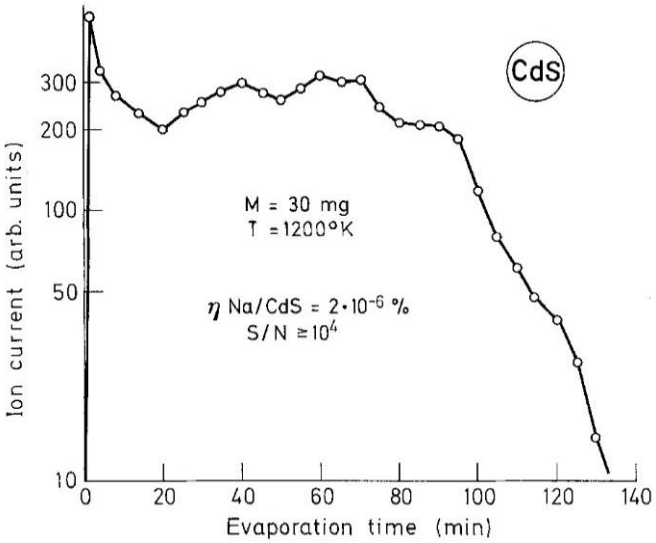


Fig. 4. Dependence of the sodium ion current i_2, on the evaporation time at $t = 940$ °C for a CdS sample with a mass of 30 mg

The content of sodium impurity in CdS was found in the following way. For every sample of CdS $< i_2 >$ and T were determined from the ion signal area. The ion current $< i_1 >$ was measured at a definite temperature of the reference beam oven. The values of $< \phi_1 >$, $< \phi_2 >$, $< \phi_0 >$ and η_1 were calculated from the known beam geometry. The values of η_0 obtained for the samples of CdS ranged from 2×10^{-6} % to 6×10^{-5} %. In most of the cases the signal-to-noise ratio was around 104 which allows, in principle, to detect impurity with $\eta_0 = 10^{-9}$ %. The factor limiting the sensitivity was the background due to nonselective multiphoton ionization of the basic substance molecules by the second-step laser radiation. Nevertheless, the result obtained for sodium with a high signal-to-noise ratio ($\eta_0 = 2 \times 10^{-6}$ %) is practically limiting for most conventional analytical methods.

3.2. Determination of the Sodium and Aluminum Contents in High Purity Germanium

Some tasks of modern technology of high purity materials, for example, determination of aluminum, boron and other third-group acceptor elements in semiconductor materials, demand that the control of impurities in materials should be at a level from 10^{-8} to 10^{-10} %. The conventional analytical methods are not able to provide such sensitivity. We studied the possibility of determining the impurities of sodium and aluminum in high-purity crystals of germanium by the method under consideration. Sodium was chosen as a model element because a scheme of effective ionization through Rydberg states had been tried for it (Sect. 3.1). The experimental technique was described above.

First the ionization efficiency of sodium atoms was studied as a function of the experimental parameters. Figure 5 presents the dependences of the sodium ion yield on the laser-pulse energy fluence of the first (*a*) and second (*b*) excitation steps and on the pulsed electric field strength (*c*).

Every second atom of sodium falling within the laser beams is ionized under saturation of all parameters [28]. The first experiments showed that, as the second step was saturated, there was a strong ion background conditioned mainly by three-photon ionization of germanium atoms in the dense beam with the second-step radiation ($\lambda_2 = 418$ nm). The second-step laser beam (its diameter determined the cross dimension of the excitation volume) was defocused from 0.5 to 1.5 mm. As a result, the ionization efficiency of sodium was reduced to 0.1 but the ion signal almost did not change because the excitation volume was increased by the same factor. The signal of three-photon ionization, however, decreased by almost 2 orders due to a nonlinear dependence of the probability of such ionization on the laser-radiation intensity.

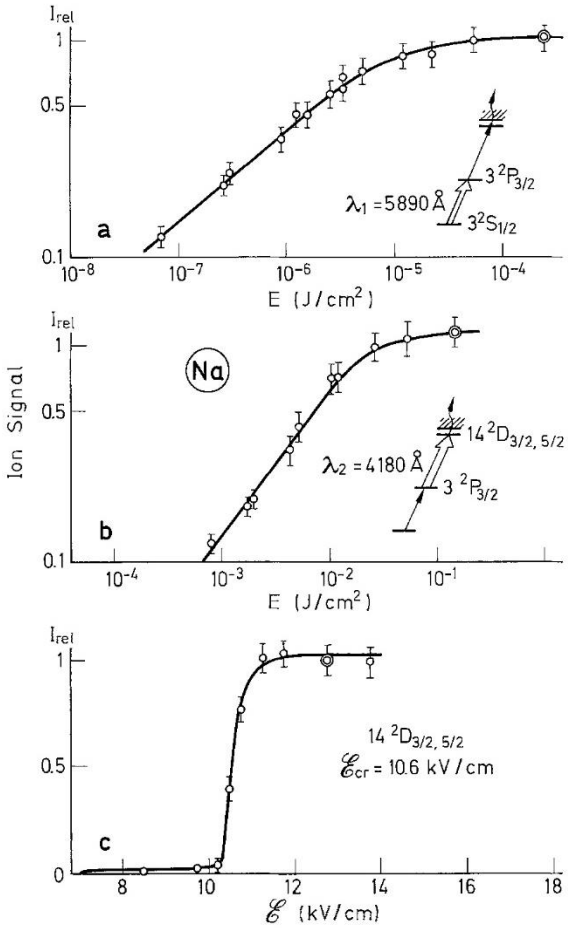


Fig. 5*a–c*. Dependence of the sodium ion yield on the laser-pulse energy fluence of the first (*a*) and second (*b*) excitation steps, and pulsed electric field strength (*c*)

Figure 6 shows the time dependence of the ion signal of sodium under different temperature conditions. Figure 6a illustrates how the crucible temperature varies in time, and Fig. 6*b* shows the time dependence of the sodium ion current for an empty crucible. The narrow peak at the beginning of heating is related to the sodium yield from the surface of the heater element. Such a peak was observed in all cases as the vacuum chamber was filled with both air and nitrogen. The intense signal observed then under gradual heating of the crucible was conditioned by the sodium yield from the surface of the crucible. This signal didn't practically vary as the time within which the crucible was kept in air increased from 1 to 30 min. During 10 to 12 min the signal was reduced to the single-ion level. Then the temperature increased, and a drastic rise of the signal and its rather rapid decrease were recorded. Such signal behaviour is probably due to the growing degree of atomization of the sodium compounds left on the crucible. Further stepwise temperature increase brought about a similar drastic rise of the signal and its subsequent quasi-exponential decrease. At

1750 °C one could record a slightly diminishing background signal caused mainly by the sodium yield from the surfaces of the construction elements of the oven under the action of the thermal radiation.

Similar investigations have been carried out for an annealed empty crucible that was kept for 10 h in a vacuum chamber at a residual pressure of $\simeq 10^{-1}$ Torr. A rather weak signal was recorded starting only from 1200 °C. This experiment showed that the crucible surface absorbed effectively the sodium compounds contained in the air.

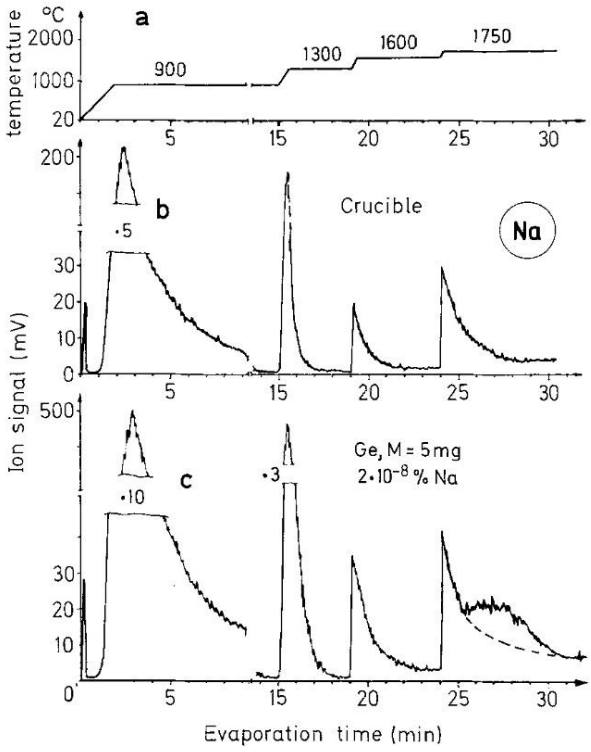


Fig. 6*a–c*. Time history of (*a*) the crucible temperature, (*b*) the sodium ion signal for an empty crucible, and (*c*) the sodium ion signal for a crucible with a 5 mg germanium sample, the sodium content was $\eta_0 = 2 \times 10^{-8}$ %

Figure 6c shows the time dependence of the sodium ion signal for a crucible with a crystal of Ge with mass $m = 5$ mg and a content of Na $\eta_{Na} = 2 \times 10^{-8}$ %[1]. It may be seen that the signal shape for the crucible with a crystal does practically not differ from the case of an empty crucible. The signals differ only by their amplitudes. As the stage of annealing is over (≦ 900 °C), the surface sodium evaporates, but the volume sodium doesn't yet emerge from the sample because the diffusion in solids is a very slow process. The situation can change when the crystal melted and the temperature increased. And really, there appeared at 1750 °C an additional sodium signal (Fig. 6c, above the dashed line) caused by the acceleration of sodium diffusion

from the volume of melted germanium. After one or two minutes this signal decreased to a certain level conditioned by the ion background of the oven and the three-photon ionization of germanium. Absolute calibration of the registration system (Sect. 3.1) allowed to determine the quantity of sodium in the sample from the area of this additional signal. The value obtained was 3×10^9 atoms of Na.

According to the results of a neutron-activation analysis, the sample must have contained 10^{10} atoms which shows that the results agree well.

Similar measurements were carried out for several samples of Ge. The time dependence of the ion signal had a form similar to that given in Fig. 6c. For samples of Ge with the Na content $\eta_0 = 2 \times 10^{-8}$ % the signal-to-noise ratio was about four.

The experiments performed have shown that the method in use enables one, with proper choice of the heating conditions, to achieve an analysis separate for surface and volume impurities even for such a background element as sodium.

The next stage in studying the potentialities of the new technique was to determine the content of aluminum in germanium. A two-step scheme of Rydberg state excitation was used, too. Figure 7 schematically shows the energy levels of the Al atom and the transitions used. A first-step laser pulse with the wavelength of $\lambda_1 = 3961.5$ Å excited the aluminum atoms to the $4^2S_{1/2}$ state from the $3^2P_{3/2}$ state lying 112 cm^{-1} higher than the ground state $3^2P_{1/2}$. At a temperature of around 1000 °C the populations of the $3^2P_{3/2}$ and $3^2P_{1/2}$ states almost level off, and it was more convenient experimentally to realize laser excitation from the $3^2P_{3/2}$ state. A second-step laser radiation pulse with $\lambda_2 = 4474$ Å performed further excitation of the atoms to the $15^2P_{1/2,3/2}$ Rydberg states. The laser radiation line width was $\Delta\nu_{1,2} \simeq 1$ cm^{-1}, and these states cannot be resolved. For the 15p state the effective principal quantum number is $n^* \simeq 14$ and the critical electric field strength $\mathcal{E}_{cr} = 10.8$ kV/cm. In the experiment 20 ns after laser excitation an electric field pulse with $\mathcal{E} = 13$ kV/cт was fed to the electrodes between which the atomic beam intersected the laser beams. This pulse ionized all the Rydberg atoms [28]. Thus, the ionization efficiency was determined by the efficiency of atomic excitation to the Rydberg state. The typical value of saturation energy fluence of the transition to a Rydberg state ranges from 1 to 5 mJ/cm^2 (Fig. 5b and [28]). The excitation volume formed by the intersection of the basic atomic beam with the laser beams was 2 mm across and 6 mm long. The energies of the first- and second-step laser pulses in the experiment were, respectively, equal to 2 and 12 μJ. From these values it was possible to find the energy fluences of laser radiation in the excitation volume: $E_1 = 60$ μJ/cm^2 and $E_2 = 400$ μJ/cm^2. The value of E_1 is quite sufficient to saturate the resonant transition $3^2P_{3/2} \rightarrow 4^2S_{1/2}$, and E_2 is almost an order lower than $E_{4s\rightarrow 15p}^{sat}$.

The ionization efficiency was determined by the second-step excitation efficiency and equaled approximately 0.1 which, in principle, was a rather high value for the ionization efficiency. The experimental technique was as before.

An important task of the experiment is to choose the proper regime of the sample heating for its evaporation. Initially the sample was annealed at 900 °C to remove surface impurities (the melting temperature of germanium is $t_{melt} = 937$ °C). Unlike the case of sodium (Fig. 6), this stage was characterized by the absence of a

background signal from surface aluminum. Then the germanium sample was heated by steps to 1800 °C. This temperature was chosen: 1) to build up, in the excitation volume, a density of aluminum atoms, which would suffice for reliable registration of the useful signal against the background level and 2) to evaporate milligram weighed samples of germanium in a period no longer than an hour.

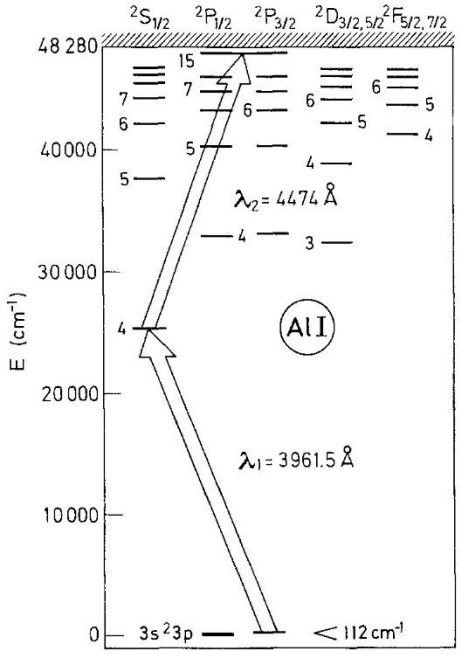


Fig. 7. Scheme of energy levels of the aluminum atom and the transitions used for excitation

Figure 8 shows the dependences of the ion signal of Al on the evaporation time at 1800 °C for an empty crucible (*a*) and a crucible with germanium samples differing in mass and surface area (*b–d*). The background signal from the empty crucible (Fig. 8*a*) is due to the thermal ions passing through the ion suppressor of the oven partially by the laser photoionization of the aluminum atoms leaving the surfaces of the oven as well as by the multiphoton ionization of germanium atoms with the second-step laser radiation. In Fig. 8*b* one can see the typical time dependence of the aluminum ion signal for a germanium sample with aluminum concentration of

The analysis of germanium for the determination of the Na content was performed by the neutron activation method at the Institute of Chemistry (Gorky), Academy of Sciences of the USSR.

2×10^{-7} %^{2} and the sample mass of 2.75 mg. It can be clearly seen that the ion signal in this case differs from the signal observed during heating an empty crucible (Fig. 8*a*). The decrease of the aluminum ion signal to the background level points to almost full yield of the Al impurity from the melted sample even though there is about one half of initial mass of germanium still left in the crucible by this time. This

is probably due to the fact that the distribution coefficient (the ratio of the impurity concentration in vapor to its concentration in a liquid) for the Ge(Al) system at liquid-vapor equilibrium, according to our estimation from [29], is above unity ($K_{distr} \approx 5$), i.e. the volatility of the impurity (Al) is higher than that of the basic substance (Ge).

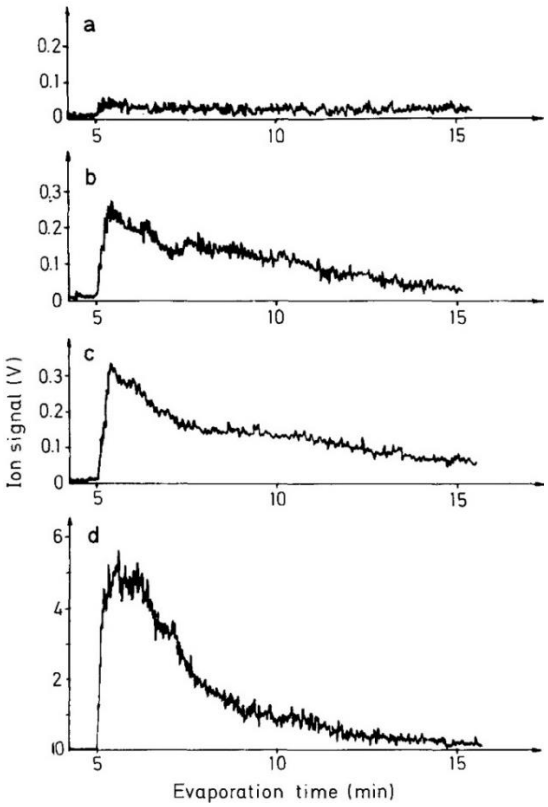


Fig. 8. Dependence of the aluminum ion signal on the evaporation time at 1800 °C for an empty crucible (*a*) and a crucible with germanium samples (*b*)–(*d*)

Calibration of the registration system allowed the total yield of ions and the content of Al in a germanium sample to be estimated from the value of the total ion signal determined by the area under the signal curve for aluminum. The value obtained 5×10^{-7} % is in satisfactory agreement with the value 2×10^{-7} % obtained in electrophysical measurements.

The influence of the surface area of the sample and its mass on the aluminum-ion signal has been studied. As seen from Fig. 8*b* and *c*, there is no essential difference between the signals from samples with almost the same masses [the sample masses are 2.75 mg (*b*) and 2.5 mg (c)] but with materially different surface areas (the surface area in Fig. 8b is 4 or 5 times smaller than that in Fig. 8*c*). The signal from the sample with a mass of 28.2 mg (Fig. 8*d*) and surface area approximating that in Fig. 8*c* has increased considerably as compared to the signals in Fig. 8*b* and *c*. These

results indicate conclusively that the signal recorded is mainly due to the aluminum atoms from the germanium volume rather than by the surface impurities. In the case illustrated in Fig. 8*d*, the signal-to-noise ratio is about 10^2 which enables one to realize the detection limit of Al in germanium at a level of 10^{-9} %.

The experiments performed have shown that it holds promise to apply the method of laser stepwise photoionization in combination with atomization of the sample in vacuum to determine the content of trace impurities. The method allows to perform direct analysis of natural specimens without preparing samples and introducing uncontrollable impurities and to register only volume impurities.

4. Analysis of Atomic Traces in Natural Waters

The development of new highly sensitive methods for analyzing microelements in natural waters, particularly aluminum, is dictated by the following reasons. Aluminum, one of the most important elements of the lithosphere, is used in lithology and geochemistry of the ocean as an indicator element of terrigenous run-off. Besides, the results obtained in [30, 31] show that aluminum dissolved in sea water is related to biological processes. Hence, correct quantitative estimation of the participation of aluminum in the processes taking place in the ocean calls for a universal method that would allow determination of the content of aluminum in water with different mineralization and a different content of organic matter. River, sea and pore waters may be placed into this category of water.

At present there is not a direct method and universally accepted technique for determining dissolved aluminum in natural water [32]. There exist many methods differing from one another in use for aluminum extraction of various chemical reagents (dyes, complex formers, etc.) which contaminate samples and form an undesirable background. The absence of reliable data on dissolved aluminum in sea and ocean waters and the presence of just single results for pore water show that these methods are complicated and unsatisfactory.

The merits of the method of laser stepwise photoionization disclosed in analyzing impurities in high purity substances have stimulated the application of the method to the analysis of natural water and more complex objects.

The procedure of determining the content of aluminum in natural water consists of the following. A water sample, 40 μl in volume, is introduced into a tantalum crucible and evaporated in air at 90 °C to a dry residium. Then the crucible with the dry residium is placed into a vacuum chamber which is pumped to a residual pressure of 10^{-6} Torr. After this the crucible is stepwise heated to 1750 °C. The subsequent technique of aluminum signal registration is similar to that described above in Sect. 3.2.

Figure 9*a* shows a typical dependence of the ion signal on evaporation time at 1750 °C for a 40 μl sample of sea water. Within the time range from 0 to 5 min the crucible was heated by steps to 1500 °C. Such gradual heating was caused by the fact that at fast ashing of the dry residium of see water considerable gassing and deterioration of the vacuum took place. In this temperature range the aluminum ion signal was practically absent. To discriminate a selective signal of aluminum from

the total ion signal, the first-step laser wavelength was periodically out of resonance with the aluminum transition $3^2P_{3/2} \xrightarrow{\lambda_1} 4^2S_{1/2}$by $3 - 5$ cm-1. The dips in Fig. 9 correspond to such detuning of λ_1 that causes the ionization efficiency of Al atoms (in the experiment it was about 0.1) to decrease by more than two orders. Such a procedure allowed for discriminating the nonselective ion background of the sea water matrix from the ion signal due only to aluminum. The nonselective background is caused apparently by the thermal ionization of easily ionized sea water components and by the laser photoionization of the molecules of the compounds constituting the sea water matrix.

The content of aluminum in the p-type germanium samples used was estimated from the results of electrophysical measurements of the difference concentrations of charge carriers and from taking account of the distribution coefficient of aluminum ($К < 1$) in germanium in zone melting.

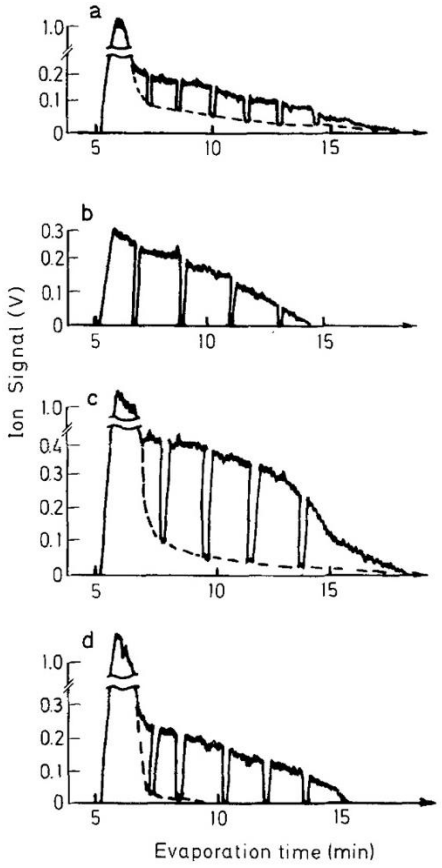


Fig. 9*a–d*. Dependence of the ion signal on the evaporation time at 1750 °C for 40 μl sample (*a*) sea water, (*b*) calibration solution of $AlCl_3$ with the aluminum content being 100 μg/1, and (*c*) mixture of sea water (9 parts) and a solution of $AlC1_3$ with the aluminum content being 1000 μg/l (1 part), and (*d*) solution of NaCl and $A1C1_3$ with *2%* concentration of NaCl and the aluminum content of 100 μg/1

In quantitative measurements the universally accepted technique consists of plotting an analytical calibration characteristic, and the calibration solutions must be prepared on the basis of the matrix being studied. Initially the aluminum yield from solutions, with Al content known, was studied. The solutions were prepared on the basis of aluminum chloride and deionized water. Figure 9b presents a typical time dependence of the ion signal for the calibration solution of $A1C_{13}$ with the content of Al being 100 μg/l ($t = 1750$ °C). It may be seen that for the $A1C_{13}$ solution the ion signal is due only to aluminum. The total yield of aluminum is determined by the area under the ion signal curve.

With the use of the addition method it was shown that the matrix composition of sea water did not distort the results of determining the aluminum content. For this purpose we prepared a solution consisting of 9 parts of sea water and 1 part of the calibration solution of $A1C_{13}$ with the content of Al being 10^3 μg/l. This corresponds to an additional aluminum concentration of 100 μg/l in sea water. The dependence of the ion signal on the evaporation time for 40 μl of such a mixture under the same conditions is shown in Fig. 9*c*. The total signal due to aluminum determined by the "selective" area under the curve is almost equal to the selective aluminum signal from sea water (Fig. 9*a*) plus the aluminum signal from the solution with the concentration of Al being 100 μg/l (Fig. 9*b*). The study of the solution with 2% of NaCl in deionized water (such a concentration of NaCl is typical of sea water) and aluminum with a concentration of 100 μg/l (Fig. 9*d*) was an attempt to analyze the nature of the nonselective ion signal in sea water (Fig. 9*a*). For such a mixture the ion signal also consists of a selective and nonselective parts. It follows from the selective signal area (Fig. 9*d*) that the yield of Al here is practically equal to that for the solution of $A1C_{13}$ (Fig. 9*b*), i.e. the presence of NaCl does not affect the yield of Al. The nonselective ion signal due to ionization of NaCl (Fig. 9*d*) differs in time behaviour from the nonselective ion signal of sea water (Fig. 9*a* and c). The nonselective signal from sea water in the time range from 5 to 7 min (Fig. 9*a* and *c*) is probably caused by ionization of NaCl. The presence of an extended nonselective signal is dictated by the entire complex composition of the sea water matrix.

On the basis of $A1C_{13}3$ solutions in deionized water an analytical calibration characteristic was constructed (Fig. 10*a*). It turned out to be linear in the concentration range from 5 μg/l to 10^3 μg/l. Above 10^3 μg/l the calibration characteristic became nonlinear due to saturation of the recording apparatus. The lower limit of the calibration curve was determined by the content of Al in deionized water and equalled 5 μg/l. The detection limit of aluminum in these experiments found by extrapolating the analytical curve to the noise level was equal to 0.01 μg/l. An analytical curve is also plotted on the basis of sea water with $A1C_{13}$ additions (Fig. 10*b*). The curves are found to be parallel, which makes it possible to use the calibration characteristic on the basis of $A1C_{13}$ solutions in quantitative measurements of aluminum content in sea water. The influence of nonselective ion background manifested itself only in the value of minimum detectable aluminum concentration in sea water since it is difficult to discriminate a small selective signal against the background of a strong nonselective one. In our experiments this value came to 1 μg/l which corresponds to an absolute amount of Al in the sample of 40 pg.

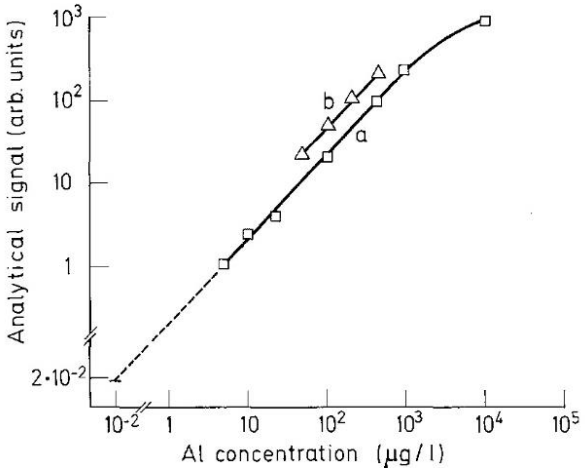


Fig. 10*a* and *b*. Analytical calibration characteristics for $AlCl_3$ solutions on the basis of deionized water (*a*) and sea water (*b*)

Twenty parallel measurements taken for sea water resulted in finding the value of the relative standard deviation. The value obtained was equal to 5.6%. The largest contribution to this value was made by the volume fluctuations of the sample introduced in the crucible.

The method was applied to determine the content of dissolved aluminum in the water samples taken in the zone where the Kura river falls into the Caspian Sea. The samples were taken with a ten-litre bathometer and were filtered through 0.45 μm membrane filters. The results of the measurements are given in Table 1. The results obtained for river water are close to the average value for the rivers of the world [32].

Table 1. Content of dissolved aluminium in the zone of the mouth of the Kura river (the Caspian Sea).

Number of station	Sampling horizon [m]	Salinity [‰]	Aluminium concentration[a] [μg/l]
1	0	< 1	190 ± 20
	2	< 1	215 ± 22
2	0	7.7	780 ± 80
	3	11.6	36 ± 4
3	0	10.1	230 ± 25
	10	12.2	260 ± 28

Number of station	Sampling horizon [m]	Salinity [‰]	Aluminium concentration[a] [μg/l]
4	0	10.4	460 ± 50
	12	12.1	380 ± 40
5	0	12.4	230 ± 25
	22	12.3	135 ± 15
6	0	12.4	95 ± 10
	30	12.4	135 ± 15

[a] The values of concentration are given with a confidence probability of 0.95.

Table 2 presents the results of measurements of the dissolved aluminum concentration in pore water samples from the Indian Ocean. Pore water was squeezed out of sediment monoliths (10–15 cm below the bottom) lifted with a bottom scoop and then it was filtered through 0.45 μm membrane filters. The results are in good agreement with the data from [31]. Pore waters of metalliferous sediments are characterized by an increased content of dissolved aluminum.

The content of dissolved aluminum in surface water samples from the Mediterranean was measured, too.

The value obtained (6.5 ± 0.7 μg/l) approximates to the average concentration of Al in the Mediterranean [33].

These results show that the method is promising and can be applied in analyzing such complex solution as natural water. To check conclusively the potentialities of the method of laser stepwise photoionization and its universality a biological object is analysed in the following.

Table 2. Content of dissolved aluminum in the pore waters of the Indian Ocean

Station coordinates: latitude	longitude	The character of sediments	Aluminium concentration[a] [μg/l]
Ocean depth [m]			
8°45′ S	102°19′ E	Pelagic slime	17 ± 2
5300			
2°63′ N	80°10′ E	Clay slime	14 ± 2
4200			
0°04′ N	80°02′ E	Clay slime	30 ± 4
4600			
10°10′ S	67°16′ E	Carbonaceous slime	34 ± 4
4060			

9°08′ S	67°16′ E	Siliceous slime	29 ± 3
6015			
26°38′ S	67°31′ E	Metalliferous sediment	220 ± 25
4780			
23°54′ S	73°56′ E	Metalliferous sediment	54 ± 6
3780			
23°00′ S	75°21′ E	Metalliferous sediment	100 ± 11
4320			

[a] The values of concentration are given with a confidence probability of 0.95.

5. Direct Determination of the Aluminum Content in Human Blood

One of the urgent analytical tasks important for biology and medicine is to determine trace amounts of metals in biological objects. Such analysis results in determining normal concentrations of metals in organisms as well as correlations between their deviation from normal concentration and various functional disorders and diseases.

Aluminum is one of the metals of interest for toxicology. The role of this element in metabolism of living organisms is still not clear. The complication of this problem consists in the fact that it is difficult to produce “aluminumless” diets because aluminum is widespread in nature. In some cases it has been ascertained that an increased content of aluminum in an organism is responsible for various diseases of the lungs and the nervous system [34].

To analyze the traces of metals in biological objects the atomic fluorescence and atomic absorption methods with flame and flameless atomization are widely applied at present. To our opinion, these methods have a number of essential shortcomings. First, before analysis, as a rule, a sample is subjected to quite a number of chemical treatments to reduce the influence of the matrix on the useful signal. In this case the sample may undergo uncontrollable pollution with the metals contained in the chemicals used, and the element to be determined may be lost during its chemical extraction. Secondly, as it has already been mentioned, in the process of atomization in a flame or in an intert gas a part of the resulting atoms is lost due to their interaction with the environment. Thirdly, at the registration of the useful signal, the spurious contribution to the signal from the molecules of the annealed matrix is not allowed for, although their absorption bands can overlap the spectral range used in the analysis. The correction introduced in the final result from the deionized water signal is thus not complete.

The method of laser stepwise atomic photoionization used in combination with thermal atomization of matter in vacuum is free of the shortcomings listed above. The possibility of direct determination of trace amounts of elements in biological objects by this method was demonstrated by determining the content of aluminum in human blood, as an example. The analytical procedure was similar to those described above and consisted of the following: a 40 μl sample of blood in its natural form was introduced into a crucible and was dried in air at a temperature from 90 to

100 °C within 3-5 min. The processes of ashing and atomization of the dry residium were carried out in a vacuum chamber evacuated to 10^{-6} Torr. In so doing it is important to choose such regimes of the crucible heating so that ashing would not deteriorate substantially the vacuum below 10^{-4} Torr. At the same time this process must run rather quickly to prevent considerable thermal evaporation of the residium without atomization. In the experiment the crucible temperature during ashing was increased to 1500 °C by five steps throughout 10 min. The technique of aluminum-atoms registration is comprehensively described in the foregoing sections.

Figure 11*a* shows a typical time dependence of the ion signal in stepwise heating of the crucible. The selective signal of aluminum was discriminated by means of the detuning technique described in Sect. 4.

The total signal from aluminum for the sample under analysis was determined by the total "selective" area under the signal curve (the difference between the total and background signals) (Fig. 11*a*). The aluminum concentration value corresponding to such a signal was determined from the calibration characteristic plotted for aqueous solutions of A_1C_{13} (Fig. 10*a*). The validity of such procedure was checked by the method of addition. In this case 40 μl of blood and 40 μl of A_1C_{13} solution with the content of Al in it being 100 μg/1 were introduced into the crucible. The aluminum signal from such a mixture turned out to be equal to the sum of the signals from the components analyzed independently within the limits of measurement error (about 10 %). This experiment proved that the blood matrix did not affect the yield of aluminum at the thermal atomization of blood in vacuum. The results for the aluminum content determination in five blood samples lie within 230 ± 50 μg/1.

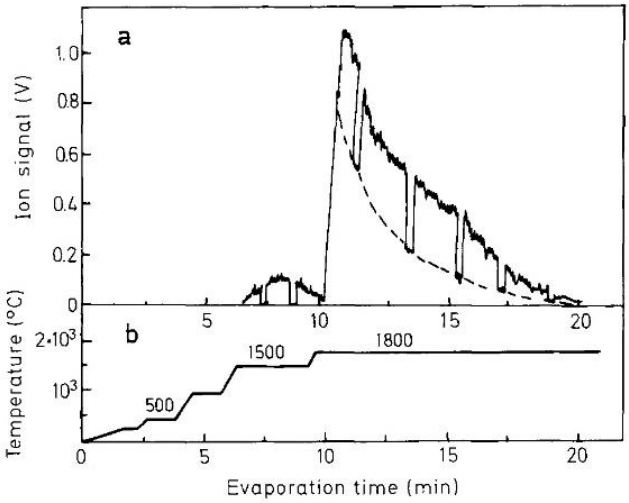


Fig. 11*a* and *b*. Dependence of the ion signal on the evaporation time for a 40 μl blood sample (*a*) at stepwise increase of the crucible temperature (*b*)

The experiments carried out support a universal character of the method of laser stepwise atomic photoionization in combination with vacuum thermal atomization of matter. It holds much promise for being used as an analytical method.

6. Conclusion. Prospects of the Method

Table 3 gives the results of analysis of traces of some elements in different substances. The experiments performed have been, in essence, the first application of the method of laser stepwise atomic photoionization for analyzing impurities and traces of elements in real objects. Under nonoptimized experimental conditions the results are limits for the most sensitive analytical methods.

Table 3. Results of laser atomic photoionization analysis of element traces in various substances

Element	Matrix	Element concentration in the matrix [at %]	Signal-to-noise ratio during recording
Yb[a]	Aqueous solution of $YbCl_3$	5×10^{-7}	200
Na	CdS crystal	2×10^{-6}	10^4
	Ge crystal	2×10^{-8}	4
Al	Ge crystal	2×10^{-7}	10^2
	Aqueous solution of $A1C1_3$	2×10^{-6}	10^3
	Sea water	5×10^{-7}	2
	Blood	3×10^{-5}	50

[a] The results are taken from [35] on determining the ytterbium content in aqueous solutions of $YbCl_3$.

Table 4 gives comparative characteristics of various methods. The method suggested is able to reduce the achieved detection limits of element traces by one or two orders. This can be done by perfecting the atomizer design, increasing the laser excitation selectivity, removing the nonselective ion background, etc. Some of these ways are discussed below in more detail.

The basic factor that does not allow improving the signal-to-noise ratio is the nonselective ion background caused by stepwise or multiphoton ionization of atoms and molecules of the substance being analyzed. Although the cross-sections of such processes are small, the ion yield in some cases proves to be very essential due to the high density of the basic beam. The resultant ion signal is the sum of this background signal and the selective signal from ionizing the Rydberg atoms of the element by an electric field pulse. These two different types of ions are separated in time by an interval of 20 ns and detected by an electron multiplier as one bunch of ions. But, if such a bunch is previously directed into a mass spectrometer that will realize spatial mass separation of ions, it is possible to separate the ions of the element under analysis from nonselective ones. Comparatively simple systems of mass

filtration enable the detection selectivity to be about 10^3 to 10^4. Such a value of nonselective background suppression will allow, in principle, the sensitivity of element trace detection to be increased to 10^{-10} %.

Now let us consider the possibilities of increasing the useful signal. As it has already been mentioned, the experiments used an atomic beam and a laser with a pulse repetition rate of 10 Hz, which was more than three orders lower than the optimal repetition rate. In this connection it is very promising to use lasers with a high pulse repetition rate, particularly the copper-vapor laser with a pulse repetition rate of 10 kHz, for dye laser pumping. Such a laser system makes it possible to generate tunable laser radiation in the region from 530 to 750 nm and its second harmonic from 265 to 360 nm with considerable average power [36]. Using several pumping lasers synchronized with one another one can obtain an energy fluence in the laser beam sufficient for transition saturation and to realize effective excitation of the atoms to Rydberg or autoionization states.

This method is of particular interest for isotopic analysis. The use of narrow-band laser radiation ($\Delta\nu_{las} < 0.01$ cm-1) and a multistep excitation scheme enables one to achieve, in principle, very high isotopic selectivity (up to 10^{-16}) [23]. A mass spectrometer applied at the stage of ion detection will allow increasing this selectivity by several orders further. The value of such ultrahigh selectivity is inconceivable for the conventional methods of analysis.

Finally, let us concern about the universality of this method. As it has been said, the laser system in use allows effective ionization of more than 80 % of the elements of the periodic table, except for elements with resonant lines in the near and vacuum uv spectral regions. Certain progress has been made in producing tunable vuv radiation by generating harmonics in metal vapor. This makes it possible to expand the applicability of the method to some more elements.

Table 4. Comparison of different methods of atomic spectral analysis of element traces

Method	Relative detection limit [%] [1] (in aqueous solutions)	Experimental detection limit [%] (in the matrix)	Selectivity for elements
Atomic absorption spectrometry	$10^{-4} \div 10^{-9}$	$10^{-4} \div 10^{-7}$	Moderate
Neutron activation analysis	$10^{-5} \div 10^{-9}$	$10^{-5} \div 10^{-9}$	Moderate
Spark mass spectrometry	$10^{-5} \div 10^{-8}$	$10^{-5} \div 10^{-7}$	High
Laser fluorescence spectrometry	$10^{-6} \div 10^{-11}$	$10^{-5} \div 10^{-8}$	High
Laser stepwise photoionization	$10^{-11} \div 10^{-14}$	$10^{-8} \div 10^{-11}$	Ultrahigh

In conclusion, it should be stressed again that the merits of the method suggested are: 1) detection sensitivity at a level of single atoms in the volume of interaction with the laser radiation; 2) the possibility of direct analysis of objects in their natural form, removal of uncontrollable impurities by atomizing matter in vacuum; 3) the possibility of discriminating the selective useful signal against the background in one measurement and separate registration of surface and volume impurities in solid samples. They allow the method to be applied to analyzing the traces of a majority of the most important elements almost in any matrix.

References

1. Trace Analysis. Spectroscopic Methods for Elements / ed. by J.D. Winefordner. New York: Wiley, 1976.

2. *Letokhov V.S.* / In: Chemical and Biochemical Applications of Lasers. Vol. 5 / ed. by C.B. Moore. New York: Academic Press, 1980. P. 1–38.

3. *Fairbank Jr. W.M., She C.Y.* Optics News. Spring, 1975. P. 4.

4. *Hurst G.S., Payne M.G., Kramer S.D., Young J.P.* // Rev. Mod. Phys. 1979. Vol. 51. P. 767.

5. *Balykin V.I., Bekov G.I., Letokhov V.S., Mishin V.I.* // Usp. Fiz. Nauk (in Russian). 1980. Vol. 132. P. 293. [Sov. Phys.-Usp. Oct. 1980. Vol. 23 (10). P. 651].

6. *Bolshov M.A., Zybin A.V., Smirenkina I.I.* // Spectrochim. Acta B. 1981. Vol. 36 B. P. 1143.

7. *Fairbank Jr. W.M., Hansch T.W., Schawlow A.L.* // J. Opt. Soc. Am. 1975. Vol. 65. P. 199.

8. *Greenless G.W., Clark D.L., Kaufman S.L., Levis D.A., Tonn J.F., Broadhurst J.H.* // Opt. Commun. 1977. Vol. 23. P. 236.

9. Balykin V.I., Letokhov V.S., Mishin V.I. // Appl. Phys. 1980. No. 22. P. 245.

10.*Letokhov V.S.* USSR Patent No. 784, 679. Appl. 30.03.1970. Published 1.08.1980.

11. *Ambartzumian R.V., Kalinin V.P., Letokhov V.S.* // Pis'ma ZhETF (in Russian). 1971. Vol. 13. P. 305. [JETP Lett. 1971. Vol. 13. P. 217].

12. *Letochow W.S.* Laserspektroskopie. Braunschweig: Vieweg, 1977. P. 150–154.

13. *Letokhov V.S., Mishin V.I., Puretzky A.A.* // Prog. Quant. Electron. 1977. Vol. 5. P. 139.

14. *Letokhov V.S.* Nonlinear Laser Chemistry // Springer Ser. Chem. Phys. No. 22. Berlin, Heidelberg, New York: Springer, 1983.

15. *Ivanov L.N., Letokhov V.S.* // Kvant. Elektr. (in Russian). 1975. Vol. 2. P. 585.

16. *Ambartzumian R.V., Bekov G.I., Letokhov V.S., Mishin V.I.* // Pis'ma ZhETF (in Russian). 1975. Vol. 21. P. 595. [JETP Lett. 1975. Vol. 21. P. 279].

17. *Stebbings R.F., Latimer C.J., West W.P., Dunning F.B., Cook T.B.* // Phys. Rev. A. 1975. Vol. 12. P. 1453.

18. *Ducas T.W., Littman M.G., Freeman R.R., Kleppner D.* // Phys. Rev. Lett. 1975. Vol. 35. P. 366.

19. *Paisner J.A., Solarz R.W., Worden E.F., Conway J.G.* In: Laser Spectroscopy III / ed. by J.L. Hall, J.L. Carlsten. Springer Ser. Opt. Sci. Vol. 7. Berlin, Heidelberg, New York: Springer, 1977. P. 160.

20. *Stebbings R.F., Dunning F.B., Rundel R.D.* In: Atomic Physics IV / ed. by G. zu Putlitz, E. Weber, A. Winnacker. London: Plenum, 1975. P. 713.

21. *Stebbings R.F.* // Science. 1976. Vol. 193. P. 537.

22. *Bekov G.I., Letokhov V.S., Matveev O.I., Mishin V.I.* // Pis'ma ZhETF (in Russian). 1978. Vol. 28. P. 308. [JETP Lett. 1978. No. 28. P. 283].

23. *Bekov G.I., Vidolova-Angelova E.P., Ivanov L.N., Letokhov V.S., Mishin V.I.* // Zh. Eksp. Teor. Fiz. (in Russian). 1981. Vol. 80. P. 866. [Sov. Phys. JETP. 1981. No. 53. P. 441].

24. *Letokhov V.S., Mishin V.I.* // Opt. Commun. 1979. Vol. 29. P. 168.

25. *Bekov G.I., Vidolova-Angelova E.P., Letokhov V.S., Mishin V.I.* In: Laser Spectroscopy IV / ed. by H. Walther, K.W. Rothe. Springer Ser. Opt. Sci. Vol. 21. Berlin, Heidelberg, New York: Springer, 1979. P. 283.

26. *Akilov R., Bekov G.I.* // Pis'ma ZhTF (in Russian). 1982. Vol. 8. P. 517.

27. *Ramsey N.F.* Molecular Beams. Oxford: Clarendon Press, 1956.

28. *Tochitsky E.I.* Crystalization and Thermal Treatment of Thin Films (in Russian). Minsk: Nauka i Tekhnika, 1976.

29. *Bekov G.I., Letokhov V.S., Matveev O.I., Mishin V.I.* // Zh. Eksp. Teor. Fiz. (in Russian). 1978. Vol. 75. P. 2092.

30. *Devyatykh G.G., Stepanov V.I., Shirobokov M.Ya., Yan'kov S.V.* In: Hydrids, Halids, and Metalorganic Compounds of High Purity (in Russian). Moscow: Nauka, 1976. P. 5.

31. *Mackenzie F.T., Wollast R., Stoffyn M.* // Science. 1978. Vol. 199. P. 4329.

32. *Caschetto S., Wollast R.* // Geochim. Cosmochim. Acta. 1979. Vol. 43. P. 3.

33. *Caschetto S., Wollast R.* // CRC Crit. Rev. Environ. Control. June 1977. P. 167.

34. *Caschetto S., Wollast R.* Marine Chemistry. 1979. Vol. 7. P. 2.

35. *Berman E.* Toxic Metals and their Analysi / ed. by L.C. Thomas. London: Heiden, 1979. P. 6.

36. *Bekov G.I., Yegorov A.S., Mishin V.I.* // Zh. Anal. Khim. (in Russian) (in press).

37. *Zherikhin A.N., Letokhov V.S., Mishin V.I., Belyaev V.P., Yevtyunin A.N., Lesnoy M.A.* // Kvant. Elektron. (in Russian). 1981. Vol. 8. P. 1340.

Phys. Rev. Lett. 1991. Vol. 67 (27). P. 3860–3863

FEMTOSECOND SPECTROSCOPY OF $YBA_2CU_3O_{7-\delta}$: ELECTRON-PHONON-INTERACTION MEASUREMENT AND ENERGY-GAP OBSERVATION

S.V. Chekalin, V.M. Farztdinov, V.V. Golovlyov, V.S. Letokhov,
Yu.E. Lozovik, Yu.A. Matveets and A.G. Stepanov
Institute of Spectroscopy, Academy of Sciences USSR

The femtosecond dynamics of reflection and transmission spectra of a $YBa_2Cu_3O_{7-\delta}$ film have been studied in the wavelength range 620–680 nm at initial temperatures T_0 both above and below the critical temperature T_c. A difference has been found to exist between the spectral responses for $T_0 < T_c$. and $T_0 > T_c$, which can be attributed to the presence of an energy gap in the spectrum at $T_0 < T_c$. Based on the experimental data, the electron-phonon-interaction parameter $\lambda<\omega^2>$ has been estimated as $(4 \pm 2) \times 10^2$ meV^2.

Real-time studies of the relaxation of charge carriers in oxide superconductors can help to obtain unique information about the nature of superconductivity in such materials, particularly the role of the electron-phonon interaction. In the works reported in Refs. [1–5], there was investigation of the femtosecond charge-carrier dynamics in cuprates using a single wavelength for both pump and probe pulses. In this work, we have studied the femtosecond dynamics of the difference reflection and transmission spectra of a $YBa_2Cu_3O_{7-\delta}$ film in the spectral range 620–680 nm at initial temperatures T_0 above and below the critical temperature T_c. The spectral dependence of the response has been found to reverse sign in the vicinity of the Fermi level. The spectra obtained with delay times between the pump and probe pulses of less than 1 ps at $T_0 < T_c$ differ drastically from those at $T_0 > T_c$, which is believed to be associated with the dynamics of destruction of superconductivity upon the heating of the sample from $T_0 < T_c$ by a high-power femtosecond pulse.

Studying the time history of electron-phonon relaxation throughout the spectral range has allowed us to estimate the electron-phonon interaction parameter [6, 7] $\lambda < \omega^2 >$ as $(4 \pm 2)\times10^2$ meV^2.

The sample under study was a 150-nm-thick $YBa_2Cu_3O_{7-\delta}$ film deposited on a $SrTiO_3$ substrate and coated with a protective MgO layer 5 nm in thickness. The superconducting and protective layers were grown by high-frequency magnetron sputtering in a single production cycle. The crystallites in the superconducting layer were around 300 nm across, their *c* axis being oriented normal to the substrate surface. The critical temperature T_c was equal to 80 K.

The sample was excited with a 150-fs laser pulse at 612 nm. The pump pulse intensity on the sample was some 10^{11}W/cm^2. The excited sample area was probed with a weak wide-band continuum pulse of the same duration. The probe pulse that passed through (or reflected from) the sample was detected with a multichannel optical analyzer built around two charge-coupled-device arrays. In our experiment, we measured the difference spectrum $\Delta A(\lambda, \tau)$ at various delay times τ between the pump and probe pulses.

In Fig. 1, which shows some of the experimental difference transmission spectra, one can see the drastic difference between the results for $T_0 > T_c$ and $T_0 < T_c$. While transmission in the former case is observed to decrease during the pump pulse over the entire spectral range under study [Fig. 1(*a*)], it grows in the region 1.93–2.01 eV in the latter case, there being only a slight drop in transmission in the range 1.89–1.93 eV [Fig. 1(*b*)]. With the delay time between the pump and probe pulses amounting to around a picosecond, a quasiequilibrium sets in, so that fast ($\simeq$100 fs) changes in the spectra cease. The only difference in the observation conditions between the spectra of Figs. 1(*a*) and 1(*b*) was that between the initial temperatures of the samples, and so it is reasonable to suppose that the changes the spectra are seen to undergo at $\tau < 1$ ps [Fig. 1(*b*)] contain information on the dynamics of destruction of the energy gap as a result of the sample being heated by the powerful femtosecond laser pulse.

Figure 2 shows the relationship between the optical density of the difference transmission spectra ΔA and the delay time τ for the most typical regions. The zero-delay time was determined from the results of independent experiments with a semiconductor-doped glass filter RG-8. At $T_0 = 92$ K (Fig. 2, curve *a*), the shape of the curves remains qualitatively the same throughout the spectral range of interest: ΔA is seen to decrease for a characteristic time of the order of 100 fs and then relax during $\tau \leq 1$ ps. The difference between the curves for various regions of the spectrum is that the asymptotic value of ΔA is less than zero at $\hbar\omega < 1.96$ eV and greater than zero at $\hbar\omega > 1.96$ eV. Similar curves, though relaxing to $\Delta A \simeq 0$, were observed at $T_0 = 70$ K for $\hbar\omega < 1.93$ eV (Fig. 2, curve *b).* The curves for $\hbar\omega > 1.93$ eV at this temperature reversed sign (Fig. 2, curve *c*); i.e., ΔA was first observed to increase and then relax to various asymptotic values, depending on wavelength. The relaxation of ΔA in the vicinity of $\hbar\omega = 1.96$ eV was nonmonotonic: two to three ΔA oscillations were observed to occur on a 300–500-fs scale. More pronounced oscillations in the transient transmissivity profile were observed in Ref. [2] only for a nonsuperconducting $YBa_2Cu_3O_{6+x}$ sample and were explained by the pulsed generation of optical phonons. An essential feature of the curves obtained at $T_0 < T_c$ is the delay of the response for $\simeq$ 200 fs in the region of 1.98 eV (Fig. 2, curve *c*), compared to that in the region of 1.91 eV (Fig. 2, curve *b*) and the response at $T_0 > T_c$ (Fig. 2, curve *a*). The magnitude of this delay is roughly 3 times the relative lag of the various spectral components of the probe pulse, observed to occur in the experiment as a result of dispersion.

To recover $\Delta\epsilon_2$ from the difference transmission and reflection spectra, use was made of ellipsometric data on the equilibrium dielectric constant, ϵ_1 and ϵ_2, of

$YBa_2Cu_3O_{7-\delta}$ [8]. The difference spectra of $\Delta\epsilon_2$ are shown in Figs. 3(*a)* and 3(*b*). As can be seen from the figures, the spectra for $T_0 > T_c$ again differ greatly from those for $T_0 < T_c$. At $\tau \geq 700$ fs, the spectral dependence of the response for $T_0 = 92$ K becomes alternating: $\Delta\epsilon_2 < 0$ for $\hbar\omega \leq 1.99$ eV and $\Delta\epsilon_2 \geq 0$ for $\hbar\omega \geq 1.99$ eV. Subsequently, starting from $\tau \simeq 1$ ps, the shape of the spectrum ceases to change – it remains alternating, with $\Delta\epsilon_2 = 0$ at $\hbar\omega = 2$ eV [Fig. 3(*a*)]. An alternating response is characteristic of the spectral range corresponding to transitions either into or out of the Fermi level region [9, 10] and is associated with the temperature smearing of the charge-carrier distribution function in the vicinity of the Fermi level. The position of the Fermi level in the spectral region $\hbar\omega \simeq 2$ eV agrees with the data of Ref. [4].

The decrease of transmission (ϵ_2 rise) for short delay times over a wide spectral range [Fig. 3(a)] is to all appearances due to the shift of the Fermi level as a result of strong heating of the charge carriers. The absence of any substantial changes in the $\Delta\epsilon_2$ spectrum at $\tau \geq 1$ ps points to the establishment of a quasiequilibrium. By this moment, the temperature of the sample reaches 500 K, and the system loses its memory of the initial conditions, so that the difference of a mere 30 K between the initial temperatures cannot bring about any significant dissimilarities in the spectra of the excited sample. It can therefore be argued that the diversities observed in the difference spectra at $\tau \geq 1$ ps [see Figs. 3(a) and 3(b)] can only result from the differences between the spectra of the sample in the initial (unexcited) state. This can be explained by the presence of an energy gap in the vicinity of the Fermi level for $T_0 = 63$ K and the shift of this level because of the difference between the T_0 values.

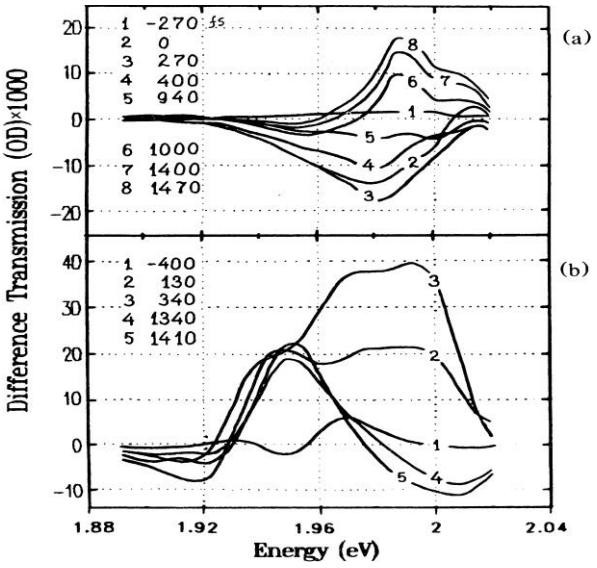


Fig. 1. Difference transmission spectra of the sample for various delay times τ (fs) of the probe pulse: (a) $T_0 = 92$ K, (b) $T_0 = 70$ K. The delay times are presented for an energy of 1.96 eV. The delay of the blue-wing probe continuum (2.02 eV) relative to its red-wing counterpart (1.9 eV) is no more than 60 fs

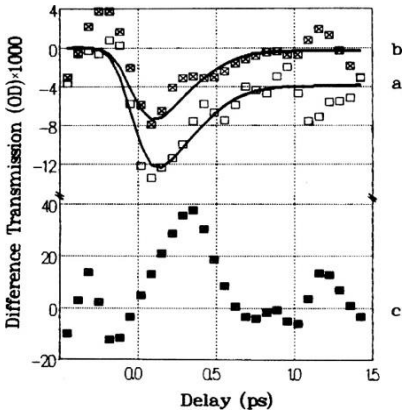


Fig 2. Difference transmission of the sample as a function of delay time for various photon energies of the probe pulse, $\hbar\omega$ (eV): Curve *a*, $T_0 = 92$ K, $\hbar\omega = 1.95$ eV ; curve *b*, $T_0 = 70$ K, $\hbar\omega = 1.91$ eV; curve *c*, $T_0 = 70$ K, $\hbar\omega = 1.98$ eV. The curves are the numerical fits to the experimental data for $\lambda\langle\omega^2\rangle 450$ meV^2, $C_e = 16$ mJ/molK^2, and $I_p = 2 \times 10^{11}$ W/cm^2

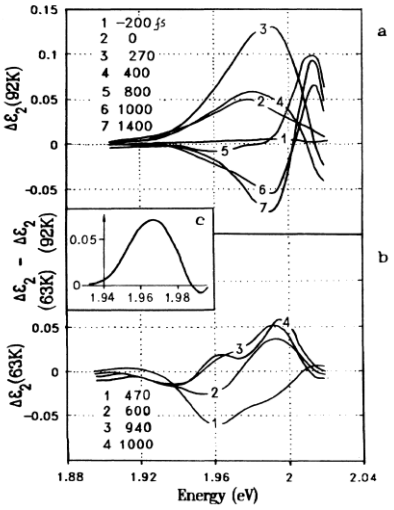


Fig. 3. Difference spectra of the imaginary part of the dielectric constant ϵ_2 for various delay times τ (fs) of the probe pulse: (*a*) T_0 = 92 K, (*b*) T_0 = 68 K, (*c*) the result of subtracting the spectra of $\Delta\epsilon_2$ for T_0 = 63 K and T_0 = 92 K (τ = 1000 fs)

Subtracting the difference spectrum $\Delta\epsilon_2$ for T_0 = 92 K at τ = 1 ps from that for T_0 = 63 K, we obtain a peak about 30 ± 10 meV wide in the neighborhood of 1.97 eV [Fig. 3(*c*)]. Relating the width of this peak to the width Δ of the energy gap (in a way similar to that used in the experiments on photoelectron spectroscopy [11, 12]), we get $2\Delta_0 / T_c = 8 \pm 3$ which agrees well with the data reported in Ref. [11].

The presence of an energy gap in the initial state can also explain the lag of the optical response maximum observed to occur for $T_0 < T_c$ in the vicinity of the Fermi level. The magnitude of this lag (≃ 200 fs) matches the time it takes for superconductivity to be destructed (see also Ref. [5]).

The experimental curves of Fig. 2 were used to estimate the electron-phonon-interaction parameter as $\lambda < \omega^2 >$ follows. The dielectric constant of the sample varies as a result of the heating of charge carriers and the shifting of energy bands due to the heating of the lattice and thermoelasticity effects. Within the framework of linear response, this variation (the change of transmission in our case) can be represented in the form [13] $\Delta A \simeq a\Delta T_e(t) + b, \Delta T_L(t)$ where T_e is the charge-carrier temperature and T_L the lattice temperature. To calculate the dynamics of ΔA, the temporal variations of T_e and T_L were determined from the set of equations [7, 13]

$$dT_e/dt = \left[\left(1 - R_f - T_f\right)/L_{sc}C_e(T_e)\right]I_p(t) - \gamma(T_e, T_L)(T_e - T_L), \qquad (1)$$

$$dT_L/dt = \gamma(T_e, T_L)[C_e(T_e)/C_L(T_L)](T_e - T_L) - (1/\tau_{esc})(T_L - T_0), \qquad (2)$$

where R_f is the reflectivity of the multilayer system, T_f the transmissivity of the superconductor layer, L_{sc} the superconductor layer thickness, I_p the pump pulse intensity, C_e and C_L the electronic and lattice heat capacities, and τ_{esc} the time it takes for phonons to escape into the substrate.

According to Allen [7], the electron-phonon relaxation rate is described by the expression ($\hbar = 1$, $k_B = 1$)

$$\gamma(t_e, T_L) = (3/\pi T_e)\lambda < \omega^2 > (1 - < \omega^4 > / 12 < \omega^2 >)(T_e T_L). \qquad (3)$$

According to the calculation results on the band structure of $YBa_2Cu_3O_{7-\delta}$ (Refs. [14, 15]), the energy interval from — 6 to + 2 eV relative to the Fermi level contains a 36-band complex made up of highly hybridized Cu *3d* and O *2p* states. Transitions across the forbidden gap in the electronic band structure start from an energy of around 3 eV. For this reason, it can be assumed that practically all of the absorbed pump pulse energy goes to the heating of the charge carriers. The quantity τ_{esc} can be estimated as ≥ 10 ps. For $C_L(T)$, we interpolated the data reported in Refs. [16, 17]. The data for $C_e = \gamma T$ differ greatly (from 13 to 54 mJ/mol K) [14, 18], and this contributes the most to the error in determining $\lambda < \omega^2 >$. According to our calculation results, the maximum temperature of charge carriers reaches some 3000 K. The maximum temperature of the lattice is around 600 K. The theoretical functions $\Delta A(t)$, calculated with due regard for the Gaussian shape of the pump and probe pulses, were compared to the experimental curves (see Fig. 2). Comparison was made for the spectral range 1.92–1.95 eV far from the Fermi level in order to avoid the possible nonlinear effects associated with the shift of the level as a result of strong heating of electrons. The parameters *a* and *b* were selected so as to make the calculated curves approximate the experimental data for the maximum ($\tau \simeq 100$ fs) and asymptotic ($\tau \geq 1$ ps) values, the temporal behavior of the experimental curves being approximated by means of the parameter $\lambda < \omega^2 >$. The resultant estimate is $\lambda < \omega^2 > = (4 \pm 2) \times 10^2$ meV^2. Using for (ω^2) the estimate $< \omega^2 > = \Theta_D^2/2$ and taking the Debye temperature Θ_D as 350 K [17], we get the following estimate for the electron-phonon coupling constant: $\lambda = 0.9 \pm 0.4$. Our data fit the results of the femtosecond pump-probe measurements [7] and the value of $\lambda \simeq 1$ found in Ref. [19] by the local-density-functional method.

We would like to thank M.E. Gershenzon and M.I. Falei for kindly providing the samples, I.B. Kedich and A.P. Yartsev for their assistance in the experiment, and also L.B. Kislichenko for her aid in calculations.

References

1. *Brorson S.D., Kazeroonian A., Moodera J.S., Face D.W., Cheng T.K., Ippen E.P., Dresselhaus M.S., Dresselhaus G., Doll G.L., Venkatesan T., Wu X.D., Inam A.* In: Ultrafast Phenomena VII / ed. by C.B. Harris, E.P. Ippen, G.A. Mourou and A.H. Zewail. Berlin: Springer-Verlag, 1990. P. 354.

2. *Chwalec J.M., Uher C., Whitaker J.F., Mourou G.A., Agostinelli J., Lelental M.* // Appl. Phys. Lett. 1990. Vol. 57. P. 1696; *Chwalec J.M., Uher C., Whitaker J.F., Mourou G.A. and Agostinelli J.* // Appl. Phys. Lett. 1990. No. 58. P. 980.

3. *Han S.G., Vardeny Z.V., Wong K.S., Symko O.G., Koren G.* // Phys. Rev. Lett. 1990. Vol. 65. P. 2708.

4. *Brorson S.D., Kazeroonian A., Face D.W., Cheng T.K., Doll G.L., Dresselhaus M.S., Dresselhaus G., Ippen E.P., Venkatesan T., Wu X.D., Inam A.* // Solid State Commun. 1990. No. 74. P. 1305; *Kazeroonian A., Cheng T.K., Brorson S.D., Ippen E.P., Wu X.D., Venkatesan T., Etemad S., Dresselhaus M.S., Dresselhaus G.* // Solid State Commun. 1991. Vol. 78. P. 95.

5. *Eesley G.L., Heremans J., Meyer M.S., Doll G.L., Liou S.H.* // Phys. Rev. Lett. 1990. Vol. 65. P. 3445.

6. *Eliashberg G.M.* // Zh. Eksp. Teor. Fiz. 1960. Vol. 38. P. 966; 1960. No. 39. P. 1437 [Sov. Phys. JETP. 1960. Vol. 11. P. 696; 1960. Vol. 12. P. 1000].

7. *Allen P.B.* // Phys. Rev. Lett. 1987. Vol. 59. No. 1460.

8. *Bjorneklett A., Borg A., Hunderi O.* // Physica (Amsterdam). 1989. Vol. 157A. P. 164.

9. *Eesley G.L.* // Phys. Rev. B. 1986. Vol. 33. P. 2144.

10. *Gershenzon M.E., Golovlyov V.V., Kedich I.B., Letokhov V.S., Lozovik Yu.E., Matveets Yu.A., Sil'kis E.G., Stepanov A.G., Titov V.D., Falei M.I., Farztdinov V.M., Chekalin S.V., Yartsev A.P.* // Pis'ma Zh. Eksp. Teor. Fiz. 1990. Vol. 52. P. 1189. [JETP Lett. 1990. Vol. 52, P. 602].

11. *Imer Y.M., Patthey F., Dardel B., Schneider W.-D., Baer Y., Petroff Y., Zettl A.* // Phys. Rev. Lett. 1989. Vol. 62. P. 336; *Shutzmann J., Ose W., Keller J., Renk K.F., Roas B., Shulz L., Saeman-Ischenko G.* // Europhys. Lett. 1989. Vol. 8. P. 679; *Collins R.T., Schlezinger Z., Holzberg F., Freidl C.* // Phys. Rev. Lett. 1989. Vol. 63. P. 422.

12. *Maksimov E.G., Savrasov S.Yu.* // Usp. Fiz. Nauk. 1990. Vol. 160. P. 155 [Sov. Phys. Usp. 1990. Vol. 33. P. 86].

13. *Brorson S.D., Kazeroonian A., Moodera J.S., Face D.W., Cheng T.K., Ippen E.P., Dresselhaus M.S., Dresselhaus G.* // Phys. Rev. Lett. 1990. Vol. 64. P. 2172.

14. Krakauer H., Pickett W.E., Cohen R.E., Supercond J. 1988. Vol. 1. P. 111.

15. *Massidda S., Yu J., Freeman A.J., Koeling D.D.* // Phys. Lett. A. 1987. Vol. 122. P. 198; *Zhao G.-L., Xu Y., Ching W.Y., Wong K.W.* // Phys. Rev. B. 1987. Vol. 36. P. 7203; *Pickett W.E.* // Rev. Mod. Phys. 1989. Vol. 61. P. 433; *Pickett W.E., Cohen R.E., Krakauer H.* // Phys. Rev. B. 1990. Vol. 42. P. 8764.

16.*Lyusternik V.E., Peletskii B.E., Bakunov V.S., Bolotnikov A.V.* // Sverkhprovodimost' (in Russian). 1990. Vol. 3. P. 2037.

17. *Kvavadze K.A., Igitkhanishvili D.D., Nadareishvili M.M., Tarkhnishvili L.A., Zinzadze G.A., Chubabriya M.Y.* // Sverkhprovodimost' (in Russian). 1990. Vol. 3. P. 1628.

18. *Nevitt M.V., Crabtree G.W., Klippert T.E.* // Phys. Rev. B. 1987. Vol. 36. P. 2398.

19. *Rodriguez C.O., Liechtenstein A.I., Mazin I.I., Jepsen O., Andersen O.K., Methfessel M.* // Phys. Rev. B. 1990. Vol. 42. P. 2692.

ЛАЗЕРНЫЙ КОНТРОЛЬ ДВИЖЕНИЯ АТОМОВ

1. *Летохов В.С.* Сужение доплеровской линии в стоячей световой волне // Письма в ЖЭТФ. 1968. Т. 7 (9). С. 348–351.

2. *Letokhov V.S., Minogin V.G., Pavlik B.D.* Cooling and trapping of atoms and molecules by a resonant laser field. //Opt. Commun. 1976. Vol. 19. P. 72–75.

3. *Андреев С.В., Балыкин В.И., Летохов В.С., Миногин В.Г.* Радиационное замедление и монохроматизация пучка атомов натрия до 1,5 К во встречном лазерном луче //Письма в ЖЭТФ. 1981. Т. 34 (8). С. 463–467.

4. *Балыкин В.И., Летохов В.С., Сидоров А.И.* Радиационная коллимация атомного пучка путем двухмерного охлаждения лазерным излучением // Письма в ЖЭТФ. 1984. Т. 40 (6). С. 251–253.

5. *Balykin V.I., Letokhov V.S.* Laser optics of neutral atomic beams // Physics Today. 1989. Vol. 42 (4). P. 23–28.

6. *Балыкин В.И., Летохов В.С., Овчинников Ю.Б., Сидоров А.И.* Отражение атомного пучка от градиента светового поля // Письма в ЖЭТФ. 1987. Т. 45 (6). С. 282–284.

7. *Balykin V.I., Letokhov V.S., Ovchinnikov Yu.B., Sidorov A.I.* Quantum-state-selective mirror reflection of atoms by laser light // Phys. Rev. Lett. 1988. Vol. 60 (21). P. 2137–2140.

8. *Balykin V.I., Letokhov V.S., Ovchinnikov Yu.B., Sidorov A.I., Shul'ga S.V.* Channeling of atoms in a standing spherical light wave // Opt. Lett. 1988. Vol. 13 (11). P. 958–960.

9. *Grimm R., Ovchinnikov Yu.B., Sidorov A.I., Letokhov V.S.* Observation of a strong rectified dipole force in a bichromatic standing light wave // Phys. Rev. Lett. 1990. Vol. 65 (12). P. 1415–1418.

10. *Balykin V.I., Letokhov V.S.* The possibility of deep laser focusing of an atomic beam into the Å-region // Opt. Commun. 1987. Vol. 64 (2). P. 151–156.

Письма в ЖЭТФ. 1968. Т. 7 (9). С. 348–351

СУЖЕНИЕ ДОПЛЕРОВСКОЙ ЛИНИИ В СТОЯЧЕЙ СВЕТОВОЙ ВОЛНЕ

В.С. Летохов
Физический Институт им. П.Н. Лебедева АН СССР

1. Линии поглощения или излучения газа низкого давления при небольшой радиационной ширине перехода имеют доплеровский контур, определяемый распределением частиц по скоростям. Цель настоящей работы — показать, что интенсивная стоячая световая волна способна так изменить распределение атомов по скоростям, что в центре доплеровской линии при наблюдении поглощения или излучения строго в направлении оси световой волны возникает чрезвычайно узкий пик. Физически это явление объясняется «пленением» между пучностями или нулями стоячей волны тех атомов, которые движутся почти параллельно волновому фронту. Этот новый эффект представляет интерес для спектроскопии внутри доплеровского контура с чрезвычайно высокой разрешающей силой и высокоточной стабилизации частоты лазера.

2. На электроны (свободные или связанные) в высокочастотном электромагнитном поле действует сила от усредненного квадрата электрического поля [1, 2]. Она определяется стрикционной силой [3], действующей на атом (молекулу):

$$f = \frac{1}{2}\kappa_\omega \mathrm{grad}(E^2)_{\mathrm{ср}} \qquad (1)$$

где κ_ω — поляризуемость атома на частоте внешнего поля ω, определяемая показателем преломления газа n_ω($\kappa = (n_\omega - 1)/2\pi N$, N — плотность частиц газа).

В случае плоской стоячей световой волны $E_0 \sin kz \sin_\omega t$ стрикционная сила является периодической функцией:

$$f = \frac{1}{4}\kappa_\omega \mathrm{E}_0^2 k \sin 2kz \qquad (2)$$

Движущиеся атомы либо втягиваются в пучности стоячей волны (при $k_\omega < 0$), либо выталкиваются из них (при $k_\omega > 0$). Изменение z-координаты атома описывается уравнением:

$$\ddot{z} = \frac{1}{4M}\kappa_\omega \mathrm{E}_0^2 k \sin 2kz, \qquad (3)$$

аналогичным уравнению колебаний маятника (M — масса атома).

Нетрудно показать, что атомы, имеющие начальную скорость в направлении z меньше некоторой критической, определяемой соотношением:

$$v_{кр} = E_0\sqrt{\frac{|\kappa_\omega|}{2M}}, \tag{4}$$

вместо свободного движения испытывают колебания в направлении с амплитудой z, не превышающей $\lambda/4$ (λ — длина световой волны). Величина $v_{кр}$ при интенсивностях в несколько киловатт на квадратный сантиметр на несколько порядков меньше средней тепловой скорости атомов $v_0 = \sqrt{2kT/M}$. Поэтому такое «пленение» между пучностями (или минимумами) волны будет иметь место лишь для атомов, движущихся под малыми углами ϕ к волновой поверхности (рис. 1):

$$|\phi| < \phi_{кр} = \frac{v_{кр}}{v_0} = E_0\sqrt{\frac{|\kappa_\omega|}{4kT}}. \tag{5}$$

Атомы, движущиеся под углом $\phi > \phi_{кр}$, свободно пересекают стоячую световую волну, но z — составляющая их скорости промодулирована осцилляциями с амплитудой $v_{кр}$.

3. При наблюдении излучения (поглощения) атомов в направлении z на длинах волн $\lambda' >> \lambda$ «плененные» атомы, которые в обычных условиях имеют доплеровскую ширину $\Delta\omega_0' = 2\left(\frac{v_{кр}}{c}\right)\omega'$, не испытывают доплеровского уширения. При осцилляциях положения атома происходит частотная модуляция частоты излучения (поглощения). Относительная интенсивность центральной несмещенной компоненты пропорциональна $J_0(\lambda/\lambda')$,а интенсивность n-й боковой компоненты — $J_n(\lambda/\lambda')$, где J — функция Бесселя n-го порядка. При $\lambda' >> \lambda$ интенсивность боковых компонент пренебрежимо мала. В результате в центре доплеровской линии возникает узкая линия (рис. 2), ширина которой определяется временем движения «плененных» атомов в стоячей волне τ. При достаточно низком давлении газа и малой радиационной ширине перехода время τ определяется временем пролета атомов через луч диаметра α. Для получения узкой компоненты необходимо выполнение условия:

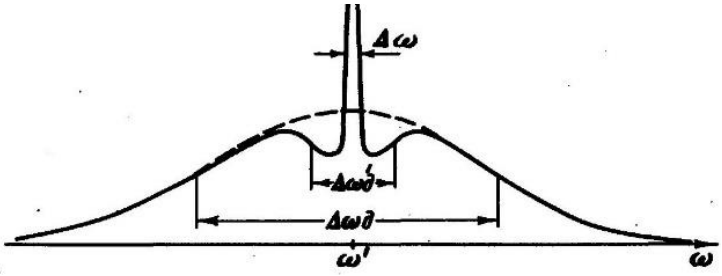


Рис. 1. Траектория движения «плененного» атома в стоячей световой волне

$$\alpha \gg d_{кр} = \frac{\lambda}{2\phi_{кр}} \tag{6}$$

Тогда ширина узкой компоненты определяется соотношением:

$$\Delta\omega = \frac{2}{\tau} = \frac{2\nu_0}{\alpha}. \tag{7}$$

4. Пусть частота световой волны лежит вне резонансов и полос поглощения атомов и поляризуемость составляет $\kappa_\omega \cong 10^{-23}$ см$^{-3}$, что соответствует показателю преломления $n_\omega - 1 \cong 2 \cdot 10^{-3}$атм$^{-1}$. При мощности стоячей световой волны $P = c(E_0^2/16\pi) = 10^5$вт/см^2, λ = 1 мк и T = 300°K критический угол $\phi_{кр} \cong 3 \cdot 10^{-4}$ рад и $d_{кр} \cong 1{,}7$ мм. В этом случае условие (6) выполнить вполне возможно. Например, при диаметре луча α = 1 см и давлении $\leq 10^{-4}$тор (для устранения столкновений) можно получить узкую компоненту с шириной $\Delta_\omega \cong 3 \cdot 10^4$ Гц на линиях с $\lambda' >> 1$ мк. В области резонансов $|\kappa_\omega|$ резко возрастает, но можно показать, что условие «пленения» атомов совпадает с условием сильного насыщения κ_ω полем. Сильное насыщение приводит к уширению однородной линии [4], что затрудняет возникновение эффекта в области резонанса.

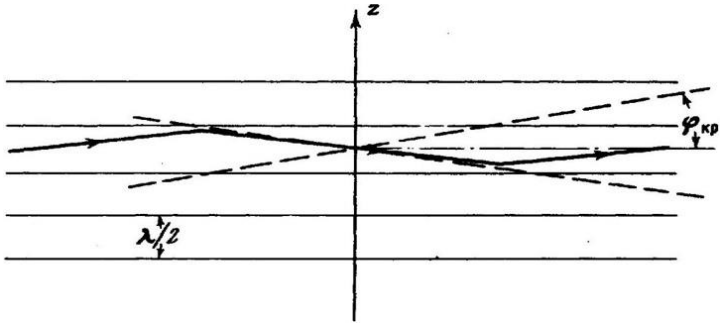


Рис. 2. Форма линии поглощения (излучения) атома в направлении оси z в присутствии стоячей световой волны (пунктирная кривая — доплеровская форма линии в отсутствие волны)

5. Узкую компоненту можно наблюдать как в поглощении, так и в излучении. Сканируя частоту ω' монохроматической волны, направленной строго вдоль интенсивной стоячей волны, можно получить форму линии поглощения. Если линия поглощения состоит из ряда линий, то узкая компонента появится в центре каждой линии. Разрешающая способность такого метода $R = (\omega'/\Delta\omega) \simeq 10^9 \div 10^{11}$. В спонтанном или индуцированном излучении атомов в направлении стоячей волны также должны возникнуть одна или несколько узких компонент, соответствующих структуре линии.

В заключение автор выражает глубокую благодарность академику Н.Г. Басову и доктору физико-математических наук О.Н. Крохину за поддержку и ценные обсуждения.

Литература

1. *Гапонов А.В., Миллер М.А.* // ЖЭТФ. 1958. Т. 34. С. 242.

2. *Аскарьян Г.А.* // ЖЭТФ. 1962. Т. 42. С. 1567.

3. *Ландау Л.Д., Лифшиц Е.И.* Электродинамика сплошных сред. М.: Гостехиздат, 1957.

4. *Karplus R., Schwinger J.* // Phys. Rev. 1948. Vol. 73. P. 1020.

Optics Communications. 1976. Vol. 19 (1). P. 72–75

COOLING AND TRAPPING OF ATOMS AND MOLECULES BY A RESONANT LASER FIELD

V.S. Letokhov, V.G. Minogin
Institute of Spectroscopy, Academy of Sciences USSR,
142092 Moscow, Podol'skii raynon, Akademgorodok, USSR
B.D. Pavlik
Physical Institute, Academy of Sciences Ukrainian SSR, Kiev, USSR

A method is suggested for simultaneous cooling and trapping of atoms and molecules in a low-pressure gas under forces caused by recoil during spontaneous or induced transitions of the particles in the resonance field of a three-dimensional standing light wave. It is shown that at light field intensities ~0.01–0.1 W/cm^2 it is possible to cool atoms and molecules to the resonance field photon momentum and to hold the particles in the light field volume during a long period of time. The proposed approach opens the way for high-resolution Doppler-free spectroscopy of a small number of atoms and molecules.

1. It is well known that the widths of narrow atomic or molecular resonances produced by up-to-date methods of non-linear laser spectroscopy are limited by broadening caused by the finite transit time of particles across the light beam and by the second-order Doppler effect [1]. These limitations are of principal importance both in the methods of saturation and two-photon Doppler-free spectroscopy because both these methods are based essentially on the interaction of light waves with free-moving atoms or molecules.

Complete or partial elimination of transit broadening and broadening due to the second order Doppler effect, and observation of narrow resonances whose widths are conditioned only by the properties of atomic or molecular quantum transitions, are possible, of course, only in the case when the particle motion in a low-pressure gas is either fully impeded or considerably limited.

At present there are two effects predicted which in principle may form the basis for laser Doppler-free spectroscopy with extremely high resolution ($>10^{12}$) and with a very small number of atoms or molecules. One of them (the effect of radiative trapping of atoms or molecules [2]) is based on using the strong field of a three-dimensional standing light wave beyond resonance transitions of an atom or a molecule for particle trapping by non-resonance forces of recoil in the nodes or loops of the light field. The practical realization of this technique has proved rather complicated because the effect appears for very slow atoms, the number of which in a low-

pressure gas at 300 K is extremely small [1]. Besides, the required field intensity is rather high (for particles with velocity 0.1 to 1 cm/sec it should be 10^3 W/cm^2).

The second effect (radiative cooling of atoms [3]) is based on atom moderation by the spontaneous light pressure force as the low-frequency part of a Doppler-broadened line of an optical transition is isotropically irradiated by an intense resonance light field. For this effect a sufficiently intense field is required too. In particular, it takes a power of 10^3 W/cm^2 to cool atoms to velocities which would correspond to the homogeneous width from 10 to 100 MHz. Besides, cooled particles quickly fly out from the region of the laser field (for instance, because of recoil effects at the probe laser field), and for long experimentation it is necessary that new particles should be cooled periodically.

It is easy to imagine a method of spectroscopy based on a combination of these effects: radiative precooling of particles by a resonance field and subsequent capture of the cooled low-speed particles by a nonresonance intense light field. This technique offers strong possibilities of realizing the spectroscopy of slow trapped particles discussed in refs. [1, 4]. The topic of our Letter however is much wider. The idea of our next suggestion is that a considerable decrease of required field intensities and a substantial widening of the trapped particle velocity range can be achieved if we use both for cooling and trapping atoms and molecules the forces caused by recoil during spontaneous and (or) induced transitions of an atom or molecule in the resonance field of a standing light wave with the frequency scanned by a certain law.

In this work we shall demonstrate that *in the resonance field of a three-dimensional standing light wave it is possible to cool particles* to velocities corresponding to the resonant photon momentum and, *simultaneously, to capture a considerable part of the cooled particles*, hence to eliminate transit broadening, and the broadening induced by the second-order Doppler effect for a considerable part of atomic or molecular transitions.

2. In the resonance field of a one-dimensional standing light wave

$$E = 2E_0 \cos \omega t \cos kz \tag{1}$$

two recoil forces act upon an atom or a molecule. One of them — the spontaneous light pressure force — is conditioned by recoil during spontaneous transitions of a particle in the field, the other one — the induced light pressure force — is conditioned by recoil during induced transitions of a particle in the field. When the lower level of the resonance transition is the ground one and the upper-level width is conditioned by spontaneous decay at the rate 2Γ only the ground level, these forces have the form:

$$F_{\text{sp}} = 2\hbar k\Gamma \times \frac{G[£(\Omega - kv) - £(\Omega + kv)]}{1 + G[£(\Omega - kv) + £(\Omega + kv)]} \sin^2 kz, \tag{2}$$

$$F_{\text{ind}} = \hbar k\Omega \times \frac{G\left[\left(1 - \frac{kv}{\Omega}\right)£(\Omega - kv) + \left(1 + \frac{kv}{\Omega}\right)£(\Omega + kv)\right]}{1 + G[£(\Omega - kv) + £(\Omega + kv)]} \times \sin 2\,kz, \tag{3}$$

where $k = \omega/c$ is the wave vector of the light wave, υ is the particle velocity projection onto the wave direction, $\Omega = (\omega - \omega_0)$ is the detuning of the field frequency about the center frequency of the resonance transition, d is the matrix element of the resonance transition dipole moment, and the following notations are introduced

$$G = \frac{1}{2}\left(\frac{dE_0}{\hbar\Gamma}\right)^2, \quad \text{£}(x) = \frac{\Gamma^2}{x^2+\Gamma^2}. \tag{4}$$

Forces (2) and (3) act on the particles in a low-pressure gas in different ways (fig. 1). The force F_{sp} conducts directed acceleration of particles: with $\Omega > 0$ the particles are accelerated by the field, with $\Omega < 0$ they are moderated. The force F_{ind} conducts either a finite motion (trapping) of particles [the average force

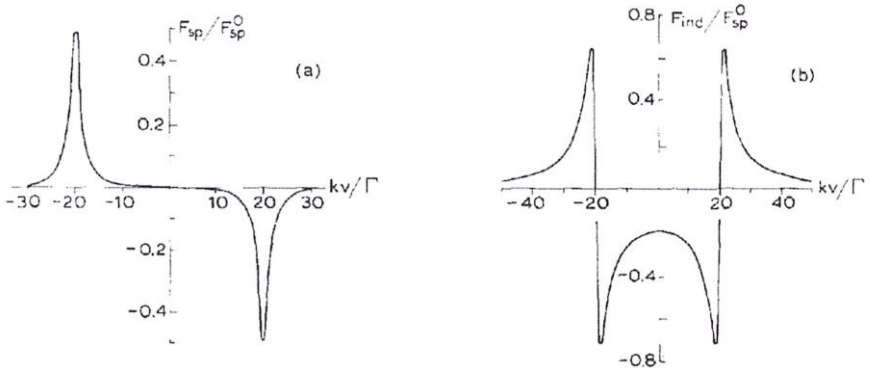


Fig. 1. Dependence of spontaneous light pressure force (a) and induced light pressure force (b), normalized to $F_8^0 = 2\hbar k\Gamma$, on particle velocity for $G = 1$, $\Omega/\Gamma = -20$. Both forces are calculated at spatial points corresponding to the maxima of F_{sp} and F_{ind}

(3) with respect to the light wavelength is equal to zero] or, if the particle velocity is high enough, conducts trebly periodic modulations of the particle velocity.

3. When the detuning $|\Omega| \gtrsim \Gamma$, the induced light field force brings about only a modulation of the resonant particle velocity $\upsilon = \pm\,\Omega/k$:

$$\left|\frac{\Delta\upsilon}{\upsilon}\right| \sim \frac{R_{rec}}{\hbar|\Omega|}\left(\frac{\Gamma}{\Omega}\right)^2 \frac{G}{1+G}, \tag{5}$$

where $R_{rec} = (\hbar\omega)^2/2mc^2$ is the recoil energy. In the important case $R_{rec}/\hbar \ll \Gamma$ this velocity modulation corresponds to the resonant frequency modulation of the atom or molecule

$$|\omega\text{-}\omega_0| \sim \Gamma\frac{R_{rec}}{\hbar|\Omega|}\frac{\Gamma}{|\Omega|}\frac{G}{G+1} \ll \Gamma. \tag{6}$$

Such relations will be apparently true for a three-dimensional standing light wave.

As the action of the induced light pressure force on particle motion with $|\Omega| \gtrsim \Gamma$ may be neglected, the spontaneous light pressure force can be used to cool the particles to velocities corresponding to the homogeneous line width by adiabatic scanning of the field frequency from $\omega \approx \omega_0 - \Delta\omega_D$ to $\omega \approx \omega_0 - \Gamma$, where $\Delta\omega_D$ is the Doppler half-width of resonance transition. The equation for particle motion in any coordinate system

$$M\frac{dv}{dt} = F_{sp} = \hbar k\Gamma\frac{G\Gamma^2}{[\Omega(t)\pm kv]^2+\Gamma^2(1+G)}. \quad (7)$$

shows that the rate of gas cooling will be maximum at time-linear scanning of field frequency, with the time required to cool the particles from the velocity $|v| \approx \Delta\omega_D/k$ to $|v| \approx \Gamma/k$ being

$$\tau_{col} = \frac{1}{2\Gamma}\frac{\Delta\omega_D}{\frac{R_{rec}}{\hbar}}\frac{1+G}{G}. \quad (8)$$

It should be noted that the time of particle cooling to velocities corresponding to the homogeneous line width of the resonance transition is practically the same both during isotropic saturation of the whole Doppler contour [3] and during saturation of its part only within the limits of the homogeneous line width by tunable radiation. In the latter case, however, much smaller field intensities are needed. For example, for the resonance transition $3^1S_0-3^1P_1$ of ^{24}Mg atoms ($\Delta\omega_D$ = 1600 MHz, $R_{rec}/\hbar$ = 0.1 MHz) with I = 0.4 W/cm^2 (G = 1) the cooling time $\tau'_{col} = 6\times10^{-5}$ sec which is much smaller than the time between collisions at pressures $\lesssim 10^3$ torr.

It is clear that rapid gas cooling during adiabatic scanning of the light field frequency is of use only down to velocities $|v| \approx \Gamma/k$, that is when the field frequency changes up to the detuning $|\Omega| \approx \Gamma$. With a further decrease of detuning the force of spontaneous light pressure tends to zero and the cooling time rises drastically.

But at constant detuning $|\Omega| \approx \Gamma$ the particles will continue to be cooled by the force of the spontaneous light pressure down to velocities corresponding to the resonance photon momentum. Indeed, with $|\Omega| \approx \Gamma$ the particles with their velocities $|v| \lesssim \Gamma/k$ are acted upon by the average force

$$F_{sp} = \hbar k\Gamma\frac{G\left(\frac{kv}{\Gamma}\right)}{\frac{1}{4}\left(\frac{kv}{\Gamma}\right)^4+\frac{1}{2}G\left(\frac{kv}{\Gamma}\right)^2+G+1}, \quad (9)$$

which moderates the particles according to the exponential law

$$v(t) = v(0)\exp\left(-\frac{R_{rec}}{\hbar}t\right) \quad (10)$$

For particles whose velocities are adiabatically moderated down to $|v| \approx \Gamma/k$ the lime of cooling to the minimum velocity $|v| \approx \hbar k/m$ with G = 1 is given by the expression

$$\tau_{\text{col}}^{''} = \frac{1}{2\Gamma}\frac{\hbar\Gamma}{R_{\text{rec}}}\ln\frac{\hbar\Gamma}{R_{\text{rec}}}. \tag{11}$$

For the transition of ^{24}Mg atoms being considered $\tau_{\text{col}}^{''} = 5 \times 10^{-6}$ sec. Note that the cooling of ^{24}Mg atoms to resonance photon momentum corresponds to the gas temperature $T = R_{\text{rec}}/k = 4.9 \times 10^{-6}$ K.

Thus, the maximum cooling of particles to the limit conditioned by quantum fluctuations can be done in a very short time, and almost all the atoms in the area of the light field can be cooled to the photon momentum.

4. An important feature of cooling atoms or molecules by the resonance field of a three-dimensional standing light wave is that it is possible to trap particles by the force of induced light pressure. When $|\Omega| \simeq \Gamma$, the force of induced light pressure not affecting, on the average, particle cooling to photon momentum forms for slow particles a potential barrier which limits the spatial movement of particles. The equation for the particle motion under force (3) shows that when the particle velocity υ is smaller than a certain trapping rate υ_{tr}

$$|\upsilon| < \upsilon_{\text{tr}}, \tag{12}$$

the particles are trapped in the loops of light field (with $\Omega < 0$). The critical velocity of trapped particles, υ_{tr}, is given by the equation:

$$\frac{1}{2}\left(\frac{k\upsilon}{\Omega}\right)^4 + \left[(3+2G)\frac{\Gamma^2}{\Omega^2} - 1\right]\left(\frac{k\upsilon}{\Omega}\right)^2 + 4(1+G)\frac{\Gamma^2}{\Omega^2}\left(1+\frac{\Gamma^2}{\Omega^2}\right)\ln\left[1-\frac{(k\upsilon/\Omega)^2}{1+(\Gamma^2/\Omega^2)}\right] + 8G\frac{R_{\text{rec}}}{\hbar\Omega}\frac{\Gamma^2}{\Omega^2} = 0. \tag{13}$$

When $R_{\text{rec}}/\hbar \ll \Gamma \ll \Gamma$ and $G \simeq 1$, the maximum of the critical velocity of particle capture will be

$$\upsilon_{\text{tr}} \approx (\Gamma/k)\sqrt{R_{\text{rec}}/\hbar\Gamma}. \tag{14}$$

It is reached with $|\Omega| \approx \Gamma$, i.e., with detuning being optimal for fast cooling of particles to photon momentum. For example, for the transition 3^1S_0–3^1P_1 of ^{24}Mg atoms with $I = 0.4$ W/cm^2 and $|\Omega| \approx \Gamma$: $\upsilon_{\text{tr}} \approx 60$ cm/sec.

The holding time of cooled particles will depend, of course, on the actual vacuum in the cell illuminated by the light field. With a typical full cross-section of atomic or molecular scattering $\sigma \approx 10^{-14}$ cm^2, an average thermal velocity of added particles $u \simeq 10^4$ cm/s and an actual vacuum pressure ~10^{-10} torr ($n = 3.6\times10^6$ cm^{-3}) this time equals

$$\tau = 1/n\delta u \simeq 1 \text{ hour}. \tag{15}$$

Thus, simultaneous cooling and trapping of particles in the resonance field of a three-dimensional standing light wave makes it possible both to hold the atoms and molecules during a long period of time in the area limited by the volume of the resonance light field and to carry out spectroscopic studies of absorption (emission) lines with their width determined by natural broadening only [4]. The probe light field used to detect narrow lines must also form a three-dimensional standing light wave because only with such a field configuration the particles will not escape from the region of the resonance field when acted upon by the recoil effect due to the probe field.

Finally, we think that cooling and keeping the cooled particles in a limited spatial region for a long time, open the way for monoatomic high-resolution spectroscopy of isolated atoms and molecules.

References

1. *Letokhov V.S.* // Science. 1975. Vol. 190. P. 344.

2. *Letokhov V.S.* // ZhETF Pis. Red. 1968. Vol. 7. P. 348.

3. *Hänsch T.W., Schawlow A.L.* // Optics Comm. 1957. Vol. 13. P. 68.

4. *Letokhov V.S., Pavlik B.D.* // Appl. Physics. 1976. Vol. 9. P. 229.

Письма в ЖЭТФ. 1981. Т. 34 (8). С. 463–467

РАДИАЦИОННОЕ ЗАМЕДЛЕНИЕ И МОНОХРОМАТИЗАЦИЯ ПУЧКА АТОМОВ НАТРИЯ ДО 1,5 К ВО ВСТРЕЧНОМ ЛАЗЕРНОМ ЛУЧЕ

С.В. Андреев, В.И. Балыкин, В.С. Летохов, В.Г. Миногин
Институт спектроскопии АН СССР

Экспериментально обнаружена скоростная монохроматизация пучка атомов натрия, замедляемого встречным резонансным лазерным излучением. При эффективной длине замедления 20 см достигнуто сужение продольного скоростного распределения атомного пучка в 19 раз, что соответствует понижению температуры относительного движения атомов до 1,5 К.

В последнее время активно разрабатываются методы лазерного охлаждения ионов [1] и атомов [2]. В экспериментальных исследованиях наибольшие успехи достигнуты при лазерном охлаждении ионов, локализованных в электромагнитных ловушках, для которых достигнута температура 10^{-2} К [3, 4]. Лазерное охлаждение движущихся нейтральных атомов, для которых пока не найдены способы пространственной локализации, является гораздо более сложной задачей.

Первое экспериментальное наблюдение лазерного охлаждения атомов было осуществлено в [5] измерением деформации скоростного распределения в пучке атомов натрия, облучаемом встречным лазерным излучением. В настоящей работе, используя более совершенную экспериментальную технику, мы впервые сообщаем о прямых исследованиях сужения скоростного распределения атомов натрия под действием интенсивного встречного двухчастотного лазерного излучения до температуры 1,5 К и о достижении степени монохроматизации $\mu \approx 19$.

Физической причиной скоростной монохроматизации является резкая резонансная зависимость силы светового давления от скорости, благодаря которой сила эффективно воздействует только на атомы, находящиеся в резонансе с волной (см. обзор [6]). При замедлении теплового атомного пучка предельная скоростная монохроматизация, определяемая отношением ширины начального скоростного распределения к ширине конечного распределения с нулевой средней скоростью, может достигать значений $\mu = (M\bar{v}/\hbar k)^{1/2} \approx 100$ [7, 8]. Это соответствует понижению температуры относительного движения атомов до $T = T_0/\mu^2 \approx 10^{-4}\ T_0$, где $\hbar k$ — импульс фотона, M, $\bar{v}$ — масса и средняя начальная скорость атомов.

На рис. 1 приведены основные элементы экспериментальной установки. Аргоновый лазер $Л_1$ накачивал два лазера на красителе непрерывного

действия, один из которых $Л_3$ осуществлял замедление атомного пучка, а другой одночастотный сканируемый лазер $Л_2$ (Spectra-Physics, Model 580 A) производил зондирование продольного скоростного распределения атомного пучка. Излучение обоих лазеров вводилось коллинеарно в вакуумную камеру навстречу основному атомному пучку. Наблюдение скоростного распределения атомов осуществлялось по сигналу флуоресценции $Ф_{1,2}$ от зондирующего лазера. Для того чтобы сигнал флуоресценции от сильного поля не мешал наблюдению слабого сигнала флуоресценции от пробного поля, были приняты меры для отделения сигнала флуоресценции, вызванного зондирующим излучением, от сигнала флуоресценции, вызванного сильным замедляющим излучением. Для этого излучение силового лазера $Л_3$ периодически прерывалось модулятором $М_1$ со скважностью 1:1 и регистрация флуоресценции от зондирующего излучения производилась только в те моменты времени, когда силовое поле было выключено. Периодическое включение регистрирующей аппаратуры осуществлялось с помощью строб-вольтметра. Вспомогательный атомный пучок, который распространялся перпендикулярно лазерному лучу, служил для частотной калибровки сигнала флуоресценции от зондирующего излучения. Частота излучения силового лазера настраивалась по максимуму флуоресценции в пределах доплеровского контура перехода $3S_{1/2} - 3P_{3/2}$ (λ = 5896 Å).

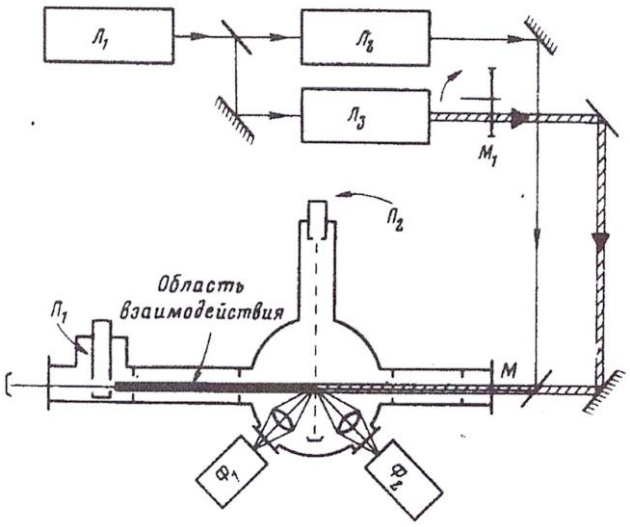


Рис. l. Схема экспериментальной установки (закрашена область взаимодействия интенсивного встречного луча с атомами в пучке): $Л_1$ — аргоновый лазер, $Л_2$ — зондирующий лазер, $Л_3$ — двухчастотный силовой лазер, $П_1$, $П_2$ — соответственно, источники параллельного и перпендикулярного атомных пучков, $Ф_1$, $Ф_2$ — фотоумножители, $М_1$ — механический прерыватель, $М$ — полупрозрачное зеркало

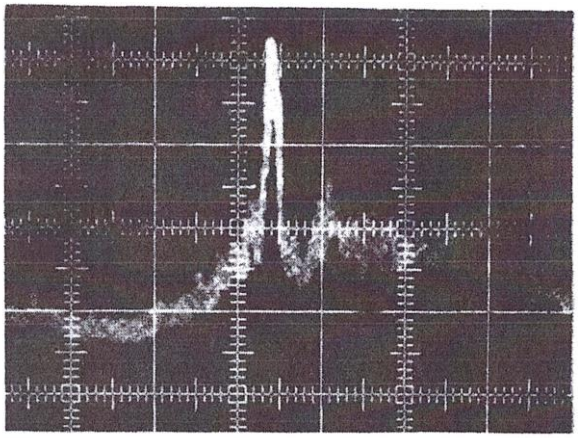


Рис. 2. Экспериментальный профиль скоростного распределения (*а*) и расчетная зависимость (*б*) деформации скоростного распределения *W(υ)* пучка атомов натрия. Пунктирная кривая представляет профиль начального распределения при температуре 573 К. Одно деление на рис. 2(*а*) соответствует 420 МГц

Поскольку основное состояние атома натрия расщеплено на два подуровня сверхтонкой структуры с расстоянием между ними $\Delta\nu = 1772$ МГц, то для обеспечения цикличности взаимодействия атомов с излучением была осуществлена генерация лазера *Л3* одновременно на двух частотах с расстоянием между ними 1770 МГц. Такой режим генерации достигался использованием трех эталонов Фабри — Перо внутри резонатора лазера для предварительного сужения спектра, выбором длины резонатора и подбором расстояния от струи красителя до «глухого» зеркала резонатора так, чтобы минимизировать конкуренцию между парами аксиальных мод, расстояние между которыми равно 1772 МГц [9]. Частота зондирующего лазера сканировалась вдоль доплеровского контура перехода $3S_{1/2}$–$3P_{3/2}$. Плавность сканирования частоты лазера контролировалась как по флуоресценции в парах натрия, так и по флуоресценции атомного пучка в отсутствие сильного поля.

Температура источника параллельного атомного пучка равнялась 300 ºС. Вакуумная камера откачивалась до давления $(3 \div 5)10^{-6}$ тор. Диаметр сильного лазерного луча вблизи выходного отверстия источника атомов равнялся $d_c' = 1{,}1$ мм, в области регистрации $d_c'' = 1{,}3$ мм соответственно, диаметры зондирующего луча равнялись $d_3' = 0{,}65$ мм; $d_3'' = 0{,}6$ мм. Геометрическая длина области взаимодействия составляла 40 см.

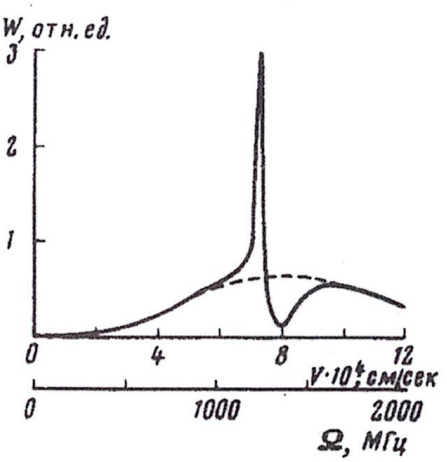


Рис. 2*б* (см. подпись к рис. 2)

На рис. 2(*а*) приведена осциллограмма сигнала флуоресценции от зондирующего излучения при сканировании его частоты вдоль деформированного сильным лазерным излучением контура скоростного распределения. Осциллограмма ясно показывает сужение продольного скоростного распределения атомов в области меньшей резонансной скорости. Следует особо подчеркнуть, что, поскольку регистрация флуоресценции производится только в моменты времени, когда сильное поле отсутствует (перекрывается модулятором M_1), то характерные провал и пик на контуре не могут быть вызваны совместным действием (например, совпадением частот в некоторые моменты времени) обоих лазерных лучей. Для приведенной на рис. 2*а* осциллограммы мощность излучения силового лазера в обеих модах составляет величину 12 мВт, мощность излучения зондирующего лазера — 0,1 мВт, а диаметры лучей — 1,3 и 0,6 мм соответственно.

Ширина пика распределения составляет 70 МГц (в единицах скорости — $4 \cdot 10^{-3}$ см/сек), что при начальной температуре пучка в 573 К соответствует степени монохроматичности $\mu = \Delta v_0 / \Delta v_{кон} \approx 19$ или эффективной температуре относительного движения 1,5 К. Смещение максимума пика относительно резонансной частоты составляет 150 МГц, что находится в хорошем согласии с простым расчетом на основе уравнения Лиувилля, который дает для сдвига максимума пика 130 МГц (рис. 2(*б*)).

В заключение подчеркнем, что деформация контура скоростного распределения была осуществлена при эффективной длине замедления 20 см. Как показывают оценки, увеличение длины взаимодействия до ~1 м позволит замедлить и монохроматизировать значительную долю атомов до нулевых скоростей.

Литература

l. *Wineland D.J., Dehmelt H.G.* // Bull. Am. Phys. Soc. 1975. Vol. 20. P. 637; *Dehmelt H.G.* // Nature. 1976. Vol. 262. P. 777.

2. *Hänsch T.W., Schawlow A.L.* // Optics. Comm. 1975. Vol. 13. P. 68.

3. *Neuhauser W., Hohenstatt M., Toschek P.E., Dehmelt H.G.* // Phys. Rev. 1980. Vol. 22. P. 1137.

4. *Wineland D.J., Itano W.M.* // Phys. Lett. 1981. Vol. 82A. P. 75.

5. *Балыкин В.И., Летохов В.С., Мишин В.И.* // Письма в ЖЭТФ. 1979. Т. 29. С. 614; ЖЭТФ. 1980. Т. 78. С. 1376.

6. *Letokhov V.S., Minogin V.G.* // Physics Reports. 1981. Vol. 73. P. 1.

7. *Краснов И.В., Шапарев Н.Я* // ЖЭТФ. 1979. Т. 77. С. 899.

8. *Зуева Т.В., Летохов В.С., Миногин В.Г.* // ЖЭТФ. 1981. Т. 81. С. 84.

9. *Hertel V.I., Stamanovic A.S.* // IEEE J. Quant. Electr. 1975. QE-11. P. 210.

Письма в ЖЭТФ. 1984. Т. 40 (6). С. 251–253

РАДИАЦИОННАЯ КОЛЛИМАЦИЯ АТОМНОГО ПУЧКА ПУТЕМ ДВУХМЕРНОГО ОХЛАЖДЕНИЯ ЛАЗЕРНЫМ ИЗЛУЧЕНИЕМ

В.И. Балыкин, В.С. Летохов, А.И. Сидоров
Институт спектроскопии АН СССР

Исследовано двухмерное радиационное охлаждение пучка атомов натрия силами светового давления в аксиально-симметричной стоячей световой волне. Температура поперечного движения атомов уменьшена до 3,5 мК.

Со времени первого наблюдения [1] охлаждения атомов лазерным излучением к настоящему времени наиболее значительные результаты достигнуты при лазерной монохроматизации и охлаждении атомных пучков [2, 3]. Полученные в указанных работах продольные скорости и температуры сравнимы с поперечными, поэтому следующим логическим шагом к достижению предельно низких температур является двухмерное охлаждение атомного пучка. Кроме того, принципиально важным для многих экспериментов является уметь сжимать пучки, уменьшать их размеры и разброс импульсов (по величине и направлению), другими словами, осуществлять их коллимацию.

О возможности уменьшения поперечных скоростей атомного пучка с помощью лазерного излучения упоминалось в работе [4].

В настоящей работе мы впервые сообщаем о достижении радиационной коллимации и двухмерного охлаждения атомного пучка под действием интенсивного лазерного излучения.

Идея радиационной коллимации атомного пучка состоит в следующем. Пучок атомов (рис. l), исходящий из источника *7*, облучается аксиально-симметричным световым полем, частота ω которого сдвинута в красную область относительно частоты атомного перехода ω_0. Аксиально-симметричное поле образовано посредством отражения лазерного излучения от зеркально-конической поверхности 5 отражательного аксиона. В аксиально-симметричном поле, создаваемом отражательным аксиконом, на атом, скорость которого направлена от оси конуса, действует сила светового давления, которая при $\omega < \omega_0$ направлена к оси конуса. Благодаря действию данной силы в области аксиально-симметричного поля происходит быстрое сужение скоростного распределения атомов поперек оси конуса. Последнее, в свою очередь, обусловливает резкое уменьшение угловой расходимости атомного пучка, то есть коллимацию пучка.

Пучок атомов натрия формировался с помощью двух диафрагм диаметром l мм, одна из которых находилась на пушке *7*, а другая — на расстоянии 14 см от пушки. Первоначальная расходимость атомного пучка $\Delta\varphi_0 = 1{,}4\ 10^{-2}$.

На расстоянии 2 см от второй диафрагмы находился конус. Длина взаимодействия атомов с излучением внутри конуса равна 35 мм. Расстояние от пушки до зоны регистрации — 52 см. Для циклического взаимодействия использовалось излучение двухчастотного лазера на красителе *1*, настроенного на компоненту D_2 — линии атома натрия. Разность частот была выбрана равной 1712 МГц так, чтобы одна частота возбуждала атомы с уровня $F = 1(^3S_{1/2})$ на уровень $F' = 2(^3P_{3/2})$, а вторая — с уровня $F = 2(^3S_{1/2})$ на уровень $F' = 3(^3P_{3/2})$. Часть двухчастотного излучения пересекала атомный пучок под углом 90° и служила для калибровки частотной шкалы.

Распределение интенсивности атомов в пучке от поперечной координаты регистрировалось по сигналу флуоресценции от одночастотного зондирующего поля, сканируемого по пространству. Пробное излучение пересекало атомный пучок под углом 10°. Частота пробного поля настраивалась на переход $F = 2(^3S_{1/2}) — F' = 3(^3P_{3/2})$ и устанавливалась в середине доплеровского контура атомного пучка, тем самым выбирались атомы с наиболее вероятной скоростью. Сигнал флуоресценции от зондирующего поля регистрировался после прерывания двухчастотного излучения. Эффективный диаметр пробного излучения в зоне регистрации равен 0,5 мм.

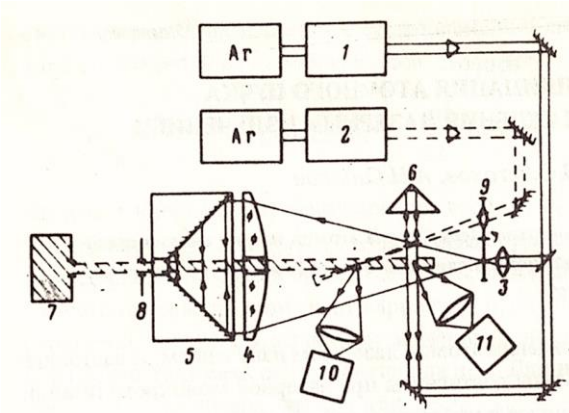


Рис. 1

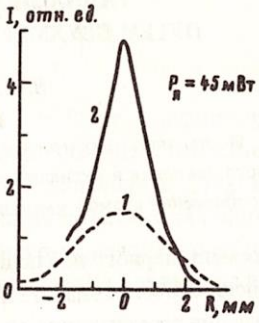


Рис. 2

Рис.1. Схема экспериментальной установки:
1, 2 — лазеры на красителях; *3, 4* — телескоп; *5* — аксион; *6* — призма; *7* — атомная пушка, *8* — диафрагма; *9* — модулятор; *10, 11* — ФЭУ

Рис. 2. Распределение интенсивности атомного пучка по поперечному сечению:
1 — интенсивность пучка до взаимодействия с лазерным излучением; *2* — после взаимодействия

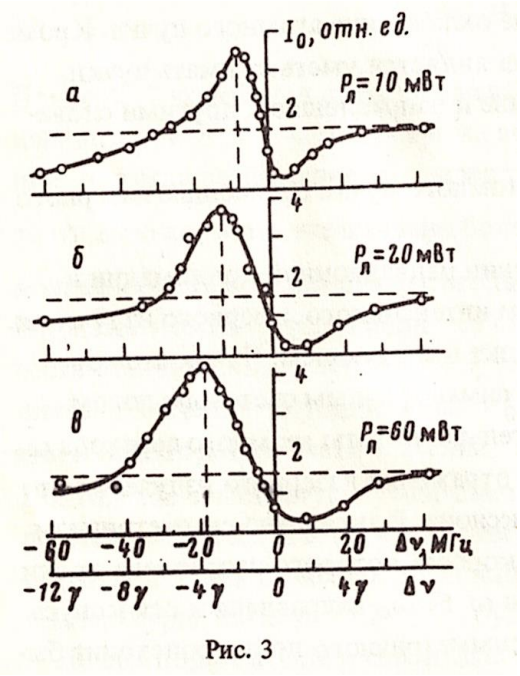


Рис. 3

Рис. 3. Зависимость интенсивности атомов в центре пучка от расстройки частот лазерного излучения относительно частоты атомного перехода при разных значениях мощности

На рис. 2 представлены профили атомного пучка до и после взаимодействия с двухчастотным излучением. Обе зависимости учитывают суммарный поток атомов на обоих подуровнях основного состояния атома натрия. Наблюдается увеличение интенсивности атомов в 3,5 раза, а также сужение (коллимация) атомного пучка. Измерение диаметра атомного пучка до взаимодействия с лазерным полем и после дает возможность рассчитать изменение поперечной скорости атомов в процессе их коллимации. Для случая, изображенного на рис. 2, расчет показывает, что поперечная скорость уменьшается с $5{,}5 \cdot 10^2$ см/с до $1{,}6 \cdot 10^2$ см/с. Это соответствует уменьшению температуры поперечного движения с 42 мК до 3,5 мК.

Нами были проведены измерения интенсивности атомов в центре пучка в зависимости от частоты коллимирующего лазерного поля (рис. 3). Как видно из рисунка, при отрицательных расстройках наблюдается коллимация пучка, при положительных, — наоборот, деколлимация. Такое поведение кривых подтверждает правильность интерпретации наблюдаемого эффекта действием силы светового давления, имеющей в поле стоячей световой волны дисперсионную зависимость от частоты лазерного поля [5]. Помимо сил светового давления на движение атомов оказывает влияние градиентная сила, используемая при больших значениях мощности для фокусировки атомных пучков [6]. Оценки показывают, что ее влияние в условиях рассматриваемого эксперимента пренебрежимо мало. Кроме того, зависимость градиентной силы от частоты излучения носит симметричный характер относительно частоты

атомного перехода в поле стоячей световой волны. Как видно из рис. 3, для каждой мощности существует оптимальное значение частоты коллимирующего поля. С точностью до ошибки измерения оптимальная расстройка частоты коллимирующего поля зависит от интенсивности лазерного поля как $\gamma(1 + I/I_{нас})^{1/2}$, где I и $I_{нас}$ — соответственно интенсивность лазера и интенсивность насыщения, γ — радиационная ширина перехода, что согласуется с расчетами, сделанными в работе [5].

В заключение подчеркнем, что коллимация атомного пучка была осуществлена при большой тепловой скорости пучка и малой длине взаимодействия. Как показывают оценки, использование коллиматора большей длины или замедленного атомного пучка позволит, во-первых, существенно увеличить их плотность, во-вторых, получить атомные пучки с предельной малой поперечной температурой.

Авторы выражают благодарность В.Г. Миногину за полезное обсуждение результатов.

Литература

l. *Балыкин В.И., Летохов В.С., Мишин В.И* // Письма в ЖЭТФ. 1979. Т. 29. С. 614.

2. *Prodan J.V., .Phillips W.D., Metcalf H.* // Phys. Rev. Lett. 1982. Vol. 49. P. 1149.

3. *Balykin V.I., Letokhov V.S., Sidorov A.I.* // Opt. Comm. 1984. Vol. 49. P. 248; *Балыкин В.И., Летохов В.С., Сидоров А.И.* // ЖЭТФ. 1984. Т. 86. С. 2019.

4. *Hänsch T.W., Schawlow A.L.* // Opt. Comm. 1975. Vol. 13. P. 68.

5. *Летохов В.С., Миногин В.Г., Павлик Б.Д.* // ЖЭТФ. 1977. Т. 72. С. 1328.

6. *Bjorkholm J.E., Freeman R.R., Ashkin A., Pearson D.B.* // Opt. Lett. 1980. Vol. 5. P. 111.

Physics Today. 1989. Vol. 42 (4). P. 23–28

LASER OPTICS OF NEUTRAL ATOMIC BEAMS

V.I. Balykin and V.S. Letokhov
Institute of Spectroscopy of the Academy of Sciences USSR

Charged-particle beams are easily manipulated by magnets. Beams of neutral atoms pose a harder problem. A new atomic-beam optics is using fields of laser light to serve as lenses and mirrors.

In ordinary optics one exploits the interaction of radiation with matter to manipulate beams of light. One can also turn the tables and control beams of charged or neutral material particles through their interaction with light. There are deep analogies and similarities between these two sorts of optics. even though they involve very different kinds of interactions between matter and radiation. Perhaps one can exploit every such interaction for some kind of "optics" — controlling beams of photons or massive particles. In this article we will describe recent developments in the laser optics of atomic beams — how experimenters are using the radiation pressure of laser light to manipulate neutral atoms.

The classical Maxwell theory tells us that light exerts pressure. In his fundamental *Treatise on Electricity and Magnetism* James Clerk Maxwell pointed out that an electromagnetic wave propagating in a medium will exert a pressure in the direction of propagation, at each point equal to its local energy density. Even though the pressure exerted by light from ordinary sources is very small, the effect was experimentally demonstrated at the turn of the century by Piotr Lebedev in Russia and E.F. Nichols and G.F. Hull in the United States. Lebedev also showed the effect of light pressure on gases, and he anticipated the possibility of dramatic pressure increases in conditions of resonance between radiation and atoms or molecules.

The next important step was taken in 1909 by Einstein. He considered light-pressure fluctuations due to the fact that atoms emit and absorb radiation in light quanta with discrete momenta. In 1933 Otto Frisch in Hamburg demonstrated such discrete momentum transfers from photons to free atoms by observing the deflection of a beam of sodium atoms by the resonant radiation of a sodium-vapor lamp.

Laser light

The invention of the laser gave us coherent light sources of high spectral brightness, monochromaticity and directivity. Light pressure, which had been a barely perceptible phenomenon, now became a plausible means of controlling atomic motion, and a variety of explicit suggestions were soon put forward. In 1968 one of us (Letokhov) proposed the use of standing light waves to localize and channel atoms [1].

Two years later Arthur Ashkin at Bell Labs demonstrated the levitation of micron-size particles at the focus of a laser beam [2]. Laser cooling of atoms was proposed in 1975 by Theodor Hänsch and Arthur Schawlow at Stanford [3]. David Wineland and Hans Dehmelt at the University of Washington made a similar suggestion for cooling ions [4]. In 1976 Letokhov and his colleagues at the Institute for Spectroscopy proposed the localization of cooled atoms in a three-dimensional standing light wave [5].

The experiments were soon under way. In 1978 Ashkin and his coworkers were able to focus a beam of atoms by means of the potential-gradient force of laser light pressure [6]. Over the next several years our group was able to decelerate [7], monochromatize and cool [8] atomic beams. In 1981 William Phillips and Harold Metcalf at the US National Bureau of Standards were able to cool a beam of sodium atoms down to 0.07 K [9]. In 1985 Steven Chu, Ashkin and colleagues at Bell Labs [10] succeeded in cooling a sodium beam down to 2.5×10^{-4} K, which we thought to be the theoretical minimum temperature achievable by laser cooling. More recently the theorists have had to rethink the issue. Last year Phillips and company [11] cooled a beam of sodium atoms far below the supposed theoretical cooling limit.

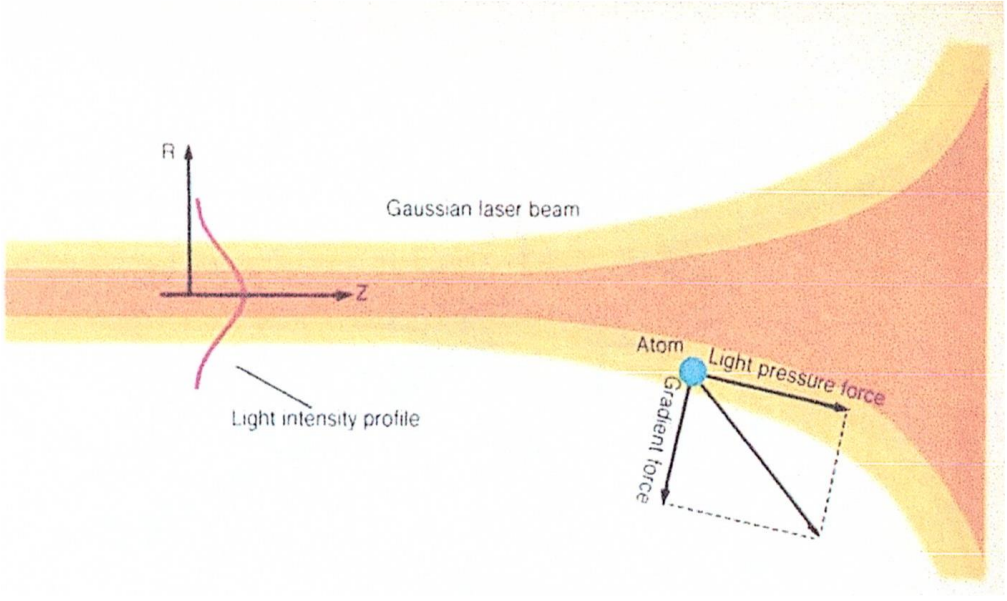


Fig. 1. A Gaussian laser beam, because its intensity profile is not uniform, exerts a gradient force on the dipole moment that intense light induces in an atom. Thus the resultant force of the laser beam is not simply in the propagation direction in which the light pressure acts

Our group achieved resonant collimation of an atomic beam by two-dimensional cooling in 1984 [12]. The following year Phillips's group [13] and another NBS group, led by John Hall [14], were able to bring atomic beams to a full stop. Phillips's group developed a magnetic trap to hold and cool the atoms of the stopped beam. A

year later Chu and company accomplished similar trapping and cooling with an optical trap [15] (See Physics Today, June 1985, page 17, and September 1986, page 17.) Our suggestion that atoms could be localized and channeled by standing waves of laser light was realized experimentally in 1987 by Claude Cohen-Tannoudji and colleagues at the Ecole Normal Superieure in Paris [16]. Also, a Bell Labs-MIT collaboration developed a hybrid "magneto-optic" trap for atoms [17].

These experiments have demonstrated that physicists now have at their disposal a new tool powerful enough to encourage the development of a new kind of optics — the optics of neutral atomic beams. This article will discuss a number of recent experiments on the collimation, focusing and mirror reflection of neutral atomic beams. We regard these experiments as beginning steps on the way to the development of optical elements for handling atomic beams.

Radiation forces on an atom

By radiation force we mean the total force due to the interaction between laser light and an atom. Depending on the wavelength, intensity and spatial-temporal structure of the light field, the radiation force can be an extremely complicated function of the atomic position and velocity. But things are simplified by the fact that all the studies of light-pressure forces have been done with only three types of light fields: plane waves, Gaussian profile beams and standing waves. We will therefore restrict ourselves to these field configurations. The theory of atomic motion in such fields is quite well developed [18]. We will consider these three cases only qualitatively.

Plane wave. Consider a plane wave directed along the z axis with its frequency tuned to resonance with the absorption frequency of an atom in the wave. The atom absorbs the laser photons directed along the z-axis and reemits them spontaneously in all directions. As a result, the atom is acted upon in the direction of the wave by a radiation force whose maximum magnitude is given simply by the product of the photon momentum $\hbar k$ and the maximum photon scattering rate γ, where k is the wavenumber of the laser light. Suppose the atomic absorption frequency ω_0 is not exactly in resonance with the laser frequency ω_1. Let them differ by a small detuning frequency shift $\Omega \equiv \omega_0 - \omega_1$. Suppose further that the atom is not initially at rest; it has velocity projection υ_z, in the direction of the light wave. Then the radiation pressure force F will be given by

$$F = \hbar k \gamma G / [1 + G + (\Omega - k v_z^2) / \gamma^2]$$

where $G = I/I_s$, I being the light intensity and I_s, the atomic-transition saturation intensity. The acceleration of a sodium atom under such a laser-light force can reach 10^8 cm/sec^2 — a hundred thousand times the acceleration of gravity.

Gaussian laser beam. An atom placed in a laser beam of finite width is acted upon by an additional gradient force due to the transverse inhomogeneity of the light field, as shown in figure 1. This force can be understood simply from the classical consideration of a dipole in an inhomogeneous field. An atom in a laser field acquires a dipole moment, and the field gradient acts on this dipole moment.

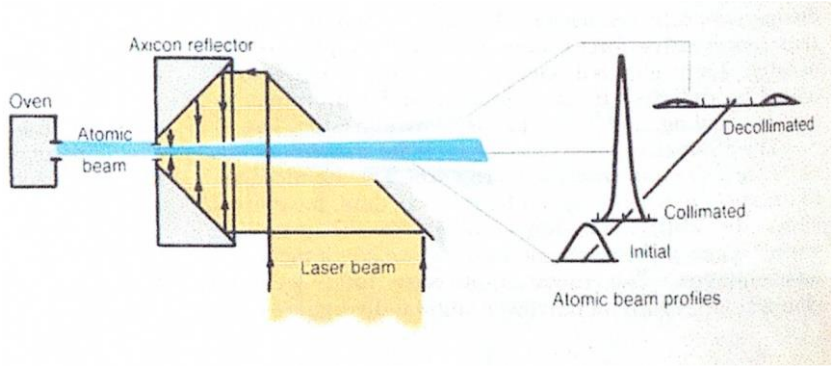


Fig. 2. Collimating an atomic beam by means of laser light. The atomic beam passing through a conical axicon reflector is irradiated from all sides by laser light detuned toward the red from the atomic absorption frequency. The resulting radiation-pressure forces narrow the angular divergence of the atomic beam (see beam profiles). Detuning the laser towards the blue decollimates the atomic beam

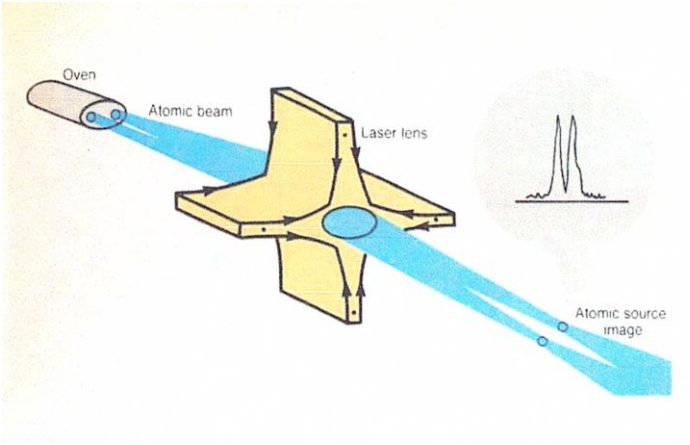


Fig. 3. Focusing and imaging an atomic beam with laser light. Four divergent laser beams impinge on the atomic beam, forming a "laser lens". Because the laser wavelength is precisely in resonance with the atomic absorption wavelength, any atom moving away from the axis is pushed back toward the axis so that a point source of atoms is imaged at another point. The beam profile in the image plane shows the double peak that images the two oven slits

Depending on the detuning of the laser frequency from the atomic-transition frequency, the field will either expel the atom out of the beam (if ω_1 is greater than ω_0) or draw it toward the beam center (ω_1 is less than ω_0). The gradient force is given by

$$F_{\text{gr}} = \frac{\hbar(\rho/\rho_0^2\ )(\Omega - kv_z)G}{1 + G + (\Omega - kv_z)^2/\gamma^2}$$

where the laser-beam radius ρ_0 is much larger than ρ, the distance from the atom to the laser-beam axis.

Plane standing wave. A standing wave can be formed by two counter propagating plane traveling waves. When the radiation intensity is low (G much less than 1), the force in the standing wave is simply the sum of the forces of the component waves. As the radiation intensity is increased, the modulation of the laser-field intensity at half the wavelength comes into play. This, in turn, causes the gradient force to become manifest. Furthermore, when the radiation intensity is high (G much greater than 1), the atomic motion is affected by stimulated reemission of photons, which, in the presence of a field inhomogeneity, give rise to a velocity-dependent gradient force component [19]. This force arises when an atom moves in an intense and highly inhomogeneous field whose strength varies significantly during the time it takes the atom to decay spontaneously. It affects atoms moving slowly along the laser-beam axis. Unlike the radiation-pressure force in a traveling wave, this retarding force can grow without limit as one increases the intensity of the laser light.

Collimating an atomic beam

We now consider how the different forces produced by these laser beams can be exploited to control atomic beams. The need to collimate a beam of particles arises whenever one has to increase their phase-space density — to compress their spatial and velocity distributions. The method of compression will depend on the particular particle species. Common to all these methods is the use of dissipative processes, because Liouville's theorem tells us that conservative forces alone cannot alter phase-space density. Light charged particles, for example, are collimated by radiative friction; protons and antiprotons by electron cooling; and heavy particles by ionization loss.

The dissipative force most effective for neutral atomic particles is the laser radiation pressure. The atomic-beam collimation experiments performed to date have used either the radiation-pressure force [20] or the retarding force [16]. Each of these schemes has its own advantages and disadvantages. The radiation-pressure force lets one obtain atomic beams of narrower angular divergence. The merit of the retarding force is faster beam collimation, but the ultimate collimation angle achievable by this means is much larger.

Let us consider collimation by the radiation-pressure force in more detail. The atomic beam illustrated in figure 2 is irradiated on all sides by an axisymmetric light field whose frequency ω_1 is shifted toward the red relative to the atomic transition frequency ω_0. The axisymmetric field is formed by reflecting a laser beam off the inner surface of a conical “axicon” reflecting surface. In the plane of the figure, this field consists of two counterpropagating light waves whose intensities are equal at any point within the axicon.

If ω_0 exceeds ω_1 an atom moving with radial velocity v_ρ in the axisymmetric light field is acted upon by a radiation-pressure force directed *against* v_ρ. Because of the Doppler shift, an atom absorbs more effectively those photons that come from the light propagating counter to its velocity vector. Therefore, the total force of the laser light converging on the atomic beam produces a rapid narrowing of the transverse velocity distribution in the inner region of the axicon. Thus, one gets the desired reduction of the angular divergence of the beam.

The joint effect of radiative friction and momentum diffusion establishes a stationary atomic velocity distribution that determines the ultimate collimation angle

$$\Delta\phi_{\min} = (1/v_z)(\hbar\gamma/M)^{1/2}$$

where M is the atomic mass and v_z, is the atomic velocity along the atomic-beam axis. For a thermal atomic beam, the ultimate collimation angle is on the order of 10^{-3} or 10^{-4} radians. If the initial beam divergence was 0.1 radian, the on-axis atomic-beam intensity can be increased perhaps a millionfold.

We did the experiment with a beam of sodium atoms. Figure 2 shows the beam profiles before and after interaction with the laser field. The collimation process is very sensitive to the precise laser frequency. To effect collimation, we detuned the laser light toward the red by 13 MHz. The longitudinal atomic velocity v_z was 7.3 10^4 cm/sec. The before and after beam profiles show a fivefold increase in the on-axis atomic-beam intensity and a considerable narrowing (collimation) of the beam. Changing over to positive detunings caused a broadening (decollimation) of the beam. The on-axis beam intensity in this latter case was observed to decrease by more than three orders of magnitude.

Focusing and imaging

The principal element in any sort of optics is a lens. It is therefore essential to create laser field configurations capable of focusing neutral atomic beams. There are at present two possibilities for focusing an atomic beam: the gradient force and the pressure force of spontaneous radiation.

The focusing of an atomic beam by means of the gradient force was first demonstrated ten years ago at Bell Labs [6]. In their scheme, the atomic beam propagated along and inside a narrow laser beam. The laser frequency was tuned below the atomic-transition frequency, so that the gradient force was directed toward the laser-beam axis. In this way the width of the atomic beam was compressed down to a minimum of 26 μm.

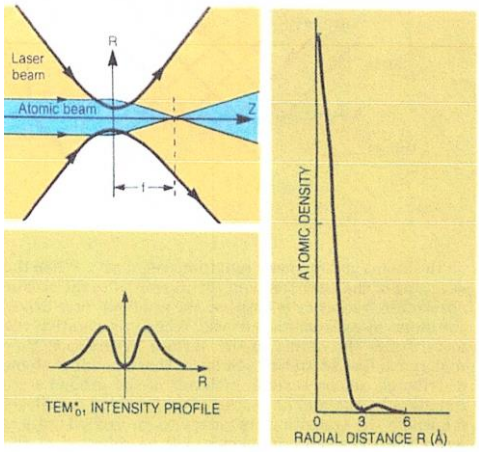


Fig. 4. Atomic objective lens is expected to focus atomic beams down to a width of a few angstroms, as shown in the calculated atomic-beam profile (rightmost graph). The atomic beam is focused by being passed through a focused laser beam. The laser field is in the TEM^*_{01} mode, whose radial intensity profile is shown at the bottom left

Our 1986 experiment [21] used a different laser field configuration, similar to that illustrated in fig. 3. In the general case, our method uses four divergent Gaussian laser beams propagating toward a point on the atomic beam. The narrow waists of the four laser beams are equidistant from this central point of the configuration. The laser frequencies are tuned to precise resonance with the atomic absorption frequency. Under such conditions, an atom moving away from the atomic-beam axis is acted upon by a spontaneous radiation-pressure force that tends to bring it back to the beam axis.

The effect of the gradient force in this case is insignificant. Such a configuration is, in effect, a “laser lens” for a beam of neutral atoms, because it can be shown that an atomic beam issuing from a point (the analog of a point source in light optics) is focused onto another point after interacting with the laser. Furthermore, one may define a focal length f for such a lens in terms of the geometric, optical and atomic parameters of the system, and derive the laser lens formula

$$1/S + 1/L = (1/f)(1 - d/2L),$$

where d is the thickness of the laser, and S and L are, respectively, the atomic-source and image distances from the lens. The laser lens is quite localized in space. Its characteristic size d along the atomic beam is much less than S and L. Under these conditions, the lens formula looks just like the usual optical lens formula.

Our first successful focusing experiment was conducted with a beam of sodium atoms and a laser lens formed by only two counterpropagating Gaussian beams. Such a laser lens is analogous to a cylindrical lens in light optics. Figure 3, which shows the more elaborate four-laser-beam lens, illustrates the imaging of a “two-point” atomic source — an atomic oven with two 0.5-mm-diameter holes spaced 2 mm apart. Without the laser lens, the atomic beam profile is a wide, diffuse spot. With the two laser beams forming the lens in the path of the atoms, we found that the atomic trajectories obeyed the laws of neutral-particle beam optics. In the image plane, the beam profile consisted of two well-defined peaks, each corresponding to one of the atomic source holes.

A serious drawback of this laser lens is its insufficient resolution: The minimum focal spot diameter is about 50 μm. As was the case in the old Bell Labs focusing experiment, the resolution limit is due to momentum diffusion, which smears the trajectories of the atoms interacting with the laser lens field.

Resolution can be materially improved by resorting to the old idea of the gradient force, but now with a different laser field configuration and a different atom-field interaction geometry. We have proposed [22] an “atomic objective lens” with a resolution of a few angstroms. Such an objective lens, illustrated in figure 4, is essentially a focused laser field with its frequency tuned well away from the atomic-transition frequency. The focused laser field is in the TEM^{*}_{01} mode, whose radia1 intensity profile is shown in the figure. The atomic beam propagates along the lens axis. The tight focusing of the laser radiation yields an effectively "thin" lens and the choice of the TEM^{*}_{01} mode and the large frequency detuning allow us to achieve a good approximation to an “ideal” objective lens. The 1978 Bell Labs paper [6] had pointed out the merits of the TEM^{*}_{01} mode.

To determine the maximum resolution of such an atomic objective lens one treats the atomic beam as a superposition of plane de Broglie waves, and the laser field through which it propagates is taken to be a transparent medium whose phase transmission function depends on the distance from the lens axis. These plane waves acquire phase advances in the laser field that lead to their subsequent focusing in the focal plane of the atomic objective lens. The minimum focal-spot diameter is determined mostly by the diffraction of the de Broglie waves by the lens aperture. Additional limitations are due to spherical and chromatic aberrations and diffusion aberration associated with the atomic momentum diffusion in the laser field. Nevertheless, the calculations show that one can choose laser-field and atomic-beam parameters such that the resolution of the lens will come very close to its diffraction limit. For instance, if the transverse dimension of the lens is taken to be equal to a few wavelengths and the laser power is about 1 W, the focal spot diameter of the atomic beam, as shown in figure 4, should not be much greater than a few angstroms.

Atomic-beam reflection

Mirrors are no less important than lenses. A mirror can be used both for focusing and reflecting. Focusing by means of a concave mirror has certain advantages over lens focusing: It avoids chromatic aberration. This is particularly important for particle-beam optics, where chromatic aberration can be especially severe. The atomic mirror idea was first suggested [23] by Richard J. Cook and Richard K. Hill at the US Air Force Institute of Technology in 1982. Figure 6 illustrates such an atomic mirror. It is formed by a very thin "evanescent" (surface) wave produced by total internal reflection of a laser beam at a dielectric-vacuum interface. The thickness of this surface wave is on the order of the wavelength. The laser radiation intensity on the surface of the dielectric equals the intensity of the initial laser wave inside the dielectric, but in the vacuum it drops almost to zero very abruptly — within a few wavelengths of the surface.

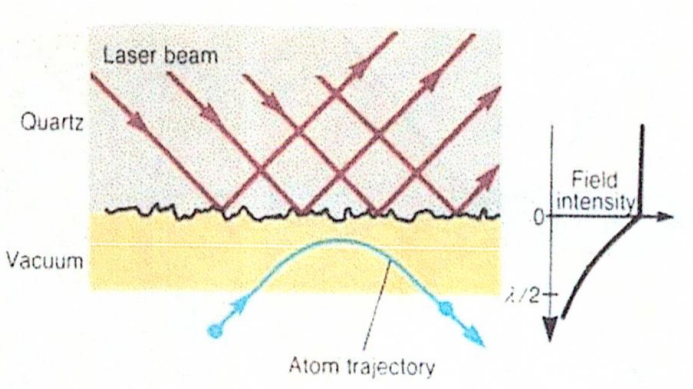


Fig. 5. Atomic mirror. A laser beam totally reflected at the inner surface of a quartz plate forms a very thin "evanescent" surface light wave just outside the plate. The enormous intensity gradient of this surface wave produces a gradient force strong enough to turn around the trajectories of approaching atoms

In such a surface wave one has an enormous light intensity gradient — the largest gradient seen anywhere in optics. An atom placed in a such a surface wave of laser frequency higher than the atomic-transition frequency experiences a gradient force tending to expel it from the wave and into the vacuum. If the atom approaches the surface wave from the vacuum side, it slows abruptly to zero normal velocity in the surface wave, then accelerates in the wave in the reverse direction away from the surface. If its transverse velocity (normal to the surface) does not exceed some critical maximum, the atom's angle of incidence will approximately equal its angle of reflection — much like light striking an ordinary mirror.

The maximum transverse atomic velocity corresponds to a kinetic energy equal to the barrier height of the surface wave. If the transverse atomic velocity is higher than this critical maximum, the atom will reach the dielectric surface and reflect from it in a diffuse manner. For typical cw laser radiation with a power of 1 watt and, for example, a sodium atom with a thermal velocity of 6×10^4 cm/sec, the critical transverse velocity will be 5×10^2 cm/sec. In that case the angle of incidence must be within 10^{-2} radian of the surface. With laser-cooled atomic beams or pulsed dye-laser radiation, there is no limitation on the angle of incidence; reflection is possible even if the atomic beam is normal to the atomic mirror.

Our group reported [24] the first observation reflection by an atomic mirror in 1987. We used a beam of sodium atoms. The atomic mirror was a plane-parallel plate of fused quartz with a beveled lateral face through which we passed laser radiation. To increase the surface area of the atomic mirror, we made use of repeated total internal reflection of the laser beam. Figure 6 shows the arrangement of the incident and reflected atomic beams, as well as a reference beam. The figure also shows profiles of these three beams. When the atomic mirror is parallel to the atomic-beam axis so that the atoms fly past it, the profile shows only the reference and incident beams. If the mirror is tilted so that it cuts off the atomic beam, the latter is observed to be reflected. As one increases the tilt angle of the mirror still further, the angle of reflection increases as well, but the number of atoms undergoing mirror reflection decreases because some atoms reach the mirror surface and suffer diffuse reflection. The maximum angle of reflection observed in the experiment was about 0.4°. The mirror reflectivity was close to 100%.

Another remarkable property of the atomic mirror is its ability to reflect atoms in a quantum-state-selective fashion. This selectivity arises from the dispersive character of the relationship between the gradient force acting on the atoms and the laser radiation frequency: When the detuning of the laser frequency with respect to the atomic absorption frequency is positive, the gradient force drives the atoms away from the surface. When it is negative, the force draws the atoms to the surface, whereupon they undergo diffuse scattering. Suppose that a beam of atoms distributed among several sublevels of the ground state impinges on the atomic mirror. The atoms in a sublevel for which the transition frequency to an excited state is lower than the laser frequency will be reflected at the mirror, whereas the rest will scatter in a diffuse manner. The reflected beam will thus contain only particles in a single energy level. Last year we observed selective reflection of atoms at two hyperfine splitting sublevels of the ground state in sodium. We found

that the mirror reflectivity for atoms in the $F = 2$ sublevel was at least 100 times greater than for the $F = 1$ sublevel.

Note that such selective reflection can also be expected for molecules. This opens up the possibility of production and spectroscopy of molecular beams in a single vibrational-rotational energy level.

It is also possible to create spherical atomic mirrors and cavities. Figure 7 shows one possible atomic-cavity configuration. It is essentially an optical cavity with the physical mirrors replaced by light-induced mirrors. One might inject atoms into such a cavity by the laser collimation of an external atomic beam. The maximum steady-state density of atoms in the cavity would be determined by the rate of their injection into the cavity and their lifetime therein. One of the parameters that characterize the light field in an ordinary optical cavity is its degeneracy — the number of photons per cavity mode. For laser radiation, the degeneracy is fairly high. Our estimates show that the realization of a pseudo-optical cavity for atomic de Broglie waves would, in principle, allow a high degeneracy to be achieved at a relatively low atomic density. This would result from the velocity monochromatization and collimation of the atomic waves in the cavity.

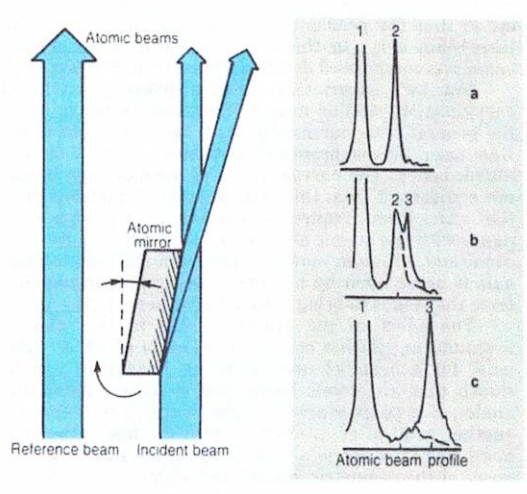


Fig. 6. Reflecting atomic beams. An atomic mirror like that in figure 5 was used in our laboratory to reflect an atomic beam. The quartz mirror can be tilted in and out of the atomic beam. When the mirror does not impinge on the beam (*a*), the beam profile (right) shows peaks for the undisturbed beam (*2*) and a reference beam (*1*). Tilting the mirror partially into the beam (*b*) produces a third peak (*3*) for the reflected beam. When the mirror is tilted further (*c*), cutting off the entire beam, the angle of reflection is increased

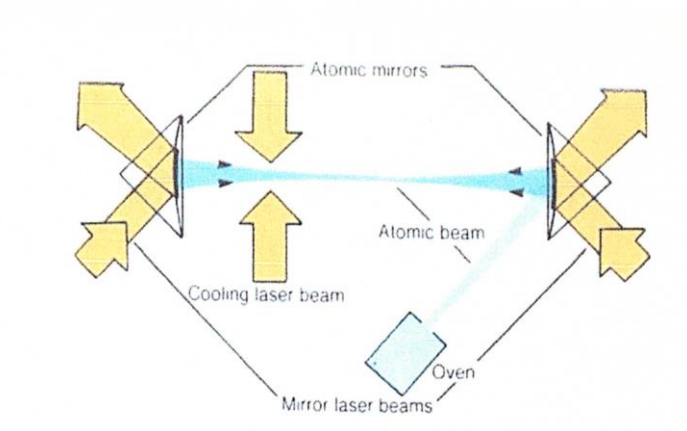


Fig. 7. Atomic-mirror cavity. An atomic beam is injected into a cavity formed by two concave atomic mirrors. The cavity collimates the beam and narrows its velocity distribution. While in the cavity, the atomic beam can also be cooled by additional lasers

Prospects

After only these first few experiments we can already say that experimenters have come into possession of an entirely new method for controlling atomic beams. As laser technology advances, it will become possible not only to perfect the elements of neutral atomic-beam optics, but also to pass on to molecular beams. Some possible applications of neutral atomic-beam optics are already clear. Collimation of atomic beams lets one shape them and improve their divergence and phase density — all this in an isotope-selective fashion. Beyond increasing atomic-beam density, atomic-beam focusing can help create an atomic microscope. It is not difficult to envisage a scanning transmission microscope or a reflection microscope of this sort. The scattered or reflected atoms could be registered by existing single-atom detection techniques.

Atomic mirrors could be used as high-speed deflectors, modulators and shutters for neutral atomic beams. They could also be used to create traps for ultracold atoms. Concave atomic mirrors could served as optical elements in an atomic microscope because they can focus atomic beams onto a spot with a diameter comparable to the de Broglie wavelength, the atom-laser interaction time being too short for momentum diffusion to become a limiting factor. Sharply focused atomic beams with focal-spot diameters of a few angstroms would let one observe atomic collisions and study atomic scattering under strictly controlled conditions. It would be interesting to extend this technique to molecular beams. This would yield better insight into molecular interact ion dynamics.

In the restricted scope of this article, we have not discussed several other analogs of conventional optical elements, nor have we covered interference phenomena. One can, for example, use configurations of laser light to serve as diffraction gratings and

beam splitters for atomic beams. Much impressive work in these areas has been done in various laboratories around the world.

We express our gratitude to V.G. Minogin, Yu.B. Ovchlnnikov and A.I. Sidorov at the Institute of Spectroscopy of the Academy of Sciences USSR for many discussions.

References

1. *Letokhov V.S.* // Pis'ma Zh. Eksp. Teor. Fiz. 1968. Vol. 7. P. 348.

2. *Ashkin A.* // Phys. Rev. Lett. 1970. Vol. 24. P. 56; Phys. Rev. Lett. 1970. Vol. 25. P. 1321; *Ashkin A., Dziedzik J.M.*//Appl. Phys. Lett. 1971. Vol. 19. P. 283.

3. *Hänsch T.W., Schawlow A.I.* // Opt. Commun. 1975. Vol. 13. P. 68.

4. *Wineland D.J., Dehmelt H.G.* // Bull. Am. Phys. Sac. 1975. Vol. 20. P. 637; *Dehmelt H.G.* // Nature. 1976. Vol. 262. P. 777.

5. *Letokhov V.S., Minogin V.G., Pavlik B.D.*//Opt. Commun. 1976. Vol. 19. P. 72.

6. *Bjorkholm J.E., Freeman R.E., Ashkin A., Pearson D.B.* // Phys. Rev. Lett. 1978. Vol. 41. P. 1361; Appl. Phys. Lett. 1980. Vol. 36. P. 99; Opt. Lett. 1980. Vol. 5. P. 11.

7. *Balykin V.I., Letokhov V.S., Mishin V.I.* // Pis'ma Zh. Eksp. Teor. Fiz. 1979. Vol. 29. P. 614.

8. *Andreev S.A., Balykin V.I., Letokhov V.S., Minogin V.G.* // Pis'ma Zh. Eksp. Teor. Fiz. 1981. Vol. 34. P. 463; Zh. Eksp. Teor. Fiz. 1982. Vol. 82. P. 1429.

9. *Phillips W.P., Metcalf H.J.* // Phys. Rev. Lett. 1982. Vol. 48. P. 596.

10. *Chu S., Hollberg L., Bjorkholm J., Cable A., Ashkin A.* // Phys. Rev. Lett. 1985. Vol. 55. P. 48.

11. *Lett P., Watt R., Westbrook C., Phillips W., Gould P., Metcalf H.* // Phys. Rev. Lett. 1988. Vol. 61. P. 169.

12. *Balykin V.I., Letokhov V.S., Sidorov A.I.* // Pis'ma Zh. Eksp. Teor. Fiz. 1984. Vol. 40. P. 251.

13. *Migdall A.L., Prodan J.V., Phillips W.P., Bergeman T.H., Metcalf H.J.* // Phys. Rev. Lett. 1985. Vol. 54. P. 2596.

14. *Ertmer W., Blatt R., Hall J., Zhu M.* // Phys. Rev. Lett. 1985. Vol. 55. P. 996.

15. *Chu S., Bjorkholm J., Ashkin A., Cable A.* // Phys. Rev. Lett. 1986. Vol. 57. P. 314.

16. *Salamon C., Dalibard J., Aspect A., Metcalf H., Cohen-Tannoudji C.* // Phys. Rev. Lett. 1987. Vol. 59. P. 1659.

17. *Raab E., Prentiss M., Cable A., Chu S., Pritchard D.* // Phys Rev. Lett. 1987. Vol. 59. P. 2631.

18. *Ashkin A.* // Science. 1980. No. 210. P. 1081; *Letokhov V.S., Minogin V.G.* // Phys. Rep. 1981. Vol. 73. P. 1; *Kazantsev A.P., Ryabenko G.A., Surdutovich G.I., Yakovlev V.P.* // Phys. Rep. 1985. Vol. 129. P. 75; Mechanical Effects of Light. Special issue of J. Opt. Soc. Am. 1985. Vol. B2; *Stenholm S.* // Rev. Mod. Phys. 1986. Vol. 58. P. 699; *Minogin V.G., Letokhov V.S.* Laser Light Pressure on Atoms. New York: Gordon and Breach, 1987.

19. *Kazantsev A.P.* // Zh. Eksp. Teor. Fiz. 1974. Vol. 66. P. 1599; *Minogin V.G., Serimaa O.T.* // Opt. Commun. 1979. Vol. 30. P. 373; *Dalibard J., Cohen-Tannoudji C.* // J. Opt. Soc. Am. 1985. Vol. B2. P. 1707.

20. *Balykin V.I., Letokhov V.S., Sidorov A.I.* // Pis'ma Zh. Eksp. Teor. Fiz. 1984. Vol. 40. P. 251; *Balykin V.I. , Sidorov A.I.*//Appl. Phys. 1987. Vol. 42B. P. 51.

21. *Balykin V.I., Letokhov V.S., Sidorov A.I.* // Pis'ma Zh. Eksp. Teor. Fiz. 1986. Vol. 43. P. 172; *Balykin V.I. , Letokhov V.S., Sidorov A.I., Ovchinnikov Yu.B.* // J. Mod. Opt. 1988. Vol. 35. P.17.

22. *Balykin V.I., Letokhov V.S.* // Opt. Commun. 1987. Vol. 64. P. 151; Zh. Eksp. Teor. Fiz. 1988. Vol. 94. P. 140.

23. *Cook R.J., Hill R.K.* // Opt. Commun. 1982. Vol. 43. P. 258.

24. *Balykin V.I., Letokhov V.S., Ovchinnikov Yu.B., Sidorov A.I.* // Pis'ma Zh. Eksp. Teor. Fiz. l987. Vol. 45. P. 282; Phys. Rev. Lett. 1988. Vol. 23. P. 2137.

Письма в ЖЭТФ. 1987. Т. 45 (6). С. 282–284

ОТРАЖЕНИЕ АТОМНОГО ПУЧКА ОТ ГРАДИЕНТА СВЕТОВОГО ПОЛЯ

В.И. Балыкин, В.С. Летохов, Ю.Б. Овчинников, А.И. Сидоров
Институт спектроскопии АН СССР

Впервые экспериментально обнаружено зеркальное отражение теплового атомного пучка от градиента лазерного поля. Коэффициент отражения «атомного зеркала» близок к 100%.

В неоднородном электромагнитном поле на атом действует сила, пропорциональная наведенному дипольному моменту атома и градиенту напряженности поля. Впервые внимание на возможность воздействия градиента светового поля на движение атомов было обращено в работе [1]. Опубликованы предложения по использованию градиентной силы для захвата атомов в узлах стоячей световой волны [2], а также в поле острофокусированного лазерного луча [3]. В работе [4] была продемонстрирована фокусировка атомного пучка градиентной силой. Авторы работы [5] предложили использовать градиент светового поля для отражения атомов.

В настоящей работе впервые экспериментально продемонстрировано зеркальное отражение теплового атомного пучка от градиента лазерного поля. Для создания «атомного зеркала» использовалось полное внутреннее отражение лазерного луча от границы «диэлектрик — вакуум» [5] (рис. 1). Поле в вакууме затухает на расстоянии $\sim\lambda/2$. При этом создается огромный градиент напряженности электрического поля. Отражение атома от «зеркала» можно рассматривать как движение атома в потенциальном поле [6]

$$U_{\text{град}}(x) = \frac{1}{2}\hbar(\Delta - kv_{\parallel})\ln\{1 + G/[1+(\Delta - kv_{\parallel})^2/\gamma^2]\}, \qquad (1)$$

где $\Delta = \omega - \omega_0$ — положительная расстройка лазерной частоты ω относительно частоты атомного перехода ω_0, 2γ — естественная ширина линии поглощения, $v_{\parallel}$ — продольная скорость атомов, $G(x) = I(x)/I_s$ — параметр насыщения атомного перехода, I_s — интенсивность насыщения перехода, $I(x)$ — интенсивность лазерного излучения. С помощью закона сохранения энергии можно доказать возможность зеркального отражения атома от такого потенциала.

В том случае, когда атом при движении в потенциальном поле все же достигнет поверхности диэлектрика, вместо зеркального должно быть обычное диффузное отражение от диэлектрика. Это накладывает ограничение на максимальную поперечную скорость

$$v_x^{max} = \left[\frac{2\,U_{\text{град}}(0)}{M}\right]^{1/2} = \left\{\frac{\hbar(\Delta - kv_{\parallel})}{M}\ln\left[1 + \frac{G(0)}{1 + (\Delta - kv_{\parallel})^2/\gamma^2}\right]\right\}^{1/2}. \qquad (2)$$

Для типичных параметров, например, атомов Na и перестраиваемого лазерного излучения: $M = 4 \cdot 10^{-23}$ г, и $\upsilon_{\parallel} = 6 \cdot 10^4$ см/с, $\gamma/2\pi = 5$ МГц, $k = 10^5$ см$^{-1}$, $P_л = 1$ Вт, $G = 10^5$, $\Delta/2\pi = 2{,}6$ ГГц можно получить значение $\upsilon_x^{max} = 410$ см/с, соответственно, максимальный угол скольжения $\alpha_{max} = \upsilon_x^{max}/\upsilon_{\parallel} = 7 \cdot 10^{-3}$ рад.

В эксперименте пучок атомов натрия формировался отверстием диаметром 0,4 мм в источнике и расположенной на расстоянии 220 мм от пушки прямоугольной щелью с размерами 0,1 мм по горизонтали и 0,4 мм по вертикали. На расстоянии 15 мм от щели находилось «атомное зеркало», которое отражало атомы в горизонтальной плоскости. Оно представляло собой плоскопараллельную пластину из плавленного кварца толщиной 0,4 мм и длиной 25 мм, в которую через скошенную грань направлялось лазерное излучение. Диаметр лазерного луча был равен 0,4 мм по уровню I/e. В пластине использовалось многократное полное внутреннее отражение лазерного луча. Мощность лазерного излучения была равна 650 мВт. Давление остаточного газа в вакуумной камере было не хуже $5 \cdot 10^{-6}$ торр.

В эксперименте использовался также второй, калибровочный атомный пучок, относительно которого измерялись смещение отраженного пучка и число отраженных атомов. Зона регистрации находилась на расстоянии 330 мм от щели. Профили атомных пучков регистрировались с помощью пробного одночастотного излучения, настроенного по частоте на переход $3S_{1/2} \rightarrow 3P_{3/2}$. Пробный луч составлял угол 83° с осью пучка по вертикали и сканировался по пространству. Мы настраивались частотой зондирующего луча в определенную часть доплеровского контура ($\Delta\nu_D \sim 250$ МГЦ) и регистрировали флуоресценцию от атомов с определенной продольной скоростью.

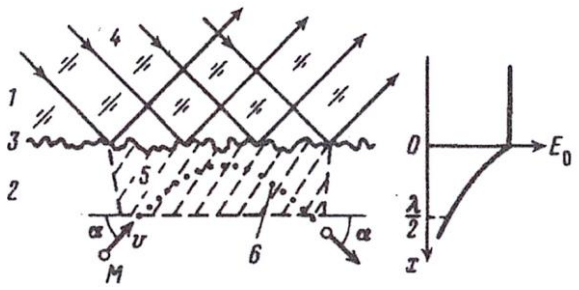


Рис. 1

Рис. 1. Схема «атомного зеркала»: *1* — диэлектрик, *2* — вакуум, *3* — граница раздела, *4* — лазерное поле в диэлектрике, *5* — лазерное поле в вакууме, *6* — траектория движения атома в лазерном поле

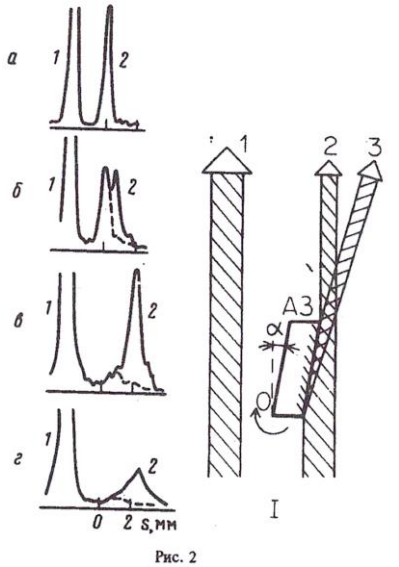


Рис. 2

Рис. 2. I — траектории атомных пучков в эксперименте по зеркальному отражению атомов: *1* — калибровочный атомный пучок, *2* — пучок атомов, проходящих мимо зеркала, *3* — отраженный атомный пучок, *АЗ* — «атомное зеркало», *О* — ось вращения «зеркала», α — угол скольжения. II — профили калибровочного (*1*), прошедшего мимо «зеркала» (*2*) и отраженного (*3*) атомных пучков в зоне регистрации. Пунктиром обозначен профиль атомного пучка при $P_л = 0$. Параметры лазерного излучения и атомного пучка: $P_л = 650$ мВт, $\Delta = 2{,}6$ ГГц, $v_{\|} = 4 \cdot 10^4$ см/с. Углы скольжения α: *а* — 0 рад, *б* — $1{,}1 \cdot 10^{-3}$ рад, *в* — $3{,}3 \cdot 10^{-3}$ рад, *г* — $5{,}5 \cdot 10^{-3}$ рад

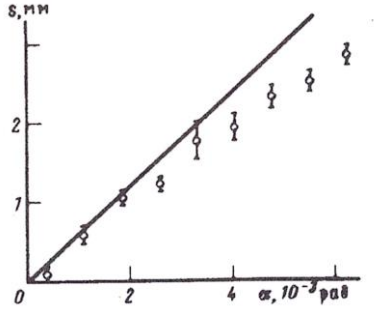


Рис. 3

Рис. 3. Зависимость смещения *s* отраженного атомного пучка в зоне регистрации от угла скольжения α падающего атомного пучка

На рис. 2 представлены профили калибровочного и отклоненных атомных пучков при частотной расстройке силового поля $\Delta = 2{,}6$ ГГц. Зондируемые атомы имели продольную скорость $4 \cdot 10^4$ см/с. Рис. 2*а* соответствует случаю, когда «атомное зеркало» параллельно оси пучка и атомы пролетают мимо зеркала. При небольшом угле наклона (рис. 2*б*) часть атомного пучка проходит мимо «зеркала», а часть отражается от него, что приводит к появлению второго пика справа. При увеличении угла наклона (рис. 2*в*) «зеркало» перекрывает

полностью атомный пучок. Число отраженных атомов растет, увеличивается и смещение отраженного пучка. При дальнейшем увеличении угла наклона (рис. 2*г*) число отраженных атомов падает, так как атомы достигают поверхности зеркала и диффузно от нее отражаются.

На рис. 3 представлен график зависимости смещения отраженного пучка s в зоне регистрации от угла скольжения α. Сплошная прямая представляет зеркальное отражение атомов. При больших значениях угла скольжения α наблюдается заметное отличие хода экспериментальных точек от расчетной прямой. Это отличие объясняется тем, что расходимость атомного пучка ($\Delta\varphi = 23\cdot10^{-3}$ рад) сравнима с углом α. Атомы с большими поперечными скоростями достигают поверхности и диффузно отражаются, поэтому поперечное скоростное распределение обрезается со стороны больших скоростей. Угол отклонения атомов становится меньше расчетного.

Важным параметром любого зеркала является его коэффициент отражения. При малых углах скольжения «атомное зеркало» по нашим измерениям имеет коэффициент отражения, близкий к 100%. По мере увеличения угла α все большее число атомов достигает поверхности и диффузно отражается от нее, поэтому коэффициент отражения падает и при $\alpha = 6{,}3\cdot10^{-3}$рад становится равным 10%.

Таким образом, полученные результаты показали, что «атомное зеркало» пригодно для отражения тепловых атомных пучков. Увеличение угла отклонения атомов и молекул может быть достигнуто применением мощных импульсных лазеров либо путем увеличения числа отражений атомов от зеркала. Отметим также возможность фокусировки теплового атомного пучка вогнутым «атомным зеркалом». Так как время взаимодействия атомов с излучением мало, скоростная диффузия из-за спонтанного переизлучения фотонов также мала. Поэтому атомный пучок можно сфокусировать в размеры, сравнимые с длиной волны де Бройля атома. Данная работа приоткрывает новые возможности создания оптики нейтральных атомов.

Литература

1. *Аскарьян Г.А.* // ЖЭТФ. 1962. Т. 42. С. 1567.

2. *Летохов В.С.* // Письма в ЖЭТФ. 1969. Т. 7. С. 348.

3. *Ashkin A.* // Phys. Rev. Lett. 1978. Vol. 40. P. 729.

4. *Pearson D.B., Freeman R.R., Bjorkholm J.E., Ashkin A.* // Appl. Phys. Lett. 1980. Vol. 36. P. 99.

5. *Cook R.J., Hill R.R.* // Opt. Comm. 1982. Vol. 43. P. 258.

6. *Миногин В.Г., Летохов В.С.* Давление лазерного излучения на атомы. М.: Наука, 1986.

Phys. Rev. Lett. 1988. Vol. 60 (21), P. 2137–2140

QUANTUM-STATE-SELECTIVE MIRROR REFLECTION OF ATOMS BY LASER LIGHT

V.I. Balykin, V.S. Letokhov, Yu.B. Ovchinnikov, A.I. Sidorov
Institute of Spectroscopy, Academy of Sciences USSR, 142 092 Troitsk, Moscow Region. USSR

We have demonstrated the specular reflection of Na atoms at a nonuniform laser field, the reflection coefficient of the "atomic mirror" being close to 100%. A specific feature of the reflection process is its quantum-state-selective character. The experimentally measured reflection selectivity (the ratio between the reflection coefficients of the sodium atoms in the ground-state sublevels with $F = 2$ and $F = 1$) was around 100.

The motion of an atom in a nonuniform quasiresonant electromagnetic field is determined by radiation force consisting of two components — the light pressure force and the gradient (dipole) force [1, 2]. In the case of a spatially inhomogeneous, sufficiently intense quasiresonant radiation, the translational motion of the atom is governed mainly by the gradient force. Proposals that this force should be used to localize or channel atoms in a standing light wave [3] or to trap atoms in the waist of a sharply focused laser beam [4] have long been known. Experiments were carried out on focusing an atomic beam [5] and trapping atoms in the waist of a Gaussian laser beam [6], and on channeling atoms in a standing light wave [7].

Of interest was the suggestion made by Cook and Hiil [8] that a nonuniform laser field can be used to reflect slow atoms. In the work reported by Balykin *et al.* [9], the mirror reflection of a thermal atomic beam from an "atomic mirror" was experimentally realized for the first time. In this paper we present experimental data on the observation of the most important property of the atomic mirror, namely, the property of quantum-state-selective reflection of atoms.

The idea of the atomic mirror is as follows [Fig. 1 (*a*)] [8]. When a plane traveling light wave is totally reflected internally at the surface of a dielectric in a vacuum a thin wave is generated on the surface. In the direction *OY* normal to the surface, this wave decays at a distance of $d = \lambda(\sin^2\theta - n^{-2})^{-1/2} / 2\pi \backsimeq \lambda/2$ [10], where λ is the length of the light wave, θ the angle of incidence of the wave, and n the refractive index of the dielectric. It is this surface wave that serves as an atomic mirror for an atom running into it. Indeed, a two-level atom near the surface experiences the gradient force [8]

$$\frac{F_{grad}(y) = \alpha\hbar(\Delta - k_1 v_x)G(y)}{1 + G(y) + (\Delta - k_1 v_x)^2/\gamma^2} \qquad (1)$$

where $a = k(\sin^2\theta - n^{-2})^{1/2}$ and $k_1 = k\sin\theta$ are the imaginary and real components of the wave vector k, $\Delta - k_1 v_x = \omega - \omega_0 - k_1 v_x$ is the detuning of the laser frequency ω relative to the transition frequency ω_0 with account being taken of the Doppler shift $k_1 v_x$, v_x is the x component of the atomic velocity, $2\gamma = 1/\tau$ is the natural linewidth, τ is the lifetime of the excited state, and $G = 1(y)/I_{sat}$ is the saturation parameter, $I(y)$ being the laser intensity and I_{sat} the transition saturation intensity.

With a positive detuning ($\Delta - k_1 v_x > 0$), the gradient force expels the atom out of the field. The reflection of the atom at the "mirror" may be considered a result of its being expelled out of a potential field whose energy is

$$U(y) = \frac{1}{2}\hbar\,(\Delta - k_1 v_x)\ln\left(\frac{1 + G(y)}{1 + (\Delta - k_1 v_x)^2/\gamma^2}\right). \qquad (2)$$

It can be demonstrated from consideration of the atomic motion in field (2) that the angle of reflection of the atom is equal to the angle of incidence, which means that what we have here is the specular reflection of the atom. With the transverse atomic velocity component v_y being great enough $\{v_y > v_y^{max} = [2U(0)/M]^{1/2}$, M being the atomic mass$\}$, the atom reaches the surface. In that case, it either adheres to the surface or is reflected from the surface. Usually reflection of atoms by surface is diffuse. Specular reflection can occur when de Broglie wavelength of atom divided by the grazing angle ψ is larger than the local surface roughness.[11] For typical atomic parameters (e.g., for the sodium atom) $M = 4 \times 10^{-23}$ g, $v_x = 6 \times 10^4$ cm/s, and $\gamma/2\pi = 5$ MHz, and tunable-laser-radiation parameters $k_1 = 10^5$ cm^{-1}, $G(0) = 10^5$, and $\Delta/2\pi = +2.6$ GHz, we have $v_y^{max} = 430$ cm/s. Accordingly, for thermal atomic velocities, the maximum grazing angle $\psi_{max} = v_y^{max}/v_x = 7\times10^{-3}$ rad.

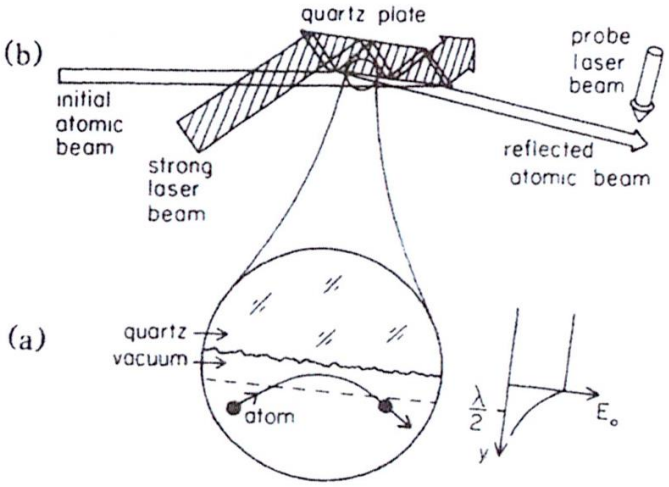


Fig. l. (*a*) Principle of mirror reflection of atoms by nonuniform laser field of surface wave. (*b*) Schematic diagram of experimental setup

That the atomic reflection is quantum-state selective follows from the character of the relationship between gradient force (l) and the detuning $\Delta - k_1 v_x$. When the detuning is positive, the gradient force repels the atom from the surface and thus the specular reflection of the atom is affected. With a negative detuning, the force attracts the atom to the surface, and so diffuse reflection is observed.

Let an atom (or molecule) have several sublevels in the ground state. For atoms, these may be, for example, fine and hyperfine ground-state splitting components (and for molecules, the vibrational-rotational sublevels of the ground state). Atoms (molecules) on a sublevel for which the frequency of transition to an excited state is lower than the laser frequency are reflected from the atomic mirror. Thus, if a beam of atoms (molecules) distributed among several ground-state sublevels is incident upon the mirror, the reflected beam will contain only atoms in one and the same quantum state. Since the expression for the gradient force (l) includes the Doppler shift, the minimum distance Between the lower sublevels at which the quantum-state-selective reflection will still obtain is determined by the magnitude of the Doppler broadening.

We have studied the quantum-state-selective reflection of the sodium atoms. The ground state of Na, $3S_{1/2}$, is split, because of hyperfine interaction, into two sublevels, one with the quantum number $F = 2$ and the other with $F = 1$, the distance between which is equal to 1772 MHz. According to the statistical weights of these sublevels, 62.5% of sodium atoms in a thermal beam are on the sublevel with $F = 2$ and 37.5% on that with $F = 1$. If the laser frequency ω is selected so that the condition $\omega_{20} + k_1 v_x < \omega < \omega_{10} + k_1 v_x$, ($\omega_{10}$ and ω_{20} being the frequencies of transitions from the sublevels with $F = 1$ and $F = 2$ to the excited state $3P_{3/2}$) is satisfied, the reflected beam will contain only atoms in the quantum state with $F = 2$.

The beam of sodium atoms [Fig. 1 (*b*)] was formed by a 400-μm-diam hole in the source and a square slit measuring 85 μm horizontally by 400 μm vertically and placed at a distance of 220 mm from the oven. The atomic mirror reflecting the atoms in a horizontal plane was at a distance of 15 mm from the slit. It was a plane-parallel plate of fused quartz 0.4 mm thick and 25 mm long into which a single-frequency laser beam was directed through a beveled side. To increase the surface area of the atomic mirror, use was made of multiple total internal reflection in the plate. The laser beam diameter was 0.5 mm at the $1/e^2$ level. The laser power was 300 mW. The grazing angle ψ was 2×10^{-3} rad. The plate surface was finished to an accuracy of $\lambda/10$. To prevent the atoms from being deposited onto the surface, the plate was heated to around 150 °C. The residual gas pressure in the vacuum chamber was no worse than 5×10^{-6} Torr.

The detection region was 330 mm distant from the slit. The atomic intensity in the beam was registered by means of a single-frequency probe laser beam which crossed the reflected atomic beam at an angle of 76° in a vertical plane. The probe laser frequency was scanned over the $3S_{1/2} \rightarrow 3P_{3/2}$ transition, which made it possible to monitor the presence in the beam of atoms on the sublevels with $F = 2$ and $F = 1$.

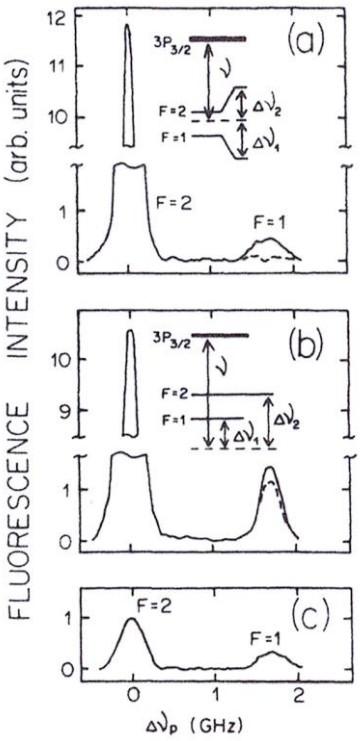


Fig. 2. Quantum-state-selective reflection of atomic sodium beam at atomic mirror. (*a*) Absorption spectrum of reflected atomic beam at detunings of intense laser field forming atomic mirror $[\omega_1 - (\omega_{10} + k_1 v_p)] / 2\pi = -1.2$ GHz, $[\omega_2 - (\omega_{20} + k_1 v_p)] / 2\pi = +0.5$ GHz ($v_p = 8.2 \times 10^4$ cm/s). (*b*) Same for the case $\Delta\omega_1/2\pi = +2.9$ GHz, $\Delta\omega_2/2\pi = +4.6$ GHz. (c) Same at $P_L = 0$ (scattered atoms). Dashed line, result of subtraction of background signal due to scattered atoms

Figure 2 demonstrates the results of the quantum- state-selective reflection of sodium atoms at the atomic mirror. The frequency ω of the intense laser radiation is measured relative to the frequency $\omega_{20} + k_1 v_p$ of the $3S_{1/2}(F = 2) \rightarrow 3P_{3/2}$ transition for the atom with the most probable velocity v_p equal to 8.2×10^4 cm/s at a source temperature of $T = 630$ K. Figure 2(a) corresponds to the case in which the laser frequency detuning is selected so as to be positive only with respect to the frequency of the transition $3S_{1/2}(F = 2) \rightarrow 3P_{3/2}$ $\{[\omega - (\omega_{20} + k_1 v_p)] / 2\pi = +0.5$ GHz$\}$. The laser frequency detuning with respect to the transition $3S_{1/2}(F{=}1) \rightarrow 3P_{3/2}$ is

$$\Delta\omega_1 / 2\pi = [\omega - (\omega_{10} + k_1 v_p)]/2\pi = -1.2 \text{ GHz}.$$

In that case, it is only the atoms on the sublevel with $F = 2$ that are being reflected. The presence of a small number of atoms on the sublevel with $F = 1$ is explained by the fact that the sodium atoms which are being scattered on the residual gas molecules reach the detection region without being reflected at the mirror [Fig. 2(*c*), no

intense laser field]. The subtraction of the signal due to the scattered atoms [dashed line in Fig. 2(*a*)] shows that there are no (accurate to within measurement error) reflected atoms on the sublevel with $F = 1$. If the detuning of the laser frequency is positive with respect to the frequencies of both transitions ($\Delta\omega_1 / 2\pi = +2.9$ GHz, $\Delta\omega_2 / 2\pi = +4.6$ GHz.), the reflected atomic beam contains both the atoms on the sublevel with $F = 2$ and those on the sublevel with $F = 1$ [Fig. 2(b)]. Note that here, too, the reflection coefficient of the atoms in the state with $F = 2$ is greater than that of the atoms in the state with $F = 1$. This is explained by the fact that the cross section of the transition [12] $3S_{1/2}(F = 2) \rightarrow 3P_{3/2}$ (and, accordingly, the saturation parameter G and the maximum transverse atomic velocity component $v_y^{\max}$) exceeds the respective parameters of the $3S_{1/2}(F = 1) \rightarrow 3P_{3/2}$ transition. For this reason, the reflected atoms in the state with $F = 2$ can have a higher longitudinal velocity than those in the state with $F = 1$. Accordingly, the integral (over the velocity distribution) reflection coefficient $R_{F=2}$ of the atoms on the sublevel with $F = 2$ is greater than $R_{F=1}$.

To obtain quantitative data on the selective reflection, account must be taken of the optical pumping of the atoms giving rise to their redistribution among the ground-state sublevels. Such a pumping can be caused, first, by the laser light at the point of intersection of the atomic and laser beams before the atoms reach the mirror [Fig. 1 (*b*)]: second, by the laser light scattered on the surface microirregularities in the plate in the course of multiple internal reflection: and third, by the surface wave interacting directly with the atoms.

The effect of optical pumping was taken into consideration as follows. Because of scattering on the residual gas molecules some atoms flew near the mirror and entered a registration region. These atoms were used to take account of optical pumping. With the laser beam brought out of the plate forming the atomic mirror, we switched the laser on and off and registered the resulting changes in the signals from these atoms on the sublevels with $F = 2$ and $F = 1$ to measure the redistribution of the atoms between the sublevels due to the first cause of optical pumping. Then we again directed the laser beam into the plate, but made the grazing angle equal to zero (no atomic reflection), and switched the laser on and off once more to measure the total effect of the first two causes of optical pumping.

Figure 3 presents the ratio between the reflection coefficients of the atoms on the sublevels with $F = 2$ and $F = 1$ (reflection selectivity) as a function of the detuning of the intense laser radiation frequency relative to the frequency of the $3S_{1/2}(F = 2) \rightarrow 3P_{3/2}$ transition of the atom with the most probable velocity in the beam. The reflection coefficient of the atoms in the state with $F = 2$ ($F = 1$) was found as the ratio of the number of reflected atoms to the number of the atoms in the state with $F = 2$ ($F = 1$) incident upon the mirror. The reflection coefficients were calculated including the effect of redistribution of the atoms between the sublevels due to optical pumping.

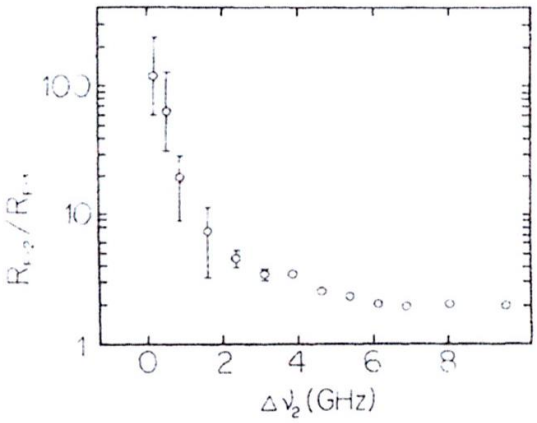


Fig. 3. Selectivity of reflection of sodium atoms on sublevels with $F = 2$ and $F = 1$ (ratio between reflection coefficients $R_{F=2} / R_{F=1}$) as a function of laser frequency detuning relative to $3S_{1/2}(F = 2) \rightarrow 3P_{3/2}$ transition frequency of atoms with the most probable velocity $v_p = 8.2 \times 10^4$ cm/s in the beam

It is evident from Fig. 3 that there is an interval of de-tunings of the laser frequency relative to the atomic transition frequency wherein the reflection selectivity reaches a sufficiently high value. The maximum experimentally measured reflection selectivity is 10^2. In our case, it was determined by the noise of the registration system. It can also be seen from Fig. 3 that the characteristic frequency interval within which selective reflection is observed amounts to a few gigahertz and coincides with the frequency interval wherein the gradient force of the surface wave of the atomic mirror acts effectively on the atoms.

In conclusion, it should be noted that such a quantum-state-selective reflection can be expected in the case of molecules as well. This will offer us the unique possibilities of preparing and spectroscopically analyzing beams of molecules in one and the same vibrational state which can be changed by varying the frequency of the reflecting laser radiation.

The authors express their gratitude to Dr. V.G. Minogin for interesting and fruitful discussions of the results.

References

1 *Opt J.* // Soc. Am. B2. 1985 (special issue on the mechanical effects of light).

2. *Minogin V.G., Letokhov V.S.* Laser Light Pressure on Atoms. N.Y.: Gordon and Breach, 1987.

3. *Letokhov V.S.* // Pis'ma Zh. Eksp. Teor. Fiz. 1968. Vol. 7. P. 348 [JETP Lett. 1968. Vol. 7. P. 272].

4. *Ashkin A.* // Phys. Rev. Lett. 1978. Vol. 40. P. 729.

5. *Bjorkholm J.E., Freeman R.R., Ashkin A., Pearson D.B.* // Phys. Rev. Lett. 1978. Vol. 41. P. 1361.

6. *Chu S., Bjorkholm J.E., Ashkin A., Coble A.* // Phys. Rev. Lett. 1986. Vol. 57. P. 314.

7. *Salomon C., Dalibard J., Aspect A., Metcalf H., Cohen-Tannoudji C.* // Phys. Rev. Lett. 1987. Vol. 59. P. 1659.

8. *Cook R.J. and Hill R.K.* // Opt. Commun. 1982. Vol. 43. P. 258.

9. *Balykin V.I., Letokhov V.S., Ovchinnikov Yu.B., Sidorov A.I.* // Pis'ma Zh. Eksp. Teor. Fiz. 1987. Vol. 45. P. 282 [JETP Lett. 1987. Vol. 45. P. 353].

10. *Born M. and Wolf E.* Principles of Optics. London: Pergamon, 1970. P. 47.

11. *Ramsey N.F.* Molecular Beams. Oxford: Clarendon, 1956.

12. *Fairbank W.M., Hänsch T.W., Schawlow A.L.* // J. Opt. Soc. Am. 1975. Vol. 65. P. 199.

Opt. Lett. 1988. Vol. 13 (11). P. 958–960

CHANNELING OF ATOMS IN A STANDING SPHERICAL LIGHT WAVE

V.I. Balykin, V.S. Letokhov, Yu.B. Ovchinnikov, A.I. Sidorov, S.V. Shul'ga
Institute of Spectroscopy, Academy of Sciences USSR,
142092 Troitsk, Moscow Region, USSR

One-dimensional localization of sodium atoms in a standing spherical light wave has been observed. The atoms have an oscillatory motion with an amplitude of approximately λ/10 along the nodes (or loops) of the wave.

The localization of atoms in a nonresonant light wave has been suggested [1]. In recent research, it has been inferred from observations of atomic fluorescence [2] and absorption [3] in a quasi-resonant standing light wave that atoms placed in such a wave undergo density redistribution [2] and channeling [3] under the action of the gradient force. In this Letter we report the first observation, to our knowledge, of the localization of atoms in the vicinity of the nodes (or loops) of a standing spherical light wave in the course of their being channeled along the curvilinear wave front of the laser field.

The basic idea of the experiment is schematically illustrated in Fig. 1. When atoms are being channeled along the nodes (or loops) of a light wave, the atomic trajectory must follow the wave front accurately to within < λ/2. Therefore, if the velocity of an atom entering a standing spherical light wave is tangent to the wave front, the localization of the atom must cause it to change the direction of its motion through an angle determined by the diameter of the laser beam forming the light wave and the wave-front curvature. If we assume that the atomic motion is determined mainly by the gradient force produced by the standing light wave, the angle a through which the atoms will be deflected from their initial direction of motion may be defined as

$$\alpha = 2\omega_0 z / [z_R(z^2 + z_R^2)^{1/2}], \tag{1}$$

where ω_0 is the beam-waist radius of the Gaussian laser beam forming the standing light wave, $z_R = \pi\omega_0^2/\lambda$, and z is the distance from the beam waist to the point of intersection between the atom and the light wave.

The maximum angular divergence of the atomic beam within which the atoms still can be localized in the standing light wave is given by

$$\Delta\phi = 2(U_{\max}/E)^{1/2} = 2(2\ U_{\max}/M)^{1/2}/v, \tag{2}$$

where v is the atomic velocity, M is the atomic mass, E is the kinetic energy of the atom, and U_{max} is the maximum atomic potential energy in the standing light wave, defined as

$$U_{max} = (h\Omega/2)/\ln(l_0 + p), \tag{3}$$

where $p_0 = 8g_0^2/(\gamma^2 + \Omega^2)$ is the atomic-transition saturation parameter in the standing-wave loop and g_0 is the Rabi frequency of the traveling light wave forming the standing light wave [4]. Equation (2) also defines the angular divergence that the localized atoms will have after leaving the standing light wave.

To produce a standing spherical light wave, we used single-frequency radiation from a cw dye laser. The laser beam was focused with a lens (F = 80 mm) into the center of curvature of a spherical mirror (R = 50 mm). The beam-waist radius ω_0 in that case was 0.015 mm. The size of the standing light wave at the point of intersection with the atomic beam was 1 mm, and the radius of curvature of the wave front was 40 mm. The beam of sodium atoms was shaped by two diaphragms. The diaphragm used in the atomic source was a round hole with a diameter of d = 0.4 mm, and the other diaphragm was a slit with dimensions l_1 = 0.17 mm and l_2 = 0.5 mm. The distance between the diaphragms was L_1 = 230 mm. In that case, the angular divergence of the atomic beam was $\theta \backsimeq 4 \times 10^{-3}$ rad.

The distance from the slit diaphragm to the laser beam was L_2 = 10 mm, with the long side of the slit parallel to the beam. The radiation power in a single traveling wave was P_1 = 0.11 W. The atoms' angle of entry into the laser beam (Fig. 1) was $\phi = 1.25 \times 10^{-2}$ rad. The atomic-beam profile was scanned by means of a probe single-frequency radiation tuned to resonance with the $3S_{1/2}$, $F = 2 \rightarrow 3P_{3/2}$, $F' = 3$ transition. The probe beam traversed the atomic beam at an angle of 76°. The detection region was at a distance of L_3 = 290 mm from the standing light wave. The probe radiation frequency was set to fall within the Doppler absorption line contour of the atomic beam, and the fluorescence of the atoms moving with a certain longitudinal velocity was detected. The velocity of the atoms subject to probing was 450 m/sec.

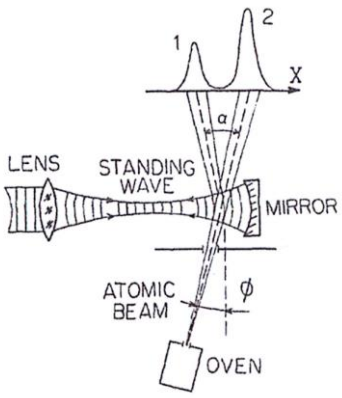


Fig. 1. Localization of atoms along the nodes (loops) of a standing light wave; (*1*) the atomic-beam intensity peak corresponding to localized atoms; (*2*) the peak corresponding to nonlocalized atoms

Figure 2(*a*) shows the experimental atomic-beam profile resulting from the interaction between the beam and the standing spherical light wave. The laser frequency ω_1 was detuned from the frequency of the $3S_{1/2}$, $F = 2 \rightarrow 3P_{3/2}$, $F' = 3$ transition, ω_0, by an amount of $\Omega = \omega_1 - \omega_0 = 300$ MHz. The interaction gave rise to the deflection of some atoms through an angle of α relative to their initial direction of motion and the appearance in the detection region of an additional atomic intensity peak [Fig. 2(*a*)]. The distance from the maximum of this peak to the center of the beam profile in the absence of the standing light wave (zero point on the *x* axis of Fig. 2) was 7.1 mm, which corresponded to a deflection angle of $\alpha = 2.5 \times 10^{-2}$ rad. Estimation of the atomic deflection angle by Eq. (1) yields $\alpha = 2.4 \times 10^{-2}$ rad, which agrees well with the measured value. It should be noted that so large a deflection angle was achieved because the gradient force in our experimental conditions exceeded the spontaneous light pressure force: $F_{\text{grad}}^{\max}/F_{\text{spont}}^{\max} \backsimeq 2G\gamma/\Omega \backsimeq 18$, where 2γ is the natural linewidth and G is the saturation parameter of the atomic transition [4].

The measured angular divergence $\Delta\alpha$ of the atoms subjected to localization also agrees with the estimate by Eq. (2) and is 5×10^{-3} rad.

The atoms entering the standing light wave at a certain angle of $\delta\phi$ comparable with the angle $\Delta\phi$ and not along the tangent to the wave front will fail to become localized. In our experiment, this was the case with $\delta\phi = \pm 3.5 \times 10^{-3}$ rad.

Figures 2(*b*)–2(*d*) show atomic-beam profiles in the detection region after interaction with the standing light wave, calculated with allowance being made for the gradient force [Fig. 2(*b*)], the gradient force and friction force[5] [Fig. 2(*c*)], and the gradient force, friction force, and momentum diffusion [6] [Fig. 2(*d*)]. The displacement of the beam profile produced by the localized atoms relative to that due to nonlocalized atoms [Fig. 2(*c*)] was used to determine the deflection angle α, which proved to be close to both the measured value and the value found by Eq. (1). Note that failure to include the friction force in calculations causes the beam profile produced by nonlocalized atoms to be displaced from its initial position [Fig. 2(b)]. Better agreement between theory and experiment occurs when both the gradient and friction forces are taken into account [Fig. 2(*c*)]. Inclusion of momentum diffusion [6–8] makes the calculated beam profiles [Fig. 2(*d*)] wider than their experimental counterparts. This effect cannot yet be explained comprehensively.

Figure 3(*a*) illustrates the calculated atomic trajectories. The three trajectories correspond to three atoms entering the spherical standing light wave at the same angle of $\phi = 1.2 \times 10^{-2}$ rad and at a distance of $\lambda/3$ from each other. The straight lines 2 and 3 in Fig. 3(*a*) correspond to the trajectories of atoms that have not been localized in the light wave and hence have not changed their direction of motion. It can also be seen from Fig. 3(*a*) that there are atoms that are localized in the vicinity of the nodes of the standing light wave. Such atoms oscillate with a characteristic amplitude of $\lambda/10$ [Fig. 3(*b*)].

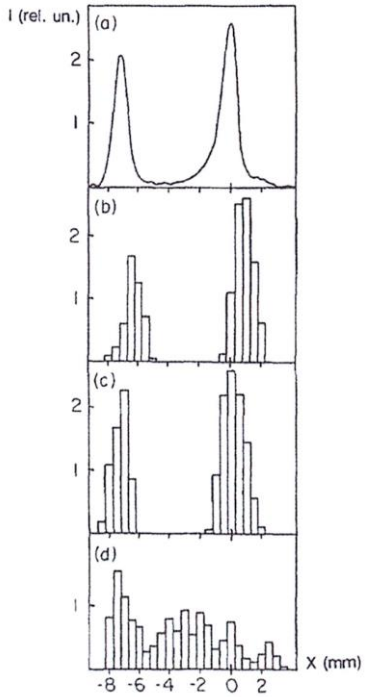


Fig. 2. Atomic-beam profile in the registration region after interaction with the standing spherical light wave: (*a*) experiment, (*b*)–(*d*) calculation. 1, atomic-beam intensity peak corresponding to localized atoms; 2, peak corresponding to nonlocalized atoms. The zero point on the *x* axis corresponds to the center of the atomic-beam profile in the absence of the laser field

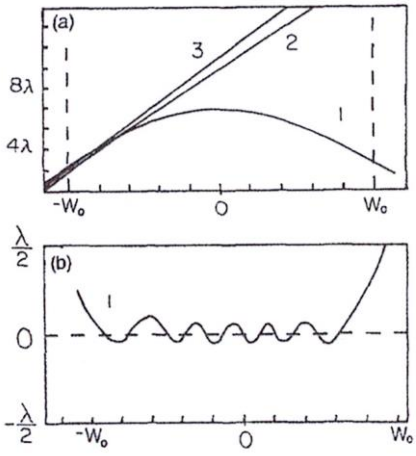


Fig. 3. Atomic trajectories in the standing light wave. (*a*) The character of motion of an atom as a function of the position of its point of entry into the standing light wave. Three atoms enter the wave at the same angle of $\phi = 1.2 \times 10^{-2}$ rad and at a distance of $\lambda/3$ from each other. The laser beam radius is $\omega = 0.5$ mm. Line 1, trajectory of a localized atom; lines 2 and 3, trajectories of nonlocalized atoms. (*b*) An enlarged scale of the trajectory of the localized atom

Calculations show that the main factor governing the localization of an atom in a standing light wave is its point of entry into the wave [1]. At $\Omega > 0$ the localization conditions are most favorable for the atoms entering the wave near its nodes. In our experiment, we also observed the localization of atoms along the loops of the standing light wave at $\Omega < 0$.

Thus, our experimental and theoretical studies have demonstrated that changes in the trajectories of atoms are due to their localization in the vicinity of the nodes of the standing light wave. On the other hand, the results obtained show that the theory of interaction between a two-level atom and a laser field cannot quantitatively describe the movement of the sodium atom in a standing light wave.

We would like to express our gratitude to Yu.E. Lozovik and V.G. Minogin for useful discussions of the results.

References

1. *Letokhov V.S.* // Pis'ma Zh. Eksp. Teor. Fiz. 1968. Vol. 7. P. 348.

2. *Prentiss M.G., Ezekiel S.* // Phys. Rev. Lett. 1986. Vol. 56. P. 46.

3. *Salomon C., Dalibard J., Aspect A., Metcalf H., Tannoudji C*. // Phys. Rev. Lett. 1987. Vol. 59, 1969.

4. *Minogin V.G., Letokhov V.S.* Laser Light Pressure on Atoms. New York: Gordon and Breach, 1987.

5. *Kazantsev A.P.* // Zh. Eksp. Teor. Fiz. 1974. Vol. 66. P. 1599.

6. *Gordon J.P., Ashkin A.S.* // Phys. Rev. Lett. 1980. Vol. 21. P. 1606.

7. Minogin V.G., Rozhdestvenskii Yu.V. // Zh. Eksp. Teor. Fiz. 1987. Vol. 93. P. 1173.

8. Baklanov E.V. // Pis'ma Zh. Eksp. Teor. Fiz. 1987. Vol. 45, 274.

Phys. Rev. Lett. 1990. Vol. 65 (12). P. 1415–1418

OBSERVATION OF A STRONG RECTIFIED DIPOLE FORCE IN A BICHROMATIC STANDING LIGHT WAVE

R. Grimm[a], Yu.B. Ovchinnikov, A.I. Sidorov and V.S. Letokhov.
Institute of Spectroscopy, Academy of Sciences USSR, 142092 Troitsk, Moscow Region, USSR

We report on the observation of a strong optical dipole force which is exerted on atoms in a bichromatic standing light wave as a result of nonlinear wave-mixing processes. This force can substantially exceed the upper limit of the spontaneous light force and, in contrast to the dipole force in monochromatic standing-wave fields, acts with constant sign on a macroscopic spatial scale.

The induced dipole force can strongly affect the motion of atoms in inhomogeneous light fields [1, 2]. In standing-wave laser fields, which have been the subject of extensive studies [3–6], a very strong dipole force can occur, greatly exceeding the principal upper limit of the spontaneous force [1]. In a single monochromatic standing wave, however, the application of this possibly strong force to manipulate the motion of atoms is restricted by the fact that the force spatially oscillates on the optical wavelength scale. Here the dipole force cannot effectively act on a macroscopic spatial scale as it vanishes in a wavelength average.

Recently, very interesting effects were considered in the works of Kazantsev and Krasnov,[7] Voitsekhovich *et al*. [8], and Javanainen [9]. Long-wavelength dipole forces are predicted to occur in bichromatic standing-wave fields as a result of a "rectification," being due to nonlinear wave-mixing processes. Different rectification schemes were investigated for two-level atoms [7, 8] and a Λ-type three-level system [9]. A relatively weak rectified dipole force may have already been observed in an experiment [10]; here, however, it at least remains unclear which rectification scheme was realized.

It is the aim of this Letter to present the first clear experimental demonstration of a strong rectified dipole force for the elementary case of two-level atoms in a bichromatic standing light wave (BSLW). Before discussing our experiment, let us explain the basic physics of the rectification effect in a simple comprehensible picture; a detailed theoretical description has already been given [7] but an illustrative explanation has not been provided up to now.

We consider the dipole force exerted on two-level atoms in a bichromatic light field under the following condition [7], allowing for a relatively easy theoretical description. We assume that one frequency component (ω_1) of the field is strongly

detuned from resonance, so that the corresponding detuning Δ_1 greatly exceeds all other relevant parameters of all points of the field:

$$|\Delta_1| >> \Omega_1(\mathbf{r}), \Omega_0(\mathbf{r}), |\Delta_0|, \gamma; \tag{1}$$

here $\Omega_0(\mathbf{r})$ and $\Omega_1(\mathbf{r})$ denote the space-dependent optical Rabi frequencies of the two field components, Δ_0 represents the detuning of the other field component (ω_0), and γ is the natural transition linewidth (HWHM). We furthermore neglect all effects induced by the atomic motion, like, e.g., friction forces [4, 5]. This approximation is justified as long as all Doppler shifts occurring in the bichromatic field remain small compared with the natural transition linewidth.

We use a Fourier expansion of the optical Bloch equations to calculate the induced atomic dipole moment [11]. From its Fourier components oscillating with the field frequencies ω_0 and ω_1 it is straightforward to calculate [7] the two corresponding contributions $\mathbf{F}_0(\mathbf{r})$ and $\mathbf{F}_1(\mathbf{r})$ to the total dipole force $\mathbf{F}_{\text{dip}}(\mathbf{r}) = \mathbf{F}_0(\mathbf{r}) + \mathbf{F}_1(\mathbf{r})$. In this way, we obtain

$$\mathbf{F}_0(\mathbf{r}) = -\frac{1}{2}\hbar\gamma \frac{\Delta_{\text{eff}}(\mathbf{r})/\gamma}{\Delta_{\text{eff}}^2(\mathbf{r})/\gamma^2 + 1 + G_0(\mathbf{r})} \nabla G_0(\mathbf{r}) \tag{2a}$$

$$\mathbf{F}_1(\mathbf{r}) = -\frac{1}{2}\hbar\gamma \left[1 - \frac{G_0(\mathbf{r})}{\Delta_{\text{eff}}^2(\mathbf{r})/\gamma^2 + 1 + G_0(\mathbf{r})}\right] \nabla G_1(\mathbf{r}) \tag{2b}$$

where $Gi(\mathbf{r}) = \Omega_i^2(\mathbf{r}) / 2\gamma^2 = I_i(\mathbf{r}) / I_{\text{sat}}$ (i=0,1) represent the optical saturation parameters determined by the intensities $I_0(\mathbf{r})$ and $I_1(\mathbf{r})$ of the two field components and the saturation intensity I_{sat} of the transition.

In Eqs. (2*a*) and (2*b*) the effective detuning parameter

$$\Delta_{\text{eff}}(\mathbf{r}) = \Delta_0 + \gamma^2 G_1(\mathbf{r})/\Delta_1 \tag{3}$$

takes into account that the field (ω_0) closer to resonance sees a *light shift* of the transition frequency induced by nonlinear wave mixing with the strongly detuned field (ω_1). We note that light-shift effects of this kind are well known in laser spectroscopy [12]; also, quite recently their possible importance in laser-cooling experiments was pointed out [13, 14]. In fact, in our case, the light-shift effect plays the essential role for the rectification of the dipole force in a BSLW, as will be demonstrated in the following.

We now consider a field consisting of two collinear standing waves (ω_0, ω_1) interacting with the optical two-level transition. The corresponding intensity profiles are described by $I_0 = \bar{I}_0[1 - \cos(2k_{0x})]$ and $I_1 = \bar{I}_1[1 - \cos(2k_{1x})]$, with $k_0 = \omega_0/c$ and $k_1 = \omega_1/c$. Because of the small wave-number difference $\delta k = k_0 - k_1$ ($|\delta k| << k_0, k_1$) the two sinusoidal standing-wave profiles display a spatial phase shift $\phi = 2\delta k_x$ with respect to each other: ϕ oscillates in space with a period $L_0 = \pi/\delta k$ greatly exceeding

the optical wavelength $\lambda = 2\pi / k \backsimeq 2\pi/k_0 \backsimeq 2\pi/k_1$ and thus can be regarded as constant over some optical wavelengths.

Figure 1 illustrates how the light-shift effect leads to the rectification of the force component $\mathbf{F}_0(x) = \mathrm{F}_0(x)\hat{\mathbf{x}}$. In our example, we assume $\phi = 3\pi/2$, $\bar{G}_0 = \bar{I}_0/I_{\mathrm{sat}} = 2000$, $\Delta_0 = 10\gamma$, $\bar{G}_1 = \bar{I}_1/I_{\mathrm{sat}} = 3000$, and $\Delta_1 = -300\gamma$; these parameters fulfill the condition $\Delta_0 + \gamma^2\bar{G}_1/\ \Delta_1 = 0$ for an optimum rectification, as will be discussed in detail elsewhere. According to Eq. (3), the light shift $\Delta_{\mathrm{eff}}(x)-\Delta_0$ occurs proportional to the intensity $I_1(x)$ of the strongly detuned field. As a consequence, the effective detuning $\Delta_{\mathrm{eff}}(x)$ displays a spatial oscillation [see Fig. 1(b)]; i.e., a spatially alternating sign reversal occurs. This leads to a corresponding spatially alternating sign reversal in the force $\boldsymbol{F}_0(x)$, which is an odd function of Δ_{eff}. In our example, the sign of $\boldsymbol{F}_0(x)$ in the BSLW [see the solid line in Fig. 1 (*c*)] is reversed exactly where it would be negative in a monochromatic standing wave [see the dashed line in Fig. 1 (c)]; otherwise, the force keeps its positive sign. This, obviously, means *spatial rectification* of the dipole force. An overall-positive force profile $\mathrm{F}_0(x)$ results. The corresponding "*rectified dipole force*", defined as force $\langle F_0 \rangle$ averaged over the rapid variations on the λ scale, is of the order of the maximum dipole force in a standing wave and thus can greatly exceed the upper limit $\hbar k\gamma$ of the spontaneous force.

The second component $F_1(x)$ [see Eq. (2*b*)] exhibits a similar rectification effect. There the underlying mechanism is a space-dependent saturation of the optical transition leading to a periodical decrease of the force; this is mathematically described by the term in square brackets in Eq. (2*b*), which directly represents the population probability difference between the ground and excited states. Without going into more details here, we note that this saturation-induced rectification in $F_1(x)$ turns out to be much less effective in obtaining a strong force than the light-shift-induced rectification in $F_0(x)$.

Quite comprehensibly, the phase $\phi = 2\pi x/L_0$ plays a crucial role for the rectification effect both in force components F_0 and F_1, and in the total force F_{dip}. For $\phi = 0,\pi$ no rectification takes place, and for $\phi = \pi/2$ ($\phi = 3\pi/2$) the maximum negative (positive) rectified force occurs. Thus, theory predicts a spatial period $L_0 = \pi / \delta k >> \lambda$ of the rectified dipole force $\langle F_{\mathrm{dip}} \rangle$.

In our experiment, schematically shown in Fig. 2, we studied the deflection of an atomic beam perpendicularly injected into a BSLW. Our beam of sodium atoms emitted from an oven with a temperature of ~620 K was shaped by two diaphragms (round holes with diameter 0.25 mm) separated by 290 mm. The residual gas pressure in the vacuum chamber was 10^{-6} mbar. The interaction of the atoms with the deflecting light took place 10 mm behind the second diaphragm.

The radiation for the deflecting light field was obtained from the two-frequency laser described in Ref. 15. This laser provided a beam consisting of two collinearly propagating Gaussian TEM_{00} modes with approximately equal power $P_1 = P_2 = 25$ mW and a frequency separation $\Delta\omega/2\pi = 1.45$ GHz; according to theory, a corresponding period of $L_0 = 10.3$ cm of the rectified dipole force can be expected.

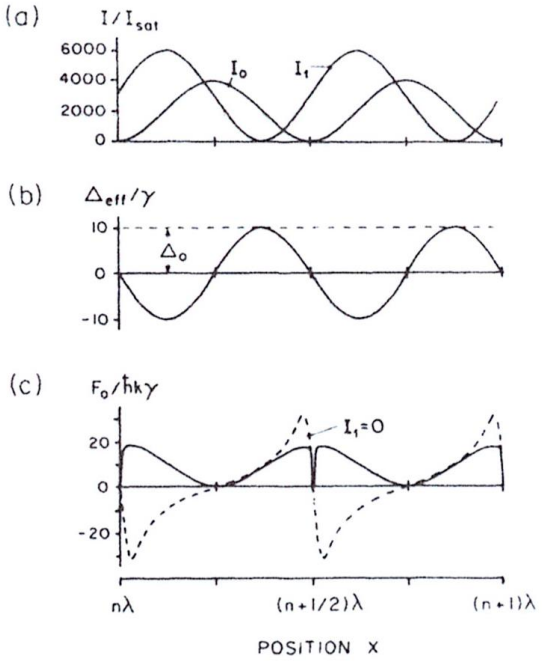


Fig. 1. Illustration of the light-shift-induced rectification of the dipole force component $\boldsymbol{F}_0(x)$ in a BSLW, where $\bar{G}_0 = 2000$, $\bar{G}_1 = 3000$, $\Delta_0 = 10\gamma$, $\Delta_1 = -300\gamma$, $\phi = 3\pi/2$ are assumed. (*a*) The intensity profiles $I_0(x)$ and $I_1(x)$ of the two standing-wave components. (*b*) Solid curve, the space-dependent effective detuning $\Delta_{\text{eff}}(x) = \Delta_0 + \gamma^2 G_1/\Delta_1$; dashed line, the initial detuning Δ_0 without the light-shift effect. (c) Solid curve, the force profile $\boldsymbol{F}_0(x)$ resulting in the BSLW; dashed curve, for comparison, the corresponding force profile which would result in the absence of the second, light-shifting standing wave ($I_1 = 0$)

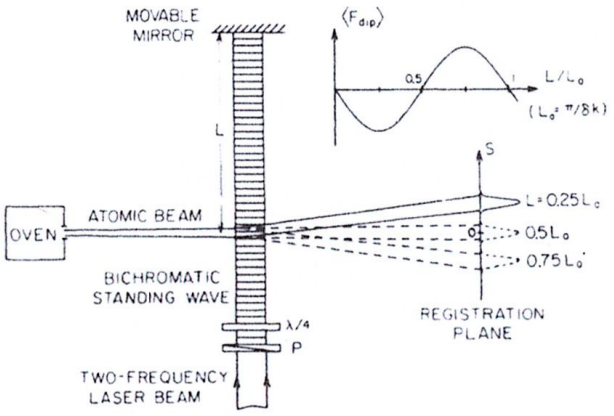


Fig. 2. Scheme of the experiment to observe the rectified dipole force in a BSLW. *P*, polarizer; $\lambda/4$, quarter-wave plate. Inset: Periodical dependence of the rectified dipole force $\langle F_{\text{dip}} \rangle$ on the distance L between interaction region and mirror

In atomic sodium, as is well known, the $F = 2 - F' = 3$ transition of the hyperfine-split D_2 line excited with circularly polarized light offers a two-level system.[16] We tuned the higher-frequency mode (ω_0) of our laser close to resonance with this transition, choosing a positive detuning $\Delta_0/2\pi = +140$ MHz. This value was, on one hand, small enough for a sufficient excitation of the two- level transition. On the other hand, it turned out to be large enough to prevent a strong unwanted excitation of the $F = 2 - F' = 1,2$ transitions, which leads to an optical pumping of the atoms into the $F = 1$ ground state. The other field component (ω_1) was strongly detuned from the two-level transition ($\Delta_1/2\pi = -1.31$ GHz) as well as from all other transitions of the hyperfine-split line. For this choice of laser frequencies, the condition of a two- level system is realized, allowing for a clear interpretation of the experimental results in terms of the light-shift effect and not in terms of optical pumping as discussed by Javanainen [9].

The plane mirror (see Fig. 2) was accurately aligned for exact backward reflection of the laser beam. An optical isolator prevented feedback into the laser and provided circular polarization of the light. The beam waist of the weakly focused laser beam with a diameter $d = 0.4$ mm (l/*e* intensity drop) was located in the mirror plane. Here the mean intensity in the beam center of each of the two standing-wave fields was $\bar{I}_0 = \bar{I}_1 \backsimeq 40$ W/cm^2, corresponding to the saturation parameters $\bar{G}_0 = \bar{G}_1 \backsimeq 6000$.

The distance L between mirror and interaction region remained small compared with the confocal parameter $b = \pi d^2 / 2\lambda \backsimeq 40$ cm in all our experiments. In this case, the wave fronts are sufficiently planar so that no significant beam deflection can result from a channeling of the atoms [17]. We also very carefully aligned the perpendicularity of laser beam and atomic beam with an accuracy of ±0.5 mrad in order to exclude a beam deflection on account of the friction force [18].

The transverse profile of the deflected atomic beam was scanned 290 mm behind the interaction region. Here the use of a single-frequency probe laser beam, intersecting the atomic beam at an angle of 76°, allowed for a velocity-selective detection [17]. We monitored the beam profile of those atoms in the ground state ($F = 2$) of the two-level transition with a longitudinal velocity of $v = 800$ m/s.

We measured the deflection profiles resulting from various positions in the BSLW; i.e., we varied the distance L between mirror and interaction region. Characteristic beam profiles, observed for the three most significant distances $L = 0.25L_0$, $0.5L_0$, and $0.75L_0$ ($\phi = \pi/2$, π, and $3\pi/2$, respectively), are shown as solid curves in Fig. 3; for comparison, the corresponding initial beam profiles observed in the absence of the BSLW are displayed as dashed curves. We are interested in the displacements of the center of mass of the beam profile since they reflect the average deflecting force. We note that the additional broadening, showing up in a similar way as for a single deflecting standing wave, occurs on account of the different atomic trajectories through the force profile, rapidly varying on the λ scale [see Fig. 1 (a)], and velocity-diffusion processes [5, 6].

For $L = 0.25L_0$, the deflection profile [see Fig. 3(a)] shows a substantial displacement $S = 0.65$ mm of the beam center, which is directed towards the mirror. From this shift we estimate an average force $\langle F \rangle = -4.0\hbar k\gamma$ acting during the transit time $d/v = 0.5$ μs of the atoms through the laser beam. For $L = 0.5L_0$ [see Fig. 3(b)], we

registered no displacement of the beam center. For $L = 0.75L_0$ [see Fig. 3(c)], we observed a displacement $S = -0.55$ mm directed away from the mirror; here we estimate an average deflecting force $\langle F \rangle = +3.4\ \hbar k\gamma$ of opposite sign and nearly the same magnitude as for $L = 0.25L_0$. Our observation that the force here appears somewhat weaker is probably explained by a less ideal experimental realization of the standing-wave field for a larger distance between mirror and interaction region. As a check, we also measured the beam deflection resulting from a traveling light wave, leaving all other experimental parameters unchanged. In good agreement with theoretical expectations, we observed a spontaneous force with magnitude $\sim 0.9\ \hbar k\gamma$.

Our atomic-beam-deflection profiles resulting from the BSLW clearly reflect an optical force with a spatial period determined by the wave-number difference of the two laser modes ($L_0 = \pi/\delta k$). This confirms that the force results from nonlinear wave-mixing processes between the two standing-wave components. Also, the strength ($\langle F \rangle > \hbar k\gamma$) and sign of the force strongly support that we, in fact, observed the *rectified dipole force* theoretically discussed above.

We note that our experimental deflection profiles cannot be expected to be fully quantitatively explained by the force described by Eqs. (2). This is mainly due to the transverse atomic velocities $v_\perp \sim \gamma/k$ occurring during the deflection process. For these velocities, exceeding our theoretical condition of weak Doppler shifts ($kv_\perp << \gamma$), both a friction force and a substantial decrease of the rectified force occur on account of motion- induced effects [7]. This may sufficiently explain that the rectified dipole force appeared weaker in our experiment ($\langle F \rangle \sim 4\hbar k\gamma$) than the corresponding theoretical force $\sim 10\hbar k\gamma$ calculated from Eqs. (2).

In summary, this Letter reports the first unambiguous experimental demonstration of a strong rectified dipole force exerted on two-level atoms in a bichromatic standing light wave. An explanation for the origin of this force is given in terms of a space-dependent light-shift effect. In accordance with theoretical predictions, the experimentally observed force considerably exceeds the spontaneous light force and keeps a constant sign over macroscopic distances. Thus the rectified dipole force may serve as a new tool for an effective manipulation of the motion of atoms. It may be, e.g., very useful for the design of optical traps for atoms with deep potential wells of macroscopic size.

We wish to thank Dr. V.I. Balykin for useful and stimulating discussions.

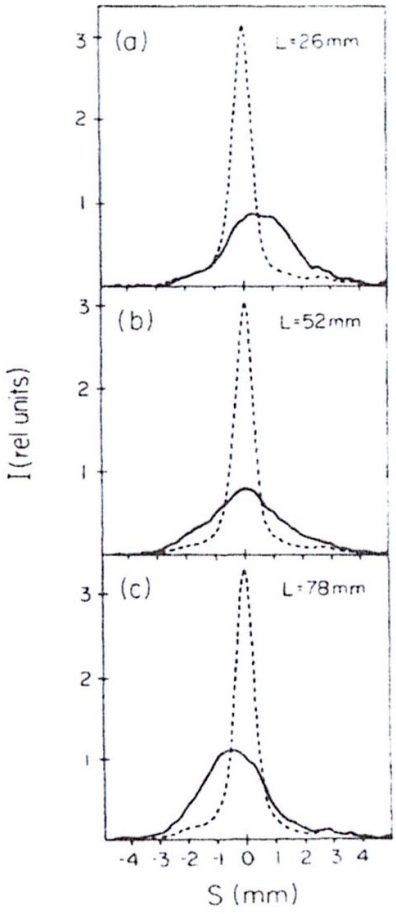


Fig. 3. Experimental atomic-beam profiles in the measured region for three different distances *L* (see Fig. 2). The dashed curves correspond to no-laser-field conditions

References

[a] On scientific exchange from Eidgenössische Technische Hochschule-Zürich, 8093 Zürich, Switzerland; now at Max- Planck-Institut für Kernphysik, 6900 Heidelberg, Federal Republic of Germany.

1. *Minogin V.G., Letokhov V.S.* Laser Light Pressure on Atoms. New York: Gordon and Breach, 1987; and references therein.

2. Special issue on laser cooling and trapping of atoms // J. Opt. Soc. Am. B. 1989. Vol. 6. P. 2019–2278; and references therein.

3. *Letokhov V.S.* // Pis'ma Zh. Eksp. Teor. Fiz. 1968. Vol. 7. P. 348 [JETP Lett. 1968. Vol. 7. P. 272].

4. *Kazantsev A.P.* // Zh. Eksp. Teor. Fiz. 1974. Vol. 66. P. 1599 [Sov. Phys. JETP. 1974. Vol. 39 P. 784].

5. *Gordon J.P., Ashkin A.* // Phys. Rev. A. 1980. Vol. 21. P. 1606.

6. *Dalibard J., Cohen-Tannoudji C.* // J. Opt. Soc. Am. B. 1985. Vol. 2. P. 1707.

7. *Kazantsev A.P., Krasnov I.V.* // Pis'ma Zh. Eksp. Teor. Fiz. 1987. Vol. 46. P. 333 [JETP Lett. 1987. Vol. 46. P. 420]; J. Opt. Soc. Am. B. 1989. Vol. 6. P. 2140.

8. *Voitsekhovich V.S., Danileiko M.V., Negrijko A.M., Romanenko V.I., Yatsenko L.P.* // Zh. Tekh. Fiz. 1988. Vol. 58. P. 1174 [Sov. Phys. Tech. Phys. 1988. Vol. 33. P. 690].

9. *Javanainen J.* // Phys. Rev. Lett. 1990. Vol. 64. P. 519.

10. *Voitsekhovich V.S., Danilciko M.V., Negrijko A.M., Romanenko V.I., Yatsenko L.P.* // Pis'ma Zh. Eksp. Teor. Fiz. 1989. Vol. 49. P. 138 [JETP Lett. 1989. Vol. 49. P. 161]. The authors claim to have observed a maximum rectified force of 0.8 *ħkγ;* their experimental data, however, rather indicate ∼0.13 *ħkγ*.

11. *Stenholm S.* Foundations of Laser Spectroscopy. New York: Wiley-Interscience, 1984.

12. *Letokhov V.S., Chebotayev V.P.* Nonlinear Laser Spectroscopy. Berlin: Springer-Verlag, 1977. P. 169.

13. *Dalibard J., Cohen-Tannoudji C.* // J. Opt. Soc. Am. B. 1989. Vol. 6. P. 2023.

14. *Sheehy B., Shange S.-Q., Van der Straten P., Hatamian S., Metcalf H.* // Phys. Rev. Lett. 1990. Vol. 64. P. 858.

15. *Balykin V.I., Sidorov A.I.* // Kvantovaya Elektron. 1984. Vol. 11. P. 2001 [Sov. J. Quantum Electron. 1984. Vol. 14. P. 1342].

16. *Balykin V.I.* // Opt. Commun. 1980. Vol. 33. P. 31.

17. *Balykin V.I., Lozovik Yu.E., Ovchinnikov Yu.B., Sidorov A.I., Shul'ga S.V., Letokhov V.S.* // J. Opt. Soc. Am. B. 1989. Vol. 6. P. 2178.

18. *Early J.W.* // Opt. Commun. 1988. Vol. 65. P. 250.

Optics Communications. 1987. Vol. 64 (2). P. 151–156

THE POSSIBILITY OF DEEP LASER FOCUSING OF AN ATOMIC BEAM INTO THE Å-REGION

V.I. Balykin and V.S. Letokhov
Institute of Spectroscopy, Academy of Sciences USSR, 142092, Moscow Region, Troitzk, USSR

An atomic beam can be focused into an angstrom size spot by the action of the gradient force of a laser field having a special configuration. The main parameters and limitations of such laser objective for atomic beam microscopy are considered.

1. Introduction

To effectuate microscopy with a spatial resolution in the Å-region, use is made of electrons [1] and X- quanta [2]. In this article, the possibility of employing beams of neutral atoms for the same purpose is discussed. The key to the realization of this idea is the possibility of focusing an atomic beam into a region of several Å, with the aid of a laser field of certain configuration, power, and frequency. The possibility of such a deep focusing of an atomic beam considered here is a logical development of the laser methods for controlling the motion of neutral atoms that have been the subject of extensive research recently [3–5], in particular the techniques for focusing an atomic beam with laser radiation [6, 7].

We consider an atomic beam in the form of the Broglie waves and then find a potential field the action of which is similar to that of an objective lens in light optics or electron optics. After that, we calculate the distribution of the field in the focal plane of the objective lens using the analogy between light and electron optics and determine the characteristics of the lens, i.e., of the potential field, such as focal length, aperture, and aberrations, and the possibility of its realization by means of modem laser technology.

2. A laser lens for an atomic microscope

In the optical image theory [8], an ideal objective lens is a transparency having the following phase transmission function:

$$T(x, y) = \exp[-ik(x^2 + y^2)/2f], \tag{1}$$

where $k = 2\pi/\lambda$ and f is the focal length of the lens. A light beam passing through such a transparency undergoes an additional phase change of $k(x^2 + y^2)/2f$.

Our task is to find such a potential field that would make the phase change of a wave function (de Broglie wave) to satisfy eq. (1) in which k now equals $2\pi/\lambda_B$. It is known that if the de Broglie wavelength λ_B is small in comparison with the characteristic size conditioning a given problem, the characteristics of the system are close to classical. In the quasiclassical approximation, the atomic wave function is defined by the expression [9]

$$\Psi = [C/(p(z)^{1/2}]\exp\big((i/\hbar)\int p(z)\mathrm{d}z\big), \tag{2}$$

where C is a constant and $p(z) = \{2M[E - U(z)]\}^{1/2}$ the atomic momentum, M being the atomic mass, E the atomic total energy, and $U(z)$ the atomic potential energy. In the text below, we will consider the atomic motion in a quasi-resonance laser field, i.e., at $\gamma << \Delta = \omega_1 - \omega_0$, $\Delta \approx (I/I_s)^{1/2}$, where 2γ is the homogeneous resonance atomic absorption line width, ω_1 the laser frequency, ω_0 the atomic transition frequency, I the laser intensity, and I_s the atomic transition saturation intensity.

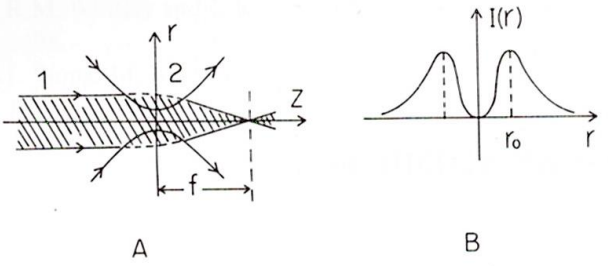


Fig. 1. Laser field configuration for focusing an atomic beam to a spot size equal to the de Broglie wavelength: (*a*) disposition of the laser and atomic beams: (*b*) cross-sectional intensity profile of the TEM_{01}^{*} laser mode field

The potential energy in a laser field is given by [10]

$$U = (\hbar\Delta/2)\ \mathrm{ln}(1+p), \tag{3}$$

where $p = (I/I_s)(\gamma^2/4)\,[(\gamma^2/4) + \Delta^2)^{-1}$ is the atomic transition saturation parameter. The phase change of the wave function (1) due to the potential (3) is

$$\Delta\varphi = \Delta\varphi_1 - \Delta\varphi_0 = (1/\hbar v_2)\int U(z)dz\,, \tag{4}$$

where $\Delta\varphi_1$ and $\Delta\varphi_0$ are the phase changes with and without the field, respectively and v_z is the atomic velocity along the z-axis.

To realize focusing, it is necessary to have a laser field providing for a phase change of the wave function equal to the exponent in eq. (1). This purpose can, for

example, be served by the TEM_{01}^{*} laser mode near the beam axis. The laser intensity in the TEM_{01}^{*} mode is defined as [11] (fig. 1)

$$I(r, z) = 4I_0[w_0^2/w^2(z)] \times [2r^2/w^2(z)] \exp[-2r^2/w^2(z)], \quad (5)$$

where w_0, is the laser beam waist radius in the plane $z = 0$, $w^2(z) = w_0^2\ (1+ z^2/z_R^2\ )$ the beam waist radius in the z-plane, $z_R = (\pi/\lambda)w_0^2$, the Rayleigh length, and $I_0 = P_0/2\pi w_0^2$, P_0 being the radiation power. In the case of paraxial optics [$\rho = r/w(z) << 1$] and subject to the condition $p < 1$, the expression for the phase change of the de Broglie wave in a laser field of the form (5) has the following form, account being taken in the expansion of the exponent of all the terms up to and including the fourth-order ones:

$$\Delta\varphi = (\pi^2\Delta z_R/\upsilon_z)\rho^2 \times [1 - (1\text{-}\alpha/2)(\rho^2/2) + (1-4\alpha)(3/16)\rho^4, \quad (6)$$

where $\alpha = (P_0\gamma^2)/(\pi I_{s\Delta}{}^2 w_0^2)$.

The phase change turns out to be proportional to the square of the radius. To a first approximation the bracketed terms proportional to ρ^2 and ρ^4 may be disregarded ($\rho << I$). In such an approximation the field (5) acts on an atomic beam as an ideal objective lens with a resolution determined by its numerical aperture and the de Broglie wavelength. The bracket terms describe spherical aberrations of the 4th and the 6th order, respectively.

By comparing the phase change (6) with the expression (1) for the transmission function of an ideal objective lens, we find the focal length of our atomic objective lens to be

$$f = \hbar(\lambda\Delta/P_0)\ (w_0^2)\ (I_s/\gamma^2 M\lambda_B^2) \quad (7)$$

The expression in the first parentheses is determined by the laser beam parameters, that in the second by the beam waist, and in the third by the atomic parameters. The expression for the focal length may be written in term of the longitudinal atomic velocity as follows:

$$f = (1/2\pi\hbar)(\lambda\Delta/P_0)\ (w_0^2)\ (I_s/\gamma^2 M\upsilon_z^2/\gamma^2). \quad (8)$$

3. The resolution of a laser lens for an atomic beam

The resolution of the laser objective lens depends mainly on the following for factors: (i) diffraction of atoms by the aperture limiting the cross-sectional size of the atomic beam, (ii) momentum diffusion caused by spontaneously re-emitted photons, (iii) chromatic aberration due to the strong atomic velocity dependence of the focal

length, and (iv) spherical aberration inevitable where a real laser field is used. Let us consider how strongly these factors affect the resolution of the objective lens.

(a) *Diffusive aberration*. An atom interacting with a quasi-resonance laser field which can absorb and then spontaneously re-emit photons is spherical symmetric; the change of the transverse atomic momentum is

$$\Delta P = (2N/3)^{1/2}\hbar k = \hbar\Delta k_{\mathrm{B}}^{\perp} \tag{9}$$

where $k_B^{\perp}$ is the change of the transverse de Broglie wave vector component. If the atomic beam diameter is equal to $2a$, then for the transverse interval of the wave vector variation due to diffraction we find

$$\Delta k_B^0 \approx 1/2a.$$

The diffusive aberration can be neglected if

$$\Delta k_{\mathrm{B}}^{\perp} < \Delta k_{\mathrm{B}}^{0} \tag{10}$$

The relation (10) is equivalent to the limitation of the number of spontaneously re-emitted photons:

$$N < (3/2)(\lambda/2a)^2. \tag{11}$$

The spontaneous decay rate is given by

$$\beta = \pi\gamma p \tag{12}$$

where

$$p = (4P_0/\pi w_0^2 I_s)\,(\gamma/2\Delta)^2\,[2r^2/w^2(z)] \tag{13}$$

is the atomic transition saturation parameter. The number of photons re-emitted during the interaction time t_{int} is

$$N = \int_{\mathrm{t_{int}}} \beta\,\mathrm{d}t = (\mathrm{l}/v_z)\int_{L_1} \beta \mathrm{d}z \tag{14}$$

where L_1 is the length of the atom-laser interaction region.

From the expressions (11)–(14) we have the following condition on which the diffusive aberration can be neglected:

$$\Delta^2 \geq (8\pi^4 P_0\gamma^3 w_0^2/3I_s v_z\lambda^3)\,(r^4/w_0^4). \tag{15}$$

(b) *Chromatic aberration*. The effect of chromatic aberration can be evaluated by considering the de Broglie wave front distortion caused by it. If the distortion is small, the new intensity of the center of the diffraction patterns is defined by the expression [12]

$$i = i_0(1 - k_B^2\overline{\Delta\varphi^2})^2, \tag{16}$$

where i_0 is the intensity at the center of the diffraction pattern disregarding the wave front distortion and $\overline{\Delta\varphi^2}$ the mean-square deviation of the wave front from true spherical shape. The local change of the wave phase is related to the defocusing Δf by the relation [12]

$$\Delta\varphi_{chr} = (2\pi/\lambda_B)\,(\Delta f)\,(r^2/2R), \tag{17}$$

where R is the wave front radius after passing through the objective lens when there are no aberrations. Using eqs. (8) for the focal length and (17) for the phase change, we get the following expressions for the mean-square phase change due to the non-monochromatic character of the atomic beam:

$$\Delta\varphi_{chr}^2 = (9k_B\,a^4/80f^2\,v_z^2)\,(\Delta v_z^2). \tag{18}$$

If the Rayleigh quarter-wave criterion is used as an image-quality criterion, the following limitation is imposed upon the nonmonochromatic character of the atomic velocities in the beam:

$$\Delta v_z \le (\sqrt{32}/6\pi)\,v_z(f/a^2)\lambda. \tag{19}$$

(c) *Spherical aberration*. It can be seen from the expression (6) for phase change that the effect of spherical aberration on the image can be eliminated in two ways. Firstly, one can reduce the atomic beam diameter. But this way leads to an increased role of diffraction and reduced beam intensity at the center of the diffraction pattern. Secondly, the laser beam parameters can be selected so as to minimize this type of aberration. For instance, it follows from eq. (6) that when $\alpha = 2$, the 4th-order spherical aberration vanishes. In this case, the laser and atomic beam parameters must satisfy the condition

$$\alpha = (P_0\gamma^2)(\pi I_s\Delta^2 w_0^2) = 2. \tag{20}$$

It is necessary to make sure that this new condition does not contradict the condition $p < 1$ used in expanding the potential (3). The saturation parameter may be expressed in term of α as

$$p = (I/I_s)\,(\gamma^2/4\Delta^2) = [I(a)/I_{max}]\,(\alpha/e), \tag{21}$$

where $I(a)$ is the laser field intensity at a distance of a from the beam axis and I_{max} the maximum intensity at a distance of $r = w_0/\sqrt{2}$ from the axis. Already at a = $w_0/4$ the parameter p becomes substantially smaller than unity.

Allowing simultaneously for the limitations imposed by the spherical and diffussive aberrations, we get the following inequality:

$$(4\pi^5\gamma\lambda/3)\,(N^4/v_z) < 1, \tag{22}$$

where $N = a/\lambda$. It is seen from this expression that for the thermal atomic beams ($v_z = 10^4$–10^5 cm/s) the diameter of the atomic objective lens should not differ greatly from the laser wavelength. For instance, at $a = \lambda$, a resolution close to the diffraction limit can be achieved with $v_z = 1.2\times10^5$ cm/s.

(d) *Thin lens condition*. In common optics, forming an image with a lens is affected in the Fresnel approximation. This approximation holds true if the following condition is satisfied [8]:

$$(\lambda/z)^{1/4} \geq (d + \rho)/z, \tag{23}$$

where z is the distance from the lens at which the diffraction pattern is being analyzed, d the lens size, and ρ the image radius. In our case, this condition assumes the form

$$f \geq (\lambda_B^{-1/4})(a^{4/3}). \tag{24}$$

At $\lambda_B = 10^{-8}$ cm and $a = w_0/4$ the focal length of the lens should be as follows: (i) $f \geq 1.4\ \lambda$ for $w_0 = \lambda$, (ii) $f \geq 28\ \lambda$ for $w_0 = 10\ \lambda$, and (iii) $f \geq 616\ \lambda$ for $w_0 = 10^2\ \lambda$. With the laser field configuration considered here, the thickness of the lens is, strictly speaking, infinite and for this reason it is necessary to evaluate the influence of the field size along the z-axis on the lens parameters. The phase change that a de Broglie wave is caused to undergo by the laser field potential covering the distance from $-z_l$ to z_l, along the z-axis is [see eq. (6)]

$$\Delta\varphi = \text{const}\ \rho^2 \times 2 \arctan z_l \tag{25}$$

If we restrict ourselves to $z_l = 5z_R$, the phase change of the de Broglie wave covering a distance of $10z_l$ will be a mere 10% at variance with that defined by eq. (6), and this difference will be expressed only in a corresponding change in the focal length of the lens.

4. Atomic beam density distribution in the focal plane

For a real atomic lens, the phase change of the de Broglie wave may be expressed in the form

$$\Delta\varphi = (k_B/2f)\, r^2\, (\alpha_{dif} + \alpha_{chr} + \alpha_{sph}) \tag{26}$$

Where

$$\alpha_{dif} = (\upsilon_z w_0^2 I_s /3\lambda\gamma P_0)^{1/2}. \tag{26a}$$

$$\alpha_{chr} = (3/2)(\Delta\upsilon_z/\upsilon_z) \tag{26b}$$

$$\alpha_{sph} = [-(1-\alpha/2)(\rho^2/2) + (1-4\alpha)(3/16)\rho^4] \tag{26c}$$

are the terms defining the contributions of the diffusive, chromatic, and spherical aberrations, respectively.

To calculate the atomic density distribution in the focal plane, we use Kirchoff's diffraction theory [8] by which the diffraction field in the image space is defined accurate to within an insignificant phase factor by the following integral:

$$i(z,\rho) = (2\pi i/\lambda z) \int_0^a \rho' f(\rho') \exp[ik_B(\rho')^2/2f] \exp[-ik_B(\rho')^2/2f] J_0(k\rho\rho'/z)\, d\rho', \tag{27}$$

where $f(\rho')$ is the field distribution at the entrance to the objective lens and J_0 the Bessel function of zero order. To allow for aberrations, the second exponent of the integrand in eq. (27) should be replaced by the expression (26). Generally speaking, to take correct account of the total effect of individual aberrations is a complicated problem [1, 13] and for this reason we will restrict ourselves to separate consideration of the effects of each type of aberration on the establishement of the atomic distribution in the focal plane.

To satisfy the thin lens condition (24), we set the focal length $f = 5z_R$ and then, using eqs. (8) and (20), find the longitudinal atomic velocity providing for such focal length:

$$\upsilon_z = [200\pi^5 (\gamma^2 w_0^2 \upsilon_r^2 P_0/ I_s\lambda^2)]^{1/4}, \tag{28}$$

where υ_r, is the atomic recoil velocity. This expression for the longitudinal atomic velocity should be substituted into eqs. (26a)–(26c) in order to find the contributions of the individual aberrations. Then we assume that the de Broglie wave incident upon the atomic objective lens is a plane wave and find the atomic density distribution in the focal plane. As would be expected from the relation (22), in the case of thermal

atomic beams an image resolved close to the diffraction limit can be achieved with a laser beam waist radius of $w_0 \approx \lambda$. At $w_0 > 10\ \lambda$ spherical and diffusive aberrations become very large, and the requirement for the chromaticity of the atomic beam very stringent ($\Delta v/v \leq 10^{-4}$).

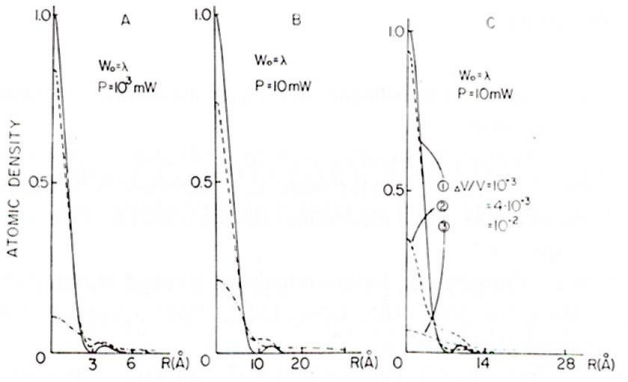


Fig. 2. Atomic beam density distribution in the focal plane: solid curve (–) corresponds to aberration-free case, dashed curve (– – –) shows the distribution with chromatic aberration taken into account, dash-and-dot curve (– .–. –.) represents that with spherical aberration allowed for, and dash -and-double-dot curve (–..–..–..) that with diffusive aberration included for $w_0 = \lambda$, $f = 15.6\lambda$, and $a = w_0/4$; (a) $P_0 = 1$ W, $v_z = 2.2 \times 10^5$ cm/s, $\Delta v_z / v_z = 10^{-3}$; (b) $P_0 = 10^{-2}$ W, $v_z = 6.9 \times 10^4$ cm/s, $\Delta v_z/v_z = 10^{-3}$; (c) $P_0 = 10^{-2}$ W, $v_z = 6.9 \times 10^4$ cm/s; $\Delta v_z/v_z = 10^{-3}$, 4×10^{-3}, and 10^{-2}

Fig. 2 illustrates the atomic density distribution in the focal plane for $w_0 = \lambda$. The solid curve corresponds to the aberration-free case. The dashed curve shows the distribution with the chromatic aberration taken into account, the dash-and-dot curve represents that with the spherical aberration allowed for and the dash-and-double-dot curve, that with the diffusive aberration included. Where figures lack some of the curves, this means that the respective aberrations are so small that the distributions coincide with that in the aberration-free case. The distribution curves of fig. 2a were calculated for the following parameters: $P_0 = 1$ W, $v_z = 2.2 \times 10^5$cm/s, $a = 0.25\ \lambda$, $f = 5z_R = 15.6\ \lambda$ and $\Delta v_z / v_z = 10^{-3}$. It is seen from the figure that with aberrations taken into consideration the atomic beam size at the focal point differs not very greatly from that governed by the diffraction limit of resolution and comes to a few Angström units. Fig. 2b shows distribution curves obtained with the same laser beam waist with a low laser power ($P_0 = 10$ mW). The atomic velocity $v_z = 6.9 \times 10^4$ cm/s is in this case close to the average velocity of a thermal atomic beam. The requirement for the atomic beam chromaticity is less stringent: the distribution with the chromatic aberration taken into account was plotted at $\Delta v_z / v_z = 10^{-3}$. The reduction of the laser power and atomic velocity impaired resolution: the atomic beam diameter at the focal point is around 10 Å. Fig. 2c illustrates the effect of the chromaticity of the atomic beam on the distribution width. It can be seen that worsening the beam chromaticity from 10^{-3} to 10^{-2} leads to a substantial spread of the beam.

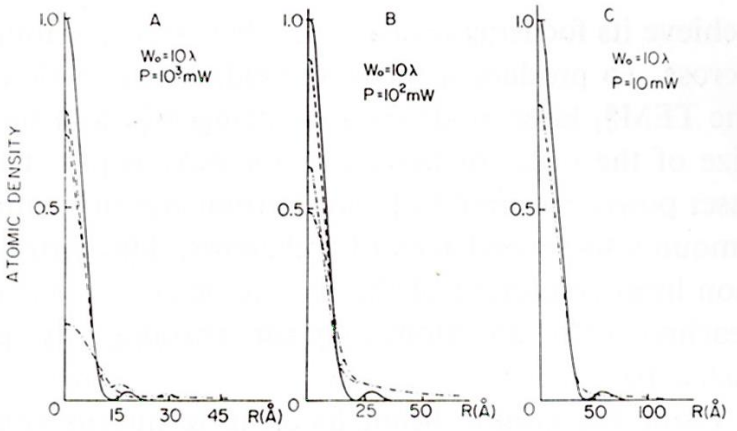


Fig. 3. Same as in fig. 2 for the case $w_0 = 10\lambda$, $f = 1570\ \lambda = 4.9 \times 10^{-2}$ cm, $a = w_0/6$, $\Delta v_z / v_z = 10^{-3}$: (a) $P_0 = 1$ W, $v_z = 6.9 \times 10^5$ cm/s; (b) $P_0 = 10^{-1}$ W, $v_z = 3.9 \times 10^5$ cm/s; (c) $P_0 = 10^{-2}$ W, $v_z = 2.2 \times 10^5$ cm/s

Fig. 3 presents similar distribution curves obtained with a different laser beam diameter: $w_0 = 10\lambda$. It can be seen that for all the three laser power values used ($P_0 = 1$ W, 0.1 W, and 0.01 W) it is possible to find such a combination of parameters as would give a distribution close to that governed by the diffraction limit. To prevent the distribution from being widened too much by spherical aberration, the atomic beam diameter a here was set to be equal to $w_0/6$. The role of this type of aberration decreases materially as the laser power is reduced. All the other types of aberration in fig. 3c are negligible and the calculated distribution curves practically coincide with that in the aberration-free case. Comparison between the three curves calculated for the three laser power values shows that the resolution of the atomic objective lens formed by a laser beam of lower power is worse. The resolution is also worse at $w_0 = 10\lambda$ than at $w_0 = \lambda$. This is due to the fact that the focal length f remains fixed at $5z_R$.

5. Conclusion

In conclusion, let us list the requirements imposed upon the laser radiation and the atomic beam to achieve its focusing into a spot a few Angström units across. To produce a focusing field, use is made of the TEM_{01}^{*} laser mode focused stringently to a spot size of the order of the radiation wavelength. The laser power required to focus thermal atomic beams amounts to several tens of milliwatts. The diffraction limit resolution of the atomic objective lens is reached with an atomic beam chromaticity of $\Delta v / v = 10^{-3}$.

Using the atomic beam focusing technique considered here, it is not very difficult to conceive of an atomic microscope similar to a reflecting or a transmission scanning electron microscope. The atoms scattered or reflected by the object under investigation can be detected by any means providing for a sufficiently high sensitivity,

especially by the laser techniques for detecting single atoms [14]. Needless to say that to realize such a scanning microscope with an Å-high resolution requires a small hole of atomic beam source. Modern technology is quite capable of making such small holes.

Acknowledgements

The authors express their gratitude to S.V. Shul'ga for his assistance in making computations and to Drs. Yu.E. Lozovik and V.G. Minogin for useful discussions.

References

1. *Glasser W.* Grundlagen der electronenoptik. Wien: Springer-Verlag, 1952.

2. *Aristov V.V., Gaponov S.V., Chekalin V.M., Gorbatov Yu.A., Erko A.I., Martynov V.V., Matveev L.A., Salashchenko N.N., Fraerman A.A.* // Pis'ma ZhETF (Russ.). 1986. Vol. 44. P. 207.

3. *Phillips W.D.,* ed. Laser-cooled and trapped atoms. Publication. 1983. No. 653. NBS, USA; Progr. Quantum Electron. 1984. Vol. 8. P. 115.

4. *Balykin V.I., Letokov V.S., Minogin V.G.* // Uspekhi Fiz. Nauk. (Russ.). 1985. Vol. 147. P. 117.

5. *Minogin V.G., Letokov V.S.* Laser light pressure on atoms (Russ.). Moscow: Fizmatgiz, 1986; Harword Academic Publ. Chur, 1987.

6. *Bjorkholm J.E., Freeman R.F., Ashkin A., Pearson D.B.* // Phys. Rev. Lett. 1987. Vol. 41. P. 1361; Optics Lett. 1980. Vol. 5. P. 11.

7. *Balykin V.I., Letokhov V.S., Sidorov A.I.* // Pis'ma ZhETF (Russ.). 1986. Vol. 43. P. 172.

8. *Papoulis A.* Systems and transforms with applications optics. McGraw-Hill Book Company, 1965.

9. *Landau L.D., Livshits E.M.* Quantum mechanics. Addison-Wesley, Reading Mass, 1985.

10. *Gordon J.P., Ashkin A.* // Phys. Rev. 1980. Vol. 21. P. 1606.

11. *Rigrod W.W.* // Appl. Phys. Lett. 1963. Vol. 2. P. 51.

12. *Marechel A., Françon M.* Diffraction structure des images. Paris, 1960.

13. *Born M., Wolf E.* Principles of optics. Pergamon Press, 1964.

14. *Balykin V.I., Bekov G.I., Letokhov V.S., Mishin V.I.* // Uspekhi Fiz. Nauk (Russ.). 1980. Vol. 132. P. 293.

ЛАЗЕРЫ И ЯДЕРНАЯ ФИЗИКА

1. *Летохов В.С.* Узкие резонансы испускания и поглощения γ-излучения ядер, индуцируемые лазерным излучением // Письма в ЖЭТФ. 1972. Т. 16 (7). С. 428–431.

2. *Letokhov V.S.* Narrow-frequency tunable γ-ray nuclear resonances induced by laser radiation // Phys. Rev. Lett. 1973. Vol. 30 (16). P. 729–732.

Письма в ЖЭТФ. 1972. Т. 16 (7). С. 428–431

УЗКИЕ РЕЗОНАНСЫ ИСПУСКАНИЯ И ПОГЛОЩЕНИЯ γ-ИЗЛУЧЕНИЯ ЯДЕР, ИНДУЦИРУЕМЫЕ ЛАЗЕРНЫМ ИЗЛУЧЕНИЕМ

В.С. Летохов
Институт спектроскопии АН СССР

Хорошо известны узкие резонансы поглощения и испускания γ-квантов без отдачи на ядерных переходах в кристаллах [1]. В настоящей статье предлагается метод получения узких ядерных резонансов в газе. Метод основан на модуляции частоты перехода ядра в молекулах, колебательно-возбужденных когерентной световой волной и имеющих одинаковую проекцию скорости движения на направление распространения волны. Метод позволяет получать резонансы как в поглощении, так и в испускании ядер, с шириной в $10^2 \div 10^4$ раз меньше доплеровской и перестраивать их частоту в диапазоне $\Delta\omega/\omega_\gamma \approx 10^{-5}$, значительно превышающем диапазон перестройки мессбауэровских резонансов.

Рассмотрим молекулы в газе низкого давления с неоднородным уширением колебательно-вращательной линии поглощения ω_0, принадлежащей некоторому i-му колебанию. Когерентной световой волной с частотой ω и волновым вектором $k_0 = n(\omega/c)$ можно возбудить молекулы со строго определенной проекцией скорости движения v [2]:

$$k_o v = \omega - \omega_o = \Omega. \tag{1}$$

Плотность возбужденных молекул определяется выражением:

$$N_2(v) = \frac{q}{2} N_0(v) \frac{x}{1+x};\ x = \frac{G\Gamma_0^2}{(\Omega - k_0 v)^2} + \Gamma_0^2, \tag{2}$$

где $N_0(v)$ — максвелловское распределение заселенности молекул на нижнем колебательном уровне в отсутствие поля; Γ_0 — однородная ширина оптического перехода, определяемая столкновениями молекул и (при очень низком давлении) конечным временем пролета молекул через световой луч; G — параметр насыщения перехода, определяемый интенсивностью световой волны; $q = g_i z_{\text{ВР}}^{-1} \exp[-(E_i/kT)]$ — число молекул на нижнем вращательном уровне E_i перехода, определяемое вырождением уровня g_i и статистической суммой вращательных состояний $z_{\text{ВР}}$.

Атомы в колебательно-возбужденных молекулах совершают вынужденные колебания с частотой ω_0 и амплитудой

$$r_{is}(t) = r_{is}^{(o)} \cos(\omega_o t + \phi), \tag{3}$$

где $r_{is}^{(o)}$ — амплитуда смещения *s*-го атома при возбуждении *i*-го нормального колебания молекулы, зависящая от силовых констант и формы колебания молекулы и ориентации ее относительно вектора поляризации световой волны. Амплитуды смещений атомов изменяются в довольно широких пределах от 10^{-9} до 10^{-11} см. Наиболее существенно то, что средняя величина смещения $r_{is}^{(o)}$ одного порядка с длиной волны λ_γ γ-квантов с энергией от 10 кэв до 1 Мэв. Колебание ядра с такой амплитудой должно вызывать значительную частотную модуляцию γ-излучения.

Спектральная линия ядра, движущегося со скоростью v, имеет центр на частоте $\omega_{\text{яд}}^{(o)} = \omega_\gamma \pm \Delta_\gamma + \mathrm{k}_\gamma \mathrm{v}$ (Δ_γ —– энергия отдачи, знаки «+» и «–» соответствуют поглощению и испусканию, k_γ — волновой вектор γ-кванта), расщепляется на ряд спектральных компонет на частотах $\omega_{\text{яд}}^{(o)} \pm \omega_o m (m = 0,1,2, \dots)$, причем интенсивность *m*-й компоненты определяется величиной

$$I_m = < J_m^2 \left(\frac{\boldsymbol{r_{is}^{(o)n}}}{\boldsymbol{\lambda_\gamma}} \right) >, \tag{4}$$

где J_m — функция Бесселя *m*-го порядка, а усреднение производится по всем ориентациям молекул. Приближенно можно принять, что $I_m \approx J_m^2 \left(r_{is}^{\text{эфф}} / \lambda_\gamma \right)$, где $r_{is}^{\text{эфф}}$ — среднеквадратичная величина проекции смещения *s*-го атома на направление световой волны, возбуждающей *i*-е колебание молекулы.

Если направление наблюдения ядерного перехода коллинеарно со световой волной ($\mathrm{k}_\gamma = \mathrm{k}_o (\omega_\gamma / \omega_o)$), то промодулированной будет только узкий спектральный интервал на частоте $\omega_{\text{ЯД}}^{(o)}$ с шириной

$$\Gamma_{\text{ЯД}} = \Gamma_o \sqrt{1 + G}\ \frac{\omega_\gamma}{\omega_o} \tag{5}$$

из всей доплеровски-уширенной линии ядерного перехода. В результате форма неоднородно уширенной линии заметно искажается. На частоте

$$\omega_{\text{ЯД}}^{(o)} = \omega_\gamma \pm \Delta_\gamma + \mathrm{k}_o \mathrm{v} \frac{\omega_\gamma}{\omega_o} \tag{6}$$

образуется провал с шириной по полувысоте $\Gamma_{\text{яд}}$ и глубиной

$$\beta^{(o)} = 1 - \frac{q}{2} J_o^2 \left(\frac{r_{is}^{\text{эфф}}}{\lambda_\gamma} \right) \frac{G}{1 + G}, \tag{7}$$

а на частотах $\boldsymbol{\omega_{\text{ЯД}}^{(m)} = \omega_{\text{ЯД}}^{(o)} \pm m\omega_o}$ образуются пики с такой же шириной и относительной величиной

$$\beta^{(m)} = \frac{q}{2} J_m^2 \left(\frac{r_{is}^{\text{эфф}}}{\lambda_\gamma} \right) \frac{G}{1 + G}. \tag{8}$$

Форма спектральной линии поглощения ядра при наблюдении в направлении световой волны, насыщающей колебательно-вращательный переход молекулы, изображена на рисунке.

Из-за относительно небольшой доли молекул $(q/2)$ [G/(1 + G)], резонирующих с когерентной световой волной (фактор q обычно лежит в интервале от 10^{-1} для простых молекул до 10^{-3} для сложных молекул), узкие резонансы имеют относительную амплитуду в интервале 0,1 + 10%. Весьма важным является автоматическая перестройка частоты резонансов при сканировании частоты световой волны вдоль доплеровского контура оптического перехода, причем абсолютная величина перестройки частоты резонансов γ-излучения в отношении ω_γ/ω_0 больше, чем для оптического перехода.

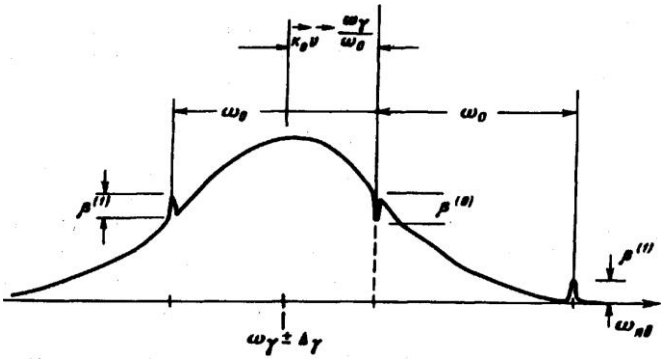


Рис. 1. Форма спектральной линии поглощения (испускания) γ-квантов на ядерном переходе в газе в поле световой волны $\mathcal{E}\cos(\omega_0 t + k_0 r)$ при наблюдении в направлении k_0

Так как коэффициент резонансного поглощения на ядерных переходах для разреженного газа мал, предлагаемый метод наиболее пригоден для получения узких линий γ-излучения с перестраиваемой частотой. Интенсивность линии излучения с шириной $\Gamma_{яд}$ в 10^2 раз у́же доплеровской ширины из вытянутой трубки с газом, заполненной молекулами с радиоактивными ядрами при давлении 10^{-2} *mop* ($q = 10^{-2}$, $G \approx 1$, длина трубки 100 см, диаметр 1 см, телесный угол наблюдения 10^{-4} стеррад) равна $10^7/r$ квантов/сек, где r — излучательное время жизни возбужденного состояния ядра.

Предлагаемый метод позволяет осуществить ряд принципиальных экспериментов. Например, перестраивая узкий резонанс γ-излучения $\omega_{яд}^{(1)} = \omega_\gamma - \Delta_\gamma - k_0 v \frac{\omega_\gamma}{\omega_0} + \omega_0$ в окрестности линии поглощения ядра $\omega_\gamma + \Delta_\gamma$ в конденсированной мишени, можно точно измерить энергию отдачи ядра, форму фононного спектра [3] и по его виду детально исследовать колебания ядер в кристаллах. Поскольку величина $k_0 v$ может быть измерена с очень высокой точностью путем измерения расстройки Ω частоты световой волны относительно центра доплеровского контура, частота резонанса γ-излучения может перестраиваться с точностью $\delta\omega_\gamma / \omega_\gamma = \delta\Omega/\omega_0$, которая в принципе может достигать значений $10^{-11} + 10^{-13}$. Это позволяет осуществить абсолютные измерения энергии

γ-квантов с точностью $\omega_\gamma/\omega_o(10^{-11} \div 10^{-13})$, которая в принципе может достигать значений 10^{-8}, и связать с такой же точностью шкалы энергии оптического и γ-диапазонов. Естественно, предлагаемый метод позволяет осуществлять γ-спектроскопию в недоступной для современных методов окрестности ядерных переходов $10^{-9} < \left|\left(\omega_{ЯД}/\omega_\gamma\right) - 1\right| < 10^{-5} \div 10^{-6}$.

Литература

1. *Mössbauer R.L.* // Z. f. Phys. 1958. Vol. 151. P. 124.
2. *Летохов В.С.* // Письма в ЖЭТФ. 1967. Т. 6. С. 597.
3. *Visscher W.M.* // Ann. of Phys. 1960. Vol. 9. P. 194.

Phys. Rev. Lett. 1973. Vol. 30 (16). P. 729–732

NARROW-FREQUENCY TUNABLE Γ-RAY NUCLEAR RESONANCES INDUCED BY LASER RADIATION

V.S. Letokhov
Institute of Spectroscopy, Academy of Sciences USSR

A method is proposed for obtaining very narrow-frequency tunable γ-ray resonances of emission and absorption in nuclear transitions. The method is based on frequency modulation of the nuclear transition in molecules vibrationally excited with a coherent laser wave and having the same tunable projection of the translational velocity on the direction of the wave propagation. Laser-induced nuclear resonances have widths 10^{-2}–10^{-4} times the Doppler width of nuclear transitions and a tuning range of about 10^{-5}.

The present Letter proposes a method for obtaining very narrow-frequency tunable nuclear resonances in gas, which extends the methods for obtaining narrow resonances by means of laser absorption saturation [1, 2] for a quite new frequency region. The method proposed is based on the frequency modulation of the nuclear transition in molecules vibrationally excited with the coherent light wave and having the same tunable projection of the translational velocity on the direction of the wave propagation. The method enables one to obtain resonances in both absorption and emission of nuclei having widths 10^{-2}–10^{-4} times the Doppler width of nuclear transitions, and to tune their frequency in $\Delta\omega/\omega_\gamma \simeq 10^{-5}$, considerably exceeding the tuning range of Mössbauer resonances [3]. The Letter also considers the principal experiments which might be carried out with these narrow resonances.

Let us consider molecules in a low-pressure gas with an inhomogeneous broadening of the vibrational-rotational absorption line ω_0, belonging to a certain *i*th vibration of the molecule. With a coherent traveling light wave of frequency ω and wave vector $\vec{k}_0 = \vec{n}\omega/c$, one can excite molecules with a quite definite projection of velocity $\vec{v}$ on the wave direction: $\vec{k}_0 \cdot \vec{v} = \omega - \omega_0 = \Omega$. The molecule density excited with a light wave on the $v'' = 1$ level is found from the expression

$$N_1(\vec{v}) = \frac{q}{2} N_0(\vec{v}) \frac{x}{1+x}, \; x = \frac{G\Gamma_0^2}{(\Omega - \vec{k}_0 \vec{v})^2 + \Gamma_0^2}, \qquad (1)$$

where $N_0(\vec{v})$ is the Maxwellian distribution of the molecule population on the lower vibrational level, $v' = 0$, when field is absent; Γ_0 is the homogeneous half-width of the optical transition determined by the collisions of molecules and (under a very low pressure) by the finite time of molecule transit through the light beam; G is the saturation parameter of the absorption transition determined by the light wave

intensity; $q = g_0 Z_{\text{rot}}^{-1} \times \exp(-E_0/kT)$ is the relative fraction of molecules occupying the rotational sublevel of the lower vibrational level of transitions determined by the g_0 level degeneracy and statistical weight Z_{rot} of the rotational states; E_0 is the rotational energy of the transition's lower level.

From the classical point of view, nuclei in vibrationally excited molecules vibrate with the frequency ω_0, which can be viewed as the average frequency of the motion from one turning point to another in the potential curve of the molecule [4]. First let us consider the simplest case to excite the lower rotational state with $J = 0$ of the vibrational level $v'' = 1$. In this case in a classical approach the time-dependent amplitude of the *S*th atom can be represented in the form

$$\vec{r}_{is}(t) = \vec{a}_{is}^{v} \cos\omega_0 t, \tag{2}$$

where $\vec{a}_{is}^{v}$ is the average oscillation amplitude of the *S*th atom in the excitation of the *i*th normal vibration of the molecule, depending upon molecular force constants and orientation of the molecule with respect to the polarization vector of the light wave. The vibration amplitudes of atoms vary from 0.1 to 10^{-3} Å [4, 5]. The most essential thing is that the nuclear displacement $\vec{a}_{is}$ is of the same order of magnitude or even more than the wavelength λ_γ of γ quanta with energy from 10 keV to 1 MeV. The vibration of the nuclear emitter with this amplitude should cause a considerable frequency modulation of γ radiation.

The transition frequency of nuclei in the molecule vibrationally excited by a light wave, for collinear observation, is equal to

$$\omega_{\text{nucl}}^{(0)} = \omega_\gamma \pm \Delta_\gamma + \vec{k}_\gamma \cdot \vec{v} = \omega_\gamma \pm \Delta_\gamma + (\omega - \omega_0)\omega_\gamma/\omega_0, \tag{3}$$

where ω_γ is the transition frequency of the recoilless nucleus; Δ_γ is the recoil energy, signs + and – denote absorption and emission, respectively; $\vec{k}_\gamma$ is the wave vector of the γ quantum. Because of the modulation of the nuclear position with frequency ω_0 and the average amplitude $\vec{a}_{is}^{v}$, there occurs a splitting of the nuclear frequency $\omega_{\text{nucl}}^{(0)}$ into a number of spectral components at frequencies $\omega_{\text{nucl}}^{(m)} = \omega_{\text{nucl}}^{(0)} \pm m\omega_0 (m = 0, 1, 2, \ldots)$. A relative component intensity at frequency $\omega_{\text{nucl}}^{(m)}$ is determined from the expression

$$I_m = \langle y_m^2 \left(\frac{\vec{a}_{is}^{v} \vec{n}}{\lambda_\gamma} \right) \rangle \simeq J_m^2 \left(\frac{\tilde{a}_{is}^{v}}{\lambda_\gamma} \right), \tag{4}$$

where J_m is the Bessel function of the *m*th order, and the averaging $\langle \cdots \rangle$ is carried out over all orientations of molecules; $\tilde{a}_{is}^{v}$ is the average value of the displacement projection of the *S*th atom on the direction of the light wave exciting the *i*th normal vibration of the molecule.

Under a collinear observation of the nuclear line ($\vec{k}_\gamma = \vec{k}_0\omega_\gamma/\omega_0$) only a narrow spectral interval will be modulated by a light wave at frequency $\omega_{\text{nucl}}^{(0)}$ with width

$$\Gamma_{\text{nucl}} = \Gamma_0(1+G)^{1/2}\omega_\gamma/\omega_0 \tag{5}$$

from the whole Doppler-broadened line of the nuclear transition. As a result, the shape of the inhomogeneously broadened nuclear line will be noticeably distorted by a light wave. At frequency $\omega_{\text{nucl}}^{(0)}$ determined by expression (3) a dip is produced with the half-width over the half-height Γ_{nucl} and the depth $\beta_0 = 1 - \frac{1}{2}qI_0G/(1+G)$; and at frequency $\omega_{\text{nucl}}^{(m)} = \omega_{\text{nucl}}^{(0)} \pm m\omega_0$ the peaks are formed with the same width and the relative value $\beta_m = \frac{1}{2}qI_mG/(1+G)$. The shape of the spectral line of the nuclear absorption (emission) for observation in the direction of the light wave saturating the vibrational-rotational transition of the molecule is depicted in Fig. 1.

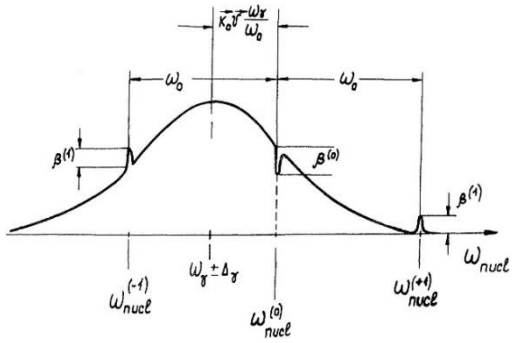


Fig. 1. Shape of spectral line of nuclear absorption (emission) for observation in the direction of the light wave saturating the vibrational-rotational transition of molecule

Because a relatively small part q of molecules is in resonance with the coherent light wave (q is a factor which determines the population of one rotational level and usually lies within the interval from 10^{-1} for simple molecules to 10^{-3} for many-atom molecules), narrow γ resonances have a relative amplitude in the interval 0.1–10%.

The principal feature of this effect is an automatic changeover of narrow γ–resonance frequency under a light-wave frequency scanning along the Doppler contour of the optical transition. A relative region of continuous tuning of the dip at frequency $\omega_{\text{nucl}}^{(0)}$ is determined by the Doppler width of transitions. However, the tuning region of all the resonances $\Delta\omega_{\text{tun}}$ exceeds the Doppler width:

$$\frac{\Delta\omega_{\text{tun}}}{\gamma} = \frac{\Delta\omega_{\text{Dopp}}\gamma}{\omega_\gamma} + \bar{m}\frac{\omega_0}{\omega_\gamma}. \tag{6}$$

The ω_0 can be changed by selecting the vibrational frequencies of the molecule in which the nucleus is incorporated, and the number m of the resonance can be raised by increasing the amplitude of the $\tilde{a}_{is}^{v}$ nucleus vibrations. The maximum

number $\bar{m}$ of peaks is approximately found by the ratio $\tilde{a}_{is}^{v}/\lambda_{\gamma}$, and in principleм $\bar{m} \gg 1$ is possible. In any case, the tuning region of the narrow resonances overlaps the interval $\Delta\omega_{\text{tun}}/\omega_{\gamma} = 10^{-5}$ in the vicinity of the nuclear transition.

In the case of the excitation of the vibrational rotational state with $J \neq 0$, it is necessary to take into account the fact that the light wave causes both the vibrational movement of the nucleus according to law (2) and an additional oscillator movement with the frequency of the molecular rotation. In the classical limit the nuclear displacement can be represented as

$$\vec{\mathrm{r}}_{is}(t) = \vec{\mathrm{a}}_{is}^{v}\cos\omega_{v}t + \vec{\mathrm{a}}_{isJ^{r}}\cos\omega_{r}t, \tag{7}$$

where $\vec{\mathrm{a}}_{isJ^{r}}$ is the average amplitude of the oscillations of the *S*th atom in the $\vec{\mathrm{k}}_0$ direction due to the molecular rotation excited on the level with angular momentum *J*. In this case the light-wave frequency is $\omega = \omega_{v} + \omega_{r}$. The peculiarity is that the amplitude of the nuclear oscillations due to the rotation can be much higher than that of the nuclear oscillations due to the vibrations. The frequency modulation of the line due to the nuclear emitter motion according to law (7) results in the splitting of each component at frequency $\omega_{\text{nucl}}^{(0)} \pm m\omega_{r}$ into many close components at frequencies $\pm n\omega_{r}$.

Since in the typical case $\tilde{a}^{r} \gg \lambda_{\gamma}$, then the modulation by the molecular rotation broadens the nuclear resonance at frequency$\omega_{\text{nucl}}^{(m)}$ by the relative value

$$\delta = \frac{\bar{n}\omega_{r}}{\omega_{\gamma}} \simeq \frac{\tilde{a}_{isJ^{r}}}{\lambda_{\gamma}}\frac{\omega_{r}}{\omega_{0}}, \tag{8}$$

where $\bar{n}$ is the number of the rotational component for which the intensity maximum is attained, i.e., the maximum value of $J_{n}^{2}(\tilde{a}_{isJ^{r}}/\lambda_{\gamma})$ as a function of *n*. If we take $\omega_{r} = 2\pi c\beta(2J+1)$ then approximately the estimate $\delta \simeq \tilde{a}_{isJ^{r}}4\pi\beta J$ is valid, where β is the rotational constant. For example, at $\tilde{a}^{r} \simeq 1$ Å, $\beta = 0.5\ \text{cm}^{-1}$, the value of the rotational broadening of the narrow nuclear resonance is $\delta \simeq 6 \times 10^{-8}\,J$. This value is much smaller than the Doppler broadening, but it exceeds the ultimate width of the resonance found with (5). Therefore, to eliminate this effect one should work either at the transition with $J = 0$, or with the nucleus placed on the rotation axis ($\tilde{a}^{r} = 0$) of the molecule, or with heavy molecules for which $\beta \ll 1\ \text{cm}^{-1}$.

The classical treatment of the modulation effect and the frequency tuning of γ-radiation resonances by the laser radiation considered above should describe correctly the qualitative aspect of the effect. The strict quantitative theory is naturally quantum mechanical. In the quantum theory the general wave function of the nucleus in the excited molecule will have oscillatory terms responsible for the additional components near the $\omega_{\text{nucl}}^{(0)}$ frequency. As a result, there arise the combination frequencies $\omega_{\text{nucl}}^{(m,n)}$ different from the central frequency $\omega_{\text{nucl}}^{(0)}$ by the frequencies of vibrational and rotational transitions. The results of the quantum-mechanical treatment of the effect considered will be presented later.

Narrow absorption resonances on the nuclear transition can be detected with a Mössbauer source of γ radiation using the same nuclei as in a molecular gas. In this case by tuning the dip frequency $\omega_{\text{nucl}}^{(0)}$ on the recoilless emission line of source frequency ω_γ one can register the absorption minimum. Similarly, by tuning the frequency $\omega_{\text{nucl}}^{(-1)}$ on the frequency ω_γ one can detect a narrow absorption peak. Since the resonant absorption coefficient for nuclear transitions in a low-pressure gas (0.01–0.1 Torr) is very small, then it is possible to observe narrow resonances in absorption through the change of the intensity of γ fluorescence of the gas. It is still more convenient to observe narrow nuclear resonances in the emission of the molecular gas with γ-active nuclei.

The method proposed enables us to fulfill several basic experiments. For example, by tuning the narrow resonance of γ radiation $\omega_{\text{nucl}}^{(+1)} = \omega_\gamma - \Delta_\gamma + \vec{k}_0 \cdot \vec{v}\omega_\gamma/\omega_0 + \omega_0$ in the vicinity of the line of the nuclear absorption ω_γ in a condensed target, one can accurately measure the phonon spectrum over the wing shape in the nuclear absorption line [6]. It is natural that in these experiments one can measure the recoil energies of nuclei with an accuracy inaccessible at present. Since the value of $\vec{k}_0 \cdot \vec{v}$ can be measured with a very high accuracy $\delta\Omega$ by measuring the detuning Ω of the frequency of the light wave with respect to the Doppler contour center ω_0, then the resonance frequency of γ radiation can change over with accuracy $\delta\omega_0/\omega_\gamma = \delta\Omega/\omega_0$. This value can reach 10^{-11}–10^{-13}. It enables absolute measurements of γ-quantum energy with accuracy $\omega_\gamma/\omega_0(10^{-11} - 10^{-13})$ which, in principle, can attain 10^{-8}. With this method one can connect the energy scales of optical and γ ranges with an accuracy of 10^{-8}. It is natural that the method suggested allows one to carry out γ spectroscopy of nuclei in the vicinity of nuclear transitions 10^{-5} with resolution 10^{-9}, inaccessible for present methods. Notice that this method is also suitable for transitions where the Mössbauer effect does not arise (for instance, for the γ-quantum energy much more than 100 keV).

References

1. *Letokhov V.S.* // Zh. Eksp. Teor. Fiz. Pis'ma Red. 1967. Vol. 6. P. 597 [JETP Lett. 1967. Vol. 6. P. 101]; *Lisitsyn V.N., Chebotayev V.P.* // Zh. Eksp. Teor. Fiz. 1968. Vol. 54. P. 419 [Sov. Phys. JETP. 1968. Vol. 27. P. 227]; Barger R.L., Hall J.L. // Phys. Rev. Lett. 1969. Vol. 22. P. 4.

2. *Letokhov V.S.* In: Proceedings of the Esfahan Conference on Fundamental and Applied Laser Physics / edited by M.S. Feld, J. Kurnit, A. Javan. New York: Academic, 1972; *Feld M.S.*, ibid.

3. *Wertheim G.K.* Mössbauer Effect. New York: Academic,1964.

4. *Herzberg G.* Molecular Spectra and Molecular Structure. N.J.: Van Nostrand, Princeton, 1950. 2nd ed. Vol. 1.

5. *Cyvin S.J.* Molecular Vibrations and Mean Square Amplitudes. Amsterdam: Elsevier Publishing Co., 1968.

6. *Visscher W.M.* // Ann. Phys. (New York). 1960. Vol. 9. P. 194.

ЛАЗЕРНЫЕ ФОТОСЕЛЕКТИВНЫЕ МНОГОФОТОННЫЕ ПРОЦЕССЫ И ЛАЗЕРНОЕ РАЗДЕЛЕНИЕ ИЗОТОПОВ

1. *Амбарцумян Р.В., Калинин В.Н., Летохов В.С.* Двухступенчатая селективная фотоионизация атомов рубидия лазерным излучением // Письма в ЖЭТФ. 1971. Т. 13 (6). С. 305–307.

2. *Ambartzumian R.V., Letokhov V.S.* Selective two-step (STS) photoionization of atoms and photodissociation of molecules by laser radiation // Appl. Opt. 1972. Vol. 11 (2). P. 354–358.

3. *Амбарцумян Р.В., Летохов В.С., Макаров Г.Н., Пурецкий А.А.* Лазерное разделение изотопов азота // Письма в ЖЭТФ. 1973. Т. 2. С. 91–94.

4. *Амбарцумян Р.В., Летохов В.С., Рябов Е.А., Чекалин Н.В.* Изотопически селективная химическая реакция молекул BC_{13} в сильном инфракрасном поле лазера // Письма в ЖЭТФ. 1974. Т. 20 (9). С. 597–600.

5. *Ambartzumian R.V., Chekalin N.V., Doljikov V.S., Letokhov V.S., Ryabov E.A.* The visible luminescence kinetics of BC_{13} in the field of a high-powerful CO_2 laser // Chem. Phys. Lett. 1974. Vol. 25 (4). P. 515–518.

6. *Амбарцумян Р.В., Горохов Ю.А., Летохов В.С., Макаров Г.Н.* Разделение изотопов серы с коэффициентом обогащения $>10^3$ при воздействии излучения CO_2-лазера на молекулуSF_6 // Письма в ЖЭТФ. 1975. Т. 21 (6). С. 375–378.

7. *Bagratashvili V.N., Doljikov V.S., Letokhov V.S., Makarov A.A., Maljavkin L.P., Ryabov E.A., Silkis E.G., Vainer Yu.G.* Stochastization limit of vibrational energy in SF_6 and CF_3I molecules at IR multiple photon excitation // Opt. Commun. 1981. Vol. 38 (1). P. 31–34.

8. *Makarov A.A., Petrova I.Yu., Ryabov E.A., Letokhov V.S.* Statistical inhomogeneous broadening of infrared and Raman transitions in highly vibrationally excited XY_6 molecules // J. Phys. Chem. A. 1998. Vol. 102. P. 1438–1449.

Письма в ЖЭТФ. 1971. Т. 13 (6). С. 305–307

ДВУХСТУПЕНЧАТАЯ СЕЛЕКТИВНАЯ ФОТОИОНИЗАЦИЯ АТОМОВ РУБИДИЯ ЛАЗЕРНЫМ ИЗЛУЧЕНИЕМ

Р.В. Амбарцумян, В.Н. Калинин, В.С. Летохов
Институт спектроскопии АН СССР

l. В настоящей работе сообщается о первом эксперименте по селективной двухступенчатой фотоионизации атомов (Rb) излучением двух лазеров, работающих на различных частотах. В двухступенчатой схеме фотоионизации излучение первого лазера переводит атомы (в данном эксперименте атомы Rb) из основного состояния в возбужденное. Одновременно атомы освещаются светом второго лазера, энергия кванта которого недостаточна для фотоионизации атомов из основного состояния, но достаточна для фотоионизации атомов с возбужденного уровня. Полученные результаты указывают на высокую селективность двухступенчатых процессов фотоионизации.

2. Схема экспериментальной установки приведена на рисунке. Рубиновый лазер с модуляцией добротности (*1*) накачивает лазер на красителе (*2*) (раствор DTTCJ в этиловом спирте). В качестве одного из зеркал лазера на красителе использовалась дифракционная решетка (600 штрих/мм), которая позволяла перестраивать частоту излучения лазера в широких пределах. Для резонансного возбуждения состояний $5^2P_{1/2}$ рубидия лазер настраивался на длину волны $\lambda_1 = 7947{,}6$ Å. Ширина спектра излучения применяемого лазера составляла 1,5–3 Å в зависимости от превышения мощности накачки над пороговым значением. Энергия излучения составляла 1,5–2 мДж. Расстояние между аксиальными модами лазера на красителе было несколько больше доплеровской ширины линий компонент тонкой структуры атомов Rb.

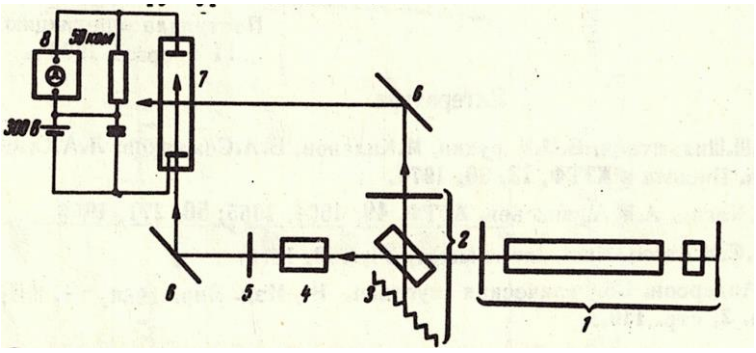


Рис. 1. Схема экспериментальной установки: *1* — рубиновый генератор с модулированной добротностью; *2* — лазер на красителе; *3* — дифракционная решетка; *4* — кристалл KDP; *5* — УФ фильтр; *6* — поворотные зеркала; *7* — ячейка с парами рубидия; *8* — осциллограф

Луч рубинового лазера далее направлялся на кристалл KDP для получения второй гармоники ($\lambda_2 = 3471$ Å), а излучение рубинового лазера отрезалось ультрафиолетовым фильтром. Энергия кванта второй гармоники (3,58 эВ) достаточна для фотоионизации возбужденных атомов Rb, но недостаточна для фотоионизации атомов из основного состояния ($E_{\text{ион}} = 4{,}12$ эВ). Энергия излучения второй гармоники составляла 1 мДж. Лучи второй гармоники и лазера на красителе сводились в одну и ту же область рубидиевой ячейки. Такая схема обеспечивала синхронность освещения паров Rb обоими импульсами. Освещаемый объем равнялся ~1 см^3, расстояние между электродами в ячейке 10 см.

Температура рубидиевой ячейки поддерживалась 116 ± 2ºС, что соответствует давлению паров 10^{-3} тор.

3. При освещении рубидиевой ячейки импульсным излучением с $\lambda_2 = 3471$ Å осциллографом регистрировался «темновой фототок», равный 1 мкА, величина которого не изменялась, если ячейка одновременно освещалась излучением лазера на красителе, длина волны которого не совпадала с линией поглощения паров Rb. Когда длина волны излучения лазера на красителе настраивалась на линию поглощения Rb, то фототок возрастал в 15–20 раз. Величина фототока примерно на порядок меньше предельного теоретического значения. Это расхождение можно объяснить: 1) небольшим запаздыванием сигнала лазера на красителе относительно сигнала второй гармоники, что связано с конечным временем развития генерации в лазере на красителе; 2) приближенным значением величины сечения фотоионизации из возбужденного состояния; 3) насыщением только части доплеровски уширенной линии атомов Rb излучением одной аксиальной моды лазера на красителе.

4. Двухступенчатая схема фотоионизации атомов лазерным излучением позволяет осуществлять селективную ионизацию различных атомов в газовой смеси, энергии ионизации которых практически совпадают, производить точные измерения сечений фотоионизации атомов из возбужденных состояний. По-видимому, высокую селективность можно получить также путем двухступенчатой фотодиссоциации молекул лазерным излучением. Эксперименты в данных направлениях ведутся в настоящее время.

Авторы считают своим приятным долгом поблагодарить академика Н.Г. Басова за поддержку работы, П.Г. Крюкова за предоставление отдельных элементов установки, а также В. М. Апатина за помощь в работе.

Appl. Opt. 1972. Vol. 11 (2). P. 354–358

SELECTIVE TWO-STEP (STS) PHOTOIONIZATION OF ATOMS AND PHOTODISSOCIATION OF MOLECULES BY LASER RADIATION

R.V. Ambartzumian and V.S. Letokhov
Institute of Spectroscopy of the Academy of Sciences USSR, Troitsk, Moscow, USSR

The general considerations for two-step photoionization of atoms and photodissociation of molecules using tunable laser sources are discussed. Experimental results are given for the (1) photoionization of rubidium vapor using a ruby-laser-pumped dye laser and a doubled ruby laser radiation, and (2) photodissociation of HCl using the Raman-shifted output and the fourth harmonic output of a tunable Nd-glass laser. The possibilities for other laser systems are also discussed.

I. Introduction

The recent achievements in tunable laser frequency control have made it possible to do systematic research on the selective action of laser radiation on matter. This problem has a unique significance for applications of coherent monochromatic light in photochemistry, biology, photosynthesis, and other sciences. The spectral response of the interaction may be used not only to determine the chemical composition of matter, but it may also be used to allow a selective reaction that could change the composition and properties of the material.

To obtain a selective action of light on matter it is necessary to observe three conditions: (1) high monochromaticity of the exciting light; (2) the selectivity of the primary process of light interaction with the matter (the existence of narrow nonoverlapping absorption lines); (3) conservation of the induced selectivity in successive physical and chemical processes.

The radiation from presently available lasers completely satisfies the first condition both in the visible and IR regions. The second condition is satisfied, for example, in the interaction of light with the discrete electronic and vibrational transitions of matter in the gaseous phase. Under special conditions it may also be obtained in condensed matter.

As far as the third condition is concerned, the selectivity obtained in the primary photochemical act may be easily lost through a number of processes and especially through collisional energy transfer between the molecules. Condition (3) may be easily fulfilled if the atoms or molecules are transformed in a stable or metastable state. This condition is achieved, for example, in the excitation of metastable states

of atoms (a well-known case is the $^3P_{0,1,2}$ state of mercury), but this requirement allows the investigation of only a very limited class of reactions. From this point of view the photoionization or photodissociation of atoms and molecules provides a great advantage, as the final state of the products is stable.

However, the elementary act of photoionization or photodissociation is not selective, and the second condition is not satisfied. From our point of view both conditions (2) and (3), may be satisfied in a more general way through the method of two-step photoionization or photodissociation.

The selective two-step (STS) photoionization or photodissociation process is carried out by two photons of different energies $\hbar\omega_1$ and $\hbar\omega_2$. The photon $\hbar\omega_1$ excites a certain state of the discrete energy spectrum belonging to an atom or molecule, and the photon $\hbar\omega_2$ produces the photoionization or photodissociation of the excited atoms or molecules. The energies of the photons satisfy the following conditions:

$$\hbar\omega_1 + \hbar\omega_2 > E_i, E_{phd} \quad (1)$$

$$\hbar\omega_2 < E_i, E_{phd} \quad (2)$$

where E_i is the photoionization energy of the atom from the ground state which is usually greater than the energy of dissociation of the molecule E_d, and E_{phd} is the photodissociation energy from the ground state. The first process (the process of excitation) is highly selective, and it contributes to the fulfillment of the second condition. As a result of the second step (photoionization or photodissociation) we get stable products, and thus the third condition is satisfied, too.

II. Two-Step Photoionization

A. General Discussion

The scheme of two-step photoionization is shown on Fig. 1. The selectivity of this process is determined by the width of the resonant transition $0 \rightarrow 1$, which, at low pressure, is equal to Doppler width $\Delta\omega_{dop}$. The maximum density of excited atoms on the first level is achieved when the $0 \rightarrow 1$ transition is saturated. The saturating power of homogeneously broadened line is given by

$$P_1 = \hbar\omega_1/\sigma_1 T_1 \quad (3)$$

where σ_1 is the cross section of the $0 - 1$ transition and T_1 is the lifetime of the particle on the upper level (in the absence of transitions from level 1 to the continuum).

The photoionization probability of the excited atom is given by

$$W_2 = \sigma_2 P_2/\hbar\omega_2, \quad (4)$$

where σ_2 is the photoionization cross section from the excited state 1, P_2 is the intensity of radiation at the frequency ω_2 in W/cm^2. To photoionize most of the excited particles it is necessary to have

$$W_2 \gtrsim \frac{1}{T_1} \tag{5}$$

from which, the required ratio between P_1 and P_2 is

$$\frac{P_2}{P_1} \gtrsim \frac{\sigma_1}{\sigma_2} \tag{6}$$

or $\omega_1 \approx \omega_2$. When we deal with allowed transitions in atoms in the visible, we have $\sigma_1 \simeq 10^{-9} - 10^{-11}$ cm^2 and the photoionization cross section $\sigma_2 \simeq 10^{-18} - 10^{-19}$ cm^2. Therefore, the ratio required should be about $P_2/P_1 \sim 10^7 - 10^{-10}$.

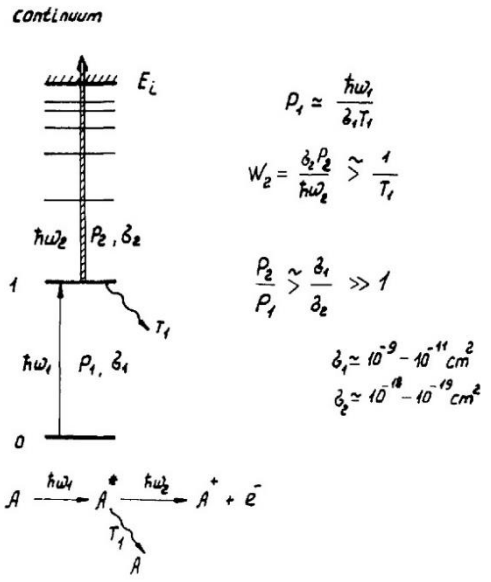


Fig. 1. Two-step photoionization scheme for atoms

To obtain the full utilization of the radiation at the both frequencies ω_1 and ω_2, various geometries for the experiments may be considered depending on the values of σ_1 and σ_2.

B. Experiment

Two-step photoionization experiments were carried out with Rb vapor [1]. An experimental ruby laser using the arrangement shown in Fig. 2 was used to pump a dye laser (DTTCI solution in ethyl alcohol). A grating with 600 lines/mm used as one of the mirrors made it possible to tune the frequency of radiation of the dye laser to $\lambda = 7947.6$ Å ($5^2P_{3/2}$ state of Rb). The width of the dye laser spectrum was $1.4 - 3$ Å depending on the intensity of the pump above threshold. The output energy was

$1.5 - 2 \times 10^{-3}$ J. The axial mode spacing of dye laser was 900 Hz, somewhat greater than the Doppler width of each hyperfine structure component of Rb atoms.

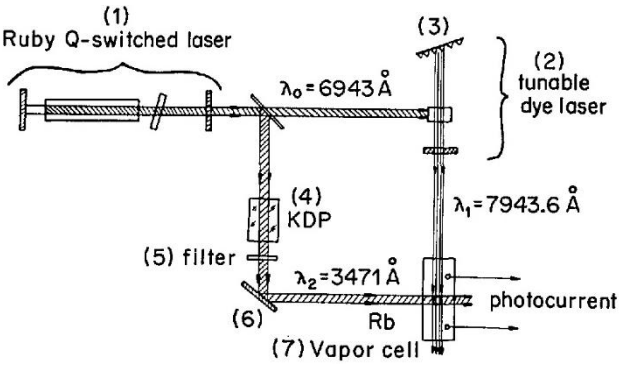


Fig. 2. Experimental setup for two-step photoionization of Rb atoms by laser radiation: (1) Q-switched ruby laser; (2) dye laser; (3) grating; (4) KDP crystal; (5) uv filter; (6) mirrors; (7) Rb vapor cell

The ruby laser beam which passed through the dye was also directed through a KDP crystal to obtain the second harmonic ($\lambda = 3471$ Å), and then the fundamental was filtered out. The quantum energy of the second harmonic (3.58 eV) is enough to photoionize the Rb atom from the excited state but not from the ground state ($E_i =$ 4.12 eV). The second harmonic energy was 10^{-3} J. The dye laser and second harmonic beams were directed to the same region of the Rb cell. The volume illuminated was about 1 cm3; the distance between the electrodes of the cell was 10 cm. The temperature of the cell was kept at 116 ± 2C°.

When the cell was illuminated by the $\lambda_2 = 3471$ Å beam only, the oscilloscope registered a dark current of 1 μA. This current did not change when the cell was simultaneously illuminated by dye laser radiation whose wavelength did not coincide with the absorption line of Rb. When the dye laser wavelength was tuned to the Rb vapor absorption line, the photocurrent increased to 15–20 μA and fluctuated between these figures although the amplitude of both lasers remained constant (Fig. 3). The value of the photocurrent was about one order of magnitude less than the value calculated from Eqs. (3) and (4). The discrepancy may be explained by (1) a small delay between the signals from the dye laser and the second harmonic associated with a finite start-oscillation time, (2) the approximate knowledge of the photoionization cross section value for the excited state; (3) saturation of a part of the Doppler broadened line of Rb by each axial mode of the dye laser (hole burning). [To saturate the whole Doppler-broadened line, multimode radiation covering the whole line or selfbroadening of the hole by a strong monochromatic field may be used. The necessary powers are: $P_1' = P_1 \Delta\omega_{dop}/\Gamma$ or $P_1'' = P_1(\Delta\omega_{dop}/\Gamma)^2$, where P_1 is the saturation power from Eq. (3)]. Using a laser with higher monochromaticity and better frequency control [2, 3] would allow us to excite and ionize the atoms through a selected hyperfine structure component.

It must be noted as well that by saturating the absorption on the $0 \rightarrow 1$ transition with a coherent standing wave, one can, in general, achieve some higher excitation degree even on one of several overlapping transitions. This is possible due to the formation of a Lamb dip when the laser frequency is tuned to the center of the selected component [4]. It is obvious that complete selectivity may not be achieved in this case.

C. Step Photoionization of Molecules

STS photoionization of molecules is more difficult than atoms because the photoionization potentials are very high ($E_i = 8—12$ eV, $\lambda_2 = 1400 - 1000$ Å) [5]. In this case the energy of each photon $\hbar\omega_1$, $\hbar\omega_2$ must be $4 - 6$ eV. Progress in uv lasers will allow us to investigate such processes in the near future. It must be noted that in the two-step case radiation with $\lambda > 1800$ Å may be used; this fact reduces the technical difficulties connected with the vacuum uv. The selectivity of the two-step photoionization of molecules may result in increasing the sensitivity of mass spectrographs.

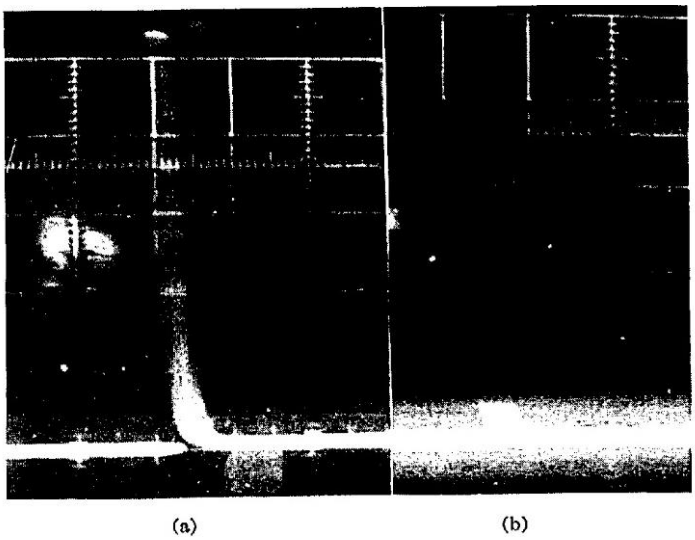


Fig. 3. Photocurrent pulses in resonance and out of resonance (100 μsec/div.)

III. STS photodissociation of molecules

A. General Notes

Various two-step photodissociation possibilities for molecules are shown schematically in Fig. 4. The selective photodissociation of molecules may be achieved by pumping on vibrational levels [Fig. 4(a)] and electronic levels [Fig. 4(b)] by photons with energy $\hbar\omega_1$. A photon with energy $\hbar\omega_2$ may also cause transitions in the molecule to a term with predissociation [Fig. 4(c)].

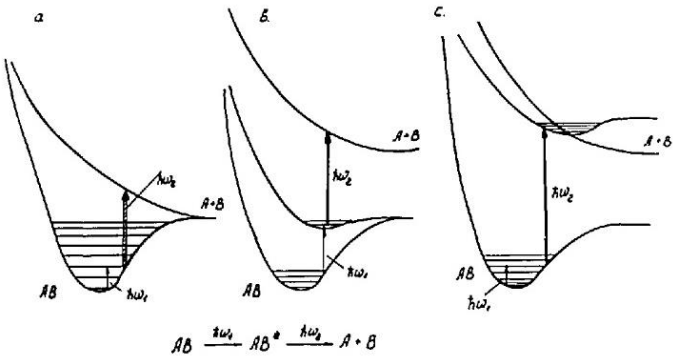


Fig. 4. Step photodissociation scheme for molecules: (*a*) excitation of vibrational level; (*b*) electronic term excitation; (*c*) photodissociation through predissociation

The intensities necessary for excitation and photodissociation of molecules are also given by Eqs. (3)–(6) with some differences that are of great importance.

When pumping on the low-lying vibrational levels the selectivity is limited by the thermal population of vibrational levels. This leads to the condition,

$$\hbar\omega_1 \gg kT. \tag{7}$$

For this reason, it is better to excite more energetic levels. This may be done by overtone pumping of complex vibrations of molecules and by multistep pumping of a high-lying level by a number of frequencies.

(1) The continuum spectrum that leads to photodissociation usually has a very wide edge. If the characteristic width of the long-wavelength wing of the continuous absorption is $\Delta\omega_{cw}$, the value $\hbar\omega_1$ should satisfy

$$\hbar\omega_1 > \hbar\Delta\omega_{cw}. \tag{8}$$

(2) Because of the Boltzmann distribution over the rotational levels of the ground vibrational state ($v' = 0$), the monochromatic wave excites molecules from one rotational sublevel. If pulse duration τ_p of frequency ω_1 is shorter than the collisional rotational relaxation time τ_{rot}, we have

$$\tau_p \ll \tau_{rot} = Z_{rot}/N_0 V_0 \sigma_0, \tag{9}$$

where N_0 is the molecule density, V_0 is the mean velocity of the molecules, σ_0 is the gas-kinetic collisional cross section, Z_{rot} is the number of collisions that is necessary to establish the equilibrium. Under these conditions only a small fraction of the molecules is excited (10^{-2}—10^{-3}). To obtain a higher density of excited molecules the pumping might be done faster than the rotational relaxation time,

$$\tau_p \gg \tau_{rot}. \tag{10}$$

In this case it is possible to obtain half of the molecules in the excited state. To increase the relaxation rate some type of buffer gas might be added so that the collisions between the buffer gas and light-absorbing molecules do not decrease the selectivity. Measures must be taken against nonselective thermal dissociation under high level pumping of the molecules at high pressures [6, 7].

B. Experiment

To obtain the two-step photodissociation case shown in Fig. 4(a), it is necessary to illuminate the molecules by two synchronized pulses, one in the ir and the other in the UV with variable wavelength. Of the now-available lasers Nd-glass is the most convenient for such experiments; the output wavelength may be tuned about 200 cm^{-1}, transformed into ir regions up to 2 μm by means of stimulated Raman scattering and also into the UV region up to 2500 Å by obtaining the second, third, or fourth harmonic of the laser radiation. It is possible to pump the overtones of simple molecules such as HF, HCl, HBr, HI, and also a number of more complex molecules.

The experimental Nd-glass laser constructed for the investigation of STS photodissociation of molecules is shown on Fig. 5. It consists of a variable wavelength oscillator whose output is split into two channels; one is the Raman laser channel that transfers the fundamental laser radiation into the IR, and the other channel is used to generate Nd-glass laser harmonics.

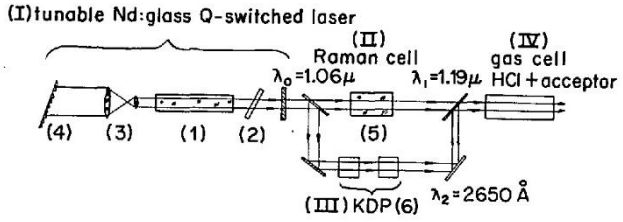


Fig. 5. Experimental setup of step photodissociation of HCl molecules: I. Nd glass Q-switched laser with variable wavelength: (1) laser rod, (2) saturable dye, (3) telescope, (4) grating; II. The laser radiation conversion into the ir (5)-pididine); III. The laser frequency conversion in the uv channel (6) amplifier and KDP crystal; IV. HCl + NO cell

The power at 2650 Å was 1 MW. Tuning the Nd-laser frequency by 200 cm^{-1} made it possible to obtain selective excitation of $v'' = 3$ state of the HCl molecule over the rotational-vibrational transitions $R(2) — R(5)$, $v' = 0 \rightarrow v'' = 3$. Changing piridine to other Raman-active media should allow pumping overtones of other molecules. Usually the absorption of molecules at the overtones is small, and long cells are required [8].

The continuous photoabsorption of HCl begins at 2500 Å [9]. For the molecules in the state $v'' = 3$ the photoabsorption edge is displaced to 3200 Å. The photodissociation cross section of HCl is $\sigma_2 \simeq 10^{-19}$ cm^2, and a pulse with an energy of $E_2 \simeq 5$ J/cm^2 is required to photodissociate all the excited molecules. The laser described above gave $E_2 \simeq 5 \times 10^{-2}$ J/cm2 and one pulse photodissociates 10–2 part of the excited molecules. Focusing the uv and ir radiation may increase this ratio.

To detect the photodissociation of HCl the cell is filled with an excess of NO gas, which reacts with Cl and produces NOCl.

IV. Possibilities of Other Laser Systems

In the experiments described above only one Q-switched laser was used (ruby in Sec. II, Nd-glass in Sec. Ill) with frequency conversion in two channels. Generally, it is possible to use two different types of lasers in synchronism.

Systematic investigation of STS processes of photoionization and photodissociation may be achieved if lasers of two types are available: (1) lasers with moderate powers and variable wavelength in the ir for selective excitation of vibrations of molecules and in the visible for electronic level excitation of atoms and molecules; (2) lasers in the UV with relatively high power density. E_2, such that $E_2 = \hbar\omega_2/\sigma_{phd}$ or $\hbar\omega_2/\sigma_{phi}$, where σ_{phd} and σ_{phi} are photodissociation and photoionization cross sections (usually $10^{-19} - 10^{-20}$ cm^2). Wavelength tuning is not required.

For lasers of the first type the following may be used (a) spinflip lasers, which, in general, may cover the range between 5 μm and 15 μm 10,11; (b) gaseous high pressure lasers when the rotational lines overlap and form very wide amplification bands covering the $2.5 - 12$- μm range with high power level; (c) Raman lasers with Nd-glass pumping that permits coverage of the $1.2 - 2.5$-μm range; (d) organic dye lasers with frequency control2,3 which covers the range from 0.4 μm to 1.2 μm; and others.

For lasers of the second type, harmonics of ruby (second harmonic 3.6 eV) and Nd glass laser (third, fourth harmonics-3.5 eV and 4.7 eV)12 might be used as well as the nitrogen laser at $\lambda_2 = 3371$ Å (3.7 eV). The progress now achieved in vacuum uv lasers13,14 may enlarge the number of powerful UV lasers.

V. Discussion

The two-step photoionization and photodissociation processes are characterized by extremely high selectivity and may be used for selective photocatalyses of chemical reactions by laser radiation.

Up to this moment only the selective photocatalysis utilizing one frequency of monochromatic light (in our terms, a one-step process) has been discussed in the literature. A number of investigators have studied reactions between excited atoms of Hg in the metastable state of Hg [15]. Schawlow and his colleagues have investigated selective photocatalysis of electronically excited Br_2 molecules [16]. Recently a selective reaction of vibrationally excited CH_3OH has been obtained [17]. These experiments indicate the generally low yield of one-step photocatalysis. The case of Hg atoms may be considered to be unique. In Ref. 16 it was impossible to fulfill the third condition of selectivity (see Sec. I). In the case of vibrational excitation [17], it was necessary to have a large difference in vibrational frequencies to obtain the needed selectivity in the mixture of gases. We consider the two-step processes to be much more generally applicable for selective photochemical reactions of atoms and molecules.

References

1. *Ambartzumian R.V., Kalinin V.P., Letokhov V.S.* // ZhETF Pis. Red. 1971. Vol. 13. P. 305 [JETP Lett. 1971. Vol. 13. P. 217].

2. *Bradley D.J., Durrent S.J.F., Gate G.M., Moore M., Smith P.D.* // IEEE J. Quantum Electron. 1968. QE-4. P. 707.

3. *Walter H., Hall J.L.* // Appl. Phys. Lett. 1970. Vol. 17. P. 239.

4. *Letokhov V.S.* // Comments on Atomic and Molecular Physics 2. 1971. Vol. 6. P. 181.

5. *Vilesov F.J.* // Usp. Phys. Nauk. 1964. Vol. 81. P. 669 [Sov. Phys. Usp. 1964. Vol. 6. P. 888].

6. *Borde C., Henry A., Henry C.* // Compt. Rend. B. 1968. Vol. 262. P. 1339; B. 1967. Vol. 263. P. 619.

7. *Karlov N.V., Petrov U.J., Prokhorov A.M., Stelmach O.M.* // ZhETF Pis. Red. 1970. Vol. 11. P. 220 [JETP Lett. 1970. Vol. 11. P. 135].

8. *Benedict W., Hecman R., Moore G.E., Silverman S.* // J. Chem. Phys. 1957. Vol. 26. P. 1671.

9. *Calvert J.G., Pitts Jr. J.N.* Photochemistry. New York: Wiley, 1966.

10. *Patel C.K.N., Shaw E.D.* // Phys. Rev. Lett. 1970. Vol. 24. P. 451; *Patel C.K.N., Shaw E.D., Kerl R.J.* // Phys. Rev. Lett. 1970. No. 25. P. 8.

11. *Mooradian J., Brueck S.R.J., Bloom F.S.*//Appl. Phys. Lett. 1970. Vol.17. P.481.

12. *Akhmanov S.A., Kovrigin A.J., Piskarascas A.S., Hohloff R.V.* // ZhETF Pis. Red. 1965. Vol. 2. P. 223 [JETP Lett. 1965. Vol. 2. P. 141].

13. *Basov N.G., Bogdankevich O.V., Danilechev V.A., Kashnikov G.N., Kerimov O.M. and Lantzov H.P.* // Phys. Short Commun. Fiz Inst. Akad. Nauk. 1970. No. 7. P. 63; *Basov N.G., Danilechev V.A., Popov J.M.*//Quant. Electron. 1970.Vol. 1.

14. *Hodgson R.T.* // Phys. Rev. Lett. 1970. Vol. 25. P. 494.

15. *Gunning H.E., Straust O.* Advances in Photochemistry / G.S. Hammond and J.N. Pitts Jr., Ed. New York: Interscience, 1963. Vol. 1. P. 209.

16. *Tiffany W.B., Moos H.W., Schawlow A.L.* // Science. 1967. Vol. 157. P. 40.

17. *Mayer S.W., Kwok M.A., Gross R.W.F. and Spencer D.J.* // Appl. Phys. Lett. 1970. Vol. 17. P. 516.

Письма в ЖЭТФ. 1973. Т. 17 (2). 91–94

ЛАЗЕРНОЕ РАЗДЕЛЕНИЕ ИЗОТОПОВ АЗОТА

Р.В. Амбарцумян, В.С. Летохов, Г.Н. Макаров, А.А. Пурецкий
Институт спектроскопии АН СССР

1. В настоящей статье сообщается о первом высокоэффективном разделении изотопов методом селективной двухступенчатой фотодиссоциации молекул. В описываемых экспериментах были разделены изотопы азота ^{14}N и ^{15}N при фотодиссоциации молекул аммиака $^{14}NH_3$ и $^{15}NH_3$. Метод двухступенчатой фотодиссоциации молекул был предложен [1] как способ селективного воздействия излучения на вещество и заключается в следующем. Монохроматическое излучение частоты ν_1 селективно возбуждает колебательный переход молекул только одного изотопического состава. Одновременно молекулы освещаются светом частоты ν_2, энергия кванта которого достаточна для фотодиссоциации только колебательно возбужденных молекул.

Схема эксперимента представлена на рис. 1. Источником монохроматического ИК-излучения частоты ν_1 (947,74 $см^{-1}$) служил импульсный CO_2-лазер с поперечным разрядом (1). Энергия импульса излучения составляла 60 мдж, длительность импульса по полувысоте — 300 нс. Источником УФ-излучения (2) на частоте ν_2 (45351 $см^{-1}$) служил разряд в воздухе (C = 0,03 мкф, U = 20 кВ). Длительность импульса УФ-излучения составляла 400 нсек по основанию. Синхронизация лазерного импульса с импульсом УФ-излучения осуществлялась путем поджига искрового промежутка частью (~30%) энергии лазерного луча, сфокусированного на один из электродов. Для полного устранения из сплошного спектра излучения искры ультрафиолетового излучения, которое могло поглощаться невозбужденными молекулами NH_3 в исследуемой кювете, перед ней устанавливался поглощающий аммиачный фильтр (3). Фильтр представлял собой кювету с окнами из кварца длиной 7,5 см, наполненную аммиаком до давления 1 атм. На частотах ν_1 и ν_2 облучалась кювета (4), которая заполнялась смесью аммиака $^{14}NH_3$ и $^{15}NH_3$, в соотношении 1:1 при суммарном давлении смеси 20 тор.

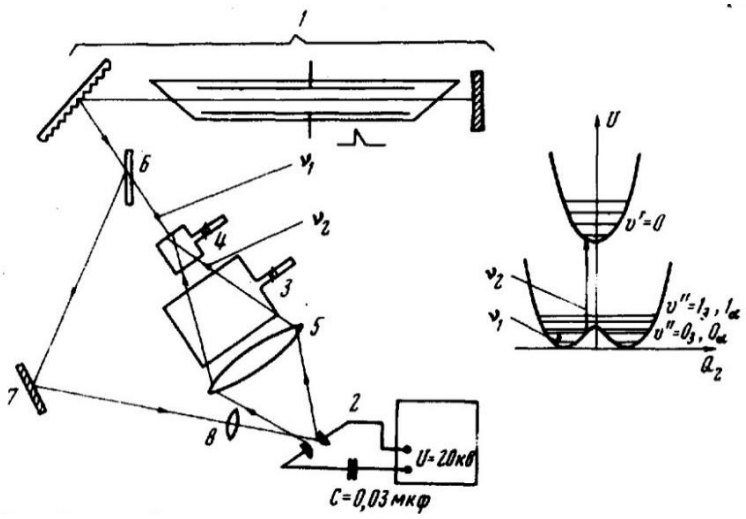


Рис. 1. Схема экспериментальной установки: (*1*) — импульсный CO_2-лазер с перестраиваемой частотой излучения, (*2*) — источник УФ- излучения, (*3*) — поглощающий аммиачный фильтр, (*4*) — кювета с исследуемым газом, (*5*) — конденсатор, (*6*) — плоскопараллельная пластинка, (*7*) — поворотное зеркало, (*8*) — фокусирующая линза

2. Как показано в [2], при накачке аммиака CO_2-лазером в электронно-колебательном спектре поглощения NH_3 возникает новая линия, соответствующая переходу $\nu' = 0 \leftarrow \nu'' = 1$. ν'', ν' — колебательные числа основного и возбужденного электронного состояния соответственно. Частота новой линии поглощения равна 45351 см$^{-1}$. В описываемых экспериментах населенность первого колебательного уровня $\nu'' = 1$ основного электронного состояния молекулы $^{15}NH_3$ в момент действия лазерного импульса составляла 35 ± 5% [3]. При такой заселенности оптическая плотность аммиака в кювете (4) на новой линии поглощения составляла 0,8 (длина кюветы 3 см). УФ-излучение, проходящее через фильтр, поглощалось на новой линии поглощения, возникающей в электронно-колебательном спектре поглощения аммиака при накачке CO_2-лазером, и приводило к диссоциации колебательно возбужденных молекул.

Неселективный фотолиз аммиака хорошо изучен [4]. При этом происходит следующий цикл реакций:

$$\begin{gathered} NH_3 + h\nu \rightarrow NH_2 + H, \\ NH_2 + NH_2 \rightarrow N_2H_4, \\ N_2H_4 + \mathrm{H} \rightarrow N_2H_3 + H_2, \\ 2N_2H_3 \rightarrow 2NH_3 + N_2. \end{gathered} \qquad (1)$$

Из (1) видно, что одним из конечных продуктов является азот.

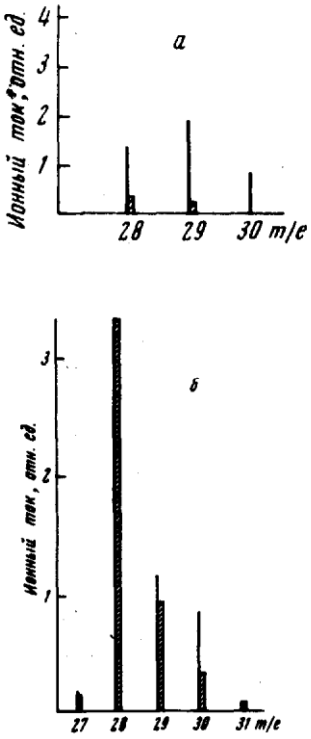


Рис. 2. Масс-спектры N_2 при: *а*) неселективной фотодиссоциации смеси, *б*) селективной двухступенчатой фотодиссоциации смеси $^{14}NH_3$ + $^{15}NH_3$. Заштрихованные линии соответствуют масс-спектрам смеси до облучения (фоновые линии)

Определим степень обогащения в продуктах реакции (в данном случае N_2) избранным изотопом (^{15}N) отношением полного числа атомов ^{15}N к ^{14}N:

$$S_{\text{обог}} = \frac{2[^{15}N_2] + [^{14}N\,^{15}N]}{2[^{14}N_2] + [^{14}N\,^{15}N]} = \frac{2I_{30} + I_{29}}{2I_{28} + I_{29}}, \tag{2}$$

где скобки обозначают концентрации указанных в них молекул, которые пропорциональны интенсивности соответствующих линий в масс-спектре. В данном случае отношение интенсивностей линий в масс-спектре из-за статистики столкновений всегда удовлетворяют соотношению:

$$\frac{I_{30}}{I_{29}} = \frac{1}{4}\frac{I_{29}}{I_{28}}. \tag{3}$$

Следовательно, степень обогащения связана с экспериментально измеряемым отношением интенсивностей линий I_{30} и I_{29} соотношением:

$$S_{\text{обог}} = \left(2\frac{I_{30}}{I_{29}} + 1\right)\left(\frac{1}{2}\frac{I_{29}}{I_{30}} + 1\right)^{-1}. \tag{4}$$

3. Было проведено два типа экспериментов: а) во-первых, исследовалось отношение интенсивностей линий а. е. м. 29 и 30 при неселективной фотодиссоциации смеси изотопов аммиака (без лазерного облучения и без фильтра (3)). Как и ожидалось, отношение интенсивностей с точностью до ошибки измерений (±5%) оказалось равным $I_{29}/\,I_{30} = 2$ (рис. 2*а*).

Проводилась селективная двухступенчатая фотодиссоциация смеси молекул $^{14}NH_3$ и $^{15}NH_3$, то есть производилась накачка молекулы $^{15}NH_3$ лазерным излучением и ее фотодиссоциация из колебательно-возбужденного состояния ($\nu'' = 1$). Отношение интенсивности линий (за вычетом постоянного с точностью до 5% фона, указанного на рис. 2 заштрихованной линией) оказалось равным $I_{29}/\,I_{30} = 0{,}5 \pm 0{,}05$ (рис. 2*б*). Достигнутая степень обогащения согласно (5), составляет $S_{\text{обог}} = 4$, то есть молекулярный азот содержит 80% атомов ^{15}N и 20% атомов ^{14}N при равной их концентрации в исходной смеси молекул аммиака.

Число фотодиссоциированных молекул $^{15}NH_3$ определяется в основном интенсивностью УФ источника и временем облучения. В наших экспериментах диссоциировано несколько % молекул аммиака. Сохранение селективности в химических вторичных реакциях служит еще одним подтверждением, что фотодиссоциация аммиака происходит по схеме, предложенной в [4].

Литература

1. *Ambartzumian R.V., Letokhov V.S.* // IREE. J.Quant. Electr. 1971. QE-7. P. 305; Appl. Optics. 1972. Vol. 11. P. 354.

2. *Амбарцумян Р.В., Летохов В.С., Макаров Г.Н., Пурецкий А.А.* // Письма в ЖЭТФ. 1972. Т. 15. С. 709.

3. *Ambartzumian R.V., Letokhov V.S., Makarov G.N., Puretzki A.A.* // Chem. Phys. Lett. 1972. Vol. 16, 252.

4. *McNesby J.R., Okabe H.* Advances in Photochemistry. Vol. 3. New York, 1964.

Письма в ЖЭТФ. 1974. Т. 20 (9). С. 597–600

ИЗОТОПИЧЕСКИ СЕЛЕКТИВНАЯ ХИМИЧЕСКАЯ РЕАКЦИЯ МОЛЕКУЛ $BC1_3$ В СИЛЬНОМ ИНФРАКРАСНОМ ПОЛЕ ЛАЗЕРА

Р.В. Амбарцумян, В.С. Летохов, Е.А. Рябов, Н.В. Чекалин
Институт спектроскопии АН СССР

Сообщается о первом наблюдении изотопически селективной химической реакции в смеси газов под действием мощного импульса инфракрасного излучения.

1. Как известно, при фокусировке импульса мощного ИК резонансного излучения поглощающем газе при мощности порядка 10^9 Вт/см^2 происходит диссоциация молекул, сопровождающаяся видимой люминесценцией продуктов диссоциации [1, 2]. В работе [2] было обнаружено, что люминесценция возникает без задержки относительно импульса лазера. Более детальное исследование, проведенное независимо в работах [3] (на молекуле BCl_3) и [4] (на молекуле SiF_4), показало, что существуют две четкие фазы в люминесценции: быстрая фаза, связанная с бесстолкновительной диссоциацией изолированных молекул в мощном ИК поле, и запаздывающая фаза, которая следует после окончания лазерного импульса и имеет, по-видимому, столкновительное происхождение.

Обнаруженный эффект мгновенной бесстолкновительной диссоциации молекул в сильном инфракрасном лазерном поле [2–4] открыл еще один путь лазерного стимулирования химических реакций, которые, в принципе, могли быть изотопически селективны при хорошо разрешенном изотопическом сдвиге в ИК спектре. В настоящей статье описываются эксперименты, впервые прямо доказывающие это предположение. Одновременно описываемый эксперимент является первым успешным разделением изотопов в естественной смеси под действием ИК излучения.

2. В эксперименте использовался импульсный CO_2-лазер атмосферного давления с энергией в импульсе до 0,5 Дж при длительности импульса 100 нс. С помощью короткофокусной линзы (f = 5 см) излучение лазера фокусировалось в кювету с газом. Излучение люминесценции из области фокуса через боковое окно с полуторакратным увеличением проектировалось на входную щель монохроматора МДР-2, с помощью которого осуществлялась запись спектров испускания радикалов и молекул, возникающих в результате диссоциации и последующих химических реакций. Полученные спектры использовались для идентификации продуктов химических реакций.

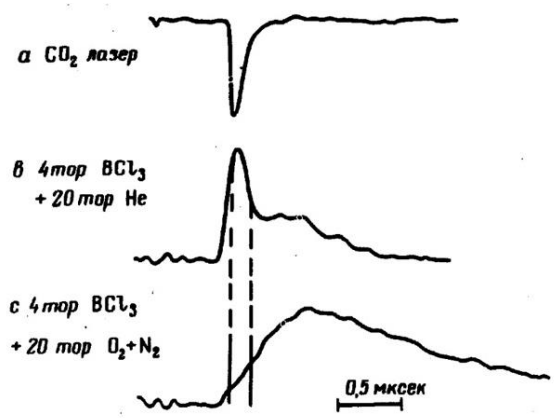


Рис. 1. Люминесценция в чистом BCl_3 и в BCl_3 в смеси с $O_2 + N_2$: *a* — импульс CO_2-лазера, *b* — импульс свечения в BCl_3, *c* — импульс свечения BO

Эксперимент проводился с естественной смесью молекул $B_{10}C_{l3}$ и B_{11} C_{l3} ($B_{10} : B_{11} = 1 : 4{,}32$). Спектр мгновенной фазы люминесценции в чистом BC_{l3} лежит в видимой области вплоть до 4400 Å и с точностью до 15 Å оказался сплошным. При добавлении в BC_{l3} смеси $O_2 + N_2$ ($O_2 : N_2 = 1{:}4$) в спектре возникала интенсивная система полос, которая была идентифицирована как α-полоса радикала BO [5]. Кроме того, происходило резкое изменение формы импульса люминесценции. На рис. 1 приведены импульсы люминесценции в чистом BC_{l3} и в смеси BC_{l3} с $O_2 + N_2$. Передний фронт импульса во втором случае соответствует скорости реакции образования BO. Использованный в эксперименте CO_2-лазер настраивался на полосу поглощения колебания ν3, либо молекулы $B_{11}C_{l3}$, либо $B_{10}C_{l3}$. Для исследования селективности бесстолкновительной диссоциации трихлорида бора и последующей реакции продуктов диссоциации с кислородом использовался сдвиг в спектре $B_{10}O$ и $B_{11}O$. Известно [5], что изотопный сдвиг между R-ветвями перехода (0,2) $2\pi 1/2 \rightarrow 2\sum$ радикалов $B_{10}O$ и $B_{11}O$ достигает 30 Å. Поэтому в эксперименте анализировался именно этот участок спектра в двух случаях: при настройке на полосу поглощения $B_{11}C_{l3}$ (линия P(26) 938,7 $см^{-1}$ CO_2-лазера) и на полосу $B_{10}C_{l3}$ (R (24) 978,5 $см^{-1}$), причем система регистрации выделяла для измерения спектра из импульса свечения BO временной интервал 150 нсек, соответствующий мгновенной фазе люминесценции в чистом BC_{l3} (рис. 1). На рис. 2 представлен полученный спектр в этих двух случаях. Давление BC_{l3} — 4 тор, $O_2 + N_2$ — 20 тор. Разрешение было не хуже 8 Å. Видно, что при возбуждении $B_{11}C_{l3}$ в основном получается $B1_{10}$, при возбуждении $B_{10}C_{l3}$ — получается $B_{10}O$. Таким образом, бесстолкновительная диссоциация молекул в мощном резонансном ИК поле является процессом селективным (по крайней мере, в случае BCl_3, когда изотопический сдвиг в полосах поглощения двух различных молекул больше 40 $см^{-1}$).

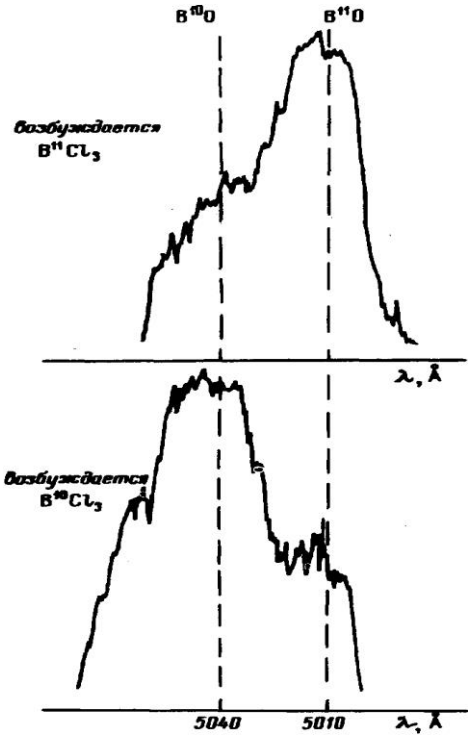


Рис. 2. Спектр испускания $B^{10}O$ и $B^{11}O$ на переходе (0,2) $^2\pi_{1/2} \rightarrow {}^2\Sigma$ при возбуждении $B^{11}Cl_3$ (вверху) и $B^{10}Cl_3$ (внизу)

Полученные результаты открывают еще один путь разделения изотопов при воздействии лазерного излучения на молекулы, существенно отличающийся от ранее предложенных и осуществленных методов двухступенчатой фотодиссоциации [6] и фотопредиссоциации [7].

Авторы выражают благодарность Е.Л. Михайлову и В.С. Должикову за помощь в подготовке эксперимента.

Литература

1. *Isenor N.R., Richardson M.* // Appl. Phys. Lett. 1971. Vol. 18. P. 225.

2. *Летохов В.С., Рябов Е.А., Туманов О.А.* // ЖЭТФ. 1972. Т. 63. С. 2025.

3. *Ambartzumian R.V., Doljikov V.S., Letokhov V.S., Ryabov E.A., Chekalin N.V.* // Chem. Phys. Lett. 1974. Vol. 25. P. 515.

4. *Isenor N.K., Merchant V., Hallsworth R.S., Richardson M.C.* // Canad. J. Phys. 1973. Vol. 51. P. 1281.

5. *Jenkins F.A., McKellar A.* // Phys. Rev. 1932. Vol. 42. P. 464.

6. *Ambartzumian R.V., Letokhov V.S.* // IEEE Journ. Quant. Electr. 1971. Vol. QE-7. P. 305; Appl. Optics. 1972. Vol. 11. P. 354.; *Амбарцумян Р.В., Летохов В.С., Макаров Г.Н., Пурецкий А.А.* // Письма в ЖЭТФ. 1973. Т. 17. С. 91.

7. *Letokhov V.S.* // Chem. Phys. Lett. 1972. Vol. 15. P. 221; *Yeung E.S., Moore C.B.* Appl. Phys. Lett. 1972. Vol. 21. P. 109.

Chem. Phys. Lett. 1974. Vol. 25 (4). P. 515–518

THE VISIBLE LUMINESCENCE KINETICS OF BCL_3 IN THE FIELD OF A HIGH-POWERFUL CO_2 LASER

R.V. Ambartzumian, N.V. Chekalin, V.S. Doljikov, V.S. Letokhov and E. A. Ryabov
Institute of Spectroscopy, Academy of Sciences USSR, Moscow, USSR

The visible luminescence in BCl_3 in the field of a high-power short-pulse CO_2 laser is studied. It is shown that there are two-time regions for the luminescence: the instantaneous, which arises simultaneously with the laser pulse, and a delayed luminescence, which is pressure dependent. Possible mechanisms which cause both types of luminescence are discussed.

1. Introduction

The visible luminescence of molecular gases in the field of cw CO_2 laser radiation has been studied by Bordé et al. [1], Losev et al. [2] and Karlov et al. [3]. This phenomenon was explained by simple heating of the absorbing gas [1, 2]. Special attention was paid to the possibility of the dissociation of irradiated molecules from high lying vibrational levels due to population by V–V transfer process in $BC1_3$ [3].

The visible luminescence was also observed in a number of molecular gases in the field of TEA CO_2 laser radiation at a power level insufficient to produce optical breakdown [4, 5]. This phenomenon was examined in more detail and it was shown that the luminescence of molecules cannot be explained by the dissociation of molecules from high lying vibrational levels, which are populated by V-V transfer process [6].

Some new results are presented here on the visible luminescence kinetics in BC_{13} at low pressures caused by short-pulse high-power TEA laser radiation. It is shown that there are two distinct time regions of luminescence — "instantaneous" (the delay is about 2×10^{-8} s) and "delayed" luminescence (the delay of which is pressure dependent).

The "instantaneous" luminescence was observed at pressures down to 0.05 torr. This rejects the V–V collisional transfer mechanism for an interpretation of instantaneous luminescence. Thus there is some other mechanism of resonant dissociation of BC_{l3} molecules caused only by the radiation field (10^9 W/cm^2), which is in resonance with the vibrational transition of molecule. The delayed luminescence arises after the laser pulse (at higher pressures and lower power levels).

2. Experimental

The laser used in the experiments was a TEA atmospheric pressure CO_2 laser analogous to that described in refs. [7, 8]. The uniform discharge was obtained between two profiled electrodes 40 cm long, and the separation of the electrodes was 2 cm. A high voltage (38 kV) pulse was applied to the electrodes. The laser worked with a mixture of CO_2:N_2:He (4:1:10) at a pressure of 1 atm. This provided a radiation pulse without any noticeable tail. The full duration of the pulse was 400 ns (150 ns at half maximum). The energy of the pulse was 0.3 J. A grating was used in the laser cavity to tune the laser frequency to the P(14) line of the 10.6 μ band of the CO_2 laser which is well absorbed by BC_{13} [9].

The detecting system included a photon drag detector for the CO_2 laser radiation and a photomultiplier for detection of visible luminescence. The time constants of both channels was slightly less than 40 ns. The photomultiplier introduced an internal delay which was 90 ns.

The CO_2 laser radiation (beam diameter 15 mm) was focused in a cell with BC_{13} by an. NaCl lens with $f = 40$ mm. The focal spot of the lens was 0.2 mm.

The visible luminescence which was investigated in this work strongly differed from optical breakdown in BC_{13}. The light intensity from the breakdown was more than 3 orders of magnitude greater compared to the luminescence. The dimensions of the luminescence region varied with pressure. For example, the length of the region varied from 5 to 20 mm under various conditions.

Magnified by a factor of 5 by a lens, the region of luminescence was projected onto a photomultiplier cathode. Insertion of a movable iris before the photocathode allowed us to detect the signal from various points in the luminous region.

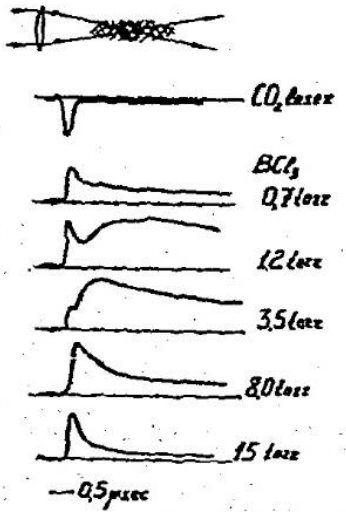


Fig. 1. Pulses of visible luminescence in $BC1_3$ at various pressures. The geometry of the experiment is shown; the squares denote the iris which confines the region of luminescence from: which the signals are picked up

The luminescence in pure BC_{l3} was observed in the pressure regions of between 0.05 and 20 torr. Typical pulses of the luminescence signal from the focal region at various pressures are shown in fig. 1 (the vertical scale is not the same for different pulses). The luminescence arises simultaneously with the laser pulse. At pressures less than 1 torr the pulse exhibits only one maximum. At low pressures the rise time of the instantaneous luminescence is independent of the pressure of BC_{13} in the cell. It was also observed that the instantaneous luminescence has a very well pronounced threshold. Under the threshold value the rise time and the delay of the luminescence pulse depends on pressure and on the laser power. As the pressure increases, a second maximum arises. The delay between these two peaks, τ, decreases with pressure. At a pressure of 6 torr the peaks cannot be resolved.

To understand the nature of these two maxima in the luminescence the dependence of the delay of the second pulse τ versus pressure was obtained.

Fig. 2 presents experimental results on the dependence of the value of the delay as a function of pressure in the case when the luminescence was registered from the focal region. It is seen that in the region of pressures $1 - 10$ torr the product of $p\tau$ is equal to 2.3 μs torr. The measurements were made at the same power level and with the same laser pulse form.

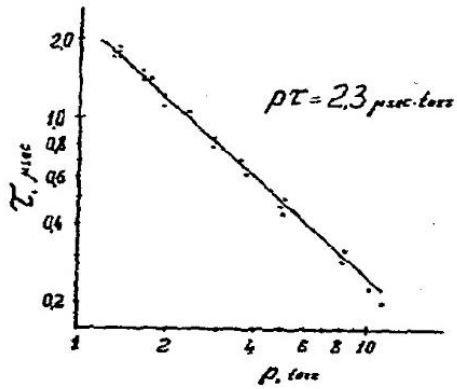


Fig. 2. The plot of delay time τ between two pulses in luminescence signal versus pressure

The form of the pulse changes significantly when the luminescence signal is taken from various other parts of the luminous region. This is clearly seen from fig. 3, where the signals from two different regions are shown: from the focal region (A) and out-of-focus region (B). In case (B), the luminescence maximum was always delayed $1 - 2$ μs after the laser pulse. The instantaneous luminescence is observed only from the focal region.

To ensure that the instantaneous luminescence is connected with the field in the focal region, the laser radiation was focused by a lens so that the focus of the lens was out of the cell. In this case the smallest laser beam diameter in the cell was 6 mm and the field intensity was 10^3 times lower compared with the field at the focus. The luminescence signal in this case is shown in fig. 4. The instantaneous luminescence is absent and the pulse begins $0.7 - 0.8$ μs after the laser pulse.

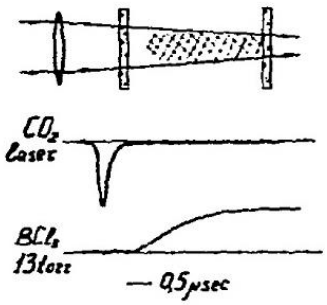


Fig. 4. The luminescence in BCl_3 when the focus of the lens was out of the cell. When a buffer gas (He) is added to BC_{13} the form of the pulses changes significantly. The second peak diminishes while the amplitude of the first changes insignificantly. This is clearly seen in fig. 5 where the pulses in pure BC_{13} at the same partial pressures are also shown

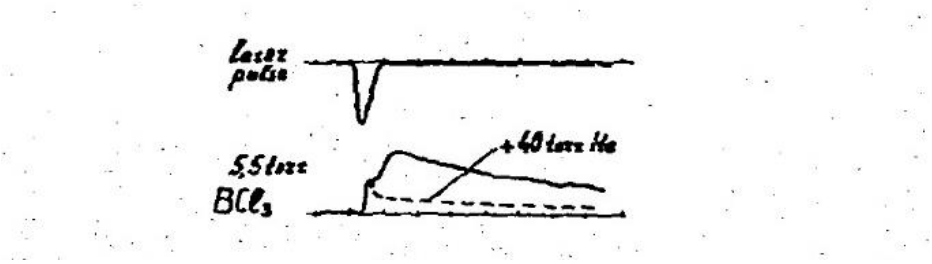


Fig. 5. The effect of He introduced into the cell with the BCl_3. The solid lines are the pulses without buffer gas, the dotted lines are the pulses with He

To add further proof that the luminescence sharply varies from breakdown, the spectrum was taken by a visible spectrograph (ISP-51, 80 A/mm). The spectrum of the luminescence was structureless, while the breakdown spectra consisted mainly of Cl^+, Cl_2^+ lines.

3. Discussion

As it was mentioned above the rise time of the instantaneous luminescence does not depend on the BC13 pressure and the value of the delay after the laser pulse is not more than 2×10^{-8} s This value is smaller than the time between successive collisions which is equal to $\tau_{col} = 4 \times 10^{-8}$ sec torr. Thus, the collisional mechanism cannot explain the instantaneous luminescence. Note that the luminescence was observed at a pressure of 5×10^{-2} torr.

The instantaneous luminescence was detected at power levels beginning from 2×10^8 W/cm2 up to 7×10^9 W/cm2. In such a field (10^9 W/cm2) the absorption lines broaden up to ≈ 1 cm-1 ($\Delta\omega = P_{12}E/\hbar$, where $P_{12} = 0.05$ debye — transitional matrix element of the ν_3 band transition in BC13 [10]).

This allows the participation of a large number of rotational lines of the ground state in the absorption of laser radiation. The estimates made in ref. [12] give 10^3

rotational lines per cm^{-1}. The broadening of the lines brings to an increase of the energy insertion rate in the molecular system. The value of the broadening coincides approximately with the anharmonicity value for die v_3 band in BC_{13}, which is according to ref. [3] equal to 1.6 cm^{-1}. This may be indicative of the probability of the radiational population of the vibrational levels with $V \gg 1$.

The induced transition rate in our case is much more than the rate of the phase relaxation $2/T_2$ in BC_{13} which is equal to 7×10^7 (s torr)-1 [10]. Therefore, the possibility of direct excitation of the vibrational levels due to multiphoton transitions $V" = 0 \rightarrow V' \gg 1$ must not be neglected.

The delayed luminescence arises at lower levels $P \approx 10^7$ W/cm^2. The dependence of the delay on the pressure of BC_{13} gas and the effect of the buffer gas indicate that collisions must be taken in account. One may assume that during the laser pulse the lower vibrational levels are highly over-populated and after the pulse V-V processes populate the higher vibrational levels from which the molecules dissociate. The time required for such processes is greater than the time required for the simple single V-V process between lowest vibrational levels. The heating and thermal dissociation of the gas also must be taken in account due to the fast V-T relaxation (5.8 μs torr [11]). But it is impossible up to now to separate these two processes, because the initial distribution of the molecules over the vibrational levels after the laser pulse and the relaxation times for $V'' \gg 1$ are unknown.

References

1. *Bordé C., Henry A. and Henry L.* // Compt. Rend. Acad. Sci. (Paris). B. 1966. Vol. 262. P. 1389.
2. *Losev V.V., Papulovski V.P., Tischinski V.P. and Fedina G.A.* High Energy Chem. 1969. Vol. 8. P. 331.
3. *Karlov N.V., Petrov Ju.N., Prokhorov A.M. and Stelmach O.M.* // Pis'ma JETPh. 1970. Vol. 11. P. 220.
4. *Isenor N.R. and Richardson M.C.* // Appl. Phys. Letters. 1971. Vol. 18. P. 224.
5. *Letokhov V.S., Ryabov E.A. and Tumanov O.A.* // Opt. Commun. 1972. Vol. 5. P. 168.
6. *Letokhov V.S., Ryabov E.A. and Tumanov O.A.* // JETPh. 1972. Vol. 63. P. 2025.
7. *Lamberton H.M. and Peaszon P.R.* // Electron. Letters. 1971. Vol. 7. P. 5–6.
8. *Denes L.J. and Farish O.* // Electron. Letters. 1971. Vol. 7. P. 12.
9. *Lavigne P. and Lachambre J.L.* // Appl. Phys. Letters. 1971. Vol. 19. P. 176.
10. *Alimpiev S.S. and Karlov N.V.* Report on Conference on Nonlinear Optics. Minsk, USSR 1972.
11. *Houston P.L., Nowak A.V. and Steinfeld J.L.* // J. Chem. Phys. 1973. Vol. 58. P. 3373.
12. *Lavigne P. and Lachambre J.L.* // Appl. Phys. Letters. 1971. Vol. 19. P. 6.

Письма в ЖЭТФ. 1975. Т. 21 (6). С. 375–378

РАЗДЕЛЕНИЕ ИЗОТОПОВ СЕРЫ С КОЭФФИЦИЕНТОМ ОБОГАЩЕНИЯ $> 10^3$ ПРИ ВОЗДЕЙСТВИИ ИЗЛУЧЕНИЯ CO_2-ЛАЗЕРА НА МОЛЕКУЛУ SF_6

Р.В. Амбарцумян, Ю.А. Горохов, В.С. Летохов, Г.Н. Макаров
Институт спектроскопии АН СССР

Сообщается о разделении изотопов серы методом селективной диссоциации молекул SF_6 в сильном поле импульсного CO_2-лазера. Получен коэффициент обогащения в одном цикле 2800 без каскадирования.

1. В настоящей статье сообщается о первом успешном разделении изотопов при воздействии на молекулярный газ мощных импульсов ИК-излучения с исключительно высоким коэффициентом обогащения в одном цикле и физическом разделении изотопов. Единственный известный эксперимент по разделению изотопов ^{10}B и ^{11}B при воздействии на молекулу BCl_3 мощных импульсов CO_2-лазера [1] требовал быстрого химического связывания атомов B акцептором O_2 и на стадии образования радикала BO позволил достигнуть коэффициента обогащения около 10. Физический принцип разделения в данных экспериментах основан на селективной химически необратимой диссоциации одного из изотопов молекулы SF_6 в сильном поле ИК-резонансного излучения лазера. Описываемый метод представляется нам наиболее простым методом лазерного разделения изотопов из всех опубликованных.

2. Эксперимент состоял в облучении кюветы с SF6 сфокусированным излучением импульсного CO2-лазера и регистрации ИК и масс-спектра остаточного газа (SF6) до и после облучения. CO2-лазер с поперечным разрядом с предварительной фотоионизацией излучал импульсы с частотой 1,5 Гц, энергией 2 Дж и длительностью по полувысоте 90 нсек. Частота генерации настраивалась дисперсионным резонатором на области поглощения отдельных изотопов молекулы SF6 природного изотопного состава на колебании ν3 (10,6 мкм). Лазерный луч фокусировался линзой с f = 50 см в кювету длиной 50 см и объемом 60 см3, содержащую SF6 природного изотопного состава (32S — 95%; 33S — 0,75%, 34S — 4,2%, 36S — 0,017%) и в некоторых случаях акцепторные молекулы. Интенсивность ИК поля в кювете в области фокуса достигала 1–2 ГВт/см2, то есть интенсивность, при которой обычно наблюдается бесстолкновительная диссоциация молекул [3]. Изотопный состав до и после облучения анализировался на масс-спектрометре МИ-1309. Кроме этого,

газ, остававшийся после облучения, в ряде экспериментов конденсировался в дополнительную кювету для исследования степени обогащения по ИК-спектрам поглощения в области 10,6 мкм.

3. При настройке частоты CO_2-лазера на пик полосы поглощения $^{32}SF_6$ на 947 см$^{-1}$ [3, 4] (линия P(16) лазера) после облучения кюветы (SF_6 — 0,18 тор, H_2 — 2 тор) $2 \cdot 10^3$ импульсами молекулы $^{32}SF_6$ в результате селективной диссоциации из смеси почти полностью исчезли. Масс-спектр SF_6 содержит в основном линии, соответствующие молекулам $^{32}SF_6$ и $^{34}SF_6$. Из отношения амплитуд масс-линий до и после облучения (рис. 1) получаем величину коэффициента обогащения смеси изотопом ^{34}S по отношению к изотопу ^{32}S

$$K\left(-\frac{34}{32}\right) = \frac{[^{34}S]_*}{[^{32}S]_*} / \frac{[^{34}S]_0}{[^{32}S]_0} \approx 2800,$$

где индекс "0" относится к необлученной смеси. Таким образом, концентрация молекул $^{34}SF_6$ увеличилась с 4,2 до 95%. Происходит также заметное обогащение смеси изотопом ^{33}S по отношению к изотопу ^{32}S. В аналогичных опытах был получен коэффициент обогащения смеси изотопом ^{36}S по отношению к ^{32}S $K(36/32) \approx 1200$.

4. При настройке частоты CO_2-лазера на полосу поглощения молекулы $^{34}SF_6$ [3, 4] (линия P(40) лазера) после облучения кюветы с тем же составом 30 импульсами коэффициент обогащения смеси изотопом ^{32}S по отношению к ^{34}S $K(32/34) = 1{,}7$, а после 500 импульсов $K(32/34) = 18$. Таким образом, концентрация изотопа ^{32}S в смеси стала выше 99%, а концентрация изотопа ^{34}S уменьшилась с 4,2 до 0,2%.

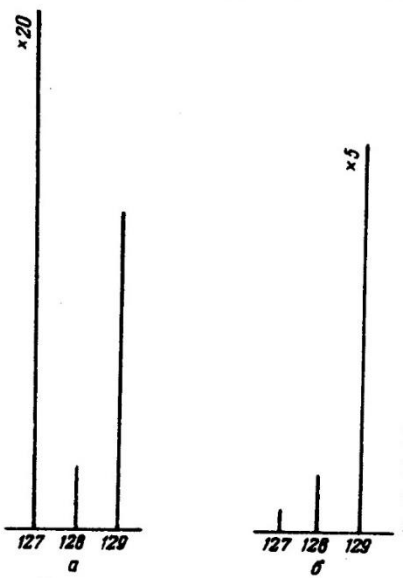


Рис. 1. Участок масс-спектра SF_6 (радикал SF_5^+): *а*) природная смесь до облучения; *б*) после облучения $2 \cdot 10^3$ импульсами CO_2-лазера (линия P(16))

5. Для наглядности и демонстрации физического разделения изотопов остаток газа после облучения вымораживался из облучаемой кюветы в малую кювету, пригодную для измерения ИК-спектра. Исходная кювета облучалась так, чтобы переработать молекулы $^{32}SF_6$ до концентрации молекул $^{34}SF_6$. На рис. 2а приведен ИК-спектр природной смеси молекул $_{SF6}$ до облучения в кювете длиной 6 см, объемом 25 см3 при давлении SF_6 — 1 тор. На рис. 2б приведен ИК-спектр, полученный после конденсации в ту же кювету остаточной смеси SF_6 после облучения 0,5 тор природной смеси SF_6 в кювете длиной 100 см, объемом 500 см3. Отчетливо видно увеличение относительной концентрации молекул $^{34}SF_6$ и $^{36}SF_6$ за счет выгорания молекул $^{32}SF_6$.

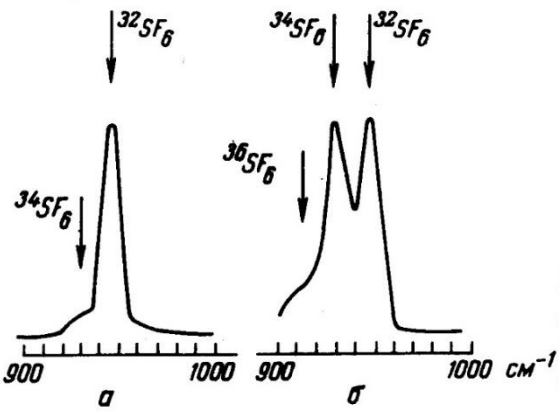


Рис. 2. ИК-спектр поглощения колебания ν_3 в SF_6: *а*) природная смесь, *б*) обогащенная в данных экспериментах смесь

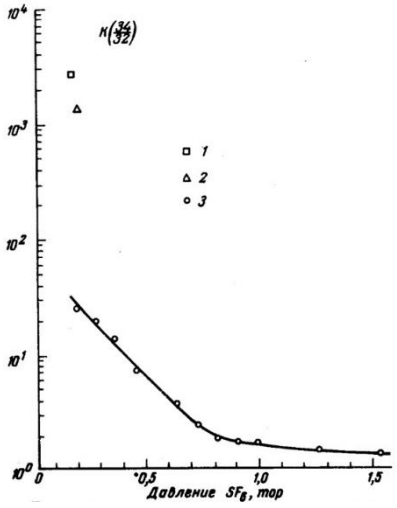


Рис. 3. Зависимость коэффициента обогащения изотопа $^{34}SF_6$ по отношению к $^{32}SF_6$ от исходного давления SF_6 в кювете

Была измерена также зависимость коэффициента обогащения K(34/32) при различных давлениях SF_6. Результаты измерений для различного числа импульсов приведены на рис. 3. В области выше 0,5 тор обогащение падает обратно пропорционально давлению.

Качественно аналогичные результаты получены при облучении как чистой SF_6, так и при добавлении акцепторов H_2, NO и HBr. Химический анализ продуктов диссоциации и химических реакций не производился, хотя в экспериментах с H_2 замечено присутствие HF.

Как показано в [1], молекула, находящаяся в сильном поле излучения ИК-лазера, может изотопически селективно вступать в химические реакции. Хотя в данном случае, в противоположность к [1], необратимая диссоциация молекул происходила без видимой люминесценции, это скорее не противоречие, а характеристика образования радикалов при ИК-фотолизе молекулы SF_6. По-видимому, не образуются радикалы в электронно-возбужденном состоянии.

Итак, в наших экспериментах было впервые осуществлено макроскопическое разделение изотопов под действием ИК лазерного излучения с выходом около 10^{-4} г SF_6 и двадцатикратным обогащением за 100 импульсов с энергией 2 Дж в течение 1 мин (при частоте повторения 1,5 Гц).

Литература

1. *Амбарцумян Р.В., Летохов В.С., Рябов Е.А., Чекалин Н.В.* // Письма в ЖЭТФ. 1974. Т. 20. С. 597.

2. *Ambartzumian R.V., Doljikov V.S., Letokhov V.S., Ryabov E.A., Chekalin N.V.* // Chem. Phys. Lett. 1974. Vol. 25. P. 1281.

3. *Brunet H., Perez M.* // J. Mol. Spectr. 1969. Vol. 29. P. 472.

4. *Климов В.Д., Лобиков Е.А.* // Оптика и спектроскопия. 1971. Т. 30. С. 48.

Opt. Commun. 1981. Vol. 38 (1). P. 31–34

STOCHASTIZATION LIMIT OF VIBRATIONAL ENERGY IN SF_6 AND CF_3I MOLECULES AT IR MULTIPLE PHOTON EXCITATION

V.N. Bagratashvili, V.S. Doljikov, V.S. Letokhov, A.A. Makarov,
L.P. Maljavkin, E.A. Ryabov, E.G. Silkis and Yu.G. Vainer
Institute of Spectroscopy Academy of Sciences USSR, SU-142092, Troitzk, USSR

By the method of double infrared-Raman resonance the stochastization limit E_{lim} in SF_6 and CF_3I molecules under IR multiple photon excitation is determined: for SF_6 molecules $E_{lim} \lesssim 3900 \pm 500 cm^{-1}$; for CF_3I molecules $E_{lim} \lesssim 6000 \pm 500$ cm^{-1}.

1. Introduction

In studies of IR multiple photon excitation (MPE) of molecules it has been proved that the intermolecular vibrational distribution formed by MPE is a nonequilibrium (see [1, 2]). This nonequilibrium may manifest itself, first of all in dividing the molecules into two ensembles: “cold” molecules not interacting with the field and “hot” molecules excited to high vibrational states. Besides, the distribution of molecules in the “hot” ensemble differs from the Boltzmann one, having a sharper high-energy tail. These features of intermolecular distribution nonequilibrium have been well disclosed in experiments for some molecules, SF_6 and CF_3I in particular, and substantiated theoretically [2]. The degree of equilibrium inside a multiple photon excited molecule, i.e. the absorbed energy distribution with respect to molecular vibrational degrees of freedom, is still not clearly understood.

It is believed [3, 4] that the vibrational motion of a molecule near its dissociation limit is stochastic and can be described by statistic methods. The equilibrium intramolecular distribution has been accepted, for example, by the authors of work [5] in the thermal model of MPE of SF_6 molecules. At the same time, it is clear that for low vibrational levels the motion can be described in terms of normal molecular coordinates. The question about the energy limit of vibration stochastization in a molecule E_{lim} at quantitative level remains to be seen [6]. The existing theoretical criteria [6, 7] allow just rough evaluation of E_{lim}. The question on the limit of mode-selective molecular excitation has been discussed for several years in literature. Some authors think that for the SF_6 molecule, for example, the MP excitation selective with respect to the ν_3 mode is possible up to the energies from 5000 to 20000 cm^{-1}. The problem of energy limit of stochastization is also of great interest for molecular spectroscopy, for the theory of nonlinear vibrations of systems with many degrees of freedom and, probably, for practical applications to laser chemistry.

This paper concerns direct experimental determination of the vibrational energy stochastization limit in SF_6 and CF_3I molecules under IR multiple photon excitation by the method of Raman light scattering (double IR-RS resonance [8]).

2. Method

For direct observation of molecular vibration stochastization and determination of the Ej_{im} value it is necessary to measure independently the vibrational energy in various vibrational molecular modes and to compare the distributions thus obtained with the equilibrium one. This can be achieved, in principle, by two methods supplementing each other: by measuring the IR fluorescence and anti-Stokes RS in vibration-excited molecules. Such a possibility is conditioned by two factors. First, in the spectra of IR fluorescence and anti-Stokes RS downward transitions occur, whereas in the spectra of IR absorption the direct and back transitions are overlapped. Besides that, the IR and RS spectra of even highly excited molecules, despite vibrational band broadening and shift, retain the structure of individual modes [2]. This allows independent measurement of signals from different modes. In our experiment [8] it has been shown that the spectrum-integrated intensity I_k^{AS} of the anti-Stokes signal corresponding to the active mode ν_k in RS is proportional to the average energy $\overline{\epsilon_k}$ stored in this mode and does not depend on type of intermolecular distribution and distribution of internal energy over other molecular modes.

The principle of measurement of the stochastization limit in IR molecular excitation is seen from fig. 1. Let a molecule be excited at a frequency coinciding with the frequency of the ν_i -th molecular mode active in IR absorption and the pulse duration of IR radiation τ_{IR} be much shorter than any collisional process. Then, by measuring the value of I_k^{AS} for different ν_k modes right after the IR pulse it is possible to determine the intra-molecular intermodal distribution formed by MPE. Increasing then the τ-delay between the instants of excitation and RS probing to a value at which the distribution is equilibrium due to collisional $\upsilon - \upsilon'$ exchange we can determine to what extend the intramolecular distribution formed in MPE differs from the equilibrium one.

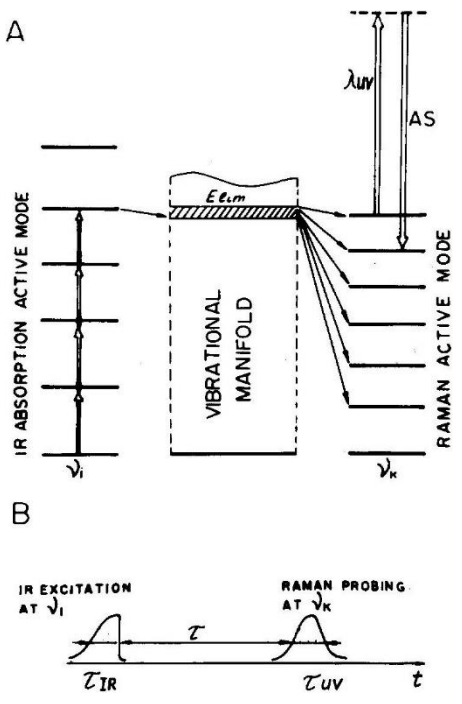


Fig. 1. On the method of stochastization limit measurement

So, to determine the E_{lim} value, one should determine, first of all, the minimum value of radiation energy flux Φ_{lim} at which the intramolecular distribution is still equilibrium and then the average level of molecular excitation in the "hot" ensemble corresponding to this Φ_{lim}.

3. Experiment

The experimental setup for RS diagnostics of vibration-excited molecules and the measuring technique are described in ref. [8]. The SF_6 and CF_3I molecules were excited by CO_2 laser radiation with $\tau_{IR} = 15 \pm 3$ ns. The second harmonic of a ruby laser with $\lambda = 3471.5$ Å and $\tau_{UV} = 20$ ns was used for RS probing. The delay between the end of the exciting pulse and the beginning of the probing pulse was set accurately to 15 ns with a synchronization system. The RS signals were recorded under the regime of photon count. In measuring I_k^{AS} the spectral region overlapping the anti-Stokes signal spectrum of just the ν_k mode was separated.

Fig. 2 shows some characteristic dependences of I^{AS} on the delay time τ for SF_6 and CF_3I. The conditions of measurement are specified in fig. 2. Within the experimental error we could not observe any variations in I^{AS} as τ changed from 15 ns, when the molecular collisions could be neglected, up to several microseconds when the collisional energy exchange was essential. (It must be noted that the decrease of the signal at $\tau > 5$ μs is related to the diffusion of the excited molecules from the area of probing, 0.2 mm in diameter). The same results were observed also in other modes of SF_6 and CF_3I active in RS. Increases in gas pressure as well as in radiation energy flux did not result in qualitative changes of the process.

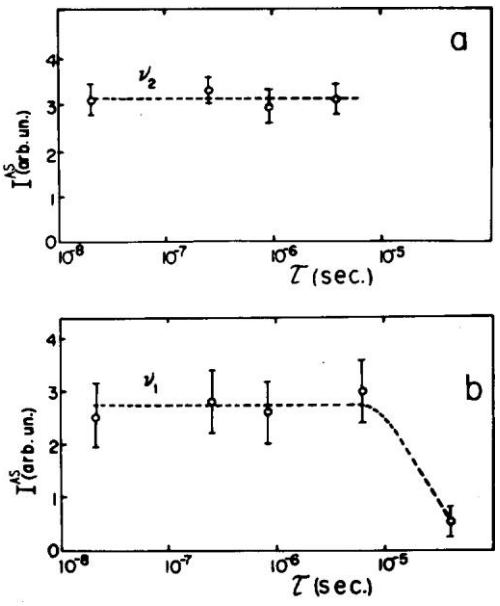


Fig. 2. Dependence of the integral anti-Stokes RS I^{AS} on the delay time τ. *a*) CF_3I, probing of ν_2 mode, excitation on 1071.6 cm^{-1}, p = 0.1 Torr, $\Phi = 0.09$ J/cm^2. *b*) SF_6, probing of ν_1 mode, excitation on 944.7 cm^{-1}, $p = 0.1$ Torr, $\Phi = 0.06$ J/cm^2

The results given unambiguously point to the fact that at MPE of SF_6 and SF_3I molecules there are states formed which correspond to the statistical-equilibrium distribution of absorbed energy between all or, at least, most vibrations of these molecules. This proves that the stochastic character of vibrational motion in the molecules concerned is formed already in the process of their interaction with IR radiation.

The results obtained have made it possible to evaluate the stochastization limit of vibrational energy E_{lim} at MPE. The minimum CO_2 laser pulse energy fluxes Φ at which the RS signals were recorded truthfully (the signal-to-noise ratio 6:1) were 0.06 J/cm^2 for SF_6 and 0.09 J/cm^2 for CF_3I. To determine the value of E_{lim} one should know the average energy absorbed by the "hot" molecular ensemble $\bar{\epsilon}_q$. It has been been found from independent measurements of the average value of absorbed energy $\bar{\epsilon}$ per all the molecules and the fraction q of molecules involved in excitation: $\bar{\epsilon}_q = \bar{\epsilon}/q$.

Fig. 3 shows the dependence of $\bar{\epsilon}_q$ and q, measured by different ways, on Φ for SF_6 and CF_3I molecules (see captions to fig. 3). From the data presented it is possible to get the upper value for the vibration stochastization limit: for SF_6 $E_{lim} \leq 3900 \pm 500$ cm^{-1}; for CF_3I, $E_{lim} \leq 6000 \pm 500$ cm^{-1}, taking into account initial vibrational energy.

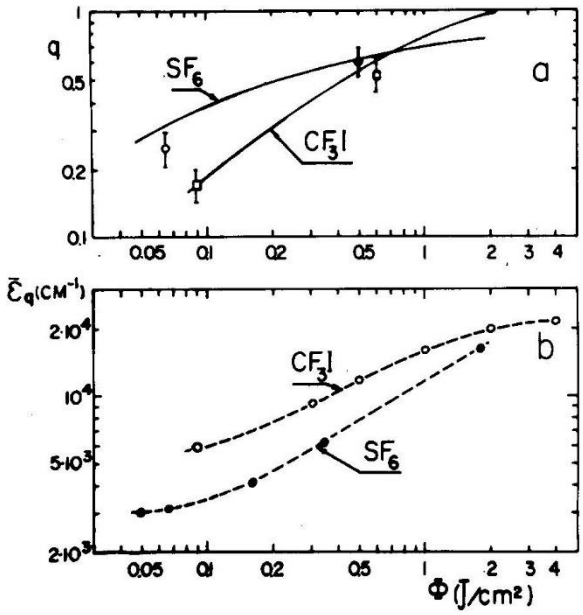


Fig. 3. Dependence of the fraction of excited molecules q (a) and $\bar{\epsilon}_q$ value (b) on the energy flux Φ. a) $q = q(\Phi)$, curves: data of [9] and [10]. ∘, • SF_6, □ CF_3I. ∘, □ measurements by anti-Stokes RS (see [8]). • measurements by Stokes RS (see [11]).b) $\bar{\epsilon}_q = \bar{\epsilon}_q(\Phi)$

4. Discussion

The values of E_{lim} obtained for SF_6 and CF_3I are upper estimates which are practicable at the sensitivity level of our equipment. In principle, we can get more accurate values of E_{lim} by increasing the sensitivity. Here we should note the following important factor. As the radiation energy flux is reduced below Φ = 0.1 ... 0.5 J/cm^2 the absorbed energy and hence the value I^{AS} decrease mainly due to a decrease in the

fraction of excited molecules (fig. 3a). The excitation level for both SF_6 and CF_3I decreases in this case very slowly (fig. 3b). This means that there are qualitative changes in transition spectrum of the molecules interacting with the field in the region of the above-given energies. The cross-sections of molecular excitation to energies corresponding to our estimation for E_{lim} are at least several times higher than the cross-sections of their further excitation to the energy region $E > E_{lim}$. This qualitatively corresponds to the vibrational energy stochastization limit near which the structure of true wave functions changes. In the region $E > E_{lim}$ the wave functions of the mode interacting with the laser radiation due to intermodal resonances mix with many other wave functions. The mechanism of such mixing (chain mixing) on account of Fermi resonances for the particular case of the CF_3I molecule has been considered in ref. [10]. More detailed theoretical analysis of the mechanism of vibration stochastization is SF_6 and CF_3I molecules will be carried out in our work [11].

References

1. *Letokhov V.S.* In: Laser spectroscopy IV, Proc. Intern. Conf., Rotach-Egern. FRG, Springer Series in Optical Sciences. Vol. 21 / eds. H. Walther and K.W. Rothe. Springer-Verlag, 1979. P. 504.

2. *Bagratashvili V.N., Letokhov V.S., Makarov A.A. and Ryabov E.A.* Multiple photon molecular processes in the IR laser field. Publication of Soviet Institute of Scientific and Technical Information. Moscow, 1980.

3. *Robinson P.J. and Holbrook K.A*. Unimolecular reactions. London: Wiley, 1972.

4. *Oxtuby D. and Rice S.A*. // J. Chem. Phys. 1976. Vol. 65. P. 1676.

5. *Bloembergen N. and Yablonovitch E.* Laser spectroscopy III / eds. J.L. Hall and J.L. *Carlsten.* Springer Series in Optical Sciences. Vol. 7. Berlin, Heidelberg, New York: Springer-Verlag, 1977. P. 86.

6. *Rice S.A.* In: Advances in laser chemistry / ed. A.H. Zewail. Springer Series in Chem. Phys. Vol. 3. Berlin, Heidelberg, New York: Springer-Verlag, 1978. P. 2–42.

7. *Shyryak E.V.* // Zh. Eksp. Teor. Fiz. (Russian). 1976. Vol. 71. P. 2039.

8. *Bagratashvili V.N., Vainer Yu.G., Doljikov V.S., Koljakov S.K., Makarov A.A., Maljavkin L.P., Ryabov E.A., Silkis E.G. and Titov V.D.* // Applied Physics. 1980. Vol. 22. P. 101.

9. *Bagratashvili V.N., Doljikov V.S. and Letokhov V.S.* // Zh. Eksp. Teor. Fiz. (Russian). 1979. Vol. 76. P. 19.

10. *Bagratashvili V.N., Doljikov V.S., Letokhov V.S., Makarov A.A., Ryabov E.A. and Tyacht V.V.* // Zh. Eksp. Teor. Fiz. (Russian). 1979. Vol. 77. P. 2238.

11. *Bagratashvili V.N., Vainer Yu.G., Doljikov V.S., Koljakov S.F., Letokhov V.S., Makarov A.A., Maljavkin L.P., Ryabov E.A., Silkis E.G. and Titov V.D.* // Zh. Eksp. Teor Fiz. (Russian). in press.

J. Phys. Chem. A. 1998. Vol. 102. P. 1438–1449

STATISTICAL INHOMOGENEOUS BROADENING OF INFRARED AND RAMAN TRANSITIONS IN HIGHLY VIBRATIONALLY EXCITED XY_6 MOLECULES

A.A. Makarov, I.Yu. Petrova, E.A. Ryabov and V.S. Letokhov*
Institute of Spectroscopy, Russian Academy of Sciences, Troitsk, Moscow Region, 142092 Russia

Simulations of the spectra of vibrational transitions in highly vibrationally excited XY_6 molecules at certain energy E_{vib} are performed. The infrared (IR) transitions in the mode ν_3, of the molecules SF_6 and WF_6 as well as the Raman ones in the mode $\nu_1$of SF_6 are studied. The shapes and parameters of the spectral bands, such as the integral intensity, the mean frequency, and the width, are obtained in a wide range of E_{vib}. The calculated widths prove to be much broader than the expected contributions to them because of intramolecular vibrational relaxation (IVR); this indicates the dominant role of statistical inhomogeneous broadening in the width formation for the investigated molecules.

1. Introduction

The multiple-photon (MP) excitation (E) of vibrations in and dissociation (D) of polyatomic molecules in the ground electronic state by intense IR laser pulses are at the root of a new line of inquiry in photochemistry that made its appearance thanks to the advent in the early 1970s of high-power pulsed CO_2 lasers operating in the range $9-11\ \mu m$. After the first successful experiments on the resonant action of CO_2 laser pulses upon molecular gases absorbing in the region of $10\ \mu m$ [1, 2] and especially after the demonstration of the isotope-selective IR MPD of polyatomic molecules (BCl_3, SF_6) [3], there followed numerous experimental and theoretical works whose results were summarized in a series of reviews and monographs [4–12]. The interest in the IR MPE/D processes persists today because of the promise they hold for the separation of isotopes on an industrial scale in the future when reliable and economical high-power tunable pulsed IR lasers with a high repetition frequency [13] are developed.

The model of IR MPD of a polyatomic molecule is schematically illustrated in Fig. 1. This qualitative model has already been discussed in the reviews and monographs cited, and here it is presented solely to make convenient the exposition of the object of the present paper. The molecule first absorbs a few IR photons in the

transitions of its vibrational mode involved in the resonant interaction with the IR radiation (see the left-hand side of Fig. 1). Thereafter, above some threshold energy Eonset (onset of vibrational chaos), there takes place the intramolecular vibrational redistribution (IVR) of the absorbed energy among the rest of the vibrational molecular modes as a result of the intermode anharmonic interaction (this is schematically shown by the broken arrows in Figure 1). This process is governed by the density of the anharmonic intermode resonances of different orders,14–17 and it may have a multiple time scale character18, 19 at that. Finally, at the third stage, the highly excited molecule keeps absorbing the IR radiation in conditions of modification of the vibrational excitation spectrum of all the modes and the intermode anharmonicity. Qualitatively this modification boils down to the shifting of the vibrational absorption band toward the red side and its broadening as a result of the intermode anharmonicity, as illustrated schematically on the right-hand side of Figure 1. Several experimental methods aimed at studying this evolution of the vibrational absorption spectrum of polyatomic molecules are described in refs 20–23. The results of these works as well as other experimental and theoretical investigations of highly vibrationally excited molecules were summarized in ref 24 and a recent review in ref 25.

The main difficulty in comparing theory and experiment is the scarcity of data on the nature of broadening (see, for example, discussion in ref. 26 related to the IR spectrum of highly vibrationally excited molecules C_2F_5I). Two effects originally contribute to the width: (1) the IVR of the energy from the vibrational mode under study (say, ν_a) which leads to the homogeneous broadening, and (2) the fact that molecular excitation near a certain vibrational energy E_{vib} can be represented by numerous combinations of occupation numbers of various vibrational modes which may lead to the inhomogeneous broadening due to different anharmonic shifts of the frequency of the mode ν_a by different combinations. The first contribution is given by the rate of IVR of the mode ν_a. In simple oscillator models, it is associated with friction, or damping, etc. For polyatomic molecules, it is calculated in the general form in refs 16 and 27. The purpose of the present work is to model theoretically only the second effect of statistical inhomogeneous broadening of IR and Raman transitions in polyatomic molecules. It can dominate at certain conditions, which are discussed below in section 2. It is useful to note here that, in the general stochastic theory of the line shape by Kubo [28], such domination is referred to as the case of slow modulation (presuming also slow damping). On the contrary, fast modulation leads to the collapse of the inhomogeneous width. This collapse is analogous, in particular, to the well-known Dicke narrowing [29]. For the highly vibrationally excited molecule, the fast modulation case roughly corresponds to the fast IVR of all the modes other than ν_a (more details are in section 2), and the remaining collapsed width is associated with the rate of the purely phase IVR [30, 31].

We have enough indications from the experiment at present to make a statement that any of the above-mentioned effects may be mainly responsible for the broadening of spectra in different specific cases. Realistic arguments have been made, for example, in ref. 32 in favor that the IR spectrum of mode ν_{27} in the molecule c-C_6F_{12} at Evib = 60 000 cm-1 is broadened due to IVR of this mode. The same conclusion has been drawn in ref 21 relating to the IR spectrum of mode ν_{21} in the molecule

$(CF_3)_3Cl$ at E_{vib} = 35 000 cm^{-1}. The pure dephasing width, however, gives probably the main contribution to the IR spectrum of the C–H stretching mode in the molecule $(CF_3)_3$-CH at room temperature, i.e. mean vibrational energy of about 2000 cm^{-1} (see the experimental results in ref. 33 and related discussion of these results in ref. 31). Eventually, inhomogeneity is considered as the principal effect in the width, at high vibrational energies, for the IR spectra of mode ν_4 of CF_3I in ref. 22 and mode ν_3 of SF_6 in ref. 34. We, as said above, will concentrate in this paper on the latter, just the statistical inhomogeneous broadening (in particular, for the ν_3 of SF_6).

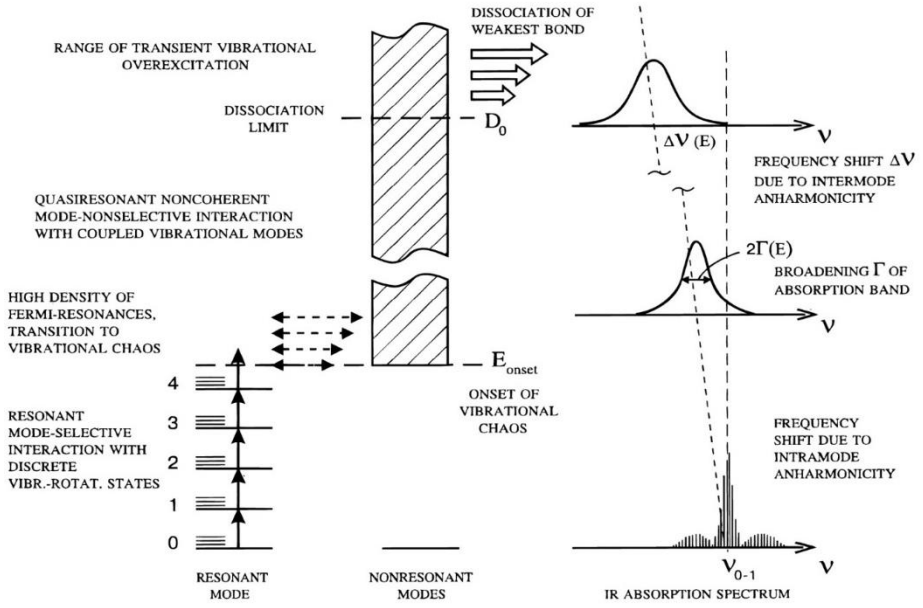


Fig. 1. Main features of IR MPE/D. See the text for details

The paper is organized as follows. Basic definitions, approximations, and equations to describe the effect of statistical inhomogeneity on spectra of vibrational transitions are given in section 2. The inhomogeneous spectral shapes can be calculated with knowledge of the fundamental frequencies ν_i of molecular vibrations and the spectroscopic anharmonicity constants x_{ij}, which are usually available from routine spectroscopy of the fundamental, combination, and overtone bands. The calculation procedure is described, in general, in section 3. Being applied to infrared transitions in the triply degenerated modes of spherical molecules like XY_6, it requires also the inclusion of anharmonic splitting. The calculation results in a wide range of vibrational energy are presented in section 4 for the molecule SF_6, and in section 5 for the molecule WF6. The rotations are not involved up to this point. Their inclusion is made in section 6, in a simple way, after finding the nonsensitivity of previous results to the Coriolis splitting. Finally, in section 7, we discuss the reliability of calculated spectra in connection with the existing estimates on the IVR rates in SF_6.

2. Theory: Definitions and Approximations

We consider optical transitions near the frequency of one mode of a molecule (say, ν_a) which start from a vibrational state $|g_\alpha\rangle$ at some energy E_{vib}. Our assumptions and definitions are as follows.

The mode ν_a is referred to as the active mode: it is implied that it is really active in either the infrared or the Raman spectrum, and correspondingly, the infrared or the Raman transitions are treated.

The upward transitions are considered for definiteness; this means that the absorptive infrared transitions or Stokes Raman ones are under treatment.

The other modes ν_i, with i = 1, ..., s, where i≠a, and s is the number of vibrational degrees of freedom, are referred to as the bath modes in accordance with the convention accepted in the literature on IVR.

The state $|g_\alpha\rangle$ is assumed to be chaotic (see, for example, discussion in ref. 35); among other things, this means that the $|g_\alpha\rangle$ has many significant projections on the regular states $|h_\beta\rangle$ the latter being described in terms of the set of mode occupation numbers n_i, with their energies $E^{(0)}_{\{n_i\}}$ near E_{vib}.

Just mentioned energies of the regular states $|h_\beta\rangle = |n_1, n_2, \ldots, n_s\rangle$ are assumed to contain the zero-order harmonic contribution and at least principal anharmonic corrections due to the spectroscopic anharmonicity constants x_{ij}, i.e.

$$E^{(0)}_\beta \equiv Ei^{(0)}_{\{n\}} \approx \sum_{i=1}^{s} n_i[\nu_i + x_{ii}(n_i - 1)] + \sum_{i=1}^{s}\sum_{j=1}^{i-1} x_{ij} n_i n_j \qquad (1)$$

For illustrative purposes, we also involve some mixing parameter δE, a typical energy interval wherein the states $|h_\beta\rangle$ with close energies (eq. 1) are strongly mixed, giving the $|g_\alpha\rangle$ as the chaotic eigenstates.

Let us consider now the upward optical transitions from the state:

$$|g_\alpha\rangle = \sum_\beta c_{\beta\alpha}|h_\beta\rangle \qquad (2)$$

with the energy E_α. For each basis state $|h_\beta\rangle$ entering the right side of eq 2, there is one relevant bright state $|h^+_\beta\rangle$ in the vicinity of the energy $E_{vib} + \nu_a$ which coincides with the $|h_\beta\rangle$ in all mode occupation numbers n_i, except n_a, being now na + 1. Next, we include the principal anharmonic corrections to the frequency of the transition $|h_\beta\rangle \rightarrow |h^+_\beta\rangle$ according to eq 1 and use the harmonic approximation for its intensity, so the frequency is

$$\omega^{(+)}_\beta \approx \nu_a + 2x_{aa}n_a + \sum_{i\neq a} x_{ai} n_i \qquad (3)$$

and intensity, in the units of the $n_a = 0 \to n_a = 1$ transition intensity, is

$$I_\beta^{(+)} \approx n_a + 1 \tag{4}$$

If the states $|h_\beta^+\rangle$ were the eigenstates, one would observe the spectrum of the upward transitions from the $|g_\alpha\rangle$ (see eq. 2) as the lines with the frequencies $\omega_\beta^{(+)}$ (see eq. 3) and the intensities $\left|c_{\beta\alpha}\right|^2 I_\beta^{(+)}$ (see eqs 2 and 4). However, they are not; the eigenstates near the energy $\mathrm{E}_\alpha + \nu_a$ are chaotic, being some superpositions of the regular states, and transition occurs, in principle, to any upper eigenstate having a nonzero projection on any of the $|h_\beta^+\rangle$. Here we involve the mixing parameter δE and notice that, in one limited case shown in Figure 2 where spreading of the frequencies $\omega_\beta^{(+)}$ is much wider than the δE, the expected spectrum, in low resolution, cannot differ much from the contour of the ($\omega_\beta^{(+)}$, $I_\beta^{(+)}$) lines. Really, in that case of small δE, each ($\omega_\beta^{(+)}$, $I_\beta^{(+)}$) line may be considered as leading to some manifold of the width δE and integral intensity $I_\beta^{(+)}$ and any of such manifolds may interfere with only a small part of them. This situation may be referred to as the statistical inhomogeneity of the spectrum, since the effect results from different frequencies (see eq. 3) of the transitions from different regular states giving the contributions to the initial chaotic state (eq. 2). Further, being interested in the low-resolution spectrum from an ensemble of the chaotic states $|g_\alpha\rangle$ with close energies, one must do the averaging in both the α and β. As long as the equality $\sum_\alpha c_{\beta\alpha}^2 = 1$ holds true, each $\omega_\beta^{(+)}$ line is present in this spectrum as a narrow manifold of lines with its integral intensity I_β inherent in the regular state $|h_\beta\rangle$, and the searched spectrum must have the same low-resolution features as the spectrum from the ensemble of regular states near the same energy. When discussing the form of this spectrum, the term inhomogeneous width may be used, in particular.

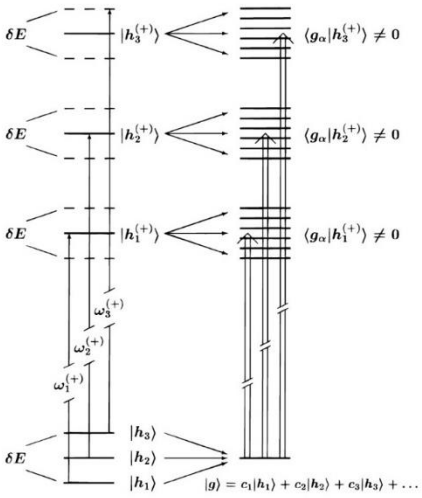


Fig. 2. Illustration of the case when similarity of the spectra for the chaotic states to the inhomogeneous spectra for the ensembles of regular states may be expected. The allowed one-to-one upward transitions between the regular states $|h\rangle$ are schematically shown on the left side. The mixing of close regular states gives the chaotic states $|g\rangle$ on the right side. The optical transitions from any state $|g\rangle$ may occur to *every* chaotic state having nonzero projection onto, at least, one of the relevant $|h^{(+)}\rangle$ states

We considered the case of the relatively small mixing parameter δE. The physical cause of the mixing is IVR, and roughly, the faster the IVR, the greater δE should be. Being reformulated in terms of the IVR rates γ_i, the adequate criterion (see, for example, ref 31) for the inhomogeneous broadening to dominate is a set of the inequalities

$$\gamma_i \ll \overline{n_i}\Delta_i \tag{5}$$

where the following assignments are used: $\overline{n_i}$, is the mean (or equilibrium) occupation number in the ith mode at the total vibrational energy E_{vib}, γ_i describes the exponential evolution (during IVR) of the current energy in the ith mode to the equilibrium energy $\overline{n_i}\nu_i$; Δ_i is equal to the shift of the average transition frequency (eq. 3) when the occupation number in the ith mode changes from n_i to $n_i + 1$ and simultaneous averaging at E_{vib} over the rest of the occupation numbers is implied. All three parameters entering the inequality eq. 5 depend on E_{vib}. The $\overline{n_i}(E_{vib})$ and Δ_i (E_{vib}) can be calculated numerically with knowledge of ν_i and x_{ij},31 but evaluation of $\gamma_i(E_{vib})$ requires either the knowledge of the anharmonic coupling terms (see, for example, ref 27) and hard calculations or the experimental data and is very far from being a routine task. So, a natural way to make things clearer is to calculate the spectral shapes due to the inhomogeneous contribution; then, this should enable us to estimate how fast IVR rates cannot be ignored. Our further consideration is limited to the systems like those where the dominant role of the inhomogeneous broadening has been assumed (and probably proved) previously.[34]

3. Calculation procedure

To simulate spectra with the dominant role of inhomogeneity, one must have tools for calculating two things as follows from the considerations of section 2. It is needed, first, to construct in explicit numerical form the representative ensemble of the regular states $|h_\beta\rangle$ lying near some energy of interest E_{vib} and, second, to get the frequencies and intensities of optical transitions from each state in the spectral region of interest. Then the resulting spectrum can be found as some average for the ensemble. Since we are interested in the spectrum also for the ensemble (now of the chaotic states also $|g_\alpha\rangle$), the averaging procedure would assume uniform contribution from all states of the constructed ensemble and, in addition, take into account (by multiplication) their statistical weights when necessary.

Construction of the $|h_\beta\rangle$ ensemble may be direct or random. The direct procedure implies trying possible combinations of the mode occupation numbers and selecting all those states whose energy (eq. 1) falls into some chosen narrow energy interval near the E_{vib}. Such procedure is computationally reasonable for small molecules, but for large molecules, it becomes expensive even with the best numerical algorithms. Of course, we tried the direct procedure for several cases of our studies below, but found that practically the same final results for the spectra could be obtained with the randomly selected ensembles which, as a rule, involved only a small part of the states near E_{vib}. We discuss, next, this random-ensemble construction and justify it in some detail.

3.1. State Ensemble Selection. The procedure starts with defining the upper and lower edges of the narrow energy interval near the current E_{vib}, usually $E_{vib} \pm \Delta E$. Then the mode occupation numbers n_i, are randomly generated using some statistics, which is mathematically approved and adjusted to the E_{vib},and each $\{n_i\}$ generation is checked to see whether the corresponding energy (eq 1) falls in the interval from $E_{vib} - \Delta E$ to $E_{vib} + \Delta E$ or not. If it does, then the generated state is included in our further calculation. The choice of the statistics must ensure the equal probabilities of generation of the nondegenerated states with equal energies. In the approximation wherein the anharmonic corrections in eq 1 are neglected, this problem can be solved using the Boltzmann statistics

$$W_i(n_i) = \left[1 - \exp\left(-\frac{\nu_i}{T}\right)\right]^{g_i} \frac{(n_i + g_i - 1)!}{n_i!\,(g_i - 1)!} \exp\left(-\frac{n_i \nu_i}{T}\right) = \\ = \left[1 - \exp(-\frac{\nu_i}{T})\right]^{g_i} G_{n_i} \exp\left(-\frac{n_i \nu_i}{T}\right) \quad (6)$$

for the independent harmonic oscillators with the frequencies ν_i and degeneracies g_i of the modes of the molecule. In fact, the probability $W_i(n_i)$ of the $\{n_i\}$ generation divided by the corresponding state degeneracy $G(\{n_i\}) = \prod_{i=1}^{s} G_{n_i}$ depends on the sum of harmonic energies n_i, ν_i only:

$$W_i(\{n_i\}) = \prod_{i=1}^{s} W_i\,(n_i) = C(T) G(\{n_i\}) \exp\,(-\sum_{i=1}^{s} n_i \nu_i) \quad (7)$$

The parameter T in eqs 6 and 7 is equivalent to the temperature and may be optimized for the rate of successful trials. The "optimum temperature" T_0 can be quite well determined by solving the equation

$$E_{vib} = \sum_{i=1}^{s} \frac{g_i \nu_i}{\exp(\nu_i / T_0) - 1} \quad (8)$$

which equalizes the current vibrational energy on the left side to the mean vibrational energy at the temperature T_0 (in the units of the Boltzmann constant) on the right side.

Choice of the window $2\Delta E$ for selection of the randomly generated states at E_{vib} is dictated by two reasons: it would be small enough for the regular dependence of the spectrum parameters on E_{vib} to be neglected inside, but would be large enough to ensure the representative statistics. The number of selected states within the $2\Delta E$ window would be also large enough to provide sufficient reproducibility of the spectrum from one computational run to another as well as quality of further smoothing procedures. These optional parameters are given below in every particular case.

In our further calculations, if there are no complete data on the anharmonicity constants (the molecule WF_6), we, selecting the generated states, limit ourselves to

the harmonic approximation, for definiteness; otherwise (the molecule SF_6), we use eq 1 in full. It should be noted, however, that anharmonic corrections do not lead to any visible effects other than some evident small compression of the vibrational energy scale (see below for details).

3.2. Transition frequencies and intensities. Upward one-quantum vibrational transitions are under treatment in the present study, as discussed in the beginning of section 2, wherein eqs 3 and 4 are given for schematic description of the transition frequency and intensity, correspondingly. These formulas, however, are adequate just for asymmetric molecules having only nondegenarate vibrations. The XY_6 molecules being the subject of this work are spherically symmetric and belong to the point symmetry group O_h; their normal modes are usually assigned to the O_h-group irreducible representations as follows:

$$\nu_1(A_{1g}), \quad \nu_2(E_g), \quad \nu_3(F_{1u}), \quad \nu_4(F_{1u}), \quad \nu_5(F_{2g}), \quad \nu_6(F_{2u})$$

We are considering the Raman transitions in the nondegenerate mode ν_1 and infrared transitions in the 3-fold degenerate mode ν_3.

Following Hecht [36], we write out (with minor, quite evident modifications) the diagonal second-order perturbation vibrational Hamiltonian:

$$\begin{aligned}\hat{H}_2{}'(vib,diag) = &\sum_{i=1}^{6} X_{ii}\hat{n}_i(\hat{n}_i-1) + \sum_{i=1}^{6}\sum_{j=1}^{i-1} X_{ij}\hat{n}_i\hat{n}_j + G_{22}\hat{m}_{2z}^2 \\ &+ \sum_{i=3}^{6}\sum_{j=3}^{i} G_{ij}\left[(\hat{l}_i\cdot l_j) - \hat{n}_i\delta_{ij}\right] + \\ &+ \sum_{i=2}^{6}\sum_{j=3}^{i} T_{ij}\hat{O}_{ij}\,(tensor) + \sum_{i=3}^{6}\sum_{j=3}^{i-1} S_{ij}\hat{O}_{ij}\,(scalar) \qquad (9)\end{aligned}$$

Here n_i is the ith mode occupation-number operator, $\hat{m}_{2z}$is the operator of the vibrational angular momentum for the 2-fold degenerate mode ν_2, $\widehat{l_\iota}$ is the operator of the vibrational angular momentum for the 3-fold degenerate mode ν_i (i = 3, ..., 6), and the operators $\hat{O}_{ij}$ (tensor) and O_{ij} (scalar) are some quartic combinations of the related vibrational coordinates and momenta explicitly given in ref 36. Further, in eq 9, the coefficients X_{ij}, G_{ij}, T_{ij}, and S_{ij} are, in fact, the spectroscopic anharmonicity constants: the constants X are responsible for the common shift of the manifold of states with the same set $\{n_i\}$ of vibrational quantum numbers (identically to eq (1)), and the other constants are responsible for the splitting inside this manifold.

Table 1. $^{32}SF_6$ Spectroscopic Constants (in cm^{-1}) Used for Calculations

i	ν_i	X_{1i}	X_{2i}	X_{3i}	X_{4i}	X_{5i}	X_{6i}
1	774.5445	-0.896	-2.358	-2.902	-1.144	-1.12	-0.3625
2	643.35		-0.43	-3.603	-1.271	-0.62	-0.348
3	948.1025			-1.7468	-1.52	-1.2	-1.102
4	615.020				-0.19	+0.13	-0.1086
5	523.56					+0.85	-1.15
6	346.076						-0.8

In this work, we limit ourselves to the perturbation Hamiltonian, eq. 9. Transitions in the mode ν_1 are, in this approximation, described by single line of the frequency (eq. 3) and intensity (eq 4) since there are no other terms than the X ones in the Hamiltonian (eq. 9) coupling the mode ν_1 with the rest of the modes, so the splittings are identical in the lower and upper manifolds of the $n_1 \rightarrow n_1 + 1$ Raman transition. On the contrary, the infrared transition $n_3 \rightarrow n_3 + 1$ consists of some number of lines. If only the vibrational quantum number n_3 is nonzero, then the $n_3 \rightarrow n_3 + 1$ transition spectrum depends on the three constants X_{33}, G_{33}, and T_{33}. This case is studied well, and related constants can be found in literature. Knowing these constants, one can find the frequencies and intensities, which belong to any $n_3 \rightarrow n_3 + 1$ transition, in general numerically, but even analytically for some first n_3 values [36]. Some general features of those spectra are that the integral intensity, assuming that the split levels are populated proportionally to their degeneracies, depends on the initial n_3 as

$$I(n_3 \rightarrow n_3 + 1) = \frac{1}{3}(n_3 + 3)I(0 \rightarrow 1) \tag{10}$$

and the weight center (mean frequency) is given by

$$\bar{\nu}(n_3 \rightarrow n_3 + 1) - \nu_3 = (2X_{33} + G_{33})n_3 \tag{11}$$

That is, it is shifted from the fundamental frequency by the value on the right side of eq 11. The effect of nonzero vibrational quantum numbers in the other modes of the molecule on the $n_3 \rightarrow n_3 + 1$ transition spectrum consists of two parts, and we encounter only one of them in this work. Namely, we assume that all the constants G_{3i}, T_{3i}, and S_{3i} $(i \neq 3)$ are equal to zero. Then the spectrum in the mode ν_3 from any selected state with the set $\{n_i\}$ of the mode occupation quantum numbers takes the structure of the $n_3 \rightarrow n_3 + 1$ transition, with the current n_3 shifted additionally by

$$\Delta\nu_{add} = \sum_{i \neq 3} X_{3i} n_i \tag{12}$$

The nonzero constants G_{3i}, T_{3i}, and S_{3i}, may lead to additional splittings. Our simplification is enforced to a certain extent, since these constants are far from being known in full for the molecules studied in this work. After presentation of the calculation results, we shall discuss this subject more.

4. Results for the molecule SF_6

After some analysis of available experimental data, we have taken for calculations the values of frequencies ν_i, and anharmonicity constants X_{ij} presented in Table 1. Our comments are as follows. The presented value of ν_3 is taken from ref. 37; it corresponds to Hecht's definition of ν^{36} and is slightly shifted from the ν_3 band origin $m(\nu_3)$ by the value $2B_0\varsigma_3 \approx 0.126$ cm^{-1}, where B_0 is the rotational constant and ς_3 is the Coriolis constant. The other frequencies are taken from ref 38 as the band origins $m(\nu_i)$ either measured or cited therein. The intramode anharmonicity constants for the mode ν_3 are taken from ref 39, where they are obtained by the interpretation of not only the $3\nu_3$ band (as in some other works on this subject) but also the $2\nu_3 - \nu_3$ band; the constant X_{33} is given in Table 1, and two other constants are

$$G_{33} = 0.9262 \text{ cm}^{-1}, T_{33} = -0.2487 \text{ cm}^{-1}$$

All other constants X_{ij} are from ref. 40, where they are defined as "effective" ones and obtained from the analysis of many combination bands, but one constant X_{35} is only estimated.

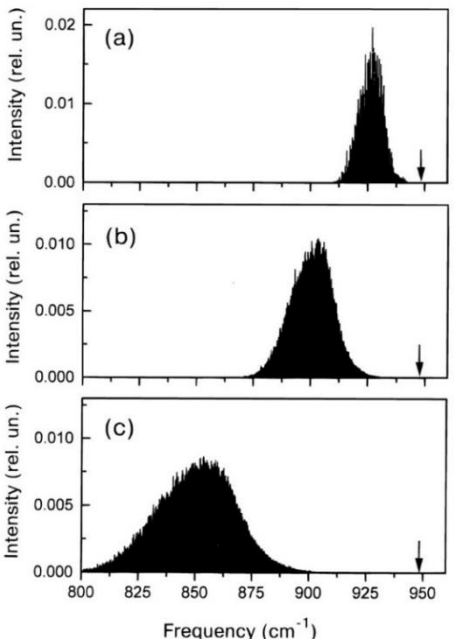


Fig. 3. Histograms of the intensity distribution of the upward transitions in the ν_3 mode of SF_6 for different vibrational energies: (*a*) 7000 cm^{-1}; (*b*) 15000 cm^{-1}; (*c*) 30000 cm^{-1}. The fundamental frequency is indicated by the arrow

Simulations of the inhomogeneous spectra in the modes ν_1 and ν_3 were performed for the energies starting from the onset of the vibrational chaos in SF_6 ($E_{onset} \simeq 5000$ cm^{-1} [41]) up to the dissociation limit, which is about 32 000 cm^{-1} [42].

4.1. Mode ν_3. As said above in section 3, our calculation of the spectrum starts from the selection of a certain number of vibrational states within used in all our computations. The reason for this choice was that the narrower ΔE (even down to 1 cm^{-1}) did not show any significant difference in the resulting spectral contour parameters for any energy E_{vib}. In addition, the procedure of selection of the states, falling into this energy interval ΔE from the randomly generated ones turned out to be fast enough to deal with the large ensembles, usually about 10^4 states.

The spectral distribution (histogram) of transition intensities is shown in Figure 3 for three energies $E_{vib} = 7000$ cm^{-1} (*a*), $E_{vib} = 15000$ cm^{-1} (*b*), and $E_{vib} = 30000$ cm^{-1} (*c*). Each of these histograms presents intensities of all allowed transitions from the states selected in one computational run divided by the number of these states (10 000 for Figure 3*a*, 10 000 for Figure 3*b*, and 5000 for Figure 3*c*). Therefore, the aggregate intensity of the histogram is equal to $(\overline{n_3} + 3)/3$ in the units of the $0 \rightarrow 1$ transition intensity (see eq 10) with the mode ν_3 mean occupation number $\overline{n_3}$ just for that run. One can see from the presented histograms the evolution of the transition spectrum: the higher the energy E_{vib}, the more intense, broadened, and red-shifted this spectrum is. Of course, the histogram characteristics at some energy E_{vib} fluctuate from run to run, but these fluctuations naturally drop ($\propto N_{run}^{-1/2}$) as the number N_{run} of selected states is increased. Such parameters of the spectrum as its integral intensity, mean frequency, and typical width converge to some well-defined values which, in addition, do not depend on ΔE. Now, we discuss how the histograms, as shown in Figure 3, are further processed for determination of the spectral contour parameters. Here it should be noted that we are treating spectra with the dominant role of inhomogeneity, but the *chaotic spectra*, nevertheless. The latter means that each transition in the histogram represents, in fact, some relatively narrow substructure due to the mixing of the regular states (see the discussion in section 2 illustrated schematically by Figure 2). From the very general considerations outlined also in section 2, the mentioned substructure is expected to be of Lorentzian contour type. So, the natural procedure of smoothing histograms is their convolution with the Lorentzian. It is preferable to use some realistic Lorentzian halfwidth, γ_L, and the halfwidths estimated by Angelié [34] for the case under consideration from his own experimental results [43] have been used. In addition, to extract the net result of the statistical inhomogeneity, the convolution with the narrow Gaussian window has been done. Its width $2\sigma_{GW}$ was taken to ensure histogram smoothing as well as to add to the histogram width not more than several percent. Particular values of $2\sigma_{GW}$ are given in the captions for the relevant figures.

The results of these convolutions are shown in Figure 4. This figure presents the transition spectra [the spectral density $I_\nu(\nu)$ of the transition intensity] for the same energies as in Figure 3. As mentioned earlier for the histograms, the transition spectrum becomes broader and shifts to the red side when the energy of the molecule

E_{vib} goes up. The resulting spectral shape may be well-approximated by the Gaussian. One example is shown in Figure 5, and rather good quality of this approximation can be seen there; another less satisfactory trial to approximate the calculated spectrum by the Lorentzian is shown for comparison.

Next, the dependences of the spectral-contour parameters are presented. It should be mentioned that, for each energy E_{vib} of SF_6, the histogram was calculated several times to estimate the accuracy of calculations and find its parameters such as the mean frequency $\bar{\nu}$, standard deviation σ_0, and integral intensity I_0. So, the points on the plots, giving the contour parameters, are obtained by averaging over several computation runs. Figure 6 shows the dependences of the mean frequency (in terms of its shift $\Delta\nu_3$ from the fundamental frequency ν_3) and contour width $2\sigma_0$ on the energy E_{vib}. Formally calculated in the course of the histogram generation, these parameters are in good agreement with the best-fit Gaussian ones. It is seen that both dependences exhibit very closely the linear law.

The linear dependence for the shift of the mean frequency v of any vibrational band from the corresponding fundamental mode frequency ν_i, i.e. $\Delta\nu_i = \bar{\nu} - \nu_i$, is frequently explored in literature in the form

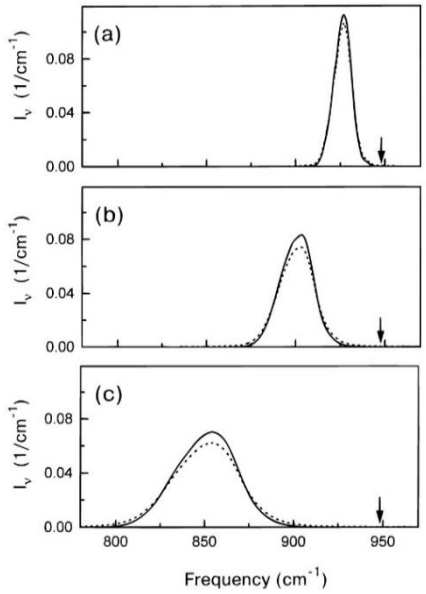


Fig. 4. Upward transition spectra in the ν_3 mode of SF_6 for different vibrational energies: (*a*) 7000 cm^{-1}; (*b*) 15000 cm^{-1}; (*c*) 30000 cm^{-1}. The solid lines present the results of convolution of the histograms in Figure 3 with the Gaussian windows of the width $2\sigma_{GW}$ equal to 1.5 cm^{-1} (*a*), 2.7 cm^{-1} (*b*), and 5.4 cm^{-1} (*c*). The dashed lines present the results of convolution of the same histograms with the Lorentzians of the widths $2\gamma_L$ equal to 1 cm^{-1} (*a*), 3 cm^{-1} (*b*), and 6 cm^{-1} (*c*)

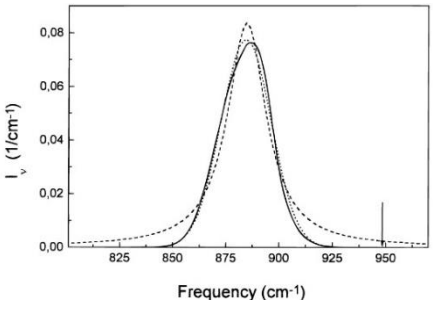


Fig. 5. Fit of the calculated upward transition spectrum in the ν_3 mode of SF_6 (solid line) by the Gaussian (dotted line) and Lorentzian (dashed line); = 20000 cm^{-1}, $2\sigma_{GW}$ = 3.6 cm^{-1}

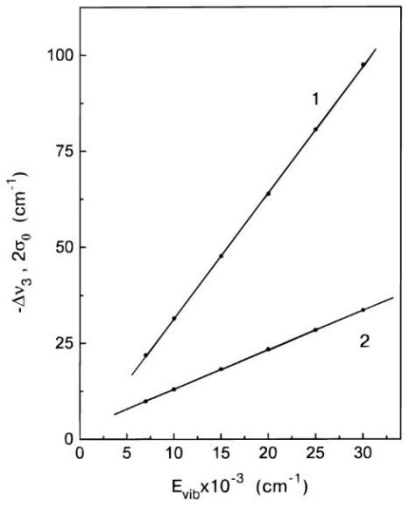


Fig. 6. Shift $\Delta\nu_3$ (line 1) of the mean frequency of the upward transitions in the ν_3 mode of SF_6 and width $2\sigma_0$ (line 2) of the spectral contour as functions of the vibrational energy

$$\Delta\nu_i = \bar{X}_\iota \frac{E_{vib}}{\nu_i} \tag{13}$$

where $\bar{X}_\iota$ is an "average" anharmonicity constant. In the case under consideration this average anharmonicity constant can be obtained from the slope of the $\Delta\nu_3(\mathrm{E}_{vib})$ dependence in Figure 6, which gives the value $\overline{X_3} = -3.11 \pm 0.01$ cm^{-1}. For interpretation of this linear law, it is ordinarily assumed that the vibrational energy is *uniformly* distributed among all vibrational degrees of freedom. Then some simple formulas expressing the $\bar{X}_\iota$ through the spectroscopic constants may be derived. In our particular case of the 3-fold degenerate mode ν_3 the formula of such a kind is

$$\overline{X_3} \approx \left(\sum_{i=1}^{6} g_i\right)^{-1} (8X_{33} + 4G_{33} + \sum_{i=1(i\neq 3)}^{6} g_i \frac{\nu_3}{\nu_i} X_{3i}) \tag{14}$$

This gives, after the substitution of the SF_6 constants, the value $\overline{X_3} = -3.136$ cm^{-1}, which agrees well with the $\overline{X_3}$ found from Figure 6.

The standard deviation σ_0 characterizes the contour width; namely, if the contour is approximated by the Gaussian, it is equal to the halfwidth at the $e^{-1/2}I_{max}$ level. One can notice that the full width $2\sigma_0$ is rather high, changing from 9.9 cm^{-1}for $E_{vib} = 7000$ cm^{-1} to 33.6 cm^{-1} for $\mathrm{E}_{vib} = 30\,000$ cm^{-1} near the dissociation limit. It is, at least, much wider than the assumed homogeneous width $2\gamma_L$ being used in the convolution procedure (the γ_L values are shown in the caption to Figure 4).

The normalized integral intensity of the spectrum $\mathrm{I}_0(\mathrm{E}_{vib})$ (see Figure 7) coincides well with the theoretical prediction $\mathrm{I}_0(\mathrm{E}_{vib}) = (\overline{n_3} + 3)/3$, where $\overline{n_3}(E_{vib})$ is the average occupation number in the ν_3 mode for the energy E_{vib}.

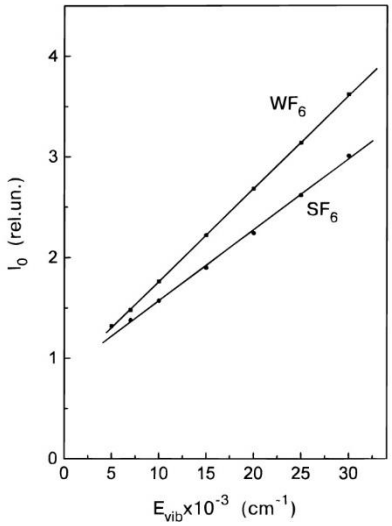


Fig. 7. Integral intensity of the upward transitions in the mode of SF_6 and WF_6 molecules as a function of the vibrational energy. This intensity $I_0$is given in the relative units of that of the $0 \rightarrow 1$ transition

It should be noted that all above calculations were performed with the inclusion of the anharmonic shifts in the state selection procedure (see section 3.1). We have checked the influence of this on the final results and found that the use of harmonic energies does not lead to significant errors. For example, at the highest E_{vib}, the errors are 3. 8% for $\Delta\nu_3$, 7.0% for σ_0, and 1.9% for I_0. In the ν_1 mode case considered in the next subsection, the similar errors are, respectively, 4.9%, 2.6%, and 2.8%.

4.1. Mode ν_1. In the case of the mode ν_1, we deal, in fact, with the Stokes Raman transitions. The histograms of their intensity distribution (see Fig. 8) look somewhat different compared to the histograms in Figure 3. Now, the groups of spectral lines with equal intensity, i.e. related to the same generated occupation number n_i are clearly seen. Also, these histograms are narrower and more asymmetric than those for the transitions in the mode ν_3. All these facts indicate what may be expected for the nondegenerate mode ν_3, whereas the anharmonic splitting in the degenerate mode ν_3 makes the spectrum broader and more symmetric. Let us clarify this.

As said, any group of the spectral lines with equal intensity joins the transitions from the states with the same and gives some fragment to the histogram. It is seen from Figure 8 that the fragment width becomes less for larger n_1. This can be easily understood as long as the energy in the other modes diminishes at the same time (the total energy E_{vib} remains constant), so deviation of the transition frequencies diminishes, too. The weight centers (mean frequencies) of different fragments do not coincide, in general. The sign of this shift of the $n_1 + 1$ fragment with respect to the n_1 fragment depends on the relations between the intramode anharmonicity constant X_{11} and the intermode anharmonicity constants X_{1i}; it is positive in the case under consideration, so one can see a sharper blue edge for the histogram.

Similar behavior could be expected for the transition spectra in the mode ν_3 if there were no anharmonic splittings. With the splitting, however, each fragment becomes wider; moreover, this additional width grows with the n_3, and any histogram asymmetry disappears.

The calculated histograms were processed as previously. The distinction was that their convolution with only the narrow Gaussian window was carried out, since there are no indications in literature of the IVR rate of the mode ν_1. The resulting spectral contours are shown in Figure 9. It is seen that these contours are narrower and less red-shifted than in the case of the mode ν_3 This is because of smaller values of the X_{1i} , anharmonicity constants. One can also see in Figure 10 that, as in the case of the mode ν_3, the spectral contour is approximated rather well by the Gaussian. Approximation by the Lorentzian is worse.

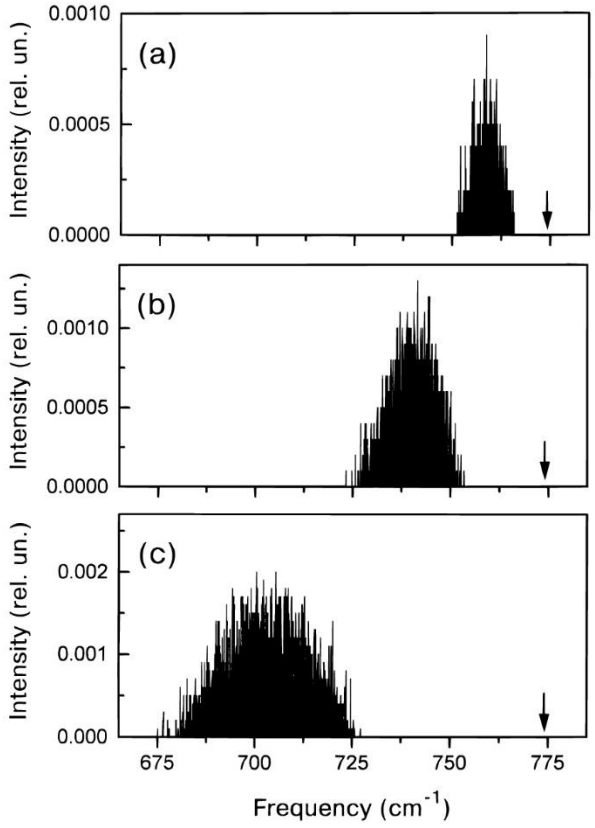


Fig. 8. Histograms of the intensity distribution of the Raman Stokes transitions in the $\nu_1$mode of SF_6 for different vibrational energies: (*a*) 7000 cm^{-1}; (*b*) 15000 cm^{-1}; (*c*) 30000 cm^{-1}. The fundamental frequency is indicated by the arrow

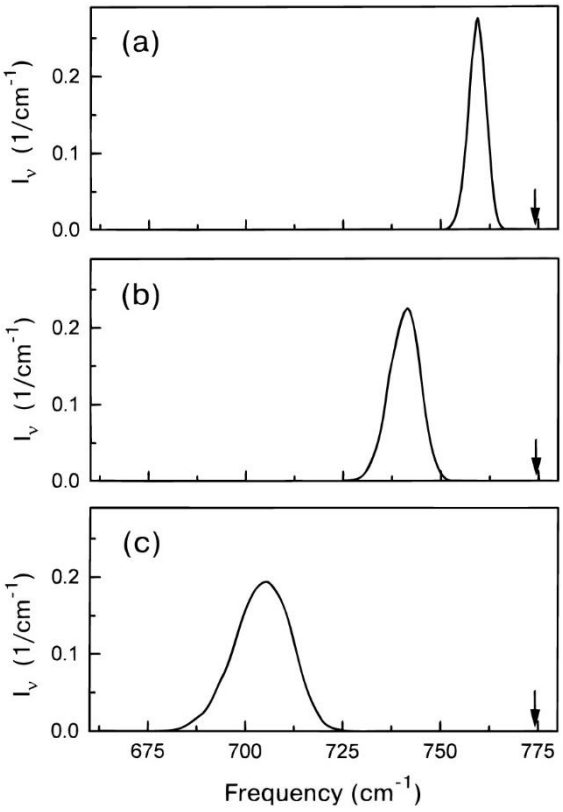


Fig. 9. Raman Stokes spectra in the ν_1 mode of SF_6 for different vibrational energies: (*a*) 7000 cm^{-1}; (*b*) 15000 cm^{-1}; (*c*) 30000 cm^{-1}. They result from convolution of the histograms in Fig. 8 with the Gaussian windows of the width $2\sigma_{GW}$ equal to 1.2 cm^{-1} (*a*), 1.6 cm^{-1} (*b*), and 2.8 cm^{-1} (*c*)

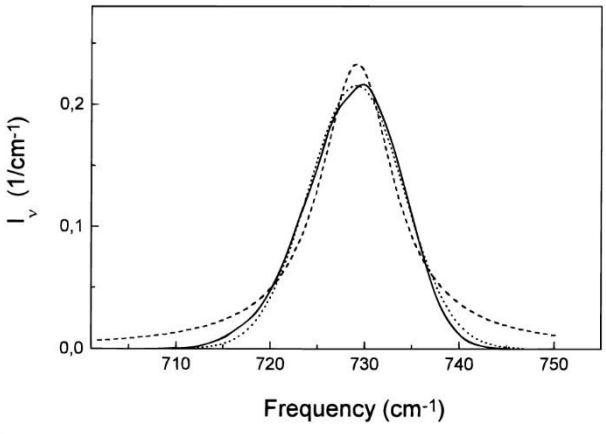


Fig. 10. Fit of the calculated Raman Stokes spectrum in the ν_1 mode of SF_6 (solid line) by the Gaussian (dotted line) and Lorentzian (dashed line); $E_{vib} = 20\,000$ cm^{-1}, $2\sigma_{GW}$=2 cm^{-1}

The shift $\Delta\nu_1$of the contour maximum and the contour width $2\sigma_0$ are shown in Figure 11 as functions of the energy E_{vib}. The average anharmonicity constant $\overline{X_1} = -1{,}85 \pm 0{,}01$ cm^{-1} can be found from the slope of the first of these dependences (see eq 13 and related discussion). The approximate formula, like eq. 14 for the 3-fold degenerated mode ν_3, is now

$$\overline{X_1} \approx \left(\sum_{i=1}^{6} g_i\right)^{-1} (4X_{11} + \sum_{i=2}^{6} g_i \frac{\nu_1}{\nu_i} X_{1i}) \qquad (15)$$

and it gives the value $\overline{X_1} = -1.873$ cm^{-1}.

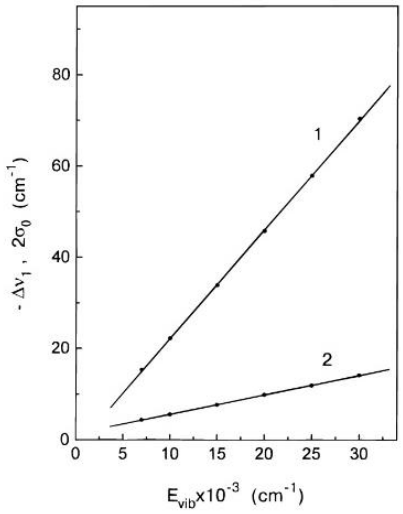


Fig. 11. Shift $\Delta\nu_1$ (line 1) of the mean frequency of the Raman Stokes transitions in the ν_1 mode of SF_6 and width $2\sigma_0$ (line 2) of the spectral contour as functions of the vibrational energy

The width $2\sigma_0$ is narrower than for the transitions in the mode ν_3 at the same vibrational energy and grows from 4.4 cm^{-1} for $E_{vib} = 7000$ cm^{-1} up to 14.2 cm^{-1} for $E_{vib} = 30\,000$ cm^{-1}. Nevertheless, these widths are again much wider than the $2\gamma_L$ for the mode ν_3. The integral normalized intensity I_0 must follow the $\overline{n_1} + 1$ prediction as the function of the vibrational energy, and it does.

Concluding this section, we stress its principal result: the widths of the SF_6 spectra in the modes ν_3 and ν_1 are determined mainly by the effect of statistical inhomogeneous broadening.

5. Results for the molecule WF_6

The developed model of statistical inhomogeneous broadening is applied here to another molecule of the XY6 type, namely, WF6. The tungsten atom is

approximately 6 times heavier than the sulfur atom, and this results in considerable change of spectral parameters of the fundamental modes. The effect of central atom substitution on the spectral features is studied in this section.

5.1. Spectroscopic parameters of WF_6. This molecule is studied much less than the SF_6. We sought complete sets of the anharmonic constants for different modes and succeeded only for the mode ν_3. Unfortunately, we did not find anywhere the experimentally measured values of intramode anharmonic constants G_{33} and T_{33}, which are responsible for splittings of the ν_3 mode energy levels. Only computed values are available from ref. 44, which are probably somewhat smaller than the actual existing ones. The latter may be deduced by comparing the SF_6 constants computed in the same ref. 44 with the experimental values. Nevertheless, we have preferred to use, for definiteness, the complete set of anharmonic constants $\{X_{33}, G_{33}, T_{33}\}$ from the same ref 44 rather than extract one of them, X_{33}, from any other source (for example, X_{33} was measured in ref. 45). As for the other spectroscopic constants, the X_{3i} and the ν_i have been taken from ref. 45, except the more precise ν_3, which was taken from ref. 46. The spectroscopic constants that are explored in the present calculations are listed in Table 2.

Table 2: WF_6 Spectroscopic Constants (in cm^{-1}) Used for Calculations

i	ν_i	X_{3i}
1	772.1	-1.7
2	678.2	-3.5
3	713.9152	$X_{33} = -0.63$ $G_{33} = 0.21$ $T_{33} = -0.105$
4	252.1	-0.5
5	320	-4.4
6	129	-2

5.2. Mode ν_3. The onset of the vibrational chaos in the molecule WF_6 is unknown, but supposedly lies lower than in SF_6 because of smaller normal mode frequencies. So, our simulations started from the energy $E_{vib} = 5000\ cm^{-1}$. As long as the anharmonicity constants of WF_6 are not known in full, we have calculated only harmonic energies of vibrational states for their selection. Figure 12 shows the inhomogeneous spectra after processing the histograms. These spectra are for the same energies as the previously shown spectra for also the mode but of SF_6 (see Figure 4). Now the spectra are about 3 times broader and more red-shifted; this may be understood from the fact that the excitations of the low-frequency modes of WF_6, due to large anharmonicity constants, lead to larger frequency shifts than in SF_6. The

spectral contour parameters $\Delta\nu_3$ and $2\sigma_0$ depending on the energy E_{vib} are shown in Figure 13. The average anharmonicity constant for the mode of WF_6 can be found from the $\Delta\nu_3 E_{vib}$ slope: $\overline{X_3} = -5.04 \pm 0.01$ cm^{-1}. The approximate formula eq. 20 gives a rather close value: $\overline{X_3} = -5.34$ cm^{-1}.

The integral normalized intensity is shown in Figure 7. As for SF_6, it follows the formula $(\overline{n_3} + 3)/3$ rather accurately.

There are no indications of the IVR rates in WF_6 anywhere in the literature. Nevertheless, numerically large inhomogeneous widths given by our simulations enable one to assume that the inhomogeneous contribution should be dominant.

Our final note concerns individual roles of scalar (mainly intermode) anharmonicity and anharmonic splitting in the formation of the inhomogeneous contour width. Looking at the values of the anharmonicity constants, one may assume that the anharmonic splitting is not very important in the specific case of WF_6. The direct calculation confirms this assumption. Another situation takes place for the same mode but of SF_6. There, these two effects give approximately equal contributions to the width. We shall discuss this point further in section 7.

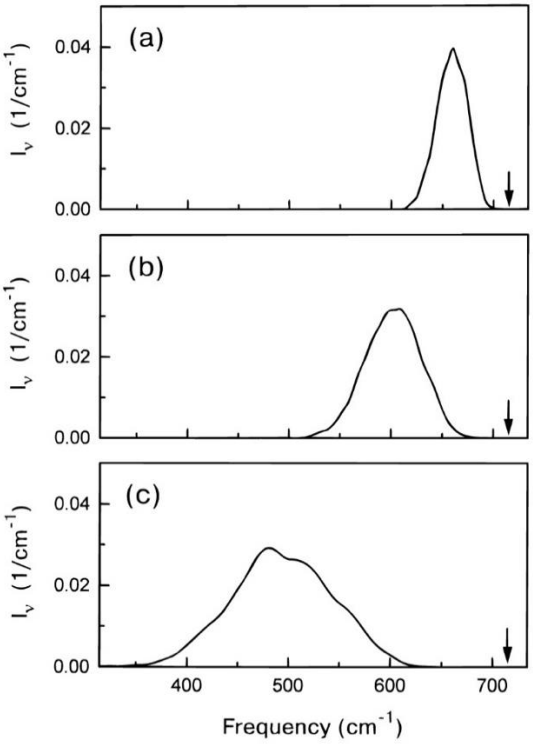


Fig. 12. Upward transition spectra in the ν_3 mode of WF_6 for different vibrational energies: (*a*) 7000 cm^{-1}; (*b*) 15000 cm^{-1}; (*c*) 30000 cm^{-1}. They result from convolution of the corresponding histograms with the Gaussian windows of the width $2\sigma_{GW}$ equal to 4.5 cm^{-1} (*a*), 8 cm^{-1} (*b*), and 15 cm^{-1} (*c*)

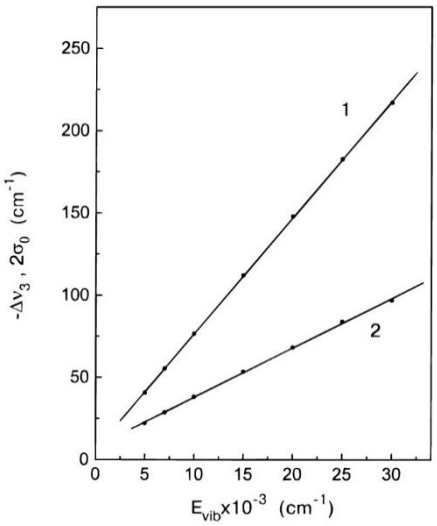


Fig. 13. Shift $\Delta\nu_3$ (line 1) of the mean frequency of the upward transitions in the $\nu_3$mode of WF_6 and width $2\sigma_0$ (line 2) of the spectral contour as functions of the vibrational energy

6. Effect of rotations on the band shapes

The above considered spectra involve only vibrational transitions but do not include any rotational substructure nor its dependence on the rotational quantum number *J*. Two effects can be added to the previous treatment in the same approximation order. They are the rotor energy, which results in different frequencies of the transitions in different rotational branches, and Coriolis splitting in the 3-fold degenerate modes, which strongly modifies the transition spectra therein. One next order effect, which is the change of the rotational constant *B* for the excited vibrational states in accordance with

$$B_{n_i} = B_0 + \alpha_i n_i \tag{16}$$

can be easily taken into account, too.

Only the latter of the mentioned effects influences spectra of the Raman transitions in the totally symmetric mode ν_1. Indeed, only the Q-branch ($\Delta J = 0$) is allowed for these transitions, and no Coriolis effect is present in the states of this nondegenerate mode. Thus, the frequency of transition from any selected state in our calculation procedure is just shifted from the previously used one by the value $\alpha_1 J(J + 1)$, and this shift does not depend on the generated mode occupation numbers, Numerically, for SF_6, the value of this shift is about 1 cm^{-1} for the typical room-temperature $J \approx 50$ cm^{-1}, i.e. small with respect to the $\Delta\nu_1$ shifts shown in Figure 11.

More complex changes may be expected, in general, for the infrared transitions in the mode ν_3.The previously calculated spectra formally correspond to the situation when both rotational constant *B* and Coriolis constant ς_3 are equal to zero.

The nonzero B and ς_3 results in the trivial fact of redistribution of the full intensity I_0 of the calculated spectra into three rotational P-, Q-, and R-branches having different mean frequencies. Their intensities are

$$I_p = \frac{2J-1}{3(2J+1)} I_0, \qquad I_Q = \frac{1}{3} I_0, \qquad I_R = \frac{2J+3}{3(2J+1)} I_0 \tag{17}$$

For the shifts of their mean frequencies from the previously calculated values caused by the rotation and Coriolis interaction, there appears the common shift for all three branches $\Delta\nu_{Cor} \approx -B\varsigma_3(n_3+2)$ and shifts for the P- and R-branches

$$\begin{aligned} \Delta\nu_p &\approx -2(1-\varsigma_3)BJ \\ \Delta\nu_R &\approx 2(1-\varsigma_3)B(J+1) \end{aligned} \tag{18}$$

which are responsible for the usual PQR-structure of the vibrational band. The main complication, however, may arise from the fact that the spectrum of any $(n_3, J) \rightarrow (n_3+1, J')$ manifold of transitions is in reality (i.e., with $\varsigma_3 \neq 0$) much more complex than the spectrum of purely vibrational transitions (with $\varsigma_3 = 0$).

One illustration is shown in Figure 14. Four spectra of $n_3 = 2 \rightarrow n_3 = 3$ transitions are presented in this figure. The spectrum in Figure 14a is one of the fragmentary spectra involved in our calculations of section 4.1 for the molecule SF_6 when any state with n_3=2 is generated, as discussed in section 3. Three other spectra in this figure are for the $(n_3 = 2, J = 15) \rightarrow (n_3 = 3, J = 14)$ transitions (b), $(n_3 = 2, J = 15) \rightarrow (n_3 = 3, J = 15)$ transitions (c), and $(n_3 = 2, J = 15) \rightarrow (n_3 = 3, J = 16)$ transitions (d). These spectra are obtained by the diagonalization of the vibration-rotation Hamiltonian H_{ν_3} of the mode ν_3, which includes the ν_3-related terms of the Hamiltonian eq. 9, the purely rotational terms, and the Coriolis interaction terms. This Hamiltonian is

$$\begin{aligned} \hat{H}_{\nu_3} = X_{33}\widehat{n_3}(\widehat{n_3}-1) + G_{33}\left(\widehat{I_3}^2 - \widehat{n_3}\right) + T_{33}\hat{O}_{33}(tensor) + \\ +(B + \alpha_3\widehat{n_3})\hat{J}^2 + B\varsigma(\hat{J}\cdot\widehat{I_3}) \end{aligned} \tag{19}$$

with the anharmonicity constants X_{33}, G_{33}, $and\ T_{33}$ of section 4 and the vibrational and Coriolis constants from ref. 37: B = 0.091 084 cm^{-1}, $\alpha_3 = -1.3106 \times 10^{-4}$ cm^{-1}, and $\varsigma_3 = 0.69344$. As the $\hat{H}_{\nu_3}$diagonalization result, one has the splittings of the (n_3, J) manifolds onto the nondegenerate levels of symmetry A_1 or A_2, 2-fold degenerate levels of symmetry E, and 3-fold degenerate levels of symmetry F_1 or F_2. Then, having the eigenvectors in the symmetry-adapted basis (see basically ref 47 and also ref. 48 for some details) and exploiting the Moret–Bailly selection rules,[47] one can calculate the intensities of allowed dipole transitions, which are, in principle, all the transitions between the states of the same symmetry; in addition, the frequencies of allowed transitions are found from the eigenvalues. After that, all the initial states (with n_3 = *2* and *J* = 15 in our case

of Figure 14) are assumed to be populated proportionally to their degeneracies, and the resulting spectra, as shown in Figure 14, are produced.

Now, two questions arise: to what extent do really more complicated fragmentary spectra modify the previous results of section 4.1, and how different are the spectra for the initial states with different J? To answer these questions, we performed the calculations of the inhomogeneous spectra in the mode ν_3 with J =15 and J = 40 in a wide range of vibrational energy. For these calculations, the state selection procedure was the same as used previously, but new, much more complex $(n_3, J) \rightarrow (n_3 + 1, J')$ transition spectra were used. The resulting spectra appear to be again nearly Gaussian, with the widths even a little narrower (e.g., about 3% for the energy 10 000 cm^{-1}) than those plotted in Figure 6. The intensity is distributed among the rotational branches in perfect correspondence with eq. 17. The mean frequencies of the different rotational branches perfectly agree with eq. 18. So, the principal conclusion from these simulations is that the vibration-rotation spectra can be produced by the purely vibrational spectra: some differences for different J in the width can be neglected, and some differences for different J in the integral intensity and mean frequency can be taken into account systematically using eqs 17 and 18.

Our final point refers to the physical reasons for the small effect of the Coriolis splitting on the spectral width. For the spectra shown in Figure 14, for example, the standard deviation that characterizes the width is 4.71 cm^{-1} for the spectrum in Figure 14*a* and 4.56 cm^{-1} for the spectra in Figure 14*b–d*. It can be derived that the standard deviation σ_{n_3} of the $n_3 \rightarrow n_3 + 1$ transition spectrum in any rotational branch may be schematically presented as

$$\sigma_{n_3} = \left(\overline{\nu_T^2} + \overline{\nu_l^2} - \bar{\nu}^2\right)^{1/2}. \qquad (20)$$

That is, the mean value of the squared frequency is the sum of two terms: the first term $\overline{\nu_T^2}$ is determined by the matrix elements of the operator $\hat{O}_{33}(tensor)$ and is therefore proportional to T_{33}^2, whereas the second term $\overline{\nu_l^2}$ is determined by the *l*-splitting of the symmetry-adapted basis states and is proportional to the value of $(G_{33} - B\varsigma_3)^2$. Hence one can easily see that the effect of the Coriolis interaction on the width is small if the ratio $B\varsigma_3/G_{33}$ is small. (For SF_6, this ratio is 0.068).

Moreover, as long as the signs of G_{33} and ς_3 are opposite, the Coriolis effect reduces the width as confirmed by the direct calculation.

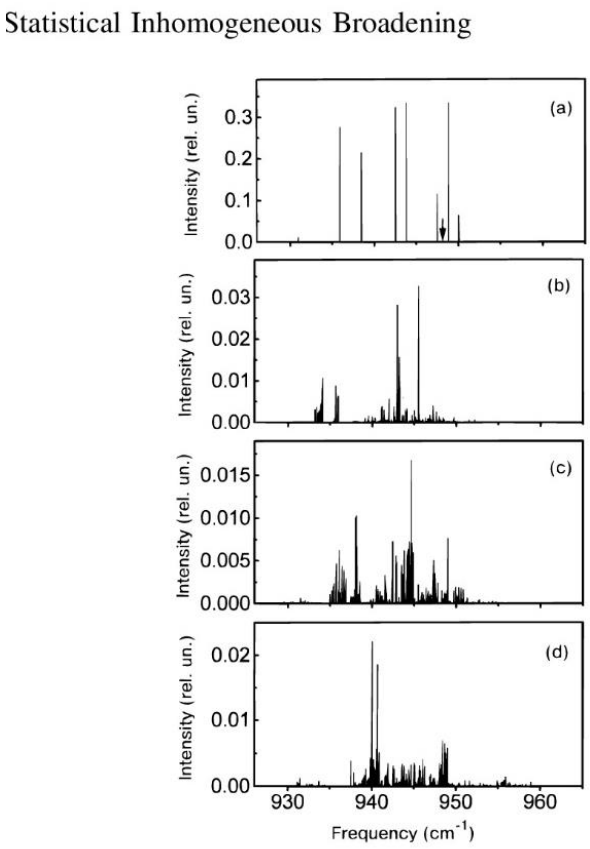


Fig. 14. Spectra of the $n_3 = 2 \rightarrow n_3 = 3$ transitions in the ν_3 mode of SF_6. (*a*) Purely vibrational spectrum; the arrow indicates the frequency of the $n_3 = 0 \rightarrow n_3 = 1$. (*b–d*) vibration-rotation spectra for the states with $J = 15$ at $n_3 = 2$ in different rotational branches: (*b*) in the P-branch, (*c*) in the Q-branch, (*d*) in the R-branch

7. Discussion and conclusions

The results of our simulations for the molecules SF_6 and WF_6 led us to consider the inhomogeneous broadening as, at least, the important effect in formation of the spectra of vibration-rotation transitions between highly excited states. The presented computational scheme has proved to be rather simple and reliable in view of several independent tests. It provides the integral intensities and peak positions very accurately in a wide range of vibrational energy from the onset of chaos up to the dissociation limit. The obtained bandwidths are much wider than those presumably caused by IVR. For the latter aspect, it should be noted that we can directly compare the widths calculated in this work with only the much narrower IVR widths for the mode ν_3 of SF_6 suggested in ref 34, but large calculated widths for the mode ν_1 of SF_6 and the mode ν_3 of WF_6, too, make the assumption for their dominant role very realistic.

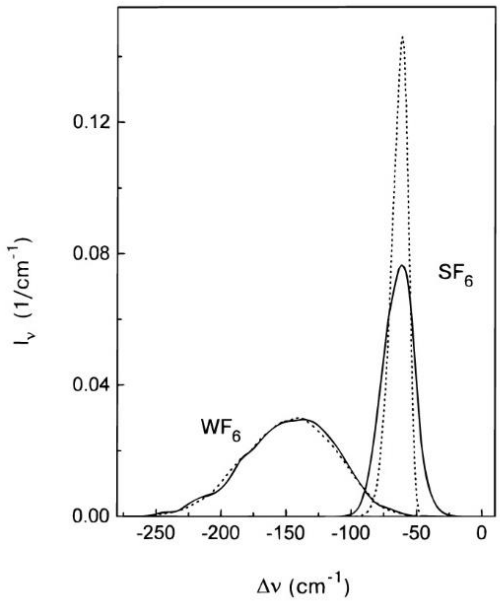


Fig. 15. Spectra of the upward transitions in the ν_3 mode of two molecules with the inclusion of the anharmonic splitting (solid line) and without it (dotted line); $E_{vib} = 20000$ cm^{-1}. Zero frequency shift in the $\Delta\nu_3$ axis refers to the fundamental frequencies 948.1025 cm^{-1} for SF_6 and 713.9152 cm^{-1} for WF_6

The Raman ν_1 band in the XY_6 type molecules is inhomogeneously broadened because of different anharmonic shifts for the excited vibrational states with different mode occupation numbers. For the infrared band ν_3, the additional effect of splitting of the states of the 3-fold degenerate mode ν_3, due to its internal anharmonicity (see section 3.2), may be significant. Its relative role can be found in the course of calculation. Figure 15 gives one illustration for the energy 20 000 cm^{-1} which shows that the contribution to the width from the anharmonic splitting is about 45% in the case of SF_6 and only about 1% in the case of WF_6. This difference is not more than the anharmonicity-constant interplay (see also the discussion at the end of section 5).

For future applications, it is useful to compare the widths calculated in this work for the mode ν_3 of SF_6 with those estimated analytically in ref. 34. The values for the width are presented there for both situations, *without* and *with* the anharmonic splitting, so it is natural to compare them with our corresponding values (as found, for example, from the dotted and solid spectral contours in Fig. 15). Such comparison shows that our "unsplit" values are 2.7 times more at $E_{vib} = 7\,000$ cm^{-1} and 2.0 times more at $E_{vib} = 30\,000$ cm^{-1} than the corresponding values of ref 34. It may be supposed that the noticed difference is due to the equipartitioning of the vibrational energy among the modes, assumed in ref 34. Since this assumption is more valid for high energies, better coincidence may be expected as the energy grows. This is really so, but the discrepancy is still large even at the dissociation limit.

Moreover, being applied to the mode ν_3 of WF_6, the analytical evaluation works much worse: it gives 5 times less values for $E_{vib} = 30\,000$ cm^{-1}and 7 times less values for $E_{vib} = 5000$ cm^{-1} than the calculated ones.

The contribution to the width from the ν_3 anharmonic splitting estimated in ref. 34 almost compensates the discrepancy with the calculation results of this work, but we believe that this fact is situational; really, the difference between the analytical evaluation and direct calculation for the ν_3 mode of WF_6 is very large: 4.5 times at $E_{vib} = 5000$ cm^{-1} and 3 times at $E_{vib} = 30\,000$ cm^{-1}.

We stress the comparison of the results of this work with the previous analytical estimates because the same effects are involved in both approaches. In reality, however, some other effects may add to the values of the widths. For example, it may occur that occasional anharmonic intermode resonances lead to redistribution of the intensity from the $n_a \rightarrow n_a + 1$ transition to some close combination transitions. In the case of SF_6, disturbance of both the ν_1 and ν_3 bands may be caused by the close intermode resonance $\nu_1 + \nu_5 \approx \nu_3 + \nu_6$, (with a defect of about 3 cm^{-1}) depending on the related anharmonicity constant value. Another effect may originate from nonzero intermode anharmonicity constants G_{ij}, $T_{ij}$and S_{ij} and lead to additional broadening of spectra of transitions in degenerate modes, as mentioned at the end of section 3.2. It should be noted that it was not computationally easy to implement the mentioned effects for the molecules like XY_6, even if all the constants are known, because of the enormous degeneracy of high vibrational states leading to the necessity of diagonalization of very large matrices for any selected state. The approaches to do this rather accurately in some indirect way are in progress now.

As for the experimental verification of the presented calculation results, we can refer to our coming publication [49]. The Raman spectrum of the mode ν_1 of SF_6 has been measured in the wide range of vibrational temperature from 850 K up to 1600 K, and rather good agreement has been found between the experimental results and spectra calculated with the use of the model presented here.

Concluding, we should note that any simple treatment of the transition spectra for highly vibrationally excited molecules is very desirable for modeling the infrared MPE dynamics. If the main features of such spectra are known on the basis of known spectroscopic constants, then the more realistic choice of other unknown parameters of the complicated MPE process can be made. Otherwise, the parameters of such spectra would be included in the list of unknown ones; making the MPE modeling much less convincing. We believe that the approach of this work, based on reasonable assumptions and computationally not hard, provides more correct and reliable spectroscopic data for transitions between highly vibrationally excited states than the prior ones.

Acknowledgment: This work was partially supported by the Russian Foundation for Fundamental Research. I.Yu.P. and E.A.R. thank Dr. A. L. Malinovsky for useful advice.

References and notes

1. (a) *Isenor N.R.; Richardson M.C.* // Appl. Phys. Lett. 1971. Vol. 18. P. 224. (b) *Isenor N.R., Merchant V., Hallsworth R.S., Richardson M.C.* // Can. J. Phys. 1973. Vol. 51. P. 1281.
2. (a) *Letokhov V.S., Ryabov E.A., Tumanov O.A.* // Opt. Commun. 1972. Vol. 5. P. 168; (b) *Ambartzumian R.V., Chekalin N.V., Doljikov V.S., Letokhov V. S., Ryabov E. A.*//Chem. Phys. Lett. 1974. Vol. 25. P. 515.
3. (a) *Ambartzumian R.V., Letokhov V.S., Ryabov E.A., Chekalin N.V.* // Sov. Phys. JETP Lett. 1974. Vol. 20. P. 273; (b) *Ambartzumian R.V., Gorokhov Yu.A., Letokhov V.S., Makarov G.N.* // Sov. Phys. JETP Lett. 1975, Vol. 21, P. 171.
4. *Ambartzumian R.V., Letokhov V.S.* In: Chemical and Biochemical Applications of Lasers / ed. Moore C.B. New York: Academic Press, 1977. Vol. 3. P. 166.
5. *Bloembergen N., Yablonovich E.*//Phys. Today. 1978. Vol.31(5). P. 23.
6. *Schulz P.A., Sudbo Aa.S., Krajnovich D.J., Kwok H.S., Shen Y.R., Lee Y.T.* // Annu. Rev. Phys. Chem. 1979. Vol. 30. P. 379.
7. *Letokhov V.S., Makarov A.A.*//Sov. Phys.-Uspekhi. 1981. Vol.24. P. 366.
8. *King D.S.* In: Dynamics of the Excited State / ed. K.P. Lawley. New York: Wiley, 1982. P. 105.
9. *Bagratashvili V.N., Letokhov V.S., Makarov A.A., Ryabov E.A.* // Multiple Photon Infrared Photophysics and Photochemistry. Chur, Switzerland: Harwood Acad. Publ., 1985.
10. Multiple-Photon Excitation and Dissociation of Polyatomic Molecules / ed. C.D. Cantrell. Berlin: Springer, 1986.
11. *Lyman J.L.* In: Laser Spectroscopy and its Applications/eds. L.J. Radziemski, R.W. Solarz, J.A.Raisner. N.Y.: Dekker, 1987. P. 417.
12. *Lupo D.W., Quack. M.* // Chem. Rev. 1987. Vol. 87, P. 181.
13. Innovative Laser Technologies in Nuclear Energy. Proceedings of the 6th International Symposium on Advanced Nuclear Energy Research. March 23–25, 1994. Mito, Ibarakie, Japan; JAERI: Japan, 1994.
14. *Bagratashvili V.N., Doljikov V.S., Letokhov V.S. , Makarov A.A., Ryabov E. A., Tyakht V.V.* // Sov. Phys. JETP. 1979. Vol. 50. P. 1075.
15. *Dűbal H.-R., Quack M.* // J. Chem. Phys. 1984. Vol. 81. P. 3779.
16. *Stuchebrukhov A., Ionov S., Letokhov V.* // J. Phys. Chem. 1989, Vol. 93. P. 5357.
17. *Stuchebrukhov A.A., Marcus R.A.*//J.Chem.Phys. 1993, Vol.98. P. 6044.
18. *Lubich L., Boyarkin O.V.. Settle R.D.F., Perry D.S., Rizzo T.R.* // Faraday Discuss. 1995, Vol. 102. P. 167.
19. *Demianenko A., Letokhov V., Makarov A., Ryabov E.* // Faraday Discuss. 1995. Vol. 102. P. 301.
20. *Evseev A.V., Krivtsun V.M., Kuritsyn Yu.A., Makarov A.A., Puretzky A.A., Ryabov E.A., Snegirev E.P., Tyakht V.V.* // Chem. Phys. 1986. Vol. 706. P. 131.
21. (a) *Bagratashvili V.N., Ionov S.I., Letokhov V.S., Lokhman V.N., Makarov G.N., Stuchebrukhov A.A.* // Sov. Phys. JETP. 1987. Vol. 66. P. 670; (b) Chem. Phys. Lett. 1988. Vol. 146. P. 599.

22. *Boyarkin O.V., Ionov S.I., Bagratashvili V.N.* // Chem. Phys. Lett. 1988. Vol. 146. P. 106.

23. *Fleming P.R., Li M., Rizzo T.R.*//J. Chem. Phys. 1991. Vol. 94. P. 2425.

24. Laser Spectroscopy of Highly Vibrationally Excited Molecules / ed. V.S. Letokhov. Bristol: Adam Hilger, 1989.

25. *Nesbitt D.J., Field R.W.* // J. Phys. Chem. 1996. Vol. 100. P. 12735.

26. *Boyarkin O.V., Ionov S.I., Kobakhidze A.A.* // Spectrochim. Acta. A. 1990. Vol. 46. P. 537.

27. (a) *Kuzmin M.V., Letokhov V.S., Stuchebrukhov A.A.* // Sov. Phys. JETP. 1986. Vol. 63. P. 264; (b) *Kuzmin M.V., Stuchebrukhov A.A.* In ref 24. P. 178.

28. *Kubo R.* In: Fluctuation, Relaxation and Resonance in Magnetic Systems / ed. D.Ter. Haar. Edinburgh: Oliver and Boyd, 1962. P. 23.

29. *Dicke R.* // Phys. Rev. 1953. Vol. 89. P. 472.

30. *Nitzan A., Persson B.N.* // J. Chem. Phys. 1985. Vol. 83. P. 5610.

31. (a) *Makarov A.A., Tyakht V.V.* // Sov. Phys. JETP. 1987. Vol. 63. P. 9; (b) *Makarov A. A.* In ref 24. P. 106.

32. *Bagratashvili V.N., Burimov V.N., Ionov S.I., Sviridov A.P., Stuchebrukhov A.A., Turovetz I.M.*//Chem. Phys. Lett. 1987. Vol.137. P.45.

33. (a) *Dűbal H.-R., Quack M.* // Chem. Phys. Lett. 1980. No. 72. P. 342; (b) *Baggot J.E., Chuang M.-C., Zare N., Dűbal H.-R., Quack M.* // J. Chem. Phys. 1985. Vol. 82. P. 1186.

34. *Angelié C.* // J. Chem. Phys. 1993. Vol. 98. P. 2541.

35. *Rice S.A.* In: Photoselective Chemistry. Part 1. / eds. J. Jortner, R.D. Levine, S.A. Rice. Advances in Chemical Physics. Vol. 47. New York: Wiley, 1981. P. 117.

36. *Hecht K.T.* // J. Mol. Spectrosc. 1960. Vol. 5. P. 355.

37. *Bobin B., Bordé C.J., Bordé J., Bréant C.* // J. Mol. Spectrosc. 1987. Vol. 121. P. 91.

38. *McDowell R.S., Krohn B.J., Flicker H., Vasquez M.C.* // Spectrochim. Acta. 1986. Vol. 42A. P. 351.

39. *Alimpiev S.S., Sartakov B.G.* // Laser Chem. 1992. Vol. 12. P. 147.

40. *McDowell R.S., Krohn B.J.*//Spectrochim. Acta.1986. Vol. 42A. P.371.

41. (a) *Malinovsky A.L., Letokhov V.S., Ryabov E.A.* // Chem. Phys. 1989. Vol. 139. P. 229; (b) *Ryabov E.A.* In ref 24. P. 55.

42. *Becker F.S., Kompa K.L.* // Nucl. Technol. 1982. Vol. 58. P. 329.

43. *Angelié C.* // J. Chem. Phys. 1992. Vol. 96, P. 8072.

44. *Halonen L., Child M.S.* // J. Chem. Phys. 1983. Vol. 79. P. 559.

45. McDowell R.S., Asprey L.B.//J. Mol. Spectrosc. 1973. Vol.48. P. 254.

46. *Takami M., Kuze H.J.* // Chem. Phys. 1984. Vol. 80. P. 5994.

47. *Moret-Bailly J.* // J. Mol. Spectrosc. 1965. Vol. 15. P. 344.

48. *Cantrell C.D., Letokhov V.S., Makarov A.A.* In: Coherent Nonlinear Optics. Recent Advances / eds. M.S. Feld, V.S. Letokhov. Topics in Current Physics. Vol. 21. Berlin: Springer, 1980. P. 165.

Malinovsky A.L., Petrova I.Yu., Ryabov E.A., Makarov A.A., Letokhov V.S. To be published.

ЛАЗЕРНАЯ БИОМЕДИЦИНА

1. *Абильсиитов Г.А., Беляев А.А., Брагин М.А., Велихов Е.П., Жданов В.С., Кару Т.Й., Летохов В.С., Рагимов С.Э., Руда М.Я., Трубецкой А.В., Фурзиков Н.П., Чазов Е.И.* Изучение фотоабляции атеросклеротических бляшек лазерным излучением // Квант. электроника. 1985. Т. 12 (10). С. 1991–1993.

2. *Karu T., Tiphlova O., Esenaliev R., Letokhov V.* Two different mechanisms of low-intensity laser photobiological effects on Escherichia coli // Lasers Surg. Med. 1993. Vol. 13. P. 470–484.

3. *Esenaliev R.O., Oraevsky A.A., Letokhov V.S., Karabutov A.A., Malinsky T.V.* Two different mechanisms of low-intensity laser photobiological effects on Escherichia coli studies of acoustical and shock waves in the pulsed laser ablation of biotissue // J. Photochem. Photobiol. B: Biol. 1994. Vol. 24. P. 155–161.

4. *Karabutov A.A., Podymova N.B., Letokhov V.S.* Time-resolved laser optoacoustic tomography of inhomogeneous media. Appl. Phys. B. 1996. Vol. 63. P. 545–563.

Квант. электроника. 1985. Т. 12 (10). С. 1991–1993

ИЗУЧЕНИЕ ФОТОАБЛЯЦИИ АТЕРОСКЛЕРОТИЧЕСКИХ БЛЯШЕК ЛАЗЕРНЫМ ИЗЛУЧЕНИЕМ

Г.А. Абильсиитов, А.А. Беляев, М.А. Брагин, Е.П. Велихов, В.С. Жданов, Т.Й. Кару, В.С. Летохов, С.Э. Рагимов, М.Я. Руда, А.В. Трубецкой, Н.П. Фурзиков, Е.И. Чазов

Научно-исследовательский центр по технологическим лазерам АН СССР, Институт экспериментальной кардиологии, Всесоюзный кардиологический научный центр АМН СССР, Москва

Исследовались механизмы и продукты разрушения атеросклеротических бляшек и стенок артерий лазерным излучением с длинами волн 308, 539 и 1078 нм при плотности энергии 0,5–8 Дж/см^2. Видимое и ИК-излучение обладают порогом разрушения тканей 3–4 Дж/см^2, причем разрушение носит «взрывной» характер с выбросом крупных фрагментов. УФ-излучение обеспечивает «мягкую» абляцию тканей во всем интервале плотностей энергии при минимальном воздействии на прилежащие слои. Удельная энергия абляции на воздухе составляет 1,1 ± 0,3 кДж/г, эффективный квантовый выход летучих продуктов (в вакууме) — 0,8 ± 0,3. Квантовый выход липидов и их фотопродуктов примерно одинаков для всех длин волн и не превышает 10^{-3}. Полученные данные подтверждают фотохимический механизм абляции тканей излучением XeCl-лазера.

Атеросклеротические поражения кровеносных сосудов служат частой причиной нарушений кровоснабжения различных органов и тканей. Специфика атеросклероза такова, что во многих случаях заболевание протекает бессимптомно вплоть до осложнений. Поэтому наряду с профилактическими мерами медицине требуются средства лечения отдаленных стадий атеросклероза. Одним из таких средств является новый и перспективный метод сердечно-сосудистой хирургии — лазерная ангиопластика.

Идея метода состоит в том, что лазерное излучение с требуемыми параметрами по гибкому световоду, введенному в русло сосуда, подводится непосредственно к атеросклеротической бляшке или тромбу и разрушает это препятствие, восстанавливая кровоток. В первых экспериментах такого типа использовалось непрерывное излучение аргонового и YAG: Nd-лазеров. Было показано, что разрушению поддаются все типы бляшек и тромбов, причем процесс можно проводить с минимальными повреждениями стенок сосудов [1–4]. Опыты применения метода на животных [5] и первые операции на людях [6, 7] дали неоднозначные результаты. В одних случаях наблюдалось улучшение кровоснабжения пораженного органа без видимых послеоперационных осложнений [6], в других — пробитый излучением канал тромбировался [7].

Возможно, причиной такого осложнения является тепловой характер разрушения препятствий непрерывным излучением. Термический режим заставляет ограничиваться малыми диаметрами каналов, чтобы не повредить стенку. Кроме того, не исключено, что образующаяся при этом поверхность канала оказывается тромбогенной.

Выходом может оказаться переход от термодеструкции к фотохимической абляции бляшек и тромбов с помощью УФ-излучения. При фотохимическом воздействии энергия излучения затрачивается непосредственно на разрыв химических связей с последующим разрушением тканей. Имеются первые сообщения о действии лазерного УФ-излучения на атеросклеротические бляшки in vitro, в которых по морфологическим признакам делается вывод об отличии механизма действия от случаев видимого и ИК излучений [8, 9]. В нашем сообщении приведены предварительные данные по исследованию механизма и продуктов разрушения бляшек лазерным излучением.

Эксперименты проводились на сегментах артерий различной локализации, полученных при вскрытиях. Образцы облучались в дистиллированной воде, на воздухе или в вакууме излучением эксимерного XeCl-лазера, Nd–$YAlO_3$-лазера и его второй гармоники. Энергия в импульсе составляла 10-50 мДж, плотность энергии на поверхности образцов 0,5–8 Дж/см^2, частота повторения импульсов достигала 12,5 Гц. Для сравнения проводились опыты с излучением непрерывного Ar-лазера мощностью 0,1–0,2 Вт во всех линиях при плотности мощности на образце от 2 до 700 Вт/см^2. Продукты абляции в воде идентифицировались по спектру поглощения в видимой и ближней УФ-областях, а летучие продукты абляции в вакууме — по спектру ИК- поглощения.

В случае Nd–$YAlO_3$-лазера и его второй гармоники разрушение начиналось только при превышении пороговой плотности 3–4 Дж/см^2 и носило «взрывной» характер с выбросом фрагментов тканей. Непрерывное излучение Ar^+-лазера при указанных параметрах не разрушало образцы. Действие излучения XeC1-лазера на образцы приводило к «мягкому» удалению вещества тканей без признаков обугливания и с минимальным выбросом конденсированных продуктов. Абляция наблюдалась во всем интервале плотностей энергии.

На рис. 1 показано сечение канала, образованного шестью импульсами излучения XeC1-лазера в стенке аорты на воздухе. Длина канала 1,5 мм, диаметр в средней части около 100 мкм. Стенки канала ровные, поврежденный слой практически отсутствует. Приповерхностные слои частично закручены кверху, вероятно, в результате выхода газообразных продуктов. Такая структура канала разительно отличается от случаев воздействия непрерывного видимого и ИК излучения, для которых характерны рваные стенки канала и наличие частиц угля на его поверхности [2, 4, 5].

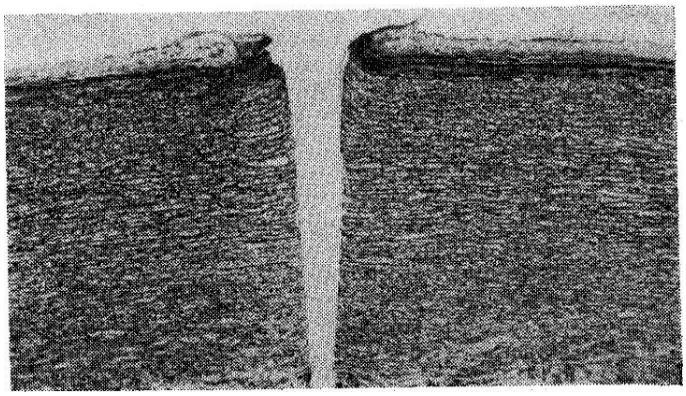


Рис. 1. Продольный срез канала в стенке аорты, образованного УФ-лазерным излучением

Дополнительное указание на фотохимический механизм абляции дает измерение ее удельной энергии. Для этого образцы массой 17–35 мг помещались на чашку торсионных весов и облучались серией из 6–30 импульсов XeCl лазера с энергией 22 мДж. Удельная энергия абляции на воздухе составила 1,1 ± 0,3 кДж/г. Она заметно не изменялась при облучении здоровой стенки или бляшки. Отметим, что удельная энергия термодеструкции тканей составляет от 3 до 10 кДж/г [10, 11], поэтому полученная нами величина говорит в пользу фотохимического механизма.

Основными продуктами УФ-абляции образцов были пары и газы. Измерения давления этих продуктов при абляции в вакууме дали квантовый выход, равный 0,8 ± 0,3. Это значение получено для свежих образцов на фоне их сублимации. Квантовый выход для сублимированных образцов падал до 0,1–0,2. ИК спектр поглощения летучих продуктов показал, что главным их компонентом является вода (рис. 2).

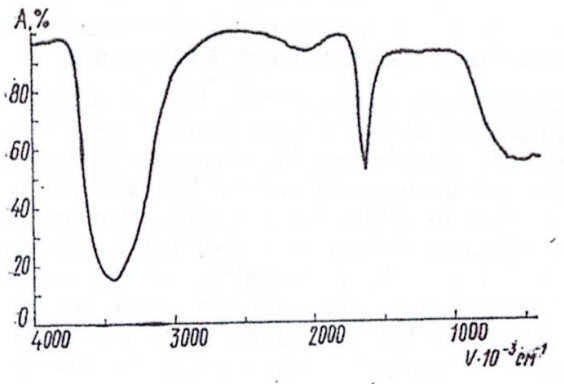


Рис. 2. ИК-спектр поглощения летучих продуктов абляции бляшки в вакууме. Толщина слоя 6 см, полное давление 14 мм рт. ст.; полосы 3430 и 1635 $см^{-1}$ принадлежат парам воды

В спектре поглощения продуктов в видимой и УФ-областях присутствуют пик с центром –200 нм (липиды), плечи на 235 и 270 нм (диеновые и триеновые гидроперекиси жирных кислот) и слабая полоса на 420 нм (аддукт цистина с сольватированным электроном) [12]. Квантовый выход этих продуктов по оценкам равен ~10^{-3}.

Таким образом, полученные результаты позволяют утверждать, что в основе абляции атеросклеротических бляшек излучением XeCl-лазера лежит фотохимический механизм.

Литература

1. *Lee G., Ikeda R.I., Kozina J., Mason D.T.*//Amer. Heart J. 1981. Vol. 102. P. 1074.

2. *Abela G.S., Normann S., Cohen D. et al.* // Amer. J. Cardiology. 1982. Vol. 50. P. 1199.

3. *Choy D.S.J., Stertzer S., Rotterdam H.Z. et al.* // Amer. J. Cardiology. 1982. Vol. 50. P. 1206.

4. *Geschwind H.J., Boussignac G., Teisseire B. et al.* // Brit. Heart J. 1984. Vol. 52. P. 484.

5. *Lee G., Ikeda R.M., Theis J.H. et al.* // Amer. J. Cardiology. 1984. Vol. 53. P. 290.

6. *Ginsburg R., Kim D.-S., Guthaner D. et al.* // Clin. Cardiology. 1984. Vol. 7. P. 54.

7. *Choy D.S.J., Stertzer S., Myler R. et al.* Conf. on Lasers and ElectroOptics, June 19–22, 1984. // Anaheim, CA, USA, techn. digest.

8. *Grundfest W., Litvack F., Forrester J. et al.* // Circulation [Suppl. II]. 1984. Vol. 70 (10). P. 11.

9. *Isner J.M., Clarke R.H., Donaldson R.F. et al.* Ibid.

10. *Алейников В.С., Бондаренко Ю.Ф., Масычев В.И., Санферова Л.И.* // Электронная промышленность. 1984. № 10 (138). С. 12.

11. *Бондаренко Ю.Ф.*// Электронная промышленность. 1984. № 10 (138). С. 16.

12. *Конев С.В., Волотовский И.Д.* Фотобиология. Минск: БГУ, 1979. С. 265, 272.

J. Photochem. Photobiol. B: Biol. 1994. Vol. 24. P. 155–161

TWO DIFFERENT MECHANISMS OF LOW-INTENSITY LASER PHOTOBIOLOGICAL EFFECTS ON *ESCHERICHIA COLI*

Tiina Karu[a], Olga Tiphlova[a], Rinat Esenaliev[b] and Vladilen Letokhov[b]
[a]*Laser Technology Centre of the Russian Academy of Sciences, 142092 Moscow Region, Troitzk, Russia*
[b]*Institute of Spectroscopy of the Russian Academy of Sciences, 142092 Moscow Region, Russia*

Bacterial suspensions in a phosphate buffer were irradiated at wavelengths λ of 632.8, 1066 and 1286 nm, incubated in Hottinguer broth for 60 min and assayed for viability by the standard surface-plating technique. The difference between the number of viable cells in the irradiated culture and the control was termed growth stimulation. Irradiation of the bacteria with an He–Ne laser (632.8 nm) or semiconductor lasers at 1066 and 1286 nm at various intensities and irradiation times produced two maxima in the growth stimulation *vs*. dose curve. The first maximum, in all cases, occurred near 50 J m^{-2}, and the reciprocity law was obeyed. The second maximum occurred at an irradiation time of 100 s irrespective of the particular radiation intensity, and the reciprocity law was not obeyed. It is assumed that two different mechanisms are responsible for these two maxima in the growth stimulation *vs*. dose curve.

Keywords: Escherichia coli WP2; He–Ne laser; Low-poser laser effects; Reciprocity law; Semiconductor lasers.

1. Introduction

According to the reciprocity law, the photobiological response is independent of the intensity of light and the irradiation time when the dose is kept constant [1]. However, this law does not always hold true, as illustrated in ref. 1, where the intensity of light or the irradiation time has been shown to be a more important factor than the total exposure dose.

The goal in previous experiments was to determine the quantitative laws governing the effect of visible monochromatic light on metabolism in various eukaryotic and prokaryotic cells [2, 3]. When studying long-term photobiological responses, such as the increase in proliferation or multiplication of microorganisms, the reciprocity law was found to be invalid. For example, when the DNA synthesis rate was measured 1.5 h after irradiation of HeLa cells with, He-Ne and dye lasers at 633 nm, the effect was found to be dependent on the laser intensity and irradiation time, with the dose

remaining constant (see refs. 2–4). A similar intensity dependence was revealed in *Escherichia coli* cells irradiated with an argon ion laser at 454 nm [5, 6]. It should be noted that both examples are concerned with long-term photobiological responses involving long chains of dark photosignal transduction reactions (see transduction mechanisms in eukaryotic cells [3] and *E. coli* [6]). The reciprocity law has also been found to be invalid in the case of human fibroblasts irradiated at 623.8 nm when measuring collagen synthesis as a final photobiological effect [7].

The aim of the experiments reported in this paper was to investigate the intensity and time dependence of the growth of *E. coli* at various red and near-IR wavelengths (632.8,1066 and 1286 nm). These experiments may be of interest not only in photobiology, but also in medicine, especially with regard to the wound-healing mechanism. The He-Ne laser (λ = 632.8 nm) has been used for many years as a main light source in low-power laser treatment of trophic ulcers and indolent wounds, as well as various pain conditions (see refs. 2 and 3 and references cited therein). Recently, various semiconductor lasers emitting in the near-IR region have been used for the same purpose. These lasers have a number of advantages over the He-Ne laser (compact size, electrical safety, simplicity of use, higher reliability), which makes them promising for medical and biological applications. An *E. coli* culture was studied as a cell population model using the method developed for the quantitative determination of the acceleration of division in these bacteria under the effect of visible light [5, 6] and near-IR radiation at 890 nm [8] and 1300 nm [9].

Materials and methods

2.1. Bacterial strain

The *E. coli* WP2 trp^- strain was supplied by the Genetic Faculty of Moscow Lomonosov University.

2.2. Chemicals

All compounds used were of reagent grade and purchased from Chemapol (Prague, Czech Republic) and Reanal (Budapest, Hungary).

2.3. Culture media and growth conditions.

Inoculation and growth conditions have been described elsewhere [5]. Cells grown to a late logarithmic state (concentration between 1×10^8 and 2×10^8 cells ml^{-1}) were harvested on a nitrocellulose filter (Millipore, 0.4, μm), washed twice with a 0.05 M K, Na-phosphate buffer solution of pH 7.0, and resuspended in the same solution to a concentration between 2×10^8 and 5×10^8 cells ml^{-1}. The suspension thus obtained was used for irradiation experiments.

2.4. Radiation sources

Continuous wave (CW) radiation at λ = 632.8 nm was obtained from an He-Ne laser (Spectra Physics, model 125A), CW radiation at λ = 1066 nm from an Nd:YAG laser pumped with a diode laser (NPO “Polyus”, Moscow, Russian Federation) and

CW radiation at λ = 1286 nm from an InGaAsP-InP laser diode (ILPN-206, NPO "Polyus", Moscow, Russian Federation). An IR filter was used to avoid exposure to short-wavelength red radiation of the Nd:YAG laser.

2.5. Irradiation procedure

A bacterial suspension (0.09 ml; 2.7 × 108 cells ml^{-1} in a 0.05 M K Na-phosphate buffer at pH 7.0) was irradiated in a round-faced quartz cell (d = 2.8 mm) (Fig. 1(a)). Another sample of the same suspension (1.0 ml) was irradiated in a glass flask with a bottom diameter of 24 mm (Fig. 1(b)). Irradiation was performed in the dark at room temperature. During irradiation, the cuvettes were placed on special holders. The beam area covered the cell suspension. The light intensity at 632.8 nm was measured with a power meter (model 404, Spectra Physics) and that at 1066 and 1286 nm with a power meter (NPO "Polyus", Moscow, Russian Federation) specially constructed for these lasers. The irradiation time was varied from 10^{-2} to 900 s, the intensity from 3 to 3 × 10^3 W m^{-2} and the dose from 5 to 2 × 105 J m^{-2}. A special automatic shutter was used for the exact control of the irradiation time.

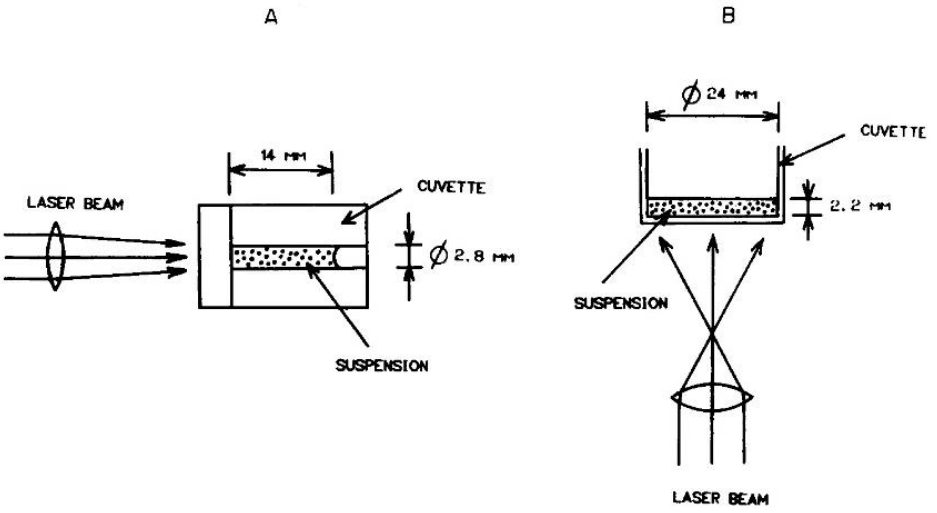


Fig. 1. Two types of cuvettes for irradiation of *E. coli* suspension

2.6. Viability assay

The irradiated and control (unexposed but placed in cuvettes for corresponding time periods) bacterial suspensions (0.05 ml) were diluted in the ratio 1:10 with a fresh nutrient medium (Hottinguer broth, pH 7.0) and incubated at 37 °C for 60 min. After incubation, the bacteria were assayed for viability by the standard surface-plating technique on agar plates (1.2% agar, Serva, Germany); the colonies were counted after incubation for 20 h at 37 °C. Five independent experiments were performed. Each experiment was performed in triplicate with individual suspension samples. Therefore, each data point is an average of 15 independent measurements.

2.7. Term "growth stimulation"

The term growth stimulation refers to the difference between the number of viable cells in the irradiated culture and the control culture, measured after 60 min incubation using the surface-plating technique.

2. Results

The irradiation of bacteria with the He-Ne laser (λ = 632.8 nm) and semiconductor lasers (λ = 1066 and 1286 nm) at a constant intensity of 157 W m^{-2} (the irradiation time was varied over a wide range from 10^{-2} to 900 s) produces two distinct maxima in the dose dependence curves (Fig. 2). The results presented in Fig. 2 show that, when the cells are exposed to radiation of the same intensity (157 W m^{-2}), the optimal doses for both maxima are practically the same for all the three wavelengths investigated (633, 1066 and 1286 nm). The first maximum (termed maximum A), in all cases, occurs near 50 J m^{-2}, and the second (referred to as maximum B) near 10^4 J m^{-2}.

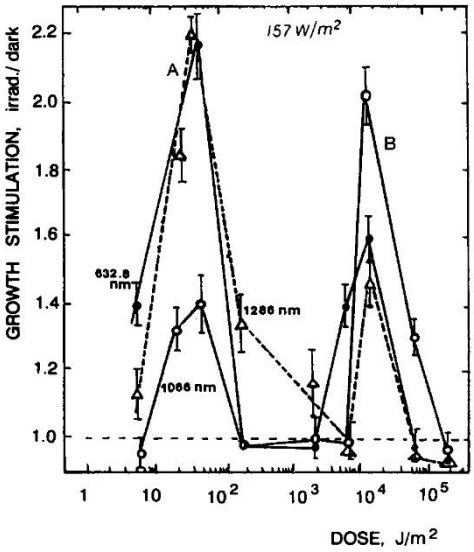


Fig. 2. Dose dependences of *E. coli* growth stimulation. The bacterial suspension was irradiated at an intensity of 157 W m^{-2} at wavelengths of 632.8, 1066 and 1286 nm

In the next series of experiments, irradiation at 632.8 nm was used at three intensities (60, 157 and 3 × 10^8 W m^{-2}), and the formation of maxima A and B was measured as a function of the irradiation time (Fig. 3). As shown in Fig. 3, maximum A in these experimental conditions depends on the irradiation time, whereas maximum B is independent. These results are analysed in Figs. 4 and 5.

Figures 4 and 5 show the irradiation dose and time corresponding to maxima A and B as a function of the radiation intensity. The irradiation time necessary for the formation of maximum A depends on the radiation intensity (Fig. 4, top): the higher

the radiation intensity I, the shorter the irradiation time τ. It can also be seen from Fig. 4 (bottom) that, for the first stimulation maximum (A) to form irrespective of the radiation intensity, the cells must be exposed to a dose of 50 ± 10 J m^{-2}. This means that the reciprocity law, in this case, is strictly obeyed.

Figure 5 (top) indicates that, for the second maximum (B) to occur, it is necessary that the cells should be irradiated for at least 100 s, regardless of the radiation intensity. The irradiation dose required for maximum B to form ranges between 6×10^3 and 3×10^5 J cm^2 (Fig. 5, bottom). It is clear from these data that, in the case of second maximum (B), the reciprocity law is not obeyed.

By analysing the data for λ = 1066 nm in the same way for three intensities (3, 157 and 721 W m^{-2}), similar results were obtained. Again, in the case of the first maximum (A), the reciprocity law was valid. This maximum formed at a dose of 40 J m-2. The second maximum (B) was observed to occur when the irradiation time reached 100 s (doses 3×10^2, 1.6×10^4 and 7.2×10^4 m^{-2}, data of Fig. 2).

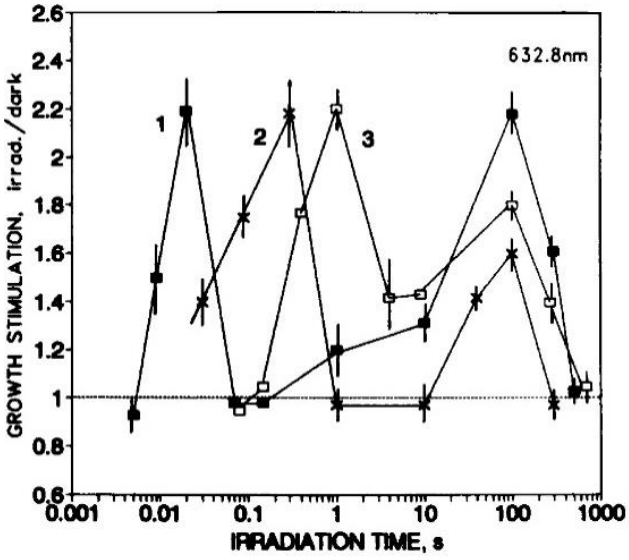


Fig. 3. *E. coli* growth stimulation as a function of the irradiation time. The bacterial suspension was irradiated at 632.8 nm at 3×10^3 W m^{-2} (1), 157 W m^{-2} (2) and 60 W m^{-2} (3)

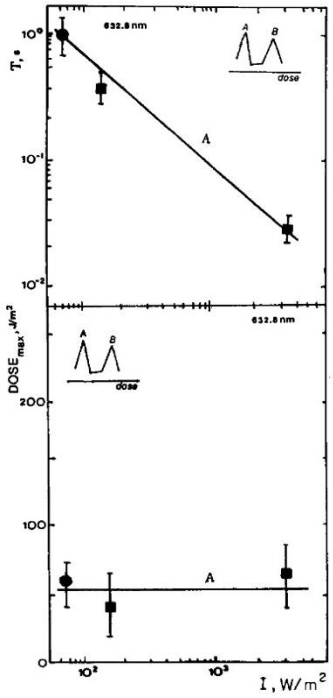


Fig. 4. Irradiation time (top) and dose (bottom) as a function of the irradiation intensity for maximum A for the bacterial suspension irradiated at 632.8 nm. The circles denote the cells irradiated in cuvette B (see Fig. 1) and the squares indicate the cells irradiated in cuvette A (Fig. 1)

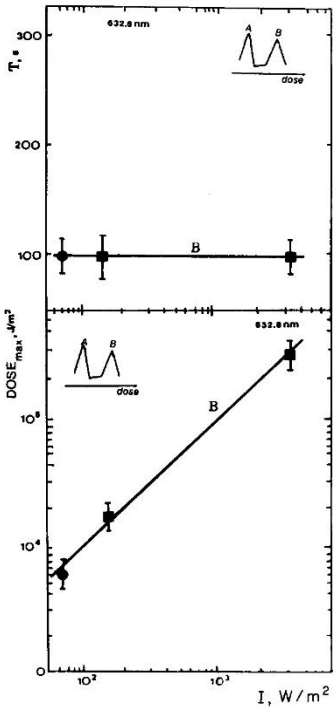


Fig. 5. Irradiation time (top) and dose (bottom) as a function of the radiation intensity for maximum B for the bacterial suspension irradiated at 632.8 nm. The circles denote the cells irradiated in cuvette B (Fig. 1) and the squares indicate the cells irradiated in cuvette A (Fig. 1)

4. Discussion

The data obtained show that there are two different maxima in the growth stimulation vs. dose curves. In the case of the first maximum (A), the reciprocity law is obeyed, and in the case of the second maximum (B), it is invalid. These data clearly indicate that the biochemical reactions (the entire photosignal transduction chain from light absorption to final photobiological response, or a part of it) providing for growth stimulation occur by two different channels, one being activated by the irradiation dose (optimal D = 50 J m^{-2}) and the other by a critical value of the exposure time (τ = 100 s).

By comparing these results with the dose dependences for other wavelengths and intensities (Fig. 6) obtained in previous experiments [5, 6], we can see that maximum B coincides with the maxima measured earlier at wavelengths of 750, 632.8, 560 and 454 nm and intensities of 60 or 100 W m^{-2}. Maximum A is very similar to the maxima measured earlier for 404 nm [5] (Fig. 6) and 890 nm [8] at low intensities (0.2 W m^{-2} and 1.2 × 10^{-2} W m^{-2} respectively).

When discussing the mechanism of E. coli growth stimulation, as well as other low-power laser effects, we should distinguish between two classes of reactions: firstly, the primary events in the photoacceptor molecules (light-induced reactions), and secondly, the subsequent biochemical reactions occurring in the dark (photosignal transduction and amplification).

The primary mechanisms by which light acts on the respiratory chain components of photoacceptor molecules (NADH dehydrogenase and cyt d in E. coli [5, 6]; NAD, nicotinamide adenine dinucleotide; cyt, cytochrome) are still not perfectly understood. One possibility discussed previously is that electron transfer in the respiratory chain is increased as a result of a change in the redox properties of the carrier due to the photoexcitation of their electronic states [3]. More recently, it has been assumed that the local pulsed heating of the absorbing chromophores may also be responsible for the growth stimulation of E. coli [10]. Therefore, let us estimate, first of all, the possibility of thermal effects for near-IR light.

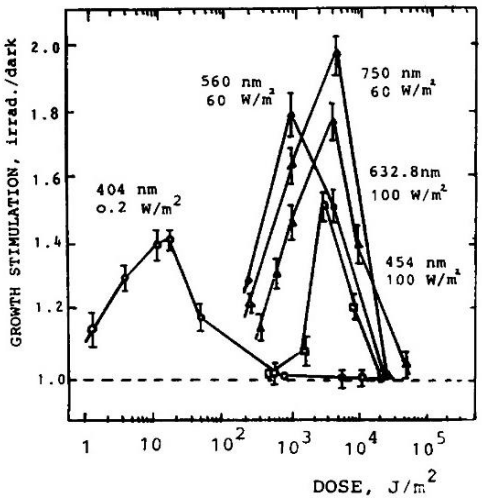


Fig. 6. Dose dependence of *E. coli* growth stimulation at various wavelengths and intensities (adapted from refs. 5 and 6)

The medium being irradiated contains weakly absorbing water molecules at concentration of nw and strongly absorbing chromophore molecules at a concentration of nchr. Heating of the suspension results from the absorption of radiation by both water and chromophore molecules. As shown in our calculations presented in Appendix A, the maximum possible volume-averaged heating in our experimental conditions does not exceed 10^{-2}–10^{-1} °C. Therefore this kind of thermal effect plays a negligible role, if any, in growth stimulation.

The situation is different when we estimate the possible transient local heating of the absorbing chromophores (e.g., cyt d complex in our case [5, 6]). As shown from the calculations presented in Appendix A, the local temperature rise around the chromophore molecule in our experimental conditions can reach tens of Kelvin. Although

it only lasts for a very short period of time, around 10^{-12} s, this overheating can cause various conformational changes both in the chromophore group itself and in the surrounding regions, which can result in significant alteration of the biological activity of the molecules.

It should be noted that reactions can also occur in the excited photoacceptor molecules, e.g., those yielding superoxide radical or singlet oxygen. These possibilities have been discussed in ref. 11.

Let us discuss the reaction channel requiring a certain irradiation period (100 s) for activation (maximum B in Fig. 2). It has been suggested [3, 6] that the absorption of light by the respiratory chain components (flavin dehydrogenases and cytochromes) causes a short-term activation of the redox chain and the oxidation of the cellular reductants, mostly the NADH pool. Redox chains, both bacterial and mitochondrial, are known to change their redox state within a period of 10 to 100 s [12]. It should be noted that the turnover numbers of individual carriers are much greater (in the range 0.7-140 s^{-1} [13]). We cannot rule out the possibility that the second maximum (B) is caused by saturation of the light-absorbing molecules. The long irradiation period needed (100 s) supports this suggestion.

The knowledge of the temporal-spatial arrangement and function of the metabolic pathways is rather limited, and so it is very difficult to draw inferences about the possible light-sensitive regulation of the respiratory chain function. It can be assumed that a reaction exists to initiate electron flow in the chain. The existence of a regulatory reaction is supported by the data presented in ref. 14, which demonstrate that the redox-state-dependent binding of proline dehydrogenase with E. coli membranes regulates the function of the electron transport chain. It should also be recalled that the growth stimulation of E. coli by He-Ne laser radiation depends on the genetic constitution of the cells [15].

5. Conclusions

In this work, it was found that there are two dose regions for the same photobiological effect, namely the stimulation of E. coli. The reciprocity law was found to be valid for one dose-response maximum and invalid for the other.

References

1. *Smith K.S., Hanawalt P.C.* Molecular Photobiology. New York and London: Academic Press, 1969.

2. *Karu T.I.* Photobiological fundamentals of low-power laser therapy // IEEE J. Quantum Electron. 1987. Vol. 26. P. 1703–1721.

3. *Karu T.I.* Molecular mechanisms of the therapeutic effect of low-intensity laser radiation // Lasers Life Sci. 1988. Vol. 2. P. 53–74.

4. *Karu T.I., Kalendo G.S., Letokhov V.S., Lobko V.V.* Dependence of biological action of low-intensity visible light upon HeLa cells on the parameters of irradiation:

coherence, dose, wavelength and intensity. II. // Sov. J. Quantum Electron. 1983. Vol. 13. P. 1169–1172.

5. *Tiphlova P.A., Karu T.I.* Stimulation of *Escherichia coli* division by low-intensity monochromatic light // Photochem. Photobiol. 1988. Vol. 48. P. 467–471.

6. *Tiphlova O.A., Karu T.I.* Action of low-intensity laser radiation on *Escherichia coli* // Crit. Rev. Biomed. Eng. 1991. Vol. 18. P. 387–412.

7. *Van Breugel H.M.F.I., Dop Bär P.R.* Power density and exposure time of He-Ne laser irradiation are more important than total energy dose in photo-biomodulation of human fibroblasts *in vitro* // Lasers Surg. Med. 1992. Vol. 12. P. 528–537.

8. *Zharov V.P., Karu T.I., Litvinov Yu.O., Tiphlova O.A.* Biological effect of radiation of a semiconductor laser in near infrared region // Sov. J. Quantum Electron. 1987. Vol. 14. P. 2131–2135.

9. *Karu T., Tiphlova O., Samokhina M., Diamantopoulos C., Sarantsev V., Shveikin V.* Effects of near-infrared laser and superluminous diode irradiation on *Escherichia coli* division rate // IEEE J. Quantum Electron. 1990. Vol. 26. P. 2162–2165.

10. *Karu T.I., Tiphlova O.A., Matveyets Yu.A., Yartsev A.P., Letokhov V.S.* Comparison of the effects of visible femtosecond laser pulses and continuous wave laser radiation of low average intensity on the clonogenicity of *Escherichia coli* // J. Photochem. Photobiol. B: Biol. 1991. Vol. 10. P. 339–344.

11. *Karu T.I.* Low power laser effects / eds. R. Waynant and G. Pettit // Lasers in Medicine. New York: Plenum Press, 1994.

12. *Lloyd D., Poole R.K., Edwards S.W.* The Cell Division Cycle. Temporal Organization and Control of Cellular Growth and Reproduction. New York: Academic Press, 1982.

13. *Wilson D.F., Owen C.S., Holian A.* Control of mitochondrial respiration: a quan-titative evaluation of the roles of cytochrome *c* and oxygen // Arch. Biochem. Biophys. 1977. Vol. 182. P. 749–762.

14. *Wood J.* Membrane association of proline dehydrogenases in *Escherichia coli* is redox dependent // Proc. Natl. Acad. Sci, USA. 1987. Vol. 84. P. 343–347.

15. *Bertoloni G., Sacchetto R., Baro E., Ceccerelli F., Jori G.* Biochemical and morphological changes in *Escherichia coli* indicated by coherent and non-coherent 632.8 nm light // J. Photochem. Photobiol. B: Biol. 1993. Vol. 18. P. 191–196.

Appendix A

Let us estimate the absorption of radiation by water and chromophores and its contribution to the heating of the medium in the following two cases: (1) volume-averaged heating of the medium; (2) local heating of the chromophore molecules.

Volume-averaged heating

The absorption of radiation by water in the spectral region of interest is well known [A1]. First, let us consider the heating of the suspension on irradiation at λ = 1066 nm. The absorptivity of water at a wavelength of 1066 nm is 0.118 cm^{-1}. That

of the chromophore molecules kchr can be estimated from the absorption cross-section ($\sigma_{\mathrm{chr}} \approx 10^{-17}$ cm^2) and concentration (nchr $\approx 10^{12}$ cm^{-3}) by the formula

$$k_{\mathrm{chr}} = \sigma_{\mathrm{chr}} \mathrm{n}_{\mathrm{chr}} \approx 10^{-5}\ \mathrm{cm}^{-1} \qquad \text{(A1)}$$

Thus, the contribution of water to the total absorptivity *(k=k_{w}+k_{chr})* at this wavelength is many orders of magnitude greater than that from the chromophore molecules. Similar estimates have been made for wavelengths of 632.8 and 1286 nm (Table Al).

Table Al. Absorption coefficient *(k)* and absorption cross-section (σ) for water (k_{w}, σ_{w}) and chromophores (k_{chr}, σ_{chr}) at wavelengths of 632.8, 1066 and 1286 nm

Parameter	Wavelength λ		
	632.8 nm	1066 nm	1286 nm
k_{w} (cm^{-1})	2.6×10^{-3}	0.118	0.88
σ_{w} (cm^2)	7.7×10^{-26}	3.5×10^{-24}	2.6×10^{-24}
σ_{chr} (cm^2)	$\approx 10^{-16}$-10^{-17}	$\approx 10^{-17}$	$\approx 10^{-17}$
k_{chr} (cm^{-1})	$\approx 10^{-4}$-10^{-5}	$\approx 10^{-5}$	$\approx 10^{-5}$

The characteristic heating time τ_{h} of the medium on irradiation depends on the geometry of the irradiated volume. If the suspension is irradiated in a long cylindrical cell (Fig. 1(a)), this time can be estimated from the relation [A2]

$$\tau_{\mathrm{h}} \approx \frac{d^2}{8\chi} \qquad \text{(A2)}$$

where d is the cell diameter and $\chi = 1.3 \times 10^{-3}$ cm^2 s^{-1} is the thermal diffusivity of water. Substituting the appropriate values, we obtain $\tau_{\mathrm{h}} \approx 7 - 8$ s. The maximum possible volume-averaged heating (at a radiation intensity of 3×10^3 W cm^{-2} and with the radiation absorbed completely at a depth of 1 mm during 10 s) does not exceed 10^{-2}–10^{-1} °C.

Local heating

The contribution to local heating from water and chromophore molecules can be estimated from the following considerations. The absorption crosssection of water σ_{w} can be calculated by the formula

$$\sigma_{\mathrm{w}} = k_{\mathrm{w}}/n_{\mathrm{w}} = k_{\mathrm{w}}\mu/\rho N_a = 0.118 \times 18/1 \times 6.023 \times 10^{23} = 3.53 \times 10^{-24}\mathrm{cm}^2$$

where μ = 18 g mol^{-1} is the molecular weight of water, ρ =1 g cm^{-3} is the density of water and N_a is Avogadro's number.

Assuming that the shape of the chromophore molecule is spherical, the volume V_{chr} occupied by one such molecule with a size of $L \approx 1$ nm can be estimated by the formula

$$V_{\mathrm{chr}} \approx (4/3)\pi(L/2)^3 = (4/3)\pi(5 \times 10^{-8})^3 = 5.24 \times 10^{-22}\mathrm{cm}^3$$

Consequently, the number of water molecules contained in the volume V_{chr} is $N_{\mathrm{w}} = V_{\mathrm{chr}}/V_{\mathrm{w}} = 17.5$. The absorption cross-section of water in the volume V_{chr} is $\sigma_{\mathrm{w}}^{*} = N_{\mathrm{w}}\sigma_{\mathrm{w}} = 6.18 \times 10^{-23}$ cm^2. The absorption cross-section of the chromophore molecule is ($\sigma_{\mathrm{chr}} \approx 10^{-17}$ cm^2, and so the absorption of radiation by a volume of water equal to the chromophore volume is a factor of 10^5–10^6 less than the absorption of the chromophore molecule itself. Thus, there can be local heating due to the absorption of radiation by the chromophore molecules.

Let us estimate the local temperature rise in the chromophore volume immediately following the conversion of the energy of the absorbed photon to heat, assuming that the entire photon energy is converted to heat. The characteristic electronic energy thermalization time, i.e. the characteristic local heating time (τ_{h}), is approximately an order of magnitude longer than the vibration period of the chromophore atoms, i.e. 10^{-12} s. The time of heat diffusion from the volume V_{chr} of the chromophore molecule can roughly be estimated from the following relation, assuming that the chromophore group is spherical in shape.

$$\tau_{\mathrm{hd}} \approx L^2/27\chi \approx 3 \times 10^{-13} s$$

Thus, the heating time and the time of heat diffusion are of the same order of magnitude, and so local overheating is possible.

Let us calculate the temperature rise ΔT_{loc} without allowing for heat diffusion. The quantum energy $E_{\mathrm{quant}} = hc/\lambda = 1.86 \times 10^{-19}$J. Therefore $\Delta T_{loc} = E_{\mathrm{quant}}/c\rho V_{\mathrm{chr}} = 1.86 \times 10^{-19}/4.2 \times 1 \times 5.24 \times 10^{-22} = 84$ K. Thus local overheating of tens of Kelvin is possible. Although it lasts only a very short period of time, around 10^{-12} s, this overheating can cause various conformational changes both in the chromophore group itself and the surrounding regions, which can result in significant alterations of the biological activity of the molecules.

References for Appendix A

Al. *Hale G.M., Querry M.R.* //Appl. Opt. 1973. Vol. 12. P. 555–563.
A2. *McKenzie A.L.* // Phys. Med. Biol. 1990. Vol. 35. P. 1175–1209.

Lasers Surg. Med. 1993. Vol. 13. P. 470–484

STUDIES OF ACOUSTICAL AND SHOCK WAVES IN THE PULSED LASER ABLATION OF BIOTISSUE

Rinat O. Esenaliev, PhD, Alexander A. Oraevsky, PhD, Vladilen S. Letokhov, PhD, Alexander A. Karabutov, PhD, and Taras V. Malinsky, MS
Institute of Spectroscopy, Russian Academy of Sciences, 142092 Troitsk, Moscow Region (R.O.E., A.A.O., V.S.L.); Physics Department, M.V. Lomonosov Moscow State University, 119899 Moscow (A.A.K.); N.E. Bauman State Technical Univ., 107005 Moscow (T.V.M.), Russia

Quantitative studies are conducted into the absolute pressure values of the acoustical and shock waves generated and propagating in a biotissue under pulsed (τ_p = 50 ns) UV (λ = 308 nm) laser irradiation (below and above the ablation threshold). Powerful (several hundreds of bars in pressure) high-frequency ($f \simeq 10^7$ Hz) acoustic compression and rarefaction pulses are found to be generated in the biotissue. The amplitudes and profiles of the acoustic pulses developing in atherosclerotic human aorta tissues and an aqueous $CuCl_2$ solution under laser irradiation are investigated as a function of the laser pulse energy fluence. The results obtained point to the absence of the cold spallation of the objects of study by rarefaction waves. Based on experimental data, the rise rates, pressure gradients, and propagation velocities of shock waves in the biotissue are calculated. The experimental data are found to agree well with the theoretical estimates.

Introduction

Laser biomedicine makes use of various types of laser-biotissue interaction, destructive interaction included. One such interaction is the ablation of biotissue by laser radiation at strong absorption wavelengths (vacuum UV, UV, and IR). The interest in pulsed ablation is due to its well-known characteristics, such as the minimum thermal damage to the surrounding biotissues and the possibility of accurate control of the pulsed evaporation depth of the biotissue. It is exactly for this reason that pulsed laser ablation holds much promise as a precision surgery tool in such diverse medical fields as ophthalmology, vascular surgery, and dermatology.

At the same time, the laser ablation mechanism, which qualitatively can be regarded as the pulsed evaporation of the overheated biotissue region [1–4], is still not clearly understood. First, there is only a qualitative understanding of the contribution of absorption microirregularities in the biotissue to the pulsed ablation characteristics [4]. Secondly, it is only recently that studies have been started of the pulsed pressure developing in the course of pulsed ablation and the resultant acoustical waves [5]

which can propagate into the areas surrounding the overheated biotissue zone subject to ablation [6–8]. The aim of this work is to study in more detail the pulsed pressures arising in biotissue under laser irradiation both below and above the ablation threshold.

The development of acoustical waves in an absorbing medium in the course of pulsed laser irradiation is due to the heating of the irradiated tissue volume, which causes the pressure in it to rise. Such an acoustical wave generation mechanism, referred to as the thermooptical type, was investigated by exposing various absorbing media to laser radiation [9–10]. It should not be confused with the striction mechanism typical of laser irradiation of transparent media.

The efficiency of laser generation of acoustical waves in absorbing media largely depends on the geometry of the irradiated volume and laser pulse duration. Most powerful acoustical fields are generated by short laser pulses whose duration, τ_{p}, is shorter than the time it typically takes for the acoustical wave to traverse the irradiated volume. For a strongly absorbing medium characterized by the attenuation coefficient μ_{eff}, this condition is expressed as $\tau_{\mathrm{p}} < \tau_{\mathrm{str}} = 1/\mu_{\mathrm{eff}}\mathrm{v_s}$, where τ_{str} is the stress relaxation time and $\mathrm{v_s}$ is the sound velocity in the medium. In that case, great mechanical stresses develop in the irradiated volume, for it has not enough time to get relieved, i.e., relax pressure, during the laser pulse.

Insofar as most biotissues are both absorbing and scattering media, the geometry of the heated volume depends on their absorptivity, μ_{a}; scattering coefficient, μ_{s}; and anisotropy factor, g. For this reason, the attenuation of a light wave in biotissue is governed by the attenuation coefficient μ_{eff} related, in the diffusion approximation, to μ_{a}, μ_{s}, and g by the well-known relation $\mu_{\mathrm{eff}} = \{3\mu_{\mathrm{a}}[\mu_{\mathrm{a}} + \mu_{\mathrm{s}}(1-\mathrm{g})]\}^{1/2}$ [11].

In the case of biotissue with an attenuation coefficient of $\mu_{\mathrm{eff}} = 10 - 10^2$ cm^{-1} (these values are typical of biotissue in the near UV region of the spectrum) at $v_s = 1.5\mathrm{x}10^5$ cm/s (for soft biotissue, v_s is close to that in water), the time $\tau_{\mathrm{str}} = (\mu_{\mathrm{eff}}v_s)^{-1}$ ranges between 10^{-6} and 10^{-8} s. Therefore, nanosecond-pulse laser irradiation of biotissue must be effective in generating pulsed stresses and acoustical waves therein.

The pulsed (explosive) ejection of the ablation products obviously gives rise to a recoil pulse which propagates inside the tissue. Studying this pressure pulse with the aid of an acoustical transducer in acoustic contact with the biotissue can provide useful information about the ablation process.

Where the amplitudes of the acoustical pulses propagating through the biotissue are great enough, shock waves can be expected to be generated in the tissue as a result of its acoustical nonlinearity which manifests itself in the velocity of the acoustical wave increasing with the rise of its amplitude.

While reflecting from a free interface (biotissue-air), the generated compression wave is transformed to a tension wave. The authors cited in references 6 and 7 believe that the powerful tension wave developing in the course of shortpulse laser irradiation of biotissue with a free interface can spall off a tissue layer. Dingus and Scammon [7] have suggested a photomechanical laser ablation mechanism (spallation of a biotissue layer, followed by its removal).

Mechanical stresses also develop in biotissues subjected to laser irradiation below the ablation threshold. These stresses relax to generate acoustical waves, the studies of which can give information on both the laser-biotissue interaction process and the optical, thermal, mechanical, and acoustical properties of the tissues.

In this work, we experimentally investigated the acoustical waves generated in biotissue under pulsed laser irradiation, both below and above the ablation threshold, by means of a nanosecond-resolution acoustical transducer designed to measure absolute pressures.

Our results point to the development of powerful high-frequency acoustical waves in biotissues subjected to irradiation with nanosecond laser pulses of high energy fluence.

The experiments conducted with atherosclerotic human aorta tissues and a model medium—a uniformly absorbing $CuCl_2$ solution— bear witness to the absence of the purely photomechanical (less evaporation) laser ablation of tissues.

Based on experimental data and theoretical estimates, we also studied the quantitative characteristics of laser-induced shock waves in biotissue, such as pressure, rise rate, pressure gradients, and propagation velocity.

Generation and propagation of acoustical pulses in an absorbing medium under irradiation with a short laser pulse (thermooptical mechanism)

Consider qualitatively the generation and propagation of acoustical pulses in an absorbing medium exposed to a laser pulse; the main associated physical effects; and the possibility of measuring optical, thermal, and acoustical parameters with the help of acoustical waves.

Condition for the generation of an acoustical wave

Let us examine for simplicity a case where the absorption of laser radiation in the medium subject to irradiation takes place in a region having the shape of a flat disc (broad laser beam, strong absorption), i.e., where the condition

$$d_L \gg 1/\mu_{\text{eff}} \tag{1}$$

holds true, d_L being the laser beam diameter (Fig. 1).

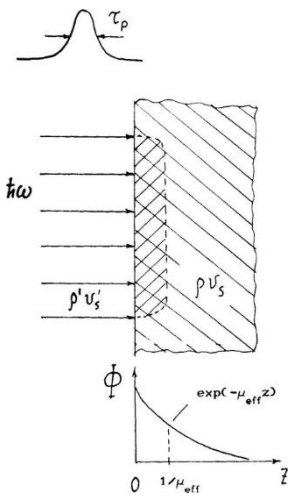


Fig. 1. Geometry of irradiating a strongly absorbing medium of absorptivity μ_{eff} with a broad laser beam ($d_L \geq I/\mu_{\text{eff}}$). The laser pulse duration at the I/e levels is τ_{p}

Let the laser pulse duration τ_{p} be shorter than the time it characteristically takes for heat to diffuse into the medium:

$$\tau_{\mathrm{p}} \ll \tau_{\mathrm{hd}} = \frac{1}{4\chi\mu_{\mathrm{eff}}^2} \tag{2}$$

where χ is the thermal diffusivity of the irradiated medium and τ_{hd} is the heat-diffusion time. In that case, the temperature rise in the absorption region is a maximum and is described, at $\mu_{\mathrm{s}} \ll \mu_{\mathrm{a}}$, by the simple relation

$$\Delta T = (\mu_{\mathrm{a}}\varphi/\rho c_{\mathrm{v}})e^{-\mu_{\mathrm{eff}}\, z} \tag{3}$$

where φ is the laser energy fluence inside the medium at the interface, ρ is the density of the medium, and c_{v} is its specific heat at constant volume. It is assumed for the sake of simplicity that the scattering coefficient μ_{s} of the medium is much lower than its absorptivity, i.e., $\mu_{\mathrm{s}} \ll \mu_{\mathrm{a}}$, so that the contribution from scattering to the distortion of the exponential law governing the attenuation of radiation in the medium can be neglected.

If the laser pulse duration satisfies the more stringent condition

$$\tau_{\mathrm{p}} \ll \tau_{\mathrm{str}} = 1/\mu_{\mathrm{eff}} v_s \tag{4}$$

there occurs an instantaneous rise of the pressure P in proportion to the temperature rise [9,10]:

$$P = \beta\rho v_s^2 \left(c_{\mathrm{v}}/c_{\mathrm{p}}\right)\Delta T = \left(\beta v_s^2/c_{\mathrm{p}}\right)\mu_{\mathrm{a}}\varphi e^{-\mu_{\mathrm{eff}}\, z} \tag{5}$$

where $\beta v_s^2/c_{\mathrm{p}} = \Gamma$ is the Grüneisen parameter, c_{p} is the specific heat of the medium at constant pressure, and β is its coefficient of volume expansion. With the laser pulse duration τ_{p} being so short, the heated volume has not enough time to relax pressure (expand), and therefore there takes place an effective conversion of the light energy into the energy of acoustical waves. Note that by ΔT is understood an "instantaneous" temperature jump occurring immediately after the laser pulse but before the heated tissue volume starts expanding.

Reflection at an Interface

Where condition 1 is satisfied, i.e., where the volume subject to heating and hence expansion has the geometry of a flat disc, two compression waves are generated, one propagating into the medium and the other, to the surface (Fig. 2a). The wave propagating towards the surface undergoes reflection at the interface, the reflectivity being given by [9, 10]

$$R = (1 - N)/(1 + N), N = \rho v_s/\rho' v_s', \tag{6}$$

where ρv_s is the acoustic impedance of the absorbing medium and $\rho' v_s'$, that of the medium from which the laser beam comes.

Where the interface is free (e.g., water-air, biotissue-air, glass-air), R =–1, and the wave changes sign while reflecting (Fig. 3, left). The profile of the wave propagating into the absorbing medium has a bipolar shape (Fig. 2b) consisting of a compression phase with the amplitude and a rarefaction phase with the amplitude P_-. If condition 4 is satisfied, the wave amplitudes P_+ and P_- will be

$$P_+ = P_- = \left(\beta v_s^2/2c_\mathrm{p}\right)\mu_\mathrm{a}\varphi \tag{7}$$

If condition 4 is but rarely satisfied, i.e., if $\tau_\mathrm{p} \lesssim 1/\mu_\mathrm{eff} v_s$ L the so-called transitory zone about τ_p in duration is formed between the compression and rarefaction phases [10]. Where the laser pulse is so long that condition 4 is not satisfied, i.e., $\tau_\mathrm{p} \gg 1/\mu_\mathrm{eff} v_s$, the efficiency of sound generation is much lower than with $\tau_\mathrm{p} \lesssim 1/\mu_\mathrm{eff} v_s$. In that case, the pressure P of the acoustical wave is proportional to the laser intensity I (Fig. 3, bottom).

If the interface is rigid (e.g., water-glass, biotissue-glass), then $R \backsimeq 1$, and in the medium there propagates only a compression wave (Fig. 3, right).

Note that in the case under consideration ($\mathrm{d}_L \gg 1/\mu_\mathrm{eff}$), the generated acoustical wave is plane. In the general case, the temporal profile and amplitude of the wave may depend in a very complicated manner on τ_p and the size and geometry of the volume being heated.

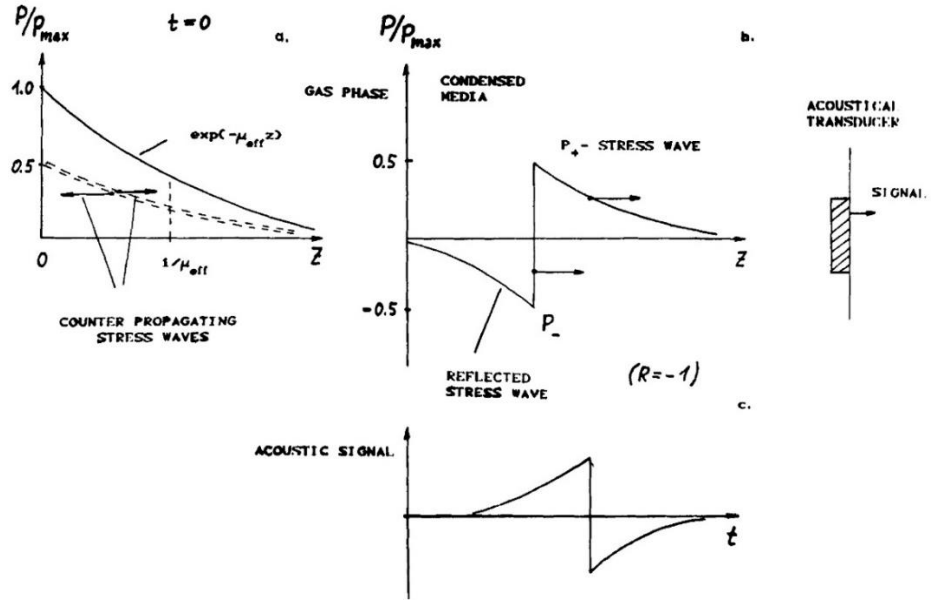


Fig. 2. Generation of an acoustical wave by an infinitely short laser pulse in a medium with a free interface (R = -1) and its propagation into the medium: a) resolution of stress into two counter-propagating waves; b) formation of a bipolar acoustical wave as a result of reflection from the free interface and the propagation of the wave into the medium; c) profile of the acoustic signal detected by means of an acoustical transducer (the case of plane wave)

Damping of the acoustical wave

When an acoustical wave propagates through a medium, its pressure gradually drops as a result of damping and diffraction. The damping of the wave is due to both its energy being absorbed and converted to heat and the scattering of sound by acoustic irregularities.

The reduction of pressure in a plane acoustical wave in the course of its propagation through a medium with a sound damping coefficient of a is described by the formula

$$P(z) = Pe^{-\alpha z}. \tag{8}$$

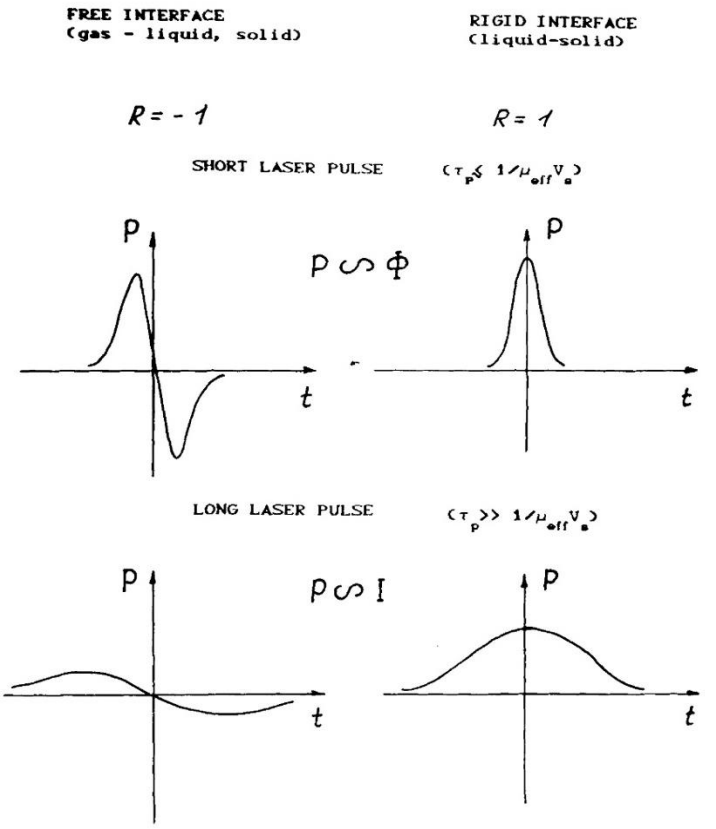


Fig. 3. Profiles of acoustic signals generated in media with a free **(left)** and a rigid **(right)** interface by a short **(top)** and a long **(bottom)** laser pulse

Attenuation dispersion of the acoustical wave

For the majority of pure liquids, the damping coefficient α rises in proportion to f^2, where f is the frequency of the acoustical wave. The literature data therefore

usually refer to the quantity α/f^2. For water at $t = 20°C$ and $f = 7 \text{ x } 10^6 - 10^8$ Hz, a $\alpha/f^2 = 25 \text{ x } 10^{-17}$ s2/cm [12,13].

Biotissues were found to show a different frequency dependence of their damping coefficient. As found in reference 14, the quantity α/f in various types of biotissue remains approximately constant in the frequency range 1.5-4.5 MHz. A linear relationship between α and f is also observed in solids whose sound damping mechanism depends first of all on their grain structure. Such a frequency dependence of damping is associated with mechanical hysteresis in the stressed medium.

The quantity α/f of biotissue depends substantially on its structure, density, viscosity, compressibility, etc. [15]. To illustrate, for fatty tissues, $\alpha = 0.07 - 0.26$ cm-1 at $f = 1 - 5$ MHz, whereas for muscular tissues in the same frequency range, $\alpha = 0.08 - 0.4$ cm-1 when measured along grain and 0.16–0.71 cm 1 across [15,16]. An abnormally high damping coefficient is observed in bony tissues: $\alpha = 1.45 - 9.2$ cm-1 at $f = 1 - 4.5$ MHz [15–17], which is probably due to their high-density inhomogeneity.

The acoustical waves generated in the experiments described below were around 107 Hz in characteristic frequency, which was much higher than the frequencies studied earlier.

However, by extrapolating the linear relationship between α and f, one can estimate the damping of sound of a higher frequency. The acoustical properties of atherosclerotic blood vessel tissues are apparently similar to those of fatty and muscular tissues, and so their sound damping coefficient α will amount to 0.8 cm-1 at $f = 10^7$ Hz. Consequently, the damping of pressure in a 2-mm-thick blood vessel tissue will be a mere 15%.

Note finally that for soft tissues, the sound velocity, v_s, and acoustic impedance, ρv_s, practically coincide with those of water [18, 19]. For hard tissues, the v_s and ρv_s values are much higher. To illustrate, for bony tissues, $v_s = 3.36 \text{ x } 10^5$ cm/s and $\rho v_s = 6.2$ g/cm2s at $f = 0.8$ MHz [19].

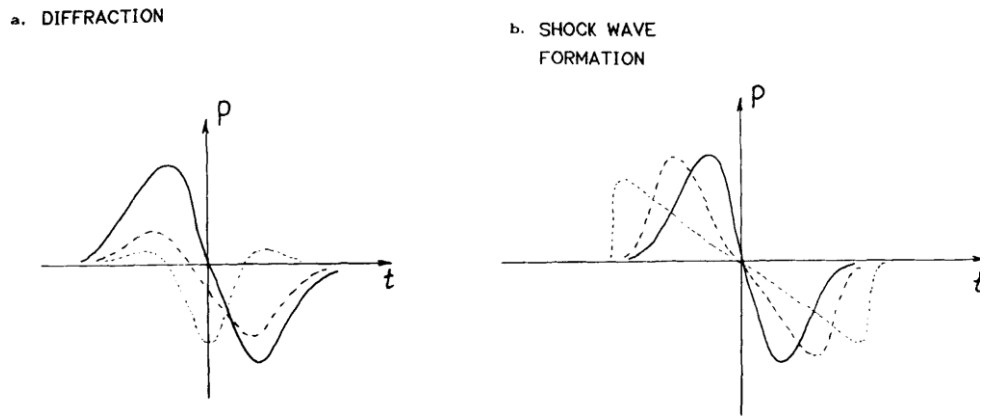


Fig. 4. Distribution of acoustical waves in the course of propagation: *a*) as a result of diffraction; *b*) as a result of acoustic nonlinearity-shock wave formation

According to formula 8, one can conclude, considering the damping coefficients for water and biotissues, that a noticeable reduction of the pressure of an acoustical wave occurs while it covers a distance of 40 cm in water and around 1 cm in a soft biotissue at $f = 10^7$ Hz.

Diffraction of the acoustical wave

The distortion of the profile of an acoustic pulse and the reduction of pressure in it also occur as a result of diffraction (Fig. 4*a*). The cause of diffraction in the case of the laser thermooptical sound generation mechanism is the limited size of the heat liberation region resulting from the finiteness of the laser spot size. Diffraction distortions augment as the acoustical wave propagates further, depending on the diffraction parameter $z\ /\ L_{dif}$, where z is the distance from the sound generation region to the observation point and L_{dif} is the diffraction length defined by the relation [10]

$$L_{dif} = \pi f r_L^2 / v_s \tag{9}$$

where r_L is the laser spot radius.

If the diffraction parameter $z/L_{dif} \ll 1$, the contribution from diffraction to the damping of the acoustical wave is small. But if $z/L_{dif} > 1$, diffraction should be taken into account. According to formula 9, the diffraction effects will manifest themselves weaker for higher-frequency acoustical waves and broader laser beams. Because of diffraction, the bipolar acoustical wave with the amplitudes $P_+ = P_-$ is transformed in the course of propagation into a wave with two compression and a single rarefaction phases, with P_+ being lower than P_- [10].

Thus, for the acoustical waves generated in strongly absorbing media under pulsed laser irradiation to be registered without distortion, one should use a broad laser beam and place the acoustic transducer as close as possible to the wave excitation region, so that the effect of damping and diffraction can be reduced.

Formation of shock waves as a result of acoustic nonlinearities

If the amplitude of the acoustical wave being generated is great enough, nonlinear acoustic phenomena become manifest as the wave propagates. A most typical manifestation of acoustic nonlinearity is the formation of a shock wave as a result of the sound velocity, v_s, being dependent on the pressure P. According to the nonlinear acoustics equations [20], the higher the pressure, the higher the sound velocity. The result is that the sound velocity in the compression phase is higher than in the rarefaction phase, the compression phase maximum propagating with the highest velocity. For this reason, as the compression phase propagates, its rise rate increases, so that the profile of the acoustical wave assumes the N-like form typical of shock waves (Fig. 4*b*).

The characteristic distance l_{NL} from the wave source to the break in the wave profile is called the shock wave formation distance and is defined by the relation [20]

$$l_{NL} = \lambda/2\pi\epsilon M\,, \tag{10}$$

where ϵ is the nonlinear acoustic parameter depending on the properties of the medium; $M = v_p/v_s$ is the Mach number for the acoustical wave in the generation zone, v_p being the velocity of particles in the wave; and $v_p = v_s/f$ is the acoustical wavelength. The particle velocity is related to the pressure in the wave by the relation

$$P = \rho v_p v_s. \tag{11}$$

Using relations 10 and 11, one can find the dependence of l_{NL} on P and f:

$$l_{NL} = \rho v_s^3/2\pi\epsilon P f. \tag{12}$$

Substituting into this formula the corresponding values for water, $\rho = 1$ g/cm^3, $v_s = 1.5 \times 10^5$ cm/s, and $\epsilon = 3.37$, we get, at $f = 10^7$ Hz and $P = 100$ bar $= 10^8$ dyne/cm^2, $l_{NL} = 1.6$ mm. Thus, an acoustical wave propagating through water at a frequency of 10^7 Hz and a pressure of 100 bar is transformed into a shock wave within a distance of the order of a millimeter.

Inasmuch as the properties of soft biotissues are close to those of water and the damping of a wave with a frequency of $f = 10^7$ Hz in such biotissues occurs within distances around 1 cm long, the development of a shock wave a few hundreds of bars in pressure can be expected there.

Informational capabilities of acoustical waves in laser ablation

By studying the shape, amplitude, and deformation of acoustical signals generated and propagating in an absorbing medium under the effect of laser radiation, one can determine all the above-mentioned parameters of the medium: optical (μ_a), thermophysical (β, c_p), and acoustic (ρ, v_s, ϵ, α, and $v_{\text{sh.w.}}$— the shock-wave velocity). What is more, such investigations can provide information on the geometry of the volume being heated by the laser, such as its size and shape, as well as the distribution of heat-liberation regions therein in the case of inhomogeneous absorption of radiation.

Of special interest is to study the optical and geometrical characteristics of absorption micro-irregularities, including those less than a micron across, by the acoustical fields generated by them under irradiation with short and ultrashort laser pulses.

In addition to the investigations mentioned above, one can also study the optical and mechanical failures of the media being irradiated, phase transitions, etc., which can manifest themselves in the form of both some distortion of the thermooptical pulse and generation of extraneous acoustical waves.

Investigations into the acoustical fields formed in the pulsed ablation of tissues allow a deeper insight to be gained into the pulsed ablation process and answer the question: whether spallation is the cause of ablation of biotissue or whether ablation proceeds by a thermal mechanism. According to formula 7, the compression and rarefaction phase amplitudes P_+ and P_- grow linearly with the increasing laser energy fluence, φ, and so no changes should occur in the shape of the acoustic pulses until the ablation threshold, (φ_{thr}, is reached (Fig. 5). If ablation proceeds by a photomechanical mechanism involving the spallation of a certain biotissue volume by a sufficiently powerful rarefaction wave, curve P_- (φ) should then level out to saturation when the spallation pressure, P_{spall}, is reached, so that $P = P_{spall}$ at $\varphi = \varphi_{thr}$ (Fig. 5).

But if ablation proceeds by a thermal mechanism giving rise to gaseous ablation products, the curve P_- (φ) should then have a minimum, the rarefaction phase vanishing altogether at fluences φ much in excess of φ_{thr}. Such a shape of the P_- (φ) curve is due to the superposition of the recoil pulse of the ablation products formed on the rarefaction wave (Fig. 5).

Thus, having studied the function P_- (φ) both at laser energy fluences below the ablation threshold and in the course of ablation, one can answer the question whether spallation is the cause of ablation of biotissue or not.

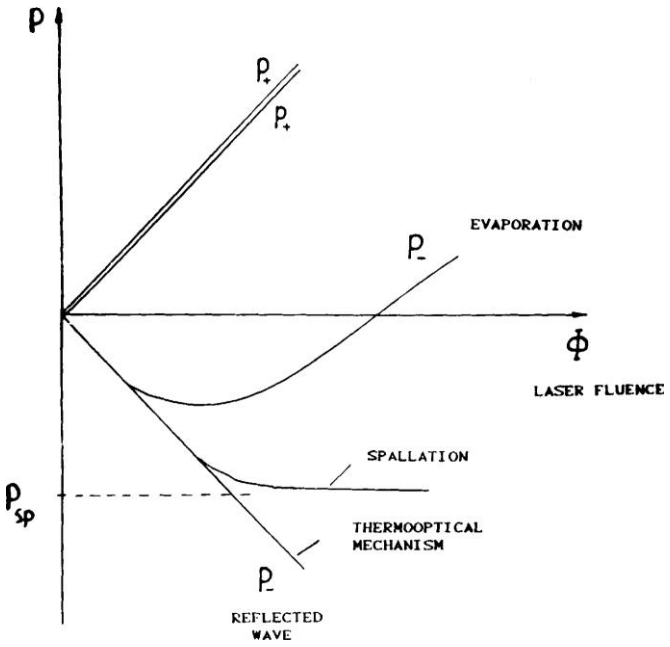


Fig. 5. Compression and rarefaction phase amplitudes, P_+ and P_-, respectively, as a function of the laser energy fluence φ

Materials and methods

The laser radiation source used in the studies of acoustical and shock waves in biotissue was a XeCl excimer laser ($\lambda = 308$ nm), for its high pulse energy $E_{\mathrm{p}} = 150$ mJ and the high attenuation coefficient $\mu_{\mathrm{eff}} = 100–120$ cm-1 at $\lambda = 308$ nm typical of atherosclerotic blood vessel tissues [4] allowed the heated tissue volume geometry to be realized in the form of a flat disc (condition 1) at laser energy fluences both below and much above the ablation threshold. Such a geometry is optimal for the generation of most powerful rarefaction waves upon reflection from a free interface, because the stress developing in a flat disc is resolved into two plane waves only.

For powerful acoustical waves to be generated effectively, use should be made of sufficiently short laser pulses whose duration satisfies condition 4. The pulse duration of the laser used was 50 ns at the I / e level and fulfilled the condition $\tau_{\mathrm{p}} \leq \tau_{\mathrm{str}}$ The leading edge of the laser pulse was somewhat steeper than the trailing one. Note that at $\tau_{\mathrm{p}} \leq \tau_{\mathrm{str}}$ the temporal profile of the laser pulse has no effect on the profile of the acoustical wave generated. It is only at $\tau_{\mathrm{p}} > \tau_{\mathrm{str}}$ that the profile of the acoustical wave depends strongly on that of the laser pulse [10].

So, the high pulse energy, high attenuation coefficient at $\lambda = 308$ nm, and short pulse duration of the XeCl laser provided for effective generation of powerful acoustical waves in atherosclerotic blood vessel tissues.

Figure 6a shows a schematic diagram of the experimental setup used to study acoustical waves in the course of laser ablation. To obtain reliable results under various irradiation conditions, acoustical waves should be generated and detected in one and the same geometry. For this reason, the laser pulse energy fluence was measured by means of calibrated light filters and not by varying the laser spot surface area. The energy of each pulse was measured by means of a calibrated photodetector and a digital voltmeter. The major proportion of radiation was focused with a positive lens onto the sample. The laser spot surface area on the surface of biotissue amounted to 1.7 mm^2.

The sample was placed on an acoustic conductor—a metal plate 3 mm in thickness and 35 mm in diameter (Fig. 6b). Cemented to the opposite side of the acoustic conductor was a nonresonant acoustical transducer—a piezoelectric ceramic (PZT-5) plate 3 mm in thickness and 6 mm in diameter. When measuring short acoustic pulses, the transducer was made to operate into a low-resistance load of $\mathrm{R}_1 = 13\ \Omega$. Its time resolution was 4 ns. The entire system (acoustic conductor, transducer, load resistor) was placed in a metal casing. The transducer was calibrated as described in [10] to read in absolute pressure units and had a sensitivity of 0.7 mV/bar with allowance made for the acoustic impedances of the biotissue and metal.

When necessary, the transducer signal was amplified and fed to a digital oscilloscope. Each acoustic pulse was read out of the oscilloscope in a point-by-point fashion, the time interval between the adjacent points amounting to 5 ns. So, the detection and registration system had a nanosecond time resolution.

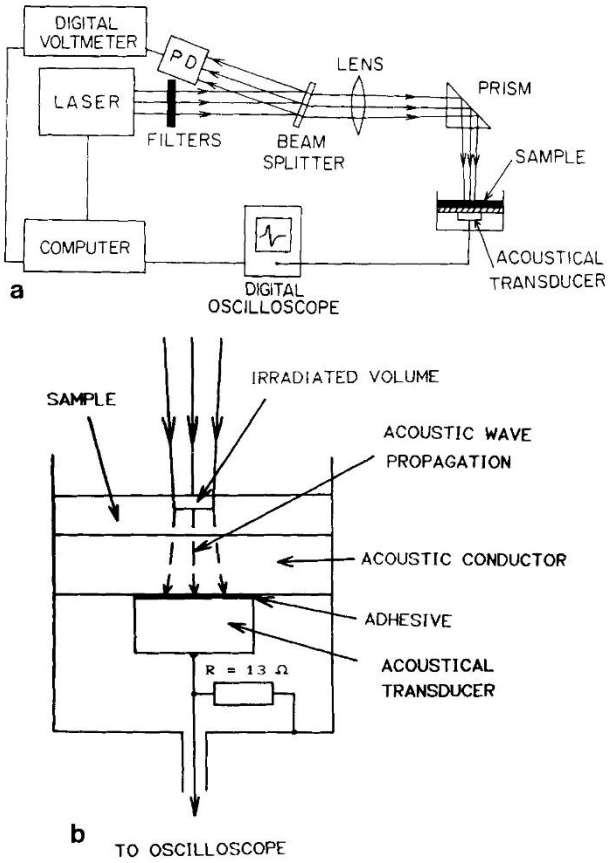


Fig. 6. *a*: Schematic diagram of experimental setup for studying laser-induced acoustical waves in the biotissue and model object; *b*: irradiation and detection geometry

Tissue samples. The experiments were conducted with sections of human cadaver thoracic aorta taken within a few hours of sudden death. Prior to experiments, the samples were stored in normal saline at 2°C for not over 24 hours. Two types of tissue–fibrous plaque and normal aorta wall — were used in the experiments. The tissue samples were 1.5–2 mm in thickness.

Model solution. Experiments were also performed with a model object—an aqueous $CuCl_2$ solution which featured a strong absorption at $\lambda = 1.064$ nm. The radiation source here was a Q-switched Nd: YAG laser with a pulse energy of $E_p = 80$ mJ. The pulse duration at the I / e level was 15 ns. Its temporal profile was almost Gaussian. The experimental setup was similar to the one described above. The solution was poured directly onto the acoustic conductor. The laser spot surface area on the surface of the solution amounted to 0.11 mm^2. The absorptivity $\mu_a$was found from the exponentially rising leading edge of the compression phase at low laser energy fluences φ (formula 5) to equal 270 cm^{-1}. Condition 1 was satisfied and the geometry of the heated solution volume was a flat disc.

Results

Model solution. The acoustic signals detected in the course of irradiation of the $CuCl_2$ solution are presented in Figure 7. Plotted on the y-axis is the acoustical wave pressure, P, normalized on the basis of the laser pulse energy fluence, φ. The pressure measurement error was 5%. At low fluences ($\varphi = 0.75$ J/cm^2, curve 1), the acoustical transducer detects first a compression phase with an exponentially rising leading edge, and then the compression phase goes over into a rarefaction phase, the duration of the transition zone being close to the laser pulse duration at the I / e level. After the rarefaction phase there is observed another compression phase with an amplitude much lower than that of the first one. The amplitude P_+ of the first compression phase is lower than the rarefaction phase amplitude P_-. Such a shape of the acoustical signal is characteristic of the thermooptical generation of sound by a short laser pulse in a strongly absorbing medium with a free interface where the acoustical wave suffers but an insignificant diffraction as it propagates from the source to the acoustical transducer [10].

The duration of each phase comes to several tens of nanoseconds, which corresponds to the generation of a high-frequency ultrasound ($f \backsimeq 10^7$ Hz).

At $\varphi = 1.5$ and 5.8 J/cm^2 (curves 2 and 3, respectively), P_+ is observed to rise and P_-, fall with the increasing φ. The slope of the leading edge of the compression phase is also observed to increase, which points to the formation of a shock wave. As the amplitude of the rarefaction phase lowers, the amplitude of the second compression phase grows higher, which is clearly observed at $\varphi = 5.8$ J/cm^2. This testifies to the development of the recoil pulse of the products of evaporation of the solution, which compresses the liquid and lowers the amplitude of the rarefaction phase.

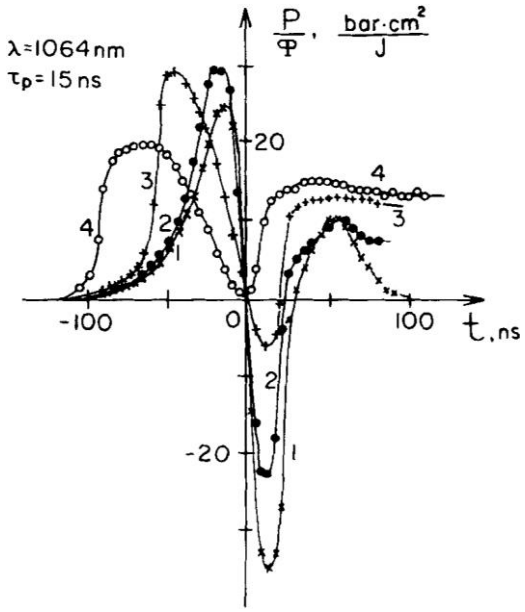


Fig. 7. Acoustic signals detected when irradiating aqueous $CuCl_2$ solution ($\mu_a = 270$ cm^{-1}) with nanosecond Nd:YAG laser pulses differing in energy fluence: $1 - \varphi = 0.75$ J/cm^2; $2 - \varphi = 1.5$ J/cm^2; $3 - \varphi = 5.8$ J/cm^2; $4 - \varphi = 15$ J/cm^2

At $\varphi = 15$ J/cm^2 (curve 4), the rarefaction phase vanishes completely, and it is only a high- amplitude compression wave that propagates through the solution. The shock wave amplitude grows even higher. A powerful recoil pulse of the evaporation products is also observed.

The relationships between the magnitudes of P_+ and P_- on the one hand and the laser energy fluence φ on the other (Fig. 8) point to the generation of acoustic pulses of a fairly high amplitude, of the order of a few hundreds of bars. The compression phase amplitude (curve 1) grows almost linearly with the increasing φ, and that of the rarefaction phase (curve 2) first grows higher and then lowers to pass into the region of positive pressure values at high φ values. Such a fluence dependence of P_- bears witness to the fact that the expulsion of a mass of the aqueous solution is due to evaporation and not to the spallation of a liquid layer.

Substituting into formula 3 the corresponding values of $\mu_a = 270$ cm^{-1} and $\rho c_v = 4.2$ cv J/cm^3, we get $\Delta T = 96^\circ$C for the temperature rise on the surface of the solution at $\varphi = 1.5$ J/cm^2. Although the density of the concentrated aqueous $CuCl_2$ solution is higher than that of pure water by approximately 20% [12,13], its specific heat is lower, also by 20%, than that of water. Therefore, the product ρc_v for the solution under study is equal to that for water to a fair degree of accuracy. The heating of water by 96°C above room temperature causes intensive evaporation.

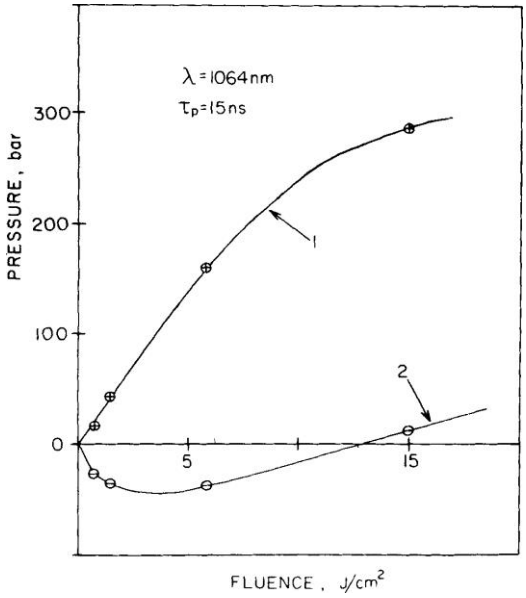


Fig. 8. Compression (curve 1) and rarefaction (curve 2) phase amplitudes as a function of the laser pulse energy fluence when irradiating aqueous $CuCl_2$ solution with nanosecond Nd:YAG laser pulses

Thus, both the function $P_-(\varphi)$ and calculated temperature point to evaporation. The slight nonlinearity of the function $P_+(\varphi)$ at $\varphi > 5$ J/cm^2 can be explained by the screening of the trailing edge of the laser pulse by the evaporation products which scatter and absorb radiation.

Biotissue. Similar results were also obtained in experiments with atherosclerotic blood vessel tissues. It should be emphasized that the experimental results for fibrous plaque and normal aorta wall samples practically did not differ from one another, which was due to the similarity of the optical properties [4] of both types of tissue, as well as their thermophysical and acoustical properties.

When irradiating the tissues of interest with XeCl laser pulses of not very high energy fluence (Fig. 9), there is also observed an acoustic pulse with compression and rarefaction phases. The amplitude of the compression phase is lower than that of the rarefaction phase, which is indicative of a slight diffraction [10].

As the laser pulse energy fluence is increased, the amplitude P_+ of the compression phase grows higher, whereas P_- lowers (Fig. 10). As in the case of the model object, shock waves are also observed to form, as evidenced by the shift of the compression phase maximum of the high-amplitude wave relative to that of the low-amplitude wave. Note that in the case of biotissue the leading edge slope of the compression phase is lower than in the case of $CuCl_2$ solution. The slope observed in the experiments with biotissue is typical of the formation of shock waves in a medium where their energy dissipates as a result of absorption and scattering [20]. At high < p values, the rarefaction phase vanishes altogether, and this is testimony to the presence of a powerful recoil pulse of the biotissue ablation products.

As with the model object, a high-frequency ultrasound ($f \simeq 10^7$ Hz) is generated in and propagates through the biotissue under study.

The function $P_+(\varphi)$ (Fig. 10, curve 1) is indicative of a practically linear rise of P_+ with the increasing φ. The amplitude of the rarefaction phase (curve 2) first grows higher and then lowers to pass into the region of positive values at $\varphi > 6$ J/cm^2, which again points to a thermal and not photomechanical biotissue ablation mechanism. The amplitudes of the pulses studied are of the order of a few hundreds of bars, which corresponds to powerful acoustical waves.

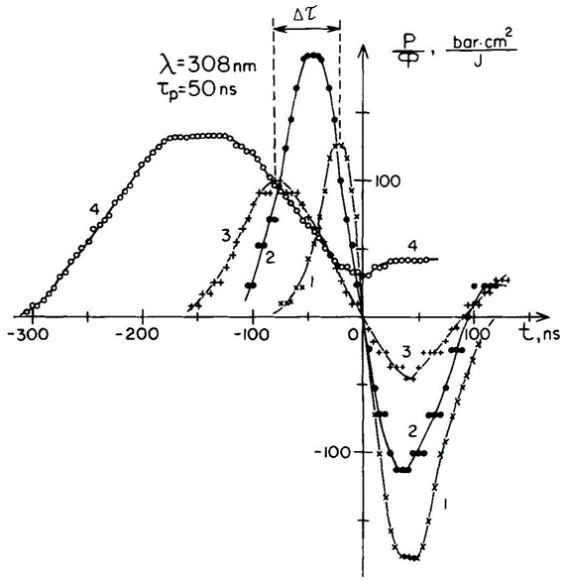


Fig. 9. Acoustic signals detected when irradiating human atherosclerotic blood vessel tissues with XeCl laser pulses differing in energy fluence: $1 - \varphi = 0.12$ J/cm^2; $2 - \varphi = 1.3$ J/cm^2 $3 - \varphi = 3.4$ J/cm^2; $4 - \varphi = 7.5$ J/cm^2. $\Delta\tau$ is the displacement of the compression phase maximum of the high-amplitude wave relative to that of the low-amplitude wave

The thermal character of ablation is also borne out by the fact that the recoil pulse of the ablation products occurs at $\varphi = 1.7 - 2$ J/cm^2, which agrees well with the ablation threshold values measured for human atherosclerotic blood vessel tissues at $\lambda = 308$ nm by many investigators $\varphi_{thr} = 1.5 - 2.7$ J/cm^2 [2, 21, 22]).

The temperature dependences of the coefficient of volume expansion, $\beta = \beta(T)$, sound velocity $v_s = v_s(T)$, and heat capacity $c_\mathrm{p} = c_\mathrm{p}(T)$ [12, 13] at high energy deposition values give rise to what is known as thermal nonlinearity. The major contribution to the thermal nonlinearity of water is made by the rise of β with the increasing T at temperatures close to 100°C. The temperature dependence of the coefficient β makes the pressure P a nonlinear increasing function of φ [10].

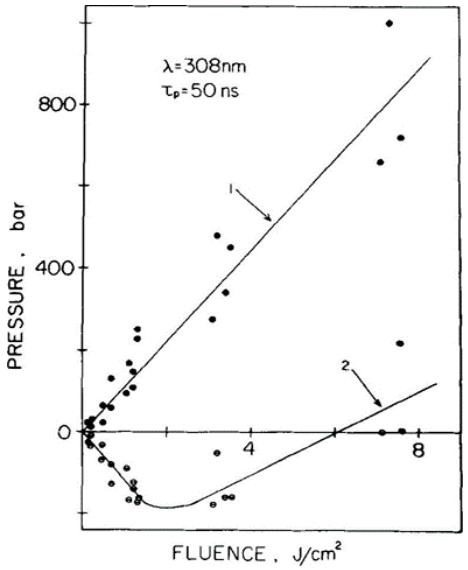


Fig. 10. Compression (curve 1) and rarefaction (curve 2) phase amplitudes as a function of the laser pulse energy fluence when irradiating human atherosclerotic blood vessel tissues with XeCl laser pulses

Thermal nonlinearity can serve to explain the nonlinear rise of P_+ as a function of φ for biotissue at $\varphi = 1 - 1.5$ J/cm^2. At $\varphi > \varphi_{\mathrm{thr}} \backsimeq 2$ J/cm2, the function $P_+(\varphi)$ is affected by the screening of laser radiation by the ablation products, and for this reason, the function $P_+(\varphi)$ observed in the experiment is almost linear. The competition between the screening of laser radiation and thermal nonlinearity is also responsible for the nonlinear rise of $P_+(\varphi)$ for the aqueous $CuCl_2$ solution at $\varphi > 1.5$ J/cm^2.

Discussion

Pulsed pressure amplitude

Let us consider separately the following two cases: the model homogeneous-absorption medium — the aqueous $CuCl_2$ solution, and the real heterogeneous-absorption biotissue.

Aqueous $CuCl_2$ solution. According to formula 7, when irradiating the solution with laser pulses having a fluence of $\varphi = 0.75$ J/cm^2, the amplitude P_+ of the compression phase must reach 110 bar, with the values of the parameters entering into the formula being as follows: ($\beta = 0.207 \times 10^{-3}$ K-1, $v_s = 1.5 \times 10^5$ cm/s, $c_\mathrm{p} =$ 4.2 J/g K, and $\mu_\mathrm{a} = 270$ cm-1. The measured value is $P_+ = 17.8$ bar. This discrepancy can be explained by the damping of the acoustical wave because of diffraction and a partial pressure relaxation during the laser pulse, for $\tau_\mathrm{p} \backsimeq \tau_\mathrm{str}$ (the absorption of the acoustical wave is insignificant).

The effect of diffraction can be allowed for as follows. As the wave propagates, its diffraction parameter increases and the amplitude of the compression phase drops faster than that of the rarefaction phase [10]. Therefore, given the ratio P_+/P_-, one can restore the initial amplitudes $P_+^0 = P_-^0$ in the sound generation region. At $\varphi =$ 0.75 J/cm^2, $P_+/P_- = 0.71$, the diffraction parameter being equal to 0.5 [10]. At such a diffraction parameter, $P_+^0 = P_-^0 = P_+/0.55 = 32.4$ bar.

The contribution from the finiteness of τ_p can be estimated from the relationship between P_+ for a finite laser pulse and the product $\mu_\mathrm{eff} v_s \tau_\mathrm{p}$ [10], where τ_p governs the width of the Gaussian laser pulse: $f(t) = 1/(\pi)^{\frac{1}{2}} \exp\left[\left(-t/\tau_\mathrm{p}'\right)^2\right]$. Obviously $\tau_\mathrm{p} = 2\tau_\mathrm{p}'$. We have $\mu_\mathrm{eff} v_s \tau_\mathrm{p} = 0.3$, which yields, in the case of free interface, $P_+^{0^*} = P_+^0/0.6 = 54$ bar, $P_+^{0^*}$ being the signal amplitude for a very short laser pulse.

Thus, considering diffraction, one may write formula 7 for finite τ_p' in the form

$$P_+ = P_- = K\left(\mu_\mathrm{eff}, v_s, \tau_\mathrm{p}'\right) D(z, d_L, f, v_s)\left(\beta v_s^2/2c_\mathrm{p}\right)\mu_\mathrm{a}\varphi \qquad (13)$$

where $K\left(\mu_\mathrm{eff}, v_s, \tau_\mathrm{p}'\right) < 1$ and $D(z, d_L, f, v_s) < 1$ play the part of correction factors for the finiteness of τ_p and the diffraction of the acoustical wave, respectively.

Biotissue. The fact that the slopes of the rectilinear sections of the curves $P_+(\varphi)$and $P_-(\varphi)$for the biotissue (Fig. 10) at low values are almost equal ($dP_+/d\varphi = 110$ bar cm^2/J and ($dP_-/d\varphi = 120$ bar cm^2/J) suggests that the diffraction of acoustic pulses is weak. Let us calculate the expected compression phase amplitude when irradiating the biotissue with laser pulses having an energy fluence of $\varphi = 1$ J/cm^2, allowing for the effect of the finiteness of τ_p' and using the well-known optical properties of biotissue at λ= 308 nm:

$$P_+^* = K\left(\mu_\mathrm{eff}, v_s, \tau_\mathrm{p}'\right)\left(\beta v_s^2/2c_\mathrm{p}\right)\mu_\mathrm{a}\varphi_\mathrm{eff}, \qquad (14)$$

where $\mu_\mathrm{eff} = 100$ cm^{-1}, $\mu_\mathrm{a} = 30$ cm^{-1}, and $\varphi_\mathrm{eff} = 2\varphi$ [22]. Since $\mu_\mathrm{eff} v_s \tau_\mathrm{p}' = 0.38$, then $K = 0.6$ [9,10] and $P^* = 30$ bar. The experimental value is P = 110 bar at $\varphi =$ 1 J/cm^2. Thus, the wave generated in the experiments with the biotissue has a substantially higher amplitude than that calculated by formula 14, notwithstanding that it takes no account of the acoustic wave attenuation as a result of diffraction.

We believe that this discrepancy can be due to the inhomogeneity of the biotissue as to absorption of radiation, which results in a stronger local heating of biotissue

regions of enhanced absorption and the ensuing thermooptical generation of waves with a higher amplitude than in the case of homogeneous moderate heating of the biotissue. On the other hand, it is more difficult to generate high peak pressures in locally heated microregions because of a faster pressure relaxation occurring there. It is probably also necessary to take account of microirregularities in the mechanical and acoustical properties of biotissue, the possibility of hydrodynamic instabilities developing in the heated biotissue, including sound focusing (hydrodynamic lenses), cavitation effects, etc. To reveal the mechanism responsible for the enhancement of pulsed pressure amplitudes in biotissue will apparently make it necessary to study the mechanism of biotissue fragmentation in the course of ablation.

Wave front slopes and pressure gradients

Table 1 lists the data on the slopes of the leading edges, $(\mathrm{d}P/\mathrm{d}t)_1$, and trailing edges, $(\mathrm{d}P/\mathrm{d}t)_1$, of acoustic pulses, calculated from the profiles of the acoustic signals obtained. The dP/dt values for the aqueous $CuCl_2$ solution are higher than those for the biotissue, which is explained by the greater dissipation of the energy of acoustical and shock waves in biotissues. Note that the $\mathrm{d}P/\mathrm{d}t$ values are rather high (0.5–30 bar/ns).

Based on the wave front slopes, one can calculate the pressure gradients $\mathrm{d}P/\mathrm{d}z = \mathrm{d}P/v_\mathrm{s}\,dt$ in the acoustical wave. The pressure gradients calculated for the leading edges, $(\mathrm{d}P/\mathrm{d}z)_1$, and trailing edges, $(\mathrm{d}P/\mathrm{d}z)_t$ of acoustic pulses are also listed in Table 1. As can be seen from the table, the pressure gradients are very high. It is probably only laser optoacoustic techniques that can help produce so high pressure gradients in biotissue. It cannot be ruled out that such great and fast pressure differentials have some biologic effects on subcellular structures and tissues, including both direct mechanical effects (deformation of various structures, destruction of membranes, etc.) and secondary biochemical effects (initiation, stimulation, or inhibition of biochemical reactions). Indeed, with cells being 1–10 μm in size, the difference in pressure between their various parts may be in the range 5–50 bar, reaching 50–500 bar for larger cells, e.g., neurons 100 μm across.

Table 1. Leading and trailing edge slopes and pressure gradients in acoustic pulses induced in the aqueous $CuCl_2$ solution and biotissue

φ, J/cm^2	P_+, *bar*	$(dP/dt)_1$, bars/ns	$(dP/dz)_1$, bar/μm	$(dP/dt)_t$, bar/ns	$(dP/dz)_t$, bar/μm
Aqueous $CuCl_2$ solution					
0.75	17.8	0.54	0.36	-2.6	-1.8
1.5	44	1.5	1	-4.3	-2.9
5.8	160	14	9.3	-5.1	-3.4
15	286	30	20	-6	-4
Biotissue					
0.1	15	0.55	0.36	-0.83	-0.55

2					
1.3	250	5.2	3.5	-7	-4.7
3.4	340	6.1	4.1	-5	-3.3
7.5	1,000	8	5.4	-7.5	-5

Research into the biologic action of such short and high mechanical stresses is of purely scientific interest and, perhaps, practical value for laser medicine.

Shock wave velocity and pressure at its front

The displacement $\Delta\tau$ of the compression phase maximum of the high-amplitude wave relative to that of the low-amplitude wave (Fig. 9) can be used to calculate the shock wave velocity $v_{\text{sh.w.}}$ as follows. The time it takes for the low-amplitude wave to cover the distance l is given by the equality

$$t_{\text{ac.w.}} = l/v_{\text{s}}, \tag{15}$$

and for the shock wave, this time is

$$t_{\text{sh.w.}} = l/v_{\text{sh.w.}}, \tag{16}$$

with the following equality being valid:

$$t_{\text{sh.w.}} = t_{\text{ac.w.}} - \Delta\tau \tag{17}$$

Proceeding from equalities (15) –(17), we get

$$v_{\text{sh.w.}} = l/(l/v_s - \Delta\tau)\,. \tag{18}$$

Table 2 lists shock wave velocities calculated by formula 18 for $l = 2$ mm.

Using the well-known relationships between the pressure $P_{\text{sh.w.}}$ at the shock-wave front, the shock wave velocity $v_{\text{sh.w.}}$, and the velocity v_{p} for water, one can calculate the pressure$P_{\text{sh.w.}}$ [23, 24]:

$$P_{\text{sh.w.}} = P_0 + \rho v_{\text{p}} v_{\text{sh.w.}} \tag{19}$$

$$v_{\text{sh.w.}} = 1.483 + 25.306 \log\left[1 + (v_{\text{p}}/5.19)\right] \tag{20}$$

where $P_0 = 1$ bar is the pressure before the wave front, $v_{\text{sh.w.}}$ and v_{p} are in km/s, and 1.483 is the velocity of an acoustical wave of infinitesimal amplitude in water, expressed in terms of km/s. The results of calculating $P_{\text{sh.w.}}$ and v_{p} by formulas 19 and 20 are also listed in Table 2. These data point to a good agreement between the experimental and theoretical values of shock wave pressures.

Table 2. Comparison between experimental and theoretical compression phase amplitudes, $P_+^{\exp}$ and P_+^{theor}. Respectively, in biotissue, based on the displacement, $\Delta\tau$, of the compression phase maximum of the high-amplitude wave relative to that of the low-amplitude wave at $\varphi = 0.12$ J/cm^2

φ (J/cm^2)	$P_+^{\exp}$ (bar)	$\Delta\tau$ (ns)	$v_{\text{sh.w.}}$ (km/s)	$v_{\text{p}} \times 10^2$ (km/s)	P_+^{theor} (bar)
0.12	15	$\backsimeq$0	$\backsimeq$1.483	$\backsimeq$0	$\backsimeq$0
1.3	250	20	1.515	1.1	160
3.4	340	55	1.57	3	460
7.5	1.000	125	1.63	7.2	1.180

Note that where the displacements $\Delta\tau$ are maximal, the velocity of shock waves exceeds that of sound in water by 10%, which corresponds to weak shock waves.

The distortion of the shock wave profile in the course of propagation through the acoustic conductor can be disregarded, acoustic wave pressures several orders of magnitude higher being necessary for acoustic nonlinearities to become manifest in metals.

Conclusion

The nanosecond laser ablation of biotissue is attended by the generation of powerful high-frequency acoustical fields propagating into the tissue at laser energy fluences both below and above the ablation threshold. As the powerful acoustical waves propagate through the biotissue, they are transformed into shock waves, giving rise to great pulsed pressure gradients in the tissue. No cold photomechanical damage–spallation by the powerful rarefaction wave formed upon the reflection of the laser-induced compression wave at the biotissue-air interface — is observed in the course of laser ablation.

The next state of this research is to study the contribution from pulsed pressures and pressure gradients to the failure of biotissue and their effect on the biological processes occurring therein.

References

1. *Isner J.M, Clarke R.H.* The paradox of thermal laser ablation without thermal injury // Lasers Med. Sci. 1987. Vol. 2. P. 165–173.

2. *Dmitriev A.K, Furzikov N.P.* Mechanism of laser ablation of biotissue // Proc. USSR Acad. Sci. Izvestia ser. Phys. (in Russian). 1989. Vol. 53. P. 1105–1110.

3. *Esenaliev R.O, Oraevsky A.A, Letokhov V.S.* Laser ablation of atherosclerotic blood vessel tissue under various irradiation conditions // IEEE Trans. BME. 1989. Vol. 36. P. 1188–1194.

4. *Oraevsky A.A, Esenaliev R.O, Letokhov V.S.* Temporal characteristics and mechanism of atherosclerotic tissue ablation by nanosecond and picosecond laser pulses // Lasers Life Sci. 1992. Vol. 5 (1–2). P. 75–93.

5. *AlDhahir R.K, Dyer P.E, Zhu Z.* Photoacoustic studies and selective ablation of vascular tissue using a pulsed dye laser // Appl. Phys. B. 1990. Vol. 51. P. 81–85.

6. *Kitai M.S, Popkov V.L, Semchishen V.A.* Dynamics of UV excimer laser ablation of PMMA caused by mechanical stresses: Theory and experiment. // Macromol. Chem. Symp. 1990. Vol. 37. P. 257–267.

7. *Dingus R.S, Scammon R.J.* Grüneisen-stress induced ablation of biological tissue // SPIE. 1991. Vol. 1427. P. 45–54.

8. *Oraevsky A.A, Esenaliev R.O, Letokhov V.S.* Pulsed laser ablation of biological tissue: Review of the mechanisms. In: Miller JC, Haglund RF / eds. "Laser Ablation. Mechanisms and Applications." Berlin: Springer-Verlag, 1992. P. 112–122.

9. *Gusev V.E, Karabutov A.A.* Laser optoacoustics. Moscow: Nauka, 1991 (in Russian).

10. *Akhmanov S.A, Gusev V.E, Karabutov A.A.* Pulsed laser optoacoustics: Achievements and perspective // Infrared Phys. 1989. Vol. 26. P. 815–838.

11. *Cheong W.F, Prahl S.A, Welch A.J.* A review of the optical properties of biological tissues // J. Quant. Electr. 1990. Vol. 26. P. 2166–2185.

12. Handbook of Chemistry and Physics. 54th edition. Cleveland, Ohio, 1973.

13. *Kikoin I.K,* ed. Tables of Physical Quantities. Handbook. Moscow: Atomizdat, 1976 (in Russian).

14. *Hüter T.H.* Messung der Ultraschallabsorption in tierischen Geweben und ihre Abhängigkeit von der Frequnz // Naturwissenschaften. 1948. Vol. 35. P. 285–287.

15. *Goss S.A, Johnson R.L, Dunn F.* Comprehensive compilation of empirical ultrasonic properties of mammalian tissues // J. Acoust. Soc. Am. 1978. Vol. 64 (2). P. 423–457.

16. *Dussik K.T, Fritch D.J, Kyriazidou M., Sear R.S.* Measurements of articular tissues with ultrasound // Am. J. Phys. Med. 1958. Vol. 37. P. 160–165.

17. *Kishimoto T.* Ultrasonic absorption in bones // Acoustica. 1958. Vol. 8. P. 179–180.

18. *Ludwig G.D.* The velocity of sound through tissues and acoustic impedance of tissues //J. Acoust .Soc. Am. 1950. Vol. 22. P. 862–866.

19. *Goldman D.E, Hueter T.F.* Tabular data of the velocity and absorption of high frequency sound in mammalian tissues // J. Acoust. Soc. Am. 1956. Vol. 28. P. 35–37.

20. *Rudenko O.V, Soluyan S.I.* Theoretical Foundations of Nonlinear Acoustics. New York: Academic Press, 1977.

21. *Singleton D.L, Paraskevopoulos G., Taylor R.S, Higginson L.A.J.* Excimer laser angioplasty: Tissue ablation, arterial response, and fiber optic delivery // IEEE J. Quant. Elect. 1987. QE-23. P. 1772–1782.

22. *Oraevsky A.A, Jacques S.L, Petit G.H, Saidi I.S, Tittel F.K, Henry P.D.* XeCl laser ablation of atherosclerotic aorta: Optical properties and energy pathways // Lasers Surg. Med. 1992 (in press).

23. *Walsh J.M, Rice N.H.* Dynamic compression of liquids from measurements on strong shock waves // J. Chem. Phys. 1957. No. 26. P. 815–823.

24. *Rice M.H, Walsh J.M.* Equation of state of water to 250 kilobars // J. Chem. Phys. 1957. Vol. 26. P. 824–830.

Appl. Phys. B. 1996 Vol. 63. P. 545–563

TIME-RESOLVED LASER OPTOACOUSTIC TOMOGRAPHY OF INHOMOGENEOUS MEDIA

A. A. Karabutov, N. B. Podymova[1], V. S. Letokhov[2]
[1]*International Laser Center of Moscow State University, Moscow, Russia*
[2]*Institute of Spectroscopy Russian Academy of Science*

The methods of time-resolved laser optoacoustic tomography of inhomogeneous media and related problems are reviewed. Time-resolved laser optoacoustic tomography allows one to measure the distribution of light absorption in turbid media with depth resolution up to several microns in real time. The theory of laser excitation of acoustic waves by absorbing of light in particles, dispersed in transparent, light-absorbing or scattering media, is developed. The distribution of light absorption can be obtained from the temporal course of acoustic pressure. Two schemes of acoustic wave detection — in the medium under testing (direct detection) and in transparent medium, coupled to the investigated one (indirect detection) — are discussed. In both cases the reconstruction of light absorption can be made by simple calculations. Test experiments with homogeneous and layered media confirm the proposed theoretical models and the possibility of using the proposed experimental schemes. Light absorption in homogeneous, inhomogeneous media and in absorbing particles dispersed in turbid media was investigated. The experimental setup allows one to measure the absorption coefficients over the range 1–500 cm^{-1} with the depth resolution 10–15 μm over the depth 1–1.5 mm.

The problem of visualization (reconstruction) of the inhomogeneities in a medium by studying the scattering of radiation of different nature in the medium is a central one in physics. To solve this problem, tomographic diagnostics methods based on recording the scattering field of radiation in various directions in the medium under study have recently gained popularity. These methods are used in different fields, such as, for example, oceanology - acoustic tomography of ocean (see, for example, [1–4]), non-destructive testing (tomography of structure and internal defects and failures with thermal [5, 6] and acoustic [7, 8] waves), medicine (optical, for example, [9] and roentgen tomography) etc. In all cases the distribution of inhomogeneities in the medium is investigated using characteristics of refracted or scattered probing radiation travelling through investigated object in various directions.

From the mathematical point of view this problem is reduced to the determination of the distribution of "refractive index" $n(\mathbf{r})$ in the wave equation

$$\frac{\partial^2 u}{\partial t^2} - \frac{c^2}{n^2(\mathbf{r})}\Delta u = 0, \qquad (1)$$

where u is the radiation field variable, and c is the velocity of probing wave in the same medium without inhomogeneities. The final goal in this case is the reconstruction

of the three-dimensional distribution of inhomogeneities using the distribution $n(\mathbf{r})$. In general, the problems of such kind do not have analytical solution and require rather complicated numerical data-processing procedures.

Let us consider optical tomography. Changes in the angular and frequency spectra of optical radiation in the course of propagation in an inhomogeneous medium are due to scattering and absorption processes. Each of these processes makes the contribution of its own to the reduction of the intensity of the wave coming to the detector. To separate these contributions is of special interest. This is most difficult to do in the case when one of the processes proves much more effective than the other.

For non-destructive testing and imaging of optical inhomogeneities, it is most promising to use laser optoacoustic methods, if inhomogeneities of acoustic properties are much smaller than the inhomogeneities of optical properties. These methods are based on the excitation of thermal and acoustic waves upon absorption of an intensity-modulated (or spatially scan) laser radiation in the medium under study. Acoustic wave occurs as a result of the thermal expansion of the medium in the course of its non-stationary and non-uniform heating. Characteristics of laser-excited thermal and acoustic waves are determined both by characteristics of absorbed radiation and by physical properties of absorbing medium.

Applications of laser optoacoustic methods include various kinds of spectroscopy [10–13], investigations of laser-matter interaction processes [14–16] and diagnostics of materials properties [5, 6, 10–13, 17–19]. Examples of the latter applications are diagnostics of microelectronic devices [5, 6, 17], polymer and ceramic coatings [5], nondestructive testing of power optics elements [18], detection of solid impurities in gases and liquids [10, 11, 19], etc.

Time-resolved detection of laser-excited acoustic pulses allows one to investigate the laser-matter interaction during the course of the laser pulse, for example, light absorption, boiling, ablation, cavitation, etc. [14–16]. Moreover, time-resolved optoacoustic method makes it possible to investigate not only the mean value of light absorption, but its distribution in the depth of the medium too [20, 21].

From the mathematical point of view the problem of optoacoustic tomography is reduced to determination of free term $\partial Q/\partial t$ in the inhomogeneous wave equation

$$\frac{\partial^2 u}{\partial t^2} - c_0^2 \Delta u = \frac{\partial Q}{\partial t}, \tag{2}$$

where c_0 is the sound velocity in the investigated medium. The free term $\partial Q/\partial t$ describes the spatial distribution of heat sources in the medium, determined by light absorption. Contrary to the tomography problem (1) mentioned above, this problem has quite simple analytical solution. The present review is devoted to theoretical analysis of different types of time-resolved laser optoacoustic tomography and their experimental realization.

Physical fundamentals of optoacoustic tomography

The laser optoacoustic effect has been investigated in detail and described in the literature (see, for example, the books and reviews [10–17, 22, 23]); however, consideration being mainly given for homogeneous media. A merit of the optoacoustic technique is the fact that the amplitude of the excited wave is proportional to the light absorption coefficient; therefore, no optoacoustic signal can occur in a scattering medium without light absorption.

The following two types of intensity-modulated laser light are most widely used in optoacoustic experiments: periodically modulated continuous-wave laser radiation and pulsed laser radiation (obtained, as a rule, in a Q-switched mode). As far as the performance of diagnostics and limitation of possible damage of the exposed sample are concerned, the second type of modulation is preferable.

Let the heating laser pulse be short enough. In this case, an inhomogeneous thermal field is "instantaneously" produced in the medium under study while the pulse propagates through it and undergoes absorption therein (Fig. 1). The stresses p' producing in the medium are given by

$$p' = \rho_0 c_0^2 \beta T', \tag{3}$$

where ρ_0 is the density of the medium, c_0 is the sound velocity in the medium, β is the thermal expansion coefficient, and T' is the temperature change. These stresses relax during the time it takes for the acoustic pulse to transit the heated region, expressed as

$$t_a \propto (\mu_a c_0)^{-1}, \tag{4}$$

where χ is the thermal diffusivity of the medium. In the case of bulk absorption of light, heat diffusion in the course of the laser pulse is insignificant as a rule.

Optoacoustic methods of studying the distribution of light absorption in a medium are based on analyzing the efficiency of excitation therein of heat or acoustic waves by laser radiation, the analysis being performed with a high temporal resolution (or within a wide range of laser radiation intensity modulation frequencies).

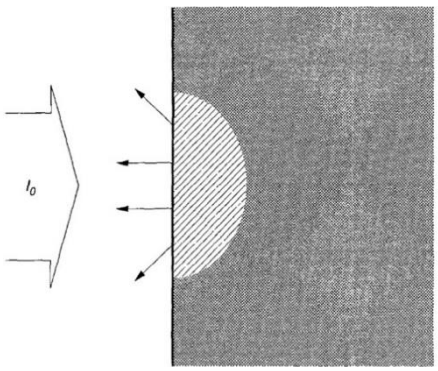


Fig. 1. Optoacoustic phenomena: the dashed area indicates the region of elevated temperature; the arrows schematically indicate the directions in which the particles of the medium move upon its thermal expansion

The frequency spectrum of the laser-induced heat waves is proportional to the Laplace transform of the heat sources distribution over the light-absorbing medium [24–28]. So, the light absorption reconstruction using this method is faced with certain mathematical difficulties of the inversion of Laplace transform [25]. Therefore, such an optoacoustic tomography version is effectively realized only for sufficiently thin specimens (particularly optically thin ones).

The frequency spectrum of the laser-excited acoustic waves is defined by the Fourier transform of the spatial distribution of the heat sources. For this reason, the solution of the inverse problem is much simpler than in the case of heat waves, and is extremely simple when short laser pulses are used [23]. In the case of optoacoustic diagnostics of inhomogeneities of a medium using short laser pulses, the inhomogeneities of the spatial distribution of the heat sources are transformed into the time modulation of the acoustic signal being detected. This is due to the delay of the arrival to the detector of the partial perturbations excited at different points in the medium under study. The time scale of the acoustic signal variation and the spatial scale of the heat sources variation are connected together by the sound velocity in the medium. So, for short laser pulses the spatial resolution of time-resolved laser optoacoustic tomography is determined by the temporal resolution of acoustic signal acquisition system multiplied by the sound velocity in the medium under study.

First experiments

The dependence of temporal shape of optoacoustic signal on the value of light absorption coefficient was established in the first experimental investigation of laser-matter interaction using time-resolved optoacoustic method [29]. The lack of theoretical basis, however, did not allow to get numerical results and the problem of optoacoustic tomography was not discussed in this work.

The relationship between the spatial distribution of heat sources and the temporal shape of the acoustic signal excited by a laser pulse was apparently first theoretically analysed in [20, 21]. The method for determining the light absorption coefficient of a homogeneous medium from the shape of an optoacoustic signal excited therein was first suggested and experimentally realized in [30, 31] (and later it was used in [32–36] for biological tissues). The distribution of the absorption coefficient in an inhomogeneous medium was for the first time reconstructed experimentally from the shape of an optoacoustic signal excited in the medium in 1987 (a detailed description of these experiments can be found in [23]). The medium comprised a set of glass plates separated by layers of aqueous solutions of $CuCl_2$ of different concentrations (Fig. 2), which caused a spatially inhomogeneous absorption of a YAG:Nd laser radiation. Acoustic wave was detected on the side opposite to the exposed side of the stack (transmission-mode tomography). By varying the solution concentration in different layers, they managed to change arbitrarily enough the shape of the acoustic signal being excited. Using the analytical relationships obtained earlier in [20], the light absorption coefficient distribution was calculated from the shape of this signal. The calculation results agreed well with the theoretically predicted distribution (Fig. 3). Similar experiments on the diagnostics of collagen gel layers differing in the

concentration of a dye were described in [35, 36]. The shape of an acoustic signal excited in a two-layer collagen layer system is presented in Fig. 4. The boundary between the layers is easily distinctive.

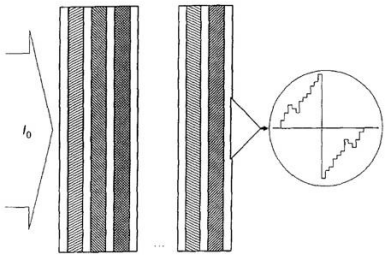


Fig. 2. Structure of an inhomogeneous, layered light-absorbing medium. Encircled is the characteristic profile of the acoustic signal being excited

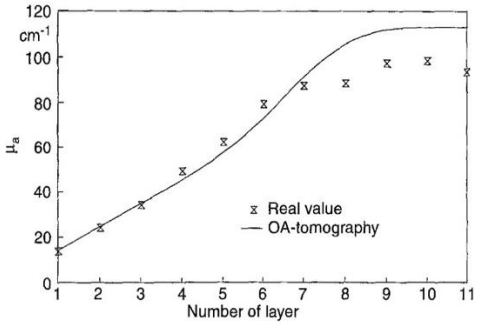


Fig. 3. Optoacoustic tomography of a model inhomogeneous, layered light-absorbing medium

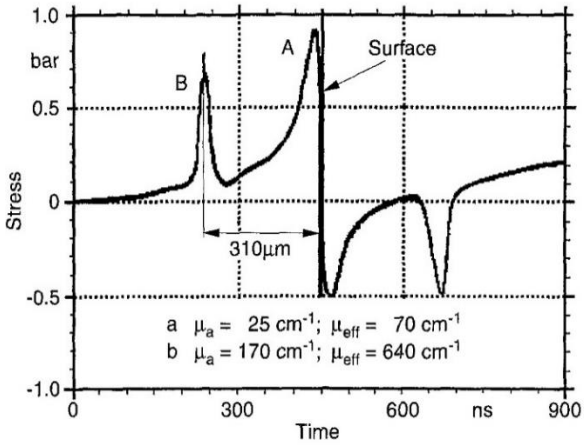


Fig. 4. Shape of the optoacoustic signal in a two-layered medium [36]. The figures denote signal profile sections due to light absorption in the individual layers

In the experiments above, acoustic wave was detected at that side of the light-absorbing medium which was opposite to the exposed side (direct signal detection, see Figs. 2 and 5*a*). In applications, however, the medium of interest is, as a rule, accessible from front side only. It is therefore necessary to modify the acoustic signal detection method so as to make it possible to implement such diagnostics technique as well. Such a modification was suggested in [35, 36] and independently realized experimentally in [37, 38]. Its schematic diagram is shown in Fig. 5b: the surface of the medium under study is irradiated through a side and a base of a transparent prism with a wide-band acoustic transducer coupled to its opposite base (indirect signal detection, in transparent medium). Piezoelectric transducers are usually used, for they are highly sensitive, simple, and miniature enough. However, more sophisticated methods (e.g. optical interferometric techniques) could also be applied to detect acoustic signals. In this case, totally contactless optoacoustic tomography would be possible.

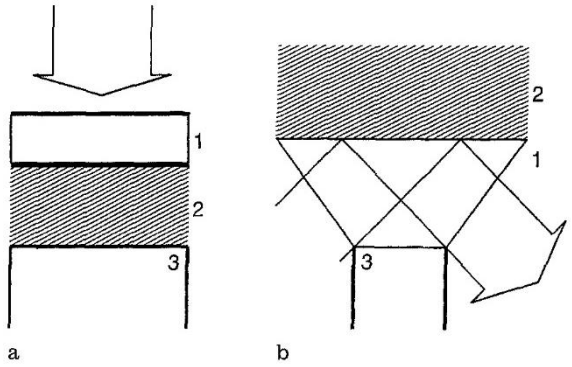


Fig. 5. (*a*) Direct and (*b*) indirect optoacoustic signal detection. The schemes include a transparent medium (*1*) a light-absorbing medium to be studied (*2*), and a wide-band acoustic transducer (*3*)

Subject of study in the above experiments [35–37] were layered (stratified) media, and the cross-sectional size of the laser beam was sufficiently large, so that the plane acoustic wave was excited. The results obtained are clear enough, and the reconstruction of the distribution of the light absorption coefficient is rather simple. In the case of inhomogeneous media containing light-absorbing particles, the procedure of reconstructing the light absorption coefficient distribution is not so trivial [39]. Moreover, even the theory of the optoacoustic effect in such media is still not yet complete.

Concerning laser excitation of acoustic waves, the principal difference between microinhomogeneous and homogeneous media consists in the appearance of "delayed" heat sources in the liquid surroundings the light-absorbing particles as a result of heat flux from the particles into the liquid. This contribution to the laser-excited acoustic wave in a microinhomogeneous medium was calculated in [40, 41]. The distribution of the particles (hence of the light absorption coefficient) was however taken to be homogeneous, and no tomography problem was discussed there. The

analysis of various extreme cases for the tomography of absorbing media was made in [39]. Formulas for reconstructing the distribution of the light absorption crosssection of particles in a microinhomogeneous medium from the shape of the optoacoustic signal excited in the medium were obtained. The medium containing light-absorbing centers may be transparent, scattering or absorbing.

Optoacoustic tomography was experimentally implemented in [37–39] for transparent homogeneously absorbing and scattering model media containing light-absorbing particles. These media were suspensions of graphite (or carbon block) particles in water, milk and an aqueous solution of $CuCl_2$. The spatial distribution of the light absorption coefficient in real homogeneous media (aqueous solutions of $CuCl_2$ differing in concentration) and macroinhomogeneous media (magnetic liquids prepared on the basis of transformer oil) was reconstructed in [42]. Q-switched YAG : Nd laser (pulse duration 10^{-12} ns, radiation wavelength $\lambda = 1.06$ μm) was used for optoacoustic tomography. This method makes it possible to reconstruct the distribution of the light absorption coefficient varying from a few cm^{-1} to a few hundreds of cm^{-1} with z-axial resolution of 15–20 μm for a liquid sample. The depth resolution achieved is at the level of the best results obtained with the *optical coherence tomography* techniques [43, 44], though the means used and mathematical treatment are much simpler.

Time-resolved detection of acoustic waves

The main technical difficulty of optoacoustic tomography is associated with the correct detection of acoustic signals with the temporal resolution which, generally speaking, has to be higher than the laser-pulse duration. Being highly sensitive and sufficiently wide-band, lithium niobate based piezoelectric transducers have proved most suitable for this purpose.

Wide-band piezoelectric transducers are usually operated in two modes: short-circuited and open-circuited. In the first case, the thickness h of the piezoelectric element should be greater than the spatial extension of the acoustic perturbation to be detected: $h > c_1 t_a$ (c_1 is the longitudinal acoustic wave velocity in the piezoelectric material). The duration of acoustic signals that can be detected correctly is accordingly limited above (as a rule, at a level of some microseconds), and the maximum depth of probing is accordingly limited. The temporal resolution is determined mainly by the recharge time of the piezoelectric element, $R_0 C$ (R_0 is the load resistance and is equal, as a rule, to the wave impedance of the connecting cable, and C is the capacitance of the piezoelectric element) and amounts to a few nanoseconds or less.

In the open-circuited mode, the thickness of the piezoelectric element should be much less than the extension of the acoustic pulse, that limits the temporal resolution. To achieve this resolution at a nanosecond level, $LiNbO_3$ piezoelectric elements thinner than 25 μm should be used. The difficulty of getting a uniform frequency response and the need to use wide-band charge preamplifiers with a high-input resistance (as a rule, not less than 100 kΩ) make it more preferable to use piezoelectric elements operating in a short-circuited mode.

Another technical difficulty in providing a high-temporal resolution in the detection of optoacoustic signals is the need for a precise adjustment of the detector face with respect to the wave front of the arriving signal. Obviously, the difference in time between the instants the perturbation arrives at the opposite edges of the piezoelectric element aperture should be less than the temporal resolution. Therefore, the angle between the wave arrival direction of the normal to the detector must be at the level of the order of $\nu \sim 3'$ or less [by the temporal resolution of $\Delta\tau \sim 10$ ns and the sensitive area aperture of $d\sim$ 3 mm ($\nu \ll c_0\Delta\tau/d$)].

The above technical difficulties are apparently the reason why the optoacoustic tomography of inhomogeneous media has not yet got wide recognition. We hope that this paper will help to overcome these difficulties.

1. Elements of the theory of laser optoacoustic tomography

In pulsed-laser optoacoustics the principal quantity being measured is traditionally the signal amplitude (or the area of the first half-wave in the case of box-car integration). This is due to the problems associated with both the adequate detection of wide-band acoustic signals and the interpretation of the influence of various factors (inhomogeneous absorption and scattering of light, inhomogeneous damping and diffraction of ultrasonic waves, thermal and acoustic non-linearities, and so on) on the profile of the optoacoustic signal. At the same time, the temporal course of the acoustic wave being excited carries detailed information about the absorption of the laser radiation, which is not, generally speaking, manifested in the signal amplitude. Possible schemes of correct detection with a high-temporal resolution of optoacoustic signals will be discussed in the next section. Here we will describe the effect of various factors on the time profile of the wave being excited.

The thermooptical excitation of acoustic wave takes place due to the absorption of light and the following thermal expansion of the medium. The absorption of light may take place both in the bulk of the medium and at individual light-absorbing centers (Fig. 6). If the depth of penetration of light into the medium is less than the average distance between the light-absorbing particles d ($d \propto n_p^{-1/3}$, n_p is the concentration of the particles), i.e. if $\mu_a d \geq 1$, the influence of particles on the absorption of light is insignificant. In this case, the thermooptical excitation of acoustic wave occurs in the same way as in a homogeneous medium. Therefore, we will take $\mu_a d \ll 1$.

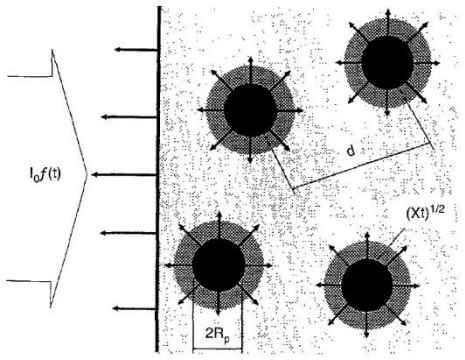


Fig. 6. Thermooptical excitation of acoustic wave in an inhomogeneous medium containing light-absorbing centers

The temperature-field dynamics is characterized by two time scales, namely, the relaxation time of the temperature of the light-absorbing particle, $\tau_p = R_p^2/\chi_p$ (χ_p is the thermal diffusivity of the particle material and R_p is the particle radius), and the time of temperature smoothing in the medium surrounding the particle, $\tau_0 = d^2/4\chi$ (χ is the thermal diffusivity of the surrounding medium). If the laser pulse duration $\tau_L > \tau_p$, the heating of the particles can be considered uniform; to fulfill this condition, the particles must be small enough: $R_p \ll \sqrt{\chi_p \tau_L}$. If the laser pulse duration $\tau_L > \tau_0$, the temperature fields produced in the medium in the course of heating of individual particles overlap, so that the contribution of the particles is reduced to some additional absorption of light. In this case, the thermooptical excitation of acoustic wave proceeds as in a homogeneous medium, provided the concentration of the particles is high enough:

$$n_p \gg (4\chi\tau_L)^{\frac{3}{2}}, \tag{6}$$

If the above condition is satisfied, the medium can be considered as microhomogeneous.

To investigate light-absorbing microinhomogeneities by means of the detection of an optoacoustic signal, it is not merely sufficient to satisfy the condition $n_p \gg (4\chi\tau_L)^{3/2}$. It is also necessary that the stress relaxation time $\tau_a = d/2c_0$ should be longer than the laser-pulse duration, i.e.

$$d > 2c_0\tau_L \qquad \left[n_p < (2c_0\tau_L)^{-3}\right]. \tag{7}$$

In this case, the stresses produced in the medium around individual particles in the course of the laser pulse do not overlap, so that the acoustic pulses excited by them can be detected separately. The time R_p/c_{0p} it takes for stresses to relax within a particle is short as a rule, and so we will hereinafter take such particles to be "acoustically small":

$$R_p \ll c_{0p}\tau_L. \tag{8}$$

(c_{0p} is the acoustic-wave velocity in the material of the particles). The finite-stress relaxation time within a particle was taken into account in [45].

Thus, the specific features or optoacoustic signals in inhomogeneous media are determined by the relationships among the laser-pulse duration τ_L, thermal relaxation times τ_p and τ_0, and stress relaxation time τ_a. Due to the adiabatic propagation of acoustic wave, $\tau_0 \gg \tau_a$. Because of the distance between the particles is greater than their diameter, $\tau_0 \gg \tau_p$. Therefore, the optoacoustic tomography of microinhomogeneous media is only possible if the conditions

$$\tau_L \leq \left(\tau_a, \tau_p\right) \ll \tau_0. \tag{9}$$

are satisfied. When $\tau_L \geq \tau_0$, no microinhomogeneities can manifest themselves in the optoacoustic signal.

1.1 Optoacoustic phenomena in a microhomogeneous medium

In a microhomogeneous medium, the temperature fields produced by individual particles overlap at the end of the laser pulse. However, the light absorption coefficient may vary in space (for example, as a result of variations in the concentration of particles). The problem of tomography therefore is reduced to the determination of these "macroinhomogeneities".

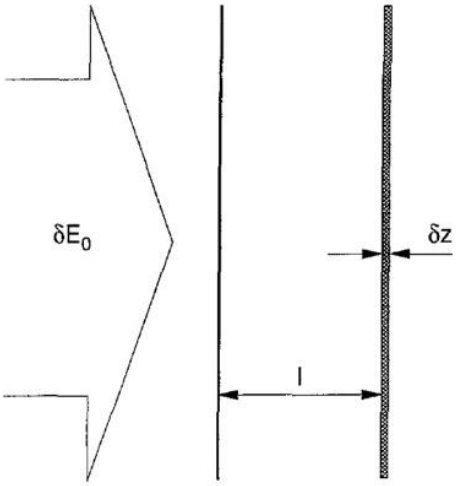


Fig. 7. Thermooptical excitation of acoustic wave by absorption of a laser pulse in a layer with a thickness of δz in the light-absorbing medium

Consider first a model situation. Let a short laser pulse with a radiant exposure δE_0 be absorbed in a thin (δz thick) layer of the medium under testing at a depth l from the surface (Fig. 7). The temperature variation in this layer will be

$$T' = \frac{\delta E_0}{\rho_0 C_p \delta z}, \tag{10}$$

where C_p is the heat capacity of the medium. This will cause stresses to develop in the medium, given by

$$p' = c_0^2 \rho' + c_0^2 \rho_0 \beta^* T', \tag{11}$$

where ρ' is the density variation and β^* is the "effective" thermal expansion coefficient of the medium: $\beta^* = \beta$ thermal expansion coefficient for liquids and gases, $\beta^* = \beta(1 - 4c_t^2/3c_0^2)$ for solids [23], where c_t is shear-wave velocity. These stresses are distributed equally between the waves running away to the left and right of the heated area (Fig. 8a). In the course of the short laser pulse, the medium has not enough time to get deformed, and so $\rho' = 0$.

The pulse R running into the medium (see Fig. 8b) suffers no influence of the boundary $z = 0$ between the transparent medium and the light-absorbing medium under study. The pulse L_0 running toward the boundary of the medium will reach the interface within the time $t_2 = l/c_0$ (see Fig. 8c). At the interface, a part of it reflects (the pulse L_r in Fig. 8d) and other part transits into the transparent medium (the pulse L_t in Fig. 8d). The pressure-wave reflection and transmission coefficients R_a and T_a depend on the ratio between the acoustic impedances Z_{tr} and Z_0 of the transparent and light-absorbing media, respectively ($Z_0 = \rho_0 c_0$, $Z_{tr} = \rho_{0tr} c_{0tr}$, ρ_{0tr} and c_{0tr} are the density and the velocity of acoustic wave of the transparent medium):

$$R_a = \frac{Z_{tr} - Z_0}{Z_{tr} + Z_0}, \tag{12}$$

$$T_a = \frac{2Z_{tr}}{Z_{tr} + Z_0}, \tag{13}$$

As can be seen from (13), the pressure wave entering the transparent medium has the same phase as the incident wave (a compression wave remains so upon the crossing of the interface, and a rarefaction wave remains a rarefaction one). The phase of the reflected wave depends on the relationship between the acoustic impedances of the contiguous media. If the transparent medium has greater acoustic impedance than the light-absorbing one ($Z_{tr} > Z_0$, for example, glass with respect to water), the reflection of a pressure wave occurs in the same phase ($R_a > 0$). In this case, the pressure amplitude in the transmitted wave is higher than in the incident one ($T_a > 1$). When the reverse acoustic impedances relationship holds true ($Z_{tr} < Z_0$, for example, air with respect to a liquid) the phase of the reflected wave will be inverted ($R_a < 0$).

Thus, the acoustic signal that will be detected by a transducer located in the transparent medium (indirect signal detection, see Fig. 5b) will only contain a single-compression pulse:

$$p'_{tr} = \frac{1}{2} T_a c_0^2 \rho_0 \beta^* T' \delta(l + z/c_{0_{tr}} - l/c_0) \tag{14}$$

(when δE_0- const and $\delta z \to 0$).

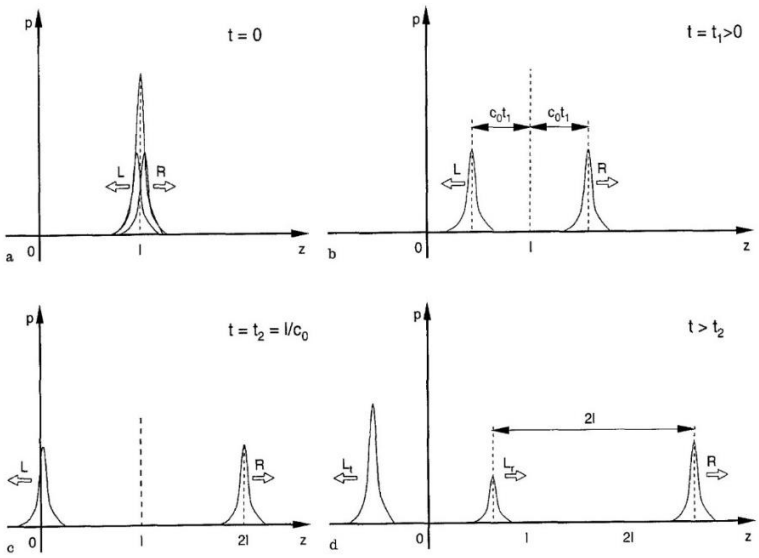


Fig. 8*a–d*. Excitation of an optoacoustic signal upon the absorption of laser radiation in a layer: (*a*) distribution of mechanical stresses immediately following the absorption of a laser pulse; (*b*) emission of acoustic waves: the impulse R propagates deep into the medium, whereas the impulse *L* runs towards its boundary; (*c*) arrival of the impulse *L* to the boundary of the light-absorbing medium; (*d*) passage of the impulse *L* through the boundary of the medium and the reflection of the impulse at the boundary

A transducer located in the light-absorbing medium (direct signal detection, see Fig. 5a) will register two pulses:

$$p' = \frac{1}{2} c_0^2 \rho_0 \beta^* T' [\delta(t - z/c_0 + l/c_0) + R_a \delta(t - z/c_0 - l/c_0) \qquad (15)$$

The first of these pulses is the compression pulse R and the second is the pulse L_r which can be either a compression pulse (at $Z_{tr} > Z_0$) or a rarefaction pulse (at $Z_{tr} < Z_0$). The pulse L_r is delayed relative to the pulse R by an interval of $2l/c_0$, and this delay grows as the depth of location of the light-absorbing layer increases. If the light-absorbing layer is located on the interface $z = 0$, these two perturbations merge together.

Let us now consider the case of thermooptical excitation of acoustic wave in a homogeneous light-absorbing medium with $\mu_a = \text{const}$. Let a wide laser beam with $\mu_a a_0 \gg 1$ (a_0 is the beam radius) be normally incident to the interface $z = 0$ (Fig. 9). If the distance $\sqrt{\chi \tau_L}$ of heat diffusion in the medium in the course of the laser pulse τ_L does not exceed the depth of light penetration into the medium, i.e. if

$$\mu_a^2 \chi \tau_L \leq 1, \qquad (16)$$

the diffusion of heat has no effect on the temperature distribution in the medium, so that its heating at the end of the laser pulse will be

$$T' = \left(\frac{\mu_a E_0}{\rho_0 C_p}\right) \exp(-\mu_a z), \tag{17}$$

where E_0 is the radiant exposure of the absorbed laser pulse.

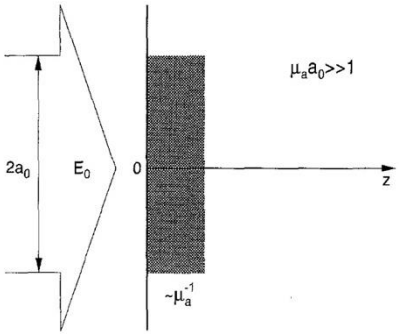


Fig. 9. Thermooptical excitation of acoustic wave in a homogeneous light-absorbing medium

This temperature field gives rise to stresses (11). If these stresses have not enough time to relax in the course of the laser pulse, i.e. if

$$\mu_a c_0 \tau_L \ll 1, \tag{18}$$

the density of the medium will not change in the course of the laser pulse, so that the pressure field will follow the temperature distribution

$$p' = \frac{c_0^2 \beta^*}{C_p} \mu_a E_0 \exp(-\mu_a z), \quad z > 0. \tag{19}$$

As in the case of light absorption in a thin layer, these stresses are equally splitted between the wave running deep into the medium and the one propagating towards the interface.

The profiles of signals that will be registered in the case of indirect or direct signal detection will be defined by the convolution of distribution (19) with solution (14) or (15), respectively,

$$p'_{tr} = T_a \frac{c_0^2 \beta^*}{2C_p} \mu_a E_0 \exp(-\mu_a c_0 \tau_{tr})\, \theta(\tau_{tr}), \tag{20}$$

$$p' = \frac{c_0^2 \beta^*}{2C_p} \mu_a E_0 [\exp(\mu_a c_0 \tau)\, \theta(-\tau) + R_a \exp(-\mu_a c_0 \tau)\, \theta(\tau)], \tag{21}$$

where $\tau = t - z/c_0$ and $\tau_{tr} = t + z/c_{0tr}$ stand for the time in the coordinate frames moving with velocities of the corresponding waves and $\theta(\tau)$ is the Heaviside unit function.

The profile of the optoacoustic signal excited by a short laser pulse in a homogeneous light-absorbing medium consists of sections of an exponential curve whose exponent depends on the light absorption coefficient (the medium is assumed clear enough) (see Fig. 10*a* for indirect signal detection and Fig. 10b for direct signal detection). The amplitude of signals (20) and (21) is directly proportional to the light absorption coefficient. It is for this reason that optoacoustic tomography is sensitive exactly to the magnitude of the light absorption coefficient.

In general case, the light-absorbing medium can also contain light-absorbing particles. However, if their concentration is high enough $[n_p \gg (4\chi\tau_L)^{-3/2}]$, such a medium can be considered as microhomogeneous [see (6)]. But if the concentration n_p of the light-absorbing particles depends on their depth in the medium and characteristic changes of n_p occur at depths of z»d, the medium is layered (stratified) and the light absorption coefficient μ_a for it will also depend on the depth z.

The expression obtained for the optoacoustic signal profile can be generalized to the case of arbitrary depth dependence of the light absorption coefficient, $\mu_a = \mu_a(z)$ [in the first case considered above, $\mu_a = \delta(z - l)$ and in the second, $\mu_a = const$]. As a result, by absorbing a short laser pulse ($\mu_a c_0 \tau_L \ll 1$) the profiles of optoacoustic signals in a stratified medium in the case of indirect and direct signal detection may be defined by the formulas

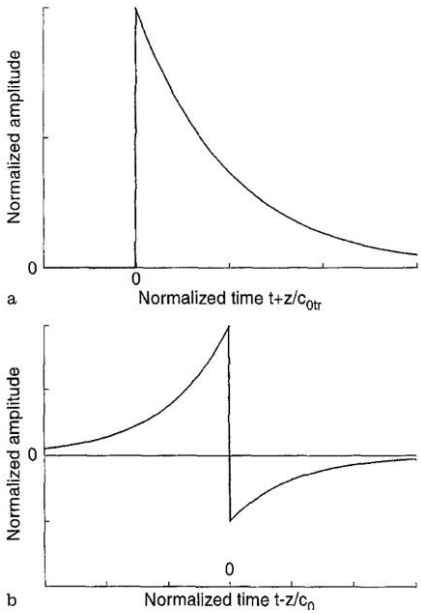


Fig. 10. Optoacoustic signals excited by a short laser pulse in a homogeneous light-absorbing medium: (*a*) indirect signal detection; (*b*) direct signal detection

$$p'_{tr} = T_a \frac{c_0^2 \beta^*}{2C_p} \mu_a(c_0\tau_{tr}) E_0 \exp\left[-\int_0^{c_0\tau_{tr}} \mu_a(\xi)d\xi\right] \theta(\tau_{tr}), \qquad (22)$$

$$p' = \frac{c_0^2 \beta^*}{2C_p} E_0 \left\{ \begin{array}{l} \mu_a(-c_0\tau) \exp\left[-\int_0^{-c_0\tau} \mu_a(\xi) d\xi \right] \theta(-\tau) + \\ + R_a \mu_a(c_0\tau) \exp\left[-\int_0^{c_0\tau} \mu_a(\xi) d\xi \right] \theta(\tau) \end{array} \right\}. \qquad (23)$$

These solutions make it possible to find the distribution of the light absorption coefficient from the shape of the optoacoustic signal. In the case of indirect signal detection, one can get from (22)

$$\mu_a(c_0\tau_{tr}) = \frac{p'_{tr}(\tau_{tr})}{c_0 \int_{\tau_{tr}}^{\infty} p'_{tr}(\xi) d\xi}, \qquad \tau_{tr} > 0. \qquad (24)$$

To determine the light absorption coefficient in the case of direct signal detection, it is convenient to use the leading edge of the optoacoustic signal [$\tau < 0$ in (23)], for the influence of the limited bandwidth of the detection on this section of the signal profile is minimal:

$$\mu_a(-c_0\tau) = \frac{p'(\tau)}{c_0 \int_{-\infty}^{\tau} p'(\xi) d\xi}, \qquad \tau < 0. \qquad (25)$$

Formulas (24)–(25) are basic in the optoacoustic tomography of layered clear media (by using short laser pulses). What is important in the fact that their application does not require absolute calibration of the acoustic detectors used. If the light scattering is strong enough, the principal features of the laser excitation of acoustic pulses are the same. But in this case the temporal shape of acoustic pulse is determined by the light extinction coefficient μ_{eff}, which depends both on light absorption and light scattering. So, μ_{eff} may be determined without absolute calibration of acoustic transducer. The amplitude of laser-excited acoustic pulse is determined by light absorption coefficient and to determine it one needs the absolutely calibrated acoustic transducer. The applicability of (24) and (25), however, is restricted to layered-inhomogeneous (macroinhomogeneous) and microhomogeneous media. The analysis of the optoacoustic effect in the more general case of microinhomogeneous medium is presented below.

1.2 Optoacoustic phenomena in a microinhomogeneous medium

The specific features of the optoacoustic effect in a microinhomogeneous medium are determined by two circumstances. First, the presence of microinhomogeneities causes the light field in the medium to change as a result of the scattering and additional adsorption of the incident radiation. In this case the attenuation of the light intensity in the medium, ***I(r)***, is determined by the extinction coefficient μ_{eff}. For collimated-laser beam $\mu_{eff} = \mu_a + \mu_s$ [46–48], μ_s is the light-scattering coefficient.

The volume heat source density $\partial Q/\partial t$ is connected to the light intensity I(**r**) by the absorption coefficient as before: $\partial Q/\partial t = \mu_a I$.

Another characteristic feature of the optoacoustic effect in a microinhomogeneous medium is due to an additional heat transfer from the light-absorbing particles into the medium. Such "delayed" heat sources acting after the end of the laser pulse course may substantially affect the shape of the acoustic pulses being excited. In general, an optoacoustic signal can be represented as a superposition of the optoacoustic signal of a microinhomogeneous medium with some "average" absorption and acoustic waves from individual light-absorbing particles. The formation of the first component of the optoacoustic signal components has been described in Sect. 1.1. As noted above, to realize the optoacoustic tomography of light-absorbing particles, it is necessary that the relation $\tau_L \ll \tau_0$ must be satisfied (in this case the thermal fields produced in the medium by the heating of individual light-absorbing particles do not overlap, see Sect. 1). In addition, if the condition $\tau_L < \tau_a$ is satisfied as well, the acoustic fields excited by the individual light-absorbing particles can also be considered practically independently.

The thermooptical generation of acoustic wave by an individual light-absorbing particle is schematically illustrated in Fig. 11. Two cases are possible, depending on the relationships among the coefficient of light absorption in the material of the particle μ_{ap}, heat diffusion depth $\sqrt{\chi_p \tau_L}$, and the side of the particle R_p. If the particle is opaque ($R_p \mu_{ap} > 1$) and thermally large ($R_p > \sqrt{\chi_p \tau_L}$), only the surface layer of the particle gets heated during the course of the laser pulse (Fig. 11a). The thickness of this layer is of the order of $\sqrt{\mu_{ap}^{-2} + \chi_p \tau_L}$ and is determined either by the absorption of light (at $\mu_{ap}^{-1} > \sqrt{\chi_p \tau_L}$) or by the diffusion of heat (at $\mu_{ap}^{-1} < \sqrt{\chi_p \tau_L}$). If the particle is thermally small ($R_p < \sqrt{\chi_p \tau_L}$), or if it is almost transparent ($R_p \mu_{ap} < 1$), it is heated uniformly all over its volume (Fig. 11b).

The diffusion of heat from the particle into the surrounding medium causes the additional non-uniform heating of the medium into the depth of $\sqrt{\chi t}$ (t is the time reckoned from the instant of the laser pulse). If the heating of the particle during the course of the laser pulse is non-uniform, the dispersion medium gets heated only on the exposed side of the particle. During the time ($t \geq R_p^2/\chi_p \gg \tau_L$), the heating of the particle tends to be uniform, so that the temperature field around it gets asymmetrical. If the heating of the particle during the course of the laser pulse is uniform, the temperature distribution is always symmetrical.

If $R_p^2/\chi_p \leq \tau_L \ll \tau_0 = d^2/4\chi$ the temperature change of each individual particle, T_p', and that of the surrounding medium, T', are found separately from the heat-diffusion equations

$$\chi_p^{-1} \frac{\partial T_p'}{\partial t} = \Delta T_p' + \frac{I_0}{\kappa_p} f(t) H(\boldsymbol{r}_\perp), \qquad (26a)$$

$$\chi^{-1} \frac{\partial T'}{\partial t} = \Delta \mathrm{T}' \qquad (26b)$$

subject to the appropriate boundary conditions

$$T_p'\big|_{r=R_p} = T'|_{r=R_p}, \tag{27a}$$

$$-\kappa_p \frac{\partial T_p'}{\partial r}\bigg|_{r=R_p} + \kappa \frac{\partial T'}{\partial r}\bigg|_{r=R_p} = 0. \tag{27b}$$

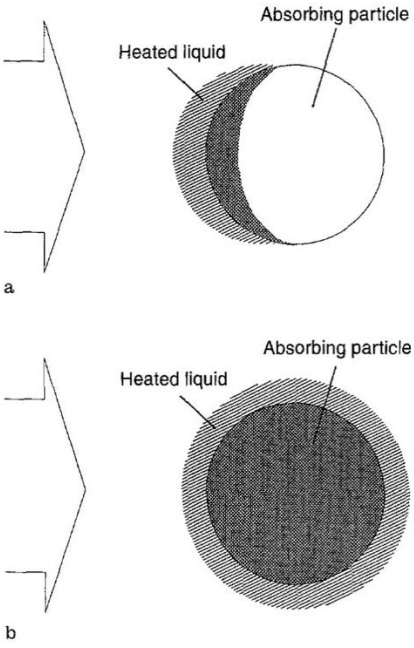


Fig. 11*a*, *b*. Thermooptical excitation of acoustic wave by absorption of light in an individual particle: (*a*) opaque and thermally large particle; (*b*) almost transparent or thermally small particle

In the expressions above, κ_p and κ are the heat conductivities of the particle and the surrounding medium, respectively, I_0 is light intensity at the particle boundary, the function $f(t)$ defines the time dependence of the laser-radiation intensity, and $H(r_\perp)$ defines the laser-radiation intensity distribution over the crosssection of the particle.

The thermal expansion of the particle and the adjacent heated layer of the surrounding medium gives rise to a spherical acoustic wave (Fig. 12). The pressure p' in this wave depends on the rate of the change of the volume V of the particle and the heated layer of the surrounding medium [52, 53]:

$$p'(\tau = t - r/c_0) = \frac{\rho_0}{4\pi r}\frac{\partial^2 V}{\partial t^2}. \tag{28}$$

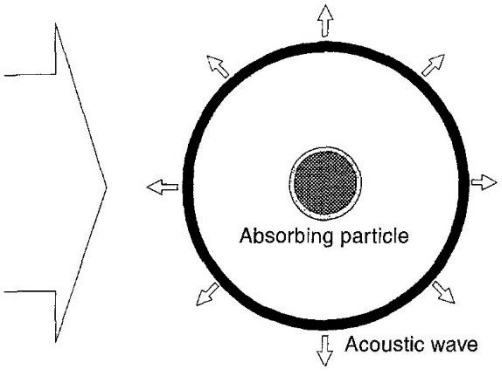


Fig. 12. Spherical acoustic wave excited as a result of the absorption of light by an individual particle

In as much as the increment δV of the volume element dV is related to the temperature by the relation

$$\delta V = \beta^* T' dV, \tag{29}$$

the change of the volume V can be found by integrating the spatial temperature distribution

$$V = 4\pi \int_0^{R_p} r^2 \beta_p^* T_p' dr + 4\pi \int_{R_p}^{\infty} r^2 \beta^* T' dr \tag{30}$$

(here β_p^* is the effective thermal expansion coefficient of the material of the particle).

In the case of thermally large particle ($R_p > \sqrt{\chi_p \tau_L}$) the pressure in the acoustic wave being emitted is defined from (28) and (30) taking into account the solution of (26)–(27):

$$p'(\tau) = \frac{\sigma_0 I_0}{4\pi r} \frac{\rho_0 \beta^* \chi}{\kappa} \frac{1 + \left(\frac{\beta_p^* \sqrt{\chi_p}}{\beta^* \sqrt{\chi}}\right)}{1 + \left(\frac{\kappa_p \sqrt{\chi_p}}{\kappa \sqrt{\chi}}\right)} \frac{\partial f(\tau)}{\partial \tau}, \tag{31}$$

where σ_0 is the light absorption cross section of an individual particle. According to (31), the temporal course of the acoustic pulse emitted upon the thermal expansion of the particle and the adjacent layer of the surrounding medium follows the shape of the derivative of the time envelope of the laser-pulse intensity.

In the case of thermally small particle ($R_p < \sqrt{\chi_p \tau_L}$), one should take into account the relationship between th radius R_p of the particle and the thickness $\sqrt{\chi \tau_L}$.

of the heated layer of the surrounding medium. For an "ultrafine" particle ($R_p \ll \sqrt{\chi\tau_L}$) the acoustic pulse being excited is defined by the expression

$$p'(\tau) = \frac{\sigma_0 I_0}{4\pi r}\frac{\rho_0\beta^*\chi}{\kappa}\frac{\partial f(\tau)}{\partial r}, \tag{32}$$

and also follows the time dependence of the derivative of the laser-pulse intensity. The amplitude of the acoustic wave excited is only determined by the thermal expansion of the surrounding medium; the role of the particle is reduced to the absorption of light and the corresponding heating of the medium. If the thickness of the heated layer of the medium is small compared to the radius of the particle ($\sqrt{\chi\tau_L} \ll R_p \ll \sqrt{\chi_p\tau_L}$) the thermal expansion of the particle is predominant:

$$p'(\tau) = \frac{\sigma_0 I_0}{4\pi r}\frac{\rho_0\beta_p^*\chi_p}{\kappa_p}\frac{\partial f(\tau)}{\partial r}. \tag{33}$$

In this case, the course of the acoustic pulse also follows the derivative of the laser-pulse intensity envelope.

Thus, in all the cases considered above, the thermooptical generation of acoustic wave by an individual light-absorbing particle gives rise to a spherical acoustic wave whose temporal course follows the derivative of the laser-pulse intensity.

Let the concentration of the light-absorbing particles be such that the acoustic fields produced by individual absorbing particles overlap during the course of the laser pulse ($\tau_L > \tau_a = d/2c_0$ or $d < 2c_0\tau_L$), but the temperature fields produced in the medium due to the heating of the individual particles do not interfere as before [$n_p < (4\chi\tau_L)^{3/2}$, $d > 2\sqrt{\chi\tau_L}$ or $\tau_L < \tau_0$]. In this case, the pressure in the acoustic wave being emitted is defined by the expression

$$p'(\boldsymbol{r}) \propto \int \sigma(\boldsymbol{r}')\frac{\partial f(t - |\boldsymbol{r} - \boldsymbol{r}'|/c_0)}{\partial t}dV', \tag{34}$$

where $\sigma(\boldsymbol{r}')$ is the spatial distribution of the light absorption cross sections of the particles. In the first approximation (relatively weak scattering of light), $\sigma(\boldsymbol{r}') = \sigma_0 n_p(\boldsymbol{r}')$, where $n_p(\boldsymbol{r}')$ is the concentration of the particles.

In general case, as noted above, an optoacoustic signal in a microinhomogeneous medium can be represented as a superposition of optoacoustic signal (22, 23) of a microhomogeneous medium with some average light absorption coefficient $< \mu_a >$ given by (24) and (25) and acoustic pulses (31)–(34) from individual light-absorbing particles. Separating these two contributions enables one to find both the distribution of the average light absorption over the bulk of the light-absorbing medium (see (24) and (25)) and the distribution of the light-absorbing particles:

$$\sigma(-c_0\tau) \propto \int_{-\infty}^{\tau} (p'(\xi) - \exp[< \mu_a > c_0\xi])\, d\xi, \tau = t - z/c_0 < 0\,. \tag{35}$$

The expression above holds true for the acoustic wave propagating into the light-absorbing medium (in the case of transmission-mode signal detection). In the case of reflection-mode signal detection,

$$\sigma(c_0\tau_{tr}) \propto \int_{\tau_{tr}}^{\infty} [p'_{tr}(\xi) - \exp(-<\mu_a> c_0\xi)]\, d\xi, \tau_{tr} = t + z/c_{0tr} > 0\,. \quad (36)$$

Thus, expression (24, 25) and (35, 36) enable one to find the spatial distribution of light-absorbing inhomogeneities in a transparent, light-absorbing, or light-scattering medium, i.e. to solve the problem of the optoacoustic tomography of an inhomogeneous medium.

1.3 Diffraction of laser-excited acoustic pulses

An optoacoustic signal excited in a microinhomogeneous medium consists of spherical waves excited by individual particles and an acoustic beam determined by the "average" (effective) light absorption. The radius of the acoustic beam coincides with that of the laser beam. Depending on the relationship between the beam radius a_0 and the light penetration depth μ_{eff}^{-1} (Fig. 13), the phase front of acoustic wave can be almost plane (at $a_0\mu_{eff} \gg 1$, Fig. 13*a*), cylindrical (at $a_0\mu_{eff} \ll 1$, Fig. 13*b*) or spherical (at $a_0\mu_{eff} \propto 1$, Fig. 13*c*). There is a vast body of literature devoted to the calculation of the optoacoustic signal profiles in these cases (see, for example, monographs [22, 23] and references cited therein).

In the case of cylindrical and spherical phase fronts, the profile of the optoacoustic signal does not change during the course of propagation [49]. But if the wave front is initially almost plane, the situation is somewhat more complicated. While propagating for a distance of z of the order of $L_D = \pi a_0^2/\lambda_s$ (λ_s is the length of the acoustic wave), the beam gets wider (its cross section doublets) due to diffraction [50], and it becomes almost spherical at distances of $\geq 3L_D$. A specific feature of optoacoustic signals is the wide band of its frequency spectrum. For this reason, the wavelengths of harmonics of optoacoustic signal vary over wide range, and accordingly, the diffraction lengths L_D of the individual harmonics differ substantially. The low-frequency components of the signal spectrum diffract earlier (at shorter distances) than their high-frequency counterparts. At the same time, to achieve a high-spatial resolution, it is necessary to detect the signal in a frequency band as wide as possible. Therefore, it is most reasonable to detect acoustic waves propagating normally to the boundary of the light-absorbing medium.

The diffraction transformation of optoacoustic signal profile in the paraxial approximation may be described by the equation [51, 23]

$$\frac{\partial^2 p'}{\partial\tau\,\partial z} = \frac{c_0}{2}\Delta_\perp p', \quad (37)$$

where $\Delta_\perp$ is the Laplace operator on the transverse coordinates $\{x, y\}$. In the case of wide beam ($\mu_{eff}a_0 \geq 3$), the boundary condition can be specified as a wave profile

calculated earlier (for example, (20)–(23)). This approach has come to be known as step-by-step [23]. Assuming a Gaussian transverse distribution of the light intensity in the beam, the boundary condition of the diffraction problem may be expressed as

$$p'(z = 0, \tau, \boldsymbol{r}_\perp) = p_0(\tau)\exp\left(-\frac{\boldsymbol{r}_\perp^2}{a_0^2}\right), \tag{38}$$

where $p_0(\tau)$ is the wave profile at the boundary of the light-absorbing medium. When the pulse propagates, the transverse light-intensity distribution remains Gaussian for every harmonic component in (38), so that the solution may be written in the form

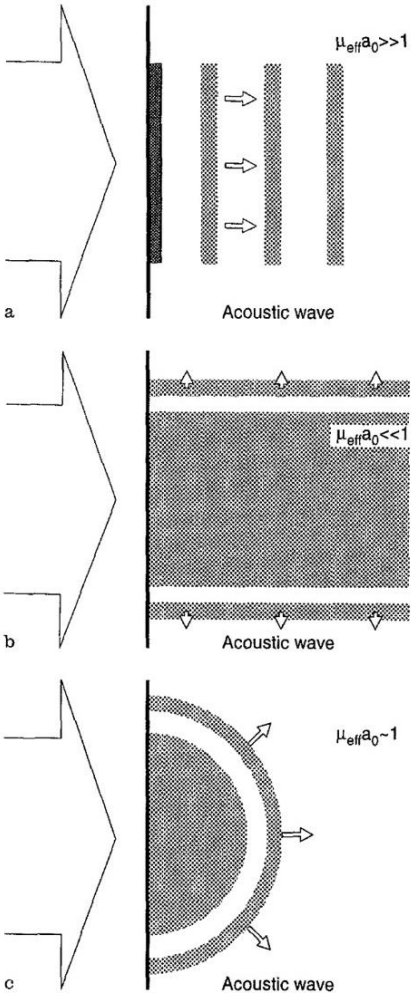


Fig. 13*a*, *b*. Phase front of an acoustic wave excited by a thermooptical source as a function of the relationship between the laser beam radius a_0 and the light penetration depth μ_{eff}^{-1}: (*a*) plane phase front; (*b*) cylindrical phase front; (*c*) spherical phase front

$$p'(z,\tau,\boldsymbol{r}_\perp)=\int\limits_{-\infty}^{\infty}p_0(t)dt\left\{\frac{1}{2\pi}\int\limits_{-\infty}^{\infty}\exp\left[-i\omega(\tau-t)-\frac{\boldsymbol{r}_\perp^2}{a_0^2}\frac{\omega}{\omega+i\dfrac{2c_0z}{a_0^2}}\right]\times\left(\omega+i\frac{2c_0z}{a_0^2}\right)^{-1}\omega\,d\omega\right\}\quad(39)$$

On the beam axis ($\boldsymbol{r}_\perp=0$), solution (39) can be simplified as follows:

$$p'(z,\tau,\boldsymbol{r}_\perp=0)=p_0(\tau)-\int\limits_{-\infty}^{\tau}\omega_D\exp[-\omega_D(\tau-t)]p_0(t)dt\,,\qquad(40)$$

where $\omega_D=2c_0z/a_0^2$. The first term in (40) follows the profile of the signal at the boundary and corresponds to plane wave without diffraction; the second term describes the effect of the limited width of the beam. The characteristic frequency ω_D grows higher with the increasing distance traveled by the wave and the decreasing cross-sectional area of the beam. In the Fraunhofer zone ($\omega_D t_a\gg 1, z\to\infty$), solution (40) becomes

$$p'(z,\tau,\boldsymbol{r}_\perp=0)=\frac{a_0^2}{2c_0z}\frac{dp_0}{d\tau}.\qquad(41)$$

As it can be seen from (41), the wave profile in the Fraunhofer zone becomes the derivative of the profile on the boundary, and its amplitude decreases inversely with the distance traveled by the wave.

The transformation of the profile of the optoacoustic signal upon its transition from the near-field to the far-field was studied in [21, 54–56] (see also [22]). In the case of uniform absorption ($\mu_a=\text{const}$) and short laser pulse (see (20) and (21)), it proves possible to express integral (40) in terms of elementary functions:

$$p_{tr}(\tau_{tr})=\frac{\beta^*E_0c_{0\,tr}\omega_a}{C_p}\frac{1}{1+N_a}\times\begin{cases}0, & \tau_{tr}<0,\\ \dfrac{\exp(-\omega_a\tau_{tr})-D\exp(-\omega_D\tau_{tr})}{1-D}, & \tau_{tr}>0,\end{cases}\qquad(42)$$

$$p_r'(\tau)=\frac{\mu_a\beta^*E_0c_0^2}{2C_p}\begin{cases}\dfrac{\exp(\omega_a\tau)}{1+D}, & \tau<0,\\ \dfrac{\exp(-\omega_a\tau)}{D-1}-\dfrac{2D\exp(-\omega_D\tau)}{D^2-1}, & \tau>0,\end{cases}\qquad(43)$$

$$p_f'(\tau)=\frac{\mu_a\beta^*E_0c_0^2}{2C_p}\begin{cases}\dfrac{\exp(\omega_a\tau)}{1+D}, & \tau<0,\\ \dfrac{\exp(-\omega_a\tau)}{D-1}-\dfrac{2D^2\exp(-\omega_D\tau)}{D^2-1}, & \tau>0,\end{cases}\qquad(44)$$

where $\omega_a = \mu_a c_0$ is the characteristic frequency of the optoacoustic signal spectrum for a short laser pulse ($\mu_a c_0 \tau_L \ll 1$), $N_a = Z_0/Z_{tr}$ is the ratio between the acoustic impedances of the light-absorbing and transparent media, and $D = \omega_D/\omega_a = 2z/\mu_a a_0^2$ is the dimensionless distance expressed in terms of the diffraction length $L_D = \mu_a a_0^2/2$ at a frequency ω_a. Formula (43) is obtained by assuming a rigid boundary $z = 0$ of the light-absorbing medium ($N_a = 0$) and (44) applies to a free boundary ($N_a \gg 1$). However, it is not very difficult to see from (11) that in the general case of finite N_a the solution can be expressed in terms of the solution $p_r'(\tau)$ and $p_f'(\tau)$presented:

$$p'(r) = \frac{1}{1 + N_a}(p_r'(\tau) + N_a p_f'(\tau)]. \qquad (45)$$

As one can see from (43) and (44), the signal leading edge ($\tau < 0$) in the case of direct detection remains exponential at any distance from the boundary. Therefore, the given section of the signal profile is most convenient for absorption coefficient measurements in the case of direct detection. At $\tau > 0$, the signal shape is formed by the difference between two exponential functions with exponents defined by the light absorption coefficient (ω_a) and diffraction (ω_D). Depending on the relationship between ω_D and ω_a (the quantity D), each of these exponents becomes manifest either at short or long τ. At short distances (D « 1) and short τ, the profile of the optoacoustic signal is determined by the absorption of light, and the diffraction term will only be important at $\omega_a \tau > 3 - 5$. At long distances ($D \geq 3$) the reverse is true; at short τ ($\omega_D \tau < 1 - 2$), the signal follows the exponent of ω_D, whereas at $\omega_a \tau > 1$, that is the exponent of ω_a.

The diffraction transformation of optoacoustic signals in the case of direct and indirect detection is illustrated in Fig. 14. In the case of direct signal detection and rigid boundary (Fig. 14*a*), the symmetrical compression pulse at the boundary $z = 0$ gradually changes, as it propagates (as the quantity D increases), to the shape of a train of alternating compression and rarefaction pulses. As can be seen, even at small enough distances ($D \cong 0.1$) the rarefaction phase is rather noticeably manifested. In the case of free boundary (Fig. 14*b*), the pulse at the boundary $z = 0$ contain both the compression and rarefaction phases. During the propagation the amplitude of the rarefaction phase grows relatively higher and its duration decreases; the subsequent compression phase appears next to it. In the case involving both the rigid and a free boundary, the shape of the leading edge of the signal ($\tau < 0$) suffers no change upon diffraction. In the case of impedance boundary, the signal shape is a weighted sum of the profiles of the pulses excited with a rigid and a free boundary (see (45)). Therefore, the leading edge of the signal undergoes no change in this case, too.

The optoacoustic pulse traveled in transparent medium and registered by indirect signal detection (Fig. 14c) has a sharp leading edge (with a rise time of the order of the laser-pulse duration) and a trailing edge determined by the difference between the two exponential functions (see (42)). At short distances, or with a sufficiently strong absorption of light ($D \ll 1$, Fig. 15a), the trailing edge of signal (3) first

follows the exponent of ω_a (1) (at $\omega_a\tau_{tr} < 1-2$) and thereafter the exponent of ω_D (2) ($\omega_D\tau_{tr} \geq 1$) (see Fig. 15a). At $D \gg 1$ (Fig. 15b), the optoacoustic signal will consist of a short pulse with a duration of $\approx \omega_D^{-1}$ on an exponential base with a drooping exponent of ω_a.

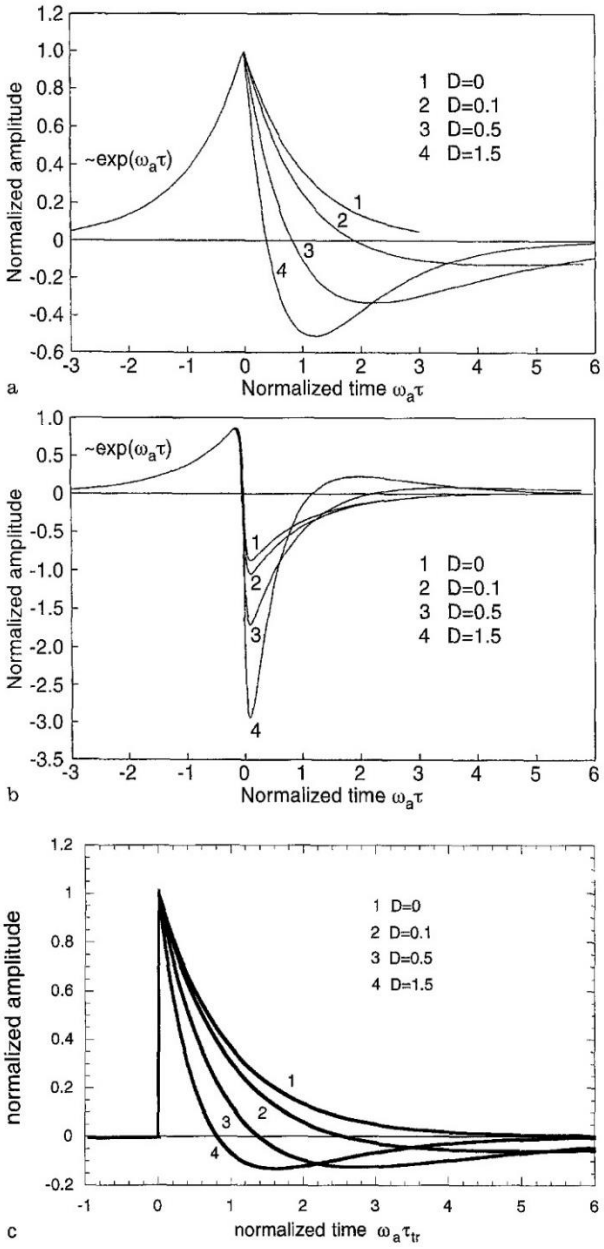


Fig. 14*a–c*. Diffraction transformation of the optoacoustic signal in the case of direct and indirect signal detection. Direct detection: (*a*) rigid boundary; (*b*) free boundary; (*c*) indirect detection

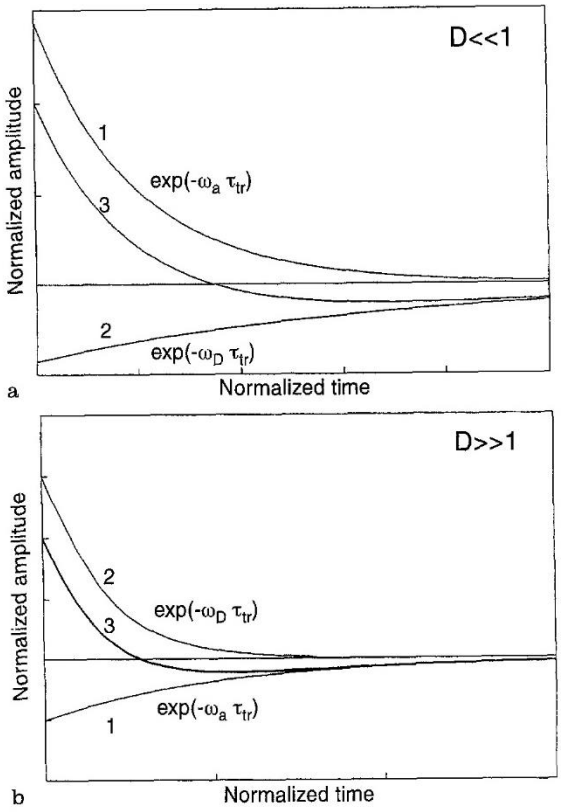


Fig. 15*a*, *b*. Optoacoustic signal components in the case of indirect signal detection: (*a*) at short distances; (*b*) in the Fraunhofer zone. *1* — exponential curve due to light absorption; *2* — exponential curve due to diffraction; *3* — resultant signal

1.4 Reconstruction of the spatial distribution of light absorption

The reconstruction of the distribution of light absorption in a microinhomogeneous medium is carried out in two steps. As noted earlier, the optoacoustic signal consists of spherical waves emitted by individual light-absorbing particles and a "basic" pulse determined by "average" absorption. If the concentration of particles is so high that acoustic fields produced by individual particles overlap, their total signal looks like the signal excited due to "average" absorption. One can therefore state that the problem of reconstruction of light absorption pattern by means of optoacoustic tomography reduces to the separation of the contributions from the "smooth" part of the light absorption distribution and point sources.

As already noted, in the case of direct signal detection, it is reasonable to use the leading edge of the optoacoustic signal. Inasmuch as the pulse from an individual particle has a symmetrical bipolar shape (see (31)–(33)), the average light absorption coefficient $< \mu_a >$ is defined so as to minimize the error integral

$$\int_{-\infty}^{0}\left[\int_{-\infty}^{\tau} p'(\xi)d\xi \frac{p_0}{<\mu_a> c_0}\exp\left(<\mu_a> c_0\tau\right)\right]^2 d\tau\,. \qquad (46)$$

Error minimization exactly for the integral of the optoacoustic signal shape makes it possible to exclude the contribution from individual point sources. This is because of the leading edge of the optoacoustic signal suffers no change on diffraction (see (43)–(44)). After this procedure, the distribution of light absorption by individual centers can be calculated using (35). Since the contributions from individual particles located in a layer with a thickness of $c_0\Delta t$ (Δt is the temporal resolution of the detection system) and "illuminated" by laser radiation add together, the calculated light absorption cross section $\sigma(z)$ is some average over the cross section of the laser beam. Thus, the spatial resolution of optoacoustic tomography is determined by the temporal resolution Δt of the detection system (in z-direction) and the laser-beam diameter. The experimental cases of the optoacoustic tomography of inhomogeneous media are discussed below.

2. Experimental investigation of light absorption with time-resolved laser optoacoustic tomography

The first experiments on the laser-optoacoustic tomography of light absorption have been reviewed in the introduction to this paper. The main difficulty in the technical realization of this technique is connected with the problem of correct detection of acoustic transients with a high-temporal resolution. The same difficulty is being overcome to some or other degree of success in various fields of acoustic diagnostics (non-destructive testing, acoustic spectroscopy, medical acoustics). But practically to solve the problem of detection of acoustic signals with a nanosecond temporal resolution has only recently proved possible.

Many hopes were pinned on various optical (primarily interference) methods for detecting acoustic vibrations (see, for example, [57–63] and references cited therein). Unfortunately, the sensitivity of such detection systems is two or three orders of magnitude lower than that of the traditional piezoelectric transducers, the frequency band being the same. Moreover, the use of optical detection methods requires a high (optical) quality of the surface under study as a rule. Therefore, their use for the optoacoustic tomography of real objects seems difficult.

For these reasons, lithium-niobate-based wide-band receiving piezotransducers operating in the short-circuited mode (WAT-04 type) were used for realization of time-resolved optoacoustic tomography. These transducers are capable to detect acoustic pulses with a duration up to 0.8–0.9 μs with a temporal resolution no worse than 3 ns. The high sensitivity of these transducers (typical sensitivity is of the order of 10^{-7} V/Pa) made it possible to operate with comparatively low-laser energy levels (of the order of 10–50 mJ).

The experimental setup of time-resolved optoacoustic tomography is quite simple (Fig. 16). A pulse of a Q-switched YAG:Nd laser ($\lambda = 1.06$ μm) is directed into the

optoacoustic cell containing the medium under testing. Schematic diagrams of optoacoustic cells are presented in Fig. 5. Laser pulses have a practically symmetrical shape with a duration of $2\tau_L = 12$ ns at the $1/e$ level; the beam diameter is 2.0 ± 0.1 mm. The laser pulse energy $E \approx 50$ mJ is attenuated to the necessary value by means of neutral light filters. The electric signal of wide-band piezoelectric transducer is processed with a transient digitizer (analog bandwidth 100 MHz). Some laser radiation is directed by means of a beam splitter onto a photodiode to monitor the radiation energy and to start the transient digitizer.

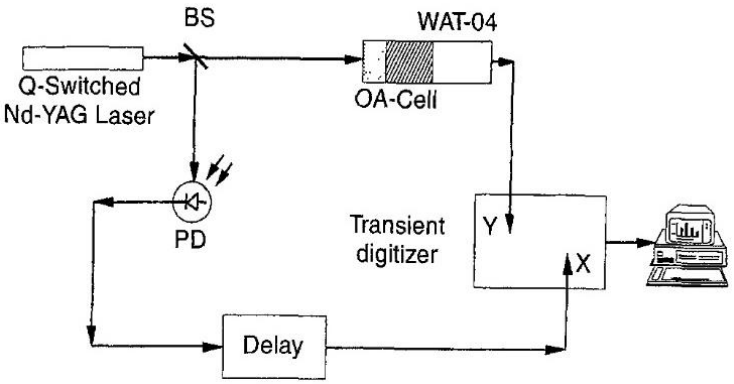


Fig. 16. Setup for the optoacoustic tomography of light absorption

The principal condition for the correct detection of wide-band acoustic signals is the acoustic wave phase front and the face of the transducer to be parallel. In our case, this achieved by precision adjustment in the case of direct signal detection and thorough fabrication of the prism (see Fig. 5*b*) in the case of indirect signal detection. Test experiments carried out with media of known light absorption coefficients showed that the temporal resolution of the acoustic wave detection system depends mainly on the limited bandwidth of the acquisition system and the laser-pulse duration. In our case, the temporal resolution of the system comes to $7 - 10$ ns.

Thus, the spatial resolution of time-resolved optoacoustic tomography can be practically as high as $10 - 15$ μm (for liquid samples) at a probing depth of up to $1.2 - 1.5$ mm. The results of studies into inhomogeneous media by the time-resolved optoacoustic tomography are described below.

2.1 Optoacoustic detection of individual light-absorbing particles in a turbid medium

The detection of individual light-absorbing particles by the optoacoustic techniques was mainly used for the purpose of impurities detection in liquids [21]. The change of the signal amplitude due to an impurity particle getting into the beam was measured with the transverse signal detection scheme (Fig. 17). The use of the transverse signal detection did not allow the position of the particle in the beam to be fixed, and so on tomography problem was posed in these works.

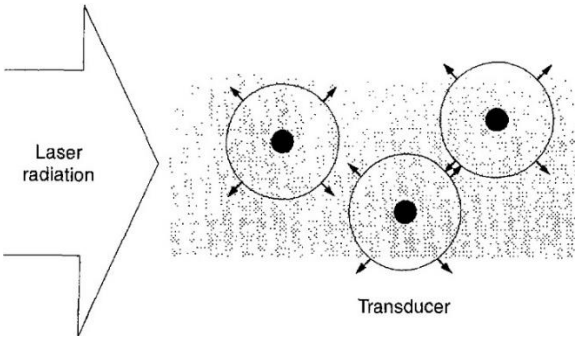


Fig. 17. Transverse detection of optoacoustic signal in a weakly absorbing medium. Individual light-absorbing centers make additional contributions to the signal

In any case, the acoustic signals coming to the transducer from centres equally distant from merge. Therefore, to fix the position of a particle in the beam, it is preferable to detect the optoacoustic signal in a direction normal to the boundary of the light-absorbing medium. However, in the case of weak light absorption and direct signal detection, the acoustic detector is strongly illuminated, which gives rise to additional noise. For this reason, in such case it is more preferable to carry out optoacoustic tomography with the indirect signal detection (see Fig. 5*b*).

Typical optoacoustic signal profiles excited in homogeneous light-absorbing medium and scattering medium with a light-absorbing particle and obtained with the indirect signal detection are presented in Fig. 18. In the case of homogeneous medium the signal consists of the leading edge defined by the integral of the laser-pulse shape (in our case, the front width is $20 - 25$ ns) and a section determined by light absorption and diffraction. The center of the leading edge corresponds to the surface $z = 0$ (the surface of the prism) with the depth of the light-absorbing particles being reckoned from this surface.

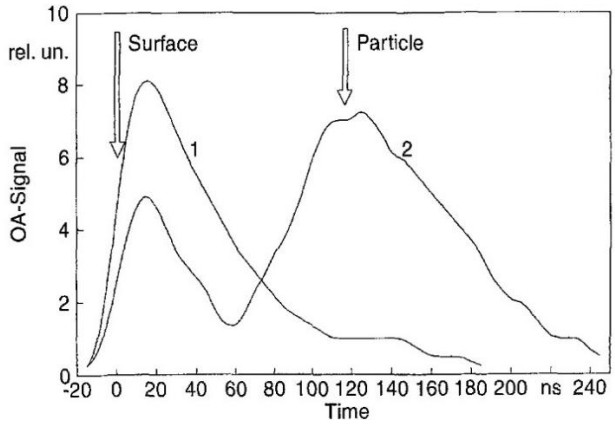


Fig. 18. Optoacoustic signal in a weakly absorbing medium in the case of indirect signal detection. Curve *1* — uniform light absorption and scattering; *2* — light-absorbing particles in a light-scattering medium

The trailing edge of the signal in the case of homogeneous light-absorbing medium (solution of $CuCl_2$ in milk, curve *1* in Fig. 18) was smooth. No visible coagulation processes in $CuCl_2$-milk solution due to chemical reactions were observed during the experiment may be due to low concentration of $CuCl_2$ ($\approx 0.2\%$). The signal amplitude is proportional to the light absorption coefficient and its measured value for used $CuCl_2$-milk solution of YAG:Nd laser radiation was $\mu_a = 3$ cm^{-1}. The signal amplitude decreased by a factor of e during the time $\tau_e \sim 50$ ns, which was much shorter than the stress relaxation time $\omega_a^{-1} = 2.2$ μs. The diffraction parameter $D \gg 1$ and the signal droop is therefore determined by the diffraction of the acoustic wave (see Fig. 15). We do not detect the optoacoustic signal in pure milk against the background of noise due to low light absorption (estimations give $\mu_a < 0.2$ cm^{-1}).

The presence of a light-absorbing particle (graphite) in milk causes a drastic change in the shape of the signal (see curve 2 in Fig. 18, particle was fixed). With the delay of approximately 100 ns (which corresponds to a distance of 150 μm from the surface of the prism) the peak due to the absorption of radiation by the particle appears. The width of the peak (≈ 70 ns at the $1/e$ level) is determined by the time difference Δt of the arrival moments of acoustic signals from the nearest and the farest to the transducer points of the illuminated area of the particle. Therefore, the size of the particle R_p may be estimated as $R_p \sim c_0 \Delta t \approx 0.1$ mm and is determined by the sound velocity in water c_0, because of the velocity of sound in graphite is approximately two times higher. Estimated value of R_p corresponds to the particle size measured microscopically. These results are, however, only qualitative, because of the stresses had not enough time to relax during the course of the laser pulse ($c_{0_p} \tau_L < R_p$).

Figure 18 clearly shows the possibility of detecting individual light-absorbing particles even in turbid (scattering) media by means of time-resolved optoacoustic tomography.

2.2 Reconstruction of light absorption by particles

Quantitative results on the reconstruction of the distribution of light absorption may be obtained using (35)–(36). However, the light-absorbing particles in this case are assumed to be acoustically small. The results of the optoacoustic tomography of fine particles with the use of the indirect signal detection (Fig. 5*b*) are presented in Fig. 19. The cell filled with water was mounted on the upper surface of the prism. Carbon-black particles (average diameter 0.5 μm) were injected into water by drop pipet (concentrated suspension of particles was used) and migrated towards the prism-water interface. The migration took place both under gravity and as a result of the thermocapillary effect under laser irradiation. Carbon-black particles were "thermally small" (see Section 1), but their concentration was low [(6) was not fulfilled]. So, the medium can be considered as microinhomogeneous.

As the particles migrated towards the interface, the course of the optoacoustic signal changed (curves 1–3 in Fig. 19a were plotted at regular intervals after the injection of the particles). At $t \geq 44$ s after droplet injection, the shape of the signal

got stable as a result of settling of all the particles on the prism surface. This shape is determined by the effect of diffraction, finite-laser-pulse duration, and the limited-frequency bandwidth of the acquisition system.

The difference in shapes between the steady-state signal and the signals detected at the preceding time moments is due to the non-uniform volume distribution of the light-absorbing particles. Insofar as the individual particles subject to radiation emit spherical acoustic waves, the dependence of this difference is connected by (34) with the spatial distribution of the cross section of light absorption by the particle. The inversion of this relation enables one to reconstruct the distribution of light absorption (see Fig. 19*b*), the quantity being reconstructed is the integral cross section of light absorption by the particles entering the laser beam, averaged over the distribution of the laser energy in the spot. One can clearly see how this distribution gets shifted in time towards the boundary water-prism. As a first approximation, one can take that the absorption cross section follows the distribution of the concentration of particles.

The rate of probing practically depends on the operating speed of the acquisition system (transient digitizer) and the repetition rate of the laser pulses. In our case, the time intervals between measurements were selected so as to make the variation of the light absorption distribution distinctive. Thus, time-resolved optoacoustic tomography enables one to study the distribution of light-absorbing particles in a transparent medium in real time.

The reconstruction of the distribution of light-absorbing particles in a homogeneous light-absorbing medium is illustrated in Fig. 20. Insofar as the absorption of light in the medium prevents the illumination of the acoustic transducer even in the absence of particles, the direct signal detection was used, which is more effective in overcoming the influence of diffraction. As noted earlier (see Sect. 1.3), to reconstruct the distribution of light absorption in the case of direct-signal detection, it is preferable to use the leading edge of the optoacoustic signal.

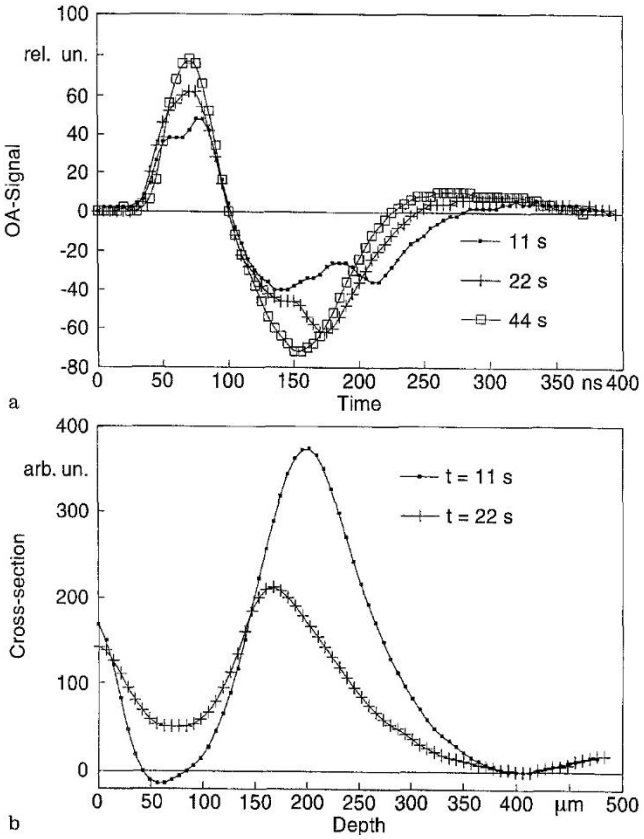


Fig. 19*a*, *b*. Optoacoustic tomography of the migration of particles in a transparent medium in the case of indirect signal detection: (*a*) optoacoustic signals; (*b)* depth distribution of the light absorption cross section

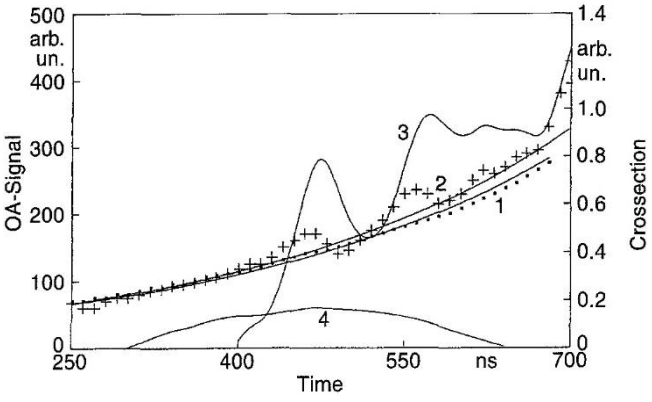


Fig. 20. Optoacoustic tomography of light-absorbing particles in the case of direct signal detection scheme: (●) optoacoustic signal in a homogeneous light-absorbing medium; (+) ditto in the presence of light-absorbing centers. Curves *1* and *2* — exponential approximations of the experimental data; *3* and *4* reconstructions of the light absorption cross section

In a homogeneous light-absorbing medium (an aqueous $CuCl_2$ solution), the leading edge of the signal is exponential (the dots in Fig. 20 are experimental data points, curve 1 is the exponential approximation). The rate of rise of the exponential curve depends on the light absorption coefficient μ_a which is 23 cm^{-1}. As can be seen, the exponential curve fits the experimental data points well enough.

The injection of fine absorbing particles (carbon black, 0.5 μm in diameter) to this solution leads to both some increase of light absorption (and the amplitude of the optoacoustic signal, crosses in Fig. 20) and the appearance of irregular oscillations in the signal profile. These oscillations are due to the irregularities in the volume distribution of the particles. These differences in the optoacoustic signal profile from that in the case of homogeneous light-absorbing medium free of particles are obvious.

To reconstruct the distribution of light absorption irregularities, one can use (35); the quantity $< \mu_a >$ is defined so as to minimize error integral (46) (the corresponding exponential curve is numbered 2 in Fig. 20). The calculated light absorption cross section for the experimental data presented is shown by curve 3 in Fig 20. One can see distribution irregularities with a characteristic size of 100-150 μm down to a depth of 0.6 mm. The probing depth is determined by the light penetration depth and comes to approximately $2\mu_a^{-1}$. The spatial resolution of the scheme amounts to 10-15 μm; however, no details of such small sizes are present in the distribution studied. Measurement errors are characterized by the "reconstruction" of the light absorption distribution for a homogeneous light-absorbing medium (curve 4). As can be seen, the values obtained are substantially lower than those for curve 3. Each curve was obtained by single laser shot without averaging. If the light absorption distribution is stable, than the accuracy may be better.

Thus, the method suggested makes it possible to investigate the distributions of light-absorbing centers, both single and clustered, in transparent, light-absorbing and scattering media easily and in real time. If the concentration of light-absorbing particles is high enough for the condition (6) of the medium microhomogeneity is satisfied, optoacoustic tomography will reveal the "macroinhomogeneities" of their distribution.

2.3 Reconstruction of light absorption in microhomogeneous media

It is convenient to reconstruct the distribution of light absorption in a microhomogeneous medium by means of the direct optoacoustic signal detection, because it is easier to reduce the effect of diffraction on the pulse profile in this case. As in the other cases, it is preferable to study the leading edge of the optoacoustic signal. The restrictions on the values of light absorption coefficient, that can be measured, are determined by several factors. On the one hand, the finiteness of the laser pulse duration τ_L and the limited frequency bandwidth Δf of the detection system set an upper limit on the permissible range of μ_a values:

$$\mu_a < \min[\frac{1}{2}(c_0\tau_L)^{-1}, \frac{\pi\Delta f}{c_0}]. \qquad (47)$$

For our conditions ($\Delta f = 100$ MHz, $\tau_L = 6$ ns), this yields $\mu_a < 500$ cm^{-1}.

On the other hand, the strong diffraction of the low-frequency components of the acoustic signal spectrum and the limited sensitivity of the detection system (the signal amplitude is proportional to μ_a) put a lower limit on the measurement range. As noted above, the lower limit is 1–3 cm^{-1}. However, the insufficient sensitivity of the signal detection system can be compensated by increasing the laser-pulse energy.

The optoacoustic diagnostics of light absorption in homogeneous media (aqueous $CuCl_2$ solutions of different concentrations) is illustrated in Fig. 21.

Figure 21*a* shows the duration of the optoacoustic signal leading edge for two various concentrations of absorber ($CuCl_2$): 1.7% and 12.5%. The representation of data on a semilog plot (Fig. 21*b*) shows that the leading edge is almost exponential and is fitted by the theoretical curve [see (43)–(44)] for a homogeneous medium. The reconstruction of the light absorption distribution by (25) (Fig. 21*b*) yields a light absorption coefficient value practically constant over the depth of the medium. The relative variation of the reconstructed $\mu_a$value does not exceed 5%. This corresponds to the linearity of the Y amplifier and the time base. Moreover, errors of digitizing may manifest for the reconstruction of the light absorption at the greater depth due to the relatively lower level of the signal.

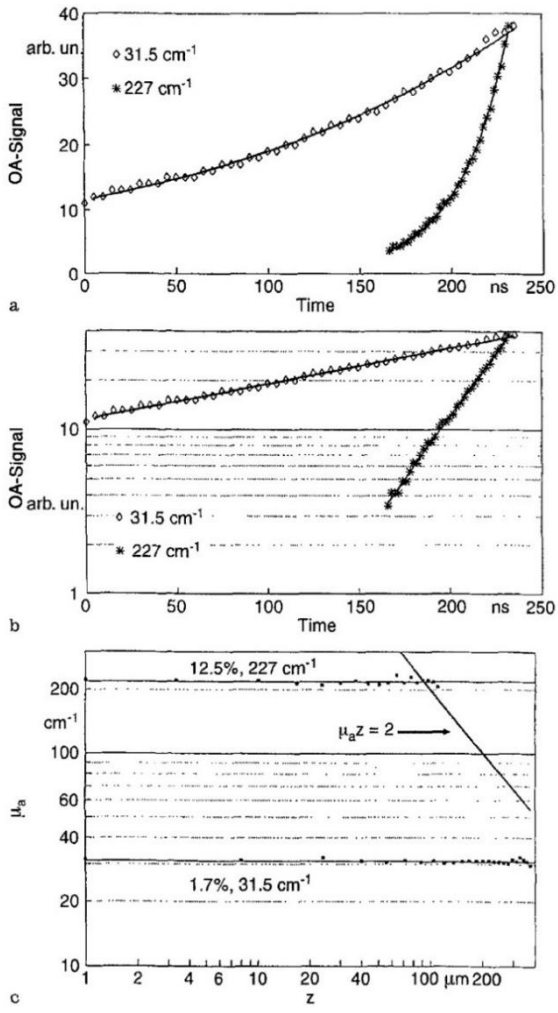


Fig. 21*a–c*. Optoacoustic tomography of homogeneous light-absorbing media: (*a*) leading edges of optoacoustic signal for two various light absorption coefficient values; (*b*) ditto on semilog plot; (*c*) reconstruction of the light absorption distribution using (25). The dots indicate the experimental data points, solid curves - exponential approximations

The maximum probing depth l_m depends on the light absorption coefficient μ_a and the dynamic range S of the acoustic signal detection system: $I_m = \mu_a^{-1} \ln S$. The lower is the light absorption coefficient (the deeper the light penetrates), the greater is the possible depth of probing. The attenuation of light during the course of propagation and the correspondent reduction of the amplitude of the optoacoustic signals coming from deep layers makes the maximum probing depth dependent on the dynamic range S: it is necessary that the signals emitted by these layers should be strong enough to be detected on the background of noise. The dynamic range of wide-band acoustic signal acquisition systems is practically $20 - 30$, and so $l_m = (2.5 + 3)\mu_a^{-1}$. Some additional restrictions are possible in the case of low light absorption (where the optoacoustic signal amplitude is initially small). This is evident from Fig. 21c: the zone $z = 2\mu_a^{-1}$is shown on the same plane, and the maximum probing depth l_m at $\mu_a = 31.5$ cm^{-1} is somewhat smaller than this quantity.

Figure 22 presents the results of reconstruction of the distribution of light absorption in microhomogeneous media. Subject to study were magnetic liquids based on magnetite particles dispersed in transformer oil. The average size of the particles was $2R_p = 200$ Å, and their volume concentration n varied from 0.08% to 1%. The distance $d = R_p\,(4\pi/3n)^{1/3}$ between the light-absorbing particles was of the order of $0.1 - 0.2$ μm, so the condition (6) for the microhomogeneity of the medium was satisfied ($n_p = d^{-3}$). In this case, one could only study the nonuniformity of the volume concentration of the light-absorbing particles (in a first approximation, the light absorption coefficient is proportional to the concentration of the particles). The medium may be considered as macroinhomogeneous in this case.

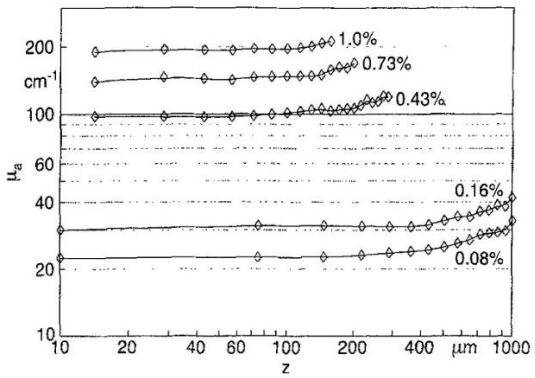


Fig. 22. Optoacoustic tomography of light absorption in microhomogeneous media (magnetic liquids)

The results obtained show that the absorption of light in a magnetic liquid grows higher from the surface into the depth (Fig. 22). The relative change of the absorption coefficient is substantial (up to 50%) at low concentrations of magnetite particles ($n = 0.08\%$) and decreases with the increasing of particle concentration. At high concentrations ($n > 1$ %), light absorption practically does not vary with depth.

The light absorption coefficient near the surface increases approximately linearly with the increasing particle concentration (Fig. 23), and the thickness of the

surface layer decreases. Considering the single-scattering approximation justifiable, one can relate the light absorption coefficient to the concentration of the light-absorbing particles:

$$\mu_a = \frac{3\sigma_0}{4\pi R_p^3} n, \tag{48}$$

where σ_0 is the light absorption crosssection of an individual particle. In our case, the absorption cross section is a small fraction of the cross-sectional area of the particle: $\sigma_0 / \pi R_p^2 = 0.03$, that is reasonable for particles whose size is much smaller than the wavelength of the light [64].

The reduction of the particle concentration near the surface can be associated with an excess energy of magnetic dipole-dipole interaction. Similar effects were noted in magnetic liquids [65], but no direct measurements of the depth distribution of the particle concentration were carried out up to now.

Thus, optoacoustic tomography makes it possible to analyze the distribution of light absorption in microhomogeneous media in the range from a few reverse centimeters to a few hundreds of reverse centimeters. The maximum probing depth depends on the dynamic range of the acoustic signal detection system and is $l_m = (2.5 + 3)\mu_a^{-1}$. The spatial resolution is limited by the temporal resolution of the acoustic signal detection system and may be as high as a few microns.

3. Conclusion

The theory of optoacoustic phenomena in homogeneous, microhomogeneous and microinhomogeneous media, that are transparent, light-absorbing or scattering media containing absorbing particles is developed. It gives a simple analytical expression connecting the temporal course of laser-excited acoustic pulses with the distribution of light absorption in inhomogeneous medium. This theory is a basis of time-resolved optoacoustic tomography discussed above. Time-resolved optoacoustic tomography makes it possible to investigate inhomogeneous media in transmission (direct detection of excited-acoustic wave in absorbing medium) and reflection mode (indirect signal detection, i.e., excitation and detection of acoustic wave from the same side of investigated medium).

Time-resolved optoacoustic tomography has been experimentally realized with Q-switched YAG: Nd laser and wide-band piezoelectric receiving transducers. This setup allows one to investigate the light absorption distribution with the spatial resolution $10 - 15$ μm over the depth of a few millimeters. The values of light absorption that can be determined by this setup are in the range $1 - 500$ cm^{-1}. The experiments have been carried out with the model layered media and confirm the developed theory of time-resolved optoacoustic tomography. This setup was used to investigate light absorption in homogeneous media ($CuCl_2$ aqueous and milk solutions), macroinhomogeneous (magnetic liquid) and microinhomogeneous media (carbon-black particles immersed in water and $CuCl_2$ aqueous solution).

The reconstruction of light absorption in homogeneous media ($CuCl_2$ aqueous solutions of different concentrations) gives constant value of light absorption coefficient (over the range $30 - 200$ cm^{-1}) with variations less than 5%. In macroinhomogeneous media (magnetic liquids of different concentrations of magnetite particles), the reconstruction of light absorption shows its dependence on the depth. The light absorption coefficient grows from the surface into the depth of liquid and then saturates. The difference is substantial for low concentrations and practically vanishes for the concentrations more than 1%. For microinhomogeneous media (carbon-black particles in liquids) the cross section of light absorption as a function of the depth was determined in real time. Such procedure allows one to visualize particles migration under laser irradiation.

The results discussed above shows time-resolved optoacoustic tomography to be a powerful method of the investigation of inhomogeneous media. One can monitor the distribution of light absorbing centers in real time with high-spatial resolution. Such experiments may be useful not only for the investigations of laser-matter interaction, but in other related fields of physics, chemistry and biology. At the same time, time-resolved optoacoustic tomography may be realized on the basis of ordinary laser sources and electronic equipment.

Acknowledgements. We gratefully acknowledge Dr. A. Oraevsky of Rice University (Houston, U.S.A.) for giving several experimental results presented here and fruitful discussions.

References

1. *Munk W., Wunsch C.* // Deep Sea Res. A. 1979. Vol. 26A. P. 123.
2. *Cornuelle B.C., Howe B.* // J. Geophys. Res. 1987. Vol. 92. P. 11680.
3. *Lee D.* // Appl. Numer. Math. 1994. Vol. 16. P. 271.
4. *Borodin V.V., Minasyan* G.R. // Acoust. Phys. 1995. No. 41. P. 27.
5. *Busse G.* In: Physical Acoustics / ed. by W.P. Mason. Vol. 18. New York: Academic Press, 1988. P. 403–497.
6. Progress in Photothermal and Photoacoustic Science and Technology / ed. by A. Mandelis. Vol. II. PTR Prentice-Hall, Englewood Cliffs. New York, 1994.
7. *Fitting D.W., Adler L.* Ultrasonic Spectral Analysis for Nondestructive Evaluation. New York: Plenum, 1981. P. 93–138.
8. *Rogerson, Murgatroyd R.A.* // Res. Techniques NDT. 1982. Vol. 5. P. 451.
9. *Levin G.G., Vishnyakov G.N.* Optical Tomography. Moscow: Radio, 1989 (in Russian).
10. Optoacoustic Spectroscopy and Detection / ed. by Y.H. Pao. New York: Academic Press, 1977.
11. *Patel C.K.N., Tam A.C.* // Rev. Mod. Phys. 1981. Vol. 53. P. 517.
12. *Zharov V.P., Letokhov V.S.* Laser Optoacoustic Spectroscopy. New York: AIP, 1986.
13. *Tam A.C.* // Rev. Mod. Phys. 1986. Vol. 58. P. 381.
14. *Sigrist M.W., Kneubühl F.* // J. Acoust. Soc. Am. 1978. Vol. 64. P. 1652.

15. *Akhmanov S.A., Gusev V.E., Karabutov A.A.* // Infrared Phys. 1989. Vol. 26. P. 815.

16. *Bunkin F.V., Kolomensky A.A., Mikhalevich V.G.* Lasers in Acoustics // Laser Science and Technology Ser. London: Gordon and Breach, 1992.

17. Phatoacoustic and Thermal Wave Phenomena in Semiconductos / ed. by A. Mandelis. Amsterdam: Elsevier, 1987.

18. *Karabutov A.A., Kubyshkin A.P., Matrosov M.P.* // Opt. Eng. 1994. Vol. 33. P. 3214.

19. *Sigrist M.W.* // J. Appl. Phys. 1986. Vol. 60. P. R83.

20. *Burmistrova L.V., Karabutov A.A., Portnyagin A.I., Rudenko O.V., Cherepetskaya E.B.* // Sov. Phys. Acoust. 1978. Vol. 24. P. 369.

21. *Karabutov A.A., Rudenko O.V., Cherepetskaya E.B.* // Sov. Phys. Acoust. 1979. Vol. 25. P. 218.

22. *Lyamshev L.M., Sedov L.V.* // Sov. Phys. Acoust. 1981. Vol. 27. P. 5.

23. *Gusev V.E., Karabutov A.A.* Laser Optoacoustics. New York: AIP, 1993.

24. *Afromowitz M.A., Yeh P.S., Yee S.* // J. Appl. Phys. 1977. Vol. 48. P. 209.

25. *Harata, Savada T.* // J. Appl. Phys. 1989. Vol. 65. P. 959.

26. *Miller R.M.* In: Photoacoustic, Photothermal and Photochemical Processes at Surfaces and in Thin Films / ed. by P. Hess // Topics in Current Physics. 1989. Vol. 47. P. 52.

27. *Mandelis* A.// J. Phys. A. 1991. Vol. 24. P. 2485.

28. *Pade O., Mandelis A.* // Inverse Problems. 1994. No. 10. P. 185.

29. *Carome E.F., Clark N.A., Mooller C.E.* // Appl. Phys. Lett. 1964. Vol. 4. P. 95.

30. *Karabutov A.A., Portnyagin A.I., Rudenko O.V., Cherepetskaya E.B.* // J. Techn. Phys. Pis'ma. 1979. Vol. 5. P. 328.

31. *Karabutov A.A., Omel'chuk N.N., Rudenko O.V., Chupryna V.A.* // Moscow Univ. Phys. Bull. 1985. Ser. 3. Vol. 26. P. 48.

32. *Cross F.W., Al-Dhahir R.K., Dyer P.E., MacRobert A.J.* // Appl. Phys. Lett. 1987. Vol. 50. P. 1019.

33. *Cross F.W., Al-Dhahir R.K., Dyer P.E.* // Appl. Phys. 1988. Vol. 64. P. 2194.

34. *Oraevsky A.A., Jacques S.L., Tittel F.K.* // SPIE Proc. 1993. Vol. 1882. P. 86.

35. *Oraevsky A.A.* // IEEE LEOS Newslett. 1993. Vol. 2. P. 6.

36. *Oraevsky A.A., Jacques S.L., Esenaliev R.O., Tittle F.K.* In: OSA Proc, on Advances in Optical Imaging and Photon Migration / ed. by R.R. Alfano. 1994. Vol. 21. P. 161.

37. *Karabutov A.A., Podymova N.B., Letokhov V.S.* // Opt. Eng. Bull. 1994. Vol. 4. P. 22.

38. *Karabutov A.A., Podymova N.B., Letokhov V.S.* //: J. Mod. Opt. 1995. Vol. 42. P. 7.

39. *Karabutov A.A., Podymova N.B., Letokhov V.S.* // SPIE Proc. 1995. Vol. 2389. P. 209.

40. *Egerev S.V., Pashin A.A.* // Acoust. Phys. 1993. Vol. 39. P. 54.

41. *Zozulya O.M., Puchenkov O.V.* // Acoust. Phys. 1993. Vol. 39. P. 60.

42. *Karabutov A.A., Podymova N.B., Letokhov V.S.* // Appl. Opt. 1995. Vol. 34. P. 1484.

43. *Tearney G.J., Hee M.R., Izatt J.A., Bouma B.E., Fujimoto J.G., Brezinski M.E., Southern J.F., Anderson R. Rox, Swanson E.A.* // SPIE Proc. 1995. Vol. 2389. P. 28.

44. *Tearney G.J., Brezinski M.E., Southern J.F., Bouma B.E., Hee M.R., Fujimoto J.G.* // Opt. Lett. 1995. Vol. 20. P. 2258.

45. *Diebold G.J., Westervelt P.J.* // J. Acoust. Soc. Am. 1988. Vol. 84. P. 2245.

46. *Chandrasekhar S.* Radiative Transfer. New York: Dover, 1960; *Kottler D.* In: Progress in Optics / ed. by E. Wolf. Vol. 3. New York: Wiley, 1964.

47. *Sobolev V.V.* Light Scattering in Planetary Atmospheres. Oxford: Pergamon, 1975.

48. *Courant R., Hilbert D.* Methods of Mathematical Physics. II. New York: Interscience, 1962.

49. *Vinogradova M.B., Rudenko O.V., Sukhorukov A.P.* Theory of Waves. New York: AIP, 1992.

50. *Novikov B.K., Rudenko O.V., Timoshenko V.I.* Nonlinear Hydroacoustics. New York: AIP, 1983.

51. *Lord Rayleigh.* The Theory of Sound, 3rd. edn. London: Macmillan, 1926.

52. *Landau L.D., Lifschitz E.M.* Fluid Mechanics. Oxford: Pergamon, 1959.

53. *Karabutov A.A., Portnyagin A.I., Rudenko O.V., Cherepetskaya E.B.* // Sov. Phys. Acoust. 1980. Vol. 26. P. 162.

54. *Musatov A.G., Rudenko O.V., Sapozhnikov O.A.* //Acoust. Phys. 1992. Vol. 38. P. 274.

55. *Andreev V.G., Veroman V.Yu., Denisov G.A., Rudenko O.V., Sapozhnikov O.A.* // Acoust. Phys. 1992. Vol. 38. P. 325.

56. *Bondarenko A.N., Kondrat'ev A.I.* // Sov. Phys. Acoust. 1981. Vol. 27. P. 46.

57. *Monchalin J.-P.* // IEEE Trans. Ultrasonics Ferroelectrics Frequency control UFFC-33. 1986. P. 485.

58. *Hutchins D.A.* In: Physical Acoustics / ed. by W.P. Mason. Vol. 18. New York: Academic, 1988. P. 21–123.

59. *Scruby C.B., Drain L.E.* Laser-Ultrasonics. Techniques and Applications. Bristol: Adam Hilger, 1990.

60. *Zhang S.Y., Paul M., Fassbender S., Scheichert U., Arnold W.* // Res. Nondestr. Eval. (2). 1990. P.143.

61. *Monchalin J.-P.* In: Physical Acoustics / ed. by O. Leroy and M.A. Breazeale. New York: Plenum, 1991. P. 65–76.

62. *Neubrand, Hess P.* // J. Appl. Phys. 1992. Vol. 71. P. 227.

63. *Born M., Wolf E.* Principles of Optics. Electromagnetic Theory of Propagation, Interference and Diffraction of Light. Oxford: Pergamon, 1964.

64. *Taketomi S.* // Jpn. J. Appl. Phys. 1980. Vol. 19. P. 1929.

НАНООПТИКА

1. *Летохов В.С.* Применение лазерного излучения в автоэлектронной и автоионной микроскопии для наблюдения биологических молекул // Квант. электроника. 1975. Т. 2 (5). С. 930–937.

2. *Chekalin S.V., Letokhov V.S., Likhachev V.S., Movshev V.G.* Laser photoion projector // Appl. Phys. B. 1984. Vol. 33. P. 57–61.

Квант. электроника. 1975. Т. 2 (5). С. 930–937

ПРИМЕНЕНИЕ ЛАЗЕРНОГО ИЗЛУЧЕНИЯ В АВТОЭЛЕКТРОННОЙ И АВТОИОННОЙ МИКРОСКОПИИ ДЛЯ НАБЛЮДЕНИЯ БИОЛОГИЧЕСКИХ МОЛЕКУЛ

В.С. Летохов
Институт спектроскопии АН СССР

Рассматривается возможность применения лазерного излучения в автоэлектронном и автоионном проекторе для селективного отрыва электрона или иона от макромолекулы. Селективную фотоионизацию определенных молекулярных связей в макромолекуле предлагается осуществлять по многоступенчатой схеме под действием нескольких лазерных импульсов на различных частотах. Рассмотрена также другая лазерная модификация автоионного проектора, которая позволяет радикально снизить напряженность электрического поля, необходимого для автоионизации атомов изображающего газа. Для этого предлагается возбуждать лазерным излучением атомы изображающего газа в квантовые состояния, находящиеся вблизи границы ионизации.

1. Введение
Постановка задачи

Одной из наиболее трудных задач является получение прямых данных о пространственно-химическом строении сложных органических молекул. Наиболее эффективным методом, который при благоприятных условиях позволяет получать данные о пространственной и химической структуре макромолекул, является рентгеноструктурный анализ. Однако этот метод требует исключительно сложной обработки наблюдаемых данных и привлечения для интерпретации результатов большого числа косвенных данных [1, 2]. Электронная микроскопия биологических макромолекул, построенных главным образом из легких атомов, не обеспечивает необходимого разрешения. Только после предварительного ввода в них тяжелых атомов удается достигнуть разрешения 10–20 Å [2, 3]. После открытия автоэлектронной, а затем и автоионной микроскопии [4, 5], делались попытки получить изображения определенных органических молекул путем их десорбции на эмиттере электронного или ионного проектора. Однако разрешение автоэлектронной микроскопии не лучше 15–20 Å, что недостаточно для разрешения атомарных деталей молекул. Даже более близкая цель — получение очертаний контура молекул на

атомарном уровне — оказалась труднодостижимой. Автоионная микроскопия требует настолько сильных электрических полей, что в них происходит испарение макромолекул и их микроскопия также сопряжена с трудностями, которые еще не преодолены [4, 5].

Об актуальности задачи пространственной локализации атомов и связей в молекулах говорит то, что она рассматривается в качестве наиболее существенного потенциального применения будущих коротковолновых лазеров на рентгеновских и гамма-лучах (молекулярная голография). Однако, на наш взгляд, лазеры в оптической области спектра могут быть также эффективно применены в задачах исследования пространственно-химической структуры биологических молекул. В частности, в данной статье рассматривается возможность принципиальных модификаций методов автоэлектронной и автоионной микроскопии, которые дают основания надеяться на эффективное применение этих методов для наблюдения биологических молекул.

Сначала, в § 2, рассматривается лазерная модификация автоэлектронного и автоионного проектора, основанная на селективном отрыве электрона или иона от макромолекулы под действием лазерного излучения, а не автоионизацией в сильном электрическом поле. За электрическим полем оставляется только функция переноса электронов или ионов по радиальным траекториям на экран проектора. Селективную фотоионизацию определенных молекулярных связей в макромолекуле, находящейся на острие проектора, предлагается осуществлять по многоступенчатой схеме [6] под действием нескольких лазерных импульсов на различных частотах. Последующая визуализация фотоэлектронов или фотоионов в проекторе позволяет получить данные о положении в макромолекуле определенных связей и комплексов. Затем, в § 3, рассматривается совершенно иная модификация автоионного проектора, которая позволяет радикально снизить напряженность электрического поля, необходимого для автоионизации атомов изображающего газа. Предлагается возбуждать лазерным излучением атомы изображающего газа в квантовые состояния, находящиеся вблизи границы ионизации. При приближении возбужденных атомов к острию автоионизация должна происходить при относительно слабых полях ($\sim 10^7$ В/см), исключающих эффект испарения молекул электрическим полем.

2. Метод селективной ионизации молекулы на эмиттере электронного или ионного проектора

Принцип действия предлагаемого фотоэлектронного лазерного микроскопа молекулярных связей ясен из рис. 1, на котором изображена его принципиальная схема. Полусферическое острие иглы с радиусом кривизны r представляет собой катод, а софокусный полусферический экран с радиусом кривизны R является анодом. Разность потенциалов между ними равна U. Материал иглы имеет высокую работу выхода электронов, так что сильное поле вблизи поверхности, составляющее величину порядка U/r, не вызывает автоэлектронной эмиссии с катода. На поверхности катода адсорбирована макромолекула с

поперечным размером $b \ll r$. Под действием серии ультракоротких импульсов света с различными частотами ω_1, ω_2, ... происходит последовательное возбуждение квантовых уровней молекулы, ответственных за выбранную молекулярную связь AB, и последующая ионизация, т. е. отрыв электрона от участка молекулы со связью AB. Схема селективной ионизации [6] определенной связи AB таким методом показана на рис. 2. Для каждой молекулы или молекулярной связи в макромолекуле подбирается определенная последовательность частот ω_1, ω_2, ..., под действием которой возможна ионизация только выбранной молекулы или связи. Под действием сильного электрического поля вблизи катода фотоэлектрон движется вдоль радиальных силовых линий к экрану, покрытому флуоресцентным слоем. Как и в автоэлектронном микроскопе Мюллера [7], на экране образуется увеличенное изображение участков катода, эмиттировавших электроны. Отличие от автоэлектронного микроскопа заключается, прежде всего, в том, что электрическое поле служит только для переноса фотоэлектронов на анод, но не для вырывания их из катода. Отрыв электронов осуществляется под действием серии лазерных импульсов с определенными частотами. Такое «мягкое» воздействие позволяет ионизовать определенный сорт молекул или определенные связи (участки) молекулы на поверхности катода, не затрагивая электроны катода. Разумеется, длина волны наиболее коротковолнового фотона должна быть больше длины волны красной границы фотоэффекта материала острия.

Увеличение фотоэлектронного лазерного микроскопа M определяется соотношением, аналогичным для автоэлектронного микроскопа [8]: $M = R/(\chi r)$, где χ — численный фактор, лежащий в интервале 1,5-2,0. При $r = 3 \cdot 10^{-5}$ см и $R = 10$ см увеличение составляет $M \approx 3 \cdot 10^5$.

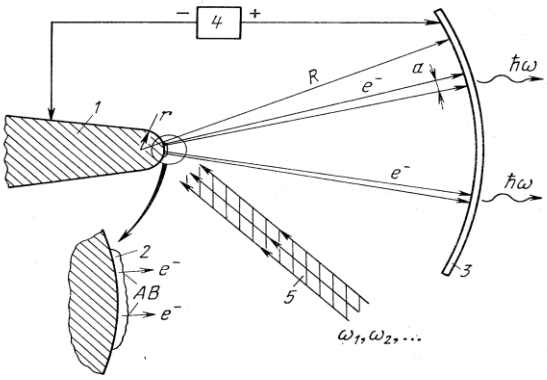


Рис. 1. Принципиальная схема фотоэлектронного лазерного микроскопа:
1 — полусферическая игла, *2* — адсорбированная на поверхности иглы макромолекула, *3* — полусферический флуоресцирующий экран, *4* — источник высоковольтного напряжения, *5* — лучи лазера с частотами ω_1, ω_2, ...

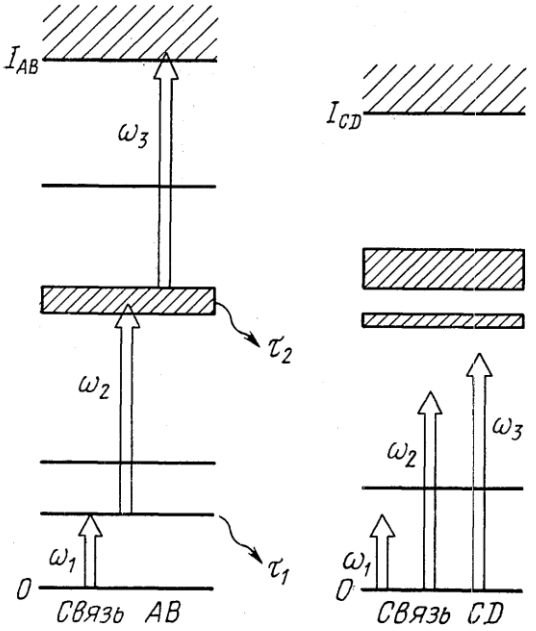


Рис. 2. Селективная многоступенчатая ионизация молекулярной связи AB с потенциалом ионизации I_{AB} в присутствии молекулярной связи CD с меньшим потенциалом ионизации I_{CD}.

Разрешающая способность фотоэлектронного лазерного микроскопа определяется теми же фундаментальными причинами (наличие тангенциальной составляющей скорости эмиттируемого электрона и соотношение неопределенностей), что и для автоэлектронного микроскопа, и описывается теми же соотношениями, но с тем отличием, что на напряженность электрического поля теперь не накладываются условия автоионизации электронов катода. Принцип неопределенности дает разброс поперечной скорости фотоэлектрона $\Delta\upsilon_1$, если его координата локализована с точностью a_1, определяемый соотношением $\Delta\upsilon_1 = \hbar/(2ma_1)$. С другой стороны, разброс поперечной скорости $\Delta\upsilon_1$ приводит к кружку рассеяния электронов на экране диаметром $d_1 = 2\,T\,\Delta\upsilon_1$, где $T = R\,[m/(2eU)]^{1/2}$ — время пролета электрона от катода до экрана, что соответствует неопределенности положения электрона на катоде $a_1 = b_1/M$. В результате разрешающая способность из-за соотношения неопределенности ограничивается величиной

$$a_1 = (2\hbar T/mM)^{1/2}. \qquad (1)$$

Наличие у фотоэлектрона начальной поперечной скорости Δv_1 ограничивает разрешающую способность на уровне:

$$a_2 = 2\Delta v_2 T/M = 2(T/M)(2\mathcal{E}_0/m)^{1/2} \quad (2)$$

где $\mathcal{E}_0$ — кинетическая энергия поперечного движения эмиттируемого фотоэлектрона. Разрешающая способность за счет суммарного действия этих двух статистически независимых эффектов равна

$$a = (a_1^2 + a_2^2)^{1/2}. \quad (3)$$

Например, при $M = 3\cdot10^5$ и $T = 3\cdot10^{-9}$ с, что соответствует $R = 10$ см и $U = 10^4$ В, величина $a_1 = 13$ Å. При $\mathcal{E}_0 = 0{,}1$ эВ и прежних остальных параметрах $a_2 = 21$ Å и суммарное разрешение $a = 25$ Å.

Потенциалы ионизации молекул и молекулярных связей лежат в области $I = 7–13$ эВ [9]. Так как полосы фотоионизационного поглощения широки и перекрываются для многих молекул, то селективность труднодостижима при одноступенчатом возбуждении молекул лазерным излучением с $\hbar\omega \gg I$. Кроме того, для прямой фотоионизации необходимо излучение в неосвоенной квантовой электроникой области вакуумного ультрафиолета (95–175 нм). Обе эти трудности устраняются естественным образом при последовательном многоступенчатом возбуждении уровней молекулы и ионизации из возбужденного состояния, как это показано на рис. 2. Эффективность этого метода для селективной фотоионизации и фотодиссоциации атомов и молекул в газовой фазе была продемонстрирована в работе [6].

Для того чтобы вероятность фотоионизации была достаточно велика, возбуждение молекулы импульсом на n-й ступени должно осуществляться за время, короче времени релаксации начального τ_{n-1} и конечного состояния τ_n, т.е. скорость индуцированных переходов W_n должна удовлетворять условию

$W_n \gtrsim 1/\tau_{n-1} + 1/\tau_n$.

Для предотвращения релаксации возбужденных молекул длительность каждого из импульсов должна быть короче любого из времен релаксации τ_n. Отсюда следует требование на энергию импульса на каждой ступени возбуждения:

$$\mathcal{E}_n \gtrsim \hbar\omega_n/2\sigma_n \text{ при } t \ll \tau_{n-1}, \tau_n, \quad (4)$$

где σ_n — сечение радиационного перехода между уровнями $(n-1) \rightarrow (n)$.

Для электронного перехода сложной молекулы $\sigma_n = 10^{-16}$-10^{-17}см^2, что приводит к энергии лазерного импульса около $\mathcal{E}_n = 3–30$ мДж/см^2 при $\hbar\omega_n = 3–4$ эВ. Время релаксации уровней лежит в интервале от 10^{-9} до 10^{-11} с. Поэтому для возбуждения электронных уровней должны использоваться субнаносекундные импульсы, например, от лазеров с самофазировкой мод. Площадь катода $2\pi r^2$ меньше типичной площадки фокусировки лазерного импульса $S_\phi \approx 10^{-5}$ см^2. Поэтому энергия импульса будет равна $E = \mathcal{E}S_\phi \approx 3\cdot10^{-8}–3\cdot10^{-7}$ Дж. Такие уровни

энергии вполне достижимы в перестраиваемых лазерах на красителях с самофазировкой мод.

Для фотоионизации возбужденной на m-й уровень молекулы необходимо, чтобы энергия и длительность импульса удовлетворяли условию (4), где под сечением надо подразумевать сечение фотоионизации σ_i, а длительность импульса должна быть короче времени релаксации возбужденного уровня τ_m. Сечение фотоионизации молекул лежит в диапазоне $\sigma_i = 10^{-18}$–10^{-19} см^2. Поэтому энергия импульса, осуществляющего фотоионизацию основной части возбужденных молекул, должна превышать энергию возбуждающих импульсов в 10^2–10^3 раз, то есть составлять $E_i = 10^{-5}$–10^{-6} Дж.

Для иллюстрации метода рассмотрим молекулы фталоцианина и хлорофилла. Обе эти органические молекулы являются плоскими и адсорбируются на поверхности металлов. Первая попытка изучить пространственную структуру молекулы фталоцианина методом автоэлектронной микроскопии была сделана еще в работе [10]. Главная трудность заключается в десорбции молекулы под действием сильного электрического поля, необходимого для автоионизации молекулы [5]. Применение лазерного излучения для отрыва электрона, очевидно, снимает эту трудность. В какой мере эмиссия фотоэлектронов будет характеризовать пространственную структуру молекулы? На рис. 3 показана схема молекулы фталоцианина меди (*а*) и распределение суммарной плотности электронного заряда (*б*) по рентгеновским данным [11]. Суммарное распределение электронной плотности обусловлено совместным вкладом σ- и π-электронов. σ-электроны локализованы с точностью до расстояния между соседними атомами, а π-электроны распределены по нескольким межатомным промежуткам, в данном случае, внутри каждого бензольного кольца. Следовательно, фотоотрыв σ-электрона определяет положение атома, а π-электрона — положение группы атомов. Структура молекулы хлорофилла имеет сходную геометрию, так как обе рассматриваемые молекулы принадлежат к одному классу органических тетрапирольных циклических соединений.

Упрощенные схемы электронных уровней молекул фталоцианина и хлорофилла приведены на рис. 4 по данным [12]. Значения энергии ионизации приняты равными значениям работы выхода фотоэлектронной эмиссии твердых слоев, которые ближе всего соответствуют случаю адсорбции молекулы на поверхности. Однако граница фотоионизации может лежать выше, поскольку образующийся положительный молекулярный ион может оказаться в возбужденном состоянии. Фотоотрыв электрона от молекулы фталоцианина может быть осуществлен под действием короткого импульса рубинового лазера и его второй гармоники по двум путям, показанным на рис. 4*а*. Фотоионизация молекулы хлорофилла также может быть выполнена при возбуждении первого возбужденного синглетного состояния и последующей ионизации его импульсом на второй гармонике как из синглетного, так и из нижнего триплетного состояния.

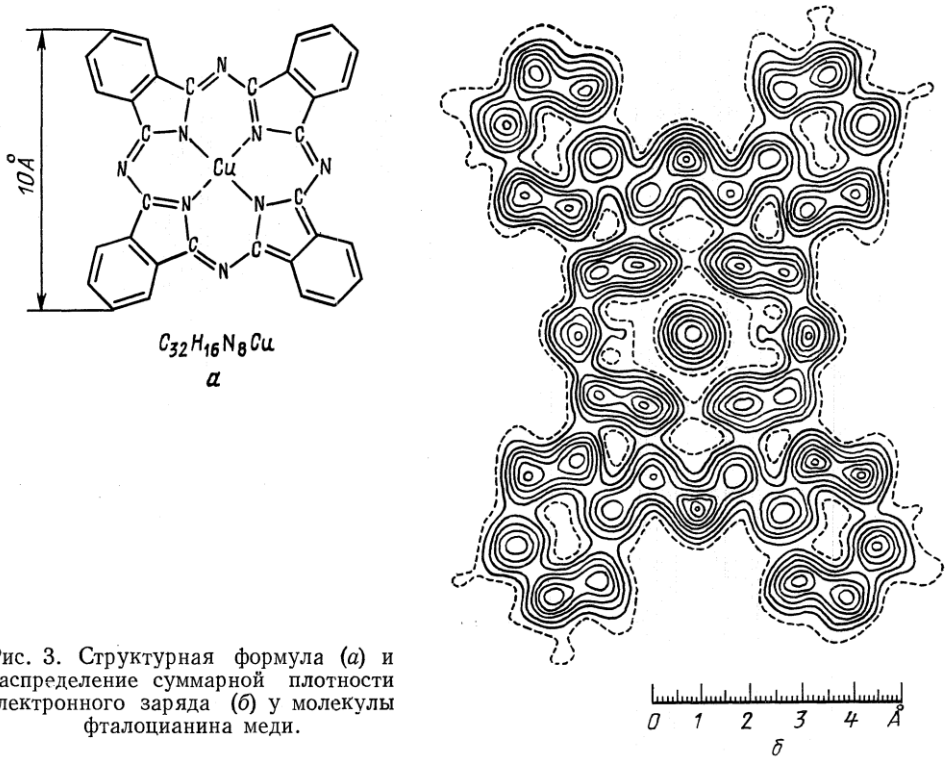


Рис. 3. Структурная формула (*а*) и распределение суммарной плотности электронного заряда (*б*) у молекулы фталоцианина меди.

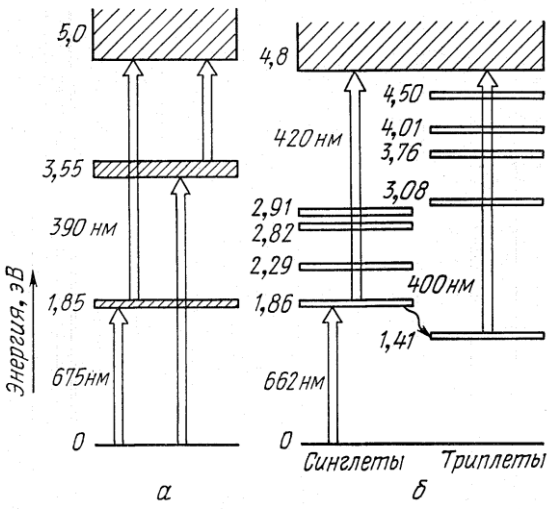


Рис. 4. Возможные схемы двухступенчатого фотоотрыва электрона у молекулы фталоцианина меди (*а*) и хлорофилла (*б*).

Согласно сделанной выше оценке (3), разрешающая способность фотоэлектронного лазерного микроскопа недостаточна для изучения структуры простых молекул типа фталоцианина и хлорофилла, и в таком простом виде метод пригоден скорее для получения информации о группах молекул, молекулярных цепочках. Тем не менее, пример относительно простой молекулы фталоцианина заслуживает внимания, так как уже была сделана попытка получить изображение ее помощью автоэлектронного микроскопа [10].

Рассмотренная идея фотоэлектронной микроскопии может быть распространена и для случая фотоотрыва ионов. Имеются данные [11], что в некоторых случаях после фотоотрыва электрона образующийся положительный молекулярный ион становится неустойчивым и самопроизвольно отделяет протон. Изменив полярность напряжения в проекторе, можно вместо электронов направлять на экран протоны. Согласно оценкам (1) и (2) пространственная локализация точки вылета протона должна быть в $(m_{\text{пр}}/m_{\text{е}})^{1/2} = 40$ выше, чем для фотоэлектрона. Такой лазерный фотоионный микроскоп может обладать разрешающей способностью, вполне достаточной для разрешения атомных деталей структуры молекул, способных к фотоотрыву протона. Нельзя также исключать возможное дальнейшее улучшение фотоэмиссионной микроскопии за счет ионизации молекул на более тяжелые молекулярные ионы. Такая возможность первичного распада молекулы на ионы под действием света была открыта Терениным еще 1930 году [13, 14]. В этом случае можно рассчитывать на дальнейшее увеличение разрешающей способности фотоионной микроскопии.

3. Метод селективного возбуждения атомов газа в автоионном проекторе

Автоионный микроскоп основан на отображении поверхности острия ионами, образующимися при автоионизации атомов остаточного (изображающего) газа в камере проектора, в момент приближения к поверхности острия. Для этого у поверхности острия создается электрическое поле с чрезвычайно высокой напряженностью (порядка 500 МВ/см). Изображение поверхности острия формируется на экране положительными ионами, летящими по нормали к его поверхности. Образец в автоионном микроскопе не эмиттирует ионы. Ионы образуются за счет автоионизации так называемого изображающего газа, введенного в рабочее пространство трубки проектора при давлении несколько тысячных миллиметра ртутного столба, в непосредственной близости у острия [4, 5]. Увеличение автоионного проектора достигает нескольких миллионов и разрешающая способность составляет 2–3 Å. Увеличение разрешения ионного проектора по сравнению с электронным достигается за счет большей массы иона и соответствующего уменьшения неопределенности локализации иона. Попытки применить автоионный проектор для получения изображения биологических молекул не оправдали возлагавшихся на них надежд. Главное препятствие при получении ионных изображений больших

органических молекул связано с необходимостью создания сильных полей. В сильных полях происходит разложение и испарение молекул, различного рода искажения [4, 5].

Напряженность электрического поля, требуемого для автоионизации атомов вблизи острия, можно существенно снизить, если предварительно возбудить атомы в состояние вблизи границы ионизации. Например, для водородоподобного атома, возбужденного в n-е главное квантовое состояние, необходимая для автоионизации напряженность электрического поля падает пропорционально n^3 [15]: $\mathcal{E}_{\text{и}} \approx \mathcal{E}^{\text{o}}_{\text{и}}/n^3$, где $\mathcal{E}^{\text{o}}_{\text{и}}$ — напряженность поля, необходимого для ионизации из основного состояния. При $n \approx 5$ критическая напряженность электрического поля должна снизиться до 10 МВ/см, то есть до значений, даже ниже обычно применяемых в автоэлектронном проекторе. При таких напряженностях можно полностью исключить испарение и разложение макромолекул электрическим полем.

Область возбуждения атомов изображающего газа в камере ионного проектора должна быть локализована вблизи острия на расстояниях $L \lesssim \tau\upsilon_0$, где τ — время радиационного распада возбужденного состояния; υ_0 — средняя тепловая скорость атомов. При возбуждении метастабильных триплетных состояний это условие легко выполнить. Однако для других состояний с $\tau \approx 10^{-8}$ с область возбуждения должна быть локализована на расстояниях порядка десятков микрон вблизи острия. Это возможно осуществить только при использовании для возбуждения атомов хорошо сфокусированного лазерного излучения.

Наиболее удобной для практического осуществления является следующая схема. Резонансным излучением обычных ламп можно достигнуть значительной населенности метастабильных состояний атомов изображающего газа. Например, нижнее триплетное состояние $^3S_1$, HeI можно заселить возбуждением вышележащего состояния $^3P_2$ излучением резонансной линии на 59,14 нм гелиевой лампы, нижнее триплетное состояние $^3P_0$HgI можно заселить линией ртутной лампы на 253,652 нм. Эти состояния можно возбуждать в объеме возбуждающего газа, а не непосредственно у острия. Метастабильные состояния He и Hg отстоят от границы ионизации на 4,03 и 5,77 эВ соответственно. Дополнительным, сфокусированным вблизи острия, излучением лазера с перестраиваемой частотой в доступной области спектра 400–500 нм можно возбудить атомы из метастабильных состояний в состояния, отстоящие на 1–2 эВ от границы ионизации. Автоионизация возбужденных атомов при приближении к острию должна происходить в относительно слабых электрических полях ($\sim 10^7$ В/см).

Прогресс в создании лазеров с перестраиваемой частотой в области 160–200 нм должен существенно упростить задачу возбуждения атомов типа Hg в состояние вблизи границы ионизации.

Литература

1. *Вайнштейн Б.К.* Дифракция рентгеновских лучей на цепных молекулах. М.: Изд. АН СССР, 1963.

2. Физические методы исследования белков и нуклеиновых кислот / сб. под ред. Ю.С. Лазуркина. М.: Наука, 1967.

3. *Вайнштейн Б.К.* // УФН. 1973. Т. 109. В. 3. С. 455.

4. *Мюллер Э., Цонь Т.* Автоионная микроскопия. М.: Металлургия, 1972.

5. Автоионная микроскопия / сб. под ред. Дж. Рена и С. Ранганатана. М.: Мир, 1971.

6. *Ambartzumian R.V., Letokhov V.S.* // IEEE J. Quantum Electronics. 1971. No. QE-7. P. 305; Appl. Optics. 1972. Vol. 11. P. 354.

7. *Müller E.W.* // Z. Physik. 1937. Vol. 106. P. 541.

8. *Dyke W.P., Do1an W.W.* In: Advances in Electronics and Electron Physics / by L. Marton. N.-Y.: Acad. Press, Inc. 1956. Vol. VIII. P. 90.

9. Handbook of Chemistry and Physics. 54-th Edition. CRC Press, 1973–1974.

10. *Müller E.W.* Naturwissensch. 1950. Vol. 37. P. 333.

11. *Теренин А.Н.* Фотоника молекул красителей и родственных органических соединений. Л.: Наука, 1967.

12. *Гуринович Г.П., Севченко А.Н., Соловьев К.Н.* Спектроскопия хлорофилла и родственных соединений. Минск: Наука и техника, 1968.

13. *Теренин А.Н.* Phys. Rev. 1930. Vol. 36. P. 147.

14. Элементарные фотопроцессы в молекулах. Сб. под ред. Б.С. Непорента, М. — Л.: Наука, 1966.

15. *Иванов Л., Летохов В.С.* // Квантовая электроника 1975.

Appl. Phys. B. 1984. Vol. 33. P. 57–61

LASER PHOTOION PROJECTOR

S.V. Chekalin, V.S. Letokhov, V.S. Likhachev, and V.G. Movshev
Institute of Spectroscopy, Academy of Sciences of the USSR

A laser photodesorption microscope has been applied to obtain 4×10^3-fold images of rhodamine crystals on a tip with a diameter of 66 μm. Peculiarities of the formation of these images have been studied with different values of electric field strength on the tip and laser pulse intensities.

The idea of a laser molecular-ion projector was discussed in [1]. Its idea is based on the assumption that it is possible to provide selective photodetachment of ions in certain functional groups of complex molecules using a sequence of ultrashort laser pulses which would allow fast multistep excitation of the chosen functional group of molecules. When the molecules are adsorbed on the surface of the Müller ion-microscope field-emitter tip, the resulting ionized photofragments will move in the radial electric field of the tip. As a result, on the fluorescent screen of the microscope one can observe an enlarged image of the relative position of molecular fragments on the tip and thus realise direct visualization of the spatial-chemical structure of the molecules.

The attempts to realize the visualization of macromolecules without lasers have been made in [2–4] and recently with alternative success in [5].

Since the suggestion was made [1], the application of lasers in ion microscopy has been developed in several ways. One group of experiments [6–10] was aimed at observing the effect of photodetachment of molecular ions from the molecules adsorbed on the surface. In [6, 7], for example, some successful experiments were performed in which authors could observe photodetachment of molecular ions from the surface of molecular crystals when the wavelength of nanosecond or picosecond laser radiation fell within the absorption band of these crystals [4]. Finally, in [8] preferential detachment of the excited chromophore (tryptophan) of the peptide molecule on the surface under uv picosecond pulsed radiation could be observed.

In work [11] Kellog and Tsong elaborated on a technique of field evaporation initiated by nanosecond laser pulses that widened considerably the scope of time-of-flight field-ion microscopy. It became possible to use semiconductor needles and to study surface chemical reactions under well-controlled conditions. Another paper [12] is concerned with experiments on laser field ionization mass-spectrometry. All these works deal basically with field photodesorption and photothermal desorption of gases condensed on the surface of the field-emitter tip and having no absorption bands within the wavelength of the lasers in use.

Our research deals with the realization of the photoion microscope and is based on selective action of ultrashort laser radiation on a molecule to detach a molecular ion. The electric field of the tip serves only for ion transport to produce an enlarged image [1].

In experiments [7] it was found that, as a thick layer of rhodamine 6G was irradiated at the 530 nm wavelength, photodetachment of $Rh6G^+$ cations from the rhodamine crystal surface took place. When irradiation was performed in the long-wavelength range at 1060 nm, rhodamine is transparent for, no detachment of molecular ions could be observed up to intensities exceeding the photodetachment threshold at 530 nm by two orders [9].

These results enabled us to proceed to the next stage; that is, to try to observe the places of rhodamine ion photodetachment on the desorption microscope screen when irradiating a thick layer of the dye on the tip at the 530 nm wavelength. The first step was to observe such a photoion image with a one-dimensional magnification in cylindrical geometry [10]. The target used in the form of a filament of 200 μm diameter, like the one used in the time-of-flight mass-spectroscopic experiments on laser photodetachment [9]. So it was possible to demonstrate the selectivity of emergence of a photoion image at varying wavelength of laser radiation.

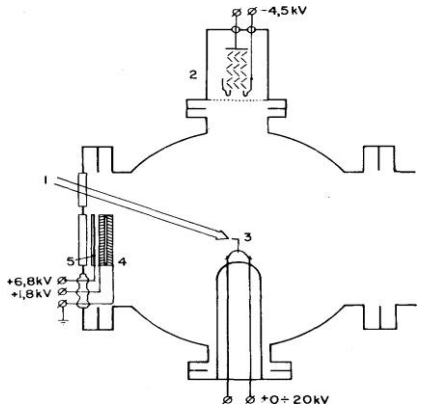


Fig. 1. Experimental setup. (*1*: laser radiation, *2*: SEM, *3*: tip, *4*: MCP, *5*: fluorescent screen)

The purpose of the work was to observe the two-dimensional photoion image of single rhodamine 6G crystals applied on the hemispherical surface of the field-emitter tip with a radius of 33 μm and to study the specific features of formation of pulsed photoion images.

Experimental Setup

The setup is schematically shown in Fig. 1. The needle used in the experiments had a hemispherical tip with a radius of 33 pm. The radius of the tip was chosen from the following consideration. As shown in [7, 9], the average density of rhodamine photoions at the photodetachment threshold ranges from about 10^6 to 10^7 ions/cm^2. As the laser-radiation intensity grows, the photoion density increases fast but due to an increase in photoion velocity spread in this case the quality of the image becomes worse [10]. It is apparent that, when operating nearby the ion photodetachment threshold, the imaged tip area should be no smaller than 10^{-6} cm^2 so that the

detectable number of ions in a pulse (10 to 10^2) can be displayed on the screen. Within the geometry of our experiment it corresponds to a hemispherical tip with a diameter of 70 μm.

The needle was made of a 200-μm tungsten wire by means of electrochemical polish. A thick layer of rhodamine 6G was applied to the needle tip from alcohol solution. The arrangement of settled crystals on the tip shape, and magnification were controlled visually using an optical microscope with 1.2×10^3 magnification. Then the needle with crystals thus applied was secured to a high-voltage input in the vacuum chamber where a pressure of 5×10^{-8} Torr was maintained by a high-vacuum pump. The needle could be supplied with a voltage of positive polarity controlled in the range from 0 to 20 kV.

The second-harmonic radiation of a Nd^{3+} YAG laser (λ = 530 nm, pulse duration 3×10^{-11} s) was directed onto the needle tip at 14° to the needle axis through the inlet quartz window. To produce a sufficiently uniform intensity distribution over the needle surface, a pinhole with its diameter of 0.7 mm was located in the laser beam within 100 cm of the target. It was made coincident with the brightest hot spot across the beam.

The ions desorbed from the tip were carried by the radial electric field to the visualization system spaced at 13.5 cm from the tip. The visualization system consisted of two microchannel plates (MCP) serving to amplify the ion current from the tip image intensifier and an aluminized screen made of ZnS·Ag, where an enlarged image of the arrangement of escaped ions from the tip was formed. The microchannel plates were placed in series (Chevron MCP). The diameter of the microchannel was 11 μm, the plates were 0.55 mm thick, each plate was supplied with +900 V. The screen was spaced at 1 mm of MCP and was charged at + 6 kV.

The magnification of the microscope is approximately equal to the ratio of the distance from MCP to the needle and the tip radius, being $M = 4 \times 10^3$. The screen diameter was D = 40 mm so the displayed section of the tip was 8 μm across. As the observations with an optical microscope show, a section of such dimensions accounted for an average of 3 to 4 crystals in size from 1 to 3 μm and for a large number of small crystals visible within optical resolution.

The electric signal appearing on the screen at the instant the ions fall within the visualization system was recorded with the type C-8-12 oscilloscope, the scanning of which was started with a laser pulse through the photodiode.

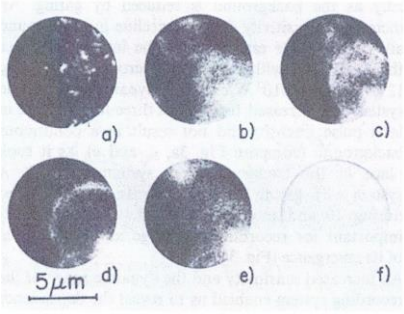


Fig. 2*a*–*f*. Photoion images produced without gating the MCP supply voltage. (*a*) The image is produced without laser-pulse irradiation as a result of field desorption of easily ionized impurities from the tip. The voltage across the needle is 14 kV. (*b*)–(*e*) Variation of the photodesorption image of rhodamine crystals with irradiation [(*b*) 10th, (*c*) 17th, (*d*) 20th, (*e*) 21st shot]. The laser-radiation intensity is 1.2×10^8 W/cm^2, the voltage across the tip is 10 kV. (f) Increase of background as the laser intensity increases to 2×10^8 W/cm^2. The voltage across the tip is 10 kV

Measuring the delay of this signal made it possible to find the time of flight of the ions desorbed by a laser pulse from the tip to the visualization system. In this way the time-of-flight technique allowed identifying the ions producing the photoion image.

In some experiments the power supply of MCP was gated to reduce the background and increase the recording-system sensitivity. In this case each MCP initially was charged at +700 V so that the brightness amplification was small and no image appeared on the screen. At the instant the ions which formed an image entered the visualization system, MCP were energized with a voltage pulse and the brightness amplification increased pulsewise by several orders. The gating pulse duration could vary from 0.2 to 10 μs. The delay time of this pulse, relatively to the laser pulse, could be varied within the same limits. By changing the gating pulse delay time one can form a photoion image using ions of different masses desorbed by a laser pulse.

The microchannel image intensifier sensitivity under gating operation was estimated with a secondary electron multiplier. It was placed at a distance of 180 nm from the needle so its axis was perpendicular to the visualization-system axis. The amplifier gain factor was 10^6 to 10^7. The signal from the SEM anode was recorded by the type C-8-12 oscilloscope, the pulse duration of a single ion in this case depended on the oscilloscope's frequency characteristic and came to 10 ns. As the image intensifier sensitivity was estimated, the needle was placed at 45° to the SEM axis and to the visualization-system axis. The needle was supplied with +15 kV, and both instruments recorded the ions arising in the field desorption from the tip. The intensity of single-ion shots was sufficient for photorecording. Under such conditions the threshold of appearance of shots from single ions on the screen coincided with that of pulses in the secondary-electron multiplier. The multistage SEM sensitivity is determined by the sensitivity of the first conversion dynode which is close to unity [9]. So it may be concluded that the efficiency of photorecording of single ions on the screen was about 50%.

Experimental Results

Figure 2*a* shows the image displayed on the microscope screen with no laser radiation. The voltage across the tip was +14 kV. At such voltage the electric field around the tip surface (10^6 V/cm) is not enough for the field desorption of rhodamine ions but can cause desorption of some easily ionized impurities. Ions of this kind form the image in Fig. 2*a*. The flux of admixed ions is rather small and therefore an exposure of about 10 s is required to record the image (several hundreds of admixed ions fall on the screen during this time). As the voltage across the tip was reduced to +10 kV, the admixed ions did not form an image on the screen at such exposure times.

Figure 2*b–f* present photodesorption images produced in irradiating the tip with rhodamine crystals charged at +10 kV by 30 ps laser pulses at the 530 nm wavelength. The visualization system operated with the MCP power supply did not gate. Each image was formed throughout one laser shot.

The correlation of Fig. 2*a* with Fig. 2*b–f* makes it possible to conclude that the photodesorption image differs essentially from the field-desorption image even

though one and the same section of the tip was imaged on the screen in both cases. The difference is caused by the image being formed by different ions. In the mass spectra taken simultaneously with the images in Fig. 2*b–e* only molecular ion of rhodamine was present. From this it followed that rhodamine crystals in size from 1 to 3 μm could be seen in the photodesorption images in Fig. 2*b–e*. Different brightness of the crystal images is apparently related to the difference in orientation of the crystals with respect to the laser beam and, respectively, to a different degree of laser radiation reflection and absorption by the crystal.

The crystals images have rather blurred boundaries which can be related to the velocity spread of rhodamine photoions. Another specific feature of the image is the formation of rings around the images of crystals (Fig. 2*b–d*). The dimensions of these rings and their arrangement change from shot to shot. With further irradiation they appear more seldom and at least disappear (Fig. 2*e*).

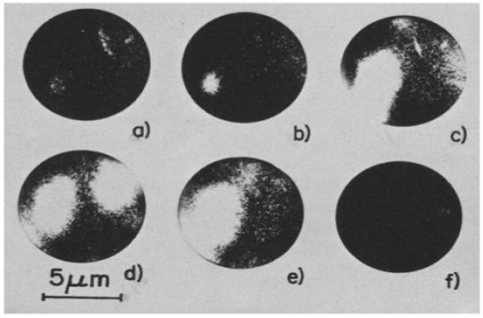


Fig. 3*a–f*. Photoion images of rhodamine crystals produced with gating the MCP supply voltage. (*a*)–(*c*) Images at the emergence threshold (laser radiation intensity of $6 \cdot 10^7$ W/cm^2). Exposure: (*a*) 1, (*b*) 12, (*c*) 30 laser shots. The voltage across the tip is 12 kV. (*d* and *e*). Images produced in two successive shots with laser intensity of 2×10^8 W/cm^2. The voltage across the tip is 12 kV. (f) Image produced during 10 laser shots with an average intensity of 2×10^8 W/cm^2. The voltage across the tip is 3 kV

As far as the small points in the image are concerned, their nature may be dual. First, these may be images of the smaller rhodamine crystals present on the tip. Second, these points may be conditioned by the admixed background ions desorbed from the tip after it is heated by a laser pulse. In experiments without gating such ions are able to contribute essentially to the formation of an image because the time of exposure in photography (~1 s) is many orders longer than the interval within which rhodamine ions arrive at the recording system (~10^{-6} s). Thus, in the absence of gating the background decreases the contrast of the image formed by rhodamine ions. Besides, the background decreases the dynamic range of the recording system, resulting a continuous background on the screen as the laser-pulse intensity is doubled over the image-emergence threshold (compare Fig. 2*d* and *f*).

Gating the voltage across MCP made it possible to improve the recording-system parameters. Figure 3*a–f* present some photodesorption images of rhodamine crystals produced with the MCP supply voltage gated at the instant rhodamine ions arrive at the plates (gating time 1 μs). It can be seen from the photographs that the image contrast increases markedly as the background is reduced by gating. An increase in sensitivity due to a decline in background allowed accurate estimation of the image-emergence threshold that, with the voltage across the tip being 12 kV, was 5.8×10^7 W/cm^2. The dynamic range of the system was increased, too. Even a three-fold increase in laser-pulse intensity did not result in a continuous background (compare Fig. 3*a*, *d*, and *e*), as it took place in the background-free system

(Fig. 2*f*). A system with gating enabled an image to be formed during 10 and more shots which was particularly important for recording an image at the threshold of its emergence (Fig. 3*a*–*c*).

An increased sensitivity and the dynamic range of the recording system enabled us to reveal the dependence of the photodesorption image-emergence threshold on the voltage across the tip. With the voltage being +12 kV, the threshold intensity of the laser pulse was 5.8×10^7 W/cm^2 (Fig. 3*a*), and at +3 kV it was possible to record a very weak image only by accumulating exposures from 10 laser shots with their average intensity of 1.3×10^8 W/cm^2 (Fig. 3*f*).

The experiments with gating unambiguously show that the observed objects in size from 1 to 3 μm are rhodamine crystals. The nature of the smaller points in the image is still not clear. This is due to the fact that the arrangement of not only small but also big crystals in the displayed area of the tip changes substantially after they are irradiated with laser pulses, especially at high intensities (compare Fig. 3*d* and e for two shots following each other). Therefore, it does not seem possible to establish an unambiguous correspondence between the points of the image during different exposures even though these points represent small crystals.

Discussion of Results

The dependence of the photodesorption image-emergence threshold on the electric field at the tip, the appearance of rings in the image as well as a blurring of the rhodamine crystal image boundary may be caused by one and the same factor, i.e. the initiation of photoconductivity in crystals irradiated by laser pulse. A high-power ultra-short pulse ($I \sim 10^{27} \div 10^{28}$ phot cm^{-2} s^{-1}) with wavelength $\lambda = 530$ nm falling within the absorption band of rhodamine creates charge carriers in the crystal. According to our tentative estimate, the density of the carriers which arises from exciton photoionization exceeds 10^{19} cm^{-3} (effect of metallization).

Figure 4 illustrates the manifestation of this phenomenon in a photoion microscope. In the absence of laser irradiation, a rhodamine microcrystal adsorbed on the tip of a metal needle acts as a dielectric.

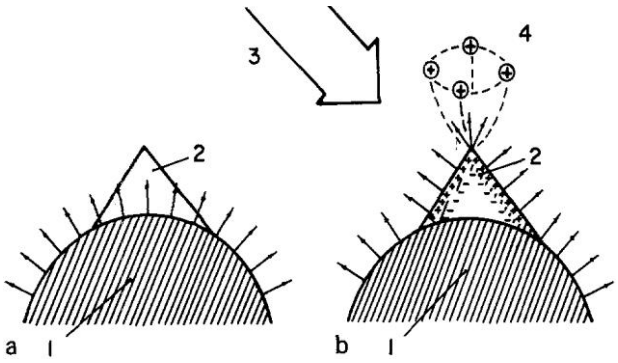


Fig. 4. Potential mechanism of emergence of rings in the photoion image. (*1*: metal, *2*: rhodamine crystal, *3:* laser radiation, *4*: photoions)

The electric field of the metal tip appearing with a voltage of + 10 kV applied across it is slightly distorted by the dielectric (Fig. 4*a*). Under laser-pulse irradiation the crystal becomes metallized. The field near the crystal is considerably distorted, there is a local-field gain in the corners and edges of the crystals (Fig. 4*b*).

This field distortion leads, first, to a distortion of the image on the screen that can contribute to the blurring of the crystal-image boundaries.

Secondly, in the corners of the crystals, where the electric-field intensity is maximum, field desorption of rhodamine ions may begin. This desorption mechanism depends on the voltage across the tip and can be responsible for the observed dependence of the image-emergence threshold on the voltage across the microscope needle.

And finally, third, the rhodamine ions thus desorbed in the corners of the crystal will at first move along the local field lines and then, starting from distances of about the crystal thickness, along the radial lines of the undistorted field. So the image formed by these ions on the screen is shaped like a ring, its centre being in the region of microinhomogeneity from where desorption occurs (Fig. 4*b*) [9].

As the crystals are exposed to laser radiation, the microinhomogeneities become smoothed out. This causes the rings in the image to disappear (Fig. 2*e*) and the photodesorption threshold to increase.

In conclusion, it must be noted that, when the photodesorption microscope is equipped with a gating recording system, it enables observing not only the photoion image of the crystals applied on the tip. The ability to record single photoions of a definite sort and the possibility to store information on the points of escape of these photoions during a lot of laser shots enable us to hope that with the use of such a system we shall manage to observe single molecules or small accumulations of molecules adsorbed on the tip. But in this case it is necessary to study the peculiarities of photodetachment of the ions of different substances applied in a submonolayer on the tip surface by varying the laser radiation parameters, the electric field, and the material the tip is made of.

References

1. *Letokhov V.S.* // Quantovaya Electron. 1975. Vol. 2. P. 930–937.
2. *Schmidt W., Krautz E.* // Surf. Sci. 1972. Vol. 32. P. 349.
3. *Graham W.R., Hutchinson F., Reed D.A.* // J. Appl. Phys. 1973. Vol. 44. P. 5155.
4. *Machlin E.S., Freilich A., Agrawal D.C., Burton J.J., Briant C.L.* // J. Microscopy. 1975. Vol. 104. P. 127.
5. *Panitz J.A.* // J. Phys. E.: Sci. Instrum. 1982. Vol. 15. P. 1281.
6. *Antonov V.S., Letokhov V.S., Shibanov A.N.* // Pis'ma Zh. Ekps. Teor. Fiz. 1980. Vol. 31. P. 471–474.
7. *Letokhov V.S., Movshev V.G., Chekalin S.V.* // Zh. Ekps. Teor. Fiz. 1980. Vol. 81. P. 480–485.
8. *Antonov V.S., Egorov S.E., Letokhov V.S., Matveetz Yu.A., Shibanov A.N.* // Pis'ma Zh. Ekps. Teor. Fiz. 1982. Vol. 36. P. 29–31.

9. *Movshev V.G., Chekalin S.V.* // Quantovaya Electron. 1983. Vol. 5 (10). P. 1425

10. *Letokhov V.S., Likhatchev V.S., Movshev V.G., Chekalin S.V.* // Quantovaya Electron. 1983. Vol. 9. P. 2117–2118.

11. *Kellog G.L., Tsong T.T.* // J. Appl. Phys. 1981. Vol. 52. P. 5320–5328.

12. *Nishigaki S., Drachsel W., Block J.H.* // Surf. Sci. 1979. Vol. 87. P. 389–409.

13. *Pottie R.F., Cocke D.L., Gingerich K.A.* // Int. J. Mass. Spectrom. Ion Phys. 1973. Vol. 11. P. 41–53.

Egorov S.E., Letokhov V.S., Shibanov A.N. In: Surface Studies with Lasers / ed. by F.R. Aussenegg, A. Leitner, M.E. Lippitsch. Springer Series in Chem. Phys., Vol. 33. Berlin, Heidelberg, New York: Springer, 1983. P. 156.

АСТРОФИЗИЧЕСКАЯ СПЕКТРОСКОПИЯ

1. *Летохов В.С.* О стимулированном радиоизлучении межзвездной среды// Письма в ЖЭТФ. 1966. Т. 4 (11). С. 477–481.

2. *Летохов В.С.* Астрофизические лазеры // Квантовая электроника. 2002. Т. 32 (12). С. 1065–1079.

Письма в ЖЭТФ. 1966. Т. 4 (11). С. 477–481

О СТИМУЛИРОВАННОМ РАДИОИЗЛУЧЕНИИ МЕЖЗВЕЗДНОЙ СРЕДЫ

В.С. Летохов
Физический институт им. П.Н. Лебедева АН СССР

1. В последнее время был обнаружен ряд аномалий в радиоизлучении молекулы OH в межзвездной среде (аномальное отношение интенсивностей линий [1–3], сильная круговая поляризация излучения при отсутствии поляризации поглощения [4], весьма малая ширина спектра [1–4]). Температура излучения по последним измерениям [5] на частоте 1665 МГц источника W3 более 2.10^6 °К. Естественно, в качестве основного механизма объяснения этих аномалий был предложен механизм когерентного усиления радиоизлучения за счет инверсной заселенности между уровнями сверхтонкой структуры молекулы OH [2–4], причем полное усиление может достигать, например, 10^7 [4]. Возможность когерентного усиления в межзвездной среде при оптической накачке рассматривалась также в [6].

Цель данного письма — показать возможность генерации радиоизлучения в усиливающей межзвездной среде за счет обратной связи при рассеянии на свободных электронах или частицах космической пыли. Свойства «космического мазера» существенно отличаются от свойств «космического мазерного усилителя», что делает возможным объяснение наблюдаемых аномалий.

2. Источники аномального радиоизлучения OH находятся в областях с высокой степенью ионизации водорода [1–4]. В них относительно высока концентрация электронов и межзвездной пыли, которые способны рассеивать радиоизлучение. Рассеяние излучения в обратном направлении может привести к самовозбуждению и генерации усиливающей области межзвездной среды. Условие самовозбуждения имеет вид:

$$e^{\alpha L} = \frac{\alpha}{\varkappa} \ , \qquad (1)$$

где α и $\varkappa$ — коэффициенты усиления и обратного рассеяния среды на единицу длины, L — размер генерирующей области.

3. Томсоновское рассеяние на электронах. Коэффициент обратного рассеяния на электронах определяется выражением:

$$\varkappa \simeq N_e Q_{\text{ген}} \left(\frac{e^2}{mc^2}\right)^2 \frac{\Delta\omega_a}{\Delta\omega_s + \Delta\omega_a}, \qquad (2)$$

где N_e — плотность электронов, $Q_{\text{ген}}$ — телесный угол генерации, определяемой формой области генерации, а последний множитель учитывает уширение

спектра излучения при обратном рассеянии на электронах. При доплеровском уширении линии усиления $\Delta\omega_a$ и спектра рассеянного излучения $\Delta\omega_s$ можно считать, что $\Delta\omega_s \gg \Delta\omega_a$ (масса усиливающей молекулы $M \gg m$) и

$$\frac{\Delta\omega_a}{\Delta\omega_s + \Delta\omega_a} \simeq \frac{1}{2}\sqrt{\frac{mT_M}{MT_E}},$$

где T_M и T_E — кинетические температуры усиливающих молекул и электронов, соответственно. Например, для случая молекул OH и $T_E \simeq 10T_M$ получаем

$$\varkappa \simeq 0{,}5 \cdot 10^{-9} N_e Q_{ген}\ пс^{-I}. \quad (3)$$

При $N_e = 10^3$ см-1 и $Q_{ген} \approx I$ стер для самовозбуждения области с размером $L = I$ пс, согласно (I), достаточно полного усиления $e^{\alpha L} \simeq 3{,}10^7$.

4. Рассеяние на космической пыли. Данные о частицах пыли в космических облаках являются весьма приближенными [8]. Для оценки рассмотрим космическую пыль в виде диэлектрических сферических частиц диаметра D с диэлектрической проницаемостью ε и концентрацией N_q. Коэффициент обратного рассеяния равен:

$$\varkappa = N_q Q_{ген} \frac{\pi^5}{3}\frac{D^6}{\lambda^4}\left(\frac{\varepsilon - 1}{\varepsilon + 2}\right)^2, \quad (4)$$

причем в этом случае $\Delta\omega_s \ll \Delta\omega_a$, так как масса частиц пыли $M_q \gg M$. Если допустить, что существуют области весьма богатые пылью, например, области с концентрацией пыли на три порядка выше средней концентрации вблизи плоскости Галактики $\langle N_q \rangle \simeq 4, I0^{-14}$ см^3 [8] и диаметром частиц $D \simeq I0^{-3}$см-1, то в принципе возможно самовозбуждение области с размером $L = I$ пс лишь при полном усилении $e^{\alpha L} \simeq 3{,}10^{I5}$ ($Q_{ген} = I$ стер, $\lambda = I8{,}5$ см, $\varepsilon \simeq 2$). Обратная связь на частицах пыли является менее эффективной, чем на свободных электронах. Однако существование плотных областей с более крупными частицами пыли может существенно облегчить условие самовозбуждения.

5. Имеется существенное отличие обратной связи на электронах и на космической пыли. В первом случае, при обратном рассеянии, происходит сильное уширение спектра излучения ($\Delta\omega_s \gg \Delta\omega_a$) и поэтому сужение спектра происходит только за один проход области усиления: ширина спектра излучения $\Delta\omega_{изл} \simeq \Delta\omega_a / \sqrt{\alpha L}$. Во втором случае, при отсутствии турбулентности рассеивающих частиц, $\Delta\omega_s \ll \Delta\omega_a$ и происходит непрерывное сужение спектра за много проходов области генерации ($\Delta\omega_{изл} \simeq \Delta\omega_a / \sqrt{\alpha ct}$, t — время) [9], вплоть до предельной ширины $\Delta\omega_{изл} \simeq \Delta\omega_s / \sqrt{\alpha L}$. При турбулентном движении рассеивающих частиц, когда уширение спектра при обратном рассеянии $\Delta\omega_s > \Delta\omega_a$, ширина спектра излучения в обоих случаях одинакова.

6. Проделанные оценки показывают, что источники аномального радиоизлучения ОН могут работать в режиме генерации. Наличие порога в режиме генерации, в отличие от режима усиления, может резко изменить свойства излучения: спектр, направленность, поляризацию и зависимость интенсивности от времени. Например, небольшая зависимость коэффициента обратного рассеяния или поглощения межзвездной среды от поляризации может сильно изменить поляризацию генерируемого излучения. При внезапном превышении порога (при импульсном возрастании усиления или уменьшении потерь) возможно экспоненциальное нарастание интенсивности излучения с последующим испусканием «гигантского» импульса.

7. Роль предложенного механизма в испускании аномального радиоизлучения в межзвездной среде может быть выяснена также по наблюдениям плотности электронов и космической пыли в источниках аномального излучения, зависимости интенсивности излучения от времени и др.

Автор глубоко благодарен академику Н.Г. Басову, Г.А. Аскарьяну и А.Г. Молчанову за обсуждение вопроса и ценные замечания.

Литература

l. *Weaver H. et al.* // Nature. 1965. Vol. 208. P. 29.

2. *Weinreb S. et al.* // Nature. 1965. Vol. 208. P. 440.

3. *Mcgee R.X., Robinson B.J., Gargner F.F., Bolton J.G.* // Nature. 1965. Vol. 208. P. 1193.

4. *Barrett A.H., Rogers A.E.E.* // Nature. 1966. Vol. 210. P. 188.

5. *Roders A.E.E. et al.* // Phys. Rev. Lett. 1966. Vol. 17. P. 450.

6. *Варшалович Д.А.* // Письма ЖЭТФ. 1966. Т. 4. С. 180.

7. *Амбарцумян Р.В., Басов Н.Г., Крюков П.Г., Летохов В.С.* // Письма ЖЭТФ. 1966. Т. 3. С. 262.

8. *Каплан С.А., Пикельнер С.Б.* Межзвездная среда. М.: Физматгиз, 1963.

9. *Амбарцумян Р.В., Крюков П.Г., Летохов В.С.* // ЖЭТФ. 1966. Т. 51. С. 1669.

Квант. электрон. 2002. Т. 32 (12). С. 1065–1079

АСТРОФИЗИЧЕСКИЕ ЛАЗЕРЫ

В.С. Летохов
Институт спектроскопии РАН, Россия, 142190 Троицк, Московская обл.

Дан обзор лазеров, работающих в естественных астрофизических условиях. Рассмотрено принципиальное отличие условий получения инверсии и усиления в астрофизическом лазере от аналогичных условий для хорошо известных астрофизических мазеров. Приведены данные о недавно открытом астрофизическом лазере на ионах Fe II. Обсуждаются характеристики астрофизического лазерного усилителя и возможности превращения его в астрофизический лазер с некогерентной обратной связью, а также методы исследования ширины спектра излучения астрофизического лазера.

Ключевые слова: астрофизические лазеры и мазеры, некогерентная обратная связь, инверсная населенность.

1. Введение

Принципы работы мазеров и лазеров были открыты в течение десятилетия (1950–1960 гг.) в ходе сначала независимых, а затем взаимосвязанных исследований, проводимых в Физическом институте им. П.Н. Лебедева АН СССР и Колумбийском университете США. Эти фундаментальные пионерские исследования получили высшее международное признание [1]. Экспериментальная демонстрация лазеров [2, 3] и последовавший экспоненциальный прогресс в области как самих лазеров, так и их применений подтвердили масштаб этого открытия. Роль Н.Г. Басова в этом прогрессе уникальна, поскольку он со своими учениками в течение нескольких десятилетий был на переднем фронте стремительного развития квантовой электроники. Однако по-существу, все эти достижения — только начало «лазерного века», так как истинный масштаб освоения оптического диапазона когерентными источниками электромагнитного излучения проявится в полной мере лишь в XXI веке.

Небезынтересно проследить истоки квантовой электроники, возникшей в результате развития и синтеза двух направлений физики: классической электромагнитной физики (назовем ее «радионаправлением») и квантовой физики (назовем ее «оптическим направлением», т.к. квантовая физика была создана на основе атомной физики и оптической спектроскопии, а уже затем стала фундаментом всей физики). Оба эти направления объединяются уравнениями Максвелла.

На рис. 1 представлена выборочная последовательность ключевых открытий, идей и экспериментов, которые привели к рождению квантовой электроники. Главная последовательность событий, в результате которых был открыт лазер, показана сплошными стрелками, а несостоявшиеся возможности

открытия лазера на пути идей усиления света в среде с инверсной населенностью уровней — штриховыми. Хотя лазеры и могли быть открыты на оптическом направлении, в действительности это произошло только после создания мазера, т.е. благодаря прогрессу радионаправления. Сначала идеи квантовой физики и создание СВЧ-источников электромагнитного излучения для радаров привели к развитию радиоспектроскопии, а затем мазеров (молекулярных генераторов). И только потом перенос идеи резонаторной обратной связи в оптическую область, где идея инверсной населенности уровней оптических переходов уже давно существовала, привел к созданию лазера. Это лишний раз подтверждает важнейшую роль взаимосвязи и синтеза различных областей науки и техники в научно-техническом прогрессе. Хотя лазеры и могли быть открыты независимо от радионаправления, этого не случилось, что опять-таки подтверждает неизбежность самого открытия, несмотря на непредсказуемость его конкретного сценария, который всегда имеет персональный, субъективный оттенок.

В этой связи уместно обратить внимание на радиоастрономическое открытие естественных мазеров в астрофизических условиях на радикале OH на $\lambda = 18{,}5$ см [4] и молекуле H_2O на $\lambda = 1{,}35$ см [5] в середине 60-х годов, спустя десять лет после создания первых лабораторных мазеров в Москве и Нью-Йорке.



Рис. 1. Последовательность открытий в оптике и радио, которые привели к рождению квантовой электроники

Яркостная температура микроволнового излучения астрофизических мазеров достигает 10^{12}–10^{18} К и поэтому может быть объяснена только усилением за счет стимулированного излучения в среде с инверсной населенностью низколежащих молекулярных уровней. Это был еще один несостоявшийся сценарий более позднего открытия мазера. Астрофизические лазеры в оптическом диапазоне, которые являются предметом данной статьи, были открыты совсем недавно, через 40 лет после создания лабораторного лазера. Однако корни их могут быть прослежены в 30-х и 40-х годах, то есть задолго до создания и лазера, и мазера. В эти годы астрофизики объясняли возникновение аномальных спектральных линий испускания (линий накачки) одного элемента совпадением с линией поглощения другого элемента (случайное совпадение Боуэна [6, 7]). Они также использовали соотношения для скоростей накачки и испускания, которые в современных терминах эквивалентны условию инверсной населенности [8] (см. ниже разд. 3). Это еще один несостоявшийся сценарий открытия лазерного эффекта на основе астрофизических наблюдений.

2. Условия действия астрофизического лазера

Усиление электромагнитного излучения ансамблем квантовых частиц возможно только при существенном нарушении термодинамического равновесия, то есть тогда, когда нарушается хотя бы одно из трех следующих условий равновесия:

1. Равновесное больцмановское распределение населенностей квантовых состояний частиц ансамбля, или средних квадратов амплитуд волновых функций состояний.

2. Равновесное состояние электромагнитного излучения, в котором находится ансамбль частиц с данной равновесной температурой, что эквивалентно отсутствию внешнего излучения помимо равновесного излучения ансамбля.

3. Равновесное (случайное) распределение фаз волновых функций квантовых состояний, то есть отсутствие средней ненулевой (нефлуктуационной) поляризуемости, или когерентности в ансамбле.

Нарушение первого условия, ведущее к образованию инверсии населенности какой-либо пары уровней, возможно многими методами, например, при избирательной некогерентной накачке возбужденного уровня по трех- или четырехуровневой схеме (рис. 2*а*, *б*), и потому оно используется практически во всех лазерах [9].

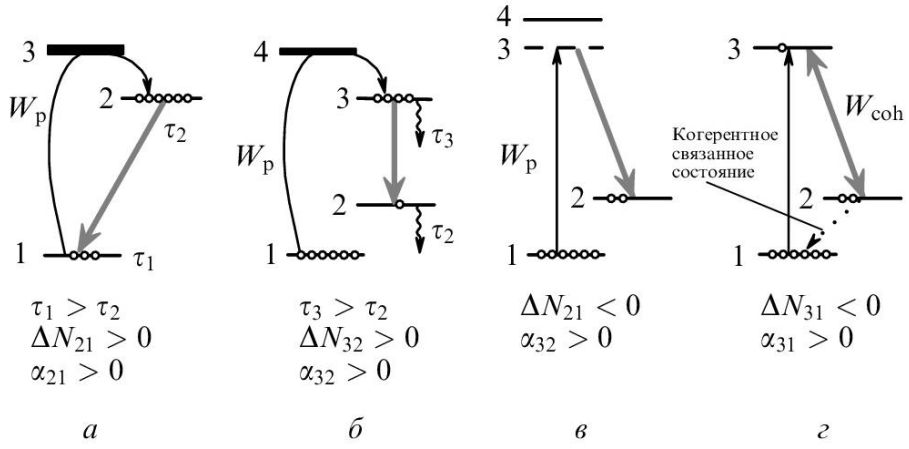


Рис. 2. Различные методы получения усиления, основанные на создании инверсной населенности по трехуровневой (*а*) и четырехуровневой (*б*) схемам, на комбинационном (рамановском) рассеянии без инверсии населенностей (*в*) и на использовании когерентной суперпозиции состояний 1 и 2 без инверсной населенности уровней 2, 3 (*г*). Получение усиления по схемам *а*, *б* требует некогерентной накачки с умеренной (особенно для схемы *б*) скоростью. Усиление по схеме *в* требует накачки с очень высокой спектральной интенсивностью (не обязательно когерентной). Усиление по схеме *г* требует когерентного возбуждения на переходе 3 → 1 и наличия когерентно-связанных (СРТ) состояний 1 и 2

Сильное нарушение второго условия равновесия способно привести к усилению даже без инверсии населенности. Примером может служить лазер на комбинационном (рамановском) рассеянии [10], когда прозрачная среда в сильном лазерном поле становится усиливающей на стоксовой частоте комбинационного (рамановского) рассеяния в среде с равновесной населенностью уровней только вследствие присутствия в ансамбле интенсивного монохроматического излучения (рис. 2*в*). Подчеркнем, что в этом случае от лазерного излучения требуются только высокая интенсивность и большая ширина спектра (порядка ширины линии рассеяния), но отнюдь не высокая когерентность.

При создании усиления путем нарушения первого и второго условий равновесия активная среда находится в некогерентном состоянии, что естественно, так как время фазовой релаксации в ансамбле обычно гораздо меньше времени релаксации населенностей. Когерентность создается только при помещении активной среды в оптический резонатор, выделяющий ограниченное число пространственных мод, в которых поддерживается высокая скорость стимулированного излучения. Другими словами, когерентность излучения создается самопроизвольно за счет «фазового перехода» в системе активная среда + излучение в резонаторе [11].

Существенно иная ситуация имеет место для случая нарушения 3-го условия равновесия, которое требует специальных обстоятельств. Нарушение равновесного (случайного) распределения фаз (точнее, разности фаз) волновых функций каких-либо двух квантовых состояний может быть достигнуто

под действием внешнего когерентного поля, которое согласует разность фаз волновых функций двух состояний, взаимодействущих с этим полем (одно- или двухчастотным). В результате такого согласования квантовая система в ансамбле может быть приготовлена в суперпозиционном антисимметричном состоянии двух стационарных квантовых состояний (1 и 2 на рис. 2*г*). Такое состояние называют когерентно-плененным (coherently population trapped (CPT) state) [12, 13]. В CPT состоянии частица не поглощает излучение ни на переходе $1 \rightarrow 2$, ни на переходе $2 \rightarrow 3$ (переход $1 \rightarrow 2$ предполагается запрещенным) из-за квантовой деструктивной интерференции двух встречных квантовых путей переходов $1 \rightarrow 3 \rightarrow 2$ и $2 \rightarrow 3 \rightarrow 1$. Этот эффект связан с электромагнитно-индуцируемой прозрачностью [14]), когда когерентное электромагнитное поле создает CPT состояние, которое не поглощает излучение. Данный эффект был использован для демонстрации лазера без инверсии за счет нарушения третьего условия равновесия по Λ-схеме, показанной на рис. 2*г* [15], и по V-схеме [16].

В астрофизических условиях вполне может быть нарушено первое условие равновесия; при этом образуется инверсная населенность, обусловленная пространственной неоднородностью астрофизической среды по плотности, температуре и т.д. (звезды и газовые облака вблизи них и т.д.), когда среда находится в стационарном, но неравновесном состоянии. При обсуждении этой возможности для астрофизических сред надо разделить импульсный [2] и непрерывный квазистационарный [3] режимы создания инверсной населенности. В импульсном режиме скорость накачки возбужденного уровня должна быть больше скорости релаксации его населенности, которая для оптических переходов обычно превышает 10^{-3} $с^{-1}$ (для запрещенных переходов иногда даже достигает значений около 1 $с^{-1}$).

В астрофизических условиях эта ситуация труднореализуема, т.к. характерные времена импульсных астрофизических явлений, пригодных для накачки, имеют гораздо большую длительность, чем времена релаксации населенностей квантовых частиц.

В непрерывном (квазистационарном) лазерном режиме используется эффект более быстрой релаксации нижнего уровня перехода по сравнению с верхним [3] (рис. 2, 6). В этом случае инверсия на таком переходе существует всегда, и требование к скорости накачки связано с достижением определенной плотности инверсии населенности уровней, необходимой для получения порогового усиления. Этот режим используется во всех непрерывных лазерах, и он наиболее вероятен для астрофизических лазеров, как было предложено в [17]. Наиболее легко он реализуется тогда, когда радиационные времена жизни двух соответствующих уровней существенно различаются (в нужную сторону). В этом случае инверсная населенность возникает в изолированной квантовой системе без участия столкновений, что типично для разреженной газовой околозвездной или межзвездной среды. Астрофизический лазер, работающий по этой схеме на высоколежащих уровнях Fe II на длине волны ~1 мкм, обнаружен недавно в газовой конденсации в окрестности наиболее массивной и яркой звезды нашей Галактики — η Car [18].

Однако в звездных атмосферах при более высокой плотности частиц столкновения, хотя они и возвращают ансамбль к равновесию населенностей, могут играть и положительную роль за счет преимущественного столкновительного опустошения нижнего уровня. Как это ни удивительно, но роль столкновений в усилении интенсивности эмиссионных линий в атмосферах звезд по типичной для лазеров схеме [19] обсуждалась еще в астрофизических работах 30-х годов [8]. Поскольку в этих работах рассматривались вопросы, связанные с вынужденным излучением, они специально обсуждаются в разд. 3.

Нарушение второго условия равновесия требует интенсивного монохроматического излучения, которое обычно генерирует только лазер. Линия комбинационного рассеяния всегда является усиливающей, а коэффициент усиления пропорционален интенсивности внешнего излучения в пределах ширины линии рассеяния. В астрофизических условиях известно только одно наблюдение комбинационного рассеяния. В работе [20] зарегистрировано комбинационное рассеяние линии O VI с λ = 1032 и 1038 Å на электронном переходе 1S–2P нейтрального водорода HI (близкий резонанс с линией Лаймана Ly_β водорода H I на λ = 1026 Å). При таком рассеянии атом водорода оказывался в состоянии 2S, а линия рассеянного излучения — в видимой области (6825 и 7082 Å). Этот эффект наблюдается в специальных астрофизических условиях симбиотических звезд, где сильные линии ВУФ излучения высокоионизованных атомов облучают области нейтрального водорода высокой плотности. Коэффициент усиления на комбинационных линиях весьма мал, и речь может идти только о спонтанном рассеянии.

Самопроизвольное, без внешнего когерентного поля, нарушение третьего условия равновесия, то есть условия случайного распределения разности фаз волновых функций квантовых состояний независимых частиц в ансамбле, представляется маловероятным. (Единственным исключением является случай ансамбля ультрахолодного газа атомов-бозонов достаточной плотности, в котором наблюдается эффект бозе-эйнштейновской конденсации.) Тем не менее, в работе [21] высказана смелая гипотеза о возможности усиления без инверсии в астрофизических условиях на линии атома водорода бальмеровской серии (переход 3P–2S). Релаксация фаз квантовых состояний в разреженной газовой среде (плотность менее 10^8 см$^{-3}$) действительно может быть весьма медленной (минуты и более), а для возбужденного 2S-состояния HI она составляет 0,12 с (из-за спонтанного двухфотонного распада). Однако для создания когерентности (или, точнее, CPT) состояний 1S и 2S водорода должен существовать механизм спонтанного возникновения CPT состояния. Авторы работы [21] полагают, что под действием двух интенсивных линий некогерентного излучения — Ly_α (λ = 1215 Å) и линии Бальмера Hα (λ = 6563 Å) — такой процесс возможен при спонтанном распаде возбужденного состояния атома по двум совершенно разным и вполне различимым каналам, но является крайне маловероятным. Обнаружение такого процесса представило бы большой физический интерес, поскольку он стал бы примером своеобразного фазового перехода ансамбля квантовых частиц из некогерентного состояния в когерентное. Известен пока только один пример такого фазового перехода — в лазере, когда

усиливающая некогерентная среда помещается в открытый резонатор, который радикально ограничивает число пространственных мод для стимулированного излучения, то есть «когерентизирует» ансамбль.

3. Астрофизические предшественники лазера

Основной движущей силой атомной спектроскопии в прошлом веке была астрофизика, так как астрономические спектры звезд, туманностей, галактик давали основную информацию о строении и развитии Вселенной. Наиболее исследованной областью является спектроскопия звездных атмосфер [22].

Принимаемое наблюдателем излучение звезды представляет собой сплошное излучение фотосферы, прошедшее через окружающую ее оболочку звезды — атмосферу, и линейчатое излучение атмосферы. Таким образом, в зависимости от того, какой из двух процессов — поглощение или спонтанное испускание — преобладает, на фоне сплошного спектра фотосферы образуются дискретные линии поглощения или испускания атмосферы. Если излучение фотосферы очень интенсивно, а яркость спонтанного излучения атмосферы невелика, то наблюдаются дискретные линии поглощения. Эта ситуация типична для большинства обычных звезд.

Однако в спектрах многих звезд присутствуют яркие линии испускания [23]. Это возможно, если излучение атмосферы на соответствующей длине волны сравнимо с излучением фотосферы в непрерывном спектре на этой длине волны. Поэтому яркие линии можно заметить только в спектрах звезд, обладающих обширными атмосферами, либо фотосферой с относительно слабым излучением. Особенно часто яркие линии наблюдаются в нестационарных (переменных) или двойных звездах [24].

Для объяснения появления ярких линий испускания используют, в основном, три механизма [22, 24]: возбуждение столкновениями, возбуждение при рекомбинации и оригинальный механизм флуоресцентного возбуждения, основанный на случайном совпадении сильной линии испускания одного элемента с линией поглощения другого [6, 7]. Однако в ряде случаев эти механизмы до сих пор не дают объяснения аномалиям интенсивности линий в звездных спектрах.

В [17] обращено внимание на возможность объяснения некоторых аномально ярких эмиссионных линий эффектом стимулированного испускания излучения в атмосфере звезды за счет инверсной населенности оптических переходов. Рассмотрим наиболее типичные аномалии, которые объясняются в [7, 8]. В этих работах высказаны идеи, являющиеся, на мой взгляд, ранними предшественниками идей получения лазерной усиливающей среды в результате инверсии населенности уровней.

Известно аномальное поведение линий кислорода O I (7774 и 8446 Å) в спектрах звезд типа Be (ранние звезды спектрального класса Be с эмиссионными линиями) [23,25]. Отношение интенсивностей линий с $\lambda = 8446$ Å ($3p3P \rightarrow 3s3S0$) и 7774 Å ($3p5P0 \rightarrow 3s5S0$) намного больше лабораторного значения. Боуэн предположил [26], что это связано с явлением флуоресценции,

вызванной совпадением яркой линии Ly_β водорода HI (1025.72 Å) с линией поглощения OI на λ = 1025.77 Å (2p3P → 3d3D0). Схема рассматриваемых переходов OI приведена на рис.3,а. Если бы это предположение было верным, то в каскадном переходе была бы яркой линия не только с λ = 8446 Å, но и с λ = 11287 Å промежуточного перехода 3d3D0 → 3p3P. Однако ничего подобного для этой линии в звездных спектрах не наблюдается [23]. Кроме того, для объяснения наблюдаемых интенсивностей компонент сверхтонкой структуры линии с λ = 8446 Å в модели совпадения линий необходимо допускать сильное различие скоростей областей испускания и поглощения линии (до 85 км/с), такое, чтобы доплеровский сдвиг мог скомпенсировать различие частот линий испускания и поглощения [27].

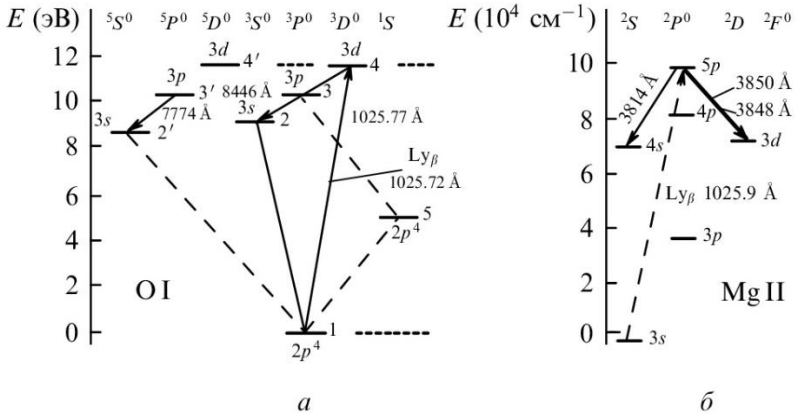


Рис. 3. Астрофизические схемы возбуждения уровня кислорода OI (*а*) и уровня Mg II (*б*) излучением Ly_β H I, объясняющие образование ярких линий O I (8446 Å) и Mg II (3848 Å)

Аномальное отношение интенсивностей можно объяснить возникновением стимулированного испускания при инверсии населенностей на переходе с λ = 8446 Å. Нижний уровень перехода 3s3S0 является более короткоживущим, чем верхний уровень 3p3P, и поэтому при умеренной накачке верхнего уровня достигается инверсия в стационарном режиме [17]. Лазерный эффект в атмосферах звезд и в туманностях (линии с λ = 8446 Å) рассмотрен в разделе 6.

Примером сходной аномалии являются линии Mg II с λ = 3848 и 3850 Å (5p2P0 → 3d2D) одного и того же мультиплета (рис. 3*б*). Первая линия бывает временами значительно более яркой [23, 28]. Делались попытки объяснить эту аномалию совпадением линии поглощения Mg II с λ = 1025.87 Å (3s2S → 5pP3/2) с линией испускания водорода Ly_β с λ = 1025.7 Å, но отсутствие аномалий на другой линии (3614 Å) с тем же верхним уровнем (5p2P0 → 4s2S) ставит под сомнение этот механизм [23].

Особенно многочисленны примеры аномалий интенсивности в спектрах долгопериодических переменных звезд поздних спектральных классов (M- и S-типа). Часто встречаются случаи, когда в испускании проявляются определенные мультиплеты, а относительные интенсивности линий отличаются от

лабораторных значений [29]. Примером может служить аномальное поведение линий In I (4101,72 и 4511 Å) на переходах между нижними термами (рис. 4*а*). Линия с λ = 4511 Å появляется преимущественно не в поглощении, а в испускании. Для того, чтобы объяснить такое поведение, привлекается механизм флуоресцентного возбуждения верхнего уровня 2S вследствие совпадения резонансной линии поглощения In I (4101,72 Å) с сильной линией испускания H_δ (4101,75 Å).

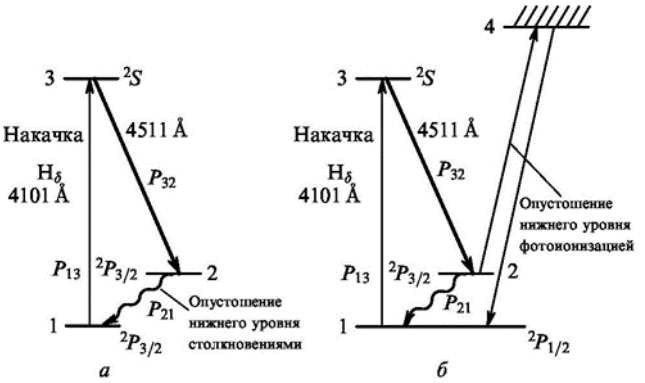


Рис. 4. Схемы циклических переходов в In I, рассмотренные в [8] для объяснения яркой эмиссионной линии 4511 Å при возбуждении линией H_δ (4101 Å), использующие столкновительное *(а)* и фотоионизационное (*б*) опустошения метастабильного уровня 2 ($^2P_{3/2}$)

На рис. 4*а* приведена схема переходов между тремя нижними уровнями In I под действием флуоресцентного возбуждения уровня 3 и непрерывного спектра, рассмотренная Таккераем еще в 1935 году [8]. Оказывается, что условие появления линии испускания, а не поглощения на переходе 3 → 2, найденное Таккераем, совпадает с условием инверсии. Действительно, пусть на резонансном переходе действует излучение с интенсивностью I13, а на аномальном переходе — с 123. Переход 2 → 1 запрещен, и в атоме невозможен циклический переход между состояниями 1, 2 и 3. Атом In имеет низкий потенциал ионизации (5,76 эВ), поэтому разумно включить в схему ионизованные атомы в состоянии 4. При условиях на вероятности переходов

$$P_{14} = P_{214}, P_{42} = 2\,P_{41}, P_{32} = P_{31}, \qquad (1)$$

учитывающих вырождение уровней и тот факт, что уровни 1 и 2 являются состояниями одного и того же терма, получим следующее выражение для населенности уровней n_i в стационарном состоянии:

$$n_1 \frac{P_{23}}{P_{23}+P_{24}} = n_2 \frac{P_{23}}{2(P_{23}+P_{24})} = n_3 P_{32}\left[2P_{13} + \frac{4}{3}P_{24} + \frac{2}{3}P_{13}\frac{P_{24}}{P_{23}}\right]^{-1}. \qquad (2)$$

Следовательно, отношение числа переходов с испусканием (3 → 2) и поглощением (2 → 3) фотонов на частоте ν_{23} есть [8]

$$\alpha = \frac{n_3 P_{32}}{n_2 P_{23}} = 1 + \frac{P_{24}(P_{13} - P_{23})}{3(P_{13} + P_{24})}. \qquad (3)$$

При $\alpha > 1$ образуется циклический переход $1 \to 3 \to 2 \to 4 \to 1$, за счет которого происходит преимущественное испускание излучения на переходе 3 → 2.

Заметим, что условие цикличности $\alpha > 1$ в направлении 3 → 2 одновременно является условием инверсии населенностей уровней 2 и 3:

$$\alpha = \frac{n_3 P_{32}}{n_2 P_{23}} = \frac{n_3 \sigma_{32}}{n_2 \sigma_{23}} = \frac{n_3}{g_3} \Big/ \frac{n_2}{g_2} > 1, \qquad (4)$$

где σ_{km} — сечение радиационного перехода k → m. Таким образом, механизм усиления излучения за счет стимулированного испускания уже давно неявно используется в теории звездных спектров для описания так называемых эмиссионных линий. Флуоресцентный механизм возбуждения Боуэна [6] (см. рис. 3) является, по-существу, астрофизическим аналогом трехуровневой схемы с оптической накачкой [30, 31]. Для объяснения аномалий в звездных спектрах астрофизиками были предложены схемы, предвосхитившие ряд лазерных схем. Например, на рис. 4*б* изображена схема переходов между нижними уровнями In I, также предложенная Таккераем [8] для объяснения эмиссионной линии с λ = 4511 Å. В этой схеме циклический переход 1 → 3 → 2 → 1 и, следовательно, инверсия населенностей состояний 3 и 2, достигается за счет быстрой столкновительной релаксации метастабильного уровня 2. Эта схема весьма схожа со схемой столкновительного лазера Гоулда [19].

Эмиссионные линии, обусловленные механизмом стимулированного излучения, должны быть уже эмиссионных линий, возникающих за счет спонтанного излучения. Сужение спектра может быть вполне достаточным для однозначного выбора механизма возникновения эмиссионной линии. Эта задача заслуживает более детального рассмотрения, учитывающего возможность существования большой оптической толщины для усиливающего перехода и резонансного рассеяния излучения. В принципе здесь возможны два режима работы: режим усиления излучения фотосферы и режим усиления собственного спонтанного излучения атмосферы. В первом случае мы имеем дело с узкополосным нелинейным лазерным усилителем внешнего широкополосного сигнала, а во втором — с резонансным лазерным усилителем спонтанного шума. В последнем случае неизбежное рассеяние излучения может легко превратить лазерный усилитель в генератор, если возвращение излучения в усиливающую область вследствие рассеяния превышает скорость ухода излучения в окружающее пространство. Тогда резонансное рассеяние приводит к возникновению в усиливающей среде некогерентной обратной связи по энергии [32, 33]. Такой эффект должен вызвать разбиение усиливающей области на множество отдельных областей, в каждой из которых достигнут порог генерации. Более

подробно эффект некогерентной обратной связи в астрофизическом лазере рассмотрен в [34, 35] (см. разд. 8).

4. Как проявляется лазерный эффект в астрофизических условиях?

Вслед за открытием космических мазеров в микроволновом диапазоне на радикале ОН [4] и молекуле H_2O [5] такие мазеры были обнаружены более чем на 100 молекулах [36], а затем на высоковозбужденных атомах водорода в миллиметровой области [37]. В ИК-области спектра (10 мкм) стимулированное излучение молекулы CO_2 было обнаружено в атмосферах Марса и Венеры [38, 39]. С лазерным эффектом всегда связывают высокую яркость излучения лабораторного лазера, тем более что это прекрасно демонстрируют астрофизические мазеры, работающие на микроволновых переходах молекул. Поскольку яркостная температура астрофизических мазеров необычайно велика (10^{12}–10^{18} К) [36], такая аналогия может оказаться ошибочной и привести к выводу о «лазерном эффекте» при наблюдении аномально высокой интенсивности и аномального отношения интенсивностей даже в отсутствие инверсии из-за неподходящего соотношения времен жизни квантовых уровней «лазерного» перехода [40]. В этом случае приходится искать другое, иногда весьма нетривиальное объяснение аномально высокой интенсивности [41] и аномального отношения интенсивностей спектральных линий [42].

Поясним «заблуждение» о высокой яркости лазерных линий в астрофизических условиях на примере сравнения астрофизического мазера в микроволновой области с астрофизическим лазером в оптической области с накачкой за счет механизма случайного совпадения спектральных линий (механизм Боуэна) [6]. Но сначала напомним о происхождении чрезвычайно высокой яркости излучения лазера. Хотя это рассмотрение тривиально, оно наглядно и полезно при сравнении лабораторного и астрофизических лазеров.

Активная среда лазера и до порога и после значительную долю энергии излучает изотропно и спонтанно во все моды окружающего пространства. Даже после заметного превышения порога доля изотропного спонтанного излучения остается сопоставимой с долей индуцированного излучения (рис. 5,а). После порога генерации населенность верхнего уровня остается фиксированной на пороговом уровне (непрерывный режим), а вся надпороговая энергия накачки расходуется на стимулированное излучение, которое, однако, происходит на ограниченном (особенно по углу) числе мод. Поэтому интенсивность направленного излучения, то есть лазерного луча, намного превышает интенсивность спонтанного излучения, попадающего в этот малый телесный угол (рис. 5*б*). В связи с этим наблюдаемая высокая интенсивность лазера связана с его малой расходимостью и с малым углом наблюдения (только в направлении распространения излучения лазера). В астрофизических условиях ситуация совершенно иная. Поскольку даже неполностью изотропное стимулированное излучение АФЛ заведомо происходит в большом телесном угле (даже в случае

рассеивающей обратной связи, см. разд. 7), оно не должно быть аномально ярким на фоне спонтанного излучения.



Рис. 5. Спонтанное и стимулированное излучение лазера, интегральное по направлению полной излучаемой мощности (*а*) и по мощности направленного излучения (*б*)

Возникает вопрос: а почему же излучение астрофизического мазера в микроволновом диапазоне так аномально ярко? Причина этого совершенно иная и обычно не обсуждается. На рис. 6 упрощенно показано происхождение излучения газового космического облака без инверсии и с инверсией на частоте микроволнового перехода ω_{21}.

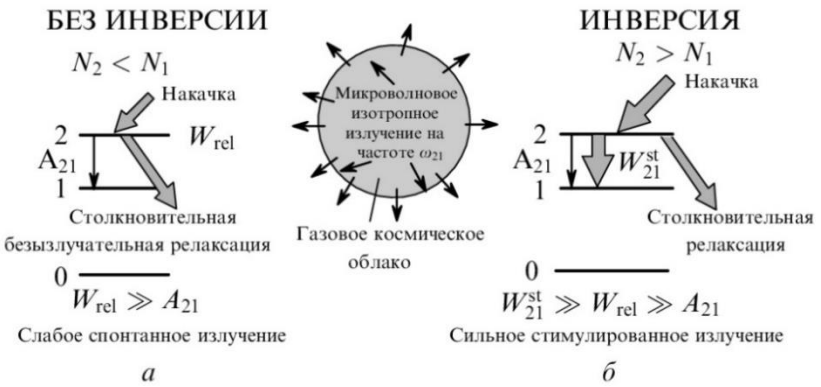


Рис. 6. Изотропное микроволновое излучение газового космического облака без инверсии (*а*) и в случае инверсии (*б*) перехода 2 → 1. Мощность накачки в отсутствие инверсии расходуется по ненаблюдаемому столкновительному каналу релаксации, а при ее наличии трансформируется в наблюдаемое интенсивное стимулированное микроволновое излучение

При отсутствии инверсии наблюдается очень слабое спонтанное микроволновое излучение, обусловленное крайней малостью коэффициента Эйнштейна в микроволновой области (A_{21} = 10^{-7}–10^{-9} $с^{-1}$), что соответствует времени

спонтанного распада 0,3 года —10 лет (!). Естественно, столкновения даже в разреженной межзвездной среде происходят чаще, и даже это слабое спонтанное излучение подавлено тушениями и основная энергия возбуждения (накачки) этого уровня деградирует по безызлучательному каналу, то есть не регистрируется наблюдателем. Если накачка достаточно интенсивна для возникновения инверсии на переходе 2 → 1, а размер газового облака L таков, что показатель усиления $\alpha L \gg 1$ способен обеспечить значительное усиление ($K = \exp \alpha L \backsimeq 10^{10} - 10^5$), то включается механизм стимулированного излучения. Поскольку скорость стимулированных переходов W_{21}^{st} может сравняться со скоростью столкновительной (ненаблюдаемой) релаксации возбуждения и даже превысить ее, то почти вся энергия накачки расходуется на наблюдаемое стимулированное излучение, которое может иметь громадную яркостную температуру. Другими словами, за счет мазерного эффекта ненаблюдаемая радиоастрономами слабая линия спонтанного излучения превращается в сильную линию стимулированного излучения, черпающего энергию из ненаблюдаемого канала. Таким образом, причина высокой яркости астрофизического лазера в том, что для его накачки не используется другое микроволновое излучение, которое является очень слабым.

Совершенно иная ситуация складывается для АФЛ в оптической области спектра (рис. 7). Пусть уровень 3 оптически возбуждается за счет другой спектральной линии какого-либо другого элемента (прямо или через высоколежащее состояние, распадающееся в состояние 3). В отсутствие инверсии в системе трех уровней (1, 2, 3) наблюдается, например, пара спектральных линий спонтанного излучения с отношением интенсивностей, равным отношению коэффициентов Эйнштейна A_{32} и A_{31}. Для наглядности на рис.7 переход 3 → 2 предполагается очень слабым ($A_{32} \ll A_{31}$) и, следовательно, почти вся энергия возбужденных на уровень 3 частиц релаксирует по каналу спонтанного излучения 3 → 1 с излучением спектральной линии на частоте ω_{31} с интенсивностью, практически равной интенсивности линии накачки уровня 3.

Пусть теперь время спонтанного распада τ_3 уровня 2, на который частицы с уровня 3 попадают сравнительно редко, гораздо меньше $1/A_{12}$, так что на переходах 3 → 2 всегда имеется инверсная населенность. Тогда переход 3 → 2 становится усиливающим, и при достаточном размере усиливающей области коэффициент усиления может превышать отношение скоростей спонтанного распада A_{31}/A_{32}. В этом случае скорость стимулированного перехода W_{32}^{st} может не только сравниться со скоростью спонтанного распада A_{31}, но и превысить ее. Основным каналом релаксации возбужденных на уровень 3 частиц является тогда канал стимулированного излучения на частоте ω_{32}. При этом интенсивность слабого перехода 3 → 2 возрастает и достигает интенсивности линии накачки уровня 3 (но не превышает ее).

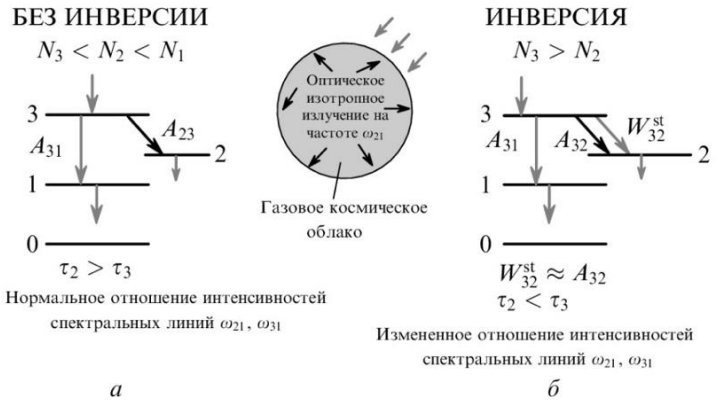


Рис. 7. Переход от режима спонтанного изотропного оптического излучения в среде без инверсии (*а*) к режиму спонтанного изотропного и стимулированного изотропного излучения в среде с инверсией (*б*)

Другими словами, лазерная линия стимулированного излучения не может быть ярче спонтанной линии, возбуждающей уровень 3. Поэтому критерий аномальной интенсивности лазерной линии по сравнению с другими яркими спектральными линиями переходов накачки неприменим для поиска лазерных линий. В этом заключается существенное отличие от мазерного случая, когда интенсивность накачки не связана с микроволновым излучением и потому может быть весьма велика. Трансформация энергии возбуждения в стимулированное микроволновое излучение делает его аномально ярким. Из этих простых качественных рассуждений ясно, что лазерный эффект должен проявляться в увеличении интенсивности очень слабых линий спонтанного излучения до уровня интенсивности линий спонтанного испускания на разрешенных переходах, то есть на переходах с малыми коэффициентами Эйнштейна ($A_{32} \simeq 1 - 10^5$ с-1).

Подчеркнем, что приведенные рассуждения относятся к случаю оптической накачки АФЛ, которая представляется наиболее вероятной для оптического диапазона. Не исключено, что существуют другие методы накачки, основанные на использовании столкновений, но следует иметь в виду, что скорость спонтанной релаксации даже метастабильных уровней очень велика по сравнению с их скоростью в микроволновом диапазоне. Это делает возможность столкновительной накачки с возникновением инверсии для оптических переходов менее вероятной, чем чисто оптическое возбуждение вследствие совпадения спектральных линий испускания и поглощения двух разных частиц.

5. Астрофизический лазер на Fe II в области газовой конденсации вблизи горячей звезды

Окрестность яркой звезды является уникальным местом, в котором атомы водорода (наиболее распространенного элемента Вселенной) в условиях глубокого

вакуума фотоионизуются под действием ВУФ излучения звезды (излучение континуума Лаймана с $\lambda < \lambda_c = 912$ Å). Образующиеся свободные протоны и электроны при последующих редких столкновениях рекомбинируют, излучая характерные спектральные линии H I, причем 70 % излучаемой энергии приходится на наиболее интенсивную линию Ly_α с $\lambda = 1215$ Å. На Земле эта спектральная линия не наблюдается из-за поглощения межзвездным водородом ультранизкой концентрации. Однако существенная роль интенсивного излучения линии Ly_α проявляется в эффектах, возникающих под его действием, в частности, при резонансном фотовозбуждении атомов и ионов других, более редких элементов. Именно в результате этого возникает лазерный эффект в области компактной газовой конденсации в окрестности звезды η Car [18].

Возможность использования резонансного оптического возбуждения накачки одного химического элемента излучением другого с целью создания инверсной населенности и лабораторного оптического лазера была рассмотрена еще в первой статье, в которой был предложен лазер [43]. Такое совпадение спектральных линий — довольно редкое явление из-за малой ширины спектральных линий свободных атомов и ионов, которое практически не используется в современных лазерах. Однако оно лежит в основе механизма образования некоторых спектральных линий туманностей, являющихся смесью многих атомов и ионов, облучаемых интенсивными спектральными линиями водорода и гелия [6]. Возможность лазерного эффекта за счет этого механизма также рассматривалась довольно давно [17], но этот эффект трудно наблюдаем на фоне интенсивного излучения самой фотосферы звезды.

Ситуация радикально изменилась с созданием космического телескопа Хаббл (HST) в сочетании со спектрографом STIS (Space Telescope Imaging Spectrograph), обеспечивающим высокое спектральное и угловое (~0.1") разрешение в широкой области спектра (1150–10400 Å) [44]. Замечательным объектом наблюдений начиная с 1998 года стала эруптивная звезда η Car [45]. Эта звезда является исключительно интересным астрономическим объектом, эжектирующим в результате многих взрывов в окружающее пространство громадное количество звездного вещества. В частности, после мощного взрыва в 1840 году эта звезда была второй по яркости на небесном своде Южного полушария. Выброшенное вещество образовало громадное (8" x 16") окружение звезды, названное Homunculus. Эта очень неоднородная и структурированная туманность является удивительным объектом нашей Галактики. В частности, в ближайшей окрестности центральной звезды (на расстоянии R_b = 100–1000 радиусов ее фотосферы) обнаружены компактные газовые конденсации (ГК) с исключительно яркими некоторыми линиями Fe II, открытые Вейгельтом и др. [46]. Эти конденсации также являются уникальными астрофизическими объектами, так как концентрация водорода в них ($N_H = 10^7$–10^{10} см$^{-3}$) [47] гораздо больше концентрации в типичной планетарной туманности (10^4 см$^{-3}$), а расположены они всего в нескольких световых днях от центральной звезды.

Из-за относительно высокой локальной концентрации водорода в ГК излучение континуума Лаймана звезды η Car почти полностью поглощается в них. Другими словами, граница Стромгрена [48], отделяющая область полностью

ионизованного водорода от области нейтрального водорода, проходит внутри ГК, как это схематично показано на рис. 8, то есть полностью ионизованная передняя часть (область H II) ГК непосредственно примыкает к нейтральной области H I. Спектральная интенсивность Ly_α-излучения, генерируемого в области H II в результате фотоионизационно-рекомбинационного цикла, в 10^3–10^4 раз больше интенсивности ослабленного излучения Ly_α, приходящего от центральной звезды. Это происходит вследствие существенной компенсации эффекта ослабления излучения звезды благодаря узости образуемого Ly_α-излучения при поглощении широкополосного континуума Лаймана и в некоторой степени — за счет пленения Ly_α в оптически плотной (для Ly_α) среде H II. В результате возникает уникальная ситуация, когда слабоионизованная смесь многих легкофотоионизуемых атомов в нейтральной области H I подвергается облучению излучением с высокой спектральной интенсивностью на длине волны Ly_α из соседней полностью ионизованной области. (Это напоминает типичную «лазерную» ситуацию, когда лампа накачки облучает находящуюся рядом активную среду лазера!) В тоже время высокое угловое разрешение HST/STIS позволяет наблюдать спектры излучения ГК отдельно от яркого излучения фотосферы центральной звезды η Car [49].

Из-за высокой плотности водорода излучение континуума Лаймана ($\lambda < 912$ Å) полностью поглощается в передней части ГК за счет фотоионизации водорода (рис. 8), и примерно 70 % этого излучения переиспускается в процессе рекомбинации на длине волны $\lambda = 1215$ Å (α -линия Лаймана). Это монохроматическое излучение сильно уширяется в процессе переноса излучения в оптически плотной нейтральной области H I ГК и способно возбуждать ряд квантовых переходов иона Fe II в неионизованной (задней) части ГК, как это показано на рис. 8. Ионы Fe II возникают за счет фотоионизации Fe с концентрацией примерно $10^{-4}\ N_{\mathrm{H}}$ излучением звезды в области $\lambda > 912$ Å; это излучение свободно проходит через фотоионизованную переднюю часть ГК.

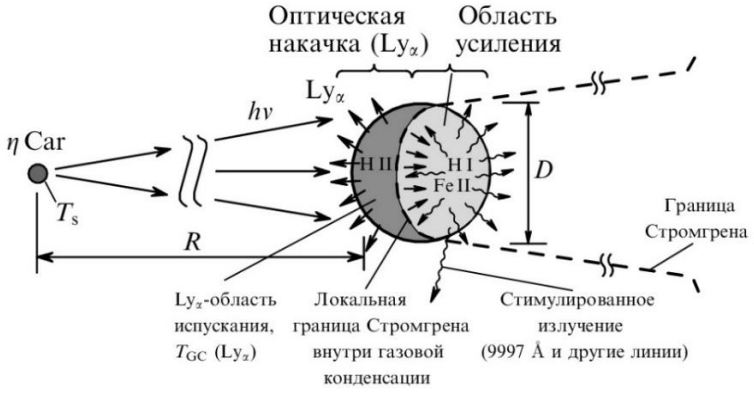


Рис. 8. Фотофизическая модель компактной газовой конденсации (ГК) вблизи горячей яркой звезды η Car с локальной границей Стромгрена между фотоионизованной (H II) и нейтральной (H I) областями внутри ГК [18]

Ионы FeII имеют богатый спектр квантовых переходов. Плотность линий поглощения FeII в области Ly_α составляет около 15 линий на 1Å. При диффузии излучения Ly_α в резонансно рассеивающей области HI с большой оптической плотностью в случае переноса излучения Ly_α происходит значительное (до сотен см$^{-1}$) уширение линий. В результате такого уширения ионы FeII фотовозбуждаются на высокие квантовые уровни [50]. Это проявляется в появлении линий флуоресценции Fe II, которые могут быть весьма яркими, как, например, FeII-линии УФ-флуоресценции (2507, 2509 Å) [51]. На рис. 9*а* показана схема возбуждения излучением линии Ly_α с λ=1215.671 Å перехода 1 → 4 Fe II [18]. Частотная расстройка $\Delta\nu$ составляет всего 30 см$^{-1}$ и компенсируется сильным уширением линии Ly_α (до 300 см$^{-1}$) в процессе переноса излучения. Главный канал распада состояния 4 — это радиационный распад в состояние 3, которое имеет довольно малый коэффициент Эйнштейна ($A_{21} \simeq 8 \times 10^4$ с$^{-1}$). Поскольку уровень 2 (рис. 9*а*) распадается очень быстро, то на переходе 3 → 2 всегда есть инверсия, так что уровень 3 является «узким горлом» радиационной релаксации высоковозбужденного Fe II.

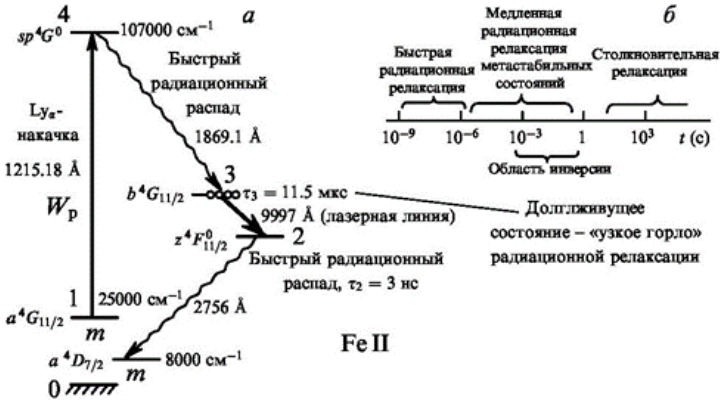


Рис. 9. Образование инверсной населенности на переходе 3 → 2 Fe II за счет резонансного фотовозбуждения высоколежащего уровня 4 и последующего каскадного радиационного распада на долгоживущий «псевдометастабильный» уровень — схема инверсии уровней и переходов (*а*) и характерные времена радиационной и столкновительной релаксации возбужденных уровней Fe II[18] (*б*)

Приведем простые оценки коэффициента усиления α_{32} в рамках рассмотренной в [41] модели фотопроцессов в ГК в близкой окрестности звезды звезды η Car. Скорость фотоселективного возбуждения состояния 4 определяется выражением

$$W_{\rm p}^{14} = A_{41}\left[\exp\left(\frac{h\nu_{14}}{T_{\rm GC}}\right) - 1\right]^{-1}, \qquad (5)$$

где A_{41} = 1,2 × 107 с$^{-1}$ — коэффициент Эйнштейна для спонтанного распада состояния 4 в состояние 1; $T_{\rm GC}$ — яркостная температура излучения Ly_α внутри

ГК. Для $kT_{\mathrm{GC}} \backsimeq$ 1,0–1,5 эВ ($T_{\mathrm{GC}} \backsimeq (12–18) \times 10^3$ К) скорость возбуждения $W_{\mathrm{p}}^{14} \backsimeq 10^3 – 10^4$ с$^{-1}$.

Основным каналом распада (97%) состояния 4 является радиационный переход на два уровня тонкой структуры b4G, один из которых (b4G11/2)-уровень состояния 3) имеет канал спонтанного радиационного распада с вероятностью $A_{32} = 8 \times 10^4$ с$^{-1}$ в состояние 2 ($z4F_{9/2}^0$) с малым временем жизни (~3 нс). Именно на переходе 3 → 2 возникает стационарная инверсная населенность уровней с плотностью ΔN:

$$\Delta N = N_3 - N_2 = N_3 = \left(W_{\mathrm{p}}^{14}\tau_3\right)N_1, \#(6)$$

где $N_2 \ll N_3$ из-за быстрого распада уровня 2; τ_3 = 11.5 мкс ; N_1 — плотность населенности начального метастабильного уровня с временем жизни $\tau_1 \backsimeq 0{,}77$ с $\gg \tau_3$.

Линейный коэффициент усиления на переходе 3 → 2 (λ = 9997 Å) определяется стандартным выражением:

$$\alpha_{32} = \sigma_{32}\Delta N, \quad (7)$$

где ΔN —плотность инверсной населенности, определяемая выражением (6). Сечение стимулированного перехода σ_{32} дается следующим выражением:

$$\sigma_{32} = \frac{\lambda_{32}^2}{2\pi}\frac{A_{32}}{2\pi\Delta\nu_{\mathrm{D}}}, \quad (8)$$

где $\Delta\nu_{\mathrm{D}}$ — доплеровская ширина перехода 3 → 2 Fe II. При температуре относительно холодной H I-области 100 — 1000 К ширина $\Delta\nu_{\mathrm{D}} \backsimeq$ 300 — 1000 МГц, то есть $\sigma_{32} \backsimeq (0{,}6 - 2) \times 10^{-13}$ см^2. Таким образом, коэффициент усиления может быть оценен следующим выражением:

$$\alpha_{32} = \sigma_{32}\left(W_{\mathrm{p}}^{14}\tau_3\right)fN_0, \quad (9)$$

где f — доля ионов FeII в начальном метастабильном состоянии по отношению ко всем остальным состояниям Fe II (все атомы FeI в области HI фотоионизованы).

Доля ионов f определяется скоростью возбуждения уровня 1 и временем его распада. Скорости столкновительных механизмов возбуждения уровня 1 (то есть рекомбинация ионов Fe_2^+ и столкновения Fe^+ с электронами) пренебрежимо малы по сравнению со скоростью распада $1/\tau_1$, поскольку вследствие фотоионизации атомов железа и других элементов с потенциалом ионизации I < 13,6 эВ концентрация электронов в области HI мала ($n_e \backsimeq 10^4 - 10^5$ см$^{-3}$).

Для заселения уровня 1 наиболее существенны каналы радиационного возбуждения широкой линией Ly_α других переходов, начинающихся с самых

нижних, более заселенных метастабильных уровней (с энергией ~ 1 эВ), при распаде которых происходит заселение уже более высоких (с энергией 2–3 эВ) низколежащих метастабильных и псевдометастабильных уровней. Эти каналы радиационного возбуждения могут обеспечивать скорость возбуждения уровня 1 порядка $1/\tau_1 \sim 1$ с$^{-1}$ и, следовательно, поддерживать относительную населенность f состояния 1 равной, например, ~10^{-2}. Это соответствует примерно одинаковому распределению ионов FeII среди 90 метастабильных и псевдометастабильных состояний, включая состояние 1. Справедливость данной оценки подтверждается наблюдением сильных линий флуоресценции FeII (2507 и 2509 Å) [51], которые возникают при селективном возбуждении линией Ly_α перехода, нижний уровень которого ($a^4D_{7/2}$) имеет энергию 0,99 эВ.

Согласно (9), в рамках таких предположений коэффициент линейного усиления на переходе 3–2 $\alpha_{32} \backsimeq (3 \times 10^{-18} - 10^{-16})N_0$, где $N_0 \backsimeq 10^{-4}N_H$ — плотность атомов железа, конвертированных в Fe II. В соответствии с данными работы [41] и результатами вычислений критической плотности атомов водорода в ГК [41], концентрация N_H в ГК, очевидно, выше 108 см-3. Таким образом, при $\alpha > 3 \times 10^{-14} - 10^{-12}$ см-1 и размере ГК $D \backsimeq 10^{15}$ [47], который можно принять в качестве размера усиливающей области (см. рис.8), $\alpha L \backsimeq 30 - 1000$ при температуре излучения линии Ly_α в ГК T_{GC} = (12–18) × 10^3 К.

Это соответствует довольно высоким значениям коэффициента линейного усиления $K = \exp \alpha_{32} L$. Однако при $K \backsimeq A_{43}/A_{42} \backsimeq 10^3$ интенсивность изотропного излучения на слабой линии λ_{32} приближается к интенсивности линии λ_{43}, обеспечивающей возбуждение уровня 3, то есть происходит истощение накачки. Другими словами, режим усиления становится насыщенным, а интенсивность слабой линии λ_{32} становится сравнимой с интенсивностью линии λ_{43}, то есть ее интенсивность (измеряемая в фот.·см$^{-2}$·с$^{-1}$) повышается в $A_{43}/A_{32} \backsimeq 10^3$ раз. Именно такой эффект наблюдается для ряда слабых линий Fe II по данным [49, 52].

Лазерное усиление и стимулированное излучение в оптическом диапазоне являются, вероятно, весьма распространенными процессами в газовых средах вблизи ярких звезд. Они возникают за счет особенностей релаксации возбуждения электронных уровней атомов (ионов) в разреженном около- или межзвездном газе. Процессы релаксации имеют различные характерные времена (см. рис. 9*б*). Радиационная релаксация, обусловленная спонтанным излучением, происходит в течение 10^{-9}–10^{-3} с (иногда даже 10^{-3} –1 с), а столкновительная релаксация длится более 100 с (при плотности газа менее 10^9 см$^{-3}$). В случае избирательного возбуждения атома (иона) со сложной структурой электронных уровней радиационная спонтанная релаксация в изолированном атоме (ионе) происходит чисто радиационным путем без участия столкновений с образованием на какой-то паре уровней инверсии из-за эффекта «узкого горла». Если размер ГК достаточен для значительного усиления на инверсном подходе, то включается механизм более быстрой излучательной релаксации, вызванной стимулированным излучением. Таким образом, лазерный эффект является механизмом радиационного охлаждения за счет стимулированного излучения ГК на инвертированных переходах наряду со спонтанным излучением на обычных переходах без инверсии населенностей.

6. Астрофизический лазер на атомах кислорода

В разд. 3 была упомянута необъясненная аномалия поведения линий кислорода с λ = 8446 и 7774 Å в спектрах звезд Be-типа [23, 25], которая естественно объясняется стимулированным излучением на инверсионном переходе с λ = 8446 Å [17] при накачке верхнего уровня яркой линией водорода H I Ly_β с λ = 1025,72 Å по схеме Боуэна [26], показанной на рис. 3*а*. Более того, на линии 8446 Å в лабораторных условиях Беннетом и др. получено лазерное действие в непрерывном режиме [53]. Инверсия достигается при электрическом разряде в смеси кислорода и благородного газа с небольшим давлением. Сходные условия вполне достижимы в атмосферах звезд. Лазерный механизм естественно объясняет нормальную интенсивность линии с λ = 7774 Å. Действительно, нижний уровень перехода данной линии метастабилен и возникновение инверсии и усиления на этом переходе невозможно. Детальный анализ возникновения инверсии населенностей и коэффициент усиления на переходе OI 3p3P → 3sSS в атмосферах звезд спектрального типа Be был представлен в [34].

Из схемы переходов на рис. 3*а* видно, что она совпадает со схемой четырехуровневого генератора и, что, благодаря удачному соотношению вероятностей спонтанных переходов A_{ij} между уровнями 3 → 2 и 2 → 1 (вероятности спонтанных переходов, рассчитанные по методу [54], и кратности вырождения уровней таковы: $A_{21} \backsimeq 5 \times 10^8$ с$^{-1}$, $A_{32} \backsimeq A_{43} \backsimeq A_{41} \backsimeq A_{4\prime1\prime} \backsimeq A_{3\prime2\prime} \backsimeq 3 \times 10^7$ с$^{-1}$, $A_{2\prime1\prime} = 10^5$ с$^{-1}$, $A_{4\prime3\prime} = 2 \times 10^6$ с$^{-1}$; g1 = 9, g2 = 3, g3 = 9, g4 = 15) на переходе 3 → 2 вполне может возникнуть инверсная населенность.

Пусть газ, состоящий из атомов кислорода с плотностью N_0 и температурой T_0, находится в поле излучения со спектральной плотностью U и частотой $\omega \approx \omega_{41}$. Уравнения баланса для населенностей в стационарном случае приведены в [34]. Как известно, в четырехуровневых лазерах существенное влияние на пороговый уровень накачки оказывает населенность уровня 2, которая зависит от температуры излучения, действующего на переходе 1 → 2 (в рассматриваемом случае безызлучательные переходы дают малый вклад). Если бы газ находился в равновесии с излучением, то температура излучения совпадала бы с температурой газа T_0. Однако в звездных атмосферах присутствует более горячее излучение, идущее от фотосферы, которое характеризуется температурой T, заметно превышающей T_0.

Плотность атомов O I в области атмосферы, расположенной близко к внешней границе фотосферы (в обращающем слое), есть $N_0 \sim 10^5 - 10^6$ см$^{-3}$, температура газа здесь $T_0 \sim 1{,}5 \times 10^4$ К, а эффективная температура фотосферы $T_* \sim 3 \times 10^4$ К [55,56]. Если принять, что температура излучения на переходе 1 → 2 равна $\sim T_*$, то, как следует из анализа в [34], необходимая яркостная температура флуоресцентной накачки на пороге должна составлять 4 x 10^4 К, а для получения инверсной населенности, например, ΔN_{32} она должна превышать это значение ($\sim 4{,}1 \times 10^4$ К).

Помимо оптической накачки оценивался вклад, который вносят столкновения с электронами в инверсию уровней 2 и 3 (возбуждение уровня 3 через

метастабильный уровень на рис. 3*а*). При действии излучения с температурой T_*, на переходе $1 \rightarrow 2$ и в отсутствие излучения на других переходах инверсия за счет этого механизма не достигается.

Теперь можно оценить возможное значение коэффициента усиления α для линии O I (8446 Å) в атмосферах звезд Be-типа. Для $A_{32} = 3 \times 10^7$ с$^{-1}$ и $\Delta\omega_D \simeq 5 \times 10^{10}$ с$^{-1}$ сечение радиационного перехода $3 \rightarrow 2$, согласно (8), $\sigma_{32} \simeq 10^{-12}$ см^2. При $\Delta N_{32} \simeq 1$ см$^{-3}$ это соответствует коэффициенту усиления в центре линии $\alpha_{32} \simeq 10^{-12}$ см$^{-1}$. Учитывая, что в звездах Be-типа протяженность атмосфер составляет 10^{13}–10^{14} см [55, 56], можно заключить, что в атмосфере звезды возникает инверсная населенность с показателем линейного усиления $\alpha L \simeq 10 - 100$.

Отметим возможность оптического возбуждения фотосферы непрерывным излучением без резонансного совпадения. При этом для получения инверсной населенности на каком-либо переходе необходимо, чтобы спектр такого непрерывного излучения был неравновесным. Мустелем [57] показано, что непрерывный спектр фотосферы может сильно отличаться от планковского распределения. Хотя в рассматриваемом конкретном примере OI указанной неравновесности в спектре оказывается недостаточно для возникновения инверсии населенности на переходе $3 \rightarrow 2$, ее следует иметь в виду при расчете других астрофизических ситуаций, в которых газовая околозвездная среда оказывается в сильно пространственно и радиационно неоднородных условиях. Среди них в первую очередь надо отметить симбиотические звезды, в которых коротковолновое излучение горячей звезды облучает атмосферу более холодной звезды. В этих условиях могут наблюдаться лазерные эффекты на многих атомах и ионах.

Другой потенциальной областью возникновения инверсии и усиления, в частности, на линии OI с λ = 8446 Å, является пограничная область Стромгрена, отделяющая ионизованную среду H II от почти нейтральной среды H I. В этой пограничной зоне яркая линия Ly_β области H I, генерируемая в область H II, облучает область H I, где кислород находится в нейтральном состоянии, так как граница потенциала фотоионизации линии O I ($I_{\text{O I}} = 13{,}618$ эВ) лежит выше границы излучения континуума Лаймана (13,5985 эВ). В этих условиях нейтральный кислород должен эффективно возбуждаться линией Ly_β именно в сравнительно тонкой пограничной области Стомгрена. Поэтому представляется весьма вероятным, что наблюдавшееся в работе [58] странное поведение линии OI (8446 Å) в туманности Ориона может быть результатом лазерного эффекта. В этой работе обнаружена уникальная интенсивная структура в переходной области H II/H I только при наблюдении высокоинтенсивной спектральной линии с λ = 8446 Å. На других линиях O I и на линии Бальмера H_α(а она должна присутствовать в областях интенсивной линии Ly_β) излучение имеет пространственно-аморфную структуру без каких-либо нитей.

Для объяснения этого уникального факта авторы [58] высказали гипотезу о существовании в данной переходной области твердых частиц, которые неким

образом влияют на морфологию и спектр излучения O I, и отметили необходимость дальнейшего изучения этой странной ситуации. Тщательная спектроскопия высокого разрешения с использованием интерферометра Фабри —Перо позволила авторам [58] наблюдать примерно 25%-ное сужение относительной ширины линии 8446 Å по сравнению с шириной другой линии (6300 Å). Мне представляется, что вся совокупность наблюдений может иметь более естественное объяснение на основе усиления на переходе с $\lambda = 8446$ Å, на котором определенно должна существовать инверсия. Особого внимания заслуживает тот удивительный факт, что в туманности Ориона наблюдается точечный (неидентифицированный) источник излучения («излучающий объект» [59]), который не наблюдается на линии с $\lambda = 8446$ Å (!). Это наводит на мысль о возможности анизотропной диаграммы направленности усиливающей интенсивность области, максимум которой не направлен к наблюдателю. Такая возможность должна стать предметом специальных наблюдений с помощью HTS/STIS.

7. Диаграмма направленности и спектр излучения усиливающей области

В отсутствие обратной связи (см. разд. 8) усиливающая среда астрофизического лазера представляет собой насыщенный усилитель спонтанного излучения. Этот тип лазерного устройства наиболее известен в квантовой электронике ВУФ и рентгеновского диапазонов, где трудно создать резонаторную обратную связь из-за кратковременности усиления и/или попутного с импульсной накачкой распространения зоны усиления. В астрофизических условиях мы имеем дело с непрерывным режимом такого насыщенного усилителя. Из-за больших размеров астрофизической области усиления всегда выполняется условие

$$\frac{a}{L} \gg \frac{\lambda}{a}, \tag{10}$$

где a, L — поперечный и продольный размеры области усиления, так что диаграмма направленности определяется геометрией усиливающей области. При близкой к сферической геометрии ($a \simeq L$) излучение должно иметь изотропный характер. Последнее утверждение, строго говоря, относится к линейному режиму усиления. В режиме насыщенного усиления небольшое отклонение от сферичности должно подчеркиваться, и из эвристических соображений можно предположить существование своеобразной нестабильности сферической геометрии излучения насыщенного усилителя. Однако этот вопрос требует отдельного рассмотрения. Так как возможность образования сферических областей усиления даже в пограничных астрофизических областях, где наиболее вероятно возникновение инверсии, весьма мала (хотя и не равна нулю), то, скорее всего, образование анизотропных диаграмм стимулированного излучения будет зависеть от геометрии областей усиления, хотя направленность таких

диаграмм вряд ли может быть острой. Последнее замечание существенно для качественного объяснения спектра излучения насыщенного усилителя в условиях, когда линия усиления уширена неоднородно из-за эффекта Доплера.

В режиме линейного усиления спонтанного излучения ширина его спектра сокращается из-за преимущественного усиления излучения в центре линии по простому закону [60–63]:

$$I = \frac{I_0(\nu)}{(1 + \alpha L)^{1/2}}, \tag{11}$$

где α — коэффициент усиления на единицу длины (см$^{-1}$). Это происходит до тех пор, пока не наступает насыщение неоднородно-уширенной линии усиления с «уплощением» ее вершины. Данный эффект был рассмотрен для астрофизического лазерного насыщенного усилителя, и был сделан вывод [62], что в насыщенном режиме сужение спектра прекращается и происходит его обратное уширение до ширины линии усиления, как это показано качественно на рис. 10. Этот вывод подтверждается многочисленными экспериментальными данными для астрофизических мазеров [1, 64–66] за одним исключением. В работе [66] наблюдался аномально узкий спектр излучения ОН мазера с λ = 18,5 см, ширина которого соответствовала доплеровской ширине при температуре $T \simeq 5$ К. Этот феномен не получил объяснения до сих пор. В [35] было обращено внимание на то, что вывод работы [62] относится только к случаю направленного излучения, когда насыщение доплеровского контура происходит с уплощением его вершины. В действительности под действием изотропного излучения насыщение доплеровского контура не сопровождается деформацией, то есть происходит однородно [68] (рис. 11), а сужение линии изотропного излучения не сопровождается уширением и должно подчиняться закону (11). В этом, вероятно, состоит объяснение аномальной узости спектра мазерной линии ОН в [67]. Тот факт, что данный случай весьма редкий, служит подтверждением того, что близкая к сферической геометрия усиливающей области также является редким событием.

В оптическом диапазоне разрешающая способность спектрометров как наземных, так и космических телескопов не превышает $R = \nu/\Delta\nu \simeq 2 \times 10^5$, то есть оказывается порядка доплеровской ширины спектральных линий излучения из областей с кинетическими температурами менее 10000 К. Поэтому, в отличие от астрофизического мазера (АФМ), экспериментальные возможности исследования АФЛ в настоящее время гораздо ограниченнее (см. разд. 9).



Рис. 10. Эволюция ширины спектра спонтанного излучения в насыщенном усилителе на доплеровски уширенном переходе для сферически-изотропного излучения сферического усилителя и направленного излучения вытянутого усилителя

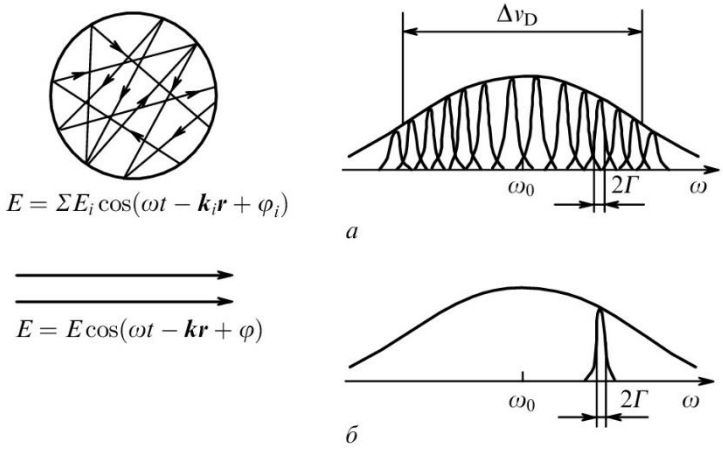


Рис. 11. Взаимодействие монохроматического изотропного (*а*) и направленного (*б*) излучения с доплеровски уширенным контуром. Изотропное излучение не «выжигает» дырки в контуре, и поэтому происходит насыщение всего доплеровского контура без деформации [68]

8. Обратная связь из-за рассеяния в АФЛ

В квантовой электронике обычно используется положительная обратная связь с помощью резонатора Фабри — Перо [43, 69] (рис. 12*а*) или его модификаций. Оптический открытый резонатор выполняет, по-существу, две функции: возвращения определенной доли энергии излучения активной среды обратно в нее и формирования довольно небольшого числа (по сравнению с огромным числом в объеме $V \gg \lambda^3$) стабильных конфигураций электромагнитного поля за счет конструктивной интерференции падающих и отраженных волн в элементах резонатора. Однако положительная обратная связь возможна только по энергии, а не по фазе, то есть без установления в активной среде стабильной конфигурации электромагнитного поля и без образования небольшого числа резонансных мод. Эта возможность была продемонстрирована в

экспериментах, проведенных под руководством Н.Г. Басова еще в середине 60-х годов [70–72], в которых кристалл рубина с высоким коэффициентом усиления на проход помещался между рассеивающими поверхностями (рис. 12*б*). При достаточно большом усилении кристалла на проход ($K \gg 1$) даже небольшой доли энергии ($\Omega_0/2\pi \ll 1$), возвращаемой из-за рассеяния в телесный угол Ω_0 усиливающей среды (т. е. при $K(\Omega_0/2\pi) > 1$), возникает генерация. Лазер, работающий в таком режиме, назван лазером с нерезонансной (или, точнее, некогерентной) обратной связью. Эта терминология отражает отсутствие пространственной когерентности генерируемого излучения, которое достигается при выполнении двух условий:

$$V \gg \lambda^3, \qquad \frac{a}{L} \gg \frac{\lambda}{a}, \tag{12}$$

где V и a / L — объем и угловой раствор генерируемого излучения в усиливающей среде соответственно. При выполнении условия (12) в пределах даже узкой линии усиления активной среды лежит громадное число (10^9 и более) пространственных мод низкой и практически одинаковой добротности, которые перекрываются между собой, создавая частотно-независимую (нерезонансную) добротность в такой рассеивающей полости (рис. 12*б*). Единственным резонансным элементом в подобном лазере остается резонансная линия усиления, и поэтому спектр генерации медленно стягивается к центру линии усиления [72]. Статистические свойства излучения такого лазера, разумеется, не соответствуют характеристикам когерентного света и близки к свойствам излучения очень яркого «черного тела» в узкой полосе частот, как это было показано экспериментально и теоретически [72].

Идея некогерентной рассеивающей обратной связи была распространена на более общий случай одновременно усиливающей и рассеивающей по объему среды [73], которая также обладает порогом генерации, эффектом сужения спектра излучения и т.д., то есть многими характеристиками лазера за исключением пространственной когерентности. Статистика излучения такого рассеивающего лазера соответствует статистике равновесного излучения с высокой температурой [74]. Осуществлены многочисленные эксперименты по реализации рассеивающего лазера на растворах красителей [75], в том числе микролазеров на рассеивающих частицах [76]. В последнем случае условие (12) находится на грани выполнения, и потому флуктуационные эффекты при интерференции сравнительно небольшого числа пространственных мод становятся заметными. Однако для астрофизических сред, имеющих громадный объем, эти эффекты не играют какой-либо роли.

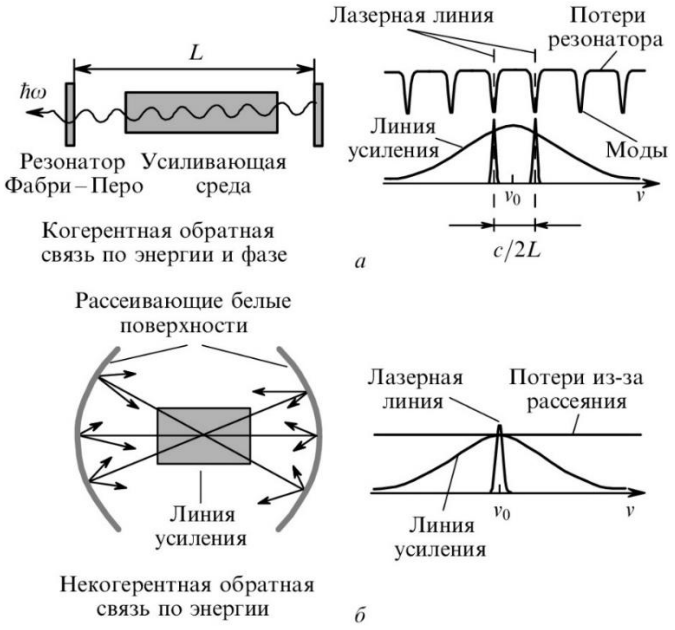


Рис. 12. Когерентная обратная связь по фазе и энергии, обеспечиваемая открытым резонатором Фабри — Перо (*а*), и некогерентная обратная связь по энергии за счет рассеивающих отражателей (*б*)

Возможность превращения астрофизического усилителя в АФМ за счет резонансного рассеяния была рассмотрена еще в [77], в частности, для усиливающих H_2O-областей. Экспериментальные данные [78] свидетельствуют, что этот эффект может действительно объяснить мерцание H_2O-мазеров. Для случая лазеров роль рассеяния в конверсии АФЛ-усилителя в лазер была детально рассмотрена в [34].

Здесь, строго говоря, надо выделить три типа рассеяния: 1) нерезонансное рассеяние на электронах с большим доплеровским случайным сдвигом частоты, величина которого значительно превышает доплеровскую ширину линии усиления (рис. 13*а*), 2) резонансное рассеяние на самих усиливающих частицах со случайным доплеровским сдвигом на величину порядка ширины линии усиления (рис. 13*б*) и 3) нерезонансное рассеяние на микрочастицах, тепловая скорость движения которых гораздо меньше атомных скоростей и поэтому вызывает малое доплеровское уширение при рассеянии (рис. 13*а*).

Первый случай малоэффективен для обратной связи из-за малой доли рассеивающих квантов, возвращающихся в пределы контура линии резонансного усиления. Второй случай вполне пригоден для обратной связи, но сужение линии генерации может происходить по закону (11). Под αL в этом случае надо подразумевать показатель усиления на среднем пути пробега фотона до его рассеяния, так как при рассеянии доплеровский сдвиг уширяет линию опять-таки до доплеровской ширины. В третьем случае сужение линии излучения из-за обратной связи может быть весьма значительным. Именно к этому случаю

относятся расчеты сужения линии излучения в АФЛ с рассеивающей обратной связью, проведенные в [34], так как в этой работе не принято во внимание доплеровское уширение при рассеянии.

Усиливающая среда с рассеянием обладает пороговым (критическим) радиусом, при котором доля фотонов, покидающих область усиления из-за рассеяния, точно компенсируется долей фотонов, рождающихся вследствие усиления [75]. Этот радиус аналогичен критическому радиусу нейтронного реактора, в котором нейтроны как размножаются, так и покидают реактор из-за рассеяния. Расчет критического радиуса АФЛ с рассеянием дан в [34]. Для случая лазера на линии OI (8446 Å) в атмосфере звезды Be-типа величина $r_{cr} \backsimeq 10^{11}$ см, что существенно меньше диаметра фотосферы звезд этого класса. Следовательно, в области усиления большего размера ($L \gg r_{cr}$) может возникать множество независимо действующих АФЛ с обратной связью из-за резонансного рассеяния.

Переход АФЛ-усилителя в АФЛ-генератор влияет не только на ширину линии излучения, но и на динамику генерации. Например, внезапное изменение скорости накачки Wp по-разному влияет на отклик усилителя и генератора, как это качественно показано на рис. 14. Конечно, характерные времена этих изменений лежат в области времен L/c, которые в астрофизических условиях могут составлять от минут до месяцев. Будущие более детальные наблюдения дадут, вероятно, ответ о действительной роли рассеивающей обратной связи в АФЛ и АФМ.

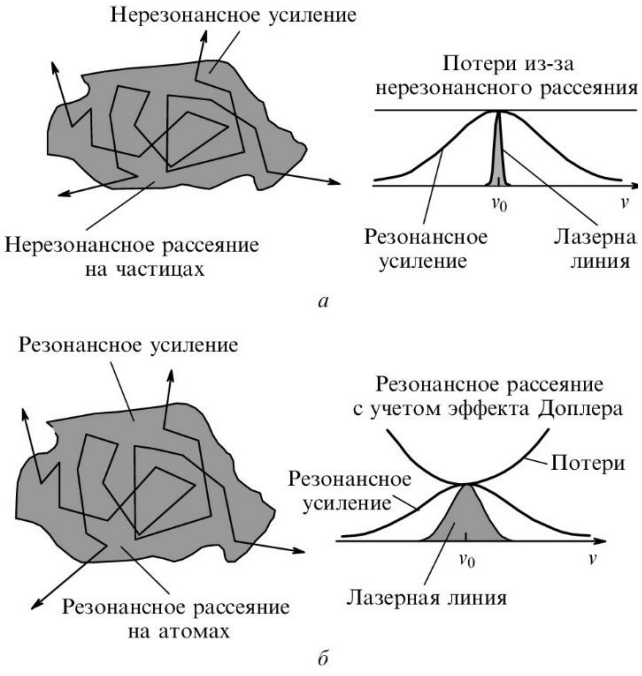


Рис. 13. Некогерентная обратная связь за счет нерезонансного (*а*) и резонансного рассеяния с учетом эффекта Доплера (*б*) на движущихся рассеивающих частицах и атомах

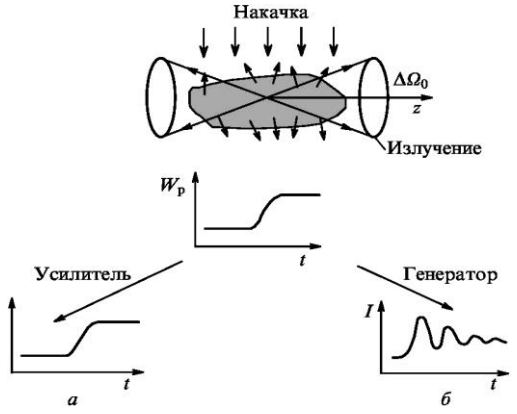


Рис. 14. Динамический отклик усилителя *(а)* и генератора (б) на быстрое изменение скорости накачки

9. О наблюдении лазерного эффекта в астрофизических условиях

Наилучшим доказательством возникновения лазерного эффекта на некоторых спектральных линиях в атмосферах звезд или их окрестностей стало бы наблюдение сужения спектра вследствие генерации. Поскольку ширина спектра при этом может быть значительно меньше доплеровской, то такие измерения можно осуществить лишь с помощью спектральных приборов с высокой разрешающей способностью (например, эталона Фабри — Перо). Обратим также внимание на возможность измерения сужения спектра корреляционным методом с помощью эффекта Брауна — Твисса [79, 80], детально рассмотренную в работе [81]; она обсуждалась также в работе [82].

Статистика флуктуаций излучения лазера с некогерентной обратной связью, наблюдаемых в узком телесном угле, совпадает со статистикой равновесного (гауссова) излучения, что теоретически и экспериментально показано в [72–74]. Поэтому при использовании корреляционного метода можно считать излучение звездного лазера некогерентным (гауссовым) светом. Для такого света функция корреляции флуктуаций интенсивности $I(t)$

$$k(\tau) = \langle \Delta I(t+\tau)\Delta I(t)\rangle, \qquad \Delta I(t) = I(t) - \langle I(t)\rangle \tag{13}$$

(скобки означают усреднение по времени) связана с шириной спектра $\Delta\nu$ соотношением

$$k(\tau) = \langle I(t)\rangle^2 |\gamma(\tau)|^2 , \tag{14}$$

где $|\gamma(t)|^2 = \exp(-\tau\pi\Delta\nu)$. Из измерений $k(\tau)$ можно получить информацию о ширине спектра $\Delta\nu$. Сужение спектра должно проявиться в возникновении корреляций с характерным временем $\tau_{kor} \approx 1/\pi\Delta\nu \gg (\Delta\nu_D)^{-1}$, где $\Delta\nu_D$ —

доплеровская ширина усиливающего перехода. Корреляционная методика выгодна для таких измерений еще по ряду причин.

Во-первых, сужение спектра приводит к соответствующему росту яркостной температуры излучения и, следовательно, увеличивает отношение S/N (сигнал/шум). Действительно, при наблюдении корреляции интенсивностей некогерентного источника, имеющего площадь Σ_S и удаленного от приемника на расстояние R [83], отношение

$$\frac{S}{N} = \kappa(t_r\tau_0)^{1/2}\Delta\nu\frac{\Sigma_S\Sigma_d}{\lambda^2R^2}\left[\exp\left(\frac{\hbar\omega_{32}}{kT_{br}}\right)\right]^{-1}, \qquad (15)$$

где κ — квантовый выход фотодетектора; t_r — время измерения; τ_0 —задержка при измерении автокорреляции; Σ_d — площадь приема излучения телескопом; T_{br} — яркостная температура. Из (15) видно, что увеличение яркостной температуры существенно увеличивает отношение S/N. Абсолютная величина S/N также лежит в пределах экспериментальных возможностей. Действительно, например, при $R = 10^{20}$ см (100 световых лет), $\kappa = 10^{-1}$, $t_r \approx 10^3$ с, $\Sigma_S = 4\pi r^2 \approx 10^{23}$ см^2, $\Sigma_d \approx 10^4$ см2, $\Delta\nu = 10^6$ с-1, $\hbar\omega_{32}/kT_{br} \approx 10^{-4}$ и $\tau_0 \approx 10^{-7}$ с получаем $S/N{\sim}100$.

Во-вторых, при приеме излучения в двух независимых пространственных точках корреляционный метод может быть использован для измерения размера области генерации, то есть критического радиуса r_0 (метод Брауна-Твисса [79]). Минимальная база b_0 (расстояние между точками наблюдения), необходимая для разрешения источника с линейным размером r_0 удаленного от приемников на расстояние $R \gg r_0$, определяется выражением [80]

$$b_0 = \frac{3{,}8\lambda R}{r_0}. \qquad (16)$$

Например, при λ = 8446 Å, $R = 10^{20}$ см, $r_0 = 10^{11}$ см необходима база $b_0 \approx 5 \times 10^5$ (5 км).

Наиболее удобным методом реализации такого эксперимента является его гетеродинный вариант; подобный эксперимент был осуществлен Ч. Таунсом с сотрудниками в области 10 мкм [84]. Прогресс перестраиваемых лазеров, волоконной оптики и малоинерционных приемников света позволяет осуществить такой эксперимент по схеме, приведенной на рис. 15. Эта схема дает возможность достичь максимальной чувствительности, спектрального и пространственного разрешения одновременно. Кроме того, эксперимент по корреляционной методике нечувствителен к неизбежным сдвигам спектральных линий из-за различных локальных скоростей АФЛ.

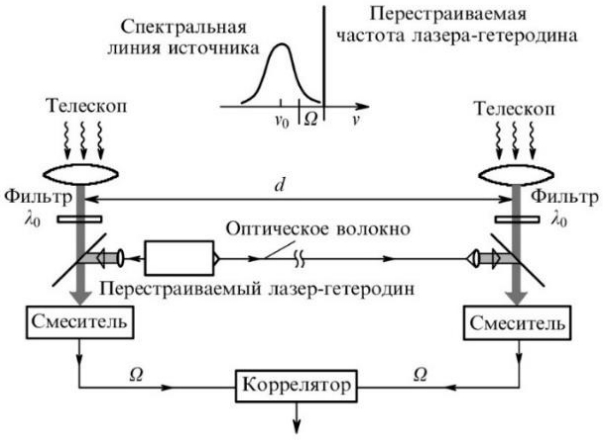


Рис. 15. Схема корреляционного наблюдения ширины узких линий АФЛ с использованием двух пространственно разнесенных телескопов и гетеродинного приема с общим перестраиваемым лазером-гетеродином

10. Заключение

Астрофизический лазер — это экстремальное по размерам природное «устройство» квантовой электроники, которое находится на краю диаграммы размер-плотность активных частиц среды лазера, представленной на рис. 16. В середине диаграммы расположены первые лабораторные мазеры и лазеры, в открытие которых Н.Г. Басов внес основополагающий вклад и, отходя от научного языка, вложил всю душу. На одном ее конце находятся полупроводниковые лазеры, также начавшиеся с пионерских работ Н.Г. Басова и его сотрудников на заре квантовой электроники, которые, благодаря открытию и реализации Ж.И. Алферовым гетропереходов [85], превратились в самый распространенный в квантовой электронике и ее многочисленных применениях тип лазера. Наконец, на противоположном конце этой диаграммы находятся астрофизические мазеры и лазеры, в которых, вероятно, действует рассеивающая некогерентная обратная связь, также открытая в 60-е годы в исследованиях под руководством Н.Г. Басова. Образно говоря, масштаб громадной и многомерной личности моего учителя Н.Г. Басова сравним с масштабом рис. 16, охватывающим 20 порядков величины.

Автор благодарит проф. С. Йоханссона за совместную работу, результаты которой использованы в разд. 5, и информацию о работе [58], а также А.А. Макарова за полезные замечания, сделанные в процессе подготовки рукописи.

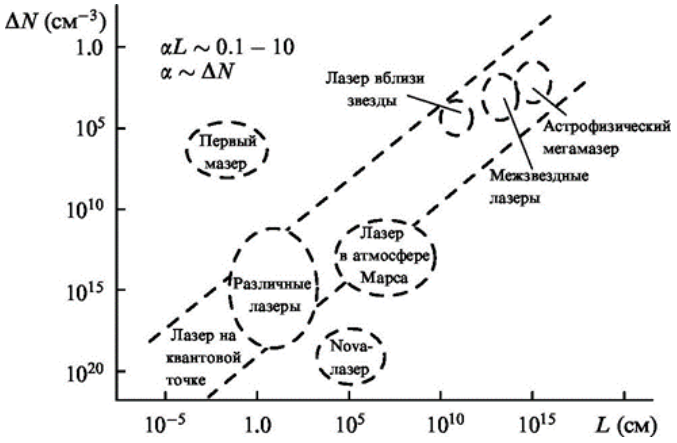


Рис. 16. Различные лабораторные и астрофизические мазеры и лазеры на диаграмме «плотность активных частиц среды — размер активной среды»

Литература

1. *Басов Н.Г., Прохоров А.М., Таунс Ч.* // УФН. 1965. Т. 85. С. 585.
2. *Maiman T.* // Nature. 1960. Vol. 187. P. 493.
3. *Javan A., Bennett W. Jr., Herriott D.R.* // Phys. Rev. Lett. 1961. Vol. 6. P. 106.
4. *Weinreb S., Meeks M.L., Carter J.C., Barrett A.H., Rogers A.E.E.* // Nature. 1965. Vol. 206. P. 440.
5. *Cheung A.C., Rank D.M., Townes C.H., Thornton O.D., Wehl W.J.* // Nature. 1969. Vol. 22. P. 626.
6. *Bowen I.* // Astrophys. J. 1935. Vol. 81.
7. *Bowen I.S.* // Publ. Astronom. Soc. Pacific. 1934. Vol. 46. P. 146.
8. *Thackerey A.D.* // Astrophys. J. 1935. Vol. 81. P. 467.
9. *Siegman A.* Lasers. University Science Book, 1986.
10. *Woodbury G.J., Ng W.R.* // Proc. IRE. 1962. Vol. 50. P. 2347.
11. *Lamb Jr. W.E., Scully M.O.* // Phys. Rev. 1967. Vol. 159. P. 208.
12. *Alzetta G.A., Gozzini L., Moi L., Orriols G.* // Nuovo Cimento. B. 1976. Vol. 36. P. 5.
13. *Arimondo E.* Progress in Optics / ed. by E. Wolf. Amsterdam: Elsevier, 1996. Vol. XXXV. P. 25.
14. *Harris S.E.* // Phys. Today. 1997. Vol. 50. P. 36.
15. *Zibrov A.S., Lukin M.D., Nikonov D.E., Hollberg L., Scully M.O, Velichansky V.L., Robinson H.G.* // Phys. Rev. Lett. 1995. Vol. 75. P. 1499.
16. *Padmabandu G.G., Welch G.R., Shubin I.N., Fry E.S., Nikonov D.E., Lukin M.D., Scully M.O.* // Phys. Rev. Lett. 1996. Vol. 76. P. 2053.
17. *Letokhov V.S.* // IEEE J. Quantum Electron. 1972. Vol. 8. P. 615; Препринт ИСАН. Троицк, 1972. № 9.

18. *Йоханссон С., Летохов В.С.* // Письма в ЖЭТФ. 2002. Vol 75. С. 591.
19. Gould G. // Appl. Opt. Suppl. on Chem. Las. 1965. Vol. 384. P. 350.
20. *Scmid H.* // Astron. Astrophys. 1989. Vol. 211. P. L31.
21. *Sorokin P.P., Glownia J.H.* // Astron. Astrophys. 2002. Vol. 384. P. 350.
22. *Унзольд А.* Физика звездных атмосфер. М.: ИИЛ, 1949.
23. *Мерилл П.* Линии химических элементов в астрономических спектрах. М.: Физматгиз, 1959.
24. *Горбацкий В.Г.* Спектры нестационарных звезд в теории звездных спектров. М.: Наука, 1966.
25. *Sletteback A.* // Astrophys. J. 1951. Vol. 113. P. 436.
26. *Bowen J.S.* // Publ. Astronom. Soc. Pacific. 1947. Vol. 59. P. 196.
27. *Burbidge E.N.* // Astrophys. J. 1952. Vol. 115. P. 418.
28. *Merrill P.W.* // Astrophys. J. 1951. Vol. 114. P. 37.
29. *Merrill P.W.* // Astrophys. J. 1952. Vol. 116. P. 22.
30. *Басов Н.Г., Прохоров А.М.* // ЖЭТФ. 1955. Т. 28. С. 249.
31. *Bloembergen N.* // Phys. Rev. 1958. Vol. 104. P. 324.
32. *Летохов В.С.* // ЖЭТФ. 1967. Т. 53. С. 1442.
33. *Ambartzumian R.V., Basov N.G., Kriukov P.G., Letokhov V.S.* // Progress in Quantum Electron. 1971. Vol. 1. P. 107.
34. *Лавринович Н.Н., Летохов В.С.* // ЖЭТФ. 1974. Т. 67. С. 1609.
35. *Letokhov V.S.* In: Amazing Light / ed. by R.Y. Chiao. Berlin: Springer, 1996. P. 409–443.
36. *Таунс Ч.* // Квант. электроника. 1997. Т. 27. С. 1031.
37. *Strelnitski V., Haas M.R., Smith H.A., Erikson E.F., Colgan S.W.J., Hollenbach D.J.* // Science. 1996. Vol. 272. P. 1459.
38. *Betz A.L., McLaren R.A., Sutton E.C., Townes C.H.* // Astrophys. J. Lett. 1976. Vol. 208. P. L145.
39. *Mumma M.J., Buhl D., Chin G., Deming D., Espenak F., Kostink T., Zipoy D.* // Science. 1981. Vol. 212. P. 45.
40. *Johansson S., Davidson K., Ebbets D., Weigelt G., Balick B., Frank A., Haman F.H., Humphreys R.M., Morse J., White R.L.* In: Science with Hubble Space Telescope-II / ed. by R. Benvenutti, F.D. Macchetto, E.J. Schreiew. Paris: ESA, 1996. P. 361.
41. *Johansson S., Letokhov V.* // Astron. Astrophys. 2001. Vol. 378. P. 266.
42. *Klimov V., Johansson S., Letokhov V.* // Astron. Astrophys. 2002. Vol. 385. P. 313.
43. *Schawlow A.L., Townes C.H.* // Phys. Rev. 1958. Vol. 112. P. 1940.
44. *Kimble R.A. et al.* // Astrophys. J. 1998. Vol. 492. P. L83.
45. *Gull T.R., Ishibashi K., Davidson K.* In: Eta Carinae at the Millenium / ed. by J.A. Morse, R.M. Humphreys, A. Damineli. ASP Conf. Ser. 1999. Vol. 179. P. 144.
46. *Weigelt G., Ebersbergen J.* // Astron. Astrophys. 1986. Vol. 163. P. L5.

47. *Davidson K., Humphreys R.M.* // Annu. Rev. Astron. Astrophys. 1997. Vol. 35. P. 1.

48. *Stromgren B.* // Astrophys. J. 1932. Vol. 89. P. 526.

49. *Gull T., Ishibashi K., Davidson K., Collins N.* In: Eta Carinae and Other Mysterious Stars / ed. by T. Gull, S. Johansson, K. Davidson. ASP Conf. Ser. 2001. Vol. 242. P. 391.

50. *Johansson S., Jordan C.* // Mon. Not. R. Astr. Soc. 1984. Vol. 210. P. 239.

51. *Johansson S., Hammann F.* // Phys. Scripta. 1993. Vol. 47. P. 157.

52. *Johansson S., Zethson T., Hartman H., Letokhov V.* In: Eta Carinae and Other Mysterious Stars / ed. by T. Gull, S. Johansson, K. Davidson. ASP Conf. Ser. 2001. Vol. 242. P. 297.

53. *Bennett Jr. W.R., Faust W.L., McFarlane R.A., Patel C.K.H.* // Phys. Rev. Lett. 1962. Vol. 8. P. 470.

54. *Вайнштейн Л.А., Собельман И.И., Юков Е.А.* Сечения возбуждения атомов и ионов электронами. М.: Наука, 1973.

55. *Аллен К.У.* Астрофизические величины. М.: ИИЛ, 1960.

56. *Боярчук А.А.* // Астрон. ж. 1957. Т. 34. С. 193.

57. *Мустель Э.Р.* // Астрон. ж. 1941. Т. 18. С. 297; 1944. Т. 21. С. 133.

58. *Münch G., Taylor K.* // Astrophys. J. 1974. Vol. 192. P. L93.

59. *Gull T., Goad L., Chin N.-Y., Maran S.P., Hobbs R.W.* // Publ. Astronomic. Soc. Pacific. 1973. Vol. 85. P. 526.

60. *Casperson L.W., Yariv A.* // IEEE J. Quantum Electron. 1972. Vol. 8. P. 80.

61. *Allen L., Peters G.I.* // Nature. Phys. Sciences. 1972. Vol. 235. P. 143.

62. *Litvak M.M.* // Phys. Rev. A. 1970. Vol. 2. P. 2107.

63. *Cook A.H.* Celestial Masers. Cambridge: Cambridge Univ. Press, 1977.

64. *Reid J.J., Moran J.M.* // Ann. Rev. Astron. Astrophys. 1981. Vol. 19. P. 231.

65. *Elitzur M.* // Rev. Mod. Phys. 1982. Vol. 54. P. 1225.

66. *Barrett A.H., Rogers A.E.E.* // Nature. 1966. Vol. 210. P. 188.

67. *Летохов В.С., Чеботаев В.П.* Нелинейная лазерная спектроскопия сверхвысокого разрешения. М.: Наука, 1990.

68. *Прохоров А.М.* // ЖЭТФ. 1958. Т. 34. С. 1658.

69. *Амбарцумян Р.В., Басов Н.Г., Крюков П.Г., Летохов В.С.* // Письма в ЖЭТФ. 1966. Т. 3. С. 261; ЖЭТФ. 1966. Т. 51. С. 274; IEEE J. Quantum Electron. 1966. Vol. 2. P. 442.

70. *Ambartzumian R.V., Basov N.G., Kryukov P.G., Letokhov V.S.* Progress in Quantum Electronics / ed. by K.W.N. Stevens, J.H. Sanders. London: Pergamon Press, 1970. Vol. 1. P. 105.

71. *Амбарцумян Р.В., Крюков П.Г., Летохов В.С.* // ЖЭТФ. 1966. Т. 51. С. 1669.

72. *Амбарцумян Р.В., Крюков П.Г., Летохов В.С., Матвеец Ю.А.* // Письма в ЖЭТФ. 1967. Т. 5. С. 378; ЖЭТФ. 1967. Т. 53. С. 1955.

73. *Летохов В.С.* // ЖЭТФ. 1967. Т. 53. С. 2110.

74. *Летохов В.С.* // Письма в ЖЭТФ. 1967. Т. 5. 262; ЖЭТФ. 1967. Т. 53. С. 1442.

75. *Lawandy N.M., Balachandran R.M., Gomes A.S.L., Sauvarn E.* // Nature. 1994. Vol. 368. P. 436.

76. *Маркушев В.М. и др.* // Квантовая электроника. 1986. Т. 13. С. 427; 1990. Т. 17. С. 854; *Cao H., Xu S.T., Chang S.-H., Ho S.T.* // Phys. Rev. 2000. Vol. 61. P. 1985.

77. *Летохов В.С.* // Письма в ЖЭТФ. 1966. Т. 4. С. 477; Астрон. ж. 1972. Т. 49. С. 737.

78. *Truitt P., Strelnitskii V.* Meeting 197 Amer. Astronom. Soc. January, 2001.

79. *Hanberry Brown R., Twiss R.Q.* // Proc. Roy. Soc. A. 1957. Vol. 242. P. 300; 1958. Vol. 243. P. 291; 1958. Vol. 248. P. 199.

80. *Mandel L.* Progress in Optics / ed. by E. Wolf. Amsterdam: Elcevier, 1963. V. 2. P. 181.

81. *Лавринович Н.Н., Летохов В.С.* // Квант. электроника. 1976. Т. 3. С. 1948.

82. *Dravins D.* In: Eta Carinae and Other Mysterious Stars / ed. by T. Gull, S. Johansson, K. Davidson. ASP Conf. Ser. 2001. V. 339.

83. *Goldberger M. L., Lewis H.W., Watson K.M.* // Phys. Rev. 1966. Vol. 142. P. 25.

84. *Johnson M.A., Betz A.L., Townes C.H.* // Phys. Rev. Lett. 1974. Vol. 33. P. 1617.

85. *Alferov Zh.I.* // ZI. Rev. Mol. Phys. 2001. Vol. 73. P. 767.

ПОЛНЫЙ СПИСОК НАУЧНЫХ ПУБЛИКАЦИЙ В.С. ЛЕТОХОВА

1. *Вацура В.В., Летохов В.С., Пухлик Ю.А.* Фотоэлектронная система для контроля направления линейного элемента изображения // Оптико-механическая промышленность. 1962. № 6. С. 29–32.

2. *Летохов В.С.* Статистический анализ изображений // Оптико-механическая промышленность. 1963. № 11. С. 7–12.

3. *Летохов В.С.* Гетеродинирование оптического шума, преобразованного с помощью интерферометров // Труды комиссии по спектроскопии АН СССР. 1963. Т. 11 (1). С. 315–322.

4. *Вацура В.В., Летохов В.С., Плотников В.С., Андреев М.И., Пухлик Ю.А., Свешников В.В.* Электронно-оптический вибродетектор // Оптико-механическая промышленность. 1964. № 3. С. 24–27.

5. *Летохов В.С.* Об измерении флуктуаций частоты колебаний методом линии задержки // Радиотехника и электроника. 1964. Т. 9 (49). С. 1628–1633.

6. *Вацура В.В., Летохов В.С., Пухлик Ю.А.* Астронавигатор // Приборы и средства автоматизации. 1964. Т. 12. С. 37–41.

7. *Летохов В.С.* Пространственные эффекты при гетеродинировании оптических волн // Радиотехника и электроника. 1965. № 10 (6). С. 1143–1145.

8. *Басов Н.Г., Беленов Э.М., Летохов В.С.* Дифракционная синхронизация оптических квантовых генераторов // Доклады АН СССР. 1965. Т. 161 (3). С. 556–559.

9. *Басов Н.Г., Беленов Э.М., Летохов В.С.* Синхронизация колебаний в полупроводниковом лазере, имеющем несколько p–n переходов // ФТТ. 1965. Т. 7 (11). С. 275–276.

10. *Басов Н.Г., Летохов В.С.* О лазерах на атомных пучках // Письма в ЖЭТФ. 1965. Т. 2 (1). С. 6–9.

11. *Басов Н.Г., Летохов В.С.* Распространение светового импульса в инвертированной среде // Оптика и спектроскопия. 1965. Т. 18 (6). С. 1042–1046.

12. *Летохов В.С., Маркин Е.П.* О статистике лазерного излучения // ЖЭТФ. 1965. Т. 48 (2). С. 770.

13. *Летохов В.С.* Дифракционные потери полости, образованной зеркалами с полосой поглощения // ЖТФ. 1965. Т. 35 (5). С. 809–812.

14. *Басов Н.Г., Беленов Э.М., Летохов В.С.* Предельное сечение пучка излучения оптического квантового генератора // Доклады АН СССР. 1965. Т. 161 (4). С. 799–801.

15. *Басов Н.Г., Беленов Э.М., Летохов В.С.* Дифракционная блокировка оптических квантовых генераторов // ЖТФ. 1965. Т. 35 (6). С. 1098–1105.

16. *Басов Н.Г., Амбарцумян Р.В., Зуев В.С., Крюков П.Г., Летохов В.С.* Скорость распространения мощного импульса света в инверсно-заселенной среде// Доклады АН СССР. 1965. Т. 165 (1). С. 58–60.

17. *Беленов Э.М., Летохов В.С.* О генерации остронаправленного когерентного излучения // Оптика и спектроскопия. 1965. Т. 19 (9). С. 465–467.

18. *Беленов Э.М., Летохов В.С.* К теории связанных оптических квантовых генераторов // ЖТФ. 1965. Т. 35 (11). С. 2126–2128.

19. *Басов Н.Г., Амбарцумян Р.В., Зуев В.С., Крюков П.Г., Летохов В.С.* Нелинейное усиление импульса света // ЖЭТФ. 1966. Т. 50 (1). С. 23–34.

20. *Басов Н.Г., Летохов В.С.* Изменения формы импульса света при нелинейном усилении // Доклады АН СССР. 1966. Т. 167 (1). С. 73–76.

21. *Амбарцумян Р.В., Басов Н.Г., Крюков П.Г., Летохов В.С.* Лазер с нерезонансной обратной связью // Письма в ЖЭТФ. 1966. Т. 3 (6). С. 261–264.

22. *Амбарцумян Р.В., Басов Н.Г., Зуев В.С., Крюков П.Г., Летохов В.С.* Короткоимпульсный лазер с модуляцией добротности и переменной длительностью импульса // Квантовая электроника. 1966. Т. 2 (9). С. 436–441.

23. *Ambartsumian R.V., Basov N.G., Zuev V.S., Kryukov P.G., Letokhov V.S.* Nichtlineare Verstarkung Von Lichtimpulsen // Experimentalle Technik der Physik. XV. Heft 4/5. 1967. P. 307–314.

24. *Летохов В.С.* Авторезонансная обратная связь в лазерах // Письма в ЖЭТФ. 1966. Т. 3 (10). С. 413–416.

25. *Амбарцумян Р.В., Басов Н.Г., Зуев В.С., Крюков П.Г., Летохов В.С.* Распространение светового импульса в нелинейно усиливающей и поглощающей среде // Письма в ЖЭТФ. 1966. Т. 4 (1). С. 19–22.

26. *Летохов В.С., Сучков А.Ф.* Динамика генерации гигантского импульса когерентного света // ЖЭТФ. 1966. Т. 50 (4). С. 1148–115.

27. *Летохов В.С., Павлик Б.Д.* Нелинейное усиление затухающей световой волны в активном оптическом волокне // ЖТФ. 1966. Т. 36 (12). С. 2181–2187.

28. *Амбарцумян Р.В., Басов Н.Г., Крюков П.Г., Летохов В.С.* Лазеры с нерезонансной обратной связью // Квантовая электроника. 1966. Т. 2 (9). С. 442–446.

29. *Амбарцумян Р.В., Крюков П.Г., Летохов В.С.* Динамика сужения линии излучения лазера с нерезонансной обратной связью // ЖЭТФ. 1966. Т. 51 (6). С. 1669–1675.

30. *Летохов В.С.* Стимулированное радиоизлучение межзвёздной среды// Письма в ЖЭТФ. 1966. Т. 4 (11). С. 477–481.

31. *Летохов В.С.* Фотоионизация атомов в когерентных состояниях// Оптика и спектроскопия. 1966. Т. 20 (2). С. 349–350.

32. *Летохов В.С.* Относительно исследования статистических свойств некогерентного света // ЖЭТФ. 1966. Т. 50. С. 765–768.

33. *Зуев В.С., Летохов В.С., Сенатский Ю.В.* Гигантские импульсы сверхлюминесценции // Письма в ЖЭТФ. 1966. Т. 4 (5). С. 182–185.

34. *Амбарцумян Р.В., Басов Н.Г., Зуев В.С., Крюков П.Г., Летохов В.С.* Структура гигантского лазерного импульса с модуляцией добротности // ЖЭТФ. 1966. Т. 51 (2). С. 406–411.

35. *Амбарцумян Р.В., Басов Н.Г., Крюков П.Г., Летохов В.С.* Оптический квантовый генератор с нерезонансной обратной связью // ЖЭТФ. 1966. Т. 51 (3). С. 724–729.

36. *Ambartsumian R.V., Basov N.G., Kryukov P.G., Letokhov V.S.* Nichtresonante Rikkopplung in lasern // Experimentalle Technik der Physik. XV. Heft 4/5. 1967. P. 280–287.

37. *Летохов В.С., Морозов В.Н.* Генерация ультракоротких когерентных световых импульсов // ЖЭТФ. 1967. Т. 52 (5). С. 1296–1302.

38. *Летохов В.С.* Стимулированное излучение ансамбля рассеивающих частиц с отрицательным поглощением // Письма в ЖЭТФ. 1967. Т. 5 (8), 262–265.

39. *Летохов В.С., Павлик Б.Д.* Генерация когерентного света с помощью пучков атомов или молекул // ЖЭТФ 1967. Т. 53 (3). С. 1107–1115.

40. *Амбарцумян Р.В., Басов Н.Г., Крюков П.Г., Летохов В.С.* Статистика излучения лазера с нерезонансной обратной связью // Письма в ЖЭТФ. 1967. Т. 5 (10). С. 378–382.

41. *Летохов В.С.* Генерация света рассеивающей средой с отрицательным резонансным поглощением // ЖЭТФ. 1967. Т. 53 (4). С. 1442–1452.

42. *Летохов В.С.* Квантовая статистика многомодового излучения атомного ансамбля // ЖЭТФ. 1967. Т. 53 (6). С. 2210–2222.

43. *Летохов В.С.* Автостабилизация частоты лазера за счёт нелинейного поглощения в газе // Письма в ЖЭТФ. 1967. Т. 6 (4). С. 597–600.

44. *Летохов В.С., Павлик Б.Д.* Теория лазера с авторезонансной обратной связью // ЖТФ. 1967. Т. 38(2). С. 343–355.

45. *Летохов В.С., Сучков А.Ф.* Динамика генерации гигантского когерентного светового импульса. II // ЖЭТФ. 1967. Т. 52 (l). С. 282–292.

46. *Богданкевич О.В., Гончаров В.А., Лаврюшин Б.М., Летохов В.С., Сучков А.Ф.* Эффекты неоднородности возбуждения в полупроводниковых лазерах с накачкой электронным пучком // ФТТ. 1967. Т. 1 (1). С. 7–14.

47. *Амбарцумян Р.В., Крюков П.Г., Летохов В.С., Матвеец Ю.А.* Статистические свойства излучения лазера с нерезонансной обратной связью // ЖЭТФ. 1967. Т. 53 (6). С. 1955–1966.

48. *Летохов В.С.* Нелинейное усиление световых импульсов. II. Скорость распространения // ЖТФ. 1968. Т. 38 (5). С. 856–864.

49. *Летохов В.С.* Формирование ультракоротких когерентных световых импульсов // Письма в ЖЭТФ. 1968. Т. 7 (l). С. 35–38.

50. *Басов Н.Г., Зуев В.С., Крюков П.Г., Летохов В.С., Сенатский Ю.В., Чекалин С.В.* Генерация и усиление мощных световых импульсов в неодимовом стекле. 1968. Т. 54 (3).С. 767–775.

51. *Амбарцумян Р.В., Басов Н.Г., Летохов В.С.* Исследование частотных характеристик Хе–Не лазера с диффузным зеркалом // Письма в ЖЭТФ. 1968. Т. 7 (3). С. 88–91.

52. *Летохов В.С.* Двухквантовое усиление короткого импульса света // Письма в ЖЭТФ. 1968. Т. 7 (8). С. 284–286.

53. *Летохов В.С.* Частотные эффекты в лазере с нелинейно поглощающим газом // ЖЭТФ. 1968. Т. 54 (4). С. 1244–1252.

54. *Летохов В.С.* Генерация ультракоротких импульсов света в лазере с нелинейным поглотителем. Errata // ЖЭТФ. 1968. Т. 55 (3). С. 1077–1089.

55. *Басов Н.Г., Крюков П.Г., Летохов В.С., Сенатский Ю.В.* Генерация и усиление ультракоротких оптических импульсов // Квантовая электроника. 1968. Т. 4 (10). С. 606–609.

56. *Летохов В.С.* Ультракороткие флуктуационные световые импульсы в лазере // ЖЭТФ. 1968. Т. 55 (5). С. 1943–1946.

57. *Ambartsumian R.V., Basov N.G., Letokhov V.S.* Frequency stability of a He–Xe laser with nonresonant feedback, IEEE Transactions Instrumentation and Measurement. IM–17. 1968. No. 4. P. 338–343.

58. *Летохов В.С.* Сужение доплеровской линии в стоячей световой волне // Письма в ЖЭТФ. 1968. Т. 7 (9). С. 348–351.

59. *Басов Н.Г., Летохов В.С.* Оптические стандарты частоты // УФН. 1968. Т. 96 (4). С. 585–631.

60. *Амбарцумян Р.В., Басов Н.Г., Зуев В.С., Крюков П.Г., Летохов В.С.* Спектр светового импульса, распространяющегося в среде с нелинейным усилением. Материалы 2-го Всесоюзного симпозиума по нелинейной оптике, г. Новосибирск, 1966. М.: Наука, 1968. С. 243–246.

61. *Летохов В.С.* Динамика генерации импульсного лазера с фазировкой мод // ЖЭТФ. 1968. Т. 54 (5). С. 1392–1401.

62. *Летохов В.С., Сучков А.Ф.* Динамика оптического квантового генератора с мгновенным включением добротности. Труды ФИАН. 1968. Т. 43. С. 169–186.

63. *Летохов В.С., Чеботаев В.Н.* Об оптическом стандарте частоты с нелинейно-поглощающей газовой ячейкой // Письма в ЖЭТФ. 1969. Т. 9 (6). С. 364–367.

64. *Летохов В.С.* Нелинейное усиление импульса света. III. Ультракороткие длительности // ЖЭТФ. 1969. Т. 56 (1). С. 402–413.

65. *Басов Н.Г., Дрожбин Ю.А., Крюков П.Г., Лебедев В.Б., Летохов В.С., Матвеец Ю.А.* Флуктуационная структура гигантского импульса света и изменение ее при прохождении через нелинейный поглотитель // Письма в ЖЭТФ. 1969. Т. 9 (7). С. 428–432.

66. *Басов Н.Г., Крюков П.Г., Летохов В.С., Матвеец Ю.А.* Исследование формирования ультракороткого импульса света при распространении в двухкомпонентной среде // ЖЭТФ. 1969. Т. 56 (5). С. 1546–1556.

67. *Крюков П.Г., Летохов В.С.* Распространение импульса света в резонансно усиливающей (поглощающей) среде // УФН. 1969. Т. 99 (2). С. 169–227.

68. *Басов Н.Г., Компанец И.Н., Компанец О.Н., Летохов В.С., Никитин В.В.* Узкие резонансы при насыщении поглощения SF_6 излучением CO_2 лазера // Письма в ЖЭТФ. 1969. Т. 9 (10). С. 568–571.

69. *Летохов В.С.* Пространственные эффекты при насыщении резонансного поглощения газа в световом поле // ЖЭТФ. 1969. Т. 56 (5). С. 1748–1754.

70. *Басов Н.Г., Летохов В.С.* Двухуровневый газовый лазер с когерентной оптической накачкой // Письма в ЖЭТФ. 1969. Т. 9 (12). С. 660–663.

71. *Басов Н.Г., Крюков П.Г., Летохов В.С., Матвеец Ю.А., Чекалин С.В.* Усиление ультракороткого импульса в двухкомпонентной среде // Письма в ЖЭТФ. 1969. Т. 10 (10). С. 479–482.

72. *Basov N.G., Letokhov V.S.* Optical frequency standards // Electron Technology. 2, 2/3, 15–20. Institute of Electron Technology. P.A.Sci. Warsaw, 1969; Conference URSI Laser measurements. Warsaw, Sept. 1968.

73. *Летохов В.С.* О возможности разделения изотопов путем резонансной атомной фотоионизации и молекулярной фотодиссоциации лазерным излучением // ФИАН. Ноябрь 1969. Институт спектроскопии АН СССР, г. Троицк. Репринт № 1. 1979. С. 1–54.

74. *Basov N.G., Kryukov P.G., Letokhov V.S.* Ultrakurze Lichtimpulse // Laser. 1969. Vol. 4. P. 39–45.

75. *Basov N.G., Kryukov P.G., Letokhov V.S.* Ultra–short laser pulse // Optical Technology and Lasers. 1970. Vol. 2 (3). P. 126–131.

76. *Богданкевич О.В., Летохов В.С., Сучков А.Ф.* Теория эффектов неоднородного возбуждения в полупроводниковых лазерах с электронно–лучевой накачкой // ФТП. 1969. Т. 3 (5). С. 665–670.

77. *Амбарцумян Р.В., Бажулин С.П., Басов Н.Г., Летохов В.С.* Спектр излучения He–Xe лазера с нерезонансной обратной связью // ЖЭТФ. 1970. Т. 58 (2). С. 441–455.

78. *Ambartsumian R.V., Basov N.G., Kryukov P.G., Letokhov V.S.* Non-resonant feedback in lasers. Progress in Quantum Electronics / ed. by J.H. Sanders and K.W.H. Stevens. Vol. 1. Pt. 3. London: Pergamon Press, 1970. P. 105–193.

79. *Басов Н.Г., Компанец О.Н., Летохов В.С., Никитин В.В.* Исследование узких резонансов в пределах доплеровской ширины линии вращательно–колебательных переходов в SF6 при насыщении поглощения // ЖЭТФ. 1970. Т. 59. № 2 (8). С. 394–403.

80. *Летохов В.С.* Селективная обратная связь для широкополосных лазеров / в сб.: Краткие сообщения по физике ФИАН. 1970. № 11. С. 14–17.

81. *Летохов В.С., Павлик Б.Д.* Стабильность частоты атомно-лучевого лазера с когерентным возбуждением // ЖТФ. 1970. Т. 40. С. 1638–1648.

82. *Knyazev I.N., Letokhov V.S.* Excitation of far vacuum UV lasers by fast heating of plasma electrons in ultrashort pulsed optical fields // Optics Commun. 1971. Vol. 3 (5). P. 332–334.

83. *Letokhov V.S.* Problems of laser frequency stabilization by nonlinear saturation of resonant absorption in gases // Comments on Atomic and Mol. Physics. 1971. 2 (6). P. 181–194.

84. *Амбарцумян Р.В., Калинин В.П., Летохов В.С.* Двухступенчатая селективная фотоионизация атомов рубидия лазерным излучением // Письма в ЖЭТФ. 1971. Т. 13 (6). С. 305–307.

85. *Компанец О.Н., Летохов В.С.* Узкие молекулярные резонансы при насыщении поглощения в разнесенных световых лучах // Письма в ЖЭТФ. 1971. Т. 14 (1). С. 20–23.

86. *Bagratashvili V.N., Knyazev I.N., Letokhov V.S.* On the tunable infrared gas lasers // Optics Commun. 1971. Vol. 4 (2). P. 154–156.

87. *Летохов В.С., Павлик Б.Д.* Газовый лазер с нелинейным поглощением в режиме квазибегущей волны // Квантовая электроника. 1971. Т. 1. С. 53–63.

88. *Летохов В.С., Павлик Б.Д.* Частотный эффект в кольцевом газовом лазере с нелинейным поглощением // Изв. вузов. сер. Радиофизика. 1971. Т. 14 (2). С. 244–251.

89. *Князев И.Н., Летохов В.С.* О стимулированном излучении в далеком вакуумном ультрафиолете при быстром нагреве электронов плазмы ультракороткими импульсами света // Оптика и спектроскопия. 1972. Т. 23 (1). С. 110–114.

90. *Летохов В.С., Мандельштам С.Л.* Проблемы лазерной спектроскопии // Вестник АН СССР. 1971. № 3. С. 40–47.

91. *Letokhov V.S., Mandel'shtam S.L.* Einige Probleme der Laser-Spectroskopie // Jenaer Rundschau. 1972. 17. 192, Heft 4.

92. *Ambartsumian R.V., Letokhov V.S.* Selective two-step (STS) photoionization of atoms and photodissociation of molecules by laser radiation // Applied Optics. 1972. Vol. 11 (2). P. 354–358.

93. *Летохов В.С.* Космический мазер с обратной связью // Астрономический журнал. 1972. Т. 49 (4). С. 737–743.

94. *Letokhov V.S.* Laser action in stellar atmospheres // IEEE Journ. Quant. Electr. 1972. QE-8 (6). P. 615; Preprint of Inst. of Spectroscopy. 1972. No. 9. P. 1–24.

95. *Kryukov P.G., Letokhov V.S.* Techiques of high-power light pulse amplification, Laser Handbook / ed. by E.O. Schulz-DuBois and F.T. Arecchi. Vol. 1, North-Holland Publ. Comp., 1972. P. 561–595.

96. *Kryukov P.G., Letokhov V.S.* Fluctuation mechanism of ultrashort pulse generation by laser with saturable absorber // IEEE J. of Quant. Electr. 1972. QE-8 (10). P. 766–782.

97. *Компанец О.Н., Летохов В.С.* Исследование узких резонансов при насыщении поглощения молекул SF_6 излучением CO_2-лазера // ЖЭТФ. 1972. Т. 62 (4). С. 1302–1311.

98. *Ambartsumian R.V., Letokhov V.S., Makarov G.N., Chekalin N.V.* Direct measurement of the relaxation rate of the HCl molecule excited to the vibrational state V"=3 by laser radiation // Chem. Phys. Lett. 1972. Vol., 13. P. 49–50.

99. *Ambartsumian R.V., Letokhov V.S.* Laser two–step photodissociation of molecules as a method of selective breaking of bonds // Chem. Phys. Lett. 1972. Vol. 13 (5). P. 446–447.

100. *Letokhov V.S., Ryabov E.A., Tumanov O.A.* Saturation of absorption and optical strength of C_2F_3Cl for CO_2 laser pulses // Opt. Comm. 1972. Vol. 5 (3). P. 168–170.

101. *Амбарцумян Р.В., Апатин В.М., Летохов В.С.* Селективное лазерное возбуждение высоких колебательных уровней молекулы HCl // Письма в ЖЭТФ. 1972. Т. 15 (6). С. 336–339.

102. *Letokhov V.S.* On selective laser photochemical reactions by means of photopredissociation of molecules // Chem. Phys. Lett. 1972. Vol. 15 (2). P. 221–222.

103. *Летохов В.С., Рябов Е.А., Туманов О.А.* Люминесценция молекулярного газа под действием импульса CO_2-лазера // ЖЭТФ. 1972. Т. 63 (6). С. 2025–2032.

104. *Летохов В.С., Макаров А.А.* Кинетика возбуждений колебаний молекул инфракрасным лазерным излучением // ЖЭТФ. 1972. Т. 6 (6). С. 2064–2076.

105. *Амбарцумян Р.В., Летохов В.С., Макаров Г.Н., Пурецкий А.А.* Двухступенчатая фотодиссоциация молекул аммиака, возбуждаемых лазерным излучением // Письма в ЖЭТФ. 1972. Т. 15 (12). С. 709–711.

106. *Ambartsumian R.V., Letokhov V.S., Makarov G.N., Puretskii A.A.* Direct measurement of population on molecular vibrational levels excited by laser radiation // Chem. Phys. Lett. 1972. Vol. 16 (2). P. 252–254.

107. *Летохов В.С.* Узкие резонансы испускания и поглощения γ-излучения ядер, индуцируемые лазерным излучением // Письма в ЖЭТФ. 1972. Т. 16 (7). С. 428–431.

108. *Letokhov V.S.* A possibility of measurement of the energy of the metastable nuclear levels by laser spectroscopy of the molecular vibrational transitions // Phys. Lett. 1972. Vol. 41A (4). P. 333–334.

109. *Knyazev I.N., Letokhov V.S., Movshev V.G.* On the collissional four–level H_2 VUV laser // Optics Comm. 1972. Vol. 6 (4). P. 424–426.

110. *Летохов В.С., Павлик Б.Д.* Нелинейное поглощение разнесённых световых лучей на доплеровски уширенном переходе. I. Слабое поле. II. Сильное поле // Оптика и спектроскопия. 1972. I: Т. 32 (5). С. 856–864; II: Т. 32 (6). С. 1057–1063.

111. *Летохов В.С., Павлик Б.Д.* Связь лазеров с нелинейным поглотителем при явлениях переноса в молекулярном газе // Радиотехника и электроника. 1972. Т. 17 (5). С. 1030–1038.

112. *Летохов В.С., Павлик Б.Д.* Колебания частоты в газовом лазере с нелинейным поглощением // Квантовая электроника. 1972. Т. 4 (10). С. 32–39.

113. *Letokhov V.S., Ryabov E.A., Tumanov O.A.* Optical strength fo molecular gas in the presence of an electric discharge // Phys. Lett. 1972. Vol. 40A (1). P. 55–57.

114. *Letokhov V.S., Pavlik B.D.* On an increase of the resolution of a nonlinear laser spectroscopy of molecules up to the natural width // Opt. Commun. 1972. Vol. 6 (2). P. 202–204.

115. *Knyazev I.N., Letokhov V.S., Movshev V.G.* TEA N_2 UV laser with reduced spectra // Optics Comm. 1972. Vol. 6 (3). P. 250–252.

116. *Голгер А.Л., Летохов В.С.* Инверсия населенности при насыщении поглощения в колебательно-вращательных молекулярных переходах // Квантовая электроника. 1973. Т. 1 (13). С. 30–40.

117. *Letokhov V.S.* Narrow resonances induced in an absorbing gas by an intense light field. In: Fundamental and Applied Laser Physics / ed. by M.S. Feld, A. Javan, N. Kurnit. Proceed. of the Estahan Symp. 1971. N.Y.: John Wiley, 1973. P. 335–367.

118. *Letokhov V.S., Makarov A.A.* Kinetics of two-step selective photodissociation of molecules by laser radiation // J. of Photochemistry. 1973/74. Vol. 2. P. 421–427.

119. *Летохов В.С., Макаров А.А., Рябов Е.А.* Определение коэффициента заселенности молекулярных колебательно-вращательных уровней методом насыщения поглощения лазерным излучением // Доклады АН СССР. 1973. Т. 212 (l). С. 74–78.

120. *Амбарцумян Р.В., Летохов В.С., Макаров Г.Н., Пурецкий А.А.* Лазерное разделение изотопов азота // Письма в ЖЭТФ. 1973. Т. 17 (2),С. 91–94.

121. *Letokhov V.S.* Possibility of the optical separation of the isomeric nuclei by laser radiation // Optics. Comm. 1973. Vol. 7 (1). P. 59–60.

122. *Letokhov V.S.* Double γ- and optical resonance // Phys. Lett. 1973. Vol. 43A (2). P. 179–180.

123. *Амбарцумян Р.В., Летохов В.С., Макаров Г.Н., Платова А.Г., Пурецкий А.А., Туманов О.А.* Исследование возбуждения колебательных уровней молекул $^{14}NH_3$ излучением CO_2-лазера // ЖЭТФ. 1973. Т. 64 (3). С. 771–784.

124. *Летохов В.С., Павлик Б.Д.* Нелинейные узкие резонансы плотности возбужденных молекул в стоячей световой волне // ЖЭТФ. 1973. 64 (3). С. 804–812.

125. *Krukov P.G., Letokhov V.S.* Examining the picosecond pulse // Laser Focus. 1973. Vol. 9 (3). P. 41–46.

126. *Gorokhov Yu.A., Kompanets O.N., Letokhov V.S., Gerasimov G.A., Posudin Yu.I.* Narrow saturation resonances in the spectrum of OsO_4 induced by CO_2 laser radiation // Opt. Comm. 1973. Vol. 7 (4). P. 320–322.

127. *Letokhov V.S.* Narrow frequency tunable γ–ray nuclear resonances induced by laser radiation // Phys. Rev. Lett. 1973. Vol. 30 (16). P. 729–732.

128. *Letokhov V.S.* Use of lasers to control selective chemical reactions // Science. 1973. Vol. 180 (4085). P. 451–458.

129. *Летохов В.С.* Лазер управляет селективными химическими реакциями // Природа. 1974. № 8. С. 13–23.

130. *Летохов В.С.* К проблеме γ-лазера на ядерных переходах // ЖЭТФ. 1973. Т. 64. (5). С. 1555–1567.

131. *Антонов В.С., Князев И.Н., Летохов В.С., Мовшев В.Г.* Водородный лазер в вакуумном ультрафиолете при атмосферном давлении // Письма в ЖЭТФ. 1973. Т. 17 (10). С. 545–548.

132. *Летохов В.С.* Накачка ядерных уровней рентгеновским излучением лазерной плазмы // Квантовая электроника. 1973. Т. 4 (16). С. 125–127.

133. *Амбарцумян Р.В., Летохов В.С., Макаров Г.Н., Пурецкий А.А.* Разделение изотопов азота методом селективной двухступенчатой фотодиссоциации молекул аммиака // Доклады АН СССР. Сер. Химия. 1973. Т. 211 (2). С. 365–368.

134. *Bagratashvili V.N., Knyazev I.N., Kudryavtsev Yu.A., Letokhov V.S.* Frequency tuning of an e-beam preionized high-pressure CO_2 laser // Optics. Commun. 1973. Vol. 9 (2). P. 135–138.

135. *Бажутин С.А., Летохов В.С., Макаров А.А., Семчишен В.А..* Селективная предиссоциация молекул орто-J_2 лазерным излучением // Письма в ЖЭТФ. 1973. Т. 18 (8). С. 515–519.

136. *Feld M.S., Letokhov V.S.* Laser spectroscopy // Scientific American. 1973. Vol. 229 (6). P. 69–85.

137. *Letokhov V.S.* New possibilities for the spectroscopy inside the Doppler line in the optical and γ-ranges. Proceed. of the Conference Methods of Spectroscopy without Doppler Broadening of Excited Levels of Simple Molecules (Aussois, France, May 23–26, 1973). 1974. P. 127–138.; Laser and Unconventional Optics. Vol. 46. 1973. P. 3–27.

138. *Компанец О.Н., Кукуджанов А.Р., Летохов В.С., Михайлов Е.Л.* Стабилизация частоты лазера на двуокиси углерода с помощью внешней нелинейно поглощающей ячейки на SF_6 // Квантовая электроника. 1973. Т. 4 (16). С. 28–34.

139. *Летохов В.С.* Оптические резонансы, индуцируемые лазерным излучением // Вестник АН СССР. 1973. Т. 10. С. 9–19.

140. *Голгер А.Л., Летохов В.С.* Инверсия населенностей на колебательных переходах в молекулярном газе высокого давления при лазерной накачке // Квантовая электроника. 1973. Т. 5 (17). С. 106–115.

141. *Баграташвили В.Н., Князев И.Н., Кудрявцев Ю.А., Летохов В.С.* Электрохимический HF-лазер высокого давления // Письма в ЖЭТФ. 1973. Т. 18 (2). С. 110–113.

142. *Летохов В.С., Чеботаев В.П.* Резонансные явления при насыщении поглощения лазерным излучением // УФН. 1974. Т. 113 (3). С. 385–434.

143. *Ambartsumian R.V., Chekalin N.V., Doljikov V.S., Letokhov V.S., Ryabov E.A.* The visible luminescence kinetics of BCl_3 in the field of a high-power CO_2 laser // Chem. Phys. Lett. 1974. Vol. 25 (4). P. 515–518.

144. *Агейкин В.А., Баграташвили В.Н., Князев И.Н., Кудрявцев Ю.А., Летохов В.С.* Спектр излучения электроионизационного лазера на двуокиси углерода с высоким давлением // Квантовая электроника. 1974. Т. 1 (2). С. 334–340.

145. *Letokhov V.S.* Vibrational satellites of γ–transitions of nuclei in the molecules, Phys. Lett. 1974. Vol. 46A. P. 257–258.

146. *Letokhov V.S., Makarov A.A.* Selectivity of chemical reactions stimulated by infrared laser radiation in molecular gas mixture // J. of Photochemistry. 1974. Vol. 3. P. 249–265.

147. *Letokhov V.S.* Electron-nuclear γ-transitions of nuclei in atoms // Phys. Lett. 1974. Vol. 46A (7). P. 481–482.

148. *Летохов В.С., Чеботаев В.П.* Квантовые стандарты частоты оптического диапазона. Обзор. // Квантовая электроника. 1974. Т. 1 (2). С. 245–267.

149. *Гольданский В.И., Летохов В.С.* О воздействии лазерным излучением на процессы распада ядер // ЖЭТФ. 1974. Т. 67 (2). С. 513–516.

150. *Ambartsumian R.V., Letokhov V.S., Makarov G.N., Puretskii A.A.* Selective two-step dissociation of ammonia molecules // Proceed. of the First International Laser Spectroscopy Conference (Vail, USA, June 29, 1973) / ed. by R. Brewer and A. Mooradian. N.Y. and L.: Plenum Press, 1974. P. 611–630.

151. *Балыкин В.И., Голгер А.Л., Коломийский Ю.Р., Летохов В.С., Туманов О.А.* CO_2-лазер на 10,6 мкм с оптической накачкой на 9,6 мкм // Письма в ЖЭТФ. 1974. Т. 19. (7). С. 482–485.

152. *Гусев В.М., Компанец О.Н., Летохов В.С., Кукуджанов А.Р., Михайлов Е.Л.* Стабилизация частоты CO_2-лазера с точностью 10^{-12} по узким резонансам SF_6 и OsO_4 // Квантовая электроника. 1974. Т. 1 (11). С. 2465–2467.

153. *Letokhov V.S.* Narrowing and frequency tuning of positronium annihilation line by laser field // Phys. Lett. 1974. Vol. A49 (4). P. 275–277.

154. *Летохов В.С.* Возможность лазерного эффекта в атмосфере звезд // ЖЭТФ. 1974. Т. 67 (5). С. 1609–1620.

155. *Амбарцумян Р.В., Летохов В.С., Рябов Е.А., Чекалин Н.В.* Изотопически селективная химическая реакция молекул BCl_3 в сильном инфракрасном поле лазера // Письма в ЖЭТФ. 1974. Т. 20 (9), 597–600.

156. *Летохов В.С., Платова А.Г., Туманов О.А.* Измерение уширения и сдвига из-за давления вращательно-колебательной линии NH_3 (5, 3)ν2 методом внерезонансного поглощения CO_2 лазера // Оптика и спектроскопия. 1974. Т. 37 (1). С. 55–58.

157. *Летохов В.С., Павлик Б.Д.* Нелинейная спектроскопия внутри доплеровского контура с помощью «конкурентных» резонансов // Квантовая электроника. 1974. Т. 1 (11). С. 2425–2434.

158. *Летохов В.С., Лозовик Ю.Е.* О магнитной предиссоциации молекул, возбужденных лазерным излучением // Квантовая электроника. 1974. Т. 1 (11). С. 2496–2499.

159. *Голгер А.Л., Летохов В.С.* Двухквантовое резонансное возбуждение колебательных уровней двухатомных молекул лазерным излучением // Квантовая электроника. 1974. Т. 1 (4). С. 870–880.

160. *Балыкин В.И., Голгер А.Л., Коломийский Ю.Р., Летохов В.С., Туманов О.А.* Исследование импульсного CO2-лазера на длине волны 10,6 мкм с накачкой излучением CO_2–N_2–He-лазера на длине волны 9,6 мкм // Квантовая электроника. 1974. Т. 1 (11). С. 2386–2397.

161. *Letokhov V.S.* Emission and absorption of γ–radiation in molecules interacting with a light field // Phys. Rev. 1975. Vol. A12. P. 1954–1965.

162. *Chebotayev V.P., Golger A.L., Letokhov V.S.* Selective two-photon laser excitation of molecules with overlapping absorption lines, Chemical Physics Vol. **7**, 316–320 (1975).

163. *Chebotayev V.P., Letokhov V.S.* Nonlinear narrow optical resonances induced by laser radiation, Progress in Quant. Electron. / ed. by J.H. Sanders. Vol. 4, pt. 2. Pergamon Press, 1975. P. 111–206.

164. *Летохов В.С., Чеботаев В.П.* Принципы нелинейной лазерной спектроскопии. М.:Наука, 1975. 279 стр.

165. *Компанец О.Н., Летохов В.С., Миногин В.Г.* Исследование возбуждения колебательных уровней молекулы четырехокиси осмия излучением CO_2-лазера непрерывного действия // Квантовая электроника. 1975. Т. 2 (2). С. 370–379.

166. *Andreev S.V., Antonov V.S., Knyazev I.N., Letokhov V.S., Movshev V.G.* Photoionization of molecules by VUV laser radiation // Phys. Lett. 1975. Vol. 54A. P. 91–92.

167. *Knyazev I.N., Letokhov V.S., Movshev V.G.* Effective and practicable VUV hydrogen laser // IEEE Journ. Quant. Electr. 1975. QE-11. P. 805–817.

168. *Иванов Л.Н., Летохов В.С.* Селективная ионизация атомов световым и электрическим полем // Квантовая электроника. 1975. Т. 2 (3). С. 585–590.

169. *Летохов В.С., Семчишин В.А.* Селективная фотохимическая реакция молекул орто-иода при возбуждении лазерным излучением // Доклады АН СССР. 1975. Т. 222 (5). С. 1071–1074.

170. *Амбарцумян Р.В., Апатин В.М., Летохов В.С., Мишин В.И.* Мощный перестраиваемый по частоте узкополосный лазер ультрафиолетового, видимого и инфракрасного диапазонов на основе неодимового стекла для селективной фотохимии // Квантовая электроника. 1975. Т. 2 (2). С. 337–342.

171. *Амбарцумян Р.В., Летохов В.С., Макаров Г.Н., Пурецкий А.А.* Исследование колебательно-возбужденных молекул аммиака методом двойного ИК-УФ резонанса // ЖЭТФ. 1975. Т. 68 (5). С. 1736–1747.

172. *Летохов В.С.* Применение лазерного излучения в автоэлектронной и автоионной микроскопии для наблюдения биологических молекул // Квантовая электроника. 1975. Т. 2 (5). С. 930–937.

173. *Амбарцумян Р.В., Должиков В.С., Летохов В.С., Рябов Е.А., Чекалин Н.В.* Исследование диссоциации молекул BCl_3 в поле мощного импульса CO_2-лазера // ЖЭТФ. 1975. Т. 69(l). С. 72–83.

174. *Letokhov V.S.* Possible laser modification of field ion microscopy // Phys. Lett. 1975. Vol. 51A (4). P. 231–232.

175. *Letokhov V.S.* Nonlinear high resolution laser spectroscopy // Science. 1975. Vol. 190 (4212). P. 344–351.

176. *Letokhov V.S.* On the possibility of selective biochemical reactions induced by a laser radiation // J. of Photochemistry. 1975. Vol. 4 (3). P. 185–191.

177. *Иванов Л.Н., Летохов В.С.* Спектр электронно–ядерных γ-переходов ядра в атоме // ЖЭТФ. 1975. Т. 68 (5). С. 1748–1756.

178. *Компанец О.Н., Кукуджанов А.Р., Летохов В.С., Миногин В.Г., Михайлов Е.Л.* Нелинейная лазерная спектроскопия колебательно-вращательных переходов моноизотопных молекул OsO_4 и стабилизация частоты CO_2-лазера // ЖЭТФ. 1975. Т. 69 (1). С. 32–47.

179. *Амбарцумян Р.В., Горохов Ю.А., Летохов В.С., Макаров Г.Н.* Разделение изотопов серы с коэффициентом обогащения $>10^3$ при воздействии излучения CO_2-лазера на молекулу SF_6 // Письма в ЖЭТФ. 1975. Т. 21 (6). С. 375–378.

180. *Bagratashvili V.N., Knyazev I.N., Letokhov V.S., Lobko V.V.* Resonance excitation of C_2H_4-molecule luminescence by pulsed high-pressure continuously tunable CO_2 laser // Optics Commun. 1975. Vol. 14. P. 426–430.

181. *Летохов В.С., Миногин В.Г.* Спектр γ-переходов ядра в двухатомной молекуле // ЖЭТФ. 1975. Т. 69 (5). С. 1569–1581.

182. *Letokhov V.S.* Prospects of dye laser applications to the selective laser photophysics // Spectroscopy Lett. 1975. Vol. 8 (9). P. 697–709.

183. *Ambartsumian R.V., Chekalin N.V., Letokhov V.S., Ryabov E.A.* Infrared molecular photolysis by high-power laser pulse // Chem. Phys. Lett. 1975. Vol. 36 (3). P. 301–304.

184. *Амбарцумян Р.В., Горохов Ю.А., Летохов В.С., Макаров Г.Н., Рябов Е.А., Чекалин Н.В.* Разделение изотопов B^{10} и B^{11} в сильном ИК-поле CO_2-лазера // Квантовая электроника. 1975. Т. 2 (10). С. 2197–2201.

185. *Амбарцумян Р.В., Беков Г.И., Летохов В.С., Мишин В.И.* Возбуждение высоколежащих состояний атома натрия излучением лазеров на красителях и автоионизация их в электрическом поле // Письма в ЖЭТФ. 1975. Т. 21 (10). С. 595–598.

186. *Letokhov V.S.* On difference of energy levels of left and right molecules due to weak interactions // Phys. Lett. 1975. Vol. 53A (4). P. 275–276.

187. *Амбарцумян Р.В., Горохов Ю.А., Летохов В.С., Макаров Г.Н.* Взаимодействие молекулы SF_6 с мощным инфракрасным лазерным импульсом и разделение изотопов серы // ЖЭТФ. 1975. Т. 69 (6). С. 1956–1970.

188. *Letokhov V.S.* Laser-nuclear spectroscopy, Proceed. of the Second International Laser Spectroscopy Conference (Megeve, France, June 23–27, 1975) // Laser Spectroscopy. Vol. 43; of Lecture Notes in Physics Springer-Verlag, 1975. P. 18–30.

189. *Амбарцумян Р.В., Горохов Ю.А., Летохов В.С., Макаров Г.Н.* Прямое наблюдение неравновесного возбуждения высоких колебательных уровней молекулы OsO_4 под действием мощного импульса CO_2-лазера и разделение изотопов осмия // Письма в ЖЭТФ. 1975. Т. 22 (2). С. 96–100.

190. *Ambartsumian R.V., Chekalin N.V., Gorokhov Yu.A., Letokhov V.S., Makarov G.N., Ryabov E.A.* Selective photochemistry in an intense infrared field, Proceed. of the Second International Laser Spectroscopy Conference (Megeve, France, June 23–27, 1975) // Laser Spectroscopy. Vol. 43; of Lecture Notes in Physics Springer-Verlag, 1975. P.121–131.

191. *Амбарцумян Р.В., Горохов Ю.А., Летохов В.С., Макаров Г.Н., Пурецкий А.А.* Селективная диссоциация при взаимодействии сильного ИК- поля на слабые составные колебания многоатомных молекул // Письма в ЖЭТФ. 1975. Т. 22 (7). С. 374–377.

192. *Летохов В.С., Лозовик Ю.Е.* Управление химическими реакциями с помощью магнитного поля // Письма в ЖТФ. 1975. Т. 1 (13). С. 609–612.

193. *Letokhov V.S., Semchishen V.A.* Selective photochemical reaction of ortho–iodine molecules excited by laser radiation // Spectroscopy Lett. 1975. Vol. 8 (5). P. 263–274.

194. *Голгер А.Л., Летохов В.С.* Усиление в смеси изотопных молекул CO_2 при накачке излучением CO_2-лазера // Квантовая электроника. 1975. Т. 2 (7). С. 1508–1518.

195. *Ambartsumian R.V., Letokhov V.S.* Isotopically selective // Laser Focus. 1975. Vol. 11 (7). P. 48–53.

196. *Амбарцумян Р.В., Летохов В.С., Максимов С.А., Мишин В.И., Фурзиков М.П.* Метод селективного возбуждения молекул излучением лазера с поглощающей ячейкой в резонаторе // Квантовая электроника. 1975. Т. 2 (8). С. 1851–1853.

197. *Князев И.Н., Кудрявцев Ю.А., Кузьмина Н.П., Летохов В.С., Мовшев В.Г., Молчанов А.Г.* Люминесценция NaCl при интенсивном возбуждении

экситонов излучением H_2 ВУФ лазера // Письма в ЖЭТФ. 1975. Т. 21 (12). С. 722–725.

198. *Амбарцумян Р.В., Горохов Ю.А., Летохов В.С., Макаров Г.Н., Рябов Е.А., Чекалин Н.В.* Разделение изотопов в сильном ИК-лазерном поле // Квантовая электроника. 1976. Т. 3(4). С. 802–810.

199. *Ambartsumian R.V., Bekov G.I., Gorokhov Yu.A., Letokhov V.S., Makarov G.N., Mishin V.I., Ryabov E.A., Puretskii A.A., Chekalin N.V.* Laser isotope separation, Proceed. IAEA Conf. “Stable Isotopes in the Life Sciences”. Leipzig, 1977 GAEA Publ., Vienna, 1977. P. 97–100.

200. *Bourimov V.N., Letokhov V.S., Ryabov E.A.* Kinetics of luminescence of BO- and BCl radicals during IR photolysis of $BCl_3$by CO_2 laser pulse, J. of Photochemistry. 1976. Vol. 5 (1). P. 49–59.

201. *Летохов В.С., Павлик Б.Д.* Метод создания квантового стандарта частоты видимого диапазона на атомных линиях поглощения на основе непрерывного лазера на красителе // Квантовая электроника. 1976. Т. 3(1). С. 60–71.

202. *Жерихин А.Н., Кошелев К.Н., Летохов В.С.* Об усилении в области далекого вакуумного ультрафиолета на переходах многозарядных ионов // Квантовая электроника. 1976. Т. 3 (l). С. 152–156.

203. *Иванов Л.Н., Летохов В.С.* Возможность разрядки метастабильных ядер при захвате отрицательного мюона // ЖЭТФ. 1976. Т. 70 (1). С. 19–28.

204. *Balykin V.I., Letokhov V.S., Mishin V.I., Semchishen V.A.* Kinetics of photophysical and photochemical processes involving selective excitation of ortho-I_2 by laser radiation // Chem. Phys. 1976. Vol. 17, 111–112.

205. *Коломийский Ю.Р., Летохов В.С., Туманов О.А.* Исследование колебательного возбуждения молекулы OCS и генерации при накачке импульсом излучения CO_2-лазера // Квантовая электроника. 1976. Т. 3 (8). С. 1771–1781.

206. *Амбарцумян Р.В., Апатин В.М., Летохов В.С., Макаров Г.Н., Мишин В.И., Пурецкий А.А., Фурзиков Н.П.* Селективная двухступенчатая ионизация атомов Rb лазерным излучением // ЖЭТФ. 1976. Т. 70 (5). С.1660–1673.

207. *Гоменюк А.С., Жаров В.П., Летохов В.С., Рябов Е.А.* Лазерный оптико-акустический метод измерения относительного содержания изотопов в молекулах // Квантовая электроника. 1976. Т. 3 (2). С. 369–373.

208. *Letokhov V.S., Ryabov E.A., Tumanov O.A., Gomenyuk A.S., Zharov V.P.* High-sensitivity method for the absorption measurement of the relative concentration of isotopes. In: Stable Isotope in the Life Sciences. Vienna: Int. Atomic Energy Agency, 1977. P. 159–164.

209. *Letokhov V.S.* Laser methods of γ-spectroscopy without Doppler broadening // Comments on Atomic and Molecular Physics. 1976. Vol. 5 (4). P. 117–127.

210. *Летохов В.С., Миногин В.Г.* Спектр гамма-перехода симметричной многоатомной молекулы // ЖЭТФ. 1976. Т. 70 (3). С. 794–804.

211. *Летохов В.С., Мур С.Б.* Лазерное разделение изотопов. Ч. 1 (обзор) // Квантовая электроника. 1976. Т. 3 (2). С. 248–287; Лазерное разделение изотопов. Ч. 2. Там же: 1976. Т. 3 (3). С. 485–516.

212. *Letokhov V.S.* Saturation spectroscopy, in: High Resolution Laser Spectroscopy / ed. by K. Shimoda. Chap. 3. Topics in Applied Physics. Springer-Verlag, 1976. Vol. 13. P. 95–171.

213. *Летохов В.С.* Проблемы лазерной спектроскопии// УФН 118(2), 199–249 (1976).

214. *Ambartsumian R.V., Letokhov V.S.* Isotopically-selective dissociation of polyatomic molecules by an intense IR laser field // Comments on Atomic and Molecular Physics. 1976. Vol. 6 (l). P. 13–25.

215. *Амбарцумян Р.В., Летохов В.С.* Лазерное разделение изотопов // Вестник АН СССР. 1976. Т. 11. С. 25–36.

216. *Ambartsumian R.V., Letokhov V.S.* Isotope separation by IR laser photoexcitation and dissociation of molecules. In: Nuclear Energy Maturity. Vol. 12, Enrichment and Fusion / ed. by P. Zaleski. Pergamon Press, 1976. P. 26–27.

217. *Амбарцумян Р.В., Горохов Ю.А., Летохов В.С., Пурецкий А.А.* Исследование механизма диссоциации молекулы SF_6 излучением CO_2–лазера // ЖЭТФ. 1976. Т. 71. С. 440–453.

218. *Letokhov V.S., Makarov A.A.* Leakage effect as an exciting mechanism of the high vibrational levels of polyatomic molecules by strong quasiresonant IR laser field // Optics Commun. 1976. Vol. 17 (3). P. 250–253.

219. *Летохов В.С., Миногин В.Г.* Нелинейные узкие резонансы без доплеровского уширения оптических переходов и аннигиляционного излучения атома позитрония // ЖЭТФ. 1976. Т. 71 (l). С. 135–147.

220. *Лавринович Н.Н., Летохов В.С.* О детектировании узких “лазерных” линий, скрытых пространственно-неоднородным уширением, в излучении звездных атмосфер // Квантовая электроника. 1976. Т. 3 (9). С. 1948–1954.

221. *Амбарцумян Р.В., Горохов Ю.А., Летохов В.С., Макаров Г.Н., Пурецкий А.А., Фурзиков Н.П.* Селективность диссоциации многоатомных молекул в двухчастотном ИК-лазерном поле // Письма в ЖЭТФ. 1976. Т. 23 (4). С. 217–220.

222. *Ambartsumian R.V., Chekalin V.N.,. Doljikov V.S, Letokhov V.S., Lokhman V.N.* Selective trans-cis isomerization of $C_2H_2Cl_2$ molecule in an intense laser infrared field // Optics Commun. 1976. Vol. 18 (3). P. 400–402.

223. *Ambartsumian R.V., Furzikov N.P., Gorokhov Yu.A., Letokhov V.S., Makarov G.N., Puretskii A.A.* Selective dissociation of SF_6 molecules in two–frequency infrared laser field // Optics Commun. 1976. Vol. 18 (4). P. 517–521.

224. *Bagratashvili V.N., Knyazev I.N., Letokhov V.S., Lobko V.V.* Optoacoustical detection of multiple photon molecular absorption in a strong IR field // Optics Commun. 1976. Vol. 18(4). P. 525–528.

225. *Letokhov V.S., Minogin V.G., Pavlik B.D.* Cooling and trapping of atoms and molecules by resonant laser field // Optics Commun. 1976. Vol. 19 (1). P. 72–75.

226. *Kompanets O.N., Kukudzhanov A.R., Letokhov V.S., Gervitz L.L.* Narrow resonances of saturated absorption of dissymmetrical molecules CHFClBr and possibility of weak current detection in molecular physics // Optics Commun. 1976. Vol. 19 (3). P. 414–416.

227. *Letokhov V.S.* Future applications of selective laser photophysics and photochemistry. Proceed. of the Conference Tunable Lasers and Their Applications (Loen, Norway, June 8–11, 1976) / ed. by A. Mooradian, T. Jaeger, P. Stokseth Berlin, Heidelberg, New York: Springer-Verlag, 1976. P. 122–139.

228. *Chekalin V.N., Doljikov V.S., Kolomiisky Yu.R., Letokhov V.S., Lokhman V.N., Ryabov E.A.* Isotope shift in the spectrum of multiquantum absorption of nitromethane molecule in intense IR field // Phys. Lett. 1976. Vol. 59A. P. 243–244.

229. *Балыкин В.И., Летохов В.С., Мишин В.И., Семчишен В.А.* Лазерное детектирование низких концентраций атомов урана, образующихся в результате химической реакции // Письма в ЖЭТФ. 1976. Т. 24 (8). С. 475–478.

230. *Потапов В.К., Мовшев В.Г., Летохов В.С., Князев И.Н., Евлашева Т.И.* Применение водородного ВУФ лазера для изучения процессов фотоионизации молекул в масс-спектрометре // Квантовая электроника. 1976. Т. 3 (12). С. 2610–2612.

231. *Баграташвили В.Н., Князев И.Н., Летохов В.С., Лобко В.В.* Исследование CO_2-лазера высокого давления с плавной перестройкой частоты // Квантовая электроника. 1976. Т. 3 (5). С. 1011–1026.

232. *Голгер Л.Л., Летохов В.С., Федосеев С.П.* Штарковский сдвиг частоты молекулярных переходов в резонансном световом поле // Квантовая электроника. 1976. Т. 3 (7). С. 1457–1470.

233. *Ambartsumian R.V., Furzikov N.P., Letokhov V.S., Puretskii A.A.* Measuring photoionization cross sections of excited atomic states // Appl. Phys. 1976. Vol. 9. P. 335–337.

234. *Ambartsumian R.V., Gorokhov Yu.A., Letokhov V.S., Makarov G.N., Puretskii A.A.* Isotope–selective dissociation of CCl_4 molecule by excitation of compound vibrational bands by intense infrared field, Phys. Lett. 1976. Vol. 56A, P. 183–185.

235. *Амбарцумян Р.В., Горохов Ю.А., Летохов В.С., Макаров Г.Н., Пурецкий А.А.* Объяснение селективной диссоциации молекулы SF_6 в сильном ИК- поле лазера // Письма в ЖЭТФ. 1976. Т. 23 (l). С. 26–30.

236. *Ambartsumian R.V., Chekalin V.N., Doljikov V.S., Letokhov V.S., Lokhman V.N.* Trans–cis isomerization of $C_2H_2Cl_2$ molecules, selective dissociation and the role of thermal processes in an intense IR laser field // J. of Photochem. 1976. Vol. 6 (l). P. 55–67.

237. *Князев И.Н., Кудрявцев Ю.А., Кузьмина Н.П., Летохов В.С., Мовшев В.Г., Молчанов А.Г.* Исследование фотолюминесценции кристаллов галогенидов щелочей под воздействием ВУФ–H_2-лазера. ФТТ. 1976. Т. 18. С. 3593–3598.

238. *Letokhov V.S., Pavlik B.D.* Spectral line narrowing in gas by atoms trapped in a standing light wave // Appl. Phys. 1976. Vol. 9. P. 229–237.

239. *Letokhov V.S.* Laser spectroscopy. Berlin: Akademie Verlag, 1977. 221 pp.

240. *Letokhov V.S.* Laser and nuclear spectrosco“crossings, in: Frontiers in Laser Spectroscopy (Les Houches, Session XXVII, 1975). Vol. 2 / ed. by R. Balian. North-Holland Publ. Co., 1977. P. 715–770.

241. *Letokhov V.S.* Principles of laser isotope separation, in: Frontiers in Laser Spectroscopy (Les Houches, Session XXVII, 1975). Vol. 2 / ed. by R. Balian. North-Holland Publ. Co., 1977. P. 771–868.

242. *Letokhov V.S., Mishin V.I., Puretskii A.A.* Selective photoionization of atoms by laser radiation and its application. Progr. of Quant. Electronics / ed. by J.H. Sanders and S. Stenholm. Oxford, New York: Pergamon Press, 1977. Vol. 5, P. 139–204.

243. *Andreev S.V., Antonov V.S., Knyazev I.N., Letokhov V.S.* Two–step photoionization of H_2CO molecule by radiation of N_2–and H_2–lasers and measurement of the lifetime of state $_1A^2$ // Chem. Phys. Lett. 1977. Vol. 45 (l). P. 166–168.

244. *Амбарцумян Р.В., Горохов Ю.А., Григорович С.Л., Летохов В.С., Макаров Г.Н., Малинин Ю.А., Пурецкий А.А., Филиппов Э.П., Фурзиков Н.П.* Очистка веществ в газовой фазе ИК-лазерным излучением // Квантовая электроника. 1977. Т. 4 (l). С. 171–173.

245. *Ambartsumian R.V., Letokhov V.S.* Selective dissociation of polyatomic molecules by intense IR laser field // Accounts of Chem. Res. 1977. Vol. 10. P. 61–67.

246. *Zharov V.P., Letokhov V.S., Ryabov E.A.* Optoacoustic laser spectroscopy of excited vibrational molecular states // Applied Phys. Vol. 12(l), 15–18 (1977).

247. *Letokhov V.S., Chebotayev V.P.* Nonlinear laser spectroscopy. Berlin, Heidelberg, New York: Springer-Verlag, 1976. 466 pp.

248. *Chekalin V.N., Doljikov V.S., Letokhov V.S., Lokhman V.N., Shibanov A.N.* Dye laser probing of primary C_2 radicals formed by IR intense field photolysis of ethylene // Appl. Phys. 1977. Vol. 12 (2). P. 191–196.

249. *Летохов В.С., Миногин В.Г., Павлик Б.Д.* Охлаждение и пленение атомов и молекул резонансным световым полем // ЖЭТФ. 1977. Т. 72 (4). Т. 1328–1341.

250. *Letokhov V.S.* Laser control of atomic motion: velocity selection, cooling and trapping // Comments on Atom. and Molecular Physics. 1977. Vol. 6. P. 119–131.

251. *Letokhov V.S., Moore C.B.* Laser isotope separation. In: Chemical and Biochemical Applications of Lasers / ed. by C.B. Moore. Orlando: Academic Press, 1977.Vol. III, Chap. 1. P. 1–165.

252. *Chekalin V.N., Doljikov V.S., Kolomiisky Yu.R., Letokhov V.S., Lokhman V.N., Ryabov E.A.* Experimental selection of molecules for isotope separation by multiple photon dissociation in an intense IR field // Appl. Phys. 1977. Vol. 13 (4), P. 311–316.

253. *Ambartsumian R.V., Letokhov V.S.* Multiple infrared photon laser photochemistry. In: Chemical and Biochemical Applications of Lasers / ed. by C.B. Moore. 1977. Vol. III, Chap. 2. P. 166–316.

254. *Letokhov V.S., Minogin V.G.* Quantum motions of ultracooled atoms in resonant laser field. Phys. Lett. 1977. Vol. 61A. P. 370–372.

255. *Беков Г.И., Летохов В.С., Мишин В.И.* Ионизация импульсным электрическим полем высоколежащих состояний атома натрия // ЖЭТФ. 1977. Т. 73 (1). С. 157–165.

256. *Bekov G.I., Letokhov V.S., Mishin V.I.* Isotopically selective Rb atoms ionization through Rydberg states by laser and electric pulsed fields // Optics Comm. 1977. Vol. 23. P. 85–89.

257. *Letokhov V.S.* Possible connection between weak interaction and the biological isomerism // Lettere al Nuovo Cimento. 1977. Vol. 20 (3). P. 107–111.

258. *Letokhov V.S.* Laser separation of isotopes // Annual Review of Physical Chemistry. 1977. Vol. 28. P. 133–159.

259. *Bagratashvili V.N., Kolominsky Yu.R., Letokhov V.S., Ryabov E.A., Baranov V.Yu., Kazakov S.A., Nizjev N.G., Pismenny V.D., Starodubtsev A.I., Velikhov E.P.* The application of high pulse repetition rate CO_2 laser with high average power for isotope separation by molecular dissociation in a strong IR field // Appl. Phys. 1977. Vol. 14. P. 217–220.

260. *Антонов В.С., Князев И.Н., Летохов В.С., Мовшев В.Г.* Фотоионизация молекул из основного и селективно возбужденного состояний с помощью излучения H_2 VUV лазера // ЖЭТФ. 1977. Т. 73(4). С. 1325–1339.

261. *Letokhov V.S.* Photophysics and photochemistry // Physics Today. 1977. Vol. 30 (5). P. 23–32.

262. *Ambartsumian R.V., Furzikov N.P., Gorokhov Yu.A., Letokhov V.S., Makarov G.N., Puretskii A.A.* Isotope-selective dissociation of OsO_4 molecule by two pulses of infrared radiation at different frequencies // Opt. Lett. 1977. Vol. 1. P. 22–24.

263. *Letokhov V.S.* Laser selective detection of ultralow concentrations of atoms // Comm. on Atomic and Molec. Phys. 1977. Vol. 7(3/4). P. 93–105.

264. *Letokhov V.S.* Laser selective detection of ultralow concentrations of molecules // Comm. on Atomic and Molec. Phys. 1977. Vol. 7 (3/4). P. 107–116.

265. *Алимпиев С.С., Баграташвили В.Н., Карлов Н.В., Летохов В.С., Лобко В.В., Макаров А.А., Сартаков Б.Г., Хохлов Э.М.* Эффект опустошения многих вращательных состояний при колебательном возбуждении молекул в сильном ИК поле // Письма в ЖЭТФ. 1977. Т. 25 (12). С. 582–585.

266. *Жерихин А.Н., Кошелев К.Н., Крюков П.Г., Летохов В.С., Чекалин С.В.* Наблюдение аномалий интенсивности в области 58–78 Å на переходах Cl VII при двухступенчатом нагреве плазмы ультракороткими лазерными импульсами // Письма в ЖЭТФ. 1977. Т. 25 (7). С. 325–328.

267. *Балыкин В.И., Летохов В.С., Мишин В.И., Семчишин В.А.* Лазерное флуоресцентное детектирование единичных атомов // Письма в ЖЭТФ. 1977. Т. 26 (6). 492–495.

268. *Akhmanov A.S., Baranov V.Yu., Pis'menny V.D., Bagratashvili V.N., Kolominsky Yu.R., Letokhov V.S., Ryabov E.A.* Multiple photon excitation of polyatomic molecules from the many rotation states by intense pulse of IR radiation // Optics Comm. 1977. Vol. 23 (3). P. 357–361.

269. *Антонов В.С., Князев И.Н., Летохов В.С., Матюк В.М., Мовшев В.Г., Потапов В.К.* Масс-спектрометр с селективной ступенчатой фотоионизацией молекул лазерным излучением // Письма в ЖЭТФ. 1977. Т. 3 (23). С. 1287–1291.

270. *Летохов В.С., Мишин В.И., Пурецкий А.А.* Селективная фотоионизация атомов лазерным излучением. В кн.: Химия плазмы / под ред. Б.М. Смирнова. Т. 4. М.: Атомиздат, 1977. 1–60.

271. *Аватков О.Н., Баграташвили В.Н., Князев И.Н., Коломийский Ю.Р., Летохов В.С., Лобко В.В., Рябов Е.А*. Многоквантовое поглощение, люминесценция и диссоциация молекул этилена в поле мощного импульса CO_2-лазера // Квантовая электроника. 1977. Т. 4 (4). С. 741–750.

272. *Антонов В.С., Князев И.Н., Летохов В.С., Матюк В.М., Мовшев В.Г., Потапов В.К.* Наблюдение двухступенчатой фотоионизации молекулы бензальдегида лазерным излучением в масс-спектрометре // Химия высоких энергий. 1978. Т. 12 (5). С. 476–478.

273. *Letokhov V.S.* Laser spectroscopy, Optics and Laser Technology Vol. 9. P. 217 (1977); ibid. Vol. 9. P. 263 (1977); ibid. Vol. 10. P. 15 (1978); ibid. Vol. 10. P 129 (1978); ibid. Vol. 10. P. 175 (1978); ibid. Vol. 10. P. 301 (1978); ibid. Vol. 11. P. 13 (1979); ibid. Vol. 13. P. 131 (1981); ibid. Vol. 13. P. 203 (1981).

274. *Летохов В.С.* Селективное действие лазерного излучения на вещество // УФН. 1978. Т. 125 (1). С. 57–96.

275. *Letokhov V.S.* Multiple photon excitation and dissociation of molecules and isotope separation by intense IR laser radiation, Multiphoton Processes, Proceed. of Intern. Confer. on Multiphoton Processes (Rochester, USA, June 6–9, 1977) / ed. by J.H. Eberly and P. Lamboropoulos. Wiley and Sons, 1978. P. 331–347.

276. *Ambartsumian R.V., Furzikov N.P., Letokhov V.S., Dyad'kin A.P., Grasyuk A.Z., Vasil'yev B.I.* Isotopically selective dissociation of CCl4 molecules by NH3 laser radiation // Appl. Phys. 1978. Vol. 15 (1). P. 27–30.

277. *Крюков П.Г., Лазарев Ю.А., Летохов В.С., Матвеец Ю.А., Терпугов Э.Л., Чекулаева Л.Н., Шарков А.В.* Пикосекундный импульсный фотолиз бактериородопсина из Halobacterium Halobium при комнатной и низких температурах // Биофизика. 1978. Т. 23 (1). С. 71–73.

278. *Letokhov V.S.* Laser selective photophysics and photochemistry, in: Progress in Optics / ed. by E. Wolf. North-Holland, 1978. Vol. XVI. P. 1–69.

279. *Беков Г.И., Летохов В.С., Мишин В.И.* Лазерное фотоионизационное детектирование единичных атомов натрия через ридберговские состояния // Письма в ЖЭТФ. 1978. Т. 27 (l). С. 52–56.

280. *Апатин В.М., Летохов В.С., Мишин В.И.* Эффект Штарка на высоковозбужденных лазерным излучением состояниях атома натрия // Квантовая электроника. 1978. Т. 5 (3). С. 632–636.

281. *Летохов В.С., Миногин В.Г.* Квантовые движения атома в резонансном поле стоячей световой волны // ЖЭТФ. 1978. Т. 74 (4). С. 1318–1335.

282. *Letokhov V.S., Makarov A.A.* Excitation of multilevel molecular systems by laser IR field. Frequency-dynamic effects // Appl. Phys. 1978. P. 47–57.

283. *Беков Г.И., Летохов В.С., Мишин В.И.* Сильно возбужденные (ридберговские) атомные состояния в электрическом поле. Лекции IV Всесоюзной школы "Физика электронных и атомных столкновений". Изд. МГУ, 1978. С. 226–241.

284. *Ambartsumian R.V., Letokhov V.S., Makarov G.N., Puretskii A.A.* Characteristics of multiple photon dissociation of OsO_4 molecule by two frequency tunable CO_2 laser pulses // Optics Comm. 1978. Vol. 25 (1). P. 69–74.

285. *Knyazev I.N., Letokhov V.S., Lobko V.V.* Role of weak transitions in multiphoton excitation of molecules by IR laser radiation // Optics Commun. 1978. Vol. 25. P. 337–342.

286. *Князев И.Н., Кудрявцев Ю.А., Кузьмина Н.П., Летохов В.С.* Изомеризация молекул при многофотонном колебательном и последующем электронном возбуждении лазерным излучением // ЖЭТФ. 1978. Т. 74 (6). С. 2017–2026.

287. *Baranov V.Yu., Kazakov S.A., Pismenny V.D., Starodubtsev A.I., Velikhov E.P., Gorokhov Yu.A., Letokhov V.S., Dyadkin A.P., Grasiuk A.Z., Vasilyev B.I.* Multiwatt optically pumped ammonia laser operation in the 12–13 μm region // Appl. Phys. 1978. Vol. 17. P. 317–320.

288. *Letokhov V.S., Minogin V.G.* Trapping and storage of atoms in laser field // Appl. Phys. 1978. Vol. 17. P. 99–103.

289. *Letokhov V.S.* Multiphoton and multistep vibrational laser spectroscopy of molecules // Comm. Atom. Mol. Phys. 1978. Vol. 8 (l/2). P. 39–49.

290. *Letokhov V.S., Minogin V.G.* Laser monochromator of a relativistic proton beam with resolution and accuracy up to 2×10^5 // Phys. Rev. Lett. 1978. Vol. 41 (12). P. 775–777.

291. *Летохов В.С., Лобашев В.М., Миногин В.Г., Мишин В.И.* Метод получения поляризованных протонов лазерным излучением // Письма в ЖЭТФ. 1978. Т. 27 (5). С. 305–308.

292. *Antonov V.S., Knyazev I.N., Letokhov V.S., Matyuk V.M., Movshev V.G., Potapov V.K.* Stepwise laser photoionization of molecules in mass–spectrometer: a new method of probing and detection of polyatomic molecules // Optics Lett. 1978. Vol. 3(2). P. 37–39.

293. *Bekov G.I., Letokhov V.S., Matveev O.I., Mishin V.I.* Single–atom detection of ytterbium by selective laser excitation and field ionization from Rydberg states // Optics Lett. 1978. Vol. 3 (5). P. 159–161.

294. *Баграташвили В.Н., Должиков В.С., Летохов В.С., Рябов Е.А.* Изотопически-селективная диссоциация молекул CF_3I при повышенном давлении под действием импульсного излучения CO_2-лазера // Письма в ЖТФ. 1978. Т. 4 (19). С. 1181–1186.

295. *Knyazev I.N., Kudriavtsev Yu.A., Kuzmina N.P., Letokhov V.S., Sarkisian A.A.* Laser isotope separation of carbon by multiple IR photon and subsequent UV excitation of CF_3I molecules // Appl. Phys. 1978. Vol. 17 (4). P. 427–429.

296. *Беков Г.И., Летохов В.С., Матвеев О.И., Мишин В.И.* Ионизационное детектирование единичных атомов лазерным излучением через ридберговские состояния // ЖЭТФ. 1978. Т. 75 (5). С. 2092–2101.

297. *Balykin V.I., Bekov G.I., Letokhov V.S., Mishin V.I.* Laser detection of single atoms. In: Atomic Physics — 6 / ed. by R.J. Damburg. Proceed. VI Intern. Conf., Riga, August, 1978 (Zinante — Riga). New York and London: Plenum Press, 1979. P. 565–584.

298. *Беков Г.И., Летохов В.С., Матвеев О.И., Мишин В.И.* Обнаружение долгоживущего автоионизационного состояния в спектре атома гадолиния // Письма в ЖЭТФ. 1978. Т. 28 (5). С. 308–311.

299. *Kryukov P.G., Letokhov V.S., Matveyev O.I., Nikogosian D.N., Sharkov A.V.* Picosecond research of some biomolecules (bacteriorhodopsin, bacteriochlorophyll and based of DNA). In: Picosecond Phenomena / ed. by C.V. Shank, E.P.Ippen, and

S.L. Shapiro. Springer Series in Chem. Phys. Heidelberg: Springer-Verlag, 1978. Vol. 4. P. 158–166.

300. *Letokhov V.S.* Laser separation of isotopes. Proceed. of IV General Meeting of EPS Trends in Physics (Sept. 25–29, 1978, York, England). Aldarad and Sons, Ltd., 1979. P. 61–73.

301. *Крюков П.Г., Летохов В.С., Матвеец Ю.А., Никогосян Д.Н., Шарков А.В.* Селективное двухступенчатое возбуждение электронного состояния органических молекул в водном растворе пикосекундными импульсами света // Квантовая электроника. 1978. Т. 5 (11). С. 2490–2492.

302. *Компанец О.Н., Летохов В.С.* Стандарты частоты и длины лазера, в кн.: Справочник по лазерам. М.:Советское радио, 1978. Т. 1, гл. 10, 221–235.

303. *Князев И.Н., Летохов В.С.* Газовые лазеры в УФ- и ВУФ-областях спектра, в кн.: Справочник по лазерам, под ред. А.М. Прохорова. Т. 1. Гл. 9. М., 1978. С. 197–220.

304. *Апатин В.М., Летохов В.С., Мишин В.И.* Эффект Штарка на высоковозбужденных лазерным излучением состояниях атома натрия // Квантовая электроника. 1978. Т. 5 (8). С. 632–636.

305. *Амбарцумян Р.В., Васильев Б.И., Грасюк А.З., Дядькин А.П., Летохов В.С., Фурзиков Н.П.* Изотопически-селективная диссоциация молекул CC_{l4} излучением мощного NH_3-лазера // Квантовая электроника. 1978. Т. 5 (8). С. 1791–1795.

306. *Летохов В.С., Чеботаев В.П.* Нелинейные узкие резонансы в оптике и их применение // Природа. 1978. № 3. С. 78–94.

307. *Letokhov V.S., Chebotayev V.P.* Narrow nonlinear resonances in optics and their applications // Europhysics News. 1978. Vol. 9 (1/2). P. 10–16.

308. *Летохов В.С., Чеботаев В.П.* Узкие нелинейные резонансы в оптике и их применение // Труды ГОИ. Ленинград, 1981. С. 182, 3–21.

309. *Баранов В.Ю., Васильев Б.И., Велихов Е.П., Горохов Ю.А., Грасюк А.З., Дядькин А.П., Казаков С.А., Летохов В.С., Письменный В.Д., Стародубцев А.И.* Импульсно-периодический режим CF4-лазера с оптической накачкой и средней мощностью генерации 0,2 Вт // Квантовая электроника. 1978. Т. 5 (4). С. 940–943.

310. *Летохов В.С., Миногин В.Г.* Монохроматизация пучка релятивистских протонов лазерным излучением // Вестник МГУ. Сер. физ., астр. Т. 19 (4). С. 146–150.

311. *Антонов В.С., Князев И.Н., Летохов В.С., Матюк В.М., Мовшев В.Г., Потапов В.К.* Лазерная спектроскопия сложных изолированных молекул методом ступенчатой фотоионизации в масс-спектрометре // Изв. АН СССР. Сер. физ. 1979. Т. 43 (2). С. 414–418.

312. *Князев И.Н., Летохов В.С., Матюк В.М., Мовшев В.Г., Потапов В.К.* Исследование процессов фотодиссоциации молекул лазерным УФ-излучением, в кн.: Кинетическая масс-спектрометрия и ее аналитические применения. М.: АН СССР, 1979. С. 189–190.

313. *Балыкин В.И., Беков Г.И., Летохов В.С., Мишин В.И.* Лазерное детектирование единичных атомов. Труды 1-й Всесоюзной школы по применению

лазеров в атомной, молекулярной и ядерной физике, г. Вильнюс, август 1978. М.: Наука, 1979. С. 41–59.

314. *Bagratashvili V.N., Dolzhikov V.S., Letokhov V.S., Ryabov E.A.* Highly efficient laser isotope separation by IR radiation, in: Proceed. of 2nd gas–flow and chemical lasers symposium (Belgium, Sept. 11–15, 1978). P. 23–26.

315. *Летохов В.С.* Применение лазеров в исследованиях ядерной физики. Труды 1-й Всесоюзной школы по применению лазеров в атомной, молекулярной и ядерной физике, г. Вильнюс, август 1978. М.:Наука,1979. С. 413–431.

316. *Летохов В.С.* Лазерная спектроскопия в ядерной физике // Вестник АН СССР. Т. 4. С. 38–48. 1978.

317. *Крюков П.Г., Летохов В.С.* Воздействие мощных ультракоротких импульсов на биоорганические молекулы. Труды международного симпозиума Сверхбыстрые процессы в спектроскопии, г. Таллин, 27 сент.–1 окт. 1978 г. Таллин: Изд. АН ЭССР, 1978. С. 145–160.

318. *Велихов Е.П., Летохов В.С., Макаров А.А., Рябов Е.А.* Разделение изотопов методом многофотонной диссоциации молекул излучением мощного CO_2-лазера. I. Пути практической реализации процесса // Квантовая электроника. 1979. Т. 6 (2). С. 317–326.

319. *Баранов В.Ю., Велихов Е.П., Казаков С.А., Коломийский Ю.П., Летохов В.С., Письменный В.Д., Рябов Е.А., Стародубцев А.И.* Разделение изотопов методом многофотонной диссоциации молекул излучением мощного CO_2-лазера. III. Исследование процесса для изотопов серы и молекулы SF_6 // Квантовая электроника. 1979. Т. 6 (4). С. 823.

320. *Chekalin N.V., Letokhov V.S., Lokhman V.N., Shibanov A.N.* Primary products of multiphoton dissociation of the C_2H_4 molecule in an intense laser field // Chem. Phys. 1979. Vol. 36 (3). P. 415–421.

321. *Баграташвили В.Н., Должиков В.С., Летохов В.С.* Кинетика спектров ИК- поглощения молекул SF_6, колебательно возбужденных мощным импульсом CO_2-лазера // ЖЭТФ. 1979. Т. 76 (l). С. 18–25.

322. *Kryukov P.G., Letokhov V.S., Nikogosyan D.N., Borodavkin A.V., Budowsky E.I., Simukova N.A.* Multiquantum photoreactions of nucleic acid components in aqueous solution by powerful ultrashort picosecond radiation // Chem. Phys. Lett. 1979. Vol. 61 (2). P. 375–379.

323. *Letokhov V.S.* Laser control of proton beam parameters // Comm. on Atom. and Mol. Phys. 1979. Vol. 8 (3/4). P. 103–112.

324. *Князев И.Н., Кудрявцев Ю.А., Кузьмина Н.П., Летохов В.С.* Изотопически-селективная фотодиссоциация молекул CF_3I при многофотонном колебательном и последующем электронном возбуждении лазерным излучением // ЖЭТФ. 1979. Т. 76 (4). С. 1281–1292.

325. *Балыкин В.И., Летохов В.С., Мишин В.И.* Наблюдение охлаждения свободных атомов натрия в резонансном лазерном поле со сканируемой частотой // Письма в ЖЭТФ. 1979. Т. 29 (10). С. 614–618.

326. *Letokhov V.S.* Laser isotope separation, Nature. 1979. Vol. 277 (5698). P. 605–610.

327. *Letokhov V.S., Mishin V.I.* Highly selective multistep ionization of atoms by laser radiation // Optics. Comm. 1979. Vol. 29 (2). P. 168–171.

328. *Баранов В.Ю., Велихов Е.П., Коломийский Ю.П., Летохов В.С., Низьев В.Г., Письменный В.Д., Рябов Е.А.* Разделение изотопов методом многофотонной диссоциации молекул излучением мощного CO_2-лазера. IV. Обогащение изотопа ^{33}S при воздействии на охлажденный газ SF_6 // Квантовая электроника. 1979. Т. 6 (5). С. 1062–1069.

329. *Баграташвили В.Н., Должиков В.С., Летохов В.С., Макаров А.А., Рябов Е.А., Тяхт В.В.* Многофотонное инфракрасное возбуждение и диссоциация молекулы CF_3I: эксперимент и модель // ЖЭТФ. 1979. Т. 77 (6). С. 2238–2253.

330. *Bagratashvili V.N., Dolzhikov V.S., Letokhov V.S., Ryabov E.A.* Isotopic selectivity of IR laser photodissociation of CF3I molecules // Appl. Phys. 1979. Vol. 20 (3). P. 231–235.

331. *Bagratashvili V.N., Dolzhikov V.S., Letokhov V.S., Ryabov E.A.* Study of primary characteristics of multiple IR photon excitation and dissociation of CF_3I, in: Laser Induced Processes in Molecules / ed. by K. Kompa and S.D. Smith, Springer Series in Chemical Physics. Berlin: Sprinder-Verlag, 1979. Vol. 6. P. 179–185.

332. *Балыкин В.И., Летохов В.С., Мишин В.И.* Лазерное флуоресцентное детектирование одиночных атомов // ЖЭТФ. 1979. Т. 77 (6). С. 2221–2237.

333. *Letokhov V.S.* Laser-induced selective multistep process: impact on nuclear physics, chemistry and biology, in: Laser Spectroscopy–IV, Proceed. of Intern. Conf. (Rottach–Egern, FRG, June 11–15, 1979), Springer Series of Optical Sciences. Berlin, Heidelberg, New York: Springer-Verlag, 1979. Vol. 21. P. 504–516.

334. *Bekov G.I., Vidolova-Angelova E.P., Letokhov V.S., Mishin V.I.* Selective detection of single atoms by multistep excitation and ionization through Rydberg states, in: Laser Spectroscopy-IV, Proceed. of Intern. Conf. (Rottach– Egern, FRG, June 11–15, 1979). Springer Series of Optical Sciences. Berlin, Heidelberg, New York: Springer-Verlag, 1979. Vol. 21. P. 283–294.

335. *Абдушелишвили Г.И., Аватков О.Н., Андрющенко В.И., Баграташвили В.Н., Бахтадзе А.Б., Вецко В.М., Должиков В.С., Есадзе Г.Г., Летохов В.С., Рябов Е.А., Ткешелашвили Г.И.* Селективная ИК-диссоциация молекул CF_3I и CF_3Br в присутствии акцепторов // Письма в ЖТФ. 1979. Т. 4 (14). С. 849–852.

336. *Домнин Ю.С., Кошеляевский Н.Б., Татаренков В.М., Шумяцкий П.С., Компанец О.Н., Кукуджанов А.Р., Летохов В.С., Михайлов Е.Л.* $CO_2/^{192}OsO_4$ лазер: абсолютная частота световых колебаний и новые возможности // Письма в ЖЭТФ. 1979. Т. 30 (5). С. 269–272.

337. *Letokhov V.S., Minogin V.G.* Cooling, trapping and storage of atoms by resonant field // JOSA. 1979. Vol. 69 (3). P. 413–419.

338. *Летохов В.С.* Прогресс в применении лазеров в атомной, молекулярной и ядерной физике. Труды 1-й Всесоюзной школы по применению лазеров в атомной, молекулярной и ядерной физике, Вильнюс, август 1979. М.: Наука, 1979. С. 24–40.

339. *Letokhov V.S.* Progress in laser applications in atomic, molecular and nuclear physics // Comm. on Atom. Molec. Phys. 1981. Vol. 10 (2/3). P. 39–46.

340. *Belogurov A.A., Zavil'gel'skii G.B., Angelov D.A., Kryukov P.G., Letokhov V.S., Nikogosyan D.N.* Effect of ultrashort laser pulses on the lambda bacteriophage // Studia Biophysica. 1980. Vol. 80 (l). P. 45–51.

341. *Angelov D.A., Kryukov P.G., Letokhov V.S., Nikogosyan D.N., Orayevskii A.A.* Selective action on nucleic acids components by picosecond light pulses, in: Lasers in Photomedicine and Photobiology, Proceed. of Intern. Conf. (Florence, Italy, September, 1979). Springer Series in Optical Sciences. Berlin, Heidelberg, New York: Springer-Verlag, 1980. Vol. 22. P. 207–215.

342. *Беков Г.И., Видолова-Ангелова Е.П., Летохов В.С., Мишин В.И.* Многоступенчатая лазерная спектроскопия высоколежащих триплетных состояний атома иттербия // Оптика и спектроскопия. 1980. Т. 48 (3). С. 435–439.

343. *Cantrell C.D., Letokhov V.S., Makarov A.A.* Coherent excitation of multilevel quantum system by laser light, in: Coherent Nonlinear Optics, ed. by M.S. Feld and V.S. Letokhov, Springer Series Topics in Current Physics Berlin, Heidelberg, New York: Springer-Verlag, 1980. Vol. 21. P. 165–269.

344. *Bekov G.I., Vidolova-Angelova E.P., Ivanov L.N., Letokhov V.S., Mishin V.I.* Double-excited narrow autoionization states of Yb atom // Optics Comm. 1980. Vol. 35. P. 194–198.

345. *Balykin V.I., Letokhov V.S., Mishin V.I.* Multiphotoelectron fluorescence selective detection of single atoms by laser radiation // Appl. Phys. 1980. Vol. 22. P. 245–248.

346. *Kudriavtsev Yu.A., Letokhov V.S.* Intermolecular vibrational energy transfer of highly excited CF3I molecules observed from transient UV absorption spectrum // Chem. Phys. 1980. Vol. 50. P. 353–359.

347. *Knyazev I.N., Kuzmina N.P., Letokhov V.S., Lobko V.V., Sarkisyan A.A.* Narrow resonances ($\Delta\nu = 2 \times 10^{-2}$ cm^{-1}) of multiple–photon IR absorption in ethylene // Appl. Phys. 1980. Vol. 22. P. 429–432.

348. *Балыкин В.И., Летохов В.С., Мишин В.И.* Охлаждение атомов Na резонансным лазерным излучением // ЖЭТФ. 1980. Т. 78 (4). С. 1376–1385.

349. *Антонов В.С., Летохов В.С., Шибанов А.Н.* Формирование фотоионизационного масс-спектра многоатомных молекул под действием УФ-лазерного излучения // ЖЭТФ. 1980. Т. 78 (6). С. 2222–2232.

350. *Angelov D.A., Kryukov P.G., Letokhov V.S., Nikogosyan D.N., Orayevskii A.A.* Selective action on nucleic acids components by picosecond light pulses // Appl. Phys. 1980. 21. P. 391–395.

351. *Antonov V.S., Letokhov V.S., Shibanov A.N.* Photoionization mass spectrometry of benzene and benzaldehyde with an excimer laser // Appl. Phys. 1980. Vol. 22. P. 293–297.

352. *Балыкин В.И., Беков Г.И., Летохов В.С., Мишин В.И.* Лазерное детектирование единичных атомов // УФН. 1980. Т. 132 (2). С. 293–344.

353. *Letokhov V.S., Minogin V.G.* Possibility of accumulation and storage of cold atoms in magnetic traps // Optics Comm. 1980. Vol. 35 (2). P. 199–202.

354. *Grasiuk A.Z., Letokhov V.S., Lobko V.V.* Molecular infrared lasers using resonant laser pumping. / ed. by T.S. Moss and S. Stenholm. Prog. in Quant. Electr. 1980. Vol. 6 (4). P. 245–293.

355. *Грасюк А.З., Летохов В.С., Лобко В.В.* Молекулярные ИК-лазеры с резонансной накачкой // Квантовая электроника. 1980. Т. 7 (11). С. 2261–2298.

356. *Антонов В.С., Летохов В.С., Шибанов А.Н.* Образование молекулярных ионов при облучении поверхности молекулярных кристаллов УФ-лазерным излучением // Письма в ЖЭТФ. 1980. Т. 31 (8). С. 471–474.

357. *Letokhov V.S.* Laser selective detection of single atoms, in: Chemical and Biochemical Applications of Lasers / ed. by C.B. Moore. New York: Academic Press, 1980. Vol. V. P. 1–38.

358. *Ангелов Д.А., Крюков П.Г., Летохов В.С., Никогосян Д.Н., Ораевский А.А.* Селективное воздействие на компоненты макромолекул ультракороткими УФ-лазерными импульсами // Квантовая электроника. 1980. Т. 7 (6). С. 1304–1318.

359. *Letokhov V.S.* Laser-induced chemical processes // Physics Today, November 1980. P. 34–41.

360. *Angelov D.A., Gurzadyan G.G., Kryukov P.G., Letokhov V.S., Nikogosyan D.N., Orayevskii A.A.* High–power UV ultrashort laser pulse action on DNA and its components. In: Picosecond Phenomena II / ed. by R.M. Hochstrasser, W. Kaiser and C.V. Shank. Springer Series in Chemical Physics. Berlin, Heidelberg, New York: Springer-Verlag, 1980. Vol. 14. P. 336–339.

361. *Летохов В.С., Устинов Н.Д.* Мощные лазеры и их применение. М.: Советское радио, 1980. 112 стр.

362. *Letokhov V.S., Ustinov N.D.* Vykonne lasery a ich vyuzitie. Bratislava: Alfa, 1981. 110 pp. (in Czech).

363. *Letokhov V.S., Ustinov N.D.* Powerful lasers and their applications. New York: Harwood Acad. Publ., 1983. 128 pp.

364. *Баграташвили В.Н., Летохов В.С., Макаров А.А., Рябов Е.А.* Многофотонные процессы в молекулах в инфракрасном лазерном поле. Итоги науки и техники. Сер. Физика атома и молекулы. Оптика. Магнитный резонанс. М.: ВИНИТИ, 1980. Т. 2, ч. 1, 192 с., ч. 2. 84 с.

365. *Letokhov V.S., Minogin V.G.* Laser radiation pressure on free atoms // Physics Reports. 1981. Vol. 73 (1). P. 1–65.

366. *Antonov V.S., Letokhov V.S.* Laser multiphoton and multistep photoionization of molecules and mass spectrometry // Appl. Phys. 1981. Vol. 24. P. 89–106.

367. *Letokhov V.S.* Is it possible to detect very rare atoms by means of laser radiation? // Comm. on Atom. Mol. Phys. 1981. Vol. 10 (6). P. 257–266.

368. *Жерихин А.Н., Кошелев К.Н., Крюков П.Г., Летохов В.С., Чекалин С.В.* Поиски усиления в далекой ВУФ области на переходах многозарядных ионов в протяженной лазерной плазме // Квантовая электроника. 1981. Т. 8 (1). С. 88–97.

369. *Ангелов Д.А., Крюков П.Г., Летохов В.С., Никогосян Д.Н., Ораевский А.А.* Эффективность двухступенчатого фоторазложения оснований ДНК мощным лазерным УФ излучением // Квантовая электроника. 1981. Т. 8 (3). С. 595–599.

370. *Беков Г.И., Видолова-Ангелова Е.П., Иванов Л.Н., Летохов В.С., Мишин В.И.* Лазерная спектроскопия узких двухкратновозбужденных автоионизованных состояний атома иттербия // ЖЭТФ. 1981. Т. 80 (3). С. 866–877.

371. *Vidolova-Angelova E.P., Ivanov L.N., Letokhov V.S.* Calculation of highly excited Rydberg states of ytterbium atoms // JOSA. 1981. Vol.71. P. 699–704.

372. *Bagratashvili V.N., Vainer Yu.G., Doljikov V.S., Letokhov V.S., Makarov A.A., Maliavkin L.P., Ryabov E.A., Silkis E.G.* Observation of nonequilibrium vibrational distrib ution of IR multiphoton excitation of molecules by Raman spectroscopy // Optics Lett. 1981. Vol. 6 (2). P. 148–150.

373. *Gurzadyan G.G., Nikogosyan D.N., Kryukov P.G., Letokhov V.S., Balmukhanov T.S., Belogurov A.A., Zavigelskii G.B.* Mechanism of high-power laser UV inactivation of viruses and bacterial plasmids // Photochem. and Photobiol. 1981. Vol. 33. P. 835–838.

374. *Летохов В.С., Макаров А.А.* Многоатомные молекулы в сильном инфракрасном поле // УФН. 1981. Т. 134(1). С. 45–91.

375. *Баграташвили В.Н., Вайнер Ю.Г., Должиков В.С., Кольяков С.Ф., Летохов В.С., Макаров А.А., Малявкин Л.П., Рябов Е.А., Силькис Э.Г., Титов В.Д.* Меж- и внутримолекулярное распределение колебательной энергии молекул при многофотонном возбуждении ИК-лазерным излучением // ЖЭТФ. 1981. Т. 80. С. 1008–1025.

376. *Antonov V.S., Letokhov V.S., Shibanov A.N.* Nonthermal desorption of molecular ions of polyatomic molecules induced by UV laser radiation // Appl. Phys. 1981. Vol. 25. P. 71–76.

377. *Bagratashvili V.N., Doljikov V.S., Letokhov V.S., Makarov A.A., Maliavkin L.P., Ryabov E.A., Silkis E.G., Vainer Yu.G.* Stochastization limit of vibrational energy in SF_6 and CF_3I molecules at IR multiple photon excitation // Optics Comm. 1981. Vol. 38 (1). P. 31–34.

378. *Minogin V.G., Letokhov V.S., Zueva T.V.* Hydrodynamical equations for atomic motion in a resonant light wave // Optics Comm. 1981. Vol. 38 (3). P. 225–229.

379. *Karu T.I., Kryukov P.G., Letokhov V.S., Matveets Yu.A., Semchishen V.A.* High quantum yield of photochemical reactions of protoporphyrin-IX induced by powerful ultrashort laser pulses // Appl. Phys. 1981. Vol. 24. P. 245–247.

380. *Балыкин В.И., Летохов В.С., Миногин В.Г.* Радиационное перераспределение скоростей свободных атомов натрия резонансным лазерным излучением // ЖЭТФ. 1981. Т. 80 (5). С. 1779–1788.

381. *Зуева Т.В., Летохов В.С., Миногин В.Г.* Теория замедления атомных пучков резонансным лазерным излучением // ЖЭТФ. 1981. Vol. 81 (l), 84–95.

382. *Letokhov V.S.* Laser visualization of molecules and spatial localization of molecular bonds // Comm. Atom. and Molec. Phys. 1981. Vol. 11(l). P. 1–12.

383. *Letokhov V.S.* Ways of laser visualization of molecules and spatial localization of molecular bonds. In: Ultrashort Phenomena in Spectroscopy, UPS-80. Proceed. of the 2nd Intern. Symp., Oct. 3 — Nov. 5, 1980. Reinhardsbrunn, GDR. Vol. 2. P. 504–526.

384. *Летохов В.С.* Способы лазерной визуализации молекул и пространственной локализации молекулярных связей. Труды 2-й Всесоюзной школы по применению лазеров в атомной, молекулярной и ядерной физике, Вильнюс, июль 1981. М.:Наука, 1983, 279–289.

385. *Antonov V.S., Letokhov V.S., Shibanov A.N.* Laser photoionization and mass–spectral detection of single naphthalene molecules // Optics Comm. 1981. Vol. 38 (3). P. 182–184.

386. *Летохов В.С., Мовшев В.Г., Чекалин С.В.* Фотоотрыв ионов молекул родамина 6G, адсорбированных на поверхности, под действием ультракороткого лазерного импульса // ЖЭТФ. 1981. Т. 81 (2). С. 480–485.

387. *Letokhov V.S., Matveets Yu.A., Semchishen V.A., Khoroshilova E.V.* UV picosecond laser induced formation of amino acids from aqueous solutions of ammonic salts of dicarboxylic acids // Appl. Phys. 1981. Vol. 12B. P. 243–245.

388. *Karu T.I., Kalendo G.S., Letokhov V.S.* Control of RNA synthesis rate in tumor cell HeLa by action of copper laser // Lettere Nuovo Cimento. 1981. Vol. 32 (2). P. 55–59.

389. *Беков Г.И., Жерихин А.Н., Летохов В.С., Мишин В.И., Федосеев В.Н.* Различие выходов многоступенчатой фотоионизации четных и нечетных изотопов Yb поляризованным лазерным излучением// Письма в ЖЭТФ. 1981. Т. 33 (9). С. 467–470.

390. *Кару Т.Й., Календо Г.С., Летохов В.С., Матвеец Ю.А., Семчишен В.А., Серебряков Н.Г.* Действие ультракоротких импульсов УФ-лазерного излучения на опухолевые клетки HeLa // Квантовая электроника. 1981. Т. 8 (12). С. 2540–2545.

391. *Letokhov V.S., Minogin V.G.* Atomic deceleration, monochromatization and trapping in laser waves. Theory and experiments. In: Laser Spectroscopy V / ed. by A.R.W. McKellar, T. Oka, and B.P. Stoicheff. Springer Series in Optical Sciences. Berlin, Heidelberg, New York: Springer-Verlag, 1981. Vol. 30. P. 377–385.

392. *Андреев С.В., Балыкин В.И., Летохов В.С., Миногин В.Г.* Радиационное замедление и монохроматизация пучка атомов натрия до 1,5 К во встречном лазерном луче // Письма в ЖЭТФ. 1981. Т. 34 (8). С. 463–467.

393. *Letokhov V.S., Minogin V.G.* Laser cooling of atoms and its application in frequency standards // J. de Physique. 1981. Vol. 42 (12). P. 347–355.

394. *Гурзадян Г.Г., Никогосян Д.Н., Крюков П.Г., Летохов В.С., Балмуханов Т.С., Белогуров А.А., Завигельский Г.Б.* Механизм инактивирующего действия ультрафиолетового лазерного излучения на вирусы и бактериальные плазмиды // Биофизика. 1981. Т. 26 (4). С. 659–663.

395. *Зуева Т.В., Летохов В.С., Миногин В.Г.* Макроскопический анализ радиационного замедления атомов. В сб.: Нелинейная оптика. Труды 7-й Вавиловской конференции, июнь 1981 г. (Новосибирск, 1982). Ч. 2. С. 90–93.

396. *Letokhov V.S.* Possibility of fast deep cooling of molecular gases by laser radiation, Appl. Phys. 1981. Vol. 24. P. 119–120.

397. *Жерихин А.Н., Летохов В.С., Мишин В.И., Беляев В.П., Евтюнин А.И., Лесной М.А.* Перестраиваемые лазеры на красителях с высокой частотой

повторения импульсов с накачкой лазером на парах меди // Квантовая электроника. 1981. Т. 8 (6). С. 1340–1343.

398. *Летохов В.С., Миногин В.Г.* Нелинейные движения атомов в световом поле. В кн.: Нелинейные волны. Распространение и взаимодействие. М.: Наука, 1981. С. 96–103.

399. *Видолова-Ангелова Е.П., Иванова Л.П., Летохов В.С.* Природа узких и аномально узких резонансов в атомах редкоземельных элементов и их отрицательных ионах // Изв. АН СССР. Сер. физ. 1981. Т. 45 (12). С. 2300–2304.

400. *Летохов В.С., Миногин В.Г.* Охлаждение атомов резонансными световыми полями. В сб.: Нелинейная оптика. Труды 7-й Вавиловской конференции, июнь 1981 г. Новосибирск, 1982.

401. *Кару Т.Й., Календо Г.С., Летохов В.С.* Действие низкоинтенсивного видимого излучения медного лазера на культуру клеток HeLa // Квантовая электроника. 1982. Т. **9**(1). С. 141–144.

402. *Antonov V.S., Letokhov V.S., Matveets Yu.A., Shibanov A.N.* Sputtering of neutral molecules and molecular ions from the adenine crystal surface induced by the UV picosecond laser pulse // Laser Chemistry. 1982. Vol. 1(1). P. 37–43.

403. *Антонов В.С., Летохов В.С., Матвеец Ю.А., Шибанов А.Н.* Распыление нейтральных молекул и молекулярных ионов с поверхности кристалла аденина, индуцированное ультрафиолетовым пикосекундным лазерным импульсом // Поверхность. 1982. 1 (12). С. 54–57.

404. *Андреев С.В., Балыкин В.И., Летохов В.С., Миногин В.Г.* Радиационное замедление и монохроматизация пучка атомов натрия во встречном луче лазера // ЖЭТФ. 1982. Т. 82 (5). С. 1429–1441.

405. *Баграташвили В.Н., Буримов В.И., Деев Л.Е., Кудрявцев Ю.А., Кузьмин М.В., Летохов В.С., Свиридов А.П.* Наблюдение электронной предиссоциации колебательно перевозбужденной многоатомной молекулы // Письма в ЖЭТФ. 1982. Т. 35 (4). 155–157.

406. *Letokhov V.S., Mishin V.I., Eshkobilov N., Tursunov A.T.* Proposal of laser radiochemical Ga detector of solar neutrino // Optics Comm. 1982. Vol. 41 (5). P. 331–334.

407. *Кару Т.Й., Календо Г.С., Летохов В.С., Лобко В.В.* Зависимость биологического действия низкоинтенсивного видимого света на клетки HeLa от когерентности, дозы, длины волны и режима облучения // Квантовая электроника. 1982. Т. 9 (9). С. 1761–1767.

408. *Акилов Р., Беков Г.И.. Летохов В.С., Максимов Г.А., Мишин В.И., Радаев В.Н., Шишов В.Н.* Определение содержания алюминия в германии высокой чистоты методом лазерной ступенчатой фотоионизации атомов // Квантовая электроника. 1982. Т. 9 (9). С. 1859–1862.

409. *Антонов В.С., Егоров С.Е., Летохов В.С., Матвеец Ю.А., Шибанов А.Н.* Наблюдение отрыва ионов хромофора от сложной молекулы на поверхности под действием пикосекундных УФ-лазерных импульсов // Письма в ЖЭТФ. 1982. Т. 36 (2). С. 29–31.

410. *Vidolova-Angelova E.P., Ivanov L.N., Letokhov V.S.* Application of model potential method in calculating Rydberg states of rare–earth elements Tm, Yb, Lu and their ions // J. Phys. B. At. Mol. Phys. 1982. 15. P. 981–991.

411. *Kudryavtsev Yu.A., Letokhov V.S.* Method of highly selective detection of rare radioactive isotopes through multistep photoionization of acceleration atoms, Appl. Phys. 1982. Vol. B29. P. 219–221.

412. *Antonov V.S., Khoroshilova E.V., Kuz'mina N.P., Letokhov V.S., Matveets Yu.A., Shibanov A.N., Yegorov S.E.* Multiple photon processes in molecules induced by picosecond UV pulses. In: Picosecond Phenomena III / ed. by R.M. Hochstrasser and W. Kaiser. Springer Series in Chemical Physics. Berlin, Heidelberg, New York: Springer-Verlag, 1980. Vol. 23. P. 310–314.

413. *Летохов В.С., Лихачев В.С., Мовшев В.Г., Чекалин С.В.* Наблюдение фотоионного изображения в лазерном десорбционном микроскопе// Квантовая электроника. 1982. Т. 9 (11). С. 2117–2118.

414. *Karu T.I., Kalendo G.S., Letokhov V.S., Lobko V.V.* Biostimulation of Hela cells by low-intensity visible light // Il Nuovo Cimento. 1982. 1D(6) P. 828–840.

415. *Абдушелишвили Г.И., Аватков О.Н., Баграташвили В.Н., Баранов В.Ю., Бахтадзе А.Б., Велихов Е.П., Вецко В.М., Гвердцители И.Г., Должиков В.С., Есадзе Г.Г., Казаков С.А., Коломийский Ю.Р., Летохов В.С., Пигульский С.В., Письменный В.Д., Рябов Е.А., Ткешелашвили Г.И.* Разделение изотопов методом многофотонной диссоциации молекул излучением мощного CO_2-лазера. Масштабирование процесса для изотопов углерод // Квантовая электроника. 1982. Т. 9(4). С. 743–758.

416. *Баграташвили В.Н., Буримов В.Н., Деев Л.Е., Заболотных А.В., Летохов В.С., Назаренко Г.И., Свиридов А.П., Шайдуров В.С.* Многофотонная ИК диссоциация молекул CF_3Br и CF_3Cl при высоких температурах // Квантовая электроника. 1982. Т. 9(2). С. 425–427.

417. *Кару Т.Й., Календо Г.С., Летохов В.С., Лобко В.В.* Реакция пролиферирующих и покоящихся опухолевых клеток на импульсно-периодическое лазерное УФ-излучение низкой интенсивности // Доклады АН СССР. 1982. Т. 262 (6). С. 1468–1501.

418. *Баграташвили В.Н., Буримов В.И., Деев Л.Е., Летохов В.С., Свиридов А.П., Шайдуров В.С.* Получение радикалов $(CF_3)_3C$ методом ИК многофотонной диссоциации молекулы $(CF_3)_3CBr$ // Квантовая электроника. 1982. Т. 9 (2). С. 423–425.

419. *Bekov G.I., Letokhov V.S., Mishin V.I.* Laser photoionization detection of impurities in solids and studies of hyperfine and isotope structures of radioactive atoms. In: Laser Techniques for Extreme Ultraviolet Spectroscopy. Proc. AIP Conf., Boulder, 1982 / ed. by T.J. Mollrath. N.Y.: R.R. Freeman, 1982. P. 101–111.

420. *Karu T.I., Kalendo G.S., Letokhov V.S., Lobko V.V.* Different responses of proliferating and resting tumor cells HeLa to high-rate repetition low intensity laser light at $\lambda = 271$ nm // Laser Chemistry. 1983. Vol. 1 (3). P. 153–161.

421. *Letokhov V.S.* Nonlinear Laser Chemistry. Multiple-Photon Excitation, Springer Series in Chemical Physics. Berlin, Heidelberg, New York: Springer-Verlag, 1983. Vol. 22. 417 pp.

422. *Летохов В.С.* Нелинейные селективные фотопроцессы в атомах и молекулах. М.: Наука, 1983. 408 стр.

423. *Bagratashvili V.N., Burimov V.I., Kuzmin M.V., Letokhov V.S., Sviridov A.P.* Multiple photon IR dissociation of $(CF_3)_3CBr$ and synthesis of $(CF_3)_3CI$ in laser-radical chemical reactions // Laser Chemistry. 1983. Vol. 1 (3). P. 133–152.

424. *Letokhov V.S.* Laser photoionization selective detection of atoms, molecules and molecular bonds. In: Advances in Laser Spectroscopy / ed. by F.T. Arecchi, F. Strumia, H. Walther. New York, London: Plenum Press, 1983. P. 417–435.

425. *Велихов Е.П., Баранов В.Ю., Летохов В.С., Старостин А.Н., Рябов Е.А.* Импульсные CO_2-лазеры и их применение для разделения изотопов. М.: Наука, 1983. 304 с.

426. *Zharov V.P., Montanari S.G., Letokhov V.S.* Application of IR laser optoacoustic spectroscopy in gas chromatography // Laser Chemistry. 1983. Vol. 1 (3). P. 163–176.

427. *Zherikhin A.N., Letokhov V.S., Mishin V.I., Muchnik M.E., Fedoseyev V.N.* Production of photoionic gallium beams through stepwise ionization of atoms by laser radiation // Appl. Phys. 1983. Vol. B30. P. 47–52.

428. *Bekov G.I., Egorov A.S., Letokhov V.S., Radayev V.I.* Direct determination of aluminium in natural waters by laser stepwise photoionization // Nature. 1983. Vol. 301. P. 410–412.

429. *Беков Г.И., Егоров А.С., Радаев В.И., Летохов В.С.* Лазерная ступенчатая фотоионизация — прямой метод определения концентрации алюминия в природных водах // Океанология. 1983. Т. 23 (1). С. 171–176.

430. *Khoroshilova E.V., Kuzmina N.P., Letokhov V.S., Matveets Yu.A.* Nonlinear laser UV photochemistry of maleic acids in aqueous solution // Appl. Phys. B. 1983. Vol. 31. P. 145–151.

431. *Khoroshilova E.V., Kuzmina N.P., Letokhov V.S., Matveets Yu.A.* Nonlinear photochemical synthesis of biomolecules by powerful UV picosecond pulses. In: Photochemistry and Photobiology / ed. by A.H. Zewail. Harwood Acad. Publ., 1983. Vol. 2. P. 1267–1275.

432. *Баграташвили В.Н., Кузьмин М.В., Летохов В.С., Шибанов А.Н.* Наблюдение процессов отрыва протона и электрона от молекулы антрацена при ее сильном ИК многофотонном перевозбуждении // Письма в ЖЭТФ. 1983. Т. 37 (2). С. 92–95.

433. *Bekov G.I., Letokhov V.S.* Laser atomic photoionization spectral analysis of element traces // Appl. Phys. B. 1983. Vol. 30. P. 161–176.

434. *Karu T.I., Tiphlova O.A., Letokhov V.S., Lobko V.V.* Stimulation of E. coli growth by laser and incoherent red light // Nuovo Cimento. 1983. 2D 4. P. 1138–1144.

435. *Алхазов Г.Д., Барзах А.Е., Берлович Э.Е., Денисов В.П., Дернятин А.Г., Иванов В.С., Жерихин А.Н., Компанец О.Н., Летохов В.С., Мишин В.И., Федосеев В.Н.* Измерение изотопических изменений зарядовых радиусов ядер европия методом трехступенчатой лазерной фотоионизации атомов // Письма в ЖЭТФ. 1983. Т. 37 (5). С. 231–234.

436. *Антонов В.С., Егоров С.Е., Летохов В.С., Шибанов А.Н.* Лазерное фотоионизационное детектирование субмономолекулярных слоев на поверхности // Письма в ЖЭТФ. 1983. Т. 38 (4). С. 185–187.

437. *Летохов В.С., Мишин В.И., Мучник М.Л., Орлов Ю.В., Черняк Е.Я.* На пути к фотоионной лазерной эпитаксии: исследование чистоты и условий зарождения кристаллических пленок индия // Квантовая электроника. 1983. Т. 10 (10). С. 1963–1964.

438. *Кару Т.Й., Календо Г.С., Летохов В.С., Лобко В.В.* Зависимость биологического действия низкоинтенсивного видимого света на клетки HeLa от когерентности, дозы, длины волны и режима облучения. II // Квантовая электроника. 1983. Т. 10 (9). С. 1771–1776.

439. *Letokhov V.S.* Laser-induced chemistry // Nature. 1983. Vol. 305 (8). P. 103–108.

440. *Letokhov V.S.* Possible new approach to free-electron lasers, in: Advances in Laser Spectroscopy / ed. by F.T. Arecchi, F. Strumia, H. Walther. New York: Plenum Press, 1983. P. 497.

441. *Yegorov S.E., Letokhov V.S., Shibanov A.N.* Molecular photoion production processes induced by laser radiation on surface. In: Surface Studies with Lasers / ed. by F. Aussenegg, A. Leither, M.E. Lippitsch. Springer Series in Chemical Physics. Berlin, Heidelberg, New York: Springer-Verlag, 1983. Vol. 33. P. 156–170.

442. *Bekov G.I., Letokhov V.S.* Laser resonant photoionization spectroscopy for trace analysis // Trends in Analytical Chemistry. 1983. Vol. 2 (11). P. 252–256.

443. *Balykin V.I., Kudryavtzev Yu.A., Letokhov V.S., Makarov A.A., Minogin V.G.* On the way to the laser highly selective detection of very rare isotopes against the background of abundant isotopes. In: Laser Spectroscopy VI. Springer Series in Optical Sciences. Berlin, Heidelberg, New York: Springer-Verlag, 1983. Vol. 40. P. 103–105.

444. *Жаров В.П., Летохов В.С., Монтанари С.Г., Туманова Л.М.* Лазерно-хроматографический метод анализа многокомпонентных смесей // Доклады АН СССР. 1983. Т. 269 (5). С. 1079–1083.

445. *Мучник М.Л., Орлов Ю.В., Паршин Г.Д., Черняк Е.Я., Летохов В.С., Мишин В.И.* Получение ионного пучка индия методом селективной ступенчатой лазерной фотоионизации атомов // Квантовая электроника. 1983. Т. 10 (11). С. 2331–2335.

446. *Яковлев Е.Н., Летохов В.С., Арманд Н.А., Бегуолев В.Б., Беков Г.И., Виноградов Б.В., Тимофеев Ю.А., Фатеева Н.С.* Волоконная эндоскопия камер высокого давления типа наковален Бриджмена // Письма в ЖТФ. 1983. Т. 9 (15). С. 924–928.

447. *Видолова-Ангелова Е.П., Иванов Л.Н., Иванова Е.П., Летохов В.С.* Узкие низколежащие состояния отрицательного иона Yb- // Оптика и спектроскопия. 1983. Т. 54 (4). С. 590–594.

448. *Zharov V.P., Letokhov V.S., Montanari S.G.* Laser optothermal detection of absorption in gas flows // J. de Physique. 1983. Vol. 44 (10). P. 573–578.

449. *Кару Т.Й., Календо Г.С., Летохов В.С., Лобко В.В.* Воздействие импульсного ультрафиолетового лазерного излучения на пролиферирующие и покоящиеся опухолевые клетки HeLa // Радиобиология. 1984. Т. 24 (2). С. 273–276.

450. *Летохов В.С.* Квантовая электроника, в кн.: Физика XX века. Развитие и перспективы. М.: Наука, 1984. С. 188–218.

451. *Bagratashvili V.N., Kuzmin M.V., Letokhov V.S.* Reduction of the pathways of photochemical reactions induced by multiple photon IR laser excitation of molecules // Laser Chemistry. 1984. Vol. 4 (3). P. 139–150.

452. *Bekov G.I., Letokhov V.S., Radayev V.N.* Direct determination of aluminium concentration in human blood through laser photoionization spectroscopy // Laser Chemistry. 1984. Vol. 5 (l). P. 11–17.

453. *Balykin V.I., Letokhov V.S., Minogin V.G.* On the possibility of highly selective detection of rare isotopic atoms by means of resonant laser light pressure, Appl. Phys. B. 1984. Vol. 33 (4). P. 247–251.

454. *Fedoseyeva G.E., Karu T.I., Letokhov V.S., Lobko V.V., Pomoshnikova N.A., Lyapunota T.S., Meissel M.N.* Effect of the He–Ne laser radiation on the reproduction rate and protein synthesis of the yeast // Laser Chemistry. 1984. Vol. 5 (l). P. 27–33.

455. *Егоров С.Е., Летохов В.С., Шибанов А.Н.* Механизм образования ионов при облучении поверхности молекулярных кристаллов импульсным лазерным излучением // Квантовая электроника. 1984. Т. 11 (7). С. 1393–1403.

456. *Chekalin S.V., Letokhov V.S., Likhachev V.S., Movshev V.G.* Laser photoion projector // Appl. Phys. B. 1984. Vol. 33. P. 57–61.

457. *Антонов В.С., Летохов В.С., Шибанов А.Н.* Лазерная резонансная фотоионизационная спектроскопия молекул // УФН. 1984. Т. 142 (2). С. 177–217.

458. *Letokhov V.S.* Laser-induced multiple photon processes in atoms and molecules and their applications in chemistry. In: Chemistry for the future, Proceed. of the 29th IUPAC Congress (Cologne, FRG, June 5–10, 1983). London: Pergamon, 1984. P. 253–260.

459. *Karu T.I., Kalendo G.S., Letokhov V.S., Lobko V.V.* Biostimulation of HeLa cells by low-intensity visible light: II. Stimulation of DNA and RNA synthesis in a wide spectral range // Nuovo Cimento. D. 1984. Vol. 3(2). P. 309–318.

460. *Karu T.I., Kalendo G.S., Letokhov V.S., Lobko V.V.* Biostimulation of HeLa cells by low-intensity visible light: III. Stimulation of nucleic acids synthesis in plateau-phase cells // Nuovo Cimento. D. 1984. Vol. 3(2). P. 319–325.

461. *Жерихин А.Н., Компанец О.Н., Летохов В.С., Мишин В.И., Федосеев В.Н. и др.* Лазерная фотоионизационная спектроскопия высокого разрешения радиоактивных изотопов европия // ЖЭТФ. 1984. Т. 86 (4). С. 1249–1262.

462. *Balykin V.I., Letokhov V.S., Sidorov A.I.* Intense stationary flow of cold atoms formed by laser deceleration of atomic beam // Optics Commun. 1984. Vol. 49 (4). P. 248–252.

463. *Балыкин В.И., Летохов В.С., Сидоров А.И.* Формирование интенсивного стационарного потока холодных атомов методом лазерного замедления атомного пучка // ЖЭТФ. 1984. Т. 86 (6). С. 2019–2029.

464. *Bagratashvili V.N., Kuzmin M.V., Letokhov V.S.* Chemical radical synthesis in gas mixture induced by IR laser multiphoton dissociation // J. Phys. Chem. 1984. Vol. 88. P. 5780–5786.

465. *Karu T.I., Tiflova O.A., Fedoseyeva G.E., Kalendo G.S., Letokhov V.S., Lobko V.V., Lyapunoma T.S., Pomoshnokova N.A., Meissel M.N.* Biostimulating action of low-intensity monochromatic visible light: is it possible? // Laser Chemistry. 1984. Vol. 5 (l). P. 19–25.

466. *Zharov V.P., Letokhov V.S., Montanari S.G., Tumanova L.M.* Laser–spectrochromatographic identification of isomers in mixture // J. Mol. Structure. 1984. Vol. 115. P. 261–266.

467. *Nikogosyan D.N., Letokhov V.S.* Nonlinear laser photophysics, photochemistry and photobiology of nucleic acids, Nuovo Cimento **6**(8), Ser. 3, 1–89 (1984).

468. *Bekov G.I., Letokhov V.S., Radayev V.N., Yegorov A.S., Baturin G.N., Kurski A.N., Nerseev V.A.* Ruthenium in the ocean // Nature. 1984. Vol. 312. P. 748–750.

469. *Bekov G.I., Letokhov V.S., Mishin V.I.* Laser selective photoionization technique: photoion beam epitaxy and semiconductor trace impurity diagnostics. In: Laser Proceed. and Diagnostics / ed. by D.Buerle. Springer Series in Chem Phys. Berlin, Heidelberg, New York: Springer-Verlag, 1984. Vol. 39. P. 437–445.

470. *Antonov V.S., Letokhov V.S.* Multiphoton ionization spectroscopy of surface molecules, in: Multiphoton Processes / ed. by P. Lambropoulos and S.J. Smith. Springer Series Atoms and Plasmas. Berlin, Heidelberg, New York: Springer-Verlag, 1984. Vol. 2. P. 182–190.

471. *Avatkov O.N., Bakhtadze A.B., Baranov V.Yu., Dolzhikov V.S., Gverdtsiteli I.G., Kazakov S.A., Letokhov V.S., Pis'mennyi V.D., Ryabov E.A., Vetsko V.M.* Carbon isotopes laser separation by multiple-photon dissociation // Appl. Optics. 1984. Vol. 23 (1). P. 26–29.

472. *Yegorov S.E., Letokhov V.S., Shibanov A.N.* Laser multiphoton ionization detection of molecules adsorbed on surface // Chem. Phys. 1984. Vol. 85. P. 349–353.

473. *Balykin V.I., Letokhov V.S., Minogin V.G., Zueva T.V.* Collimation of atomic beams by resonant laser radiation pressure // Appl. Phys. B. 1984. Vol. 35. P. 149–153.

474. *Балыкин В.И., Летохов В.С., Сидоров А.И.* Радиационная коллимация атомного пучка путем двухмерного охлаждения лазерным излучением // Письма в ЖЭТФ. 1984. Т. 40 (6). С. 251–253.

475. *Fedoseyev V.N., Letokhov V.S., Mishin V.I., Alkhazov G.D., Barzakh A.E., Denisov V.P., Dernyatin A.G., Ivanov V.S.* Atomic lines isotope shifts of short-lived radioactive Eu isotopes studied by high-sensitive laser photoionization method in "on-line" experiments with proton beams // Optics Comm. 1984. Vol. 52 (1). P. 24–28.

476. *Алхазов Г.Д., Барзах А.Е., Берлович Э.Е.,. Денисов В.П, Дернятин А.Г., Иванов В.С., Летохов В.С., Мишин В.И., Федосеев В.Н.* Оболочечный эффект в изотопической зависимости среднеквадратичных зарядовых радиусов короткоживущих ядер европия, измеренной методом лазерного фотоионизационного детектирования "в линию" с ускорителем // Письма в ЖЭТФ. 1984. Т. 40 (3). С. 95–98.

477. *Letokhov V.S.* Multiple-photon IR vibrational overexcitation of polyatomic molecules // Comm. Atom. Molec. Phys. 1984. Vol. 15 (3). P. 107–117.

478. *Letokhov V.S.* Laser picosecond excitation of highly-lying electronic states of biomolecules // Comm. Atom. Molec. Phys. 1984. 14 (6). P. 307–320.

479. *Кару Т.Й., Календо Г.С., Летохов В.С.* Сравнение действия ультракоротких УФ-мощных лазерных импульсов на репликативную и транскрипционную функцию ДНК в пролиферирующих и покоящихся клетках HeLa // Радиобиология. 1984. № l. С. 17–20.

480. *Кару Т.Й., Летохов В.С., Лобко В.В., Новиков В.Ф., Парамонов Л.В.* Светолечение больных язвенной болезнью желудка и двенадцатиперстной кишки на основе стимуляции клеток низкоинтенсивным красным цветом // Вопросы курортологии, физиотерапии и лечебной физкультуры. 1984. № 1. С. 36–39.

481. *Акилов Р., Беков Г.И., Девятых Г.Г., Летохов В.С., Максимов Г.А., Радаев В.Н., Шишов В.Н.* Определение примесей алюминия и натрия в высокочистом германии методом лазерной ступенчатой фотоионизации атомов // Журнал аналитической химии. 1984. Т. 39 (l). С. 31–34.

482. *Alkhazov G.D., Barzakh A.E., Berlovich E.E., Denisov V.P., Dernyatin A.G., Ivanov V.S., Fedoseyev V.N., Letokhov V.S., Mishin V.I., Kompanets O.N.* Isotopic variations of mean-square charge radii of Eu nuclei measured by resonant atomic photoionization, in: Proceed. 7th Intern. Conf. on Atomic Masses and Fundamental Constants. Darmstadt, FRG, Sept. 1984. P. 334–340.

483. *Egorov S.E., Letokhov V.S.* Laser photoionization surface mass spectrometry, in: Proceed. III Sump. of Optical Spectroscopy (Reinhardsbrunn, Sept. 26–28, 1984). Leipzig, 1985. P. 82–87.

484. *Дорофеев В.С., Жаров В.П., Жемчужин С.Г., Летохов В.С., Монтанари С.Г., Туманова Л.М.* Лазерный оптико-акустический детектор для определения гербицидов методом газовой хроматографии // Агрохимия. 1984. № 8. С.116–121.

485. *Bagratashvili V.N., Letokhov V.S., Makarov A.A., Ryabov E.A.* Multiple photon infrared laser photophysics and photochemistry. In: Laser Chemistry. 1983. Vol. 1. P. 211; 1984. Vol. 4. P. 171–174; 1984. Vol. 4. P. 311–423; 1984. Vol. 5. P. 53–105.

486. *Жаров В.П., Летохов В.С.* Лазерная оптико-акустическая спектроскопия, под ред. А.М. Бонч-Бруевич. М.: Наука, 1984. 320 стр.

487. *Балыкин В.И., Зуева Т.В., Летохов В.С., Миногин В.Г.* Коллимация атомных пучков давлением резонансного лазерного излучения // ЖТФ. 1985. Т. 55 (9). С. 1755–1762.

488. *Letokhov V.S., Ryabov E.A.* Time-resolved Raman spectroscopy of highly excited vibrational states of polyatomic molecules, in: Time-resolved Vibrational Spectroscopy / ed. by A. Laubereau and M. Stockburger. Springer Proceed. in Physics. Berlin, Heidelberg, New York: Springer-Verlag, 1985. Vol. 4. P. 53–57.

489. *Karu T.I., Letokhov V.S.* Biological action of low–intensity monochromatic light in the visible range. In: Laser Photobiology and Photomedicine / ed. by S. Martellucci, A.N. Chester. London: Plenum Press, 1985. P. 57–66.

490. *Karu T.I., Letokhov V.S., Lobko V.V.* Biostimulation of HeLa cells by a low-intensity visible light: IV dichromatic irradiation // Nuovo Cimento. 3D 5. Ser. 3. 1985. No. 6. 483–496.

491. *Ivanov L.N., Letokhov V.S.* Double-excited autoionization states of multielectron atoms // Comm. Atom. Molec. Phys. 1985. Vol. 16 (4). P. 169–183.

492. *Evseev A.V., Letokhov V.S., Puretzky A.A.* Multiphoton excitation and dissociation of molecules in multiple-frequency IR laser fields, in: Recent Advances in Molecular Reaction Dynamics, CNRS Symp. (Aussois, France, June 10–14, 1985). Paris: CNRS, 1985. P. 409–423.

493. *Abil'siitov G.A., Belyayev A.A., Bragin M.A., Velikhov E.P., Zhdanov V.S., Karu T.I., Letokhov V.S., Ragimov S.E., Ruda M.Ya., Trubetskoi A.V., Furzikov N.P., Chazov E.I.* Study of photoablation of atherosclerotic plaques by laser radiation // Sov. J. Quantum Electron. 1985. Vol. 15. P. 1314–1316.

494. *Bagratashvili V.N., Ionov S.I., Kuzmin M.V., Letokhov V.S., Mishakov G.V., Stuchebrukhov A.A.* Infrared transitions spectra and dynamics of strongly vibrationally excited CF3I molecules. In: Recent Advances in Molecular Reaction Dynamics, CNRS Symp. (Aussois, France, June 10–14, 1985). Paris: CNRS, 1985. P. 425–436.

495. *Кару Т.Й., Летохов В.С., Лобко В.В.* Существенна ли когерентность низкоинтенсивного лазерного света при его воздействии на биологические объекты? // Биофизика. 1985. Т. 30 (2). С. 366–371.

496. *Bagratashvili V.N., Letokhov V.S., Makarov A.A., Ryabov E.A.* Multiple photon infrared laser photophysics and photochemistry. Chur: Harwood Acad. Publ., 1986. P. 512 pp.

497. *Bagratashvili V.N., Kuzmin M.V., Letokhov V.S., Stuchebrukhov A.A.* Theory of multiple-photon IR excitation of polyatomic molecules in the model of active and passive modes of vibrational reservoir // Chem. Phys. 1985. Vol. 97. P. 13–29.

498. *Letokhov V.S.* Laser photoionization spectroscopy of single atoms and molecules // Optica Acta. 1985. Vol. 32 (9/10). P. 1191–1210.

499. *Летохов В.С.* Лазерная спектроскопия одиночных атомов и молекул// Природа. 1985. № 2. С. 15–25.

500. *Evseev A.V., Letokhov V.S., Puretzky A.A.* Highly selective and efficient multiphoton dissociation of polyatomic molecules // Appl. Phys. 1985. Vol. B39. P. 93–103.

501. *Никогосян Д.Н., Ораевский А.А., Летохов В.С.* Сенсибилизированное разложение жидкого растворителя при двухступенчатом лазерном возбуждении растворенных молекул // Доклады АН СССР. 1985. Т. 283 (6). С. 1425–1427.

502. *Balykin V.I., Letokhov V.S., Minogin V.G.* Cooling of atoms by laser radiation pressure // Sov. Phys. Usp. 1985. Vol. 28 (9). P. 803–826.

503. *Nikogosyan D.N., Orayevskii A.A., Letokhov V.S., Arbieva Z.Kh., Dobrov E.N.* Two-step picosecond UV excitation of polynucleotides and energy transfer // Chem. Phys. 1985. Vol. 97. P. 31–41.

504. *Kudryavtsev Yu.A., Letokhov V.S., Petrunin V.V.* Laser detection of 40K in a beam of accelerate atoms by the isotope–selective ionization technique // JETP Lett. 1985. Vol. 42. P. 26–28.

505. *Bekov G.I., Letokhov V.S., Radayev V.N.* Laser photoionization spectroscopy of ruthenium traces at the 1 part in 1012 // JOSA B. 1985. Vol. 2 (9). P. 1554–1560.

506. *Balykin V.I., Letokhov V.S., Minogin V.G., Rozhdestvensky Yu.V., Sidorov A.I.* Radiative collimation of atomic beams through two–dimensional cooling of atoms by laser radiation pressure // JOSA B. 1985. Vol. 2 (11). P. 1776–1783.

507. *Letokhov V.S.* Laser biology and medicine // Nature 316, July 25, 1985. P. 325–330.

508. *Балыкин В.И., Летохов В.С., Миногин В.Г., Сидоров А.И.* Интенсивные пучки холодных атомов для задач лазерной спектроскопии // Изв. АН СССР. Сер. физ. 1985. Т. 49 (3). С. 479–486.

509. *Коробейник Г.С., Летохов В.С., Монтанари С.Г., Туманова Л.М.* Лазерный спектрохроматографический анализ компонентов нефти // Квантовая электроника. 1985. Т. 12 (1). С. 120–125.

510. *Сазонов А.М., Романов Г.А., Портной Л.М., Одинокова В.А., Кару Т.Й., Лобко В.В., Летохов В.С.* Низкоинтенсивный некогерентный красный свет в комплексном лечении язвенной болезни желудка и двенадцатиперстной кишки // Советская медицина. 1985. № 12. С. 42–46.

511. Беков *Г.И., Курский А.Н., Летохов В.С., Радаев В.Н.* Определение следов рутения в рудах методом лазерной фотоионизационной аналитической спектроскопии // Журнал аналитической химии. 1985. XL (12). С. 2208–2215.

512. *Антонов В.С., Летохов В.С.* Многофотонная ионизация молекул, в кн.: Физические основы масс-спектрометрии (методы ионизации). Уфа, 1985. С. 68–83.

513. *Letokhov V.S.* Introduction to laser analytics. In: Laser Analytical Spectrochemistry / ed. by V.S. Letokhov. Bristol — Boston: Adam Hilger, 1986. P. 1–51.

514. *Летохов В.С.* Введение в лазерную аналитику. В кн.: Лазерная аналитическая спектроскопия / под ред. В.С. Летохова. М.: Наука, 1986. Гл. 1. С. 5–42.

515. *Bekov G.I., Letokhov V.S.* Laser atomic photoionization spectral analysis. In: Laser Analytical Spectrochemistry / ed. by V.S. Letokhov. Bristol — Boston: Adam Hilger, 1986. P. 98–151.

516. *Беков Г.И., Летохов В.С.* Спектральный анализ лазерной атомной фотоионизации. В: Лазерная аналитическая спектроскопия / под ред. В.С. Летохова. М.: Наука, 1986. Гл. 3. С. 77–119.

517. *Antonov V.S., Letokhov V.S.* Laser photoionization spectroscopy and mass-spectrometry of molecules. In: Laser Analytical Spectrochemistry / ed. by V.S. Letokhov. Bristol — Boston: Adam Hilger, 1986. P. 314–352.

518. *Антонов В.С., Летохов В.С.* Лазерная фотоионизационная спектроскопия и масс-спектрометрия молекул. В кн.: Лазерная аналитическая спектроскопия / под ред. В.С. Летохова. М.: Наука, 1986. Гл. 7. С. 242–272.

519. *Balykin V.I., Letokhov V.S., Sidorov A.I.* Atomic beam focusing by the dissipative radiation pressure force // JETP Lett. 1986. Vol. 43 (4). P. 217–220.

520. *Letokhov V.S.* Laser detection of very rare isotopes. In: Proceed. of the 3rd Vilnius School on Laser Applications in Atomic, Molecular and Nuclear Physics (1984) / ed. by V.S. Letokhov. Harwood Acad. Publ., 1986. P. 1–22.

521. *Oraevsky A.A., Nikogosyan D.N., Letokhov V.S.* Two-quantum picosecond UV photolysis of nucleic acid components in aqueous solution in comparison with γ-radiolysis // Lasers in Life Sciences. 1986. Vol. 1 (1). P. 49–60.

522. *Летохов В.С.* Лазерно-индуцированные процессы в спектроскопии, разделении изотопов и фотохимии // УФН. 1986. Т. 148 (1). С. 123–141.

523. *Doljikov V.S., Doljikov Yu.S., Letokhov V.S., Makarov A.A., Malinovsky A.L., Ryabov E.A.* Intramolecular and intermolecular redistribution of vibrational energy at MP IR excitation: CF2HCl molecule // Chem. Phys. 1986. Vol. 102. P. 155–163.

524. *Doljikov Yu.S., Letokhov V.S., Makarov A.A., Malinovsky A.L., Ryabov E.A*. Raman probing of overtone and combinations bands to study vibrational energy distribution produced by multi-photon excitation // Chem. Phys. Lett. 1986. Vol. 124 (4). P. 304–308.

525. *Kuz'min M.V., Nemov I.V., Stuchebrukhov A.A., Bagratashvili V.N., Letokhov V.S.* Chaotic nonergodical vibrational motion in a polyatomic molecule // Chem. Phys. Lett. 1986. Vol. 124 (6). P. 522–526.

526. *Zharov V.P., Letokhov V.S.* Laser optoacoustical spectroscopy. Springer Series in Optical Sciences. Berlin, Heidelberg, New York: Springer-Verlag, 1986. Vol. 37. 327 pp.

527. *Andreev S.V., Mishin V.I., Letokhov V.S.* High-efficiency laser resonance photoionization of Sr atom in a hot cavity // Optics Commun. 1986. Vol. 57 (3). P. 317–320.

528. *Балыкин В.И., Летохов В.С., Миногин В.Г., Рождественский Ю.В., Сидоров А.И.* Коллимация и деколлимация атомных пучков давлением лазерного излучения // ЖЭТФ. 1986. Т. 90 (3). С. 871–880.

529. *Кузьмин М.В., Летохов В.С., Стучебрюхов А.А*. Пороговая энергетическая зависимость скорости внутримолекулярной колебательной релаксации изолированной многоатомной молекулы // ЖЭТФ. 1986. Т. 90 (2). С. 458–470.

530. *Stuchebrukhov A.A., Kuz'min M.V., Bagratashvili V.N., Letokhov V.S.* Threshold energy dependence of the intramolecular vibrational relaxation rate of a polyatomic molecules // Chem. Phys. 1986. Vol. 107. P. 429–443.

531. *Баграташвили В.Н., Ионов С.И., Летохов В.С., Лохман В.Н., Макаров Г.Н., Стучебрюхов А.А.* Однородный спектр колебательных переходов и время внутримолекулярной колебательной релаксации сильновозбужденной многоатомной молекулы // Письма в ЖЭТФ. 1986. Т. 44 (10). С. 450–453.

532. *Должиков Ю.С., Летохов В.С., Макаров А.А., Малиновский А.Л., Рябов Е.А.* Меж- и внутримолекулярное распределение колебательной энергии при ИК-многофотонном возбуждении молекулы CF_3Br // ЖЭТФ. 1986. Т. 90 (6). С. 1982–1994.

533. *Баграташвили В.Н., Ионов С.И., Кузьмин М.В., Летохов В.С.* Сильное вибрационное перевозбуждение выше предела диссоциации и мономолекулярный распад большого $(CF_3)_3CI$ в инфракрасном лазерном поле // ЖЭТФ. 1986. Т. 91. С. 766–778.

534. *Apatin V.M., Bagratashvili V.N., Ionov S.I., Letokhov V.S., Lokhman V.N., Makarov G.N.* Direct photoionization measurements of slow decay rates of vibratio-

nally overexcitated $(CF_3)_3CI$ molecules in the ground electronic state in a beam // Chem. Phys. Lett. 1986. Vol. 127 (5). P. 438–444.

535. *Андреев С.В., Летохов В.С., Мишин В.И.* Лазерное резонансное фотоионизационное детектирование следов радиоактивного изотопа ^{221}Fr в образце // Письма в ЖЭТФ. 1986. Т. 43 (12). С. 570–572.

536. *Letokhov V.S.* Laser ultrasensitive high-resolution spectroscopy of short-lived radioactive atoms // Commun. Atom. Molec. Phys. 1986. Vol. 18 (5). P. 209–211.

537. *Антонов В.С., Летохов В.С., Московец Е.В.* Лазерно-стимулированная десорбция ионов в сильном электрическом поле // Изв. АН СССР. Сер. физ. 1986. Т. 50 (4). С. 690–694.

538. *Алхазов Г.Д., Барзах А.Е., Буянов Н.Б., Денисов В.П., Дернятин А.Г., Иванов В.С., Летохов В.С., Мишин В.И., Секацкий С.К., Федосеев В.Н., Чубуков И.Я.* Исследование сверхтонкой структуры и электромагнитных моментов изотопов тулия // Изв. АН СССР. Сер. физ. 1986. Т. 50 (12). С. 2366–2371.

539. *Миногин В.Г., Летохов В.С.* Давление лазерного излучения на атомы, в книге Современные проблемы физики. М.:Наука,1986, 224 стр.

540. *Зюзиков А.Д., Летохов В.С., Мишин В.И., Федосеев В.Н.* Лазерная резонансная фотоионизационная спектроскопия возбужденных и автоионизационных состояний атомов редкоземельнных элементов. 1. Европий // Оптика и спектроскопия. 1987. Т. 63 (5). С. 973–981.

541. *Летохов В.С.* Лазерный свет, атомы и ядра // УФН. 1987. Т. 153 (2). С. 311–344.

542. *Letokhov V.S.* Laser light, atom, and nuclei, in: Lasers in Atomic, Molecular and Nuclear Physics. Proceed. of IV Intern. School in Vilnius. Singapore: World Scient. Publ., 1989. P. 3–42.

543. *Mishin V.I., Sekatskii S.K., Fedoseyev V.N., Buyanov N.B., Letokhov V.S., Barzahk A.E., Denisov V.P., Dernyatin A.G., Ivanov V.S., Chubukov I.Ya., Alkhazov G.D.* Resonance photoionization spectroscopy and laser separation of ^{141}Sm and ^{164}Tm nuclear isomers // Optics Commun. 1987. Vol. 61 (6). P. 383–386.

544. *Balykin V.I., Letokhov V.S., Ovchinnikov Yu.B., Sidorov A.I.* Reflection of an atomic beam at a light field gradient // JETP Lett. 1987. Vol. 45. P. 353–356.

545. *Andreev S.V., Letokhov V.S., Mishin V.I.* Laser resonance photoionization spectroscopy of Rydberg levels in Fr. // Phys. Rev. Lett. 1987. Vol. 59 (12). P. 1274–1276.

546. *Letokhov V.S.* Laser control of neutral atomic beams // Comm. Atom. Mol. Phys. 1987. Vol. 19 (3). P. 119–132.

547. *Letokhov V.S.* Laser Photoionization Spectroscopy. New York: Academic Press, 1987. 353 pp.

548. *Летохов В.С.* Лазерная фотоионизационная спектроскопия. М.: Наука, 1987. 318 стр.

549. *Bagratashvili V.N., Kuz'min M.V., Letokhov V.S.* Kinetics of nonequilibrium gas phase reactions induced by vibrational multiple photon IR laser excitation of molecules // Laser Chemistry. 1987. Vol. 7. P. 1–28.

550. *Батурин Г.Н., Беков Г.И., Егоров А.С., Курский А.Н., Летохов В.С., Нарсеев Н.А., Радаев В.Н.* Рутений в донных отложениях и железомарганцевых конкрециях океана // Океанология. 1987. Т. 27 (3). С. 445–449.

551. *Kuzmin M.V., Letokhov V.S., Stuchebrukhov A.A.* Intramolecular vibrational relaxation and IR absorption spectrum of vibrationally excited polyatomics-I and II // Comm. Atom. Molec. Phys. 1987. Vol. 20 (3). P. 127–152.

552. *Летохов В.С.* Лазерное разделение изотопов // Атомная энергия. 1987. Т. 62 (4). С. 252–262.

553. *Мишин В.И., Секацкий С.К., Федосеев В.Н., Буянов Н.Б., Летохов В.С., Алхазов Г.Д., Барзах А.Е., Денисов В.П., Иванов В.С., Чубуков И.Я.* Ультрачувствительная лазерная резонансная фотоионизационная спектроскопия цепочки радиоактивных изотопов $^{157–172}$Tm на протонном ускорителе // ЖЭТФ. 1987. Т. 93 (2). С. 410–423.

554. *Иванов Л.Н., Летохов.* Спектр электронно-ядерных γ-переходов ядра в многозарядном атомном ионе // ЖЭТФ. 1987. Т. 93 (2). 396–404.

555. *Minogin V.G., Letokhov V.S.* Laser light pressure on atoms. New York: Gordon and Breach Science Publ., 1987. 248 pp.

556. *Миногин В.Г., Летохов В.С.* Давление лазерного излучения на атомы. М.: Наука. ФМЛ, 1986. 224 стр.

557. *Егоров С.Е., Летохов В.С., Московец Е.В.* Эффект Франца-Келдыша в лазерно-стимулированной полевой десорбции тонких молекулярных слоев // Письма в ЖЭТФ. 1987. Т. 46 (6). С. 233–235.

558. *Алхазов Г.Д., Барзах А.Е., Буянов Н.Б., Денисов В.П., Дернятин А.Г., Иванов В.С., Летохов В.С., Мишин В.И., Секацкий С.К., Федосеев В.Г, Чубуков И.Я*. О различиях в изотопических изменениях зарядовых радиусов ядер в области $50 \leq (N, Z) \leq 82$ // Письма в ЖЭТФ. 1987. Т. 46 (4). С. 136–138.

559. *Letokhov V.S., Mishin V.I.* Ultrasensitive laser photoionization spectroscopy of short-lived isotopes and very rare atoms. In: Laser Spectroscopy VIII / ed. by S. Svanberg and W. Persson. Springer Series in Optical Sciences. Berlin, Heidelberg, New York: Springer-Verlag, 1987. Vol. 55. P. 167–175.

560. *Orayevskii A.A., Letokhov V.S., Omelyanenkh V.G., Ragimov A.E., Belayev A.A., Akchurin R.S.* Laser spectral analysis of human atherosclerotic vessels. In: Laser Spectroscopy VIII / ed. by S. Svanberg and W. Persson. Springer Series in Optical Sciences. Berlin, Heidelberg, New York: Springer-Verlag, 1987. Vol. 55. P. 370–371.

561. *Balykin V.I., Letokhov V.S.* The possibility of deep laser focusing of an atomic beam into the Å-region // Commun. 1987. Vol. 64 (2). P. 151–156.

562. *Letokhov V.S.* Ultrashort laser pulses in studies of biomolecules, in: Laser Picosecond Spectroscopy and Photochemistry of Biomolecules / ed. by V.S. Letokhov. Bristol: Adam Hilger Publ. Co., 1987. P. 1–55.

563. *Летохов В.С.* Ультракороткие лазерные импульсы в исследовании биомолекул. В кн.: Лазерная пикосекундная спектроскопия и фотохимия биомолекул. М.: Наука, 1987. Гл. 1. С. 5–46.

564. *Furzikov N.P., Karu T.I., Letokhov V.S., Belyaev A.A., Ragimov S.E.* Relative efficiency and products of atherosclerotic plaque destruction by pulsed laser radiation // Lasers in the Life Sciences. Vol. 1(4), 265–274 (1987).

565. *Баграташвили В.Н., Ионов С.И., Летохов В.С., Лохман В.Н., Макаров Г.Н., Стучебрюхов А.А.* Инфракрасная фотодиссоциационная спектроскопия колебательно-перевозбужденных молекул // ЖЭТФ 93(4), 1188-1198 (1987).

566. *Летохов В.С.* Лазерно-индуцированные процессы в атомах и молекулах // В мире науки. № 1. С. 46–58 (1987).

567. *Kozlov A.A., Lobko V.V., Matveets Yu.A., Nikogosyan D.N., Letokhov V.S.* Decomposition of thymine sensitized by hematoporphyrin and its derivative at one- and two-step laser excitation // Lasers in Life Sciences. 1987. Vol. 1. P. 247–264.

568. *Letokhov V.S.* Detecting individual atoms and molecules with lasers, Scientific American, Sept. 1988. P. 44–49.

569. *Balykin V.I., Letokhov V.S., Ovchinnikov Yu.B., Sidorov A.I., Shul'ga S.V.* Recent progress in the control of the motion of atomic beams by laser field. In: Atomic Physics II, Proceed. 11 Intern. Conf. on Atomic Physics. 1988. P. 229–242.

570. *Балыкин В.И., Летохов В.С.* Глубокая фокусировка атомного пучка в Å-область с помощью лазерного излучения // ЖЭТФ. 1988. Т. 94 (1). С. 140–150.

571. *Egorov S.E., Letokhov V.S., Moskovets E.V.* Laser-stimulated field desorption of molecular ions from tungsten emitter // Appl. Phys. B. 1988. Vol. 45 (1). P. 53–57.

572. *Balykin V.I., Letokhov V.S., Ovchinnikov Yu.B., Sidorov A.I.* Focusing of an atomic beam and "imaging" of atomic source by means of a "laser lens" based on resonance-radiation pressure // J. Modern Optics. 1988. Vol. 35 (1). P. 17–34.

573. *Bekov G.I., Letokhov V.S., Radayev V.N., Badyukov D.D., Nazarov M.A.* Rhodium distribution at the Cretaceous. Tertiary boundary analysed by ultrasensitive laser photoionization // Nature. 1988. Vol. 332. P. 146–148.

574. *Козлов А.А., Летохов В.С., Матвеец Ю.А., Чекалин С.В., Ярцев А.П.* Десорбция ионов, образованных на поверхности молекулярных кристаллов фемтосекундным лазерным импульсом // Письма в ЖЭТФ. 1988. Т. 47 (6). С. 294–296.

575. *Letokhov V.S.* Laser-induced chemistry-basic nonlinear processes and applications // Appl. Phys. B. 1988. Vol. 46, 237–251.

576. *Balykin V.I., Letokhov V.S., Minogin V.G.* Laser control of the motion of neutral atoms and optical atomic traps // Physica Scripta. 1988. Vol. T22. P. 119–127.

577. *Kudryavtsev Yu.A., Letokhov V.S., Petrunin V.V.* Collinear laser photoionization of helium isotopes in a fast atomic beam // Optics Commun. 1988. Vol. 68. P. 25–30.

578. *Balykin V.I., Letokhov V.S., Ovchinnikov Yu.B., Sidorov A.I.* Quantum–state–selective mirror reflection of atoms by laser light // Phys. Rev. Lett. 1988. Vol. 60. P. 2137–2140.

579. *Bekov G.I., Radayev V.N., Letokhov V.S.* Laser photoionization spectroscopy of atomic traces at part per trillion levels // Spectrochimia Acta. 1988. Vol. 43B (4/5). P. 491–499.

580. *Orayevskii A.A., Letokhov V.S., Ragimov A.E., Omelyanenkh V.G., Belayev A.A., Shekhonin B.V., Akchurin R.S.* Spectral properties of human atherosclerotic blood vessel walls // Lasers in the Life Sciences. 1988. Vol. 2 (4). P. 257–270.

581. *Letokhov V.S.* Use of lasers for ultrasensitive trace analysis, in: Euroanalysis VI. Reviews of Analytical Chemistry / ed. by E. Roth. Paris: Les Editions de Physique, 1988. P. 117–135.

582. *Egorov S.E., Letokhov V.S., Moskovets E.V.* Laser-stimulated ionization and desorption of molecules in an electric field. In: Laser Optics of Condensed Media / ed. by J.L. Birman, H.Z. Cummins, A.A. Kaplyanskii. New York, London: Plenum Press, 1988. P. 183–191.

583. *Алхазов Г.Д., Барзах А.Е., Денисов В.П., Иванов В.С., Чубуков И.Я., Буянов Н.Б., Летохов В.С., Мишин В.И., Секацкий С.К., Федосеев В.Н.* Среднеквадратичный зарядовый радиус магического ядра ^{14}Gd // Письма в ЖЭТФ. 1988. Т. 48 (7). С. 373–375.

584. *Bagratashvili V.N., Ionov S.I., Stuchebrukhov A.A., Letokhov V.S., Lokhman V.N., Makarov G.N.* The homogeneous Lorentzian IR absorption spectrum of $(CF_3)_3CI$ at twice the threshold vibrational energy // Chem. Phys. Lett. 1988. Vol. 146 (6). P. 599–604.

585. *Ionov S.I., Stuchebrukhov A.A., Bagratashvili V.N., Lokhman V.N., Makarov G.N., Letokhov V.S.* Evolution of the homogeneous IR spectrum of a highly vibrationally excited molecule as a result of a change in its vibrational energy // Appl. Phys. 1988. Vol. B47. P. 229–232.

586. *Alkhazov G.D., Barzakh A.E., Chubukov I.Ya., Denisov V.P., Ivanov V.S., Panteleev V.N., Starodubsky V.E., Buyanov N.B., Fedoseyev V.N., Letokhov V.S., Mishin V.I., Sekatskii S.K.* Nuclear electromagnetic moments and charge radii of deformed thulium isotopes with the mass numbers A = 157–172 // Nucl. Phys. A. 1988. Vol. 477 (1). 37–54.

587. *Andreev S.V., Mishin V.I., Letokhov V.S.* Rydberg levels and ionization potential of francium measured by laser-resonance ionization in hot cavity // JOSA B. 1988. Vol. 36. P. 2190–2198.

588. *Chekalin S.V., Golovlev V.V., Kozlov A.A., Matveets Yu.A., Yartsev A.P., Letokhov V.S.* Femtosecond laser photoionization mass–spectrometry of tryptophan-containing proteins // J. Phys. Chem. 1988. Vol. 92. P. 6855–6858.

589. *Balykin V.I., Letokhov V.S., Ovchinnikov Yu.B., Sidorov A.I., Shulga S.V.* Channeling of atoms in a standing spherical light wave. Opt. Lett. 1988. Vol. 13 (11). P. 958–960.

590. *Антипенко А.Г., Беков Г.И., Девятых Г.Г., Компанец О.Н., Летохов В.С., Максимов О.А., Радаев В.Н., Щапин С.М.* Лазерный атомно-фотоионизационный спектрометр для анализа твердых высокочистых веществ. Определение фемтограммовых содержаний примеси галлия в германии // Высокочистые вещества. 1988. № 2. С. 136–143.

591. *Chekalin S.V., Golovlev V.V., Letokhov V.S., Kozlov A.A., Matveets Yu.A., Yartsev A.P.* Femtosecond laser photoionization mass spectrometry of molecules on surfaces. In: Ultrafast Phenomena VI / ed. by T. Yajima, K. Yoshihara, C.B. Harris, S. Shionoya. Berlin, Heidelberg, New York: Springer-Verlag, 1988. P. 414–419.

592. *Furzikov N.P., Letokhov V.S., Oraevskii A.A.* Fundamentals of laser angioplasty: photoablation and spectral diagnostics. In: Laser Sciences and Technologies

/ ed. by A.N. Chester, V.S. Letokhov, S. Martellucci. New York: Plenum Press, 1988. P. 243–258.

593. *Алхазов Г.Д., Барзах А.Е., Буянов Н.Б., Денисов В.П., Иванов В.С., Летохов В.С., Мишин В.И., Секацкий С.К., Федосеев В.Н., Чубуков И.Я.* Изотопные изменения среднеквадратичных зарядовых радиусов и электромагнитных моментов ядер изотопов самария и неодима при N < 82 // Изв. АН СССР. 1988. Т. 52 (8). С. 1651–1655.

594. *Kudriavtsev Yu.A., Petrunin V.V., Sitkin V.M., Letokhov V.S.* Laser photoionization detection of rare isotope He // Appl. Phys. B. 1989. Vol. 48. P. 93–96.

595. *Letokhov V.S.* Recent results in laser biomedicine and some prospects of the future, Ber. Bunsenges // Phys. Chem. 1989. Vol. 93. P. 233–238.

596. *Balykin V.I., Letokhov V.S.* Laser optics of neutral atomic beams // Physics Today. 1989. P. 23–28.

597. *Stuchebrukhov A., Ionov S., Letokhov V.S.* IR spectra of highly vibrationally excited large polyatomic molecules and intramolecular relaxation // J. Phys. Chem. 1989. Vol. 93. P. 5357–5365.

598. *Balykin V.I., Letokhov V.S.* Atomic cavity with light–induced mirrors // Appl. Phys. B. 1989. Vol. 48. P. 517–523.

599. *Letokhov V.S.* Introduction to the physics of multiple–photon excitation of vibrations in polyatomic molecules. In: Laser Spectroscopy of Highly Vibrationally Excited Molecules / ed. by V.S. Letokhov. Bristol and Boston: Adam Hilger, 1989. P. 1–54.

600. *Balykin V.I., Lozovik Yu.E., Ovchinnikov Yu.B., Sidorov A.I., Shul'ga S.V., Letokhov V.S.* One-dimensional localization of atoms in a standing spherical light wave // JOSA. 1989. Vol. 6B (11). P. 2178–2187.

601. *Беков Г.И., Курский А.Н., Летохов В.С., Пахомов Д.Ю., Радаев В.Н.* Определение родия методом лазерной фотоионизационной спектроскопии в породах, рудах и природных водах // Журнал аналитической химии. 1989. Т. 44(4). С. 689–694.

602. *Алхазов Г.Д., Летохов В.С., Мишин В.И., Пантелеев В.Н., Романов В.И., Секацкий С.К., Федосеев В.Н.* Высокоэффективная Z-селективная фотоионизация атомов в горячей металлической полости с последующим электростатическим удержанием ионов // Письма в ЖТФ. 1989. Т. 15 (10). С. 63–67.

603. *Bekov G.I., Letokhov V.S., Radaev V.N.* Laser photoionization spectroscopy for ultrasensitive trace element analysis // Freseniys Zh. Anal. Chem. 1989. Vol. 335. P. 19–24.

604. *Ryabov E.A., Letokhov V.S.* Time-resolved Raman spectroscopy studies of intramolecular vibrational dynamics. In: Recent Trends in Raman Spectroscopy. Proceed. of Intern. Conf. Singapore: World Scient. Publ., 1989. P. 28–39.

605. *Bekov G.I., Letokhov V.S.* Ultrasensitive laser photoionization analysis in oceanology, geochemistry and geology. In: Resonant Ionization Spectroscopy. Proceed. of 4th Intern. Symp. Bristol: Adam Hilger, 1989. P. 331–336.

606. *Malinovskii A.L., Ryabov E.A., Letokhov V.S.* Laser time–resolved Raman spectroscopy of mode selectivity and vibrational energy distribution for IR MP excited polyatomic molecules // Chem. Phys. 1989. Vol. 139. P. 229–238.

607. *Esenaliev R.O., Oraevsky A.A., Letokhov V.S.* Laser ablation of atherosclerotic blood vessel tissue under various irradiation conditions // IEEE J. of Biomedicine Engineering. 1989. Vol. 36. P. 1188–1194.

608. *Letokhov V.S.* Laser light interaction with biomolecules, cells and tissue. In: Dosimetry of Laser Radiation in Medicine and Biology / ed. by G.J. Muller and D.H. Sliney. SPIE Proceed. 1989. Vol. 155. P. 2–4.

609. *Алхазов Г.Д., Барзах А.Е., Буянов Н.Б., Денисов В.П., Иванов В.С., Летохов В.С., Мишин В.И., Секацкий С.К., Федосеев В.Н., Чубуков И.Я.* Исследование радиоактивных редкоземельных изотопов методом лазерной резонансной атомной фотоионизации // Известия АН СССР. Сер. физ. 1989. Т. 53 (6). С. 1208–1214.

610. *Balykin V.I., Letokhov V.S., Ovchinnikov Yu.B., Sidorov A.I., Shul'ga S.V.* Recent progress in the control of the motion of atomic beams by laser field. In: Frequency Standards and Metrology (Proceed. of the 4th Int. Sym., Ancona, Italy, September 5–9, 1989). Berlin: Springer-Verlag, 1989. P. 248–263.

611. *Letokhov V.S.* Recent progress in the control of the motion of atomic beams by laser field. In: Atomic Physics 11 (Proceed. of the 11th Intern. Conf. on Atomic Physics, 4–8 July, 1988, Paris). Singapore: World Scientific, 1989. P. 229–242.

612. *Letokhov V.S.* Multiple-photon laser resonant excitation of molecules", in: Laseres y Reactiones Quimicas (Proceed. Cursos de Verano, El Escorial, 1989). Publ. of Universidad Complutense de Madrid, 1990. P. 67–99.

613. *Letokhov V.S.* Multiple-photon laser chemistry, Chinese J. of Lasers. B. 1994. Vol. 3 (14). P. 289–313.

614. *Alkhazov G.D., Barzakh A.E., Chubukov I.Ya., Denisov V.P., Ivanov V.S., Buyanov N.B., Fedoseyev V.N., Letokhov V.S., Mishin V.I., Sekatskii S.K.* Nuclear deformation of holmium isotopes, Nuclear Physics. A. 1989. Vol. 504. P. 549–561.

615. *Letokhov V.S.* Prospects of laser spectroscopy of biomolecules with nanometer spatial resolution. In: Laser Spectroscopy IX / ed. by M. Feld, J. Thomas, A. Mooradian (Proceed. of the Ninth Int. Laser Spectroscopy Conf., Bretton Woods, N.H., June 18–23, 1989). Boston: Academic Press, 1989. P. 494–499.

616. *Balykin V.I., Letokhov V.S., Ovchinnikov Yu.B., Sidorov A.I., Shul'ga S.V.* Localization of atoms with light-induced mirrors and in a standing light wave. In: Laser Spectroscopy IX / ed. by M. Feld, J. Thomas, A. Mooradian (Proceed. of the Ninth Int. Laser Spectroscopy Conf., Bretton Woods, N.H., June 18–23, 1989). Boston: Academic Press, 1989. P. 452–454.

617. *Балыкин В.И., Летохов В.С.* Лазерная оптика нейтральных атомных пучков // УФН. 1990. Т. 160 (1). 141–154.

618. *Letokhov V.S., Tyakht V.V.* Coherent vibrational wave packet dynamics in femtosecond excitation of diatomic molecules // Israel J. of Chem. 1990. Vol. 30. P. 189–195.

619. *Balykin V.I., Letokhov V.S., Ovchinnikov Yu.B., Sidorov A.I., Shul'ga S.V.* Collimation of atoms localized in a spherical standing light wave // Optics Commun. 1990. Vol. 77. P. 152–156.

620. *Есеналиев Р.О., Ораевский А.А., Летохов В.С., Рабкин Е.И., Нацвалишвили З.Г., Кавтеладзе З.А., Бабунашвили А.М.* Исследование процесса

лазерной абляции тканей атеросклеротических сосудов при различных условиях облучения // Известия АН СССР. Сер. физ. 1990. Т. 54 (8). С. 1586–1593.

621. *Grimm R., Ovchinnikov Yu.B., Sidorov A.I., Letokhov V.S.* Observation of a strong rectified dipole force in a bichromatic standing light wave // Phys. Rev. Lett. 1990. Vol. 65. P. 1415–1418.

622. *Kudryavtsev Yu.A., Letokhov V.S.* Detection of very rare isotopes // Physics World. 1990. Vol. 3. P. 48–52.

623. *Chekalin S.V., Golovlev V.V., Matveets Yu.A., Yartsev A.P., Letokhov V.S., Greulich K.-O., Wolfrum J.* Laser femtosecond MPI mass-spectrometry of dye–labeled nucleotides // IEEE J. Quant. Electron. 1990. Vol. 26 (12). P. 2158–2161.

624. *Гершензон М.Е., Головлев В.В., Кедич И.Б., Летохов В.С., Лозовик Ю.Е., Матвеец Ю.А., Силькис Э.Г., Степанов А.Г., Титов В.Д., Фалей М.И., Фарзтдинов В.М., Чекалин С.В., Ярцев А.П.* Прямое измерение характеристик электрон-фононного взаимодействия в YBa2Cu3O7 методом фемтосекундной лазерной спектроскопии // Письма в ЖЭТФ. 1990. Т. 52 (11). С. 1189–1192.

625. *Ораевский А.А., Летохов В.С., Рагимов С.Э., Омельяненко В.Г., Беляев А.А.* Спектральная диагностика атеросклеротических бляшек в сосудах человека // Известия АН СССР. Сер. физ. 1990. Т. 54 (10). С. 1900–1903.

626. *Bekov G.I., Letokhov V.S., Radayev V.N.* Laser photoionization spectroscopy for ultrasensitive determination of element traces. Proceed. of Intern. Trace Analysis Symposium 90. Senday and Kiryu, Japan, 1990. P. 37–46.

627. *Bekov G.I., Letokhov V.S.* Laser ultrasensitive photoionization detection of rare elements in geochemistry, oceanology and study of geological catastrophes, in: Optoelectronics and Environmental Science / ed. by S. Martelucci and A.N. Chester. N.Y.: Plenum Press, 1990. P. 177–183.

628. *Kudriavtsev Yu.A., Letokhov V.S., Petrunin V.V.* Laser detection of very rare long-lived isotopes. In: Applied Laser Spectroscopy / ed. by W. Demtroder and M. Inguscio // Plenum Press. No. 4. 1990. P. 329–338.

629. *Alkhazov G.D., Barzakh A.E., Denisov V.P., Ivanov V.S., Chubukov I.Ya., Fedoseyev V.N., Letokhov V.S., Mishin V.I., Sekatskii S.K.* Laser photoionization spectroscopy of rare-earth elements: new results on nuclear electromagnetic moments and charge radii of Eu, Gd, Tb isotopes // Hyperfine Interactions. 1990. Vol. 61. P. 1335–1338.

630. *Alkhazov G.D., Barzakh A.E., Bolshakov V.A., Denisov V.P., Ivanov V.S., Sergeyev Ya.Yu., Chubukov I.Ya., Tikhonov V.I., Letokhov V.S., Mishin V.I., Sekatskii S.K., Fedoseyev V.N.* Odd-even staggering in nuclear charge radii of neutron-rich europium isotopes // Z. Phys. A. Atomic Nuclei. 1990. Vol. 337. P. 257–259.

631. *Alkhazov G.D., Barzakh A.E., Denisov V.P., Ivanov V.S., Chubukov I.Ya., Letokhov V.S., Mishin V.I., Sekatskii S.K., Fedoseyev V.N.* Electromagnetic moments and nuclear charge radii for neutron-deficient Tb isotopes and the deformation jump near Z = 64 // Z. Phys. A. Atomic Nuclei. 1990. Vol. 337. P. 367–370.

632. *Aseyev S.A., Kudryavtsev Yu.A., Letokhov V.S., Petrunin V.V.* Laser detection of the rare isotopes ^{3}He at concentrations as low as 10^{-9} // Optics Lett. 1991. Vol. 16 (7). P. 514–516.

633. *Fedoseev V.N., Kudryavtsev Yu.A., Letokhov V.S., Mishin V.I., Ravn H., Sundell S., Kluge H.J., Scheerer F.* A laser ion source for on-line isotope separation. In: Resonance Ionization Spectroscopy — 90. Inst. Phys. Conf. Ser. No. 114. Bristol, London, 1991. P. 129–32.

634. *Aseyev S.A., Kudryavtsev Yu.A., Letokhov V.S., Petrunin V.V.* Detection of very rare isotopes by collinear resonance ionization of accelerated atoms. In: Resonance Ionization Spectroscopy — 96 inst. Phys. Conf. Ser. No. 114, Bristol, London, 1991. P. 7–12.

635. *Alkhazov G.D., Barzakh A.E., Denisov V.P., Fedoseyev V.N., Letokhov V.S., Mishin V.I., Sekatskii S.K.* Laser resonance ionization spectroscopy of radioactive isotopes of rare-earth elements. In: Resonance Ionization Spectroscopy — 90 inst. Phys. Conf. Ser. No. 114, Bristol, London, 1991. P. 13–18.

636. *Schultz Ch., Arnold E., Borchers W., Nen W., Neugart R., Neuroth M., Otten E.W., Scherf M., Wendt K., Lievens P., Kudriavtsev Yu.A., Letokhov V.S., Mishin V.I., Petrunin V.V.* Resonant ionization spectroscopy of fast atomic beam. In: Resonance ionization Spectroscopy — 90, Inst. Phys. Conf. Ser. No. 114, Bristol, London, 1991. P. 27–30.

637. *Grimm R., Ovchinnikov Yu.B., Sidorov A.I., Letokhov V.S.* Dipole force rectification in a monochromatic laser field, Optics Commun. 84(12), 18–22 (1991).

638. *Letokhov V.S.* Effects of transient local heating of spatially and spectrally heterogeneous biotissue by short laser pulses // Nuovo Cimento. 1991. Vol. 13D (17). P. 939–948.

639. *Karu T.I., Tiphlova O.A., Matveets Yu.A., Yartsev A.P., Letokhov V.S.* Comparison of the effects of visible femtosecond laser pulses and continuous wave laser radiation of low average intensity on the clonogenicity of Escherichia coli // J. Photochem. Photobiol, B: Biol. 1991. Vol. 10. P. 339–344.

640. *Aseyev S.A., Kudryavtsev Yu.A., Letokhov V.S., Petrunin V.V.* Method of detecting the rare isotopes 85Kr, and 81Kr by means of collinear laser photoionization of atoms in an accelerated beam // J. Phys. B: At. Mol. Opt. Phys. 1991. Vol. 24. P. 2755–2763.

641. *Летохов В.С., Секацкий С.К., Миров С.Б.* Лазерный ступенчатый резонансный фотоэффект на примесных ионах Nd3+ на поверхности кристалла ZrO2 // Письма в ЖЭТФ. 1991. Т. 54 (8). С. 438–441.

642. *Гримм Р., Овчинников Ю.Б., Сидоров А.И., Летохов В.С.* Наблюдение магнито-оптической радиационной силы // Письма в ЖЭТФ. 1991. Т. 54 (11). С. 611–614.

643. *Oraevskii A.A., Esenaliev R.O., Letokhov V.S.* Pulsed laser ablation of biological tissue: review of the mechanisms. In: Laser Ablation. Mechanisms and Applications / ed. by J.C. Miller and R.F. Haglund. Berlin: Springer-Verlag, 1991. P. 112–122.

644. *Ovchinnikov Yu.B., Sidorov A.I., Grimm R., Letokhov V.S.* Behavior of the friction force in a biochromatic standing light wave // J. Phys. B: At. Mol. Opt. Phys. 1991. Vol. 24. P. L539–L543.

645. *Sidorov A.I., Grimm R., Letokhov V.S.* Rectification of the gradient force acting on a three-level atom in a bichromatic standing light wave // J. Phys. B: At. Mol. Opt. Phys. 1991. Vol. 24. P. 3733–3740.

646. (a) *Chekalin S.V., Farztdinov V.M., Golovlev V.V., Letokhov V.S., Lozovik Yu.E., Matveets Yu.A., Stepanov A.G.* Femtosecond spectroscopy of $YBa_2Cu_3O_7$–δ electron–phonon interaction measurements and energy-gap observation // Phys. Rev. Lett. 1991. Vol. 67. P. 3860–3863; (b) in: Ultrafast Processes in Spectroscopy / ed. by A. Laubereau, Proceed. Int. Symp., Bayreuth, 1991 inst. Phys. Conf. Ser. No. 12, 1992. P. 261–266.

647. *Alkhazov G.D., Batist L.Kh., Bykov A.A., Vitman V.D., Letokhov V.S., Mishin V.I., Panteleyev V.N., Sekatskii S.K., Fedoseyev V.N.* Application of a high efficiency selective laser ion source at the IRIS facility // Nuclear Instr. and Methods in Phys. Res. 1991. Vol. A 306. P. 400–402.

648. *Schultz Ch., Arnold E., Borchers W., Neu W., Neugart R., Neugart M., Otten E.W., Scherf M., Wendt K., Lievens P., Kudriavtsev Yu.A., Letokhov V.S., Mishin V.I., Petrunin V.V. and ISOLDE collaboration*. Resonance ionization spectroscopy on a fast atomic ytterbium beam // J. Phys. B: At. Mol. Opt. Phys. 1991. Vol. 24. P. 4831–4844.

649. *Oraevskii A.A., Esenaliev R.O., Letokhov V.S.* Temporal characteristics and mechanism of atherosclerotic tissue ablation by nanosecond and picosecond laser pulses // Lasers in the Life Sciences. 1992. Vol. 5. P. 75–93.

650. *Ovchinnikov Yu.B., Letokhov V.S.* Channeling of atoms in a standing laser light wave // Comm. At. Mol. Phys. 1992. Vol. 27(4). P. 185–201.

651. *Letokhov V.S.* Atomic optics with tunable dye lasers. In: Dye Lasers: 25 Fears / ed. by M. Stuke. Berlin: Springer-Verlag, 1992. P. 153–168.

652. *Grimm R., Letokhov V.S., Ovchinnikov Yu.B., Sidorov A.I.* A strong magneto-optical force exerted on neutral atoms // J. Phys. II. France. 1992. Vol. 2. P. 593–599.

653. *Balaban P., Esenaliev R., Karu T., Kutomkina E., Letokhov V., Oraevsky A., Ovcharenko N.* He–Ne laser irradiation of single identified neurons // Lasers in Surgery and Medicine. 1992. Vol. 12. P. 329–337.

654. *Ovchinnikov Yu.B., Grimm R., Sidorov A.I., Letokhov V.S.* Action of strong rectified dipole forces on atoms. In: Laser Spectroscopy X / ed. by M. Ducloy, E. Giacobino, G. Camy. Singapore: World Scientific, 1992. P. 21–26.

655. *Letokhov V.S., Sekatskii S.K.* Laser photoelectron microscopy for imaging impurity ions, color centers, and small-size irregularities in dielectric media // Appl. Phys. B. 1992. Vol. 55. P. 177–179.

656. *Moskovets E.V., Letokhov V.S.* Laser-stimulated field desorption of organic molecules in high electric fields // Surface Science. 1992. Vol. 266. P. 81–87.

657. *Головлев В.В., Матвеец Ю.А., Санов А.Н., Летохов В.С.* Исследование релаксации электронной температуры медной пленки при возбуждении фемтосекундными лазерными импульсами // Письма в ЖЭТФ. 1992. Т. 55 (7–8). С. 441–444.

658. *Dobryakov A.L., Lozovik Yu.E., Puretsky A.A., Letokhov V.S.* Comments on small superconducting clusters // Appl. Phys. A. 1992. Vol. 54. P. 100–102.

659. *Letokhov V.S., Sekatskii S.K.* Towards laser photoelectronic resonance ionization spectromicroscopy (RISM). In: Resonance Ionization Spectroscopy 1992 / ed. by C.M. Miller and J.E. Parks IOP Publ. Bristol, 1992. P. 241–248.

660. *O1'shanny M.A., Letokhov V.S., Minogin V.G.* Role of interaction time in light pressure force on atoms // Nonlinear Opt. 1992. Vol. 3. P. 183–294.

661. *Letokhov V.S., Mishin V.I., Sekatskii S.K., Fedoseyev V.N., Alkhazov G.D., Barzahk A.E., Denisov V.P., Starodubsky V.E.* Laser spectroscopical studies of nuclei with neutron number N < 82 (Eu, Sm, and Nd isotopes) // J. Phys. G: Nucl. Part. Phys. 1992. Vol. 18. P. 1177–1193.

662. *Alkhazov G.D., Barzahk A.E., Denisov V.P., Mezilev K.A., Novikov Yu.N., Panteleyev V.N., Popov A.V., Sudentas E.P., Letokhov V.S., Mishin V.I., Fedoseyev V.N., Andreev S.V., Vedeneyev D.S., Zyuzikov A.D.* New highly efficient method of atomic spectroscopy for nuclids far from stability // Nucl. Instr. and Methods in Physics Research. B. 1992. Vol. 69. P. 517–520.

663. *Letokhov V.S.* Laser cooling and trapping of atomic particles. In: Atomic and Molecular Physics and Quantum Optics / ed. by H.-A. Bachor, K. Kumar, B. Robson. Singapore: World Scientific, 1992. P. 467–511.

664. *Oraevsky A.A., Letokhov V.S.* Pulsed laser ablation of atherosclerotic plaque in blood vessels. In: The Practice of Interventional Cardiology / ed. by J.H.K. Vogel and S.B. King III. Mosby, St. Louis, 1993. P. 203–214.

665. *Alkhazov G.D., Barzahk A.E., Panteleyev V.N., Letokhov V.S., Mishin V.I., Fedoseyev V.N.* Nuclear radii and moments of rare-earth elements from laser spectroscopy, in: Proceed. 5th Int. Conf. on Nuclei Far from Stability and 9th Int. Conf. on Atomic Masses and Fundamental Constants, Bernkastel-Kues, 1992 (Publ. of IOPP, No. 132, 1993). P. 145–150.

666. *Sekatskii S.K., Letokhov V.S., Mirov S.B.* External photoelectronic effect in CaF2:Sm2+ crystals under irradiation with visible light // Optics Comm. 1993. Vol. 95. P. 260–264.

667. *Ol'shanny M.A., Ovchinnikov Yu.B., Letokhov V.S.* Laser guiding of atoms in a hollow optical fiber // Optics Comm. 1993. Vol. 98. P. 77–79.

668. *Klimov V.V., Letokhov V.S.* Radio emission of an optical soliton propagating in a ring fiber // Optics Commun. 1993. Vol. 100. P. 437–442.

669. *Mishin V.I., Fedoseyev V.N., Kluge H.-J., Letokhov V.S., Ravn H.L., Scheerer F., Shirakabe Y., Sundell S., Tengblad O. and the ISOLDE collaboration.* Chemically selective laser ion-source for the CERN- ISOLDE online mass separator facility, Nucl. Instr. and Meth. in Physics Research. B. 1993. Vol. 73. P. 550–560.

670. *Kardash I.E., Letokhov V.S., Lozovik Yu.E., Matveets Yu.A., Stepanov A.G., Farztdinov V.M.* Ultrafast relaxation of photoinduced darkening in fullerites // JETP Lett. 1993. Vol. 58. P. 138–141.

671. *Ovchinnikov Yu.B., Grimm R., Sidorov A.I., Letokhov V.S.* Rectified dipole force in a bichromatic standing light wave // Optics Commun. 1993. Vol. 102. P. 155–165.

672. *Esenaliev R.O., Oraevsky A.A., Letokhov V.S., Karabutov A.A., Malinovsky A.V.* Studies of acoustical and shock waves in the pulsed laser ablation of biotissue // Lasers in Surgery and Medicine. 1993. Vol. 13. P. 470–484.

673. *Balykin V.I., Letokhov V.S., Ovchinnikov Yu.B.* Channeling of atoms in a standing laser light wave, in: Frontiers in Nonlinear Optics, ed. by H. Walther, N. Koroteev. M.O. Scully. Bristol: Publ. of IOP, 1993. P. 1–16.

674. *Golovlev V.V., Letokhov V.S.* Laser ablation of absorbing liquids: acoustical microfragmentation mechanism // Appl. Phys. B. 1993. Vol. 57. P. 417–423.

675. *Golovlev V.V., Esenaliev R.O., Letokhov V.S.* Ablation of an optically homogeneous absorbing medium by scattered pulsed laser radiation // Appl. Phys. B. 1993. Vol. 57. P. 451–457.

676. *Letokhov V.S.* Ultrasensitive laser spectroscopy of trace elements // Ber. Bunsen Ges. Phys. Chem. 1993. Vol. 97 (12). P. 1512.

677. *Farztdinov V.M., Lozovik Yu.E., Matveets Yu.A., Stepanov A.G., Letokhov V.S.* Femtosecond dynamics of photoinduced darkening in C60 films // J. Phys. Chem. 1994. Vol. 98. P. 3290–3294.

678. *Klimov V.V., Letokhov V.S.* A simple theory of the near field in diffraction by a round aperture // Optics Commun. 1994. Vol. 106. P. 151–154.

679. *Dobryakov A.L., Farztdinov V.M., Lozovik Yu.E., Letokhov V.S.* Energy gap in the superconductor optical spectrum // Optics Commun. 1994. Vol. 105. P. 309–314.

680. *Letokhov V.S.* Partial population inversion for electron-nuclear transitions in multiply charged ions // Optics Commun. 1994. Vol. 106. P. 227–230.

681. *Bezel I.V., Chekalin S.V., Matveets Yu.A., Stepanov A.G., Yartsev A.P., Letokhov V.S.* Two-photon absorption of powerful femtosecond pulses in C_{60} films // Chem. Phys. Lett. 1994. Vol. 218. P. 475–478.

682. *Letokhov V.S., Sekatskii S.K.* Laser resonance photoionization of absorbing centers on surface // Opt. and Spectr. 1994. Vol. 76 (2). P. 303–310.

683. *Ovchinnikov Yu.B., Grimm R., Sidorov A.I., Letokhov V.S.* Resonant light pressure on atoms by bichromatic standing wave // Optics and Spectroscopy. 1994. Vol. 76 (2). P. 210–220.

684. *Асеев С.А., Кудрявцев Ю.А., Летохов В.С., Петрунин В.В.* Лазерная коллинеарная ионизация ускоренных атомов в пучке как метод детектирования редких изотопов криптона // Оптика и спектроскопия. 1994. Т. 76 (2). С. 227–236.

685. *Балыкин В.И., Летохов В.С., Климов В.В.* Эффект острой фокусировки атомного пучка ближним полем лазерного излучения // Письма в ЖЭТФ. 1994. Т. 59 (4). С. 219–222.

686. *Karu T., Letokhov V.S.* Possible benefits of two-quantum excitation in ALA-PDT // J. Photochem. B: Biol. 1994. Vol. 23. P. 261–262.

687. *Sekatskii S.K., Letokhov V.S., Basiev T.T., Ter-Mikirtychev V.V.* Laser resonance external photoelectric effect in F_2- color centers of LiF crystals // Appl. Phys. A. 1994. Vol. 58. P. 467–470.

688. *Klimov V.V., Letokhov V.S.* Selection of particles by a gradient force in the near field of laser light // JETP Lett. 1994. Vol. 59 (9). P. 609–612.

689. *Farztdinov V.M., Lozovik Yu.E., Letokhov V.S.* Saturation of the fullerite photodarkening at high laser energy fluences // Chem. Phys. Lett. 1994. Vol. 224. P. 493–500; Err. Chem. Phys. Lett. 1995. Vol. 233. P. 490.

690. *Esenaliev R.O., Karabutov A.A., Podymova N.B., Letokhov V.S.* Laser ablation of aqueous solutions with spatially homogeneous and heterogeneous absorption // Appl. Phys. B. 1994. Vol. 59. P. 73–81.

691. *Klimov V.V., Letokhov V.S.* Selective sorting of neutral atoms and molecules by the gradient dipole force in the near field of laser radiation // Optics Commun. 1994. Vol. 110. P. 87–93.

692. *Lozovik Yu.E., Merkulova S.P., Sekatskii S.K., Letokhov V.S.* The possibility of nanolocal reactions on surface // Phys. Letts. 1994. Vol. 189. P. 131–133.

693. *Ashikhmin M.V., Belyaev Yu.E., Dem'yanenko A.V., Ryabov E.A., Letokhov V.S.* Laser [2+1] REMPI detection of Br atoms in unimolecular decomposition reactions // Chem. Phys. Lett. 1994. Vol. 227. P. 343–348.

694. *Karu T., Tiphlova O., Esenaliev R., Letokhov V.* Two different mechanisms of low-intensity laser photobiological effects on Escherichia Coli // J. Photochem. Photobiol. B. 1994. Vol. 24. P.155–161.

695. *Добряков А.Л., Головлев В.В., Летохов В.С., Лозовик Ю.Е., Матвеец Ю.А., Степанов А.Г., Фарзтдинов В.М., Чекалин С.В.* Фемтосекундная спектроскопия сверхпроводников $YBa_2Cu_3O_7$–δ. Измерение параметра электрон-фононного взаимодействия и наблюдение энергетической щели // Оптика и спектроскопия. 1994. Т. 76 (6). С. 975–983.

696. *Hurst G.S., Letokhov V.S.* Resonance ionization spectroscopy. // Phys. Today. 1994. P. 38–45.

697. *Balykin V.I., Klimov V.V., Letokhov V.S.* Laser near field lens for atoms // J. Phys. II. France. 1994. Vol. 4. P. 1981–1997.

698. *Moskovets E.V., Letokhov V.S.* Cat's-eye reflectron // Appl. Phys. B. 1994. Vol. 59 (5). P. 547–552.

699. *Конопский В.Н., Секацкий С.К., Летохов В.С.* Исследование поверхности кристалла LiF:F с субволновым пространственным разрешением // Письма в ЖЭТФ. 1994. Т. 60 (9–10). С. 691–693.

700. *Esenaliev R.O., Golovlyova O.A., Golovlyov V.V., Letokhov V.S.* Effect of erythrocyte of acoustic waves generated upon absorption of laser radiation // Lasers in the Life Sciences. 1994. Vol. 6. P. 153–161.

701. *Letokhov V.S., Yukov E.A.* Excitation of isomeric low-lying levels of heavy nuclei in a laser-produced plasma // Laser Physics. 1994. Vol. 4 (2). P. 382–386.

702. *Karabutov A.A., Podymova N.B., Letokhov V.S.* Laser optoacoustic investigation of light absorption by homogeneous, inhomogeneous, and scattering media // Bull. SPIE. 1994. No. 4. P. 22–25.

703. *Karabutov A.A., Podymova N.B., Letokhov V.S.* Time-resolved optoacoustic detection of absorbing particles in scattering media // J. Mod. Optics. 1995. Vol. 42. P. 7–11.

704. *Alekseev V.A., Krylova D.D., Letokhov V.S.* Sympathetic cooling of two trapped ions // Physica Scripta. 1995. Vol. 51. P. 368–372.

705. *Letokhov V.S., Ol'shanii M.A., Ovchinnikov Yu.B.* Laser cooling of atoms: a review // Quantum Optics. 1995. Vol. 7. P. 5–40.

706. *Климов В.В., Летохов В.С.* Пленение атомов в ближнем поле лазерного излучения // Письма в ЖЭТФ. 1995. Т. 61 (1). С. 15–19.

707. *Letokhov V.S.* Towards laser control of molecular motion // Ber. Bunsenges. Phys. Chem. 1995. Vol. 99. P. 498–503.

708. *Letokhov V.S.* Impact of laser and nuclear technologies, Proceed. of 6th Int. Symp. Innovative Laser Technologies in Nuclear Energy. March, 1994. Publ. of Japan Atomic Energy Research Institute, 1995. P. 11–24.

709. *Letokhov V.S.* Multiphoton photochemistry and photobiochemistry with ultrashort laser pulses. In: Ultrafast Processes in Chemistry and Photobiology / ed. by M. El-Sayed, Tanaka, Y. Molin. Oxford: Blackwell Science, 1995. P. 195–214.

710. *Асеев С.А., Кудрявцев Ю.А., Ларюшин Д.В., Летохов В.С., Петрунин В.В.* Ионизация быстрых ридберговских атомов в магнитном поле // Письма в ЖЭТФ. 1995. Т. 62 (5). С. 368–370.

711. *Balykin V.I., Letokhov V.S.* Atom optics with laser lightю Harwood Acad. Publ. Chur, 1995. P. 1–115.

712. *Karabutov A.A., Podymova N.B., Letokhov V.S.* Time-resolved optoacoustical measurement of absorption of light by nonhomogeneous media // Appl. Opt. 1995. Vol. 34 (9). P. 1484–1487.

713. *Летохов В.С.* Фокусировка электронного пучка дипольной силой ультракороткого лазерного импульса // Письма в ЖЭТФ. 1995. Т. 61 (10). С. 787–790.

714. *Klimov V.V., Letokhov V.S.* Laser-near-field-based atomic lens: Quantum wave optics consideration // J. Modern Opt. 1995. Vol. 42 (7). P. 1485–1503.

715. *Климов В.В., Летохов В.С.* Селекция частиц градиентной силой в ближнем поле лазерного излучения // ЖЭТФ. 1995. Т. 108 (1). С. 91–104.

716. *Добряков А.Л., Коваленко С.А., Летохов В.С., Лозовик Ю.Е., Маровский Г., Матвеец Ю.А., Фарзтдинов В.М., Эрнстинг Н.Р.* Когерентные фононы в фуллеритах при фемтосекундном лазерном возбуждении // Письма в ЖЭТФ. 1995. Т. 61 (11–12). С. 957–961.

717. *Овчинников Ю.Б., Ларюшин Д.В., Балыкин В.И., Летохов В.С.* Охлаждение атомов при отражении от поверхностной световой волны // Письма в ЖЭТФ. 1995. Т. 62 (2). С. 102–107.

718. *Letokhov V.S.* Laser Maxwell's demon // Contemp. Phys. 1995. Vol. 36 (4). P. 235–243.

719. *Lozovik Yu.E., Popov A.M., Letokhov V.S.* Possibility of selective adsorption of molecules on modified surface // J. Phys. Chem. 1995. Vol. 99. P. 13480–13486.

720. *Венгрус И.И., Добряков А.Л., Коваленко С.А., Летохов В.С., Лозовик Ю.Е., Маровский Г., Матвеец Ю.А., Фарзтдинов В.М., Эрнстинг Н.Р.* Спектральная зависимость релаксации в YBa2Cu3O7-δ при фемтосекундном лазерном возбуждении // Письма в ЖЭТФ. 1995. Т. 62 (9). С. 739–743.

721. *Demianenko A., Letokhov V., Makarov A., Ryabov E.* Multiphoton IR laser-induced unimolecular decay of $(CF_3)_3CBr$ molecule // Faraday Discuss. 1995. Vol. 102. P. 301–309.

722. *Klimov V.V., Letokhov V.S.* New atom trap configurations in the near field of laser radiation // Optics Commun. 1995. Vol. 121. P. 130–136.

723. *Конопский В.Н., Секацкий С.К., Летохов В.С.* Первая реализация метода лазерной селективной проекционной фотоэлектронной микроскопии:

исследование поверхности кристалла LiF:F2 с субволновым пространственным разрешением // Изв. РАН. Сер. физ. 1995. Т. 59 (12). С. 13–18.

724. *Ovchinnikov Yu.B., Laryushin D.V., Balykin V.I., Letokhov V.S.* Inelastic reflection of atoms from an evanescent light wave. In: Modern problems of laser physics / ed. by S.N. Bagayev and V.I. Denisov. Publ. of Sib. Branch of Russian Acad. Sci., 1996. P. 173–179.

725. *Dobryakov A.L., Ernsting N.P., Farztdinov V.M., Kovalenko S.S., Letokhov V.S., Lozovik Yu.E., Marowsky G., Matveetz Yu.A.* Coherent photons in fullerites under femtosecond laser excitation. In: Ultrafast Processes in Spectroscopy / ed. by O. Svelto et al. N.Y.: Plenum Press, 1996. P. 95–99.

726. *Dobryakov A.L., Farztdinov V.M., Kovalenko S.S., Letokhov V.S., Lozovik Yu.E., Matveetz Yu.A.* Observation of coherent photons generation in C_{60} films // Proceed. of SPIE. 1996. Vol. 2797. P. 102–107.

727. *Ovchinnikov Yu.B., Laryushin D.V., Balykin V.I., Letokhov V.S.* Inelastic reflection of atoms from an evanescent light wave // Laser Phys. 1996. Vol. 6 (2). P. 264–267.

728. *Konopsky V.N., Sekatskii S.K., Letokhov V.S.* First realization of laser selective projection photoelectron microscopy: Studying of LiF:F_2 crystal surface with the subwavelength spatial resolution. Proc. of SPIE, Atomic and Quantum Optics: High-Precision Measurements 2799. 1996. P. 344–350.

729. *Letokhov V.S.* Noncoherent feedback in space masers and stellar lasers. In: Amazing Light / ed. by R.Y. Chiao. Berlin: Springer. 1996. P. 409–443.

730. *Klimov V.V., Letokhov V.S.* Increase of spontaneous quadrupole transition rate in the vicinity of a dielectric microsphere // Optics Commun. 1996. Vol. 122. P. 155–162.

731. *Sekatskii S.K., Letokhov V.S.* Scanning optical microscopy with nanometer spatial resolution based on resonance excitation of fluorescence from one–atom excited center // JETP Lett. 1996. Vol. 63. P. 319–323.

732. *Letokhov V.S.* Laser resonance photoelectron spectromicroscopy with a subwavelength spatial resolution. In: Quantum Optics of Confined Systems / ed. by M. Ducloy and D. Bloch. Dordrecht: Kluwer Academic Publ., 1996. P. 327–340.

733. *Klimov V.V., Ducloy M., Letokhov V.S.* Spontaneous emission rate and level shift of an atom inside a dielectric microsphere // J. Modern Opt. 1996. Vol. 43 (3). P. 549–563.

734. *Klimov V.V., Letokhov V.S.* Gradient optical force on atoms: Beyond dipole approximation // Optics Commun. 1996. Vol. 126. P. 45–48.

735. *Konopsky V.N., Sekatskii S.K., Letokhov V.S.* Laser photoionization spectroscopy with subwavelength spatial resolution: First observation of single color centers on the surface. In: Laser Spectroscopy XII Intern. Conf. (June 11–16, 1995, Capri, Italy) / ed. by M. Inguscio, M. Allegrini, A. Sasso. Singapore: World Scientific, 1996. P. 433–439.

736. *Konopsky V.N., Sekatskii S.K., Letokhov V.S.* Laser resonance photoelectron spectromicroscopy with subwavelength spatial resolution. In: Modern Optics of Laser Physics / ed. by S.N. Bagayev and V.I. Denisov. Publ. of Sib. Branch of Russian Acad. Sci., 1996. P. 461–467.

737. *Балыкин В.И., Ларюшин Д.В., Субботин М.В., Летохов В.С.* Увеличение атомной фазовой плотности в полом лазерном волноводе // Письма в ЖЭТФ. 1996. Т. 63 (10). С. 763–767.

738. *Klimov V.V., Letokhov V.S.* Atom optics in laser near field // Laser Physics. 1996. Vol. 6. P. 475–500.

739. *Balykin V.I., Subbotin M.V., Letokhov V.S.* Reflection of an electron beam by femtosecond light waves // Optics Commun. 1996. Vol. 129. P. 177–183.

740. *Konopsky V.N., Sekatskii S.K., Letokhov V.S.* Laser photoelectron projection microscopy with subwavelength spatial resolution // Appl. Surface Science. 1996. Vol. 94/95. P. 148–155.

741. *Letokhov V.S.* Multiple photon laser chemistry: from nanoseconds to femtoseconds. In Femtochemistry / ed. by M. Chergui. Singapore: World Scientific, 1996. P. 25–34.

742. *Letokhov V.S.* Some future trends of laser biomedicine. In: Biomedical optical istrumentation and laser-assisted biotechnology / ed. by A.M. Verga Scheggi, S. Martellucci, A.N. Chester, R. Pratesi. Dordrecht: Kluwer Acad. Publ., 1996. P. 3–20.

743. *Karu T., Kurchikov A., Letokhov V., Mokh V.* He–Ne laser radiation influences single-channel ionic currents through cell membranes: a patch-clamp study // Lasers in the Life Sciences. 1996. Vol. 7 (1). P. 35–48.

744. *Klimov V.V., Letokhov V.S.* SPIE Proceedings of Low-power light on biological systems / ed. by. G. Bottiroli, T. Karu, R. Lubart. 1997. 3198. P. 57–66.

745. *Klimov V.V., Letokhov V.S.* Hard X-radiation emitted by a charged particle moving in a carbon nanotube // Physics Lett. A. 1996. Vol. 222 (6). P. 424–428.

746. *Konopsky V.N., Sekatskii S.K., Letokhov V.S.* Laser resonance photoelectron microscopy with a subwavelength-high spatial resolution: the first observation of single color-centers on surface // Optics Commun. 1996. Vol. 132. P. 251–256.

747. *Konopsky V.N., Sekatskii S.K., Letokhov V.S.* Resonance ionization spectromicroscopy (RISM) with subwavelength spatial resolution: the first observation of single color centers. In: Resonance Ionization Spectroscopy 1996 / ed. by N. Winograd, J. Parks. ATP Conference Proceeding, 388, Am. Ins. Ph., Woodbury, N.Y. 1997.

748. *Klimov V.V., Ducloy M., Letokhov V.S.* Radiative frequency shift and linewidth of an atom dipole in vicinity of a dielectric microsphere // J. of Modern Optics. 1996. Vol. 43. P. 2251–2267.

749. *Klimov V.V., Letokhov V.S.* Quadrupole radiation of an atom in the vicinity of dielectric microsphere // Phys. Rev. A. 1996. Vol. 54 (3). P. 4408–4423.

750. *Sekatskii S.K., Letokhov V.S.* Single fluorescence centers on the tips of crystal needles: first observation and prospects for application in scanning one-atom fluorescence microscopy // Appl. Phys. B. 1996. Vol. 63. P. 523–530.

751. *Aseyev S.A., Petrunin V.V., Letokhov V.S.* Ionization of fast Rydberg atoms in a magnetic field // Comm. Atom. Molec. Phys. 1996. Vol. 33(1). P. 41–52.

752. *Letokhov V.S.* Mixed electron-nuclear transitions in multiply charged ions: potentialities for X-γ-laser. In: X-ray Lasers 1996 / ed. by S. Svedberg and C.G. Wahlström. Proceed. of 5th Intern. Conf., Lund, Sweden, June 1996. Publ. of Inst. of Physics. Vol. 151. Bristol, 1996. P. 483–490.

753. *Karu T.I., Ryabykh T.P., Antonov S.N., Letokhov V.S.* Different sensitivity of cells from tumor-bearing organisms to continuous-wave and pulsed laser radiation (λ = 632.8 nm) evaluated by chemiluminescence test. Proc. of SPIE 2929, Effects of low-power light on biological system II / ed. by G. Jori and T. Karu, 2–11. 1996.

754. *Karu T.I., Ryabykh T.P., Letokhov V.S.* Different sensitivity of cells from tumor-bearing organisms to continuous-wave and pulsed laser radiation (λ = 632.8 nm) evaluated by chemilumenescence test: III Effect of dark period between pulses // Lasers in the Life Sciences. 1997. Vol. 7(13). 141–146.

755. *Laryushin D.V., Ovchinnikov Yu.B., Balykin V.I., Letokhov V.S.* Reflection cooling of sodium atoms in an evanescent light wave // Optics Commun. 1996. Vol. 135. P. 138–148.

756. *Konopsky V.N., Letokhov V.S., Sekatskii S.K.* Field- and photoassisted field emission studies of calcium fluoride coated silicon tips // J. de Physique. 1996. IV. 6. P. 129–134.

757. *Karabutov A.A., Podymova N.B., Letokhov V.S.* Time-resolved laser optoacoustical tomography of inhomogeneous media // Appl. Phys. B. 1996. Vol. 63. P. 545–563.

758. *Dobryakov A.L., Farztdinov V.M., Lozovik Yu.E., Matveetz Yu.A., Stepanov A.G., Yartsev A.P., Letokhov V.S.* Femtosecond optical spectroscopy of fullerites.Proc. of SPIE. 1996. 2797. P. 97–101.

759. *Konopsky V.N., Letokhov V.S.* Toward direct observation of the atomic structure of biomolecules with nanometer spatial resolution by visible light // Laser Phys. 1997. Vol. 7. P. 173–178.

760. *Klimov V.V., Letokhov V.S.* Monochromatic γ-radiation emitted by a relativistic electron moving in a carbon nanotube // Phys. Lett. A. 1997. Vol. 226. P. 244–252.

761. *Fedorov M.V., Goreslavsky S.P., Letokhov V.S.* Pondermotive forces and stimulated compton scattering of free electrons in a laser field // Phys. Rev. 1997. E 55. P. 1015–1027

762. *Klimov V.V., Letokhov V.S.* Vacuum splitting of the energy levels of a system consisting of an atom and a dielectric microsphere // JETP. 1997. Vol. 84 (1). P. 24–28.

763. *Subbotin M.V., Balykin V.I., Laryushin D.V., Letokhov V.S.* Laser controlled atom waveguide as a source of ultracold atoms // Opt. Commun. 1997. Vol. 139. P. 107–116.

764. *Ivanov L.N., Letokhov V.S.* The splitting of excited electronic states in optically inactive molecules due to the parity-violating electron-nuclear interaction // J. Chem. Phys. 1997. Vol. 106 (14). P. 6045–6050.

765. *Секацкий С.К., Летохов В.С.* Наблюдение одиночного лазерно-возбужденного центра на острие кристаллической иглы // Письма в ЖЭТФ. 1997. Т. 65 (6). С. 441–444.

766. *Klimov V.V., Ducloy M., Letokhov V.S.* Vacuum Rabi splitting of an atom dipole near a dielectric microsphere // J. Modern Opt. 1997. Vol. 44 (6). P. 1081–1092.

767. *Badikov V.V., Blinov P.S., Kosterev A.A., Letokhov V.S., Malinovskii A.L., Ryabov E.A.* Efficient parametric oscillators of picosecond mid-IR pulses based on $AgGaS_2$ crystals // Quant. Electron. 1997. Vol. 27 (6). P. 523–526.

768. *Minogin V.G., Fedorov M.V., Letokhov V.S.* Formation of ultrashort electron pulses on scattering of an electron beam by a standing laser wave of ultrashort duration // Optics Commun. 1997. Vol. 140. P. 250–254.

769. *Letokhov V.S.* Femtosecond laser control of electronic beams for ultrashort diffraction. In: Chemical Reactions and their Control on the Femtosecond Time Scale / ed. by P. Gaspard and I. Burghardt. Proced. of XXth Solvay Conference on Chemistry. Adv. in Chem. Phys. Vol. 101. Wiley, 1997. P. 185–192.

770. *Letokhov V.S.* Femtospectrochemistry: Novel possibilities with three-dimensional (space-time) resolution. In: Chemical reactions and their control on the femtosecond time scale / ed. by P. Gaspard and I. Burghardt. Proceed. of XXth Solvay Conference on Chemistry. Adv. in Chem. Phys. Vol. 101. Wiley, 1997. P. 873–887.

771. *Letokhov V.S.* Concluding remark on XXth Solvay conference on chemistry. In: Chemical reactions and their control on the femtosecond time scale / ed. by P. Gaspard and I. Burghardt.Proceed. of XXth Solvay Conference on Chemistry, Adv. in Chem. Phys. Vol. 101. Wiley, 1997. P. 896–898.

772. *Farztdinov V.M., Dobryakov A.L., Letokhov V.S., Lozovik Yu.E., Matveetz Yu.A., Kovalenko S.A., Ernsting N.R.* Spectral dependence of femtosecond relaxation and coherent photon excitation in C_{60} films // Phys. Rev. B. 1997. Vol. 56 (7). P. 4176–4185.

773. *Klimov V.V., Ducloy M., Letokhov V.S.* Vacuum Rabi splitting of energy levels in a strongly coupled system of two-evel atom and dielectric microsphere // Phys. Rev. A. 1997. Vol. 56 (3). P. 2308–2315.

774. *Lapshin D.A., Balykin V.I., Letokhov V.S.* Diffraction of atoms by an evanescent-wave grating formed by a periodical surface structure // Laser Phys. 1997. Vol. 7 (2). P. 361–368.

775. *Balykin V.I., Laryushin D.V., Subbotin M.V., Letokhov V.S.* A bright coherent source of de Broglie waves // Laser Phys. 1997. Vol. 7 (2). P. 358–360.

776. *Letokhov V.S., Sekatskii S.K.* Laser spectroscopy with subwavelength spatial resolution: Recent achievements and future perspectives // J. Korean Phys. Soc. 1997. Vol. 30 (2). P. 353–358.

777. *Sekatskii S.K., Letokhov V.S.* Laser femtosecond photoelectron projection microscopy with an ultrahigh spatial resolution. Proceed. of the 5th Symp. on Laser Spectroscopy, Korea, Nov. 1997. Vol. 5 (3). P. 33–50.

778. *Aseev S.A., Kunets A.V., Letokhov V.S.* Development of a laser method for the detection of a rare aluminium isotope // Laser Phys. 1997. Vol. 7 (2). P. 356–357.

779. *Афанасьева Н.И., Артюшенко В.Г., Кольяков С.Ф., Пахомов Д.Ю., Соколов В.В., Франк Г.А., Летохов В.С.* Спектральная диагностика опухолевых тканей методом волоконно-оптической спектроскопии // ДАН. 1997. Т. 356 (1). С. 118–121.

780. *Afanasyeva N., Kolyakov S.F., Letokhov V.S., Golovkina V.N.* Diagnostics of cancer tumors by fiberoptic evanescent wave. Fourier transform IR (FEW FTIR) spectroscopy, SPIE Proceed. 1997. 2979. P. 478–486.

781. *Klimov V.V., Letokhov V.S.* Hard directional X–radiation emitted by a positron moving in a carbon nanotube // Physica Scripta. 1997. Vol. 56. P. 480–486.

782. *Klimov V.V., Letokhov V.S.* Hard highly directional X–radiation emitted by a charged particle moving in a carbon nanotube. In: Atomic Physics Methods in Modern Research / ed. by K. Jungman, J. Kowalski, I. Peinard, F. Trager (Berlin, Springer, 1997), 167–164.

783. *Klimov V.V., Letokhov V.S.* Dynamics and radiation of charged particle moving in a carbon nanotube. In: Nanostructures: Physics and Technology. Proceed. of Int. Symp. / ed. by Zh. Alferov and L. Esaki. St.-Petersburg, 1997. P. 407–410.

784. *Demyanenko A.V., Letokhov V.S., Puretskii A.A., Ryabov E.A.* Emission spectroscopy of a carbon plasma formed by laser ablation of graphite. I. Ablation by XeCl laser radiation // Quant. Electron. 1997. Vol. 27 (11). P. 983–987.

785. *Letokhov V.S., Sekatskii S.K.* Laser-excited one-atom source of electrons // J. of Nonlinear Optical Physics and Materials. 1997. Vol. 6 (4). P. 411–420.

786. *Гордеев В.В., Егоров А.С., Лисицин А.П., Летохов В.С., Пахомов Д.Ю., Гулевич В.М.* Растворимое золото в поверхностных водах северо–восточной Атлантики // Геохимия. 1997. № 11. С. 1139–1148.

787. *Letokhov V.S.* Multiphoton nanosecond-to-femtosecond laser chemistry. In: Femtochemistry and femtobiology: ultrafast reaction dynamics at atomic-scale resolution / ed. by V. Sundström, Proceed. of Nobel Symposium, Sept. 9–12, 1996, Bjorkborn. Imperial College Press, 1997. P. 597–628.

788. *Letokhov V.S.* Ultrafast processes: from the past to the future. In: Femtochemistry and femtobiology: ultrafast reaction dynamics at atomic-scale resolution / ed. by V. Sundström, Proceed. of Nobel Symposium, Sept. 9–12, 1996, Bjorkborn. Imperial College Press, 1997. P. 755–763.

789. *Balykin V.I., Lapshin D.A., Subbotin M.V., Letokhov V.S.* Near field diffraction grating for atoms, // Optics Commun. 1998. Vol. 145. P. 322–328.

790. *Makarov A.A., Petrova I.Yu., Ryabov E.A., Letokhov V.S.* Statistical inhomogeneous broadening of infrared and Raman transitions in highly vibrationally excited XF_6 molecules // J. Phys. Chem. A. 1998. Vol. 102. P. 1438–1449.

791. *Лапшин Д.А., Решетов В.Н., Секацкий С.К., Летохов В.С.* // Письма в ЖЭТФ. 1998. Т. 67 (4). С. 245–250.

792. *Letokhov V.S., Sekatskii S.K.* On the possibility of ultra-high density WROM based on the using of laser and corpuscular beams // Optics Commun. 1998. Vol. 147 (1–3). P. 19–25.

793. *Dem'yanenko A.V., Letokhov V.S., Puretskii A.A., Ryabov E.A.* Emission spectroscopy of a carbon plasma formed by laser ablation of graphite-2. Ablation by a CO_2 laser and also simultaneously by XeCl and CO_2 lasers // Quant. Electron. 1998. Vol. 25 (1). P. 36–40.

794. *Lapshin D.A., Balykin V.I., Letokhov V.S.* Imaging of the near-field over the reflection phase grating by the apertureless photon scanning tunneling microscope // J. of Modern Optics. 1998. Vol. 45. P. 747–758.

795. *Klimov V.V., Letokhov V.S.* Resonance energy exchange at nanoscale curved interface // Chem. Phys. Lett. 1998. Vol. 285. P. 313–320.

796. *Dem'yanenko A.V., Ryabov E.A., Letokhov V.S.* IR multiple-photon dissociation of $Br(CF_2)_4COI$ molecules by excitation via C = 0 (1794 cm^{-1}) stretching and sceleton (961 cm^{-1}) vibrations // Chem. Phys. Lett. 1998. Vol. 286. P. 277–283.

797. *Afanasieva N., Artjushenko V., Kolyakov S., Lerman A., Pakhomov D., Sokolov V., Letokhov V.* Fiberoptic evanescent mid–IR Fourier transform spectroscopy of cancer tissue // Lasers in the Life Sciences. 1998. Vol. 8 (2). P. 65–79.

798. *Секацкий С.К., Серебряков Д.В., Летохов В.С.* Лазерная фотоионная фотоселективная микроскопия с разрешением 5 нм // Письма в ЖЭТФ. 1998. Т. 67 (7). С. 450–454.

799. *Sekatskii S.K., Chekalin S.V., Ivanov A.L., Matveets Yu.A., Stepanov A.G., Letokhov V.S.* Femtosecond two-photon laser photoelectron microscopy // J. Phys. Chem. A. 1998. Vol. 102. P. 4148–4153.

800. *Климов В.В., Летохов В.С.* Резонансная флуоресценция системы атом+диэлектрическая микросфера, возбужденная единичным фотоном // Письма в ЖЭТФ. 1998. Т. 68. С. 115–120.

801. *Klimov V.V., Letokhov V.S.* Resonance interaction between two atomic dipoles separated by the surface of a dielectric nanosphere // Phys. Rev. A. 1998. Vol. 58. P. 3235–3247.

802. *Malinovsky A.L., Petrova I.Yu., Ryabov E.A., Makarov A.A., Letokhov V.S.* Transition spectra in the vibrational quasicontinuum of polyatomic molecules. Raman spectra of highly excited SF_6 molecules // J. Phys. Chem. 1998. Vol. 102. P. 9353–9359.

803. *Sekatskii S.K., Serebryakov D.V., Letokhov V.S.* Direct observation of light–absorbing nanocrystals in glass matrices by the projection laser photoion microscopy technique // Rev. Sci. Instr. 1998. Vol. 69 (11). P. 3885–3888.

804. *Иванов Л.Н., Летохов В.С.* Влияние заряда и положения атома на нарушение четности и различие в энергии молекулярных энантиомеров // ДАН. 1998. Т. 43 (9). С. 36–39.

805. *Sekatskii S.K., Serebryakov D.V., Letokhov V.S., Zhirnov V.V., Meshcheryakova A.L., Alvarez J.C., Sokolov N.S.* Field desorption imaging of insulator surfaces: High-resolution images of Calcium Fluoride epitaxial layers // Appl. Surface Science. 1999. Vol. 140. P. 46–51.

806. *Klimov V.V., Letokhov V.S.* Enhancement and inhibition of spontaneous emission rates in nanobubbles // Chem. Phys. Lett. 1999. Vol. 301. P. 441–448.

807. *Lapshin D.A., Reshetov V.N., Sekatskii S.K., Letokhov V.S.* Contact mode near-field microscopy // Ultramicroscopy. 1999. Vol. 76. P. 13–20.

808. *Klimov V.V., Ducloy M., Letokhov V.S.* Strong interaction between a two-level atom and the whispering gallery modes of a dielectric microsphere: Quantum-mechanical consideration // Phys. Rev. A. 1999. Vol. 59 (4). P. 2996–3014.

809. *Klimov V., Ducloy M., Letokhov V.* Quasiorbital motion of ultracold excited atomic dipole near dielectric microsphere // Eur. Phys. J. 1999. D5. P. 345–350.

810. *Shubeita G.I., Sekatskii S.K., Chergui M., Dietler G., Letokhov V.S.* Investigation of nanolocal fluorescence resonance energy transfer for scanning probe microscopy //Appl. Phys. Lett. 1999. Vol. 74 (23). P. 3453–3455.

811. *Климов В.В., Летохов В.С.* Спектр двухфотонной флюоресценции в системе атом + диэлектрическая микросфера // Письма в ЖЭТФ. 1999. Т. 70. С. 192–197.

812. *Климов В.В., Летохов В.С.* Точное решение задачи о лазерной фокусировке атомного пучка // Письма в ЖЭТФ. 1999. Т. 70. С. 654–659.

813. *Секацкий С.К., Чекалин С.В., Иванов А.Л., Компанец В.О., Матвеец Ю.А., Степанов А.Г., Летохов В.С.* Проекционная фотоэлектронная микроскопия сверхвысокого пространственного разрешения с использованием фемтосекундных лазеров // ЖЭТФ. 1999. Т. 115 (5). С. 1680–1688.

814. *Lokhman V.N., Petin A.N., Ryabov E.A., Letokhov V.S.* Transition spectra in the vibrational quasicontinuum of polyatomic molecules. IR multiple-photon absorption in SF_6. I. Experimental studies // J. Phys. Chem. 1999. Vol. 103. P. 11293–11298.

815. *Lokhman V.N., Makarov A.A., Petrova I.Yu., Ryabov E.A., Letokhov V.S.* Transition spectra in the vibrational quasicontinuum of polyatomic molecules. IR multiple-photon absorption in SF6. II. Theoretical stimulations and comparison with experiment // J. Phys. Chem. 1999. Vol. 103. P. 11299–11309.

816. *Letokhov V.S.* How to rebuild Russian science // Phys. World, Jan. 1999. P. 14–15.

817. *Letokhov V.S., Sekatskii S.K.* Laser resonance photoelectron/photoion microscopy with subwavelength spatial resolution. In: Advances in Laser Physics, vol. 21 / ed. by V. Letokhov, P. Meystre. Laser Science and Technology. Harwood Academic Publ., 2000. P. 85–115.

818. *Sekatskii S.K., Chekalin S.V., Ivanov A.L., Kompanetz V.O., Matveets Yu.A., Stepanov A.G., Letokhov V.S.* Quantitative measurements of the local coefficient of two-photon photoelectric effect by the femtosecond laser photoelectron microscopy // J. Nonlinear Opt. 2000. Vol. 23. P. 157–170.

819. *Lapshin D.A., Kobylkin E.E., Letokhov V.S.* Shear force distance control in near-field optical microscopy: Experimental evidence of the frictional probe-sample interaction // Ultramicroscopy. 2000. Vol. 83. P. 17–23.

820. *Klimov V.V., Letokhov V.S.* Effect of the curvature of nanostructures on radiative multipole transitions rates // Comm. Modern Phys. 2000. Vol. 2(1). P. D15–27.

821. *Летохов В.С.* Принципы лазерного разделения изотопов. В кн.: Изотопы / под ред. В.Ю. Баранова. М., 2000. С. 291–307.

822. *Летохов В.С., Рябов Е.А.* Многофотонная изотопически-селективная ИК диссоциация молекул. Изотопы: свойства, получение, применение. В кн.: Изотопы / под ред. В.Ю. Баранова. М., 2000. С. 329–342.

823. *Sekatskii S.K., Shubeita G.T., Chergui M., Dietler G., Mironov B.N., Lapshin D.A., Letokhov V.S.* Towards the fluorescence resonance energy transfer (FRET) scanning near-field optical microscopy: investigation of nanolocal FRET processes and FRET probe microscope // JETP. 2000. Vol. 90 (5). P. 769.

824. *Balykin V.I., Minogin V.G., Letokhov V.S.* Electromagnetic trapping of cold atoms // Reports on Progr. in Physics. 2000. 63 (9). P. 1429–1510.

825. *Балыкин В.И., Летохов В.С.* Возможность «информационного» охлаждения нейтральных атомов // Письма в ЖЭТФ. 2000. Т. 72 (1). С. 18–22.

826. *Klimov V.V., Letokhov V.S.* Coherent radiation scattering by resonant nanostructures // Phys. Rev. B. 2000. Vol. 62(3). P. 1639–1642.

827. *Kosterev A.A., Makarov A.A., Malinovsky A.L., Petrova I.Yu., Ryabov E.A., Letokhov V.S.* Transition spectra in the vibrational quasicontinuum of polyatomic molecules: Raman spectra of highly excited UF6 molecules // J. Phys. Chem. A. 2000. Vol. 104. P. 10259–10264.

828. *Dem'yanenko A.V., Lokhman V.N., Ogurok D.D., Ryabov E.A., Letokhov V.S.* Direct observation of S^+ and SF^{++} ions resulting from the IR+UV laser irradiation of SF_6 molecules // Chem. Phys. Lett. 2000. Vol. 320. P. 594–600.

829. *Baranov V.Yu., Dyadkin A.P., Malyuta D.D., Kuzmenko V.A., Pigulsky S.V., Mezhevov V.S., Letokhov V.S., Laptev V.B., Ryabov E.A., Yarovoi I.V., Zarin V.B., Podoryashy A.S*. Production of carbon isotopes by laser separation. In: Progress in Research and Development of High-Power CO_2 Lasers / ed. by V. Panchenko, V. Golubev. Proceed. of SPIE 4165. 2000. P. 314–323.

830. *Миронов Б.Н., Лапшин Д.А., Секацкий С.К., Летохов В.С.* Эмиссионная проекционная микроскопия диэлектрических образцов со сверхвысоким пространственным разрешением // Письма в ЖЭТФ. 2001. Т. 74 (4). С. 263–266.

831. *Sekatskii S.K., Mironov B.N., Lapshin D.A., Dietler G., Letokhov V.S.* Analysis of scanning near-field optical microscopy fiber probes by field emission microscopy // Ultramicroscopy. 2001. Vol. 89 (1–3). P. 83–87.

832. *Johansson S., Letokhov V.S.* Resonance-enhanced two-photon ionization of ions by Lyman radiation in gaseous Nebulae // Science. 2001. Vol. 291. P. 625–627.

833. *Johansson S., Letokhov V.S.* Multiple two-photon resonance-enhanced ionization of elements in natural conditions // Письма в ЖЭТФ. 2001. Т. 73 (3). С. 134–136.

834. *Johansson S., Letokhov V.S.* Mysterious UV lines of FeII from car blobs. In: Eta Carinae and other mysterious stars / ed. by T. Gull, S. Johansson, K. Davidson // ASP Conf. Series. 2001. Vol. 242. P. 297–308.

835. *Johansson S., Zethson T., Hartman H., Letokhov V.S.* Fluorescence lines in Carinae and other objects. In: Eta Carinae and Other Mysterious Stars / ed. by T. Gull, S. Johansson, K. Davidson // ASP Conf. Series 2001.Vol. 242. P. 309–324.

836. *Balykin V.I., Letokhov V.S.* Information cooling of neutral atoms // Phys. Rev. A. 2001. Vol. 64 (6). P. 3410.

837. *Sekatskii S.K., Letokhov V.S.* Electron tunneling time measurements by field emission microscopy // Phys. Rev. B. 2001. Vol. 64. P. 233311.

838. *Lokhman V.N., Ogurok D.D., Ryabov E.A., Letokhov V.S.* IR multiple-photon + UV multiphoton laser selective fragmentation and ionization of SF_6 and CF_2HCl molecules // Zeitschrift für Physikalische Chemie. 2001. No. 215 (12). S. 1469–1485.

839. *Климов В.В., Дюклуа М., Летохов В.С.* Спонтанное излучение атома в присутствии нанотел//Квантовая электроника. 2001. Т. 31 (7). С. 569–586.

840. *Johansson S., Letokhov V.S.* A model for the origin of the anomalous and very bright UV lines of FeII in gaseous condensations of the star Eta Carinae // Astron. and Astrophys. 2001. 378 (1). P. 266–278.

841. *Letokhov V.S.* Possibility of ESCA microscopy with laser femtosecond EUV–X-ray pulses // Письма в ЖЭТФ. 2001. Т. 74 (9). С. 520–522.

842. *Johansson S., Letokhov V.S.* Successive resonance-enhanced two-photon ionization of elements inside Nebulae: I. Atoms and ions C, N, and O // Astron. and Astrophys. 2001. Vol. 376. P. 319–327; [Erratum: AA, 395, 345 (2002)].

843. *Letokhov V.S.* Electromagnetic trapping of cold atoms: an overview. Trapped Particles and Fundamental Physics / S.N. Atutov, R. Calabrese, L. Moi (eds.), Kluwer Acad. Publ., 2002. P. 11–40.

844. *Klimov V., Johansson S., Letokhov V.* The origin of the anomalous intensity ratio between very bright UV FeII lines and its satellites in gaseous condensations of the star Eta Carinae // Astronomy and Astrophysics. 2002. Vol. 335. P. 313–327.

845. *Serebryakov D.V., Cherkun A.P., Loginov B.A., Letokhov V.S.* Tuning-fork based fast highly-sensitive surface-contact sensor for AFM/SNOM // Rev. Sci. Instr. 2002. Vol. 73. P. 1795–1802.

846. *Shubeita G.T., Sekatskii S.K., Dietler G., Letokhov V.S.* Local fluorescent probes for the fluorescence resonance energy transfer scanning near-field optical microscopy // Appl. Phys. Lett. 2002. Vol. 80. P. 2625–2627.

847. *Klimov V.V., Ducloy M., Letokhov V.S.* Emission of an atom placed near prolate nanospheroid // European J. of Physics. 2002. D 20. P. 133–148.

848. *Klimov V.V., Ducloy M., Letokhov V.S.* A model of an apertureless near-field scanning microscope with a prolate nanospheroid as a tip and excited molecule as an object // Chem. Phys. Lett. 2002. Vol. 358. P. 192–198.

849. *Letokhov V.S.* Some prospects of EUV-X-ray femtosecond pulses in chemical pulses. In: Femtochemistry and Femtobiology / ed. by A. Douhal and J. Santamaria // Proceed. of Femtochemistry-V, 2–6 September, 2001, Toledo, Spain. Singapore: World Scientific Publ. Co., 2002. P. 459–471.

850. *Johansson S., Letokhov V.S.* Laser action in space: 1 μm lines of FeII in gaseous condensations in the vicinity of η Car // Письма в ЖЭТФ. 2002. Т. 75 (10). С. 591–594.

851. *Lapshin D.A., Shubeita G.I., Sekatskii S.K., Dietler G., Letokhov V.S.* Direct measurements of the absolute value of the interaction force between fiber probe and sample in scanning near-field optical microscopy // Appl. Phys. Lett. 2002. Vol. 81 (8). P. 1503–1505.

852. *Секацкий С.К., Летохов В.С.* Визуализация волновой функции квантовой частицы в импульсном пространстве методом автоэлектронной микроскопии // ЖЭТФ. 2002. Т. 122 (2). С. 245–257.

853. *Летохов В.С., Секацкий С.К.* Новый класс источников монохроматического пространственно-некогерентного излучения: безрезонаторные порошковые лазеры с накачкой от полевых эмиссионных катодов // Квантовая электроника. 2002. Т. 32 (11). С. 1007–1008.

854. *Letokhov V.S.* Femtosecond laser pulses and their applications // Herald of Russ. Acad. of Sci. 2002. Vol. 72 (9). P. 779–785.

855. *Летохов В.С.* Астрофизические лазеры // Квантовая электроника. 2002. Т. 32 (12). С. 1065–1079.

856. *Летохов В.С.* Лазерный эффект в космосе // УФН. 2002. Т. 172 (12). С. 1468–1470.

857. *Makarov A.A., Letokhov V.S.* Comment of scheme for multistep photoionization of atoms // Phys. Rev. A. 2002. Vol. 66. P. 047401–2.

858. *Letokhov V.S.* Laser light in biomedicine and life sciences: present to the future, Biomedical Photonics Handbook / ed. by Tuan Vo-Dinh. CRC Press, Boca Raton, 2003. P. 5.1–5.15.

859. *Johansson S., Letokhov V.S.* Radiative cycle with stimulated emission from atoms and ions in an astrophysical plasma // Phys. Rev. Lett. 2003. Vol. 90 (1). P. 011101.

860. *Lokhman V.N., Makarov A.A., Ogurok D.D., Ryabov E.A., Letokhov V.S.* UV multiphoton fragmentation and ionization of SF_5 radicals and highly excited SF_6 molecules // Chem. Phys. 2003. Vol. 286. P. 385–397.

861. *Klimov V.V., Letokhov V.S.* Laser focusing of cold atoms: analytical solution of the problem // Laser Physics. 2003. Vol. 13 (3). P. 339–349.

862. *Dobryakov A.L., Letokhov V.S.* On the physics of ultraweak bioluminescence and intercellular photon signaling, Proceed. Int. Workshop "Energy and information transfer in biological systems / ed. by F. Musumeci et al. (18–22 Sept., 2002, Catania, Italy). Singapore: World Scientific. 2003. P. 205–216.

863. *Letokhov V.S.* Atomic physics at accelerators: Laser spectroscopy and applications // Physica Scripta. 2003. 68. P. 6–9.

864. *Sekatskii S.K., Mironov B.N., Kompanets V.O., Matveets Yu.A., Chekalin S.V., Dietler G., Letokhov V.S.* Nonperturbating observation of optical near field by means of two-photon ionization by ultrashort laser pulses // Appl. Phys. Lett. 2003. Vol. 83 (24). P. 4900–4902.

865. *Секацкий С.К., Миронов Б.Н., Компанец В.О., Матвеец Ю.А., Чекалин С.В., Летохов В.С., Dietler G.* Невозмущающая визуализация света в ближнем поле с помощью фемтосекундных импульсов // Нанофотоника. 2003. С. 489–492.

866. *Balykin V.I., Letokhov V.S.* Atomic opto-spintron correlator based on selective specular reflection // Quant. Electron. 2003. Vol. 33 (7). P. 628–632.

867. *Makarov A.A., Letokhov V.S.* Spontaneous decay of two spatially separated atoms (one-imensional case) // JETP. 2003. Vol. 97 (4). P. 668–701.

868. *Johansson S., Letokhov V.S.* Anomalously bright UV lines of Fe II as a probe for gas condensations in vicinity of hot stars // Astronomy and Astrophysics. 2003. Vol. 412. P. 771–776.

869. *Балыкин В.И., Климов В.В., Летохов В.С.* Атомная нанооптика на основе фотонных точек и фотонных дырок // Письма в ЖЭТФ. 2003. Т. 78 (1). С. 11–15.

870. *Johansson S., Letokhov V.S.* Anomalous spectral effects Fe II lines and high temperature HI Lyα in gaseous condensations in vicinity of η Carinae // Astronomy Lett. 2004. Vol. 30 (1). P. 58–63.

871. *Letokhov V.S.* Nanooptics: atoms in the near field. Tribute to Emil Wolf. Bellingham, WA: SPIE Press, 2004. P. 477–490.

872. *Letokhov V.S., Ryabov E.A.* Laser isotope separation. In: Optical Encyclopedia / ed. by Th.G. Brown et al. (Wiley–VCH). Vol. 2. 2004. P. 1015–1028.

873. *Джохансон С., Летохов В.С.* Возможность последовательной резонансно-усиленной двухфотонной ионизации Ne и Ar в астрофизической плазме // Астроном. журнал. 2004. Т. 81 (4). С. 1–9.

874. *Lapshin D.A., Letokhov V.S., Shubeita G.T., Sekatskii S.K., Dietler G*. Shear force distance control in a scanning near-field optical microscope in resonance excitation of the fiber probe versus out of resonance excitation // Ultramicroscopy. 2004. 99 (4). P. 227–233.

875. *Balykin V.I., Klimov V.V., Letokhov V.S.* Atom nanooptics // 2005. OPN. 16 (3). P. 44–48.

876. *Johansson S., Letokhov V.S.* Stimulated amplification in spatially nonhomogeneous conditions: Astrophysical Fe II laser in vicinity of Eta Carinae // Physica Scripta. 2005. 120. P. 99–104.

877. *Cherkun A.P., Serebryakov D.V., Sekatskii S.K., Morozov I.V., Letokhov V.S.* Double-resonance probe for scanning near-field optical microscopy // Rev. Sci. Instr. 2006. Vol. 77. P. 033703.

ИЗБРАННЫЕ НАУЧНЫЕ ТРУДЫ ПРОФЕССОРА В.С. ЛЕТОХОВА

Составители:
В.И. Балыкин, В.Н. Задков,
Е.А. Рябов, С.В. Чекалин

Формат 70x100 1/16
Гарнитура Times
Усл.-п. л. 43,23. Уч.-изд. л. 36,35
Тираж 300 экз.

Издатель – Российская академия наук

Публикуется в авторской редакции

Корректура и верстка – ООО «ВИН»
Отпечатано в экспериментальной цифровой типографии РАН

Издается по решению Научно-издательского совета
Российской академии наук (НИСО РАН) от 31.03.2023 г.

Распространяется бесплатно